

ANL-05/04

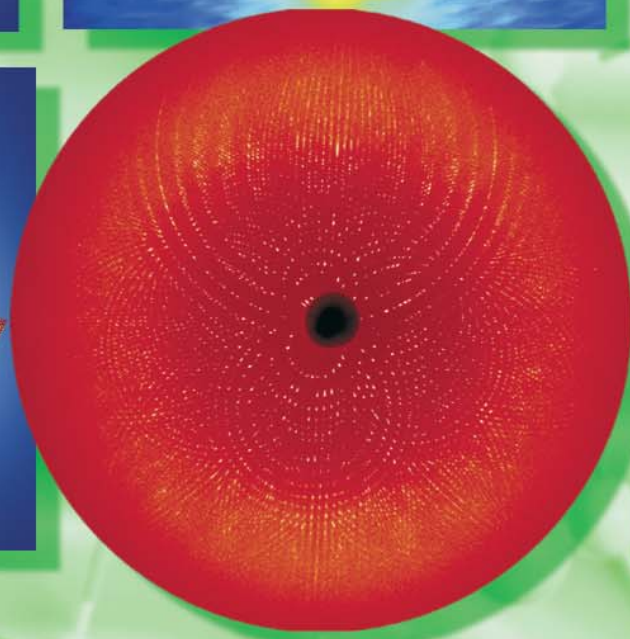
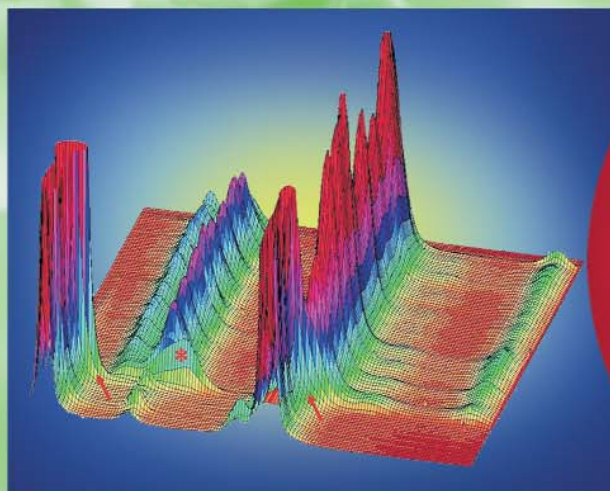
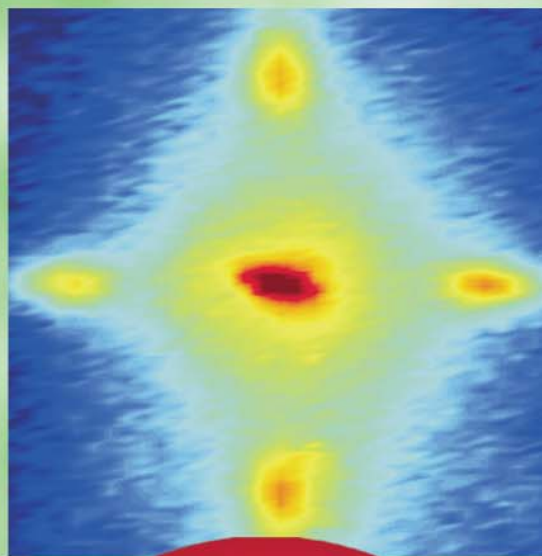
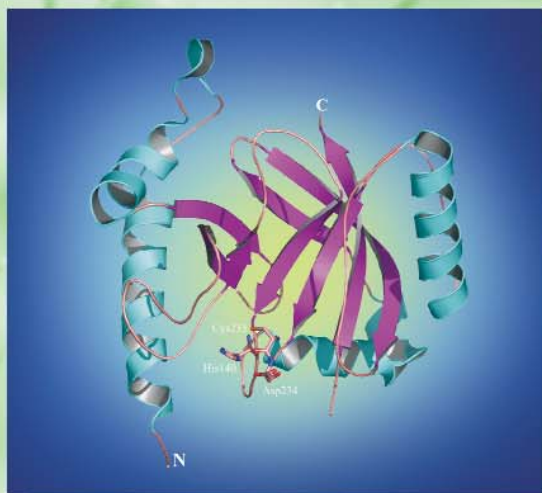
APS SCIENCE

2004

The annual report of the
Advanced Photon Source
at Argonne National Laboratory

May 2005

Includes the special section: "Five-Year Scientific Vision for the Advanced Photon Source"



Argonne National Laboratory is operated by The University of Chicago for the U.S. Department of Energy Office of Science



APS SCIENCE 2004 • May 2005 • Argonne National Laboratory • ANL-05/04

Support for the Advanced Photon Source

Argonne National Laboratory's Advanced Photon Source is supported by the U.S. Department of Energy, Office of Science, Office of Basic Energy Sciences.

About Argonne National Laboratory

Argonne is operated by The University of Chicago for the U.S. Department of Energy Office of Science, under contract W-31-109-Eng-38. The Laboratory's main facility is outside Chicago, at 9700 South Cass Avenue, Argonne, Illinois 60439. For information about Argonne and its pioneering science and technology programs, see www.anl.gov.

Availability of This Report

This report is available, at no cost, at <http://www.osti.gov/bridge>. It is also available on paper to U.S. Department of Energy and its contractors, for a processing fee, from:

U.S. Department of Energy
Office of Scientific and Technical Information
P.O. Box 62
Oak Ridge, TN 37831-0062
phone (865) 576-8401
fax (865) 576-5728
reports@adonis.osti.gov

APS SCIENCE

**The annual report of the
Advanced Photon Source
at Argonne National Laboratory**

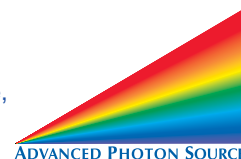
2004

May 2005 ANL-05/04

Includes the special section: "Five-Year Scientific Vision for the Advanced Photon Source"



The Advanced Photon Source is funded by the U.S. Department of Energy, Office of Science,
Office of Basic Energy Sciences,
under Contract W-31-109-ENG-38.



HOWARD K. BIRNBAUM 1932-2005



Dr. Howard Birnbaum, an expert in the science of materials who developed new concepts to prevent materials from failing, passed away on Monday, January 24, 2005. Dr. Birnbaum was a founding member and chair of the APS Proposal Evaluation Board (later the Program Evaluation Board) and its successor, the Scientific Advisory Committee (SAC), serving from 1989 to the present. In his advisory capacity from the earliest days of this facility, Howard played a major role in shaping the direction of the APS, thanks to his thoughtful recommendations and strategic vision. The APS and the entire materials research and synchrotron communities greatly miss his wit and wisdom.

"I owe a personal debt to Howard," said APS Director Murray Gibson, "both for his unflagging commitment to the APS, and for his support when I was a professor at the University of Illinois. Howard combined intelligence and integrity in a manner that defines scientific nobility."

Dr. Birnbaum's research interests involved physical metallurgy, the physics and mechanical properties of solids, dislocation theory, hydrogen in solids, interstitial diffusion, and hydrogen embrittlement. He was the Director Emeritus of the Materials Research Laboratory at the University of Illinois at Urbana-Champaign. In 1988, he was elected to the National Academy of Engineering for his exceptional work on the effects of hydrogen and hydrogen embrittlement on the properties of metal. In 2002, Dr. Birnbaum received the Materials Research Society's highest honor, the Von Hippel Award.

Dr. Birnbaum attended Columbia University (B.S., 1953, and M.S., 1955), then studied with Professor Tom Read at the University of Illinois (Ph.D. in metallurgy, 1958). He taught at The University of Chicago as an instructor and then as an assistant professor at the Institute for the Study of Metals. In 1961, he returned to the University of Illinois as an associate professor and was promoted to a full professor in 1963. His tenure at The University of Chicago Institute of Metals (the first interdisciplinary materials laboratory) and the University of Illinois' Materials Research Laboratory taught him the great promise of the interdisciplinary approach to research. After teaching in the field of materials science, he became the Director of the Frederick Seitz Materials Research Laboratory in 1987 and served in that capacity until his retirement in 1999.

Dr. Birnbaum's career, spanning the period in which several fields of science and engineering coalesced into the new field of materials science, was devoted to teaching, research, and the support of interdisciplinary materials science. He worked with about 40 Ph.D. graduate students and 20 research associates in a number of research areas, including defects in solids, deformation and fracture, hydrogen diffusion, and hydrogen behavior in materials. He is the author of many publications in these fields.

He was a fellow of the American Academy of Arts and Sciences, the American Association for the Advancement of Science, the American Physical Society, the Materials Society, and the American Society for Metals, and a member of the National Academy of Engineering.

WELCOME

J. MURRAY GIBSON...

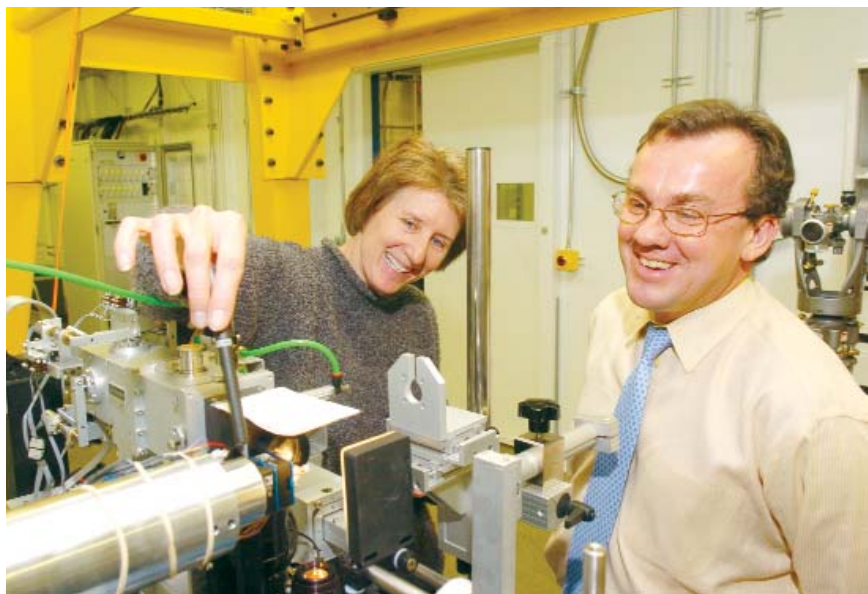
... is Associate Laboratory Director for Scientific User Facilities at Argonne National Laboratory and Director of the Advanced Photon Source.

Whether you are an existing user of the APS, a prospective user, or simply curious about our unique facility, I welcome your interest and hope that you find our 2004 annual report valuable. This was another milestone year for the APS. Growth was observed in most of our metrics; for example, the number of user visits increased by over 6% to 8,531 and our publication output increased by 17%. This healthy growth results from the availability of new beamlines, enhanced support, and increased time at existing beamlines. The machine operated at its most reliable yet—the mean time between faults exceeded two days for the first time ever. And the machine performance increased. For example, our real-time feedback system has been implemented to give a more stable beam using insertion device x-ray beam position monitors (see page 149).

For me, the highlight of 2004 was the culmination of our strategic planning for new scientific directions at the APS. A series of workshops involving more than 300 scientists (many not experienced users of synchrotrons) was held in the summer and resulted in the “Five-Year Scientific Vision for the APS” (page 12). In that document, we lay out compelling opportunities for instrumentation and new user communities to continue the growth of the APS into the next decade. I want to thank all the people who participated, especially the organizers of all the workshops: Gopal Shenoy (APS) and Sunil Sinha (U.C., San Diego).

Promising new construction is going on at the APS. The Center for Nanoscale Materials is being built, and we will soon see the construction of the final lab/office module at the APS—LOM 437. Sectors 30 (Inelastic X-ray Scattering), 26 (Nanoprobe), and 11-BM (Powder Diffraction) are under construction. And in the last year, three canted undulator beamlines for structural biology moved forward (see inset for a picture from the General Medicine and Cancer Institutes Collaborative Access Team [GM/CA-CAT] at sector 23, which achieved the first dual monochromatic beams into their research stations in early 2005). This year our activities in support of the next-generation x-ray laser—the Linac Coherent Light Source (LCLS) at Stanford—made significant progress as procurement began for the ~130 m of undulator

The APS increased its responsibility for the operation of beamlines that were previously supported by the U.S. Department of Energy, Office of Science, Office of Basic Energy Sciences. As of the time of this writing, we are now responsible for 12 sectors—a majority of the physical sciences beamlines at APS. The consolidation of these capabilities has added more stability and efficiency



Janet Smith (University of Michigan), Director of GM/CA-CAT, and Murray Gibson in the 23-ID-D research station.

in operation, and we work with these sectors, our partner users, and other CATs to best serve the user community. We recognize that a compelling need at our facility is the optimization of a larger number of dedicated beamlines in techniques such as small-angle scattering and high-energy x-ray scattering, and we have developed a strategic plan for our beamlines to accomplish this. This plan complements the APS five-year scientific vision, which focuses on completely new capabilities. The APS and our partner CAT users are evolving a strategic plan for the future of our beamlines that offers the broadest and most powerful spectrum of techniques to serve the scientific community.

In other news, Argonne National Laboratory went through a major change. What used to be Argonne West, in Idaho, is in 2005 now a part of the new Idaho National Laboratory. As a result, Argonne East underwent reorganization, which led to the creation of a new Directorate: Scientific User Facilities (SUF), which combines the APS and the Intense Pulsed Neutron Source (IPNS) into one Directorate, under my leadership. There are many shared interests between IPNS and APS and further opportunities to exploit the scientific complementarity of x-rays and neutrons.

The year 2004 saw a number of important safety innovations at APS, some the positive outcome of lessons learned from unfortunate events at APS and elsewhere. In particular, we have strengthened our user-accessible laser facilities at APS for improved safety of non-expert users. Internally, we have developed a robust and general series of policies and procedures for

Please see “Welcome” on page 7

THE APS SCIENTIFIC ADVISORY COMMITTEE

J. MICHAEL ROWE...

... (Chair, APS Scientific Advisory Committee) was the Director (now retired) of the Center for Neutron Research at the National Institute of Standards and Technology.

The Scientific Advisory Committee (SAC) met on January 25, 2005, having just received the sad news of the passing of Howard Birnbaum. His passing is a deep loss to the SAC, to all of the APS, and to me personally. Howard was a man who spoke truth to power; he was a man of the highest integrity, who was fearless in his dealings with any and all bureaucracies. At the same time, he was a man of learning and culture outside science, renowned for his personal kindness. In his final years, as he faced personal health problems that would have stopped lesser men, he was indomitable, continuing to function as only Howard could. He was the Chair of the original Proposal Evaluation Committee and continued to serve on its successor committee until his death. He will be sorely missed.

This meeting of the SAC was devoted to strategic planning, Sector Review Panel (SRP) reports, and user programs, along with a half-day cross-cut review on science using the time structure of the APS (which will be reported separately). The model

of operation for the APS has been changing over the past three years, along with the scientific environment in which it operates. That, along with budget pressures on all scientific activities, makes it imperative that priorities be set for future investment and emphasis. To this end, and in light of the small number of APS sectors left for allocation, during the 2003 meeting, the SAC requested that Gopal Shenoy and Sunil Sinha organize a survey of future opportunities for science at the APS. As always, they rose to the challenge and arranged a series of workshops that are described elsewhere in this annual report. The output from these workshops became a vision for the future direction of the APS that will guide future decision making and planning. After a presentation of this vision by Murray Gibson, it was discussed in great detail by the SAC over the course of the meeting. Needless to say, we had many thoughts and suggestions, but, on the whole, we were very pleased that the process was

Please see "Advisory" on page 7



The APS Scientific Advisory Committee, photographed on January 25, 2005. **Seated, l. to r.:** Wayne Hendrickson, J. Murray Gibson, Mike Rowe (SAC Chair, 2003-2005), ANL Director Hermann Grunder, and Partner User Council Chair P. James Viccaro. **Standing, l. to r.:** Paul Bertsch, William Bassett, Joachim Stöhr, Denis McWhan, Pierre Wiltzius (SAC Chair, 2005-2007), Peter Ingram, John Helliwell, Paul Percy, James Norris, APSUO Chair Mark Rivers, and Gerhard Materlik. **Not pictured:** Kathleen Taylor.

THE APS USERS ORGANIZATION

MARK L. RIVERS...

... (Chair, APSUO Steering Committee) is an Associate Director of the Center for Advanced Radiation Sources (CARS) at The University of Chicago and GeoSoilEnviroCARS Principal Investigator.

The highlight of the year was the 2004 Users Meeting for the APS on May 3-6, where over 600 APS users set a new attendance record. They were rewarded with an outstanding collection of scientific talks and workshops. The meeting was dedicated to the memory of Cullie Sparks, who was a pioneer in synchrotron radiation research, and whose career was recalled in a wonderful talk by Gene Ice (Oak Ridge National Laboratory). The meeting also saw the presentation of the first Rosalind Franklin Young Investigator Award to Alexis Templeton for her work on the role of microorganisms in the environment. (For a complete report on the meeting and the Franklin Award, see page 144.)

The Advanced Photon Source Users Organization Steering Committee (APSUOSC) plays an important role in representing the interests of the APS general user community. The APS General User Program has now been running in its current form for more than two years, and we felt it was time to conduct a review and assess how the program was working. A subcommittee was formed, chaired by Keith Brister (BioCARS), to study the program and make recommendations to APS management. The committee worked hard to solicit input from all of the stakeholders in the system, and over 300 people provided input in some form. While the program is felt to be generally working well, the committee has formulated a number of recommendations for improvement and submitted them to APS management for consideration.

At the quarterly meetings throughout the year, the APSUOSC has been called upon to advise APS management on issues including the recently released strategic plans for the APS and for the XOR beamlines, the upcoming Department of Energy review of the APS, the centralized general user proposal system, the partner user proposal system, non-resident user access issues, and the transfer of Office of Basic Energy Sciences sectors to APS operations support. The policy initiated last year to help keep the steering committee up to date on new developments among users by inviting user group representatives to join the committee for lunch and give short presentations was continued. In the course of the year, all APS user



The 2004 APSUO Steering Committee. L. to r.: Malcolm Capel (Cornell University), Carol Thompson (Vice Chair, Northern Illinois University), Keith Brister (The University of Chicago), Julie Cross (University of Washington), Ward Smith (Argonne National Laboratory), Mark Rivers (Chair, The University of Chicago), Stephen M. Durbin (Purdue University), Timothy Graber (The University of Chicago), Thomas Gog (Argonne National Laboratory), Stephan Ginell (Argonne National Laboratory). **Not pictured:** Gene Ice (Oak Ridge National Laboratory).

groups have this opportunity to share issues and concerns with the steering committee.

The APS management has taken a number of steps to increase user input into management decisions. These include inviting the chairs of the APSUOSC and the Partner User Council or their representatives to attend the weekly APS Operations Directorate Meeting; to participate in all Sector Review Panel meetings where APS sectors undergo their three-year reviews; and to attend the annual meeting of the APS Scientific Advisory Committee. This involvement gives the user community a genuine voice in the APS decision making process.

Washington outreach continues to be a focus for the APSUOSC. In April 2005, a team of user-group chairs from the APS, as well as from our sister DOE labs, the National Synchrotron Light Source, the Advanced Light Source, and the Stanford Synchrotron Radiation Laboratory, will travel to Washington, D.C., to expound on the importance of the DOE investment in synchrotron science. ○

THE APS PARTNER USER COUNCIL

P. JAMES VICCARO...

... (Chair, APS Partner User Council) is the Executive Director of the Center for Advanced Radiation Sources (CARS) at The University of Chicago and ChemMatCARS Principal Investigator.

In its second year, the APS Partner User Council (PUC), which is made up of member representatives from each sector on the experiment hall floor, continued to solidify its role as the primary forum for discussion of management issues involving the APS and the collaborative access teams (CATs). I was re-elected as Chair for another year, and John Quintana accepted the invitation to continue as Deputy Chair.

As an *ex-officio* member of the APS Scientific Advisory Committee (SAC), the Chair or his designee participated in all of the Sector Review Panels during the year, as well as the annual SAC meeting in January 2005. In addition, Quintana attended the APS Weekly Operations Meeting as the PUC representative. He then presented a summary of the Operations Meeting issues at the PUC executive sessions. As usual, either the Chair or Deputy Chair contributed to setting the agenda for the APS/Users' Operations Monthly Meeting.

Four PUC meetings were held in 2004, all of which were well attended by the sector representatives. The principal thrust of the meetings continued to be discussions of issues related to current and future beamline operations, APS facility development, and the relationship between the APS and partner users. In the opinion of the Chair, discussions at the meetings continue to be at times lively and most often relevant and productive.

Perhaps one of the more challenging issues faced by the PUC in 2004 related to the new "Policy and Procedures for Proprietary Research at the APS." Essentially every industrial participant was represented at a special ad hoc meeting organized by the PUC and attended by APS management. As a result of this meeting and subsequent interactions, the new policy was discussed and modified with input from the PUC and from the industrial community, and procedures for implementation of the policy were developed.

As part of the same ad hoc meeting, discussions were held regarding possible APS guidelines for evaluating the impact of beam time usage by non-academic partner-user researchers. As a result of the dialog, new guidelines that included relevant input by the community were accepted by the PUC.



The 2004 APS Partner User Council. **Front row, l. to r.:** Andrzej Joachimiak (SBC-CAT), Robert Fischetti (GM/CA-CAT), Larry Lurio (IMMY/XOR), John Chrzas (SER-CAT), Lisa Keefe (IMCA-CAT), Douglas Robinson (MU-CAT), Barry Lai (XOR). **Second row, l. to r.:** Murray Gibson (APS), Denny Mills (APS), Bruce Bunker (MR-CAT), Edward Stern (PNC-CAT), P. James Viccaro (ChemMatCARS, PUC Chair), Raul Barrea (Bio-CAT). **Third row, l. to r.:** Kevin D'Amico (SGX-CAT), Brian Stephenson (Nanoprobe-CDT), John Quintana (LS-CAT & AOD), George Srajer (XOR), Thomas Gog (CMC/XOR). **Fourth row, l. to r.:** Paul Zschack (UNI-CAT), Steve Heald (PNC-CAT), Dean Haefner (XOR), Eric Dufresne (MHATT/XOR), Reinhard Pahl (BioCARS), Denis Keane (DND-CAT), Mark Beno (BESSRC/XOR & XFD).

A second highlight in 2004 was the formation of the APS Advocacy Committee, composed of PUC members and chaired by Ed Stern from the University of Washington. As a direct outcome of this committee, a letter was drafted (with input from the APS Users Organization, or APSUO) to the national Inter-agency Working Group (IWG) on Synchrotron Facilities. The letter, which was signed by the Chairs of the PUC and the APSUO, stressed the importance of the partner user access mode at synchrotron facilities and requested that this mode be considered in the IWG analysis and in recommendations regarding U.S. synchrotrons.

More recently, the PUC meeting has proved to be an effective forum for discussion of the APS strategic plan for the near-term development of the facility. In addition to providing input on the plan for the APS-managed sectors through the X-ray Operations and Research groups, PUC members have begun work-

Please see "Partner" on next page

“Advisory” from page 4

off to a good start, and we commend all involved. Of special interest was a discussion of the joint mission of the APS and the Center for Nano-scale Materials, for which Director Eric Isaacs joined the meeting. I urge you to read the APS vision document (which is printed in this volume pXX), in order to understand the many future scientific opportunities that are foreseen. While this is not a detailed road map for the future, it is the first step in that process. In the area of strategic planning, it is often the planning that is important, rather than the plan.

One of the next steps in the strategic planning process is an operational plan for the future of the X-ray Operations and Research (XOR) beamlines that incorporates the overall APS vision, along with the needs of the current users and programs. Gabrielle Long, Associate Division Director in the Experimental Facilities Division, presented a first draft of this plan to the SAC, which discussed it at length and offered its own suggestions. The plan provides a road map for the future development of the XOR sectors, with an emphasis on more dedicated beamlines to better and more effectively meet the needs of the users. This plan was developed with input from all of the stakeholders. Continuing input from beamline staff and internal and external users will be sought and welcomed. While there will inevitably be changes as the plan goes forward, this step is the beginning of a major transformation of activities at the APS that will set the stage for the next decade of accomplishment.

The SAC also discussed the SRP reports for sectors 1-4, 7, 10, 18, 31, 33, and 34. In each case, the SRP was chaired by a member of the SAC, who presented the results to the whole committee. These reports are endorsed by, and become the

recommendations, of the SAC. This process now is working well, and we thank all those involved for their assistance.

The final item on the agenda was a discussion of the user program at the APS. This session started with a presentation by Keith Brister (The University of Chicago/Center for Advanced Radiation Sources), Chair of the General User Program Evaluation Committee. This committee was set up to look at the APS-run general user program, now that it has been operational for several cycles. The committee's report suggested several possible improvements, but no major change in the fundamentals of the program. Dennis Mills (Deputy Associate Laboratory Director, APS) presented a report on partner users and led a discussion of the accomplishments and outputs of this program to date. The discussion centered on criteria for acceptance of a Partner User Proposal (PUP) and mechanisms for review of the accomplishments of the program (at present, PUPs are reviewed by the SRPs, and the investigators are required to write a summary of accomplishments at the end of the PUP). After a stimulating discussion, the SAC concluded that the user programs are working to meet the needs and goals of the users, the APS, and its sponsors, but that minor changes should be considered.

On a personal note, this was my last meeting as Chair of the SAC; after one more meeting, I will no longer be a member of the committee. With the departure of Wayne Hendrickson and the loss of Howard Birnbaum this year, the evolution from the PEB to the SAC is nearly complete. It has been both interesting and challenging to be associated with the APS over these somewhat turbulent years and to have helped in some way to implement necessary changes. I look forward to watching your accomplishments over the coming years. ○

“Welcome” from page 3

carrying out work on our radiation safety systems, and we have heightened attention to electric safety and instituted appropriate training for our employees and our users. Personal and environmental safety always comes first at the APS, to the benefit of our users, employees, and the public.

Educational outreach is a very important activity for the facility. A highlight this year has been the creation of an international Web site (lightsources.org), which provides information and news on synchrotron sources worldwide. The APS took a leadership role in building this partnership, which involves support from some 17 facilities across the world, and helps educate the public, politicians, and potential users about our unique tools. The light source community is tightly integrated, and this activity is just one of many that is mutually beneficial.

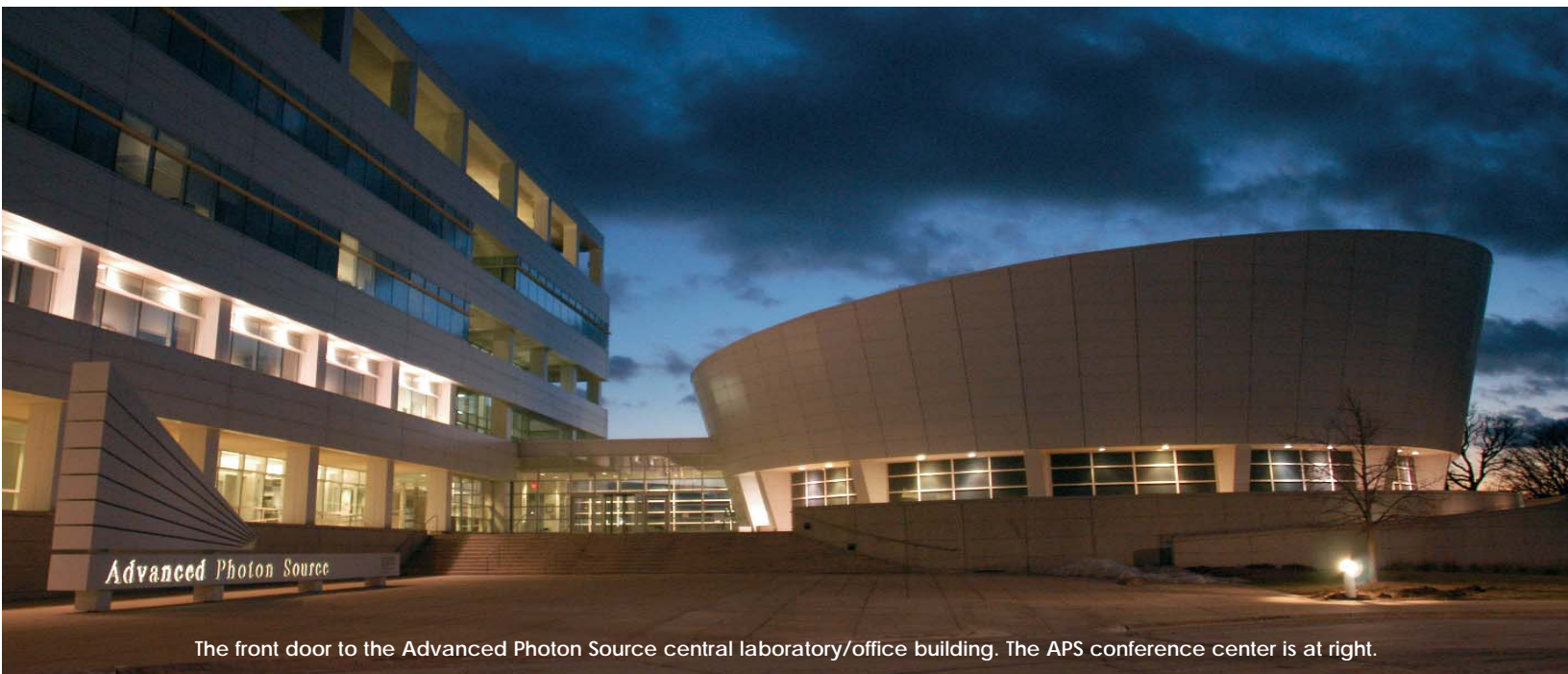
You can find in this annual report write ups on many of the high-profile scientific discoveries that resulted from studies at the APS; I hope you enjoy reading them. Our success is based on the hard work of our users and employees, and I thank you all. We are also grateful to our sponsor, the Department of Energy Office of Science, Office of Basic Energy Sciences, for their continuing support. ○

“Partner” from page 6

ing with the APS to coordinate the strategic plan with the user-operated sectors.

In addition to these highlights, the PUC proved in its second year of existence, to be an effective nexus for focused discussions on user concerns relating to operations and development, as well as other user-related issues. In one of the last meetings of the year, the Chair formed two ad hoc committees: one to consider strategies for promoting user access to the structural biology beamlines at the APS, and the other to make recommendations concerning the current PUC mission statement, policy, and leadership of the council in the coming year.

The first year of the PUC was a learning experience for the user groups who participated. The new responsibility placed on the partner users to define and to pursue to closure issues that are relevant to effective scientific productivity at the sectors is at times a daunting challenge. In the opinion of the Chair, during this second year, PUC representatives have risen to this challenge, and the council is establishing itself as a relevant member of the APS team. I look forward to continued success in the coming years. ○



The front door to the Advanced Photon Source central laboratory/office building. The APS conference center is at right.

The Advanced Photon Source (APS) facility occupies an 80-acre site on the Argonne National Laboratory campus, about 25 miles from downtown Chicago, Illinois.

For maps of the Argonne/Chicago area, see <http://www.aps.anl.gov/user/maps/maps.html>.

For directions to Argonne, see <http://www.anl.gov/visiting/anlil.html>.

ACCESS TO BEAM TIME AT THE APS

There are two ways to obtain beam time at the APS: as a general user (a researcher not associated with a particular beamline) or as a partner user (a member of a collaborative access team, or CAT). If you are a CAT member, contact your CAT for instructions on applying for CAT beam time. At minimum, 25% of the time at all operating beamlines is available to general users, but many offer considerably more general user time, up to 80%.

How general users can apply for beam time at the APS:

- 1) First-time users should read the information for new users found on our Web site at http://www.aps.anl.gov/user/new_users.html before applying for beam time. Also, certain administrative requirements must be completed. In particular, a user agreement between the APS and each research-sponsoring institution must be in place.
- 2) To choose the appropriate technique(s) and beamline(s), see the techniques and beamlines directories in the "Data" section of the volume, or at: http://beam.aps.anl.gov/pls/apsweb/beamline_display_pkg.technique_dir for techniques, and http://beam.aps.anl.gov/pls/apsweb/beamline_display_pkg.beamline_dir for beamlines.
- 3) Submit a proposal via the Web-based system. Proposals are evaluated before each user run. For more information and the current proposal schedule, see the proposal system overview (http://www.aps.anl.gov/user/beam_time/prop_submission.html).

For news from, and information about, light sources worldwide, see lightsources.org



TABLE OF CONTENTS

HOWARD K. BIRNBAUM—1932-2005	2
WELCOME	3
THE FUTURE OF THE ADVANCED PHOTON SOURCE	10
THE WORKSHOPS ON FUTURE SCIENTIFIC DIRECTIONS	
FOR THE ADVANCED PHOTON SOURCE	10
FIVE-YEAR SCIENTIFIC VISION FOR THE ADVANCED PHOTON SOURCE ...	12
RESEARCH HIGHLIGHTS	18
STRUCTURAL STUDIES	20
ELECTRONIC & MAGNETIC MATERIALS	26
ENGINEERING MATERIALS & APPLICATIONS	38
SOFT MATERIALS & LIQUIDS	43
CHEMICAL SCIENCE	54
LIFE SCIENCE	58
PROTEIN CRYSTALLOGRAPHY	66
ATOMIC, OPTICAL, & MOLECULAR PHYSICS	90
ENVIRONMENTAL, GEOLOGICAL, & PLANETARY SCIENCE	91
NANOSCIENCE	102
NOVEL X-RAY TECHNIQUES & INSTRUMENTATION	110
APS USERS	141
THE APS LIGHT SOURCE	147
APS DATA	157
APS PUBLICATIONS—2004	165
ACKNOWLEDGEMENTS	196

THE WORKSHOPS ON FUTURE SCIENTIFIC DIRECTIONS FOR THE ADVANCED PHOTON SOURCE

Devising a menu of new possibilities for the APS experimental program defies the conventional wisdom about too many cooks. Workshops that brought together an abundance of experts from a wide range of scientific disciplines to consider “Future Scientific Directions for the Advanced Photon Source” have produced a bounty of ideas for expanding the already robust research at this national user facility.

The workshops, which were held in May, July, August, and September 2004, were organized and chaired by Gopal Shenoy (ANL-XFD) and Sunil Sinha (U. of C., San Diego). They brought



Sunil Sinha (left) and Gopal Shenoy at the workshops on future scientific directions for the APS.

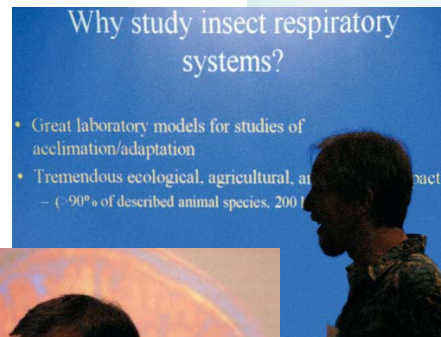
APS users and personnel into contact with leaders from the broad scientific community who are both experts in their fields and newcomers to the use of x-ray techniques. The workshops had as a primary goal “the expansion of both the scientific leadership of APS users and the boundaries of science’s frontiers in the next decade” by identifying new opportunities for scientific discovery and impact using synchrotron radiation sources during the next 5 to 10 years and seeking ways of bringing new scientific communities to the use of synchrotron x-ray

beams. Speakers at the workshops also dealt with the (literally) nuts-and-bolts questions of new instrumentation and operational requirements needed for these programs. Also considered were evaluations of existing APS beamline capabilities in terms of the future beamline capabilities that would be needed for new programs.

A sampling of the topics presented at the workshops includes a new source of x-ray beams that deliver pulses of light on the picosecond time scale; using x-rays to capture the detailed mechanisms of molecular functions as they occur; a wide range of new (or newly combined) synchrotron x-ray techniques to provide unprecedented insights about materials structures on the atomic scale; and the behavior of a wide range of biological functions on the molecular scale. Strategies for fabrication, characterization, and understanding of nanoscale materials; emphasizing new



What are the Grand Challenges for Biological Crystallography ?





functionalities; and a beamline dedicated to the use of a 40-MW super magnet to be used for the study of materials under extreme magnetic forces were also discussed.

The conclusions of each workshop are summarized as follows:

- 1) Emerging areas of biological crystallography will address the essence of living systems through the measurement of structural dynamics at the molecular level and the responsible chemical forces.
- 2) High-energy x-ray tools will focus on understanding the relationships between the structure and the properties of materials over several hierarchical length scales ranging from the atomic to the nanoscopic to the mesoscopic scale.
- 3) The emerging research topics in membrane science are truly interdisciplinary and represent the interfaces among materials chemistry, physics, molecular biology, and medicine. They will have the broadest industrial impact in areas ranging from gas-phase separation to the hydrogen economy to drug delivery.
- 4) Basic understanding of environmental materials and processes at the molecular scale will be provided by x-ray techniques. This knowledge is essential for risk assessment and management and for reduction of environmental pollutants at field, landscape, and global scales.
- 5) X-ray phase analysis lends itself to numerous emerging opportunities in x-ray imaging with ultra-high spatial resolution. The impact of both 2-D and 3-D x-ray imaging on many areas such as medical diagnostics, new materials discovery, paleontology, etc. is huge.
- 6) It is of paramount importance to understand the magnetic behavior of individual nanomagnetic building blocks, which are combined into more complex structures leading to the development of spintronics devices with new functionalities. The spin-sensitive x-rays techniques will have a major impact on the field of confined magnetism.
- 7) Rearrangement of atoms or electronic states or protein structures in response to various external stimuli takes place over 15 orders in time domain. The time-resolved x-ray techniques utilized at storage rings can be the most powerful probes of this important science, which has broad applications in astrophysics, atomic physics, chemical physics, materials science, and biology.
- 8) Understanding the behavior of confined matter when the length scales range from the mesoscopic to the nanoscopic has attracted recent attention because of the potential nanotechnology applications. The x-ray methods that offer atomic resolution will provide considerable understanding of nanomaterials and processes that occur at the nanoscale.

The workshop summaries were presented at the second APS Strategic Planning Meeting (SPM), held on September 2–3, 2004, and co-chaired by Shenoy and Gabrielle Long (ANL-XFD). The SPM served to summarize all of the workshops in the series, highlighting scientific opportunities identified during each of the workshops and leading to the “Five-Year Scientific Vision for the Advanced Photon Source,” which follows. Workshop and SPM slides can be accessed on the Web at <http://www.future.aps.anl.gov/Future/future.htm>. The study is documented through a report, based on the summaries from each of the workshops, available at <http://www.future.aps.anl.gov/Future/report.pdf>.

FIVE-YEAR SCIENTIFIC VISION FOR THE ADVANCED PHOTON SOURCE

The Advanced Photon Source in 2005 is beginning its eleventh year since producing first light and has seen its user base grow to nearly 3,000 individual scientists per year. Today, the APS has 46 instrumented beamlines occupying 30 sectors. Nonetheless, there remain four uncommitted sectors, opportunities to optimize existing insertion device beamlines or expand others with canted undulators, and over a dozen undeveloped bending magnet beamlines. Furthermore, the highest priority identified for the facility by the most recent University of Chicago Review Committee was the evolution of a greater number of dedicated, and fewer multipurpose, beamlines.

For these reasons, the APS and its Scientific Advisory Committee have developed plans that address priorities for new or improved beamlines over the next 5 to 10 years. To make choices that will have the most positive scientific impact, we have engaged the wider community in developing our plans. We recognize that powerful new instrumentation is needed, but that, in many cases, outreach to new user communities can be just as important. We commissioned a broad study on “Future Scientific Directions for the Advanced Photon Source,” which looked at the scientific opportunities where synchrotron radiation could play new roles, and we connected these with instrumentation and community needs. The study chairs, Gopal Shenoy, of the APS, and Professor Sunil Sinha, of the University of California, San Diego, made use of extensive community input in organizing a series of nine workshops that were held in 2004. Each workshop focused on a compelling scientific area and brought together synchrotron experts with scientists who had not previously used synchrotron radiation. Every workshop provided an executive summary and aims to publish a full report in a scientific journal.

Following the conclusion of the workshops, that in total involved over 300 scientists, a summary strategic planning meeting was held at which the workshop highlights and other relevant input were presented and discussed with a broadly representative audience. This document is based on that summary meeting. It briefly summarizes the scientific opportunities in the fields identified through the study and categorizes the major needs for instrumentation and community activities to maximize APS scientific impact in the next decade. Our scientific vision and its followup serve as a blueprint for the development of new instrumentation, including entire beamlines, and for APS management decisions on staffing, accelerator operations, and improvements. It also puts flesh on Phases I and II of the APS 20-year plan submitted to the Department of Energy in 2003 (<http://www.aps.anl.gov/aps/downloads/20030223-roadmap.pdf>). If the vision for new instrumentation and community support in this document is fulfilled, we have every confi-

dence that the scientific impact of the APS will grow dramatically in the next decade.

This vision for the next five years at the APS has been reviewed by the APS Scientific Advisory Committee. Input was also sought from the two representative user bodies at the APS—the APS User Organization Steering Committee and the APS Partner User Council. Of course, this is not intended to be an all-encompassing, detailed plan. Instead, it identifies a menu of persuasive opportunities at the time of writing. As in the past, new beamline construction at the APS is expected to involve external partnerships and will remain proposal-driven. This document will provide a context in which existing and future proposals can be reviewed, and it is expected to stimulate successful proposals.

Because this is an executive summary, further details will be made available elsewhere. There are three sections here: a summary of fields in which new impacts from synchrotron radiation science are anticipated, a high-priority list of necessary major beamline-scale instrumentation, and a discussion of areas and approaches to build new APS user communities. Where major new instrumentation needs are identified, the APS has appointed technical liaisons for each instrument, who will coordinate the technical aspects of instrument design with internal and external teams, as appropriate. In recent beamline construction projects, partners (in the form of collaborative development teams) are involved in initial development and commissioning through close collaboration with the APS. During operation, the APS expects to take primary responsibility for beamlines in the physical sciences and operate them for open access through the general user and partner user programs.

NEW SCIENTIFIC OPPORTUNITIES FOR SYNCHROTRON RADIATION

Across the wide spectrum of scientific areas covered by the workshops, several general themes emerged. The need for simultaneous characterization with high spatial and temporal resolution was appreciated in diverse fields—from biology to condensed-matter physics. This frontier challenges the limits of third-generation sources, and exciting development opportunities will be built upon by the next generation of ultra-fast, ultra-brilliant x-ray laser sources. Second, in many fields, the unique capabilities of hard x-rays to perform *in situ* studies of materials in real environments will become increasingly important. Last, but by no means least, it is apparent that close juxtaposition, if not integration, of complementary tools is invaluable. For example juxtaposition of tools and expertise for electron, optical, and x-ray microscopy, or x-ray and neutron scattering, offers the most compelling resource for users. Co-location of tools for materials synthesis and processing, such as

in the new Center for Nanoscale Materials at Argonne, is an excellent example. This integration of capabilities should also extend to theory and modeling.

The pulsed structure of synchrotron x-ray sources offers access to **Time Domain Science** down to the tens-of-picosecond (ps) scale. Future x-ray lasers promise three orders of magnitude improvement. Stimulating scientific opportunities are found in atomic and molecular physics, chemistry, biology, and condensed matter physics—from the study of chemical reactions and excited states to the transport of carriers in semiconductors. This group of scientists can take much greater advantage of existing sources such as the APS and grow a community that will use x-ray lasers in a decade or more. There is great interest in pushing the capabilities from the current time structure of the APS toward shorter time scales and in better utilizing experiments from the current limits up to much longer time scales. A novel approach to generating 1-ps pulses is under serious consideration within the APS. Developments in choppers and detectors are also very important to maximum utilization of the time structure of the beam.

Whereas high-energy machines like the APS are often associated with hard x-rays, the performance of the machine promises new **Frontier Science Using Soft X-rays**. At 0.5–3 kV x-ray energy, the APS ring (with a suitable undulator) can produce exceptionally brilliant beams that are very stable and

can be controllably polarized. There are several exciting areas of science that this capability can impact, including nanomagnetism. Soft x-ray imaging was identified, in the APS 2003 cross-cut review of microbeam science, as an important frontier. A unique and interesting opportunity involves the use of angle-resolved photoemission spectroscopy (ARPES) and related spectroscopies at these energies. Such experiments would provide access to the momentum-resolved electronic structure that ARPES gives so well, while at the same time being less surface-sensitive. Applications include understanding electronic transport in exotic conductors and untangling the role of magnetic and charge transport in materials.

There are abundant **Emerging Scientific Opportunities Using X-ray Imaging** in fields including geology, paleontology, biology, engineering materials, and complex systems. In fact, the interest from new user communities in full-field x-ray imaging is probably the widest of any x-ray technique. The ability to study structure in materials on scales from nanometers to centimeters is very powerful. For example, it can be applied to understanding materials failure by crack propagation, to real-time imaging of physiological processes in insects and small animals, to understanding gene expression in plants, and to the study of micro-fossils to find clues to the origins of the earliest life in the solar system.

The excitement of producing new **Mesoscopic and Nanoscopic Materials** that are not found in nature, and that have unique properties, has driven the burgeoning field of nanoscience in the last decade. Such properties include improved catalysis through tailored nanoparticle surfaces, better information storage and computation, and self-organized structures for better drug encapsulation and delivery. Many of these materials are complex and hierarchical. Key frontiers to enable progress include the understanding and control of self-assembly, where x-ray techniques, especially *in situ*, will play a major role. It is also becoming clear in nanoscale systems, that knowledge not only of structure, but of dynamics, will be key, and so x-ray spectroscopy will be important.

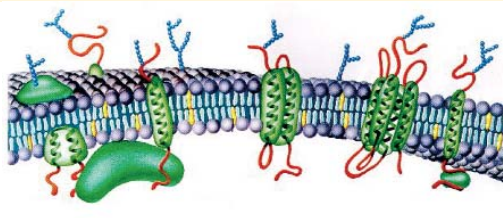
The goal of research in **Nanomagnetism** is to build, from nanoscale building blocks, complex integrated systems with new functionalities. It is clear that the ability to characterize both the magnetic structure and the dynamics of individual and assembled nanostructures will enable progress, and that synchrotron radiation will offer important capabilities. Frontier science will juxtapose high spatial resolution (the ~5-nm scale of the exchange interaction) and ultrafast studies (the ~1-ps time scale of spin-orbit coupling and other intrinsic magnetic phenomena) to revolutionize our understanding of nanoscale magnetism. Areas of impact include magnetoresistive memory, spintronics, and tailored magnetic materials for energy applications.

Measurement of short- and medium-range atomic structure in nanomaterials is one powerful application of **High-Energy X-rays**, which provide a unique tool to study real materials in realistic conditions. The penetrating power rivals that of neutron sources, but adds a finer microfocusing capability for inhomogeneous materials and the higher Q-space range needed for disor-

Membrane Science

Membrane technology has advanced the state of the art in water treatment and purification; in the electronics, semiconductor, chemical, petrochemical, and pharmaceutical industries; and in environmental applications, such as low-cost control of carbon dioxide absorption to combat greenhouse gases. New research opportunities include medical and biological processes (such as

hemodialysis used in artificial kidneys); essential components for the fuel-cell and hydrogen-energy economies and technologies; and separation of



proteins in the food, beverage, pharmaceutical, and biotech industries. Biomembrane science takes this field back to its source: a better understanding of cell membranes themselves. These complex, heterogeneous systems are highly adaptable and are critical to a wide range of biological processes, including ion transport and signal transduction. The evolution of a wide range of synchrotron-radiation-based techniques is proving to be essential to gaining molecular-level structural information about membranes, membrane interfaces, and interacting supramolecules. Moreover, applying these varied techniques to real-time studies can provide information on the time evolution and molecular interactions in membranes. (Image: A natural membrane. Courtesy of Garrett & Grisham)

dered materials. Revolutions in the micromechanics of materials and improved disordered and nanophase materials can all be anticipated from increased synchrotron research with high-energy x-rays.

Membrane Science is a truly interdisciplinary emerging field, at the interfaces amongst chemistry, materials, physics, molecular biology, and medicine. There is synergy to be exploited between inorganic membranes—of importance for chemical separation such as hydrogen fuel—and organic membranes, including the vital cell wall. Techniques of particular value include small-angle x-ray scattering, reflectometry, and photon correlation spectroscopy. The major technical challenges are extending experiments to the time domain and enabling specialized *in situ* experiments.

Synchrotron radiation has had a stunning impact on **Biological Crystallography** in the last 20 years, to the extent that most structures are now solved on synchrotron sources. In particular, the tunability and intensity of insertion devices has permitted the development of anomalous dispersion techniques for structure solution. Given the great importance of this field to human health and biology, it is imperative that facilities such as the APS remain at the forefront, anticipating the scientific needs of the community. The scientific impact from expected developments will involve understanding molecular machines, the critical role played by membranes, and the dynamics of proteins. In all these areas, x-ray techniques will play a role, but it is increasingly apparent that integration of x-ray techniques with other methods (e.g., electron cryomicroscopy) will also be essential.

Environmental Science presents multidisciplinary challenges in complex systems that have tremendous societal importance. Synchrotron radiation is playing a large and growing role, especially through its ability to characterize on the molecular scale with high spatial resolution, for example, to elucidate bioremediation in soils. Challenges include understanding and controlling the transport of contaminants in the ground, developing approaches to environmental remediation based on understanding at the molecular level, and ensuring the stability of environmental repositories.

NEW, LARGE-SCALE INSTRUMENTATION PRIORITIES

In almost all of the workshops, it was evident that the evolution of dedicated and well-supported beamlines is of paramount importance at the APS. Nonetheless, many science areas, such as nanosciences, will not rely on just a single x-ray technique but will need access to many. Better technique-dedicated facilities are the most effective solution, except where a technique will be almost exclusively used by one community, in which case the advantage of staff and ancillary infrastructure specific to the science will be highly desirable.

The following prioritized list contains compelling new instrument capabilities, all of which are needed in the near term to realize the scientific promise of the APS. More details about each instrument can be found in the workshop reports and through the appropriate APS technical liaisons (page 17).

Environmental Science

The largest poisoning in history is believed to have occurred due to natural arsenic (As) contamination of the wells in Bangladesh. These deep wells, sunk in the 1970s, were introduced to avoid surface cholera contamination. Controversy still brews as to the origin of the arsenic contamination,



but recent micro-x-ray absorption spectroscopy studies carried out at the APS suggest that cyclic changes in mineral hosts of arsenic are the culprits. Depth profiles of As concentration and oxidation state suggest As bearing sulfides account for a majority of arsenic at well depth and that arsenic is being liberated from this source during natural seasonal redox cycles.

This study is only one example of the growing role to be played by synchrotrons in advancing environmental science. (Photo: <http://asp.grameen.com/annualreport/2001/arsenic.htm>)

• SHORTER PULSE CAPABILITIES FROM THE STORAGE RING

As a result of stimulating discussions at the time domain science workshop, the APS has investigated a scheme (due to Zholents, et al.) for the creation of picosecond pulses by a transverse radio frequency kick and x-ray crystal optics compression. The initial study was just completed, and the results indicate that this is feasible. The capability can be applied to one or two sectors without disturbing the storage ring and offers extremely exciting and unique possibilities to extend the capabilities for time-domain science by two orders of magnitude. This would be associated with dedicating either one or two adjacent sectors to ultrafast time-domain science and parallel efforts elsewhere to support such science at longer time scales.

• LONG BEAMLINE FOR FULL-FIELD IMAGING

Phase-contrast imaging and tomography require coherent beams with large illuminated fields of view. At present, this is best achieved with a very long (~200 meters) beamline free of focusing optics. Options still remain at APS to construct a new beamline, or modify an existing beamline, for these purposes, and it is strongly believed that we need such a dedicated facility to foster the tremendous needs of the imaging community.

• BIO-NANOPROBE

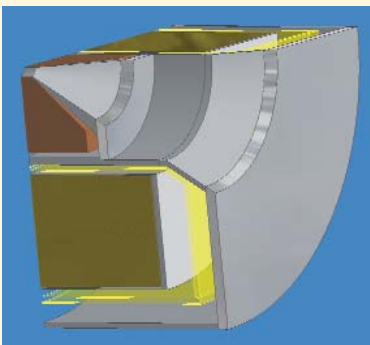
This tool is focused on the study of metals in cells, which is very important to biology and medicine. There is a large community of users who could take advantage of the unique and complementary aspects of x-ray spectromicroscopy. The APS could serve this community with a dedicated beamline offering high spatial resolution and spectroscopic sensitivity. This oppor-

Science with a High-Field Magnet

In the study of matter, going to extremes is often the path to startling and useful discoveries. Just as extremes in pressure and temperature have provided fruitful experimental environments, the use of high-field magnets to study the properties of matter remains

a frontier. High magnetic fields interact with charge and spin in materials but, until now, any structural effects of the highest fields could not be measured with synchrotron radiation. The National High Magnetic Field Laboratory at the University of Florida, and the APS are proposing construction of the largest high-field magnet beamline facility in the world, to be

located at the APS. To achieve the desired steady fields of up to 35 T, the magnet would marry resistive and superconducting technology to produce a hybrid “magnet within a magnet” that has demonstrated the world’s highest fields to date. (Image: Proposed “down-bore” magnet for APS beamline. Courtesy of G. Boebinger, National High Magnetic Field Laboratory)



tunity emerged from a number of workshops held at the APS in recent years. The large demand justifies a dedicated facility, and the advantage would be an expert staff to interact with novice users and a close connection with related facilities such as those for optical and electron cryomicroscopy. It is expected that the user base at the APS will sustain several nanoprobe instruments such as this. The nanoprobe, for the Center for Nanoscale Materials (under construction at sector 26), will focus on nanoscience in non-biological, or biologically inspired materials. The bio-nanoprobe would focus on biology itself. A third instrument for environmental sciences, for which the resolution demands are often less severe, could likely be accommodated at an existing or improved beamline.

• DEDICATED MICROFOCUSING STATION FOR STRUCTURAL BIOLOGY

There is an important subset of structural biology problems which need a small-crystal (<10 μm) capability, where no such dedicated capability exists today at the APS. It makes sense that one of the structural biology sectors at the APS should offer such a dedicated capability. It is not anticipated that a new sector need be constructed. Other innovations in structural biology can be accommodated at existing sectors.

• HIGH-MAGNETIC-FIELD FACILITY AT THE APS

High magnetic fields offer a unique probe to understand, and ultimately control, the transport properties of materials. A recent National Research Council report emphasizes the need

for *in situ* x-ray scattering tools at high magnetic fields. This could be accommodated at a new dedicated scattering sector for magnetism. We propose that one beamline should have a high-DC magnetic field capability (at least 20 T), with both horizontal and vertical field geometries, which would be unique in the world. Collaboration with the National High Magnetic Field Laboratory, and related plans to establish facilities at neutron sources, are being explored.

• DEDICATED HIGH-ENERGY X-RAY CAPABILITIES

Particularly, there is a need for a high-energy undulator line dedicated to applications requiring high brilliance, especially microfocusing. In addition, dedicated beamlines with high flux will be needed for pair-distribution-function and other work (e.g., in solution). The latter could likely be accommodated by restructuring existing beamlines.

• IMPROVED SOFT X-RAY CAPABILITIES

A dedicated soft x-ray beamline in the approximate energy range of 0.5–3 kV should be produced with a specially designed undulator to allow ARPES and related spectroscopies with sub-surface sensitivities. The brilliance from a specially designed source, combined with the stability and polarizability of the beam, would lead to a unique capability for those experiments requiring illumination of small volumes. Additional soft x-ray capabilities for imaging, scattering, and magnetism should also be provided.

• INELASTIC X-RAY SCATTERING

The Phase I design of the Inelastic X-ray Scattering beamline (APS sector 30) involves the co-existence of medium-energy-resolution (MERIX) and high-energy-resolution (HERIX) capabilities at one sector. Whilst we have investigated options for increasing the length of the straight section to accommodate more and longer insertion devices, it seems clear that a sector dedicated to HERIX and a sector dedicated to MERIX should be Phase II of this plan. The best choice would be to accommodate dedicated HERIX capabilities at sector 30 and to establish another insertion device sector with a dedicated MERIX beamline. The latter might be accommodated without constructing a completely new sector. Because of the brilliance needs of both techniques, the MERIX sector requires a longer straight section with multiple permanent magnet undulators, and the HERIX sector a dedicated superconducting undulator (now under design).

• IMPROVED DETECTORS

Optimized detector systems will be critical to fully realize the expected increase in productivity from dedicated beamlines and specialized insertion devices. We recognize that a sustained effort in detector development could have the most scientific leverage, and we aim to be aggressive in securing advanced detectors for our users. We will be preparing detailed plans in the near future for detector development in areas such as avalanche-photodiodes and pixel-array detectors. We will work in close collaboration with other facilities in the U.S. and abroad.

Note that this list neglects important capabilities already existing or under construction at the APS. For example, a need expressed by the materials science and structural biology communities for powder studies will be accommodated by the dedicated bending magnet powder diffraction beamline under construction at sector 11. Also, this list does not include many techniques that are very important yet do not yet exist in dedicated form at the APS, such as small-angle x-ray scattering, because we believe that such dedicated facilities will emerge from reorganizing our internal X-ray Operations and Research (XOR) beamlines. A strategic plan for the development of XOR sectors has recently been prepared.

While the list above focuses on large-scale instrumentation, there is strong support from the existing and potential user community for broader instrumentation development. This includes improving the x-ray source, which is a high priority for the APS, and x-ray optics and end station instrumentation, where responsibilities are shared with partner users.

Intrinsic to the success of all these plans is the need for the APS to develop insertion devices optimized for each of our dedicated beamline capabilities. For example, superconducting undulators are being developed for high-energy and inelastic scattering. Development of such devices represents Phase II of our 20-year strategic plan and goes hand-in-hand with creating dedicated beamlines, which is the principal aspect of Phase I.

OUTREACH TO NEW SCIENTIFIC COMMUNITIES

In this section, we discuss some important issues, which emerged from the workshops, related to nurturing and building new user communities. As a general observation, it is well-recognized that APS scientific staff or resident partner users, who are expert in the fields of the user, are best suited to maximizing the scientific impact of user research. Such resident scientists provide expert assistance, and they reach out to the relevant scientific communities. Not only is this best for the users and the facility, but it is also very effective for career development of beamline research staff. Given the balance of time available for user support versus personal research, it is highly effective for a beamline scientist to collaborate with outsiders and to specialize in a particular field, at least for a period of time. Whilst the APS staff will strive to provide more expertise, the partner user program offers a vehicle to leverage this expertise by bringing in expert users who may choose to reside for extensive periods at the facility. In almost all the areas covered by the workshops, the need for this expertise is established, but particular needs stand out in environmental molecular science, biology, imaging science, and membrane science. In addition, industrial partner users offer an important conduit from industry to general users and strengthen the coupling of science and technology.

Critical to the success of all our beamlines is adequate staffing, and we are committed to using our resources in the best way possible to foster productive and well-supported beamlines.

A powerful method for preserving scientific specialization as beamlines become optimized by technique is the use of *virtual portals*. In this concept, a group (typically partner users) acts as a conduit for all experiments into a number of APS beamlines and provides the high-level scientific expertise and advice that is most effective. Although this model has not yet been tested, we are anxious to begin exploring it. An example could be in structural biology, where access to specialized beamlines—for systems under extreme conditions, for powder diffraction, and for small-angle scattering, to name a few workshop priorities—could be coordinated by an existing resource in cooperation with the APS and other partners.

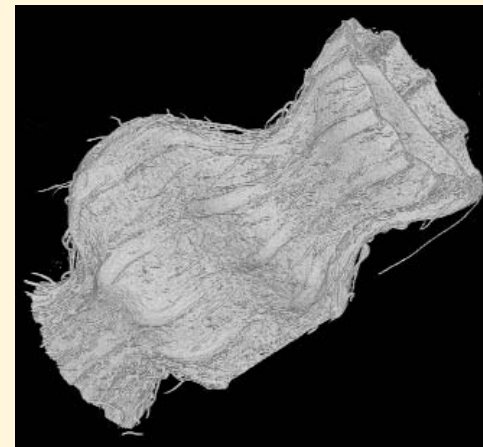
Another vehicle recommended during several workshops was the establishment of advisory panels in strategic scientific areas to help guide the APS as programs and capabilities evolve.

Joint appointments between the APS and other Argonne divisions, universities, and other institutions offer a special kind of partnership that can be very effective.

The need to facilitate *in situ* experiments, which may take a longer time than typical experiments and may often be effective in partnership, is clear in many areas. These experiments can be fostered through dedicated end stations. Frontiers of *in situ* experiments include time-resolved measurements at high spatial resolution.

X-ray Imaging for the Life Sciences

Many objects, from seeds (picture) to cracked concrete, exhibit complex hierarchical internal structures that cannot be properly preserved or studied by sectioning, and are thus not amenable to study with conventional microscopes. Many objects share a low-density matrix and a low-absorption cross section for x-rays. For such objects, x-ray phase-enhanced imaging is uniquely able to reveal complex internal structures on the submicron level



in macroscopic objects without sectioning. A dedicated long-imaging beamline is necessary for sufficient coherence and field-of-view to study problems in food science, genetics, engineering materials, biology, and a wide range of other subjects.

(Image: A mustard fruit rendered in three dimensions from tomographic data.. Diameter of the fruit is about 3 mm; length of image is 6 mm. Image taken at the European Synchrotron Radiation Facility, courtesy of W.-K. Lee [ANL] and K. Donohue [Harvard U.])

As we bring in new communities of scientists requiring synchrotron methods, but having little synchrotron research experience, we recognize that they will need help with the acquisition and processing of data. This means that we will have to raise the level of APS staff support in terms of guiding researchers in synchrotron x-ray techniques and that we will need to increase the quantity and accessibility of robust data reduction and analysis packages. This implies a substantially higher level of APS involvement in data handling, but we see it as key to the realization of the promise in emerging areas of science.

Many enabling research areas that do not explicitly involve new instrumentation also became clear as priorities. One example is fundamental studies on radiation damage, both to understand the consequences of this limiting issue in biological crystallography and soft materials and possibly to use knowledge of

the nature of damage for better structural insight. Details can be found in the workshop reports and summaries.

A LAST WORD

Strategic planning is essential, and for a national user facility, current and potential users must be fully engaged. We are delighted at the outcome of our series of vibrant planning workshops held in 2004. That outcome is embodied in this vision. The new directions identified here will undoubtedly pay off in high scientific impact, and we are committed to aggressively pursuing these opportunities with the help of our user community. Our plans for new scientific directions complement our equally strong commitment to improve the machine performance and productivity for our existing users. ○

TECHNICAL LIAISONS

Shorter pulse capabilities from the storage ring:

Dennis Mills (DMM@aps.anl.gov)

Long beamline for full-field imaging:

Wah-Keat Lee (WKLEE@aps.anl.gov) and Qun Shen (QSHEN@aps.anl.gov)

Bio-nanoprobe:

Stefan Vogt (VOGT@aps.anl.gov)

Dedicated microfocusing station for structural biology:

John Quintana (JPQ@aps.anl.gov)

High-magnetic-field facility at the APS:

George Srajer (SRAJERG@aps.anl.gov)

Dedicated high-energy x-ray capabilities:

Dean Haeffner (HAEFFNER@aps.anl.gov)

Improved soft x-ray capabilities:

Richard Rosenberg (RAR@aps.anl.gov)

Inelastic x-ray scattering:

Ercan Alp (EEA@aps.anl.gov)

Improved detectors:

John Quintana (JPQ@aps.anl.gov)

APS RESEARCH HIGHLIGHTS

APS Research Groups:

XOR—sectors 1-4

X-ray Operations and Research

DND-CAT—sector 5

DuPont-Northwestern-Dow Collaborative Access Team (CAT)

MU-CAT—sector 6

Midwest Universities CAT

MHATT/XOR—sector 7

Center for Real-Time X-ray Studies

IMMY/XOR—beamline 8-ID

IBM-McGill-MIT-Yale

CMC-CAT—sector 9

Complex Materials Consortium CAT

MR-CAT—sector 10

Materials Research CAT

BESSRC/XOR—sectors 11 & 12

Basic Energy Sciences Synchrotron Radiation Center

CARS-CAT

Center for Advanced Radiation Sources

GeoSoilEnviroCARS-CAT—sector 13

BioCARS-CAT—sector 14

ChemMatCARS-CAT—sector 15

HP-CAT—sector 16

High Pressure CAT

IMCA-CAT—sector 17

Industrial Macromolecular Crystallography Association CAT

Bio-CAT—sector 18

Biophysics CAT

SBC-CAT—sector 19

Structural Biology Center CAT

PNC/XOR—sector 20

Pacific Northwest Consortium

LS-CAT—sector 21

Life Sciences CAT

SER-CAT—sector 22

South East Regional CAT

GM/CA-CAT—sector 23

General Medicine and Cancer Institutes CAT

NE-CAT—sector 24 & beamline 8-BM

Northeastern CAT

Nanoprobe-CDT—sector 26

Nanoprobe Collaborative Development Team (CDT)

IXS-CDT—sector 30

Inelastic X-ray Scattering CDT

SGX-CAT—sector 31

Structural GenomiX CAT

COM-CAT—sector 32

Commercial CAT

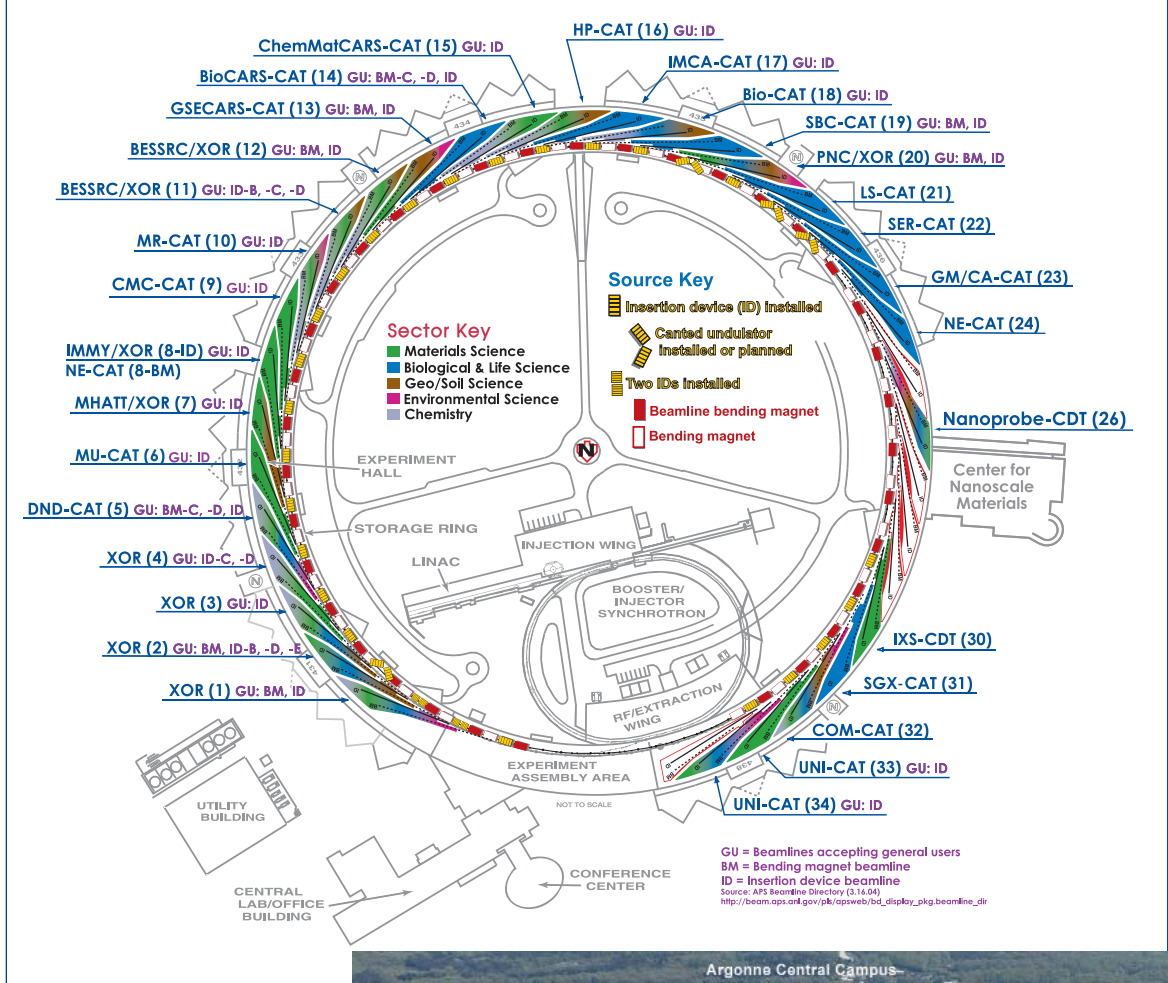
UNI-CAT—sectors 33 & 34

A University-National Laboratory-Industry CAT

THE ADVANCED PHOTON SOURCE

Sector Allocations & Disciplines

Source Configuration



Right: The Advanced Photon Source facility at Argonne National Laboratory.

Below: The Center for Nanoscale Materials (as of March 2005), under construction on the west side of the APS experiment hall.



HOW CRYSTALS FORM VIA ORDERING IN GLASS CERAMICS

Because it is symmetric, glass is generally not expected to demonstrate the non-linear optical properties that are characteristic of some crystals. But recent studies are changing the way we look at glass. When heat is used to form crystallites, a glass ceramic arises—one that exhibits optical second harmonic generation (SHG). One of these glass ceramics contains tellurium (Te) and niobium (Nb) oxide, which have been the subject of some debate regarding the final structure of the crystalline phase. A new model for this tellurium-niobium oxide, resulting from x-ray and neutron diffraction studies carried out at the DND-CAT beamline 5-BM and the XOR 1-BM beamline, refutes previously proposed models and suggests a more direct route to crystallization by means of an ordering of the existing structure.

Using data collected at the APS, investigators from Indiana University, Dalhousie University, and Argonne National Laboratory studied the $(\text{K}_2\text{O})_{15}(\text{Nb}_2\text{O}_5)_{15}(\text{TeO}_2)_{70}$ glass ceramic (15-15-70) and found no evidence of previously proposed fluorite crystallization and cation ordering. Rather, their work demonstrated that (1) the crystalline phase is a distortion of the $\text{K}_2\text{Te}_4\text{O}_9$ structure, and (2) SHG activity does not require the major chemical changes previously thought necessary. This polymorph of $\text{K}_2\text{Te}_4\text{O}_9$ is in space group $P2_1/c$ with a tetragonal lattice ($a = 7.821 \text{ \AA}$, $b = 16.590 \text{ \AA}$) and is consistent with all observed diffraction data, including the cubic arrangement of cations in the x-ray patterns, as well as the bond lengths, angles, and additional features from the neutron diffraction data.

The melt quench method was used to synthesize glass samples, which were treated at 425°C for 14 h to produce ceramics. The 5-BM (Te edge) and 1-BM (Nb edge) beamlines at the APS were used to collect anomalous powder x-ray diffraction data. At the Nb and Te absorption edges, x-ray absorption spectra (XAS) were measured and analyzed by using the computer program CHOOCH. Powder patterns were taken for Nb and Te with photon energies representing 5, 30, 50, and 120 eV below absorption edges.

Powder neutron diffraction data were collected and analyzed by using the General Purpose Powder Diffractometer instrument at the Intense Pulsed Neutron Source at Argonne.

The researchers used five different data sets to corroborate the proposed model: (1) XAS of 15-15-70 glass ceramics for Te and Nb; (2) the lowest energy and tetragonal polymorph crystal structures of $\text{K}_2\text{Te}_4\text{O}_9$ along the b -axis, which showed a cubic motif; (3) the neutron diffraction data compared to the calculated

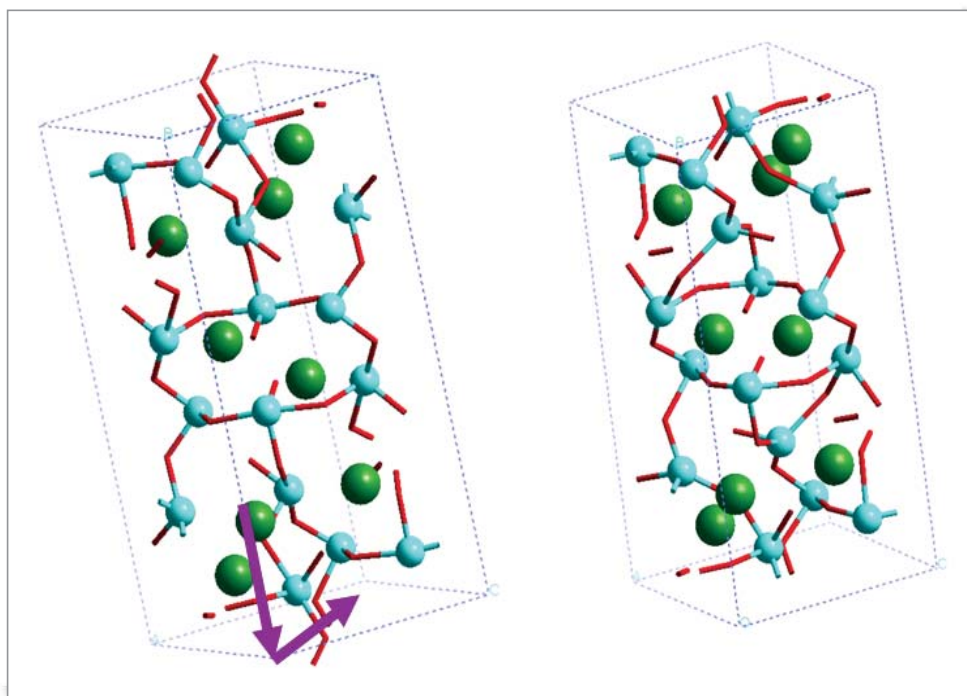


Fig. 1. Polymorphs of $\text{K}_2\text{Te}_4\text{O}_9$. Left: stable crystal structure from single-crystal x-ray diffraction. Right: pseudo-cubic $\text{K}_2\text{Te}_4\text{O}_9$ structure. This is a prototype for the crystalline phase of the 15-15-70 glass ceramic that satisfies all diffraction data and topological and chemical constraints. The violet arrows on the stable structure symbolize the shortening of the b -axis and stretching of the $a \cdot c$ distance, resulting in the pseudo-cubic structure.

pattern for the tetragonal polymorph, and the face-centered cubic fluorite model previously proposed; (4) the results of the powder x-ray diffraction experiments compared to the tetragonal polymorph and the fluorite model; and (5) the total correlation functions for the x-ray and neutron data compared to that calculated for the $\text{K}_2\text{Te}_4\text{O}_9$ polymorph model and the fluorite model.

Consistent with their earlier work, the researchers found 15-15-70 glass to be a phase-separated mixture with droplet morphology, although the new model shows the droplet/crystalline phase to be rich in Te. Such a conformation is expected when a melt lies between two stable crystalline compositions, that being the case here because $\text{K}_{18}\text{Te}_{41}\text{O}_{91}$ differs minimally from $\text{K}_2\text{Te}_4\text{O}_9$ when Nb is left out. Similarities between $\text{K}_2\text{Te}_4\text{O}_9$ and the cube suggested by the x-ray pattern imply a distortion

that can be explained without significant changes to bonding geometries or connectivities (Fig. 1). Such a model can account for the discrepancies between the x-ray diffraction patterns and the neutron diffraction patterns, which lacked the cubic characteristics, by addressing the different relative scattering strengths of oxygen and the metals. The model also explains observed phase separation behavior.

The model, as described for the crystalline phase, shows inversion symmetry. Current research is aimed at exploring 15-15-70 glass ceramic to characterize an additional mechanism that leads to SHG from an isotropic distribution of inclusions that is small when compared to the length of incident light. Taken together with the existing data, these results will lead to a much greater understanding of the complex optical behavior (especially the non-linear response) of glass ceramics. — *Mona Mort*

See: R.T. Hart¹, J.W. Zwanziger², and P.L. Lee³, "The Crystalline Phase of $(K_2O)_{15}(Nb_2O_5)_{15}(TeO_2)_{70}$ Glass Ceramic is a Polymorph of $K_2Te_4O_9$," *J. Non-Cryst. Solids* **337**, 48 (2004).

Author Affiliations: ¹Indiana University, ²Dalhousie University, and ³Argonne National Laboratory

Correspondence: jzwanzig@dal.ca

This research was funded by NSF grant DMR9870246. R.T.H. has been supported by a Graduate Assistance in Areas of National Need (GAANN) Fellowship administered by the Department of Education. This work was also supported in part by a fellowship from Merck Research Laboratories. Use of the Advanced Photon Source and the Intense Pulsed Neutron Source was supported by the U.S. Department of Energy, Office of Science, Office of Basic Energy Sciences under Contract No. W-31-109-ENG-38.

CHARACTERIZING LOCAL CRYSTALLOGRAPHIC MICROSTRUCTURE EVOLUTION IN THREE DIMENSIONS

Researchers from Oak Ridge National Laboratory have combined sophisticated theoretical and experimental techniques to gain detailed knowledge of the three-dimensional (3-D) structure of complex crystalline samples. The samples were probed using high-intensity x-rays from the UNI-CAT 34-ID beamline at the APS.

The polychromatic x-rays were concentrated in a very narrow (500nm) beam and diffracted from microscopic portions of a small sample of iridium (Ir) that had been subjected to a weld, which caused a portion of its volume to melt, and then recrystallize as it cooled. Due to the heating and cooling around the weld, a heat-affected zone was produced. Internal stresses were pronounced within that zone. Some of those internal stresses were relieved through plastic deformation (which is a permanent change in the structure of a material). The plastic deformation of the crystalline iridium could largely be attributed to dislocations in the crystal's structure. In general, an edge dislocation occurs when a partial plane of atoms in the crystal's structure is sandwiched between two full planes of atoms. Because the x-ray microbeam penetrated just a few microns into the iridium, at most only a couple of distinct crystalline grains within the sample were encountered at any beam position on the sample.

When a polychromatic x-ray beam is intercepted by a single crystal, it reflects some of the x-rays into a characteristic geometrical pattern that depends on the crystalline structure and on the orientation of the crystal. From a nearly perfect crystal, the Laue pattern will appear as a series of sharp spots on

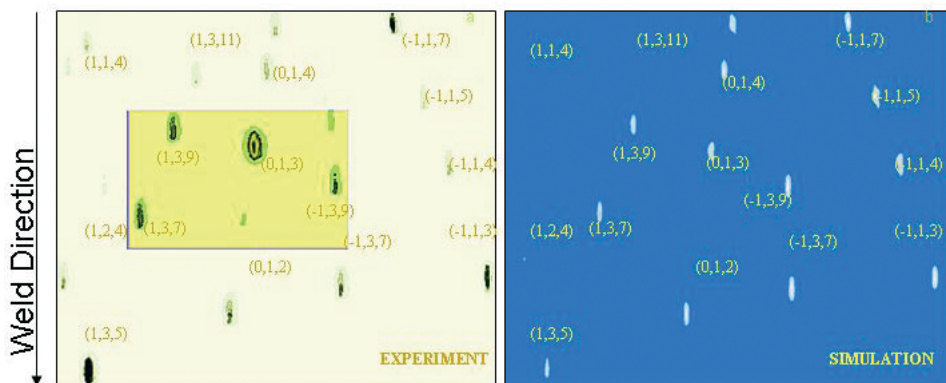


Fig 1. Comparison of Laue diffraction patterns: the left-hand graphic displays experimental data, while the right-hand side is based upon computer simulation.

an area detector. The spots correspond to wavelengths at which the x-ray scattering from atomic planes in the crystal interfere constructively. When portions of the sample's heat-affected zone were probed by the microbeam of polychromatic x-rays, the resulting diffraction patterns show pronounced streaking of the Laue spots. The streaks are largely a result of dislocations within the crystalline iridium. (Streaking can also be attributed to effects of elastic strain within a crystal; however, in this case elastic strain was considered to have a negligible impact upon the resulting diffraction pattern.) The researchers

Continued on next page

showed that streaking direction and intensity are related to the unpaired dislocation density tensor.

For a particular crystalline grain, there are many possible dislocations that can cause streaking of a Laue pattern. The researcher's task was to determine which type of dislocation—known as a “slip system”—was responsible for the particular Laue pattern seen in their experiment. The researchers conducted computer simulations for the grain probed in their experiment, which indicated that only two of the possible twelve slip systems would yield Laue images closely resembling the images produced in the experiment. Further mathematical analysis identified the slip system that best matched the experimental data and theory (Fig 1).

It was also found that crystalline deformation near the weld was closely correlated to the thermal gradients and to the local crystallographic orientation in that region. Furthermore, misorientations of the crystal's lattice structure in the heat affected zone appeared mainly about an axis perpendicular to the weld direction.

The researcher's results demonstrate that a combination of sophisticated computer modeling, modern experimental tech-

niques, and high-intensity x-ray sources, such as Argonne's APS, can give important insights into the microscopically inhomogeneous behavior of materials. These methods can be further extended by the use of differential aperture x-ray microscopy, a new method that allows for the measurement of distinct small volumes deep within low *Z* samples. — *Phil Koth*

See: G.E. Ice and R. Barabash, “Polychromatic X-ray Microdiffraction Characterization of Local Crystallographic Microstructure Evolution in 3D,” Proceedings of the 25th Risø International Symposium on Materials Science: Evolution of Deformation Microstructures in 3D, C. Gundlach, K. Haldrup, N. Hansen, X. Huang, D. Juul Jensen, T. Leffers, Z.J. Li, S.F. Nelson, W. Pantleon, J.A. Wert, and G. Winter, eds.; 351 (Risø National Laboratory, Roskilde, Denmark, 2004).

Author Affiliations: Oak Ridge National Laboratory
Correspondence: barabashom@ornl.gov

This research was supported by the U.S. Department of Energy, Office of Basic Energy Sciences under contract No. DE-AC05-00R22725 with UT-Battelle LLC. Use of the Advanced Photon Source was supported by the U.S. Department of Energy, Office of Science, Office of Basic Energy Sciences, under contract No. W-31-109-ENG-38.

PROBING BOND CHANGES IN BORON NITRIDE AT HIGH PRESSURE

In its wurtzite and cubic phases, boron nitride is one of the hardest materials known and has many industrial uses. Although the process of forming the superhard phases from the flaky graphite-like hexagonal boron nitride (h-BN) has been known for nearly 50 years, our understanding of how the bonds change as the material transforms from one phase to another is limited, based primarily on theoretical calculations and indirect experimental evidence. The lack of a direct *in situ* experimental probe for electronic structure at high pressure had left researchers with a number of unanswered questions. Recent developments in high-pressure inelastic x-ray scattering (IXS), however, gave researchers from the Carnegie Institution of Washington, The University of Chicago, and the Brookhaven and Argonne national laboratories a direct method for probing electronic bonding changes under these challenging conditions. The research team used this method to investigate how BN changes at high pressure.

Standard spectroscopic techniques for light (low-*Z*) elements, such as soft x-ray absorption spectroscopy (SXAS) and electron energy-loss spectroscopy (EELS), are limited in high-pressure environments because the diamond anvils typically used for generating high pressure absorb x-rays in the energy range of interest. Although IXS has potential for high-pressure studies, it has been limited by the small differential scattering cross section in combination with the small sample size.

The research group carrying out this experiment was able to use IXS by making several equipment modifications: they used a cylindrical diamond anvil cell with a beryllium gasket through which x-rays can enter and exit. They obtained a usable signal by focusing the full undulator beam on the sample and using a post-sample slit to discriminate signal from background. This method measures loss of the incident hard x-

ray photon energies with ever better resolution, allowing the study of light elements.

As the anvil-cell pressure increased, the group observed the conversion of h-BN's (in-plane) sp² and weaker (out of plane) p bonds into wurtzite's very hard and stable (diamond-like) sp³ bonds and found that the bonds convert simultaneously in both crystallographic directions. The revealing experiments were conducted at the HP-CAT beamline 16-ID and the GSECARS-CAT beamline 13-ID at the APS.

The group obtained spectra in two crystallographic directions as they put the h-BN sample under increasing pressure, transforming it into wurtzite or w-BN (Fig. 1). The bonding information from the spectra suggests that the sp³ bonds form simultaneously in both directions without relative displacement or rotation between the layers of h-BN structure. Each nitrogen atom appears to bond with three boron atoms in the same plane

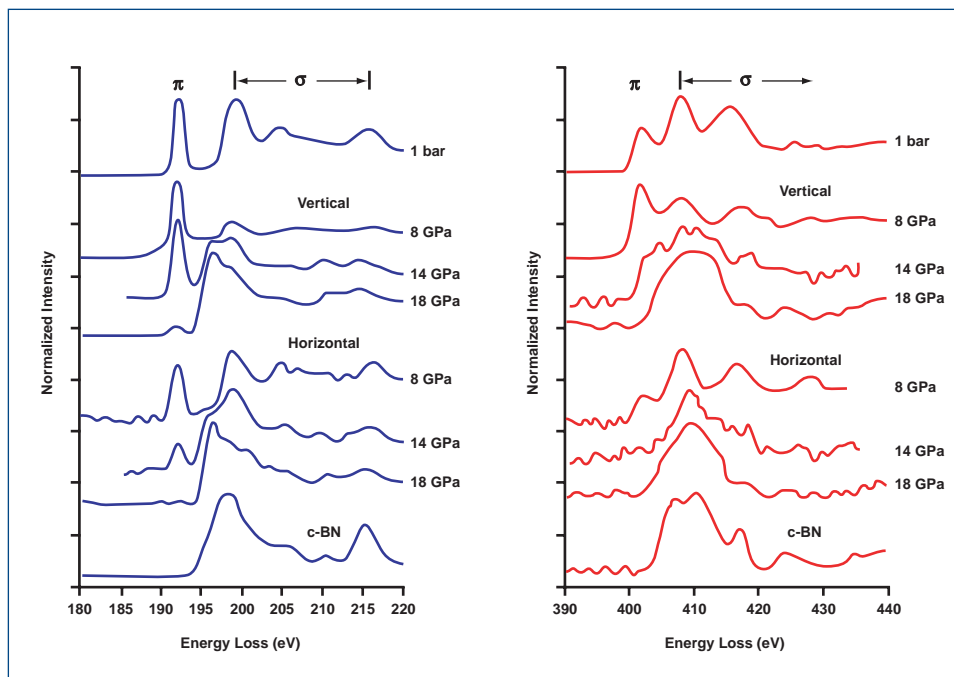


Fig. 1. Spectra of boron's K absorption edge (left) and nitrogen's K absorption edge (right) at varying pressures, obtained using inelastic x-ray scattering. As pressure increases, the peaks corresponding to sp^2 and p bonds recede and are replaced by those of sp^3 bonds. The scattered intensity is normalized to the incident intensity. High-pressure spectra were taken in horizontal and vertical geometries to probe bonds in directions parallel and perpendicular to the c -axis. The top spectra are from the starting h-BN sample at 1 bar. The bottom spectra are from cubic BN.

and a boron atom from the next layer down. At the same time, each boron atom forms a bond with a nitrogen atom buckled down from an adjacent layer above. This results in a much stronger solid. Yet, although the bonding is similar, w-BN is still distinct from crystalline c-BN.

The new IXS method and the results obtained thus far will allow researchers to investigate a number of pressure-induced phenomena in boron and nitrogen materials, including polymerization, metallization, superconductivity, semiconductivity, and superhardness. It should also offer some contrast between BN and the properties of carbon. — *Yvonne Carts-Powell*

See: Y. Meng^{1,2}, H.-K. Mao², P.J. Eng³, T.P. Trainor³, M. Newville³, M.Y. Hu^{1,2}, C. Kao⁴, J. Shu², D. Hausermann^{1,2}, and

R.J. Hemley¹, "The Formation of sp^3 Bonding in Compressed BN," *Nat. Mater.* **3**, 111 (February 2004).

Author Affiliations: ¹Argonne National Laboratory, ²Carnegie Institution of Washington, ³The University of Chicago, ⁴Brookhaven National Laboratory

Correspondence: ymeng@hpcat.aps.anl.gov

Use of the HP-CAT facility is supported by the U.S. Department of Energy (DOE) Office of Basic Energy Sciences; the DOE National Nuclear Security Administration; the National Science Foundation; the Department of Defense Tank, Automotive and Armaments Command; and the W.M. Keck Foundation. Use of the Advanced Photon Source is supported by the DOE Office of Science, Office of Basic Energy Sciences under Contract No. W-31-109-ENG-38.



NEW IMAGES OF SURFACE PHASE TRANSITIONS

A vast range of chemical and materials science phenomena occur on surfaces, so it is important to understand how atomic-layered structures form on substrates. Of particular interest are surface phase transitions, in which one ordering of atoms on a surface changes to a different ordering. The starting point for unraveling the details of surface phase transitions is an accurate picture of the surface on an atomic scale. Despite many experimental investigations, the dynamics of a wide range of structural transitions remain unresolved. Recently, researchers from Northwestern University, using the DND-CAT 5-ID-C beamline at the APS, have developed a technique for examining arrangements of adsorbed atoms on surfaces in three dimensions (3-D) as a function of temperature by means of x-ray standing wave (XSW) imaging.

A particularly puzzling surface phase transition is the reconstruction of tin (Sn) atoms on a germanium (Ge) surface. When a Ge (111) surface is covered by approximately one-third of a monolayer of Sn at room temperature, the adsorbed layer forms the so-called $\sqrt{3} \times \sqrt{3}$ pattern (Fig. 1). As the substrate is cooled to 100K, the Sn atoms undergo a reversible phase transition to a 3×3 structure. When this 3×3 structure is examined by means of scanning tunneling microscopy, some of the Sn sites appear different from the others. Previous studies with x-ray diffraction measurements have yielded conflicting results, so the research team used XSW observations to examine the surface reconstruction.

X-ray standing wave imaging is an element-specific analysis tool that relies on x-ray fluorescence induced by the interference pattern created near a surface by an incoming x-ray beam and its Bragg reflection. XSW has advantages over conventional x-ray diffraction in interpreting the data, because it yields both phase and amplitude information, as opposed to x-ray diffraction, which loses the phase component.

To create the samples, Sn was evaporated onto the sputter-cleaned Ge surface at room temperature, then annealed at 473K in an ultrahigh-vacuum chamber. X-rays at 7 keV energy from 5-ID-C were directed onto the Ge surface, and the Sn x-ray fluorescence was collected at various temperatures by a solid-state detector. To form the XSW image, the Ge crystal was rotated relative to the incident beam, causing the standing wave pattern to move in and out from the surface.

The researchers used the XSW data to obtain a set of Fourier components that were added together to derive a real-space 3-D atomic density map of the adsorbed Sn atoms relative to the Ge substrate lattice. In the room temperature structure, the map showed that the Sn atoms aligned laterally over a Ge atomic position in the second layer down of Ge atoms. Furthermore, the Sn distribution was found to be vertically split—with one-third of the Sn atoms 0.45 Å higher than the remaining two-thirds. This distribution showed no change when going through the surface reconstruction (when the Ge crystal was cooled), consistent with an order-disorder picture. Below the transition temperature, the Sn atoms are locked in place, while above the transition temperature, they undergo fluctuations between the two vertical positions. The use of XSW to study this particular surface reconstruction has resolved a num-

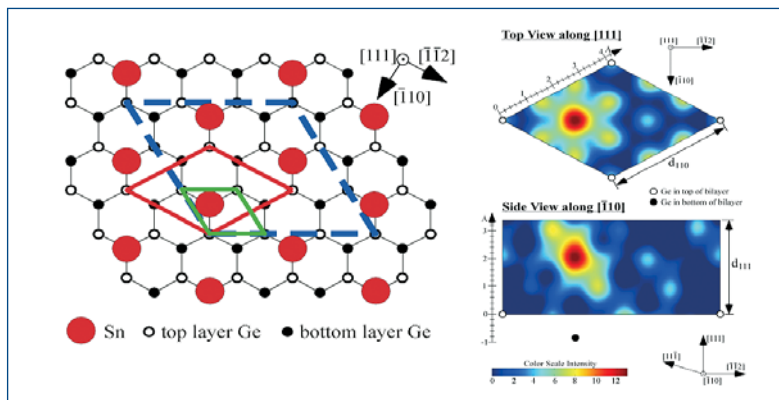


Fig 1. (left) Schematic of $1/3$ monolayer of Sn atoms (red) adsorbed on a Ge (111) surface (top Ge layer: open circles; bottom Ge layer: filled circles). The 1×1 two-dimension unit cell is outlined in green, the $\sqrt{3} \times \sqrt{3}$ in red, and 3×3 as dashed blue lines. (right) A lateral cut (top) and vertical cut (bottom) through the Sn 3-D atomic density map that was generated by a summation of a small set of x-ray standing wave measured Sn Fourier components. The cuts were selected to coincide with the maximum (dark red) in the Sn density. The subsidiary maxima are due to unmeasured Fourier components being artificially set equal to zero in the summation (i.e., truncation error). The small open circles represent the positions of the Ge top layer of atoms that forms the 1×1 unit cell.

ber of controversies over the structure of the Sn adsorbate layer and the nature of the phase transition involved. In addition, the work highlights the value of third-generation synchrotron facilities such as the APS to provide the very bright monochromatic x-ray beam essential to these kinds of surface structural probes. — David Voss

See: J.S. Okasinski, C.-Y. Kim, D.A. Walko, and M.J. Bedzyk, "X-ray Standing Wave Imaging of the $\frac{1}{3}$ Monolayer Sn/Ge(111) Surface," *Phys. Rev. B* **69**, 041401 (2004).

Author Affiliation: Northwestern University
Correspondence: bedzyk@northwestern.edu

This work was supported by the NSF under Contract Nos. DMR-9973436, DMR-0076097, and CHE-9810378; the State of Illinois under Contract No. IBHEHECANWU96 to NU, and the U.S. DOE under Contract Nos. W-31-109-ENG-38 to ANL and DE-FG02-03 ER 15457 to NU. Use of the Advanced Photon Source was supported by the U.S. Department of Energy, Office of Science, Office of Basic Energy Sciences, under Contract No. W-31-109-ENG-38.

OCTAHEDRAL TILT PROVIDES CATALYST CLUES

The smallest of structural changes can lead to large changes in the properties of technologically important materials. Take perovskites, for instance. The perovskite structure is an archetypal crystal structure found in a diverse range of minerals, including materials with useful catalytic and electronic properties. But subtle distortions from the archetypal structure can turn an active catalyst into an inactive one or a superconducting material into an insulator. Now, researchers from the State University of New York at Stony Brook, Brookhaven National Laboratory, Michigan State University, and Argonne National Laboratory have used high-energy x-rays from the XOR 1-ID beamline at the APS to study the structure-dependent properties of a perovskite-related mineral: alpha-aluminum trifluoride (α -AlF₃). Their findings show how new x-ray diffraction methods can allow researchers to detect and model subtle changes of structure more accurately than before, and confirm that these new methods have many significant applications in chemistry, materials science, and for geologically important materials.

The mineral α -AlF₃ is commonly used in the chemical industry as a catalyst for fluorocarbon manufacture and as an additive for improving the electrolysis of aluminum ore in aluminum production. The material has a distorted perovskite structure related to the compound rhenium oxide at room temperature. However, heat it above 468°C, and the material changes, adopting the cubic rhenium oxide structure.

According to the team, using conventional approaches—such as powder diffraction and neutron diffraction—to analyze

this phase change does not provide enough detailed information as to how the change occurs. These techniques yield useful long-range information that is averaged but cannot reveal the dynamics of the process. By necessity, it is the movement of ions or atoms that underlies the structural change. Recently, the team obtained data from the XOR 1-ID beamline that are detailed enough to reveal the dynamics of structure-changing processes.

Earlier studies have explained the structural changes in perovskites and other minerals in terms of the rotation of rigid octahedral sub-units in the crystal structure. Indeed, scientists use the rigid unit model with great success to describe the phase changes in silica and various natural perovskites. In the case of aluminum trifluoride, these octahedra comprise a central aluminum atom surrounded by six fluorine atoms, one at each vertex of the octahedron. By combining two distinct techniques—so-called “Rietveld refinement” and a pair distribution function—the team was able to observe the shifting octahedra within the material's structure at temperatures just below the phase change, at the temperature at which the phase change occurs, and temperatures just above it.

The group also ran molecular dynamics simulations in parallel with their refinement of the beamline data. The simulations gave them a way to “animate” the phase transition as one form of aluminum trifluoride is converted into the other as the temperature increases. The simulations then allowed the researchers to refine their model still further by comparing the simulation with their experimental results.

The study shows that the high-temperature structure of aluminum trifluoride is highly dynamic and is essentially composed

Continued on next page

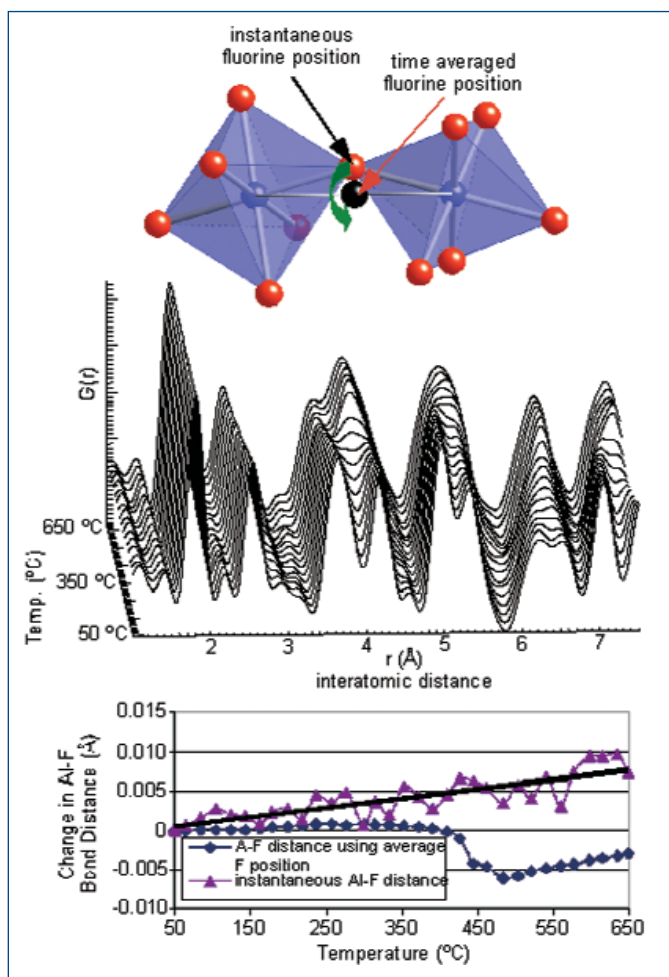


Fig. 1. Two corner-sharing AlF₆ octahedra, bridged by a single fluorine atom (top). The time-averaged fluorine position is shown as a black sphere and the actual fluorine position is shown in red, which rapidly rotates around the average position at high temperature. The pair distribution functions as a function of temperature are shown in the middle graph. The first peak corresponds to the aluminum-fluorine bond distance and shows a gradual increase as a function of temperature. The bottom plot shows the difference between the average and instantaneous fluorine positions as a function of temperature.

of a superposition of tilted AlF_6 octahedra that rotate between the different tilted structures, leading to an apparent cubic, undistorted structure.

The researchers hope to extend their approach to other materials, including other perovskites; catalysts such as CeO_2 (cerium dioxide); negative thermal expansion materials, such as zirconium molybdate; and perovskite minerals of geological relevance. One such mineral, magnesium silicate, comprises the bulk of the Earth's mantle and is the subject of investigations to explain anomalous seismic behavior observed at the boundary between the mantle and the Earth's core. The researchers anticipate that the combined experimental approach, in which both local atomic structure and long-range structure are probed, will provide valuable insight into how local structural distortions couple with physical properties or reactivity in this and other related mineral structures. — *David Bradley*

See: P.J. Chupas^{1,5}, S. Chaudhuri¹, J.C. Hanson², X. Qiu³, P.L. Lee⁴, S.D. Shastri⁴, S.J.L. Billinge³, and C.P. Grey¹,

"Probing Local and Long-Range Structure Simultaneously: An *In Situ* Study of the High-Temperature Phase Transition of $\alpha\text{-AlF}_3$," *J. Am. Chem. Soc.* **126**, 4256 (2004).

Author Affiliations: ¹State University of New York at Stony Brook, ²Brookhaven National Laboratory, ³Michigan State University, ⁴Argonne National Laboratory, ⁵Present address: Argonne National Laboratory

Correspondence: cgrey@mail.chem.sunysb.edu

REFERENCE

S. Chaudhuri, P.J. Chupas, M. Wilson, P. Madden, C.P. Grey, "Study of the Nature and Mechanism of the Rhombohedral-to-Cubic Phase Transition in $\alpha\text{-AlF}_3$ with Molecular Dynamics Simulations," *J. Phys. Chem. B.* **108**, 3437 (2004).

This work was supported through DOE grants DEFG02-96ER14681 and DE-AC02-98CH10086. Use of the Advanced Photon Source was supported by the U.S. Department of Energy, Office of Science, Office of Basic Energy Sciences under Contract no. W-31-109-ENG-38.

QUANTUM MUSIC: INFLUENCES ON THIN-FILM GROWTH



As most concert musicians and all good piano tuners know, two musical notes of similar pitch will interfere with each other and produce an undulating "beating" effect that indicates how well-tuned the instrument is. A similar beating phenomenon has been shown to be influential in the realm of quantum physics, where the wave-like nature of electrons interferes with the atomic structure of a nanoscale metal film. Such effects may prove very important for future technologies as the size of devices quickly shrinks to atomic dimensions. Many researchers have already predicted these effects in theoretical studies, but experimental observation of them has been more elusive. Recently, a team of researchers from the University of Illinois at Urbana-Champaign, using the UNI-CAT 33-ID beamline at the APS tackled the problem with an experiment using x-ray scattering from thin lead films on silicon.

Because of the penetrating nature of x-rays, detailed information not only about the surface of a film, but also about the substrate that supports it can be obtained by means of x-ray diffraction. Such an ability allows for measurement of absolute film thicknesses over a wide surface area. With this technique, the researchers observed the structural evolution of nanoscale films as they passed through various phases at different temperatures; the technique also revealed quantum influences caused by electron confinement on the physical properties of the films.

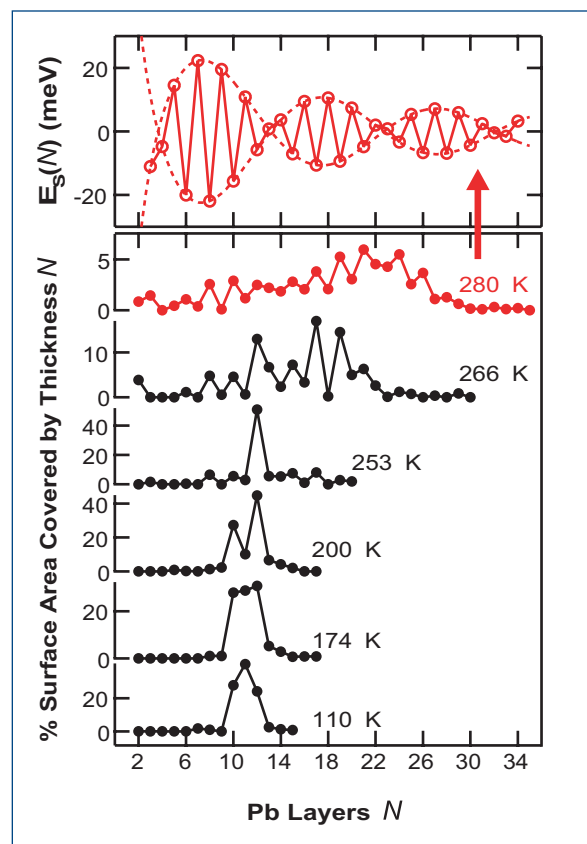
Thin-film samples were fabricated by evaporating Pb onto Si(111) substrates in an ultra-high-vacuum chamber at the UNI-CAT facility. Each substrate was cleaned and pretreated before growing a Pb film of a specific thickness. The films were then slowly warmed from 110K to room temperature while examining the surface morphology at select times by measuring the extended x-ray reflectivity. The data were then analyzed to reveal the distribution of nanostructure heights, which showed that the surface energy of a film, and hence its relative stability, is strongly dependent on its thickness.

The samples were found to undergo an unusual set of structural changes as they warmed: At 110K, the deposited Pb

atoms form smooth closed films in a layer-by-layer fashion. The bottom panel of Fig. 1 shows such a film, which is 11 atomic layers thick. At around 200K, the film transforms into a state often referred to as the "magic height" phase since all of the nanostructures on the surface are the same height (12 atomic layers in Fig. 1). Finally, at higher temperatures (around 280K), the films roughen and the height distribution greatly broadens, reflecting the broader energy landscape of the system. By analyzing the distribution of nanostructure heights at the final temperature, researchers can obtain a measure of the relative stability of each thickness with respect to its neighbors. This quantity can, in turn, be related to the surface energy for that height (Fig. 1, top), which exhibits an unusual oscillation pattern as a function of thickness. This oscillation strongly resembles the beating pattern that arises from the interference of two sinusoidal functions that have nearly the same frequency, as with two musical notes of similar pitch.

The oscillations and beating pattern can be explained by quantum confinement of the electrons in the thin layers of Pb. In the case of a thin film in the classical limit, where the electrons can occupy a continuum of energy levels, the surface

Fig. 1. Curves in the bottom panel show the percent surface area covered by different thicknesses of Pb. Starting at 110K, the morphology evolves from an initial thickness of 11 atomic layers, through various preferred thickness states, and to a final state at 280K that exhibits pronounced oscillations. The corresponding relative surface energy for the 280K curve is shown in the top panel, exhibiting a beating pattern that decays with increasing thickness. The beating pattern is attributable to quantum confinement of electrons in the thin film layers.



energy is constant with thickness. But electrons in a quantum well structure only occupy discrete levels, leading to oscillations in the surface energy. The beating pattern arises from the interference of the electron waves with the atomic lattice structure of the crystalline films. These results show that x-ray diffraction affords a detailed look at quantum effects in nanostructured surfaces unavailable with other probes. Moreover, such diffraction experiments are made possible by the high brilliance and excellent resolution of third-generation synchrotron facilities such as the APS — *David Voss*

See: P. Czoschke, H. Hong, L. Basile, and T.-C. Chiang, "Quantum Beating Patterns Observed in the Energetics of Pb Film Nanostructures," *Phys. Rev. Lett.* **93**, 036103-1 (16 July 2004).

Author Affiliation: University of Illinois at Urbana-Champaign
Correspondence: chiang@mrl.uiuc.edu

This work is supported by the U.S. Department of Energy (Grant No. DEFG02-91ER45439). The UNI-CAT facility at the APS is supported by the University of Illinois at Urbana-Champaign, Frederick Seitz Materials Research Laboratory (U.S. DOE and the State of Illinois-IBHEHECA), the Oak Ridge National Laboratory (U.S. DOE under contract with UT-Battelle LLC), the National Institute of Standards and Technology (U.S. Department of Commerce), and UOP LLC. We also

acknowledge partial equipment and personnel support from the Petroleum Research Fund, administered by the American Chemical Society, and the U.S. National Science Foundation (Grant No. DMR-02-03003). Use of the Advanced Photon Source was supported by the U.S. Department of Energy, Office of Science, Office of Basic Energy Sciences, under Contract No. W-31-109-ENG-38.

HOW THIN CAN A FERROELECTRIC BE?

Thin films of ferroelectric material for use in future "electronic" devices can be as thin as 1.2 nanometers without loss of function, according to a synchrotron x-ray study carried out by researchers using the BESSRC/XOR beamline 12-ID at the APS. The results show that a thin film of one particular ferroelectric material, lead titanate, is still stable even in a layer that is a mere 1.2 nanometers (three unit cells) thick.

An electric field can control the permanent polarization in a ferroelectric material in much the same way that a magnetic field controls the magnetization of a ferromagnet. Ferroelectric materials known as perovskites, of which lead titanate is one, share their crystal structure with the mineral perovskite. They are being keenly investigated for new applications in microelectronics.

Ferroelectric materials are already being used in microelectronic devices, such as non-volatile random access memory (NVRAM), that exploit ferroelectricity to store information. An

electric field can switch the permanent polarization from one direction to the other, representing the switch from a 0 bit of information to a 1. The development of NVRAM could provide computers and ever-smaller portable information devices with high-density solid-state memory that, unlike conventional RAM, does not lose its information when switched off. The Argonne research removes a potential limitation on how dense these devices can be when fabricated.

Perovskites also have other potentially useful properties. They are piezoelectric materials, for instance, which means

Continued on next page

that they change shape when a voltage is applied, or generate a voltage when they are deformed. They are also pyroelectric, producing a voltage when the temperature changes. Electronically controlled switches, valves, pumps, and sensors in so-called "lab-on-a-chip" devices, or microelectromechanical systems, could exploit such properties.

Technologists hoping to exploit the novel electrical and magnetic properties of such advanced materials in thin-film form have often encountered problems maintaining their properties in very thin films. Researchers found that films of lead titanate thinner than 100 nanometers, for instance, have reduced polarizability and sometimes exhibit no ferroelectric behavior at all. If this problem proved to be the result of a fundamental incompatibility between ferroelectricity and reduced thickness, it might present a lower limit on the size of microelectronic components based on such materials.

Researchers from Argonne National Laboratory and Northern Illinois University were not convinced that the size effects seen in previous studies would arise in all ferroelectric samples. It can be very difficult to separate the effects of true size dependence from those of uncontrolled experimental variables, such as stress and composition, that can vary with sample size. Recent theoretical calculations carried out by other researchers had also predicted that perovskite films would still have ferroelectric properties, even in films just a few nanometers thick.

The group set about making detailed experimental observations that would unambiguously settle the long-standing question of the thickness limit for ferroelectricity. The team used metalorganic chemical vapor deposition to grow thin layers of the perovskite lead titanate on single crystals of strontium titanate. By carrying out x-ray scattering experiments during the deposition process, they were able to control the thickness of the layer very precisely to an integer value of the film's unit cell. By using this *in situ* approach and the high-brilliance synchrotron x-ray beam from the APS, the team obtained accurate data from high-quality samples as thin as 1 unit cell.

In these thin films, the ferroelectric phase forms in nanometer-scale stripes of alternating polarity, which produce characteristic signals, or satellite peaks, in the x-ray scattering results. The researchers used these satellite peaks to identify the ferro-

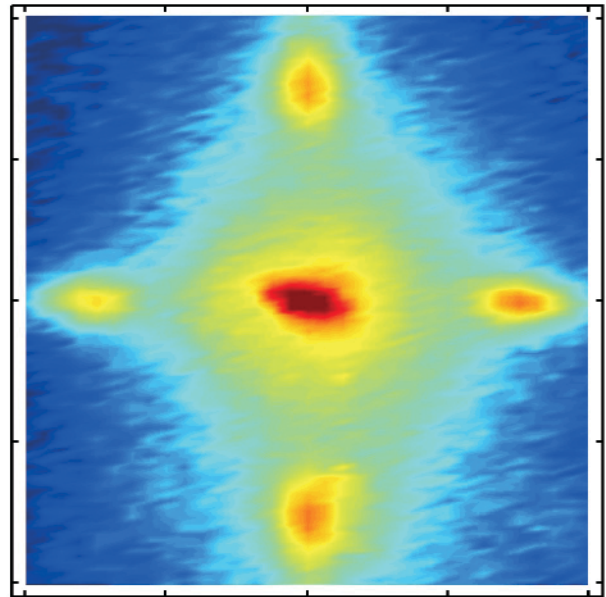


Fig. 1. X-ray scattering pattern from ferroelectric stripe domains in a thin film of lead titanate 3-unit-cells thick.

electric phase. Fig. 1 shows the scattering pattern from a 3-unit-cell- (1.2-nanometer) thick film that is shown to be ferroelectric. The team found thinner (2- and 1-unit-cell-thick) films to be non-ferroelectric. This tiny thickness limit for ferroelectricity bodes well for fabricating submicroscopic layers for use in various novel applications. — *David Bradley*

See: D.D. Fong¹, G.B. Stephenson¹, S.K. Streiffer¹, J.A. Eastman¹, O.Auciello¹, P.H. Fuoss¹, and C. Thompson², "Ferroelectricity in Ultrathin Perovskite Films," *Science* **304**(5677), 1650, 11 June 2004).

Author Affiliations: ¹Argonne National Laboratory, ²Northern Illinois University

Correspondence: stephenson@anl.gov

Work supported by the State of Illinois and by the U.S. Department of Energy, Office of Science, Office of Basic Energy Sciences under Contract no. W-31-109-ENG-38.



SiC CRYSTALS EXAMINED UNDER HIGH PRESSURE WITH X-RAY AND ULTRASONIC TECHNIQUES

Silicon carbide (SiC) is currently the focus of intensive research. Its favorable attributes include high mechanical hardness, excellent thermal conductivity, and tolerance to high temperatures (over 600°C) without significant structural degradation. Because of these and other positive features, SiC is thought to have great potential for application in a variety of important technologies, such as high-temperature and high-current electronic devices. In this research, a team consisting of investigators from the University of Hawaii, the State University of New York at Stony Brook, and Argonne National Laboratory examined small samples of SiC utilizing synchrotron x-rays and ultrasonic sound waves. For both types of measurements, the SiC samples were subjected to a range of pressures in order to reveal certain key properties of the material, including the bulk and shear modulus, along with their corresponding pressure derivatives. The x-ray measurements were carried out at the HP-CAT 16-ID beamline at the APS.

For the x-ray measurements, a powdered sample of SiC crystals was obtained. The powder was then compressed to form a pellet, placed into a diamond anvil cell (DAC), and surrounded by a pressure-transmitting fluid consisting of methanol and ethanol. The DAC device was used to exert high pressures on the sample, which reached a maximum of 50 GPa. The highly monochromatic synchrotron x-rays derived from the HP-CAT beamline were focused by Kirkpatrick-Baez mirrors to a square area of just 10 μm per side (1 $\mu\text{m} = 10^{-6}$ m). The x-ray wavelength was $\lambda = 0.4246$ Å. Angle dispersive x-ray diffraction (XRD) was the technique employed to decipher the crystalline structure of the sample at various pressures.

Silicon carbide crystals come in a variety of distinct forms called “polytypes.” All SiC polytypes share a common building block or bilayer, which in the case of SiC, can be conceptualized as two planar sheets of atoms bonded together—one sheet of silicon atoms, the other of carbon atoms. The x-ray diffraction patterns obtained from this research showed that, at all pressures, the SiC crystals in the sample were all of the 6H polytype. The “6” means that the bilayer is repeated six times, while the “H” denotes the crystals’ hexagonal structure. Pressures exerted on the sample were determined by measuring the fluorescence of tiny ruby chips placed in the sample chamber. The volumes of the SiC crystals, which decreased as the pressure increased, were deduced from the x-ray diffraction data. From those measurements it was determined that from zero pressure to the maximum of 50 GPa, the linear compressibility of the SiC crystals was very nearly isotropic (i.e., the same in every lattice direction).

The ultrasonic measurements, carried out at the State University of New York at Stony Brook, were performed at pressures up to 13.6 GPa. The SiC sample was held in a specialized hydraulic press. Both compressional P and transverse S ultrasonic waves were induced in the sample. Measurement of the velocities of those waves allowed the volume of the sample to be determined at various pressures (Fig. 1).

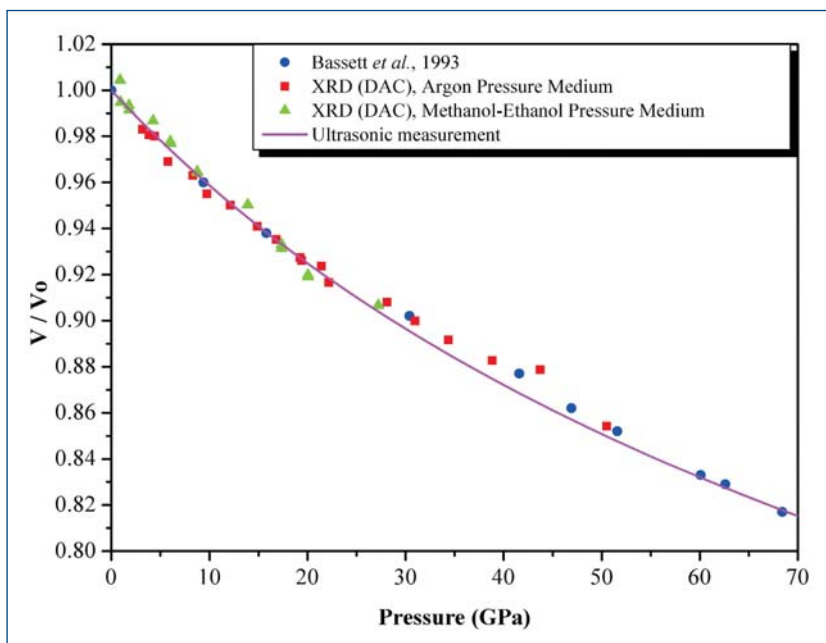


Fig. 1. Comparison of the variation of the unit cell volume ratio with pressure. Data from four experiments are compared: the x-ray diffraction and ultrasonic experiments described in this summary; a subsequent x-ray diffraction experiment that used a different pressure media than the one described here; and finally, a previous experiment conducted by Bassett et al, *J. Appl. Phys.* 74, 3824 (1993).

A prime goal of the x-ray and ultrasonic experiments was the determination of the bulk modulus (K_0) and bulk modulus pressure derivative (K'_0) of the SiC crystals. Both K_0 and K'_0 can be determined using an equation of state. The equation of state is basically a model that expresses the pressure exerted on the crystals as a function of volume, K_0 , and K'_0 . The pressure and volume data from the x-ray and ultrasonic experiments were fit to the equation of state and the values of the bulk modulus and its pressure derivative were determined independently for each of those two techniques. From the x-ray diffraction measurements, the researchers found $K_0 = 218.46 \pm 4.9$ GPa, which overlaps the value of the bulk modulus derived

Continued on next page

from the ultrasonic measurements, $K_0 = 216.56 \pm 1.1$ GPa. Notably, the two experimental techniques yielded the same value for the bulk modulus pressure derivative of $K'_0 = 4.19 \pm 0.09$. The values of K_0 and K'_0 were close to those determined by several other research teams that employed similar techniques and materials. — *William Arthur Atkins*

See: G. Amulele¹, M.H. Manghnani¹, B. Li², D.J.H. Errandonea³, M. Somayazulu³, and Y. Meng³, "High Pressure Ultrasonic and X-ray Studies on Monolithic SiC Composite," *J. Appl. Phys.* **95**, 1806 (15 February 2004).

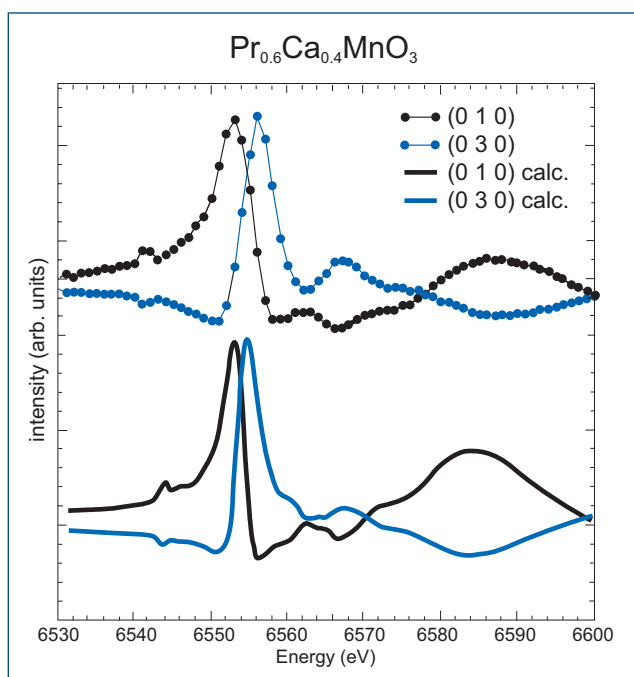
Author Affiliations: ¹University of Hawaii; ²State University of New York at Stony Brook; ³Argonne National Laboratory
Correspondence: gamulele@soest.hawaii.edu

Use of the HP-CAT facility was supported by DOE-BES, DOE-NNSA, NSF, DOD-TACOM, and the W.M. Keck Foundation. HP-CAT is a collaboration among the Carnegie Institution, Lawrence Livermore National Laboratory, the University of Hawaii, the University of Nevada Las Vegas, and the Carnegie/DOE Alliance Center CDAC. This research project was supported by TACOM Contract No. DAAE07-01-C-L055. Use of the Advanced Photon Source was supported by the U.S. Department of Energy, Office of Science, Office of Basic Energy Sciences under Contract No. W-31-109-ENG-38.

TEASING OUT THE ELECTRONIC STRUCTURE OF PEROVSKITE MANGANITES

Perovskites are the parent minerals for an increasingly important group of oxides. Perovskites have remarkable electronic properties that depend on the different electronic degrees of freedom—spin, charge, orbital degeneracy, and electron-lattice coupling—and the way these interact. Even after 50 years of research, scientists are still unclear about what electronic arrangements account for perovskite's unusual properties. Researchers from Rutgers University, Brookhaven National Laboratory, Hamburger Synchrotronstrahlungslabor (HASYLAB), the Joint Research Center for Atom Technology, and Argonne National Laboratory used resonant x-ray diffraction (RXD) at the CMC-CAT 9-ID beamline at the APS and beamline X22C at the National Synchrotron Light Source to better understand the electronic ground state of a perovskite manganite. Their results provide new information about the material and led them to suggest an orbital ordering scheme.

The group studied a particular perovskite manganite: $\text{Pr}_{0.6}\text{Ca}_{0.4}\text{MnO}_3$. Spectra were obtained at the material's Mn-K transition edge both above and below the structural phase transition temperature.



The oldest theory regarding the ground-state of half-doped manganites is a charge and orbital ordering model by Goodenough: the Mn^{3+} and Mn^{4+} sites form a checkerboard, and the molecular orbitals form zig-zag magnetic chains. In 1997, Radaelli and others proposed a structure supporting this theory. But x-ray spectroscopy experiments did not show any charge ordering. A conflicting "Zener polaron" theory published in 2002 suggested a different crystal structure, with no checkerboard ordering.

The research team observed the presence of inequivalent Mn atoms but not the charge ordering. Their work is evidence against the Zener polaron theory. It does show that inequivalent Mn atoms order as suggested in the older theory. However, the results also imply a new pattern of orbital ordering. The data suggest that all the Mn sites have similar charge density with different $3d$ orbitals orientations. Because this orientation is crucial to the magnetic and transport properties, the work suggests new considerations for the physics of manganites.

Fig. 1. Resonant x-ray diffraction allows researchers to obtain spectra that sheds light on the higher orbitals of Mn in the crystal structure of perovskite manganites. The RXD data shows very different curves for Mn in different positions within a crystal unit cell. Although standard crystallographic methods barely distinguish the two inequivalent sites, RXD converts some hundredths of an Angstrom difference into a 500% variation in the signal intensity.

Resonant x-ray-diffraction is an excellent tool for investigating the electronic ordering of the material because it is extremely sensitive to the environment of the resonant ions. RXD involves measuring the intensity of a reflection as a function of the incident photon energy. This technique obtains spectroscopic information regarding the molecular orbitals of the material. It also provides diffraction and scattering information because of the coherence of the resonant process.

By tuning the incident energy to the Mn K-edge, the researchers probed the unoccupied density of p-orbital states. The probe was a 6.550 keV photon with enough energy to be absorbed by a deep core electron, which was then promoted above the Fermi level (from the 1s to 4p orbital). This 4p orbital extends beyond the closest oxygen neighbors. The 4p mappings of the different Mn sites in the crystal unit cell are dramatically different (Fig. 1). — *Yvonne Cartz-Powell*

See: S. Grenier^{1,2}, J. P. Hill², D. Gibbs², K.J. Thomas², M. v. Zimmermann³, C. S. Nelson⁴, V. Kiryukhin¹, Y. Tokura⁵, Y. Tomioka⁵, D. Casa⁶, T. Gog⁶, and C. Venkataraman⁶, "Resonant X-ray Diffraction of the Magnetoresistant Perovskite: $\text{Pr}_{0.6}\text{Ca}_{0.4}\text{MnO}_3$ " *Phys. Rev. B* **69**, 134419 (15 April 2004).

Author Affiliations: ¹Rutgers University, ²Brookhaven National Laboratory, ³Deutsches Elektronen-Synchrotron (DESY), ⁴Brookhaven National Laboratory, ⁵Joint Research Center for Atom Technology, ⁶Argonne National Laboratory
Correspondence: grenier@bnl.gov

Brookhaven National Laboratory is supported under DOE Contract No. DE-AC02-98CH10886. The research received support from the NSF MRSEC program, Grant No. DMR-0080008. Use of the Advanced Photon Source was supported by the U.S. Department of Energy, Office of Science, Office of Basic Energy Sciences, under Contract No. W-31-109-ENG-38.

NEW DETAILS OF FERROELECTRIC SWITCHING



All of our current information technology relies on devices that process information as binary ones and zeroes. Ferroelectric materials are of special interest to developers of the next generation of such devices because they exhibit polarized electronic states that can represent bits of information. Moreover, these materials retain their polarization states without consuming electrical power, making ferroelectrics the subject of intense study for non-volatile memory applications in which data are stored even when the power is turned off. One problem, however, is polarization fatigue: after a number of cycles, the switchable polarization begins to taper off, rendering the device unusable. A team of researchers from the University of Wisconsin, Bell Laboratories, and the University of Michigan used the MHATT/XOR beamline 7-ID at the APS to study the micron-scale details of polarization fatigue in ferroelectric oxides.

Polarization fatigue is a well-known problem in ferroelectric capacitor technology. One problem that may cause polarization fatigue stems from the migration of oxygen atoms to the electrode region. This migration, in turn, leads to formation of oxygen vacancies which can pin polarization domain walls and inhibit switching. Another mechanism involves the formation of a layer near the electrode interface that reduces the total electric field in the ferroelectric material and shuts down its ability to reverse polarization. Both of these proposed mechanisms appear to be microscopic in nature; to study them in detail requires a precise, high-resolution structural analysis tool. X-ray microdiffraction can be used to image the evolution of polarization domains in buried ferroelectric thin films during switching with submicrometer resolution.

The ferroelectric devices studied here were made in the University of Wisconsin group of Chang-Beom Eom by first depositing an SrRuO_3 bottom electrode on an insulating

Continued on next page

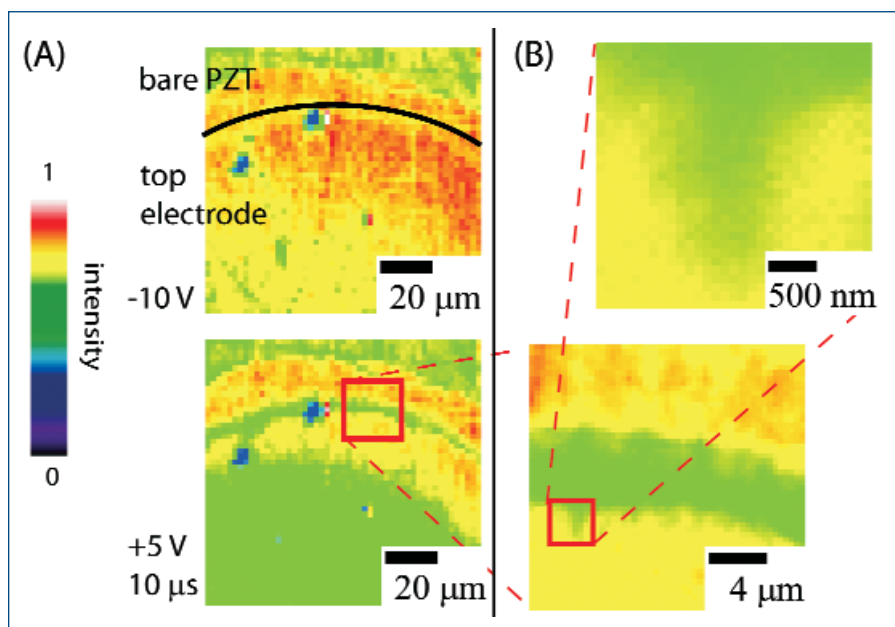


Fig. 1. Microdiffraction images of polarization switching in a $\text{Pb}(\text{Zr},\text{Ti})\text{O}_3$ thin film capacitor. (A) Images made following a -10 V pulse (top) and a shorter 10 μs +5 V pulse (bottom) show nearly complete polarization switching. Longer electrical pulses completely switch the device. (B) The boundary between two regions with opposite polarizations.

SrTiO₃ substrate. Epitaxial PbZr_{1-x}Ti_xO₃ (PZT) films with a nominal composition of $x = 0.55$ and thicknesses of 80 or 160 nm were grown on top of the electrodes by means of radio frequency sputtering, followed by a top electrode layer consisting of sputtered polycrystalline platinum. A beam of 10-keV x-rays from the 7-ID beamline was focused onto a 0.8- μm spot on this ferroelectric structure, and the diffracted x-rays were detected by using conventional x-ray diffraction techniques. Images of the stored polarization with the ferroelectric layer were obtained by scanning the x-ray beam across the device. An advantage of this configuration is that electrical measurements can be made *in situ* during x-ray diffraction experiments. As a baseline, diffraction images were collected for each of the two stable polarization states to establish that x-ray microdiffraction was an accurate probe of the ferroelectric behavior.

The results of this study showed that polarization fatigue was qualitatively different when the switching was driven by lower-amplitude electric-field pulses (0.625 MV per cm peak) switching versus higher-amplitude field pulses (1.2 MV per cm peak). Fatigue was observed in both regimes as the polarization-field hysteresis loops collapsed after repeated cycling with triangle wave pulses at 1 kHz. Low electric-field fatigue was observed within 10⁴ pulses as the PZT layer structure became pinned into an unswitchable state, which could be restored by exposure to higher electric-field pulses.

A different process was found for fatigue induced by high field pulses. Although the onset of fatigue occurred after a much higher number of electric-field cycles, the decrease in switchable polarization and the structural changes were more dramatic and irreversible. The x-ray microdiffraction images

showed that isolated regions of severely decreased x-ray scattering intensity begin to form and that these eventually coalesce to encompass the entire region under the electrodes. The diffraction data indicate that there is a drastic loss of structural order as the fatigue progresses to failure of the device.

These measurements, made possible by the high brightness of the third-generation synchrotron at the APS, confirm that several mechanisms may be at play during fatigue and failure of ferroelectric devices. The results also indicate that x-ray microdiffraction is an ideal tool for high-resolution studies of structural changes in thin-film devices under a wide range of conditions, especially when structural and electronic phenomena are deeply enmeshed. ○

See: D.-H. Do¹, P.G. Evans¹, E.D. Isaacs^{2,†}, D.M. Kim¹, C.B. Eom¹, and E.M. Dufresne³, "Structural Visualization of Polarization Fatigue in Epitaxial Ferroelectric Oxide Devices," *Nat. Mater.* **3**, 365 (1 June 2004).

Author Affiliations: ¹University of Wisconsin, Madison; ²Bell Laboratories, Lucent Technologies, ³University of Michigan (†Present address: Argonne National Laboratory)

Correspondence: evans@engr.wisc.edu

This work was supported by the National Science Foundation through the University of Wisconsin Materials Research Science and Engineering Center (grants number DMR-0079983 and DMR-0313764 [C.B.E.]). E.D. acknowledges support from the U.S. Department of Energy (grants number DE-FG02-03ER46023 and DE-FG02-00ER15031) and from the NSF FOCUS Physics Frontier Centre. Use of the Advanced Photon Source was supported by the U.S. Department of Energy, Office of Science, Office of Basic Energy Sciences under Contract No. W-31-109-ENG-38).

AROUND THE EXPERIMENT HALL



Julie Cross (Argonne National Laboratory) in the PNC/XOR 20-ID-C research station, using a video microscope to center a 70 μm -diameter molybdenum wire on the rotational axis of a six-circle Huber Psi goniometer.

RESONANT X-RAY MAGNETIC SCATTERING IN NONMAGNETIC/MAGNETIC LAYERED SAMPLES

Probing the partially magnetic structures of compound materials or alloys can be difficult. Neutron scattering to tell one type of atom from another works only in well-ordered structures. Now, using the technique of resonant x-ray magnetic scattering (RXMS) at the XOR 4-ID beamline at the APS, researchers from the Nara Institute of Science and Technology, the Rigaku Corporation, and Argonne National Laboratory have employed the faster properties of an avalanche photodiode detector (APD), which can count x-rays at rates up to 10^7 photons s^{-1} , to detect and measure the weaker magnetism induced on nonmagnetic metals, even in the nearby presence of ferromagnetic atoms.

There are two ways to isolate RXMS from charge scattering: analyze the polarization of x-rays with a linearly polarized probing x-ray beam, or use circularly polarized x-rays of alternating helicities and calculate the difference of I^+ and I^- (respectively, the scattering intensities of the + and - helicities of the primary x-rays). For multilayered samples, the use of circularly polarized x-rays is preferable because the $\cos^2\theta$ polarization factor retains a large value at small scattering angles. Because of its ability to detect high count rates in reasonably short times, an avalanche photodiode detector is optimal for investigating the weaker magnetism induced in nonmagnetic metals.

The research team used this technique in an experimental setup based around an APD with a homemade 1-GHz bandwidth amplifier and an SR400 photon counter. The linearly polarized source hard x-rays are converted into circularly polarized beams using a rotary oscillating 0.45 mm-thick diamond crystal. To minimize instabilities, a quarter-wavelength phase plate is rotary oscillated to flip the helicity of the x-ray beam, and I^+ and I^- are synchronously measured (digital lock-in technique). Experiments using the SPring-8 light source at the Japan Synchrotron Radiation Research Institute demonstrated that this detector system could measure RXMS at superlattice Bragg peaks at various peak count rates in a multilayered sample near the K absorption edge of Co. With count-loss corrections in the peak profiles taking into account the electron bunch rates in the light source, the APD measures RXMS of 0.1% in flipping ratios at observed count rates up to low seven in I^+ and I^- .

The experimenters used this setup on the XOR 4-ID beamline to measure RXMS from “nonmagnetic” Cu layers in a Co/Cu multilayer on a silicon substrate. To maximize difference scattering intensity, the x-ray energy was tuned to 8991 eV (close to the K edge of Cu), and RXMS flipping ratios were observed at first-, second-, and third-order Bragg peaks. The research group could quantitatively measure RXMSs as small as 0.01% in flipping ratio at APD peak count rates of $\sim 3 \times 10^6$ cps.

The peak profiles obtained demonstrate nonuniform spin polarization in the out-of-plane direction in the 4p-state electrons of Cu between the Co layers of the sample, and are either positive or negative. However, at the Co K edge, the 4p states are all spin polarized in the negative direction, as would be expected since 4p states in the ferromagnetic Co layers should be polarized to the same extent throughout. With the Co/Cu multilayer sample placed in a strong in-plane external field, the exchange coupling was measured across the multilayers, providing a model polarization profile that

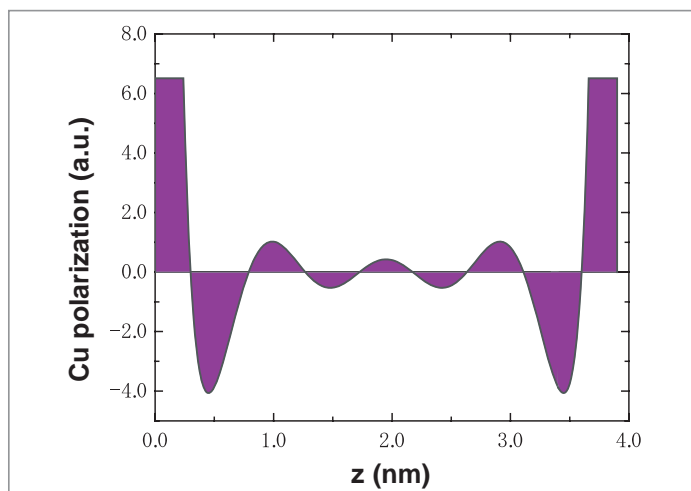


Fig. 1. Magnetic polarization profile induced in the 3.88-nm-thick Cu layers used to calculate RXMS patterns. A Cu layer is sandwiched between ferromagnetic Co layers with their interfaces located at $z = 0$ and 3.88 nm. Theoretical patterns assume this polarization profile for the 50 Cu layers in the sample.

shows an oscillatory behavior across the 3.9 nm-thick Cu layers that is consistent with RKKY (Rutherford-Kittel-Kasuya-Yosida) theory adapted to a planar geometry. Thus, this APD detector system enabled the study of the indirect exchange coupling and magnetic structures of “nonmagnetic” materials using RXMS and provided data in a relatively short time using synchrotron-generated circularly-polarized x-rays, even for nonmagnetic materials sandwiched between ferromagnetic layers in a sample. — Mark Wolverton

See: Y. Hayasaki¹, K. Ishiji¹, H. Hashizume¹, N. Hosoito¹, K. Omote², M. Kuribayashi², G. Srajer³, J.C. Lang³, and D. Haskel³, “Measurement of Resonant X-ray Magnetic Scattering from Induced Cu Polarizations in Exchange-coupled Co/Cu Multilayers,” *J. Phys. Condens. Matter* **16**, 1915 (2004).

Author Affiliations: ¹Nara Institute of Science and Technology, ²Rigaku Corporation, ³Argonne National Laboratory. Correspondence: hhashizu@ms.naist.jp

The experiment at SPring-8 was supported under proposals nos. 2002B0462 and 2003A0480; the one at APS under proposal no. GUP-100. This work supported by Collaborative Research Projects of the Materials and Structures Laboratory, Tokyo Institute of Technology. Use of the Advanced Photon Source was supported by the U.S. Department of Energy, Office of Science, Office of Basic Energy Sciences under Contract No. W-31-109-ENG-38.

COMPENSATING FOR STRESS FROM DOPANTS IN THE GROWTH OF ROOM-TEMPERATURE FERROMAGNETIC SEMICONDUCTORS

Spintronics—the science and application of electronics based on electron spin and charge—is a burgeoning field with vast potential applications. But the full realization of its potential depends on the development of semiconductors that are ferromagnetic at room temperature and also compatible with traditional silicon-based circuits. Such semiconductors have proven devilishly difficult to create, however, because doping at the high levels needed for room-temperature ferromagnetism induces too much epitaxial strain, which can lead to disorder and phase separation in the crystal lattices. How is it possible to achieve the high doping percentage required while preserving the semiconductor? A team of researchers from the University of North Carolina and Argonne National Laboratory, using beamlines MHATT/XOR 7-ID-C, XOR 2-BM, and XOR 2-ID-E has found a possible answer to this question. Employing two different elements as dopants, the experimenters were able to compensate for the epitaxial strain and suppress the phase separation effects manifested at higher doping levels.

The team grew crystals highly doped with Co and Mn in sequence with 2 Å intervals of Ge(001) by using combinatorial molecular beam epitaxy. The total concentration (x) of dopants was varied, while the relative concentration (a/b) between Co and Mn was maintained. The epitaxial growth process and the structural evolution and composition of the samples were studied by using real-time *in situ* scanning reflection high-energy electron diffraction (RHEED), x-ray diffraction (XRD), and x-ray fluorescence spectroscopy (XFS) from 2-BM, 2-ID-E, and 7-ID-C.

Above a doping concentration x , a roughening transition occurs, which is confirmed by RHEED and XRD and also by complementary scanning probe microscopy (SPM) and high-resolution transmission electron microscopy. Around this transition, as the atomically smooth two-

dimensional (2-D) RHEED intensity diminishes and peak width increases, rough three-dimensional (3-D) RHEED features begin to appear, turning completely 3-D at higher x values. As x increases further, growth becomes still more disordered. An epitaxial phase diagram derived from these measurements shows that this transition depends on the relative doping concentration. With $a/b \sim 3$ up to maximum doping of ~ 14 at. %, there is coherent 2-D epitaxial growth. Within this window, promising Ge magnetic semiconductors have been discovered with ferromagnetic transition temperature T_C near room temperature. As a/b deviates from ~ 3 , lattice strain increases and growth becomes unstable, with the films exhibiting lattice relaxation, surface roughening, and phase separation. The differing tetrahedral covalent radii of Mn and Co compared to Ge (Mn is larger, Co smaller) make it possible for Co and Mn to compensate for each other's strain effects. Specifically, the expansion caused by Mn doping can be offset by the compression resulting from Co doping.

Further studies show that the onset of the roughening transition also depends on the film thickness. The observed thickness dependence indicates that phase separation, along with strain, is a major factor in controlling the epitaxial growth. In other words,

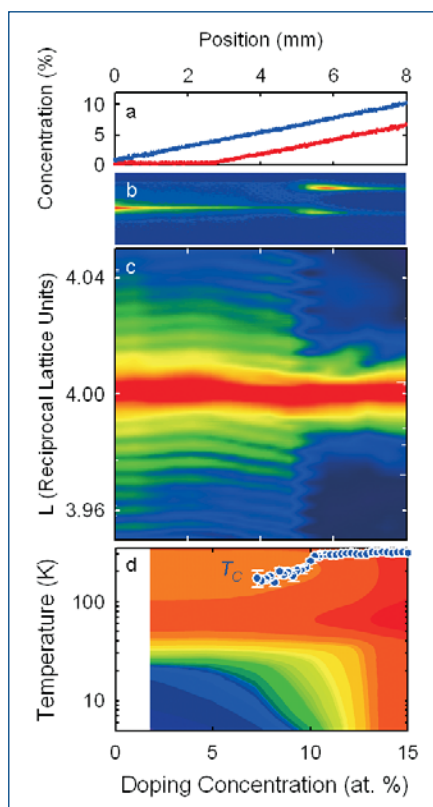


Fig. 1. The evolution of structure, magnetism, and electronic transport of highly doped Ge(001) epitaxial films using combinatorial approach. a. The composition profile versus position on the sample measured by XFS (blue for Co and red for Mn). b. Surface morphology measured by RHEED: the 0th order specular intensity in log scale versus q perpendicular to the surface (vertical) and composition. c. X-ray diffraction intensity in log scale versus reciprocal lattice vector L in the $[11L]$ direction of Ge (vertical) and composition. d. Conductivity in log scale and Curie temperature (points) versus temperature and composition. The structure exhibits a transition from smooth coherent epitaxy to rough/disordered growth at doping concentration ~ 10 at. % (b and c) that correlates with a semiconductor to metal transition (d) and an anomaly in Curie temperature. Within the ordered semiconducting regime, the correlation between the doping profile (a) and epitaxial strain as indicated by the fringes in (c) demonstrates the strain compensation effect due to the two dopants in Ge lattice.

when compared to systems with low solubility alone, the added lattice strain can lead to earlier onset of defective and inhomogeneous crystal growth as doping concentration increases.

The research team has shown that using complementary transition metal dopants, such as Mn and Co, can reduce internal stress and thus resist phase separation and stabilize epitaxial growth at the higher doping levels needed for the production of room-temperature ferromagnetic semiconductors. Because not all potential dopants possess the complementary characteristics to compensate for each other's individual strain profiles, it is possible to narrow the search for appropriate materials based on known structural and chemical characteristics. Moreover, the team's work demonstrates the practicality of engineering the semiconducting materials with tailored electronic and magnetic

properties, thus bringing the great promise of spintronics technology much closer to realization. — Mark Wolverton

See: F. Tsui¹, L. He¹, A. Tkachuk², S. Vogt², and Y.S. Chu², "Evidence for Strain Compensation in Stabilizing Epitaxial Growth of Highly Doped Germanium," *Phys. Rev. B* **69**, 081304 (2004).

Author Affiliations: ¹University of North Carolina, ²Argonne National Laboratory

Correspondence: ftsui@physics.unc.edu

The work supported in part by the U.S. National Science Foundation, Grant No. DMR-0108605. Use of the Advanced Photon Source was supported by the U.S. Department of Energy, Office of Science, Office of Basic Energy Sciences, under Contract No. W-31-109-ENG-38.

SHORT-RANGE ORDERED SUPERSTRUCTURES IN YBCO SUPERCONDUCTORS

There is mounting evidence that high- T_C cuprates are inhomogeneous even in the superconducting phase. Although the driving force for these inhomogeneities might well be electronic instabilities, lattice strain, or a combination of both, a consensus on the nature of these inhomogeneities and their role in the overall phase diagram remains elusive. In the case of yttrium-barium cuprates ($\text{YBa}_2\text{Cu}_3\text{O}_{6+x}$, or YBCO), x-ray diffuse scattering studies carried out at the XOR 4-ID beamline at the APS by researchers from Argonne National Laboratory; the University of California, San Diego; the University of Houston; and the Max-Planck-Institut für Metallforschung revealed superstructures characterized by a wave-vector of the form $q_0=(q_x, 0, 0)$ throughout the superconducting region of its electronic phase diagram.

The magnitude of the modulation vector (q_0) decreases with increasing oxygen concentrations (or "hole" doping) from 1/2 (2-unit-cell) in the heavily underdoped compound to 1/5 in the overdoped material. At optimal doping a 4-unit-cell superstructure was observed (Fig. 1).

These superstructures correspond to short-range ordered regions of correlated displacements, as indicated by the *intensity asymmetry* between the two satellite peaks on either side of a Bragg point (Fig. 1). Furthermore, measurements of the intensity of a given satellite along a direction corresponding to the normal to the CuO_2 planes (i.e., c^* -axis) indicated that atomic displacements on only three neighboring CuO , BaO , and CuO_2 planes are mutually coupled. A model displacement pattern (Fig. 2) has been deduced by fitting integrated intensities (Fig. 1). The model portrays a pattern remarkably similar to that obtained via first-principles atomic-relaxation calculations in the presence of oxygen-vacancy ordering, a study carried out by D. de Fontaine and coworkers (University of California, Berkeley). Thus, the 4-unit-cell lattice modulation at optimal doping is consistent with the presence of an oxygen-ordered ("Ortho-IV") phase, or "nanodomains."

These nanodomains induce a long-range strain in the host, creating an intrinsically inhomogeneous lattice. The strain

Continued on next page

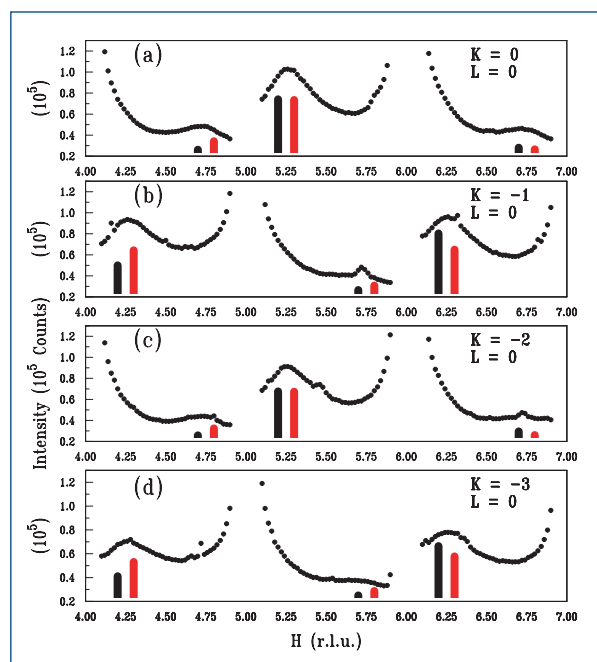


Fig. 1. (a)-(d) H-scans for different values of K and $L=0$ ($7K$). Black and red vertical lines are experimental and calculated intensities.

manifests below $\sim 200\text{K}$ as Huang diffuse scattering (HDS) around the Bragg points (Fig. 3) in both *twinned* (left) and *de-twinned* (middle) crystals. HDS has a distinct symmetry compared to the expected thermal diffuse scattering (TDS) pattern (Fig. 3, right). Intensity along a line near the Bragg point clearly reveals a pair of lobes, as opposed to the central peak expected from TDS. Thus, HDS is independent of stress detwinning of the crystal and is intrinsic to YBCO. Note the satellite peaks on either side of the Bragg point.

T-dependent measurements of superlattice peaks revealed that the intensity at $\sim 300\text{K}$ is more than two-fold smaller than that at $\sim 7\text{K}$, which cannot be explained simply in terms of a Debye-Waller-factor effect from the average lattice. It seems that these "nanodomains" are elastically softer than the host, which can be important in influencing electronic properties in these cuprates.

In summary, YBCO compounds are intrinsically inhomogeneous because of the formation of O-vacancy ordering. Thus, the treatment of superconductivity in these cuprates in terms of a single homogeneous phase seems unrealistic. — *Z. Islam*

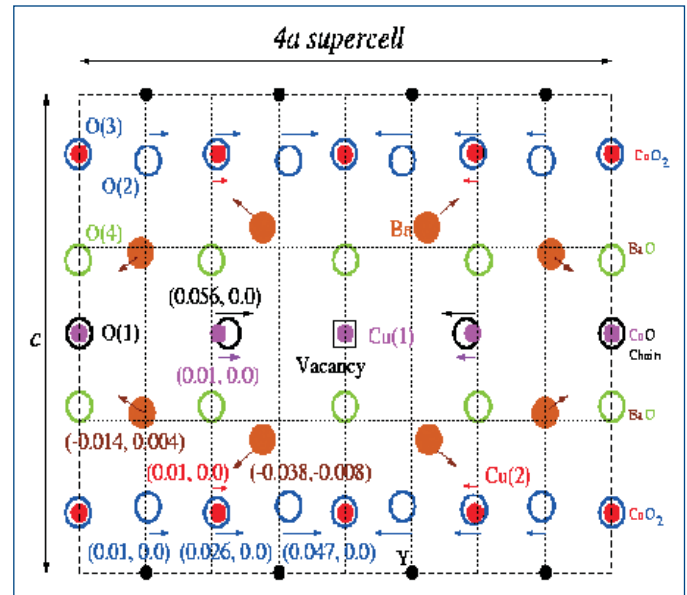


Fig. 2. An ideal atomic displacement pattern in optimally doped YBCO, projected on the ac plane (7K).

See: Z. Islam¹, X. Liu², S.K. Sinha², J.C. Lang¹, S.C. Moss³, D. Haskel¹, G. Srajer¹, P. Wochner⁴, D.R. Lee¹, D.R. Haefner¹, and U. Welp¹, "Four-Unit-Cell Super-structure in the Optimally Doped $\text{YBa}_2\text{Cu}_3\text{O}_{6.92}$ Superconductor," *Phys. Rev. Lett.* **93**, 157008 (2004).

Author Affiliations: ¹Argonne National Laboratory, ²University of California, San Diego, ³University of Houston, ⁴Max-Planck-Institut für Metallforschung
Correspondence: zahir@aps.anl.gov

S.C.M. thanks the NSF for support on DMR-0099573. Use of the Advanced Photon Source was supported by the U.S. Department of Energy, Office of Science, Office of Basic Energy Sciences, under Contract No. W-31-109-ENG-38.

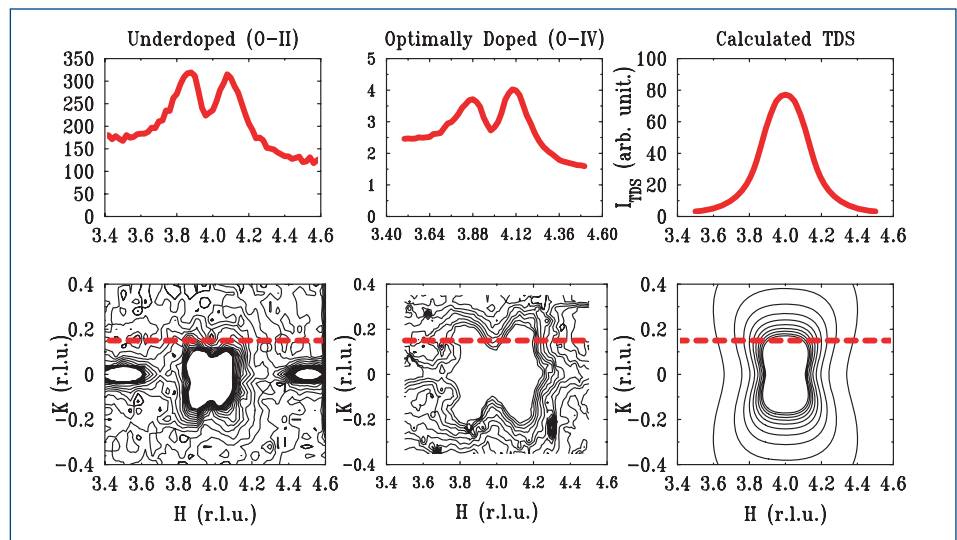


Fig. 3. Bottom: Contour plots of HDS and calculated TDS around $(4,0,0)$ Bragg point. Top: Intensity profile along the red-dashed line (see bottom panels) in reciprocal space.



ULTRATHIN CO FILMS ON GE SHOW ENHANCED ORBITAL MAGNETIC MOMENTS

The next major revolution in microelectronics may come from the ability to manipulate flows of electrons by using both their spin-related magnetic moments and their electrical charge. Much needs to be learned, however, before the potential of spin-based electronics (spintronics) can be fully exploited. One outstanding issue concerns interface formation between semiconductors and ferromagnetic metals, where interfacial roughness and intermixing and mismatch-induced strain tend to disrupt the passage of spin-aligned currents. Researchers using the XOR 4-ID beamline at the APS have gained new insights into several characteristics of one important ferromagnetic semiconductor.

The Co/Ge ferromagnetic/semiconductor system is of interest because hcp (hexagonal close packing) cobalt has the largest magnetocrystalline anisotropic energy (MAE) of the ferromagnetic transition metals, and because germanium can readily interface with silicon, the material from which most semiconductor devices are made. The MAE is a measure of the tendency of ferromagnetic magnetic moments to assume specific orientations. This orientation-related energy is mediated by the orbital magnetization through the spin-orbit interaction, which links the spin to the atomic structure of the ferromagnet.

Researchers from the Argonne and Los Alamos national laboratories and from the University of Arizona studied the growth, electronic structures, and magnetic characteristics of Co/Ge boundary layers in experiments performed at the APS. Their on-line analysis chamber was equipped with *in situ* growth and surface preparation capabilities, which were used to grow ultrathin Co films on a Ge(100) substrate (sample 1). The cobalt was deposited by means of e-beam evaporation,

while the substrate was maintained at a low temperature (~170K) to minimize intermixing and avoid alloy formation. Photoemission spectroscopy and low-energy electron diffraction were used to characterize the quality of the prepared surfaces. A Co wedge (sample 2) was grown separately to gain easier access to a wider thickness range and to study temperature dependence. The 0-Å to 50-Å Co wedge was grown at room temperature on a substrate taken from the same wafer as the *in situ* sample and capped with a 30-Å Au protective layer.

A circularly polarizing undulator provided an intense flux of >96% circularly polarized photons, while an electromagnet supplied a controllable field for x-ray magnetic circular dichroism (XMCD) measurements. XMCD was measured by means of the total electron yield with samples in remnant magnetic states (Fig. 1); sum rule analysis of the XMCD data yielded the ratios of the orbital and spin magnetic moments of the Co films. To measure the orbital and spin moments independently, the researchers determined the electron occupancies of Co 3*d* states by integrating the x-ray absorption spectra for the thin Co films. These measurements yielded an occupancy measurement once a thick Co film was referenced to an averaged figure for bulk Co (taken from previously published theoretical studies).

Photoemission data indicated the formation of a <4.8-Å Co/Ge mixed interfacial region for the *in situ*-grown sample. Rocking curves of the Co wedge system provided evidence of a similar but larger (~7.5-Å) intermixed region. The thicknesses of nonmagnetic Co were estimated at 2.1 Å and 4 Å for the *in situ* and the wedge samples, respectively. Coercivity measurements along the wedge showed a dramatic change due to a bcc (body-centered cubic)-to-hcp phase transition. The growth of Co beyond the magnetically inactive Co/Ge intermixed region was uniform for both samples, with the wedge showing a typical perpendicular roughness of ~2 Å.

XMCD indicated an enhanced orbit-to-spin moment ratio for the narrow region of Co growth above the Co/Ge interfacial region for the *in situ*-grown sample, where a loss of perpendicular symmetry enhanced the orbital moment. The Co wedge showed a constant but larger orbit-spin ratio, possibly due to the presence of the Au overlayer (see Fig. 1 inset). The total moment per atom was measured at 1.53 μ_B (at 36 Å), which compared well with published data. *Continued on next page*

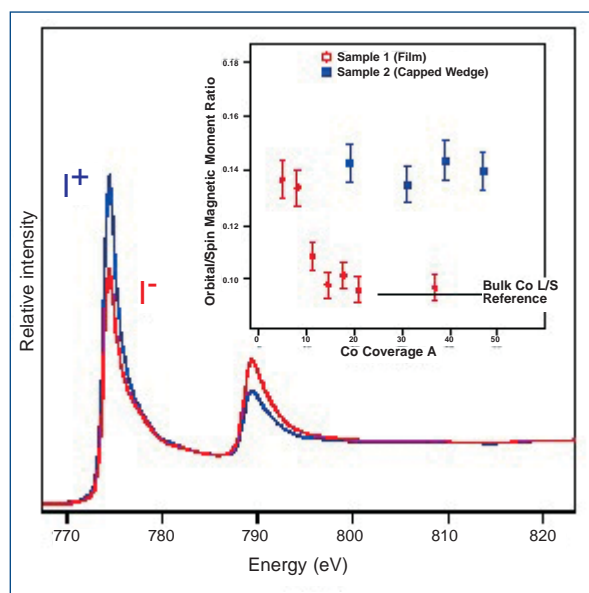


Fig. 1. Absorption spectra for both antiparallel spin directions, with the difference being the dichroic signal. Inset: Orbital-to-spin magnetic moment ratios as a function of Co coverage calculated from a sum rule analysis of the XMCD data for both samples.

The data demonstrate, among other things, that low deposition temperatures are not sufficient to avoid interfacial intermixing with this ferromagnetic/semiconductor system. — *Vic Comello*

See: P. Ryan¹, R.P. Winarski¹, D.J. Keavney¹, J.W. Freeland¹, R.A. Rosenberg¹, S. Park², C.M. Falco³, “Enhanced Magnetic Orbital Moment of Ultrathin Co Films on Ge(100),” *Phys. Rev. B* **69**, 054416 (2004).

Author Affiliations: ¹Argonne National Laboratory, ²Los Alamos National Laboratory, ³University of Arizona
Correspondence: pryan@aps.anl.gov

Work at the University of Arizona was supported by the U.S. Department of Energy under Grant No. DE-FG03-93ER45488. Use of the Advanced Photon Source was supported by the U.S. Department of Energy, Office of Science, Office of Basic Energy Sciences under Contract No. W-31-109-ENG-38.

TOWARD SUPERCONDUCTING WIRES

In the energy industry, as much as 10% of all the power converted and transmitted is lost because of electrical resistance in wires and components. The development of high-critical-temperature superconducting wire could revolutionize the industry by cutting these losses to near zero, allowing electricity to be carried without resistance. Now, researchers from the Illinois Institute of Technology and the Argonne, Los Alamos, and Oak Ridge national laboratories are using the MR-CAT 10-ID beamline at the APS to gather new clues about the chemistry of candidate superconductor materials, such as ceramic oxide compounds composed of yttrium (a rare earth element), barium, and copper. This particular class of superconducting oxides exhibits promising properties, including a critical temperature above the boiling temperature of liquid nitrogen, excellent current transport characteristics, and good performance in strong magnetic fields—such as those that occur in motors and transformers.

Numerous research groups around the world have focused on growing epitaxial films of $\text{M}\text{Ba}_2\text{Cu}_3\text{O}_{7-x}$ (known as the M-123 phase), in which M is either the metal yttrium or another rare earth element, such as erbium or neodymium. Such films become superconducting at around -183°C . But more information is needed about how to control the growth of these ceramic films if they are to be made into viable zero-resistance wires for use in electrical conversion and transmission equipment.

One approach to making superconducting wire involves coating a textured metal substrate with M-123 to produce an epitaxial film. Such coated conductors are seen as the way forward for high-current and high-voltage applications because they should cost about the same as copper wires and be commercially viable even when the required cooling is taken into account.

Current synthetic schemes for making these coated conductors require the deposition of a film of M-123 onto a textured substrate in such a way that the texture of the substrate is adopted by the film. In order to make this happen, several buffer layers are applied to the substrate first to prevent substrate atoms from diffusing into the film. Each step of the substrate fabrication and film synthesis process requires meticulous attention to detail.

The researchers are exploiting the combined techniques of Raman spectroscopy and synchrotron-based x-ray diffraction to help them understand how the multilayered superstructure needed to form such coated conductors evolves during processing.

Raman spectroscopy data are providing information about phase purity, crystal morphology, and overall texture development, leading to identification of the best specimens for detailed x-ray diffraction analysis at MR-CAT. The spatially resolved diffraction measurements (Fig. 1) have allowed the researchers to discern how well the M-123 film texture mimics the underlying substrate, as well

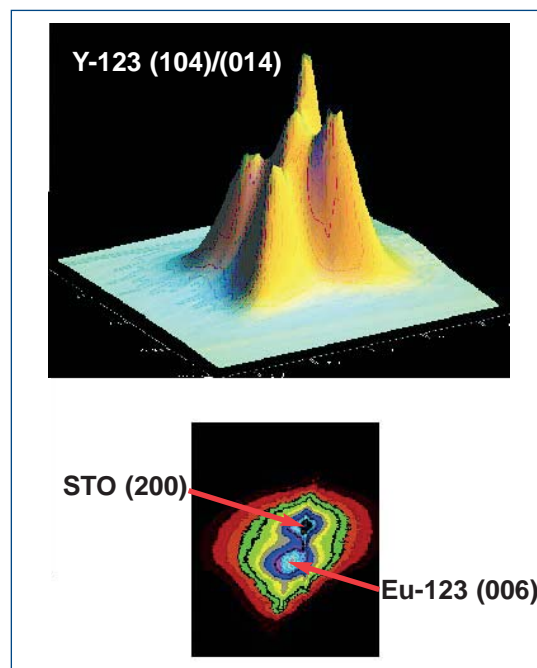


Fig. 1. The features revealed by this high-resolution diffraction space mapping have shed new light on the consequences of structural changes in the M-123 films, which will help researchers choose appropriate procedures for depositing the buffer layer and the M-123 film itself. This, in turn, will allow them to fabricate high-performance coated conductors more effectively and bodes well for rapid progress in electric power technology programs worldwide.

as to observe the influence of the buffer layer on the quality of the M-123 films.

An important aspect of this research is that the diffraction space mapping measurements were performed at high resolution with a robust signal-to-noise ratio, which allowed the researchers to examine in detail the features that reveal structural effects in the films. Such studies would not have been possible without the brilliance and concomitant energy resolution afforded by the APS.

The lower image in Fig. 1 shows the diffraction space map in the vicinity of the Eu-123 (006) reflection which occurs in close proximity to the (200) reflection of the strontium titanate (STO) substrate. From the precisely measured two-theta and omega values we can determine the degree of strain in the Eu-123 layer near the interface with the STO surface. The upper image in Fig. 1 is the diffraction space map in the vicinity of the (104)/(014) reflections of twinned Y-123 on STO. The map evidences the proper development of the twin structure required for optimum superconducting properties. A detailed explanation of the results in Fig. 1 is presented in the appended reference.

The features revealed by this high-resolution diffraction space mapping have shed new light on the consequences of structural changes in the M-123 films. Such information will

help researchers make high-performance coated conductors, which bodes well for rapid progress in electric power technology programs worldwide. The implementation of M-123-based superconducting generators, transformers, and transmission lines might be possible in the coming decade. — *David Bradley*

See: K. Venkataraman¹, A.J. Kropf¹, C.U. Segre², Q.X. Jia³, A. Goyal⁴, B.W. Kang⁴, S. Chattopadhyay¹, H. You¹, and V.A. Maroni¹, "Detection of Interfacial Strain and Phase Separation in $\text{M}\text{Ba}_2\text{Cu}_3\text{O}_{7-x}$ Thin Films Using Raman Spectroscopy and X-ray Diffraction Space Mapping," *Physica C* **402**, 1 (2004).

Author Affiliations: ¹Argonne National Laboratory, ²Illinois Institute of Technology, Chicago, ³Los Alamos National Laboratory, ⁴Oak Ridge National Laboratory

Correspondence: maroni@cmt.anl.gov

This research was sponsored by the U.S. Department of Energy (DOE), Energy Efficiency and Renewable Energy, as part of the DOE program to develop electric power technology. Work performed at MR-CAT is supported, in part, by funding from the DOE under grant number DEFG0200ER45811. Use of the Advanced Photon Source is supported by the U.S. Department of Energy, Office of Science, Office of Basic Energy Sciences under Contract No. W-31-109-ENG-38.

DISLOCATION FORMATION IN NICKEL SINGLE-CRYSTAL ALLOY WELDS

Single-crystal nickel-based superalloys are used in advanced aircraft and land-based turbine engines because the materials offer excellent high-temperature properties. The high cost of the material encourages users to repair (rather than replace) damaged or worn parts and to refurbish as-cast parts that contain defects. Both repairing and refurbishing require welding of nickel-based single crystals, which can result in major problems, such as dislocation structure changes. Researchers from Oak Ridge National Laboratory, using the UNI-CAT 34-ID beamline at the APS, analyzed structural changes arising from welding operations, including how dislocations form in the area outside the weld, where the temperature does not reach the melting point.

The researchers quickly heated a nickel-based, single-crystal superalloy to the melting temperature, then studied the heat-affected zone (HAZ) using polychromatic microbeam synchrotron diffraction from the UNI-CAT beamline, as well as electron and optical microscopy. In particular, the researchers looked at the changes in the gamma prime particles in this zone.

Nickel-based, single-crystal turbine engine components consist primarily of a two-phase microstructure: a face-centered cubic gamma solid-solution matrix phase and a uniform distribution of ordered gamma prime precipitates. Advanced single-crystal superalloys typically contain 50 to 70 volume percent gamma prime. In order to maintain the high-temperature mechanical properties, both the fusion zone of the weld and the HAZ must retain the single-crystal nature of the microstructure and the high-volume fraction of gamma prime precipitates.

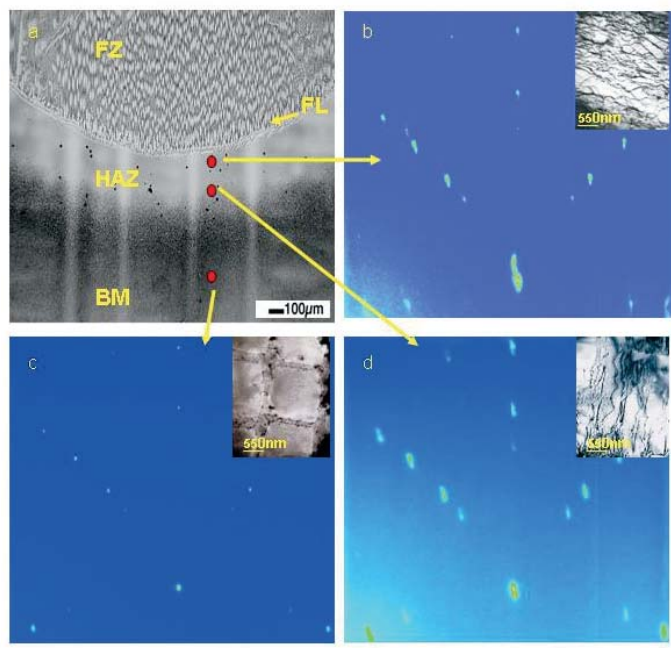
The group found that, during welding, the material near the fusion line is heated so much that the gamma prime particles

dissolve entirely or partially. As the area cools, they precipitate again. Near the fusion line, the process is particularly intense, and after cooling, the gamma prime phase particles that form are only about 10–20 nm across—about an order of magnitude smaller than before.

The heating and cooling also cause thermal expansion and contraction of the material, resulting in a strong plastic deformation of both the HAZ and the entire weld. This cycle produces dislocations, the arrangement of which depends on both the thermal gradient field and the dissolution and reprecipitation of gamma prime particles. The highest density of dislocations is located at the edge of the fusion line, where the temperature gradient and its rate of change are highest. The dislocations are concentrated in the gamma matrix of the single-crystal superalloy. Furthermore, the researchers pinned down the major type of dislocations to dislocation slip systems that form Z-shaped lines.

Continued on next page

Fig. 1. Microstructure of a single-crystal alloy weld (a) including the fusion zone (FZ), fusion line (FL), heat-affected area (HAZ), and bulk material (BM). Laue patterns from different locations (b-d) collected on the 34-ID beamline of the APS with inset transmission electron microscopy images.



The experiments to support these conclusions involved examination of heated samples of the alloy. The microstructures of the materials were examined by using transmission electron microscopy, optical microscopy, and both conventional Laue diffraction and Laue diffraction using high-energy polychromatic x-rays from the 34-ID beamline of the APS (Fig. 1). Analyzing the Laue streaks allowed the researchers to determine the density of unpaired dislocations and dominating slip systems.

The experiments provided much more localized information. The x-ray synchrotron measurements provided three-dimensional maps of the crystalline phase, orientation, and plastic deformation with 1- μm spatial resolution. Dimensions of the beam were $0.5 \times 0.5 \mu\text{m}$ with a penetration depth of about 30 μm . — *Yvonne Carts-Powell*

See: O.M. Barabash, J.A. Horton, S.S. Babu, J.M. Vitek, S.A. David, J.W. Park, G.E. Ice, and R.I. Barabash, "Evolution of Dislocation Structure in the Heat Affected Zone of a Nickel-Based Single Crystal," *J. Appl. Phys.* **96**(7), 3673 (1 October 2004).

Author Affiliation: Oak Ridge National Laboratory

Correspondence: barabashom@ornl.gov

The research was sponsored by the Division of Materials Sciences and Engineering, Office of Basic Energy Sciences, U.S. Department of Energy under Contract DE-AC05-00OR22725 with UT-Battelle, LLC. Use of the Advanced Photon Source was supported by the U.S. Department of Energy, Office of Science, Office of Basic Energy Sciences, under Contract No. W-31-109-ENG-38.

HOW OXIDE STRUCTURES ON ZIRCONIUM ALLOYS INFLUENCE CORROSION RESISTANCE

The fuel utilization of light-water nuclear reactors depends greatly on the corrosion resistance of the zirconium (Zr)-based alloys used as fuel cladding and structural components. To provide insight into the relationship between the structures of the oxide layers formed on Zr-based alloys and their resulting corrosion behavior, scientists from Pennsylvania State University, Westinghouse Electric Co., and Argonne National Laboratory used the XOR 2-ID beamline at the APS for a detailed study of oxides formed in 360°C water on four Zr-based alloys.

Past efforts to increase corrosion resistance of Zr-based alloys have relied primarily on empirical development, which has resulted in practical thermo-mechanical processing schemes for achieving improved corrosion responses. This empirical approach has about run its course, suggesting that further significant improvement in corrosion resistance requires a mechanistic model of the corrosion process. Efforts to develop a model of this complex process have been hampered by the resolution limitations inherent in the experimental techniques that have been employed.

The high brilliance of x-ray beams from the APS allowed data acquisition with a lateral resolution that had heretofore been unobtainable. Microbeam x-ray diffraction was used, along with transmitted light optical microscopy, to obtain

information on these oxide structures as a function of distance from the oxide/metal interface. For this study, the alloys were selected on the basis of their wide variation in corrosion rates. This work resulted in the first spatially resolved sub-micron observations of the oxide structures formed on Zr alloys while the oxides were still attached to the base metal.

The experiments performed at beamline 2-ID utilized the x-ray microprobe, which produces a monochromatic $0.2\text{-}\mu\text{m} \times 0.3 \mu\text{m}$ x-ray beam with a flux of 5×10^9 photons/s and an energy bandwidth of 0.01%. The distance between the oxide/metal interface and the oxide/water interface measured by using this method agreed with optical determinations of oxide thickness to within 0.5 μm .

Optical microscopy revealed a layered oxide structure in which the average layer thickness was inversely proportional to the accelerated (post-transition) corrosion rate. The detailed diffraction studies showed that the oxide contained both tetragonal and monoclinic ZrO_2 , with a higher fraction of tetragonal oxide near the oxide/metal interface. Evidence of a cyclic variation of the tetragonal and monoclinic oxides across the oxide thickness was also observed, with a period of the layer thickness. The regularity of the layered structures indicates that the corrosion process remained the same from the beginning to the end of the corrosion test.

The detailed spatial resolution of the experiment is demonstrated by Fig. 1, which shows diffracted intensity versus the diffraction angle as the beam is scanned from the metal, across the oxide/metal interface, and through the oxide to the oxide/water interface. The peaks are associated with particular crystallographic planes in the various phases present in the metal and oxide, providing information about the phases present and their crystal orientation at various locations in the oxide layer.

Diffraction peaks associated with the hexagonal close-packed Zr phase (subscript Zr) may be observed in the left part of the figure (in the metal). Closer to the oxide/metal interface are hydride peaks (subscript hydr) resulting from the ingress into the metal of hydrogen released in the corrosion reaction, and which forms hydrides ahead of the advancing oxide/metal interface. The red arrows indicate a Zr_3O sub-oxide phase that also forms ahead of the advancing oxide. Just inside the oxide, the peaks of the majority oxide phase (monoclinic ZrO_2 , subscript m) become dominant, but a strong tetragonal peak is also seen (101_t). It is apparent from the figure that the monoclinic and tetragonal peaks are both periodic in the oxide layer. In fact, their periodicity is exactly out of phase (when one is high, the other one is low), indicating a process in which the advancing oxide front forms alternatively tetragonal or monoclinic oxide as it reacts with the metal.

The peak shown with an asterisk at the oxide/metal interface is visible only in the first 0.2-0.3 μm near the oxide/metal interface. This peak is an indication that at the oxide/metal inter-

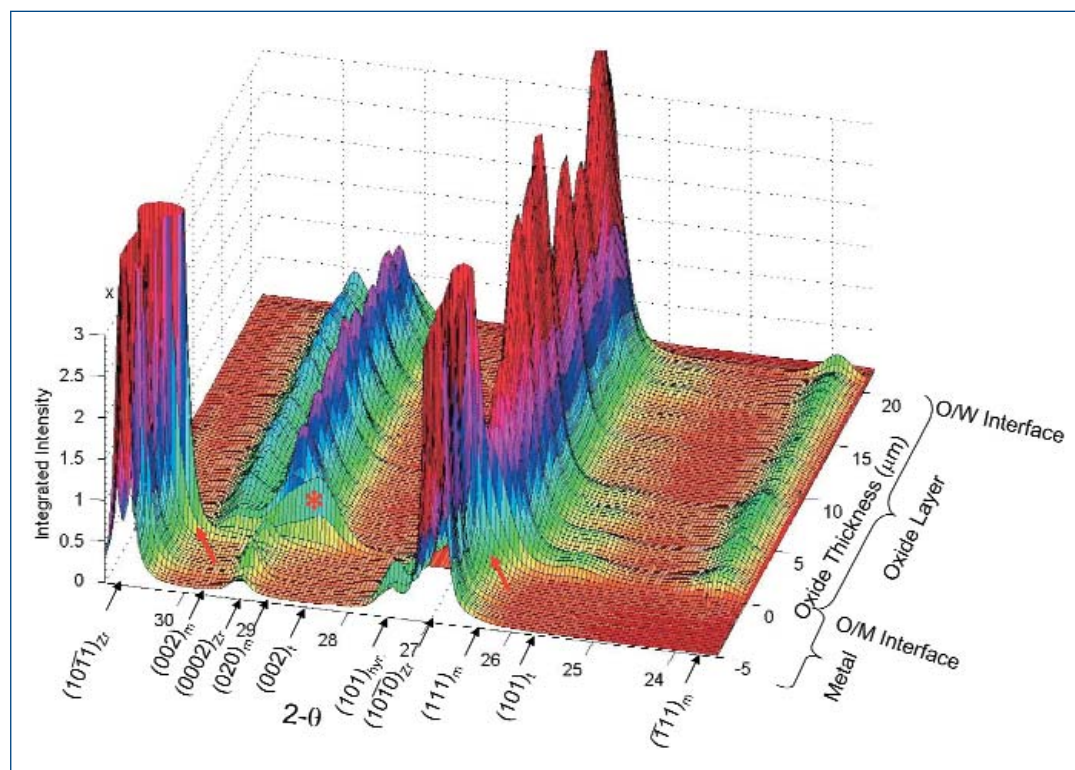


Fig. 1. X-ray diffracted intensity versus diffraction angle, from the oxide/metal interface to the oxide/water interface of a ZIRLO oxide layer formed in a 360°C pure-water environment. The subscripts "m" and "t" stand for monoclinic and tetragonal oxide peaks, "hydr" for hydride peaks, and "Zr" for zirconium metal peaks.

face, a highly oriented tetragonal phase is formed, which serves as a precursor of the monoclinic phase seen in the bulk of the oxide. Such detailed information about near-interface oxide structure would not have been obtainable by using bulk diffraction methods. The information obtained in the experiment allowed the researchers to propose a model for the advancement of the oxide layer that will be useful in comparing the oxides formed in different alloys. — *Vic Comello*

See: A. Yilmazbayhan¹, A.T. Motta¹, R.J. Comstock², G.P. Sabol³, B. Lai⁴, Z. Cai⁴, "Structure of Zirconium Alloy Oxides Formed in Pure Water Studied with Synchrotron Radiation and Optical Microscopy: Relation to Corrosion Rate," *J. Nucl. Mat.* **324**, 6 (2004).

Author Affiliations: ¹The Pennsylvania State University, ²Westinghouse Electric Co., ³Consultant to Westinghouse Electric Co., ⁴Argonne National Laboratory
Correspondence: atm2@psu.edu

This research was sponsored by the U.S. Department of Energy, Nuclear Engineering Research Initiative (DOE-NERI) program, under grant number DE-FC03-99SF21918, and International Nuclear Energy Research Initiative (DOE I-NERI) grant no. DE-FG07-03RL14530. Use of the Advanced Photon Source was supported by the U.S. Department of Energy, Office of Science, Office of Basic Energy Sciences under Contract No. W-31-109-ENG-38.

HIGH-RESOLUTION, 3-D MEASUREMENTS IN DEFORMED POLYCRYSTALLINE ALUMINUM

Materials such as diamond are exceedingly hard in single-crystal form; but soft metals, such as aluminum and alloys, obtain the strength needed for industrial and technological applications through a three-dimensional (3-D) mosaic of tiny crystals with varying orientations that form grain boundaries where they meet. Although the resistance of grain boundaries and junctions to deformation is known to be the source of their increased strength, the details of the process are highly complex and it is still not possible to predict theoretically how to make stronger, lighter, cheaper alloys without expensive trial-and-error materials development. Researchers from Oak Ridge National Laboratory and the Alcoa Technical Center have employed the recently developed technique of differential-aperture x-ray microscopy (DAXM) on the UNI-CAT 34-ID and MHATT/XOR 7-ID beamlines at the APS to study the effect of grain boundaries on the crystal microstructure generated during the deformation of a ductile metal, aluminum.

Using the DAXM technique, .5- μm -diameter polychromatic x-ray micro-beams were used to study crystal deformation near a grain boundary in compressed aluminum. In order to study the underlying science of deformation at grain boundaries using the DAXM technique, the research group exploited the fact that polychromatic x-rays generate full Laue diffraction patterns from each position along the microbeam. Obtaining full x-ray diffraction patterns from each position along the microbeam means, in turn, that it is possible to determine the precise crystal orientation for each point along the microbeam. Hence, it is possible to determine crystal orientation changes with micron resolution from all points along the x-ray beam, as described in detail previously [1] and discussed in a recent review [2].

Figure 1 is a composite showing a vertically strained three-grain aluminum sample and indicating the position along the grain boundary between grain A and grain B at which DAXM measurements of the crystal rotations (i.e., deformation) were performed. The figure also shows a color-coded, 3-D mapping of the crystal rotations near the (16°) grain boundary. These rotation results for four positions parallel to the grain-boundary demonstrate the ability to measure deformation microstructure, non-destructively, in 3-D with micron spatial resolution using DAXM. When compared to $2\text{--}5^\circ$ rotations found away ($\sim 1\text{ mm}$) from the grain boundary, the $5\text{--}8^\circ$ rotations found in grain A near the A-B grain boundary represent pile up of deformation at grain boundaries; moreover, the observation of larger lattice rotations in the grain A side of the boundary compared to the grain B side of the boundary demonstrates the impact of grain orientation. Such measurements are of qualitative interest by themselves, but they will be of quantitative importance, when compared to computer simulations and multi-scale modeling, in developing an overall predictive understanding of materials properties.

This research focused on revealing the detailed structure of a polycrystalline aluminum sample subjected to plastic deformation. However, the underlying technology of DAXM, when combined with highly intense x-ray sources such as the APS, holds bright promise for the high-resolution, 3-D examination of a large range of diverse materials, including metallic alloys, advanced composites, and functionally graded materials.

— B.C. Larson

REFERENCES

- [1] B.C. Larson et al., *Nature* **415**, 887 (2002).
- [2] B.C. Larson and B. Lengeler, *MRS Bulletin* **29**, 152 (2004).

See: B.C. Larson¹, W. Yang¹, J.Z. Tischler¹, G.E. Ice¹, J.D. Budai¹, W. Liu¹, and H. Weiland², "Micron-Resolution 3-D Measurement of Local Orientations Near a Grain-Boundary in Plane-Strained Aluminum Using X-ray Microbeams," *Int. J. Plasti.* **20**, 543 (2004).

Author Affiliations: ¹Oak Ridge National Laboratory, ²Alcoa Technical Center

Correspondence: bcl@ornl.gov

Use of the Advanced Photon Source was supported by the U.S. Department of Energy, Office of Science, Office of Basic Energy Sciences, under Contract No. W-31-109-ENG-38.

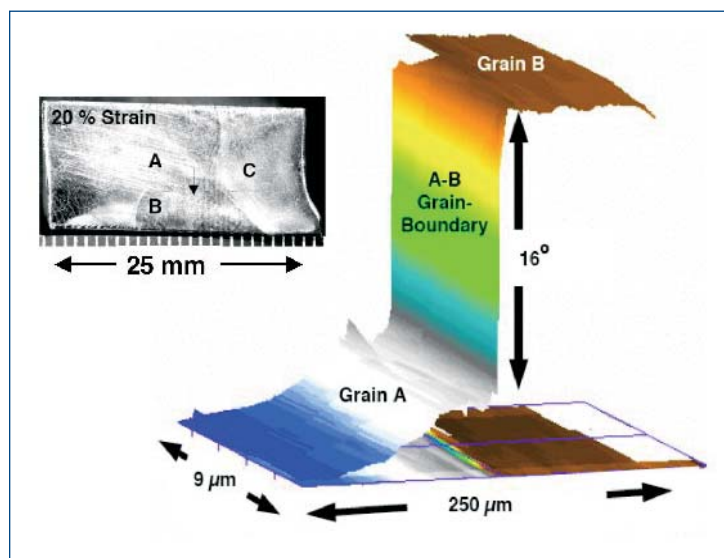


Fig. 1. Aluminum tri-crystal after 20% vertical compression showing grains A, B, and C and an arrow denoting the position of DAXM orientation measurements at the A-B grain-boundary; the color coded 3D orientation mapping shows the magnitude of lattice rotations increasing in grain-A within $\sim 50\text{ }\mu\text{m}$ of the 16° A-B grain-boundary and it indicates smaller changes within grain-B.

IMAGING PLASMONS IN WATER AT 41.3-ATTOSECOND RESOLUTION

A host of modern techniques employ x-ray beams to decipher the microscopic structure of materials. But many researchers also want to understand how processes within materials change dynamically (that is, over time). Toward that end, researchers from Cornell University used synchrotron x-rays to dynamically image a disturbance in the electrons of water molecules on extremely small scales of time and space. The Cornell team completed their project at the CMC-CAT beamline 9-ID of the APS after extensive preliminary research at the Cornell High Energy Synchrotron Source (CHESS).

The distribution of electrons in various materials can be determined by measuring how a beam of radiation aimed at a sample is absorbed and/or scattered. In the research discussed here, electron distributions within a sample of water were examined by using inelastic x-ray scattering (IXS). "Inelastic" means that the x-ray photons lost energy as they interacted with the atoms of water. As a result of that interaction, lower-energy x-rays emanated from the sample in a variety of directions (hence the term "x-ray scattering"). The energies and frequencies of the scattered x-ray photons were then measured using a device the researchers designed and constructed themselves.

The experimental setup consisted of a tiny volume of water in a small glass tube. The APS provided synchrotron x-rays with very uniform energies and momenta. When the synchrotron x-rays impinged on the water, they interacted with the valence electrons of the water's oxygen atoms, creating a plasmon. A plasmon is a collective oscillation of free electrons within a material. The researchers measured the energy of the resulting scattered photons, as well as the angles at which they were scattered. One key piece of information, however, could not be measured: the phase of the electric

field of the scattered x-rays. This uncertainty is commonly termed the "phase problem," and it appears not only in IXS measurements, but in other x-ray techniques as well. The team solved the phase problem by deriving new mathematical formulas to obtain meaningful results from x-ray measurements, and then used those formulas to, in effect, reconstruct the missing x-ray phases. That phase reconstruction was essential for calculating the electron dynamics in the water sample.

Using the data collected over a two-day period at the APS, the researchers were able to calculate the state of the plasmon over extremely short spans of time and space. Specifically, the electron dynamics were resolved to a time of 41.3 attoseconds (1 attosecond = 10^{-18} seconds), with a spatial dimension of 1.27 Å (1 Å = 10^{-8} centimeters).

The mathematical techniques described in the paper were strictly applicable only to point sources (i.e., a stationary point charge, such as a single electron). However, the researchers modified those techniques in order to model the effects on electron density caused by "extended" sources. Two hypothetical cases were considered. The first case

Continued on next page

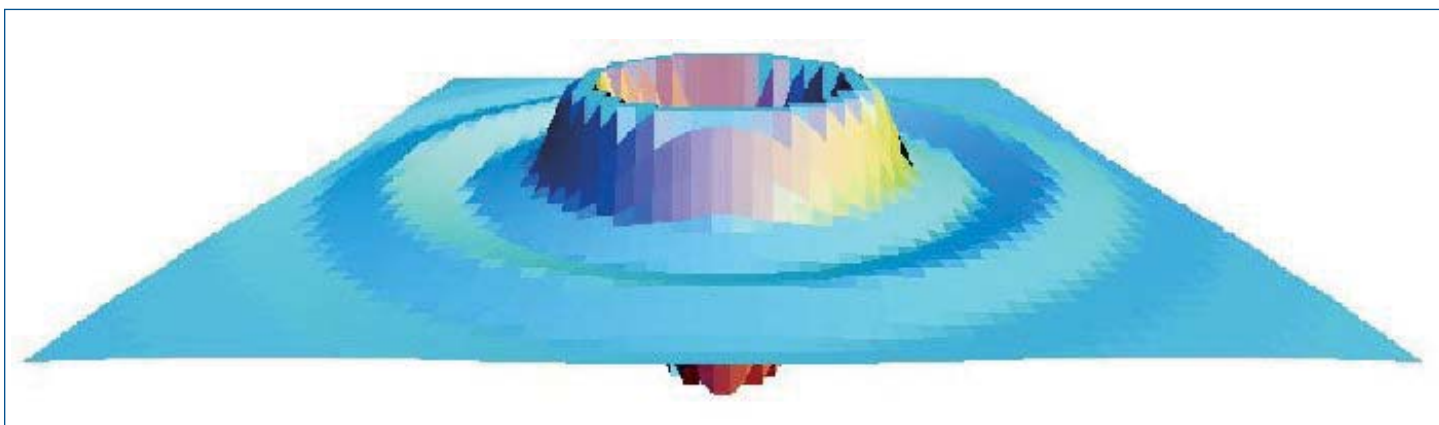


Fig. 1. Image depicting the disturbance to the distribution of outer (valence) electrons in a microscopic sample of water. The "dips" (or valleys) shown in the figure indicate regions of net negative charge (surplus electrons), while the peaks indicate a region of net positive charge (electron deficiency). At $t=0$ the system was "struck" with a positive point charge at the center of the figure. Around 16 attoseconds (1.6×10^{-17} s) after the impulse, the figure shows a large negative recoil centered at the origin (the dip at the center) and surrounded by a ring of compensating positive charge lying at a distance of 1.3 Å from the origin. Outside the large, central ring is a second, smaller dip (again, depicting negative charge) that is followed by a smaller secondary ring of positive charge at 3.8 Å from the center. The disturbance to the valence electrons depicted in this figure is similar to electron disturbances that can occur around point impurities in metals, known as Friedel oscillations.

entailed modeling an oscillating dipole within a solution. The dipole consisted of two charges possessing opposite signs, and separated by a distance of 1 Å. (Many excited states in molecules can be modeled as electric dipoles because they exhibit dipole selection rules.) The distribution of electrons close to the dipole was calculated via a computer program. The results were subsequently depicted in a computer-generated color image with different colors indicating different electron densities. Figure 1 is a computer-generated depiction of the change in electron density after a perturbing event. One possible application of the dipole model relates to the measurement of distances in microscopic biological systems.

The second case entailed calculating the disturbance to an electron distribution caused by an ion of gold traveling through a sample of water at one percent the speed of light. As in the previous case, the disturbance to the sample's electron density was depicted by a computer-generated color image.

The achievements of the researchers were two-fold. First, data collected from IXS from a sample of water was used to calculate, and graphically represent, the actual density distribution of electrons within the sample over incredibly short

spans of time and space. Second, theoretical modeling was developed to show how ultra-fast processes in certain materials can potentially be imaged using synchrotron x-rays. It is also worth noting the symbiotic role the two synchrotron facilities played in making this project possible. Approximately one year of background research carried out at Cornell's CHES facility was validated with the aid of Argonne's APS facility and its staff. — *Phil Koth*

See: P. Abbamonte, K.D. Finkelstein, M.D. Collins, and S.M. Gruner, "Imaging Density Disturbances in Water with a 41.3-Attosecond Time Resolution," *Phys. Rev. Lett.* **92**, 237401 (2004).

Author Affiliations: Cornell University
Correspondence: abbamonte@bnl.gov

This study was supported by the U.S. Department of Energy Grant No. DEFG02-97ER62443. CHES is supported by the National Science Foundation and the National Institute of General Medical Sciences under cooperative agreement DMR-0225180. Use of the Advanced Photon Source was supported by the U.S. Department of Energy, Office of Science, Office of Basic Energy Sciences, under Contract No. W-31-109-ENG-38.

HOW WATER MOLECULES ARE CONNECTED

Water may be the most important molecule on Earth, but our understanding of its properties is embarrassingly limited. In solid ice form, water takes on numerous phases and structures that can be studied by means of diffraction techniques. As a liquid, however, water poses a frustrating structural puzzle because of the complex hydrogen bonding that forms a disordered network. Recently, researchers from the Stanford Synchrotron Radiation Laboratory, the BESSY laboratory, Stockholm University, Linköping University, and Utrecht University have used the Bio-CAT 18-ID beamline at the APS, as well an Advanced Light Source (ALS) beamline, to obtain detailed information about the nearest neighbor coordination geometry in liquid water.

Previous experimental efforts to understand water structure have relied on several methods including infrared spectroscopy and neutron and x-ray diffraction. Unfortunately, the structural information provided by infrared spectra is ambiguous for water, and diffraction provides only radial distribution functions that do not allow unique assignment of local hydrogen bonding configurations. In the work reported by Wernet et al., x-ray absorption spectroscopy (XAS) and x-ray Raman spectroscopy (XRS) were used to investigate local bonding in the first coordination shell of water. In XAS, x-rays are absorbed by core electrons close to the nucleus of the oxygen atoms in water; in XRS, the x-ray photons are inelastically scattered by the oxygen atoms. Both processes are highly sensitive to the hydrogen bonds formed by the water molecules. The XRS data were collected at the Bio-CAT18-ID beamline at the APS; the XAS measurements were carried out at the ALS.

The researchers found that the hydrogen bonding of liquid water was very similar to that seen in the surface layers of ice but very different from the bonding observed in bulk ice, in

which water molecules are tetrahedrally coordinated. This new finding indicates that, contrary to the conclusions of earlier work, bulk water is not predominantly four-fold coordinated. Instead, it appears that the x-ray spectroscopy results are consistent with quantum chemical models in which the water molecules form two hydrogen bonds with their neighbors. In this case, liquid water appears to consist of structures made of chains and rings, which are, in turn, weakly hydrogen-bonded to other chains and rings.

Members of the research group believe that the work will be controversial because many computer simulations over the last 10 years tell a very different story. Because computer power has increased rapidly and experimental techniques have been more difficult to develop, the simulations have outpaced the empirical data. Based on the recent models, many scientists have concluded that, in changing from ice to liquid, water molecules maintain their four-fold tetrahedral network structure, but the liquid acquires more defects and disorder in the form of different bond lengths and bond angles. The new x-ray spec-

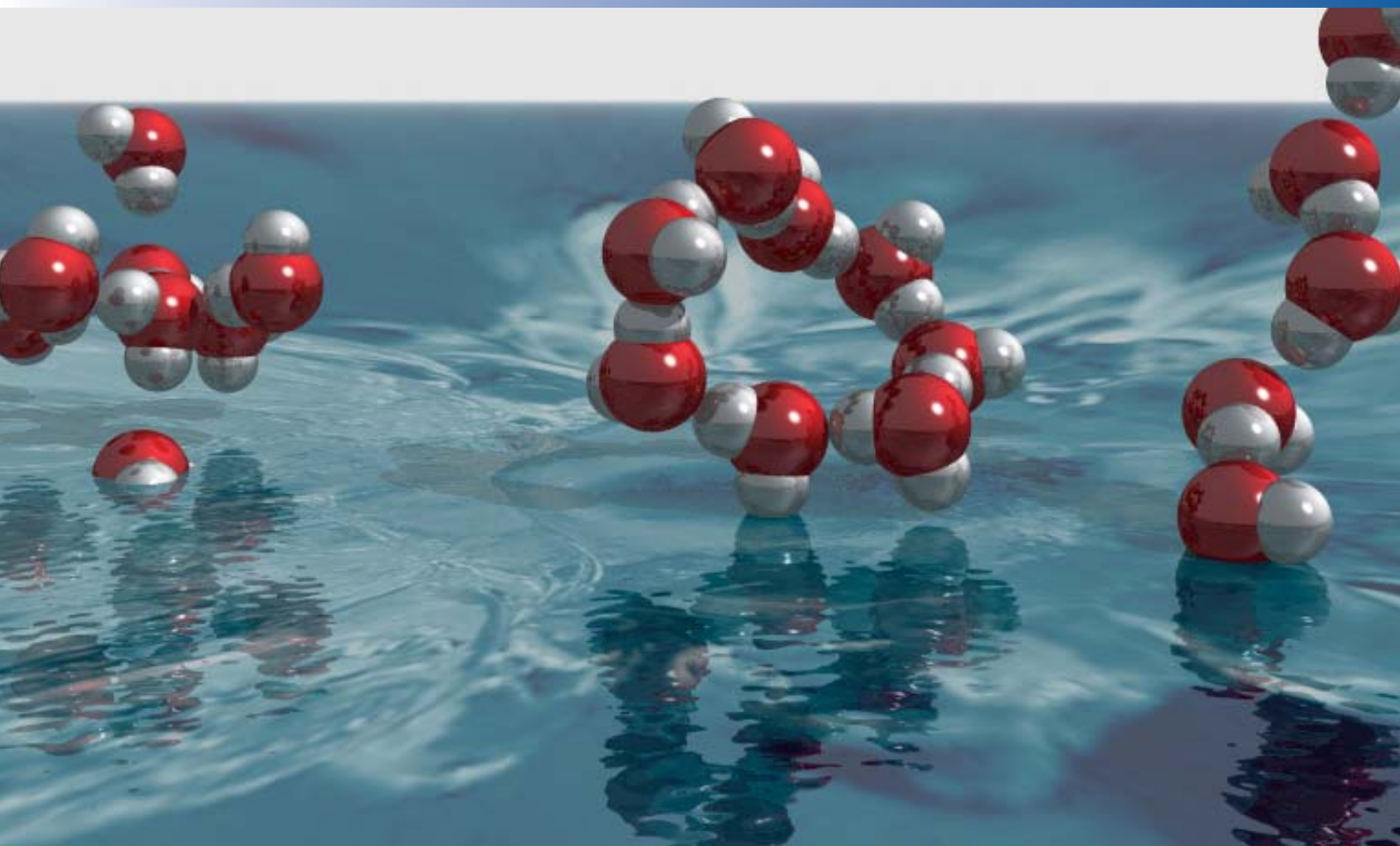


Fig. 1. In ice, each water molecule is surrounded by four other molecules in a tetrahedral arrangement (left). This new result on liquid water shows that the molecules are connected only with two others. This implies that most molecules are arranged in strongly hydrogen-bonded rings (middle) or chains (right) embedded in a disordered cluster network connected mainly by weak hydrogen bonds. The oxygen atoms are red, and the hydrogen atoms are gray in the water (H_2O) molecules. (Figure courtesy of H. Ogasawara, Stanford Synchrotron Radiation Laboratory.)

troscopy data discussed here do not support this conclusion, however, yielding a two-fold bonding picture instead.

The debate on the structural picture is likely to continue, but these new data show the importance of third-generation facilities such as the APS synchrotron. Core excitation spectroscopies—especially XRS, which can only be done at the newest x-ray sources—are vital to understanding the local structure of a complex system such as water. — *David Voss*

See: P.H. Wernet^{1,2}, D. Nordlund³, U. Bergmann¹, M. Cavalleri³, M. Odellius³, H. Ogasawara^{1,3}, L.Å. Näslund^{1,3}, T.K. Hirsch³, L. Ojamäe⁴, P. Glatzel⁵, L.G.M. Pettersson³, A. Nilsson^{1,3}, "The Structure of the First Coordination Shell in Liquid Water," *Science* **304**, 995 (14 May 2004).

Author Affiliations: ¹Stanford Synchrotron Radiation Laboratory, ²BESSY, ³Stockholm University, ⁴Linköping University, ⁵Utrecht University

Correspondence: nilsson@slac.stanford.edu

This research was supported by the Swedish Foundation for Strategic Research, Swedish Natural Science Research Council, and U.S. National Science Foundation grant CHE-0089215. Generous grants of computer time at the Swedish National Supercomputer Center and the Center for Parallel Computing are gratefully acknowledged. Stanford Synchrotron Radiation Laboratory is a national user facility operated by Stanford University on behalf of the U.S. Department of Energy, Office of Basic Energy Sciences. The Advanced Light Source is supported by the Director, Office of Science, Office of Basic Energy Sciences, Materials Sciences Division, of the U.S. Department of Energy under Contract No. DE-AC03-6SF00098 at Lawrence Berkeley National Laboratory. The Biophysics Collaborative Access Team (Bio-CAT) is a National Institutes of Health-supported research center RR-08630. Use of the Advanced Photon Source was supported by the U.S. Department of Energy, Office of Science, Office of Basic Energy Sciences, under Contract No. W-31-109-ENG-38.

DISTORTED ICOSAHEDRAL SHORT-RANGE ORDER SEEN IN LIQUID EARLY TRANSITION METALS

Though they lack long-range order, liquids contain a surprising amount of short-range order. The structure of this order is reasonably well understood for closed-shell inert gas liquids, but not for metallic or covalently bonded systems. While various theoretical approaches produce results that agree reasonably well with experimental data for late transition metals, they fail for the early transition metals (e.g., Sc, Ti, V), for which the theories cannot even reproduce the experimentally measured peak positions in the liquid structure factors. Because of the difficulty in obtaining experimental data, it was unclear whether these failures pointed to inadequacies in the theories or in the quality of the experimental data. This situation was clarified by more precise experimental studies carried out on the MU-CAT 6-ID-D beamline at the APS by researchers from Washington University, the University of Massachusetts, the NASA Marshall Space Flight Center, the University of Alabama in Huntsville, and Iowa State University.

Using the recently developed beamline electrostatic levitation (BESL) technique [1], which enables *in situ* x-ray diffraction experiments to be made on electrostatically levitated droplets, the researchers studied the short-range order in equilibrium and supercooled liquids of early (Ti) and late (Ni) transition metals. The structure factor $S(q)$ data for Ni, above and below the melting temperature, are shown in Fig. 1a. The dashed line represents the results of first-principles calculations of $S(q)$ from the embedded atom method for the equilibrium liquid [2]. While the theoretical calculations give a reasonable prediction of the peak locations for $S(q)$, they fail to predict the developing shoulder on the high- q side of the second peak that was observed in the experimental data (indicated by the arrow), which becomes more prominent in the undercooled liquid. This shoulder is a signature of icosahedral short-range order (ISRO) in the supercooled liquid [1] and is consistent with a half-century-old hypothesis of Frank [3], which links icosahedral order in supercooled metallic liquids to the observed barrier for the nucleation of crystal phases. The measured $S(q)$ for Ti liquids (Fig. 1b) agrees better with the predictions of theoretical calculations (dashed lines) than do earlier data [4] (dotted line), although the second peak in the experimental data is wider than predicted. The high- q side of this peak is different than that for Ni (inset of Fig. 1b).

As shown in Fig. 2, the profile of the second peak in $S(q)$ for Ti is consistent with a distorted ISRO in the liquid. Although such distortions, resulting from a competition between structural (maximum number of bonds) and electronic (Jahn-Teller effect) factors, have been predicted in atomic cluster studies, the present results are the first direct experimental observations of such distortions in a liquid. This is also the first time that the degree of distortion has been correlated with atomic interactions. The findings signal a competition between a tendency for atomic close packing in the nearly filled d-band of late transition metals, which favors local icosahedral order, and the importance of the angular dependence of the d-band bonding in the early transition metals. Distorted icosahedral (or decahedral) short-range order is also expected in other early transition metal liquids. While the nucleation barrier for simple crystal phases is expected to be little affected by the degree of perfection of ISRO in alloy liquids, the latter could have a dramatic

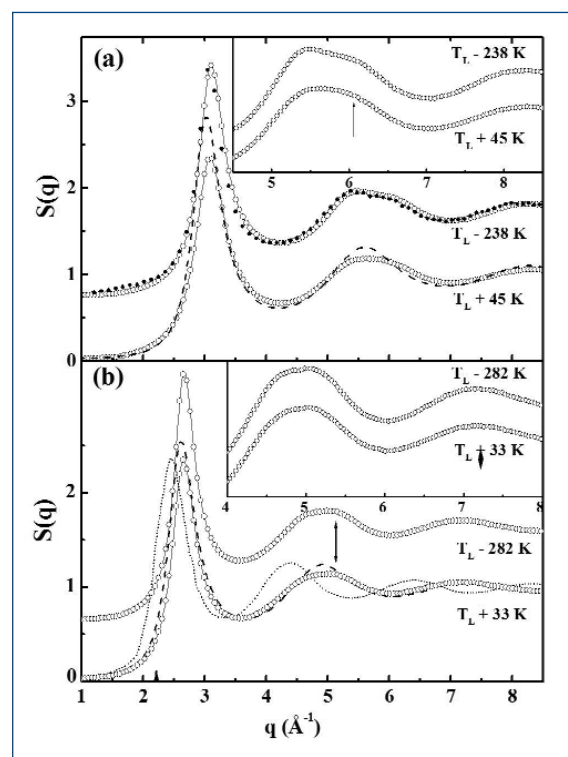


Fig. 1. X-ray structure factor for liquid (a) Ni (liquidus temperature $T_L=1728$ K) and (b) Ti ($T_L=1940$ K) as a function of temperature; the curves are displaced vertically for clarity. (a) Dashed line from theory [2]; these BESL data are in good agreement with recent neutron diffraction studies using electromagnetic levitation [5] (closed circles; selected data points are shown for clarity). (b) Dashed line from theory [2], dotted line from previous work [4]. The differences between Ni and Ti are more clearly observed in the insets, showing only the 2nd and 3rd peaks of $S(q)$.

effect on the nucleation of ordered phases with ISRO, as occurs in icosahedral quasicrystals. — *Vic Comello*

REFERENCES

- [1] K.F. Kelton, G.W. Lee, A.K. Gangopadhyay, R.W. Hyers, T. Rathz, J. Rogers, M.B. Robinson, and D. Robinson, *Phys. Rev. Lett.* **90**, 195504 (2003).

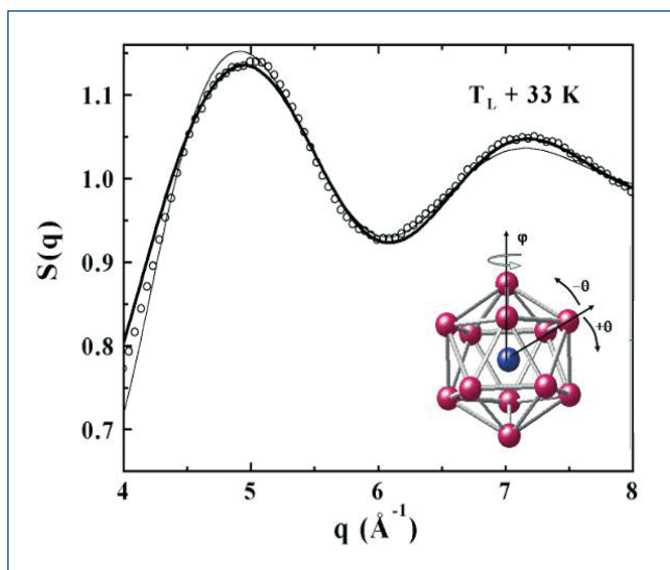


Fig. 2. Comparison of experimental data (open circles) with the calculated structure factors for Ti for an undistorted (thin line) and distorted (thick line) icosahedron ($\theta = -6^\circ$ and $\phi = 10^\circ$) including the Debye-Waller factor ($r_o = 2.871 \text{ \AA}$ and $\langle dr_o^2 \rangle = 0.034 \text{ \AA}^2$). The inset indicates the θ and ϕ distortions of the icosahedron.

[2] G.M. Bhuiyan, M. Silbert, and M.J. Stott, Phys. Rev. B. **53**, 636 (1996).

[3] F.C. Frank, Proc. Royal Soc. London **215A**, 43 (1952).

[4] Y. Waseda and S. Tamaki, Phil. Mag. **32**, 273 (1975); Y. Waseda, *The Structure of Non-Crystalline Materials* (McGraw-Hill, New York, 1980).

[5] T. Schenk, D. Holland-Moritz, V. Simonet, R. Bellissent, and D.M. Herlach, Phys. Rev. Lett. **89**, 075507 (2002).

See: G.W. Lee¹, A.K. Gangopadhyay¹, K.F. Kelton¹, R.W. Hyers², T.J. Rathz³, J.R. Rogers⁴, and D.S. Robinson⁵, "Difference in Icosahedral Short-Range Order in Early and Late Transition Metal Liquids," Phys. Rev. Lett. **93**, 037802 (2004).

Author Affiliations: ¹Washington University, ²University of Massachusetts, ³University of Alabama in Huntsville, ⁴NASA Marshall Space Flight Center, ⁵Iowa State University

Correspondence: drobinsn@iastate.edu

The research at Washington University was supported by the National Aeronautics and Space Administration under Contracts NAG8-1682 and NNM04AA016 and the National Science Foundation under Grant DMR 03-07410. The use of MU-CAT was funded by DOE Contract No. W-7405-ENG-82 through the Ames Laboratory. Use of the Advanced Photon Source was supported by the U.S. Department of Energy, Office of Science, Office of Basic Energy Sciences, under Contract No. W-31-109-ENG-38.

DIGGING IN THE DIRT

Common wisdom has it that each of us will eat a pound of dirt before we die. But how do materials respond to the presence of dirt? In most cases, dirt is detrimental, but in some systems, it can help. Impurities in superconductors, for instance, enhance their ability to conduct an electric current without energy loss. A recently asked question is, how might dirt affect the diverse class of compounds known as liquid crystals, which are not only ubiquitous in modern electronic display devices, but also exist in biological systems, such as cell walls? Finding strategies to attack this problem is at the core of experiments done at the IMMY/XOR beamline 8-ID at the APS and at the National Synchrotron Light Source by researchers from the Johns Hopkins University and the Massachusetts Institute of Technology.

Real condensed matter systems (i.e., materials) have imperfections, so understanding disorder is essential to a complete understanding of materials. Physicists face a problem in trying to understand real-world conditions. Theoretical frameworks that are ideal for neat, pure systems often have a hard time standing up to those with externally imposed randomness. Such systems are at the frontier of physics.

The Johns Hopkins/Massachusetts Institute of Technology group hope to answer important questions about one of the most fragile states of matter: the smectic liquid crystal. Liquid crystals are fluids in which the molecular constituents possess a degree of order between fully ordered crystalline materials and fully disordered simple liquids. There are many types of well characterized liquid crystal phases, which makes them an ideal test bed for discovering the effects of imposed randomness. Smectic liquid crystals normally form a layered arrangement in which their long, rod-like molecules align parallel to each other and stack into layers. Understanding how these liq-

uids respond to the presence of externally imposed disorder (dirt, in other words) is a rather vexing question. The group notes that the smectic doesn't handle the dirt well at all. The phase is destroyed, which is not surprising. What remains, however, is far more intriguing. From disorder, the theory goes, a new state of matter known as a "Bragg glass" might emerge. The research group is using a controlled chemical environment to see if they can observe this new state.

The key to the group's experiments is trapping the liquid crystals in a gel. The structure of a gel imparts random constraints that the smectic must accommodate in its effort to form neat layers. The group has focused on the behavior of smectic liquid crystals based on the organic compound octylcyanobiphenyl (8CB), which they can trap in a colloidal silica gel, an aerosil. By exploiting beamline 8-ID, the degree of success that the liquid crystal has in forming orderly layers can directly be determined.

Continued on next page

The liquid crystal molecules interact with the gel surfaces and a competition arises between the liquid crystal's natural tendency to order and the pull of the randomness of the gel. These x-ray studies are revealing the nature of this conflict in detail as well as the forces that are involved in disturbing the liquid-crystal order.

The research group found that the effect of the imposed randomness on the smectic is profound, revealing a host of interesting consequences. However, they note that they are ultimately reporting a negative result. The specific motivation for the experiment was to find evidence that, once the smectic phase is destroyed by the externally imposed disorder, the new state of matter, the "Bragg glass," would emerge in its place. In contrast to theoretical predictions, they did not find a Bragg glass. The group believes that the jury is still out on whether the theory is correct, and believes the answer may lie in exploring systems with weaker disorder. Perhaps then, researchers will see the new state latent in smectic liquid crystals and a new phase of matter will emerge from the dirt.

— David Bradley

See: D. Liang¹, M.A. Borthwick², and R.L. Leheny¹, "Smectic Liquid Crystals in Anisotropic Colloidal Silica Gels," *J. Phys. Condens. Matter* **16**, S1989 (30 April 2004).

Author Affiliations: ¹Johns Hopkins University, ²Massachusetts Institute of Technology

Correspondence: leheny@pha.jhu.edu

Funding was provided by the NSF under Grant No. DMR-0134377 (D.L. and R.L.) and Grant No. DMR-0071755 (M.B.). Acknowledgement is also made to the donors of The Petroleum Research Fund, administered by the ACS, for partial support of this research. Research was car-

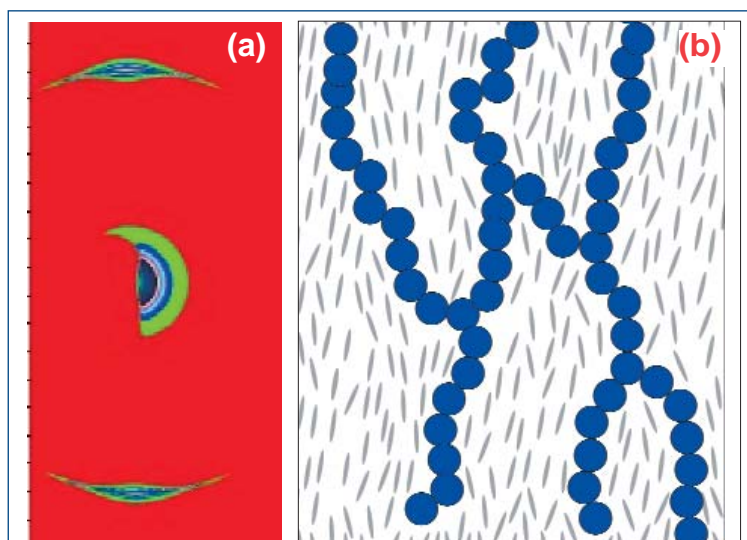
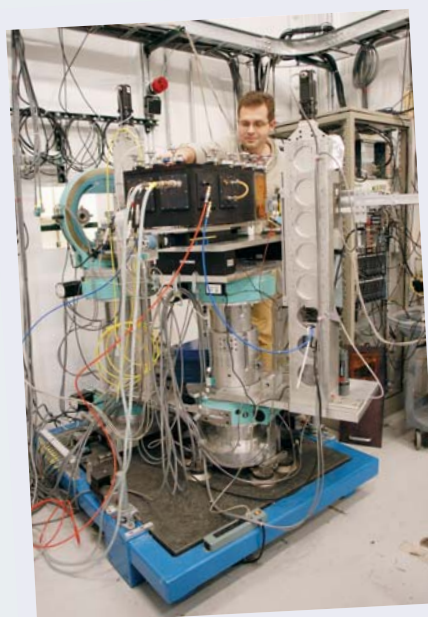


Fig. 1. (a) Liquid crystals held within a gel produce an imperfect x-ray scattering pattern. The less than pristine shape of the two lobes at the top and bottom of the image reflect the degree to which the randomness of the gel distorts the liquid crystal layering. (b) Schematic of the liquid crystal (molecules shown in gray) entrained by the randomly cross-linked network of the silica gel (blue).

ried out at the National Synchrotron Light Source, Brookhaven National Laboratory, which is supported by the U.S. Department of Energy, Division of Materials Sciences and Division of Chemical Sciences, under Contract No. DE-AC02-98CH10886. Use of the Advanced Photon Source was supported by the U.S. Department of Energy, Office of Science, Office of Basic Energy Sciences under Contract No. W-31-109-ENG-38.

AROUND THE EXPERIMENT HALL

Joe Strzalka (University of Pennsylvania) in the CMC-CAT 9-ID-C research station, leveling the Langmuir trough on the sample stage of the liquid surface spectrometer.



UNDERSTANDING PHASES AND TRANSITIONS WITHIN COPOLYMER-HOMOPOLYMER SYSTEMS

Basic modeling of the structure and phase behavior of polymeric materials can be accurately achieved through the use of self-consistent field theory (SCFT), which was first formulated for polymers by S.F. Edwards and given new utility for ordered block copolymers by M. A. Matsen and M. Schick. The study of polymer amphiphiles, which consist of blocks of mutually incompatible polymers chemically attached to each other, offers the promise of a detailed understanding of generic complex fluid phases that appear not only in polymer systems, but also routinely in small-molecule-based complex fluids. Researchers from Yale University, the Massachusetts Institute of Technology, and the University of Massachusetts worked with block copolymer-homopolymer systems in order to identify the symmetric-to-asymmetric (S-to-A) transition between the symmetric sponge-phase (L_3 phase or S phase) and the asymmetric vesicle-phase (L_4 or A phase). Using small-angle x-ray-scattering (SAXS) at the IMMY/XOR 8-ID beamline at the APS, and cryo-transmission electron microscopy (CTEM) to determine structure and phase behavior, they found microstructures formed from a random dispersion of poly(ethylene/butylene) membranes within polystyrene. The microstructures consist of two unique solvent volumes—each dependent on the particular size of the membrane's volume fraction.

The first experiment (for the SAXS measurements) involved dissolving samples of symmetric poly(styrene-ethylene/butylene-styrene) (PSEBS) tri-block copolymer and a short-chain polystyrene homopolymer (PS) in toluene, filtering the resultant solution, precipitating it into cold propanol, annealing the solution under vacuum at the 8-ID beamline, collecting scattered x-rays by means of a charge-coupled device-based detector; and finally, obtaining supplemental point-detector data at beamline X22A of the National Synchrotron Light Source. The second experiment (for the CTEM measurements) required annealing the solution under vacuum, microtoming it, and staining the solution with ruthenium tetroxide before carrying out the CTEM measurements.

The SAXS and CTEM results reveal the existence of two polymeric, membrane-based, equilibrium phases (Fig. 1): an L_3 symmetric-sponge phase and an L_4 asymmetric-sponge phase. On the basis of these results, the collaborators suggest that PSEBS-PS forms (1) an L_4 phase that consists mostly of equilibrium vesicles (spherical cavities) for volume fractions $f < 0.22$ and (2) an L_3 phase for $0.22 < f < (\text{at least}) 0.43$. In addition, for the first time, the collaborators found an S-to-A transition between the two phases in a copolymer-homopolymer blend. The S and A phases are distinguished by the two distinct volumes, which are separated by the sponge-phase membrane: one labeled “inside” (I) and the other “outside” (O). Specifically, when I and O volumes are equivalent, the L_3 phase occurs, but when I and O volumes are not equivalent, the symmetry is broken, and the L_4 phase occurs.

Because of this research, future microscopic calculations of polymers should result in a better understanding of these complex fluid phases and more accurate determination of key membrane parameters—such as modulation wave vector, correlation length of the I-O order parameter, amphiphile correlation length, membrane thickness, and coupling characteristics between the I-O order parameter and the amphiphile density. — *William Arthur Atkins*

See: P. Falus^{1,2}, H. Xiang³, M.A. Borthwick², T.P. Russell³, and S.G.J. Mochrie¹, *Phys. Rev. Lett.* **93**(14), 145701 (1 October 2004).

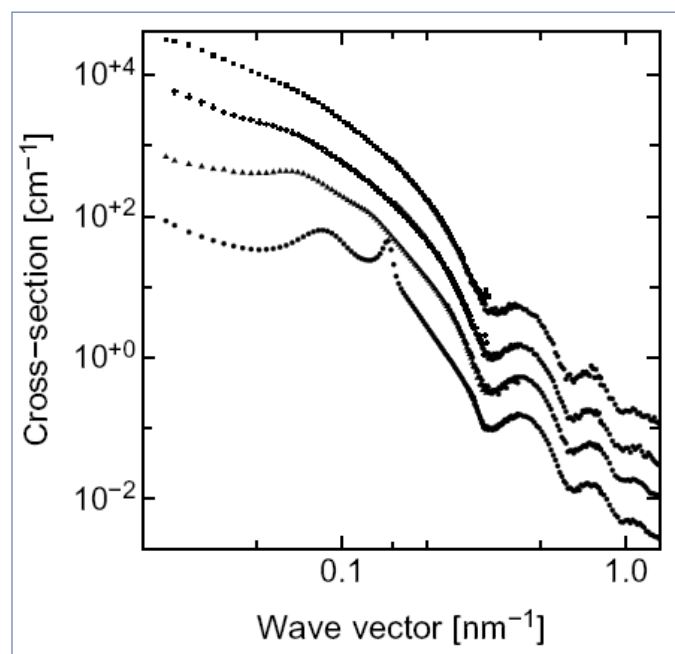


Fig. 1. SAXS intensity from PSEBS-PS blends with PSEBS volume fractions of (from top to bottom) 0.015, 0.19, 0.30, and 0.40 for wave vectors from 0.02 to 1.3 nm^{-1} . For clarity, these profiles have been multiplied by 125, 25, 5, and 1, respectively. The 0.32-inverse-nm-period intensity oscillations clearly point to a membrane-based microstructure for all compositions, while the behavior at smaller wave vectors distinguishes L_3 and L_4 phases.

Author Affiliations: ¹Yale University, ²Massachusetts Institute of Technology, ³ University of Massachusetts
Correspondence: simon.mochrie@yale.edu

This work was supported by the NSF via DMR 0071755, and by the MRSEC at the University of Massachusetts. The NSLS is supported by the U.S. DOE. Use of the Advanced Photon Source was supported by the U.S. Department of Energy, Office of Science, Office of Basic Energy Sciences, under Contract No. W-31-109-ENG-38.

A VIABLE METHOD OF CHARACTERIZING BROMINE-LABELED LANGMUIR MONOLAYERS

Langmuir monolayers are important interfacial systems for the study of organic, bio-organic, and polymeric amphiphilic macromolecules and their interactions with polar and nonpolar atomic and molecular species. Their numerous biomedical and materials science applications, however, often require localizing the positions of particular molecular, submolecular, or atomic components within the monolayers. Researchers from the University of Pennsylvania and the Brookhaven and Argonne national laboratories, using the CMC-CAT 9-ID beamline at the APS, applied resonance reflectivity to locate resonant bromine atoms that were covalently bound to the hydrocarbon chain of an organic fatty acid in a Langmuir monolayer at an air/water interface.

Although resonance x-ray reflectivity has been used extensively in the structural characterization of inorganic and bio-organic multilayer films, its use with single monolayer films is much more problematic because of the relatively low number of resonant atoms, the small magnitude of the resonant effect, and the lack of periodicity in the samples. Measurements on liquid surfaces are inherently more difficult because interferometric techniques cannot be applied to enhance the diffraction signal from the monolayer. Nevertheless, the development of a resonance x-ray reflectivity technique for the structural characterization of Langmuir monolayers in amphiphilic macromolecules would be of great value because, among other things, it would open the door to localizing resonant-atom-labeled single-amino-acid residues within the scattering length density profiles of monolayers of vectorially oriented proteins.

In the study at CMC-CAT, a monolayer of bromostearic acid was used as a test case to confirm that known resonant atom stoichiometry and location of the monolayer within the chemical structure of the macromolecular species would demonstrate that resonance reflectivity at the air/water interface could specify atomic positions with sub-angstrom precision. Resonance reflectivity requires that the alignment of the liquid surface spectrometer be precisely maintained as the x-ray energy is varied about the resonant atom's absorption edge and that model-independent data analysis techniques be used. Furthermore, accurate measurement of the resonance effect necessitated that x-ray radiation damage of the monolayer film be avoided, even though the small total number of resonant atoms in the monolayer requires long data acquisition times to obtain satisfactory statistics.

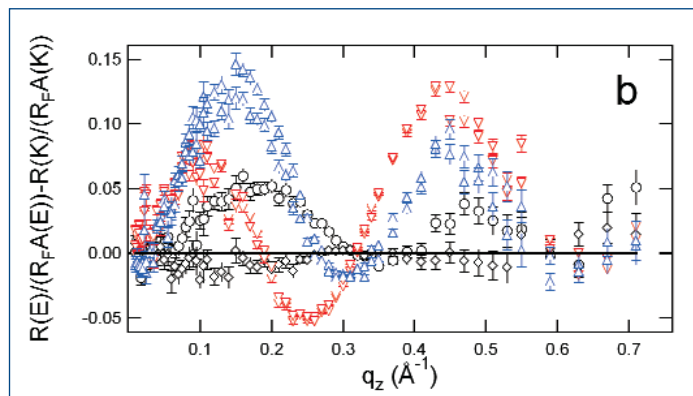
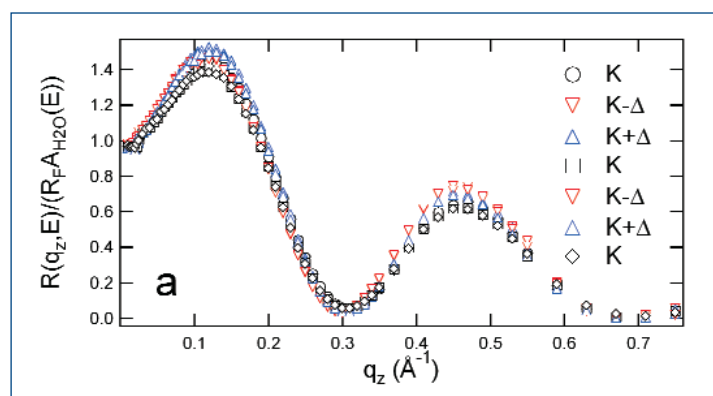
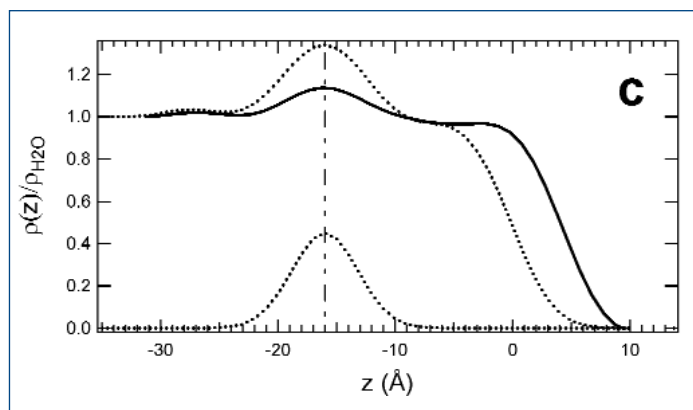


Fig. 1. (a) Fresnel- and energy-normalized reflectivity data collected from a 2-bromostearic acid monolayer at various energies: $K = K_{Br} = 13,474$ eV; $\Delta = 200$ eV. (b) Differences between the second data set at $E = K$ in (a) and the data at $E = K$ reproduce well and indicate that energy-dependent resonant effects exist in the data at $E = K \pm \Delta$. (c) The electron density distributions derived via box refinement for the stearic acid (solid) and 2-bromostearic acid (dotted curve) monolayers. The contribution to the monolayer from Br, as determined from the resonance data, is shown as the lower dotted Gaussian curve, centered at $z = -16.0 \pm 0.2$ Å, with a width of 2.8 ± 0.2 Å. For such small molecules, labeling with Br does not preserve the isomorphism of the monolayer, but for larger molecules such as proteins, substitution of Br for H should not perturb the structure as significantly.



The resonance x-ray reflectivity measurements were performed at CMC-CAT's 9-ID beamline because a constant-exit-height monochromator permits changes in the energy of the beam while keeping downstream optics in alignment. To avoid radiation damage, samples were translated transversely relative to the x-ray beam between data points and between successive scans. The data collection protocol employed cycles through several energies in the vicinity of the Br K absorption edge. The protocol verified that the observed energy dependencies were indeed resonant effects and demonstrated the correct energy dependence of the resonance effect in the brominated sample and the absence of an effect in a control sample without Br. The protocol also confirmed the absence of radiation damage to either sample.

Determination of the Br atom's location within the monolayer profile structure required simultaneous fitting of all available data at different energies. For the analysis to specify the location of the Br atoms with sub-angstrom precision, both the real and the imaginary parts of the changes in the scattering factor, as reported in the literature, needed to be considered.

This study demonstrates the feasibility of combining resonance x-ray reflectivity measurements on Br-labeled Langmuir monolayers with the approaches to data collection and analysis that are required to obtain reliable information on the locations of the resonant species. A best-practice approach would also measure the changes in the real and imaginary parts of the scattering factor directly from the sample, thereby constraining the locations of the resonant atoms even further. — *Vic Comello*

See: J. Strzalka¹, E. DiMasi², I. Kuzmenko³, T. Gog³, and J.K. Blasie¹, "Resonant X-ray Reflectivity from a Bromine-Labeled Fatty Acid Langmuir Monolayer," *Phys. Rev. E* **70**, 051603 (November 2004).

Author Affiliations: ¹University of Pennsylvania, ²Brookhaven National Laboratory, ³Argonne National Laboratory

Correspondence: strzalka@sas.upenn.edu

This work was supported by the NIH under Grant No. GM-55876 and by the MRSEC program of the NSF under Award No. DMR96-32598. Use of the Advanced Photon Source was supported by the U.S. Department of Energy, Office of Science, Office of Basic Energy Sciences, under Contract No. W-31-109-ENG-38.

THE SURFACE AFFECTS POLYELECTROLYTE-SURFACTANT COMPLEX FORMATION

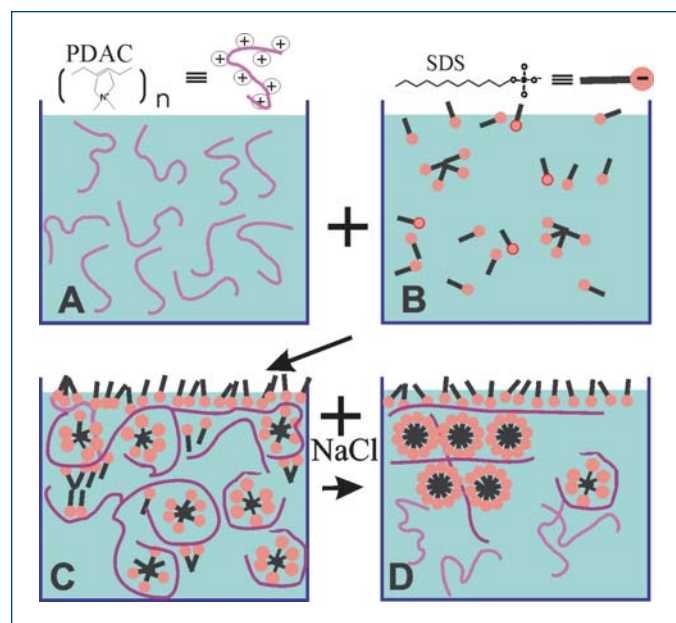
Understanding the behavior of polymer-surfactant mixtures is important for a host of applications as diverse as detergents, paints, cosmetics, and DNA transfection. Charged flexible or semi-flexible polyelectrolytes (PEs) are a subset of the larger group that contains interesting and useful molecules including DNA and actin. Most studies focused on bulk properties of the mixtures, but researchers at Iowa State University and Hebrew University of Jerusalem took a different approach. Using the MU-CAT 6-ID-B beamline at the APS to perform surface-sensitive x-ray diffraction studies of the gas-liquid interface in PE-surfactant, they discovered that the interface plays an important role in forming these complexes and inducing their aggregation.

The ways in which polymer-surfactant mixtures phase-change, aggregate, and precipitate are not well understood. By measuring surface tension and performing x-ray reflectivity (XR) and grazing incidence x-ray diffraction (GIXD) studies, the researchers examined the role of the surface on the formation of PE-surfactant complexes and investigated how adding salt to the mixture induces crystal formation.

The group experimented using solutions of the PE polydiallyldimethylammonium chloride (PDAC) at 2% by weight in pure water, the surfactant sodium dodecyl sulfate (SDS), and

Continued on next page

Fig. 1. Procedures leading to the crystallization of PE-surfactant complexes. (A) Surface x-ray scattering shows that the polyelectrolyte PDAC (positively charged) at 2% wt. is completely water soluble. (B) Similar studies of SDS (negatively charged) at concentrations smaller than 10^{-4} M show that the surfactant is practically water soluble. (C) By mixing the two solutes, hydrophobic complexes (PE-induced micelles) are formed and detected at the interface. (D) The addition of NaCl to the PE-surfactant mixture solution induces crystallization of cylindrical PE-micelles at the interface.



NaCl. In addition to performing surface tension experiments, the group performed XR and GIXD experiments using the Ames Laboratory Liquid Surface Diffractometer with highly monochromatic beams at 8 and 16.2 keV. The x-ray beam can be deflected onto the liquid surface to a desired angle of incidence, yielding information on the density profile across the interface and the in-plane ordering at the surface (within the penetration depth of the beam). From these measurements, the molecular arrangements in the film can be deduced.

Based on their measurements, the group confirmed that when the PE is first added to water (without a surfactant or salt in the solution), it dissolves and is repelled from the surface because of interfacial discontinuity in the dielectric constant (Fig. 1). If a very small amount of surfactant is added to the solution (at concentration levels so low that the surfactant would otherwise be totally soluble in pure water), it decreases the surface tension. This is caused by the formation of hydrophobic PE-surfactant complexes that migrate to the surface, where the surfactant forms a monolayer. Above a critical surfactant concentration—when the ideal linear bulk separation among surfactants is about 250 Å—micellization occurs. The researchers

believe that, when salt is added, the micelles are transformed into a cylindrical shape, and because the ions screen electrostatic interactions, the micelles stack into hexagonal, columnar crystals growing from the interface.

The researchers hope to use anomalous XR and GIXD techniques with heavier ions to further investigate the internal structure of the crystals. — *Yvonne Carts-Powell*

See: D. Vaknin¹, S. Dahlke¹, A. Traveset¹, G. Nizri², and S. Magdassi², “Induced Crystallization of Polyelectrolyte-Surfactant Complexes at the Gas-Water Interface,” *Phys. Rev. Lett.* **93**, 218302-1 (2004).

Author Affiliations: ¹Iowa State University, ²Hebrew University of Jerusalem

Correspondence: vaknin@ameslab.gov

The MU-CAT sector at the APS and the measurements described here are supported by the U.S. DOE, Office of Science, Office of Basic Energy Sciences. Use of the Advanced Photon Source was supported by the U.S. Department of Energy, Office of Science, Office of Basic Energy Sciences, under Contract No. W-31-109-ENG-38.

A CLOSER LOOK AT MATERIAL AGING



A variety of materials, from glasses to polymers and gels, all undergo a lengthy structural relaxation after being disturbed. This process is called “aging,” and the fact that such different substances share this behavior suggests a common underlying mechanism. While there has been extensive theoretical effort to elucidate the microscopic details of aging in materials, experimental efforts have typically been limited to temporal studies that are sensitive to macroscopic changes. A clearer microscopic picture of aging would have practical benefits, both for a better understanding of the fundamental physics of materials and for technological applications. Recently, collaborators from Johns Hopkins University, the Massachusetts Institute of Technology, and Yale University have used x-ray correlation spectroscopy at IMMY/XOR beamline 8-ID at the APS to untangle the dynamic details of material aging on the scale of individual particles.

Aging is a manifestation of non-equilibrium behavior. Although many systems settle down quickly after undergoing a change in conditions, some continue a long evolution toward a state that is never quite reached. For example, the density of water assumes a certain value that depends on its temperature and pressure. However, for aging materials that are perpetually evolving, a simple question such as, “What is the density?” can be problematic. And just as the macroscopic transformation of liquid water to ice can be understood at the molecular level, scientists would like to understand material aging at the level of individual particles. For this reason, the research team employed x-ray photon correlation spectroscopy, a method by which the motion of particles in relation to their neighbors can be probed in detail.

As a test system, the researchers studied laponite, a synthetic silicate clay consisting of highly monodisperse nanoscale disks, in water suspension with a volume fraction of 0.012. When dispersed in water at such low concentrations, the

laponite suspension undergoes a remarkable transformation from low viscosity liquid to a jelly-like solid over the course of days. The 8-ID beamline employs a silicon monochromator and precision slits to select a micron-scale piece of the incident beam to produce a partially coherent source of x-rays incident on the sample. X-rays scattered from the suspension were collected with a CCD array configured for a range of wave vectors from 0.05 nm⁻¹ to 0.3 nm⁻¹, a range tuned for the distance between nearest neighbor disks. Sequences of CCD images were used to determine the intensity autocorrelation function for correlation delay times of 1.6 to 1000 seconds at various stages after formation of the sample, from 1.3 × 10⁴ to 2 × 10⁵ seconds, during which time the suspension evolved from fluid to solid.

By analyzing the correlation data, the research team found that the transformation displays the hallmarks of aging. However, surprisingly, the microscopic behavior was not consistent with the slowing of diffusive fluid-like motion of the clay particles. Instead, the dynamics seem to be best explained by a

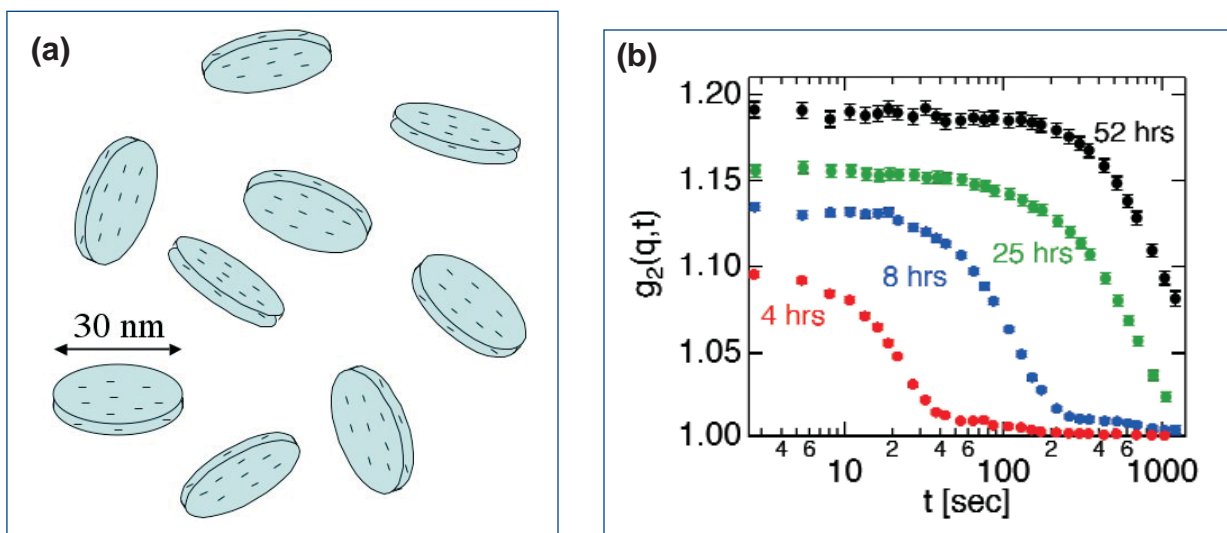


Fig. 1. (a) Cartoon of a laponite suspension — charged, monodisperse clay disks in aqueous solution. (b) Intensity auto-correlation function $g_2(q,t)$ measured with multispeckle x-ray correlation spectroscopy for a laponite suspension at wave vector, $q = 0.10 \text{ nm}^{-1}$, at various stages after the formation of the sample. The evolution of the decay to larger times t is a signature of aging in the system. The increase in the plateau value at short times indicates a growing repulsion between particles with increasing age.

model in which the particles constantly shift in response to local, isolated rearrangements of disks. The rate of motion of the shifting steadily decreases, leading to aging. Moreover, by comparing the x-ray results with conductivity measurements of the suspension, the team concluded that the process can be explained by a picture in which the repulsive force between disks gradually increases over time. This interpretation raises the interesting question: What other examples of material aging might be explained by similar scenarios?

These photon correlation measurements have opened a long-sought window into the detailed dynamics of such non-equilibrium systems at length scales of the individual particles. Such techniques have only recently become available because of the advent of third-generation facilities, such as APS, which provide sufficiently bright sources to enable the partially coherent x-ray beams needed for these scattering experiments. Future work of this nature will permit a more comprehensive

understanding of the general dynamics and underlying principles of aging materials. — *David Voss*

See: R. Bandyopadhyay¹, D. Liang¹, H. Yardimci¹, D.A. Sessoms¹, M. A. Borthwick², S.G.J. Mochrie³, J.L. Harden¹, and R.L. Leheny¹, “Evolution of Particle-Scale Dynamics in an Aging Clay Suspension,” *Phys. Rev. Lett.* **93**, 228302 (26 November 2004).

Author Affiliations: ¹Johns Hopkins University, ²Massachusetts Institute of Technology, ³Yale University
Correspondence: leheny@pha.jhu.edu

Funding was provided by the NSF (DMR-0134377 and DMR-0071755). Acknowledgement is also made to the donors of The Petroleum Research Fund, administered by the ACS. Use of the Advanced Photon Source was supported by the U.S. Department of Energy, Office of Science, Office of Basic Energy Sciences, under Contract No. W-31-109-ENG-38.



UNTANGLING THE STRUCTURE OF BORON CARBIDE

Boron compounds exhibit mechanical and electronic properties that are of substantial interest to physicists and materials researchers. Boron compounds with five-fold icosahedral symmetry, especially boron carbide (B_4C), are particularly important because of their extreme mechanical strength, which makes them valuable as abrasive agents, reinforcements in composite materials, and armor plate. In addition, B_4C is commonly used in control rods in nuclear reactors. However, there has been continuing debate about the details of the site-substitutional disorder present in B_4C , where the boron and carbon atoms can occupy each other's places in the lattice. This issue is one of the contributors to the continuing difficulties in calculating the electronic properties of this system, which is already challenging because of the presence of boron's unique 3-center chemical bonding. Recently, a research team from the University of Washington and Argonne National Laboratory used the PNC/XOR 20-ID beamline at the APS to carry out x-ray spectroscopic studies in order to provide information about site occupation in B_4C . The results of these studies can be used to constrain theoretical models of the structure.

Previous structural studies of boron carbide by means of neutron and x-ray diffraction, while revealing the general properties of the crystal structure, have been less useful for studying the substitutional disorder in B_4C because these probes cannot distinguish easily between boron and carbon atoms at a given site. In the past, spectroscopic techniques such as x-ray near-edge structure (XANES) and electron energy loss spectroscopy (EELS) have been used in these kinds of studies because of their ability to probe element-specific energy states with high resolution. But the technique known as nonresonant x-ray Raman scattering (XRS) affords an additional degree of freedom, namely the ability to observe scattering as a function of momentum, as well as energy. This ability can, in turn, provide unique insights about chemical occupancy of sites with different local *symmetry* in a unit cell. XRS is an inelastic spectroscopy in which x-rays are scattered by K shell electrons; in the process, some energy and momentum is transferred to these electrons, so the scattered x-rays are observed at a slightly lower energy.

To carry out the experiments, the researchers packed polycrystalline B_4C powder having micrometer-scale grains into 3-mm-thick disks. X-rays of 10-keV energy (far higher than the boron K-shell binding energy, which is only 190 eV) from beamline 20-ID were directed at the samples, and inelastically scattered x-rays were collected and analyzed in transmission mode. Boron XRS spectra were collected at 8 different momentum transfers from 1.05 \AA^{-1} to 9.01 \AA^{-1} . The Compton background was subtracted to yield background-free XRS spectra.

The Raman spectra were combined with site-specific *ab initio* calculations to unravel the near-edge spectroscopic features. Simulations of the expected scattering cross sections were carried out for various models of the site occupancy of carbon in B_4C and compared with the experimental data. Of particular interest is a peak near the boron K edge in the experimental spectra.

The main result of the study is a strong q -dependence of the near-edge peak, demonstrating a strongly p -type character. A pure state with such properties must come from an atom located in a highly symmetric position in the unit cell. In the case of B_4C , only the so-called chain-center site has the nec-

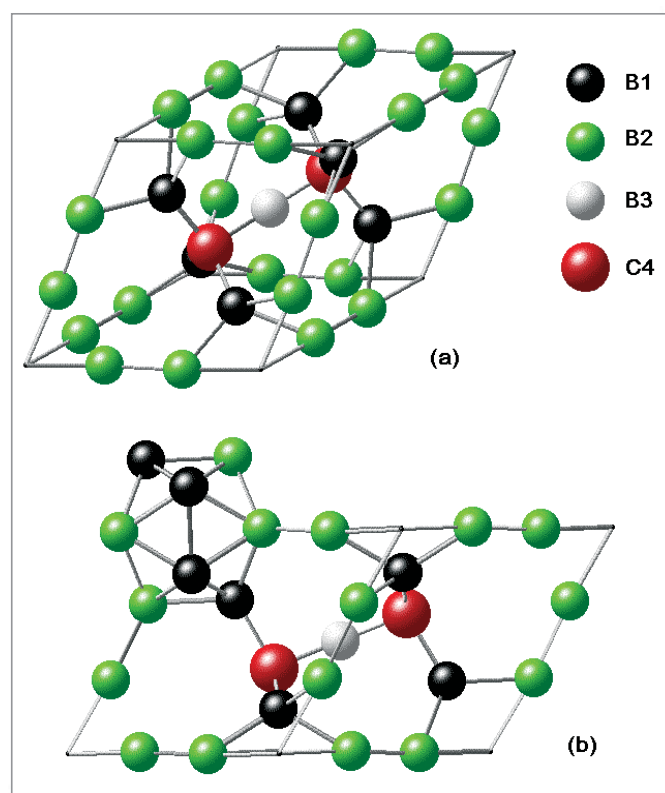


Fig. 1. (a) The unit cell of icosahedral boron carbide for structure model B12-CBC, with four distinct crystallographic sites specified as 1 to 4 with different colors. Other structure models with boron or carbon on different crystallographic sites would have specifications such as B4 or C1. The sticks are not indications of chemical bonds but the nearest neighbor relationship and the boundary of the unit cell. (b) View of the unit cell from a different angle. The six B1 equatorial sites and six B2 polar sites form an icosahedron, as shown on the corner of the unit cell.

essary high symmetry; as a consequence, the study concludes that there must be dominant boron occupation of this site. This assignment is consistent with site-specific *ab initio* calculations on different structural models. In previous studies, this feature

has been attributed to a π -bonding resonance in the carbon-boron-carbon chain, but the new results indicate that the observed feature is not consistent with this interpretation. Instead, the strong near-edge peak seen in the actual spectra indicates an excited core electron-hole pair (an exciton) being formed during the measurement process. Moreover, the exciton appears to be spatially extended, again requiring an *ab initio* treatment instead of a molecular orbital approach.

This study shows that a combination of XRS and *ab initio* calculations can be a very useful method for prying apart the details of site-substitutional disorder in materials. Further, the formation of excitons in these materials may provide a new way to probe the local symmetry properties of solid lattices.

— David Voss

See: Y. Feng¹, G.T. Seidler^{1,2}, J.O. Cross^{1,2}, A.T. Macrander³, and J.J. Rehr¹, "Role of Inversion Symmetry and Multipole Effects in Nonresonant X-ray Raman Scattering from Icosahedral B₄C," *Phys. Rev. B* **69**, 125402-1 (8 March 2004).

Author Affiliations: ¹University of Washington, ²Argonne National Laboratory

Correspondence: seidler@phys.washington.edu

This research was supported by the L.X. Bosack and B.M. Kruger Charitable Foundation; the Mellam Family Foundation; U.S. DOE Grant Nos. DE-FGE03-97ER45628, W-31-109-ENG-38, and DE-FG03-97ER45623 facilitated by CMSN; the University of Washington; and the Natural Sciences and Engineering Research Council of Canada. Use of the Advanced Photon Source was supported by the U.S. Department of Energy, Office of Science, Office of Basic Energy Sciences, under Contract No. W-31-109-ENG-38.

USING REPEATED EXCITATIONS TO REVEAL REAL-TIME RAPID GEOMETRIC CHANGES



A new x-ray technique that uses laser light to excite molecules and x-rays in order to capture a "snapshot" of the molecules as they change shape can provide chemists and biologists with detailed information about important catalytic, photochemical, and biological processes. The technique, developed by researchers from the State University of New York (SUNY) at Buffalo and employed at the ChemMatCARS-CAT 15-ID beamline at the APS, can provide atom-by-atom detail about the short-lived chemical species that exist in the short time-span between reactant and product. This work can help researchers improve industrially important reactions and better understand biochemistry.

Crystallography traditionally provides detailed snapshots of molecules only in their lowest energy state, which is commonly referred to as the "ground state." However, the ground state is not necessarily the most interesting one when it comes to understanding the behavior of different molecules and how they interact with each other. The ability to probe other energy states by using x-ray techniques could provide an opportunity to watch geometric changes as they take place at the molecular level. The collaboration in this study has pioneered a stroboscopic technique that uses laser light to repeatedly excite the molecules in a sample combined with x-ray pulses from the 15-ID beamline to capture an image of the short-lived species that exist in a transient excited state between reactant and product.

This experiment, which explores the reaction of a molecule containing two atoms of the metal rhodium, shows how these atoms react to exposure to intense light from a laser source. The resulting excited (i.e., high-energy) species are highly reactive. The team used a burst of laser light lasting only a fraction of a millionth of a second and having an energy of a few hundreds of a microjoule. Immediately after excitation, they exposed the molecules to a short pulse of x-rays from the 15-ID beamline. This allowed them to probe the structure of the excited molecule several ten thousand times a second as it changed and dropped back to its non-excited state, ready for

Continued on next page

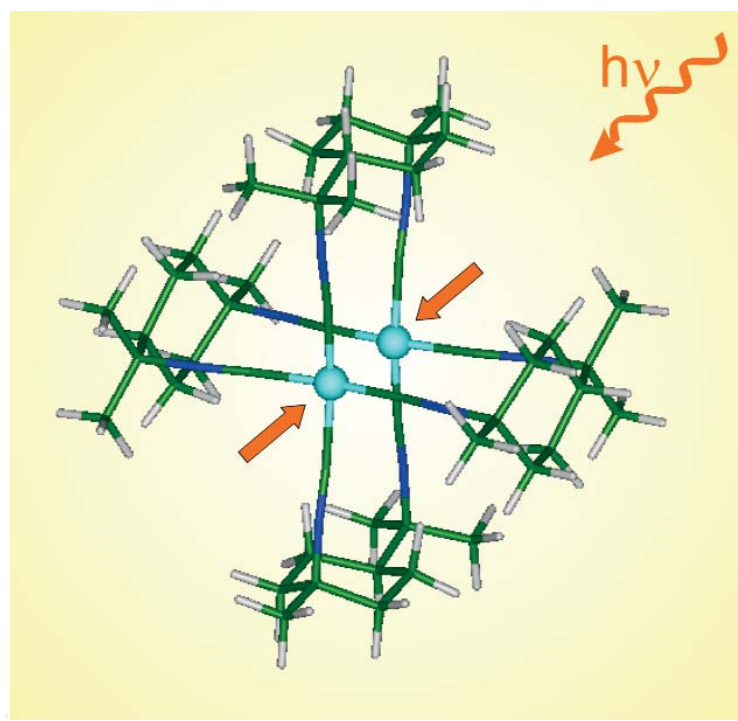


Fig. 1. Light excites an organometallic complex of rhodium, allowing researchers to observe its excitation with a short burst of x-rays.

the next burst of laser light. The method provides an instantaneous snapshot of the molecule as it is distorted in the high-energy laser beam.

In an application of their new approach, the team performed a study on an organometallic compound of rhodium in which the rhodium atoms are held together by a “bridging” organic compound. When this compound is excited by a burst of laser light, the rhodium atoms become linked by a direct bond and are drawn much closer together than they are in the ground state of the molecule. This is the first time that scientists have been able to observe such a light-induced molecular contraction directly, with detail revealed at atomic resolution.

Chemical and biological processes proceed through the formation of transient chemical species that exist for only a few millionths of a second or less. By probing the structure of such transient species, researchers can gain insights into the workings of all kinds of chemical and biochemical reactions, from the catalytic conversion of raw materials into products to the metabolic reactions that turn sugars into energy in our cells.

The energy stored for very brief times in such molecules can in turn be used to initiate other chemical reactions. Related compounds, several of which the SUNY-Buffalo group have also studied, are used to capture energy from sunlight for the development of renewable energy resources.

Further development of this technique to obtain shorter time resolution will allow even shorter-lived light-emitting species to be studied in great detail and permit researchers to monitor light-induced reactions at the atomic level in real time. The insights that will become available from such studies will allow chemists to synthesize new complexes with desirable properties, such as strong light emission and light-to-energy conversion, that mimic such biochemical processes as photosynthesis. — *David Bradley*

See: P. Coppens¹, O. Gerlits¹, I.I. Vorontsov¹, A. Yu. Kovalevsky¹, Y.-S. Chen², T. Graber³, M. Gembicky¹, and I.V. Novozhilova¹, “A Very Large Rh-Rh Bond Shortening on Excitation of the $[\text{Rh}_2(1,8\text{-diisocyno-}p\text{-menthane})_4]^{2+}$ Ion by Time-Resolved Synchrotron X-ray Diffraction,” *Chem. Commun.* **19**, 2144 (2004).

Author Affiliations: ¹State University of New York at Buffalo, ²University of Toledo, ³The University of Chicago
Correspondence: coppens@acsu.buffalo.edu

Time-resolved experiments at the ID-15 beamline are supported through DOE grant DE-FG02-02ER15372. Work at SUNY-Buffalo funded by the National Science Foundation (CHE0236317). The 15-ID beamline is funded through NSF CHE0087817. Use of the Advanced Photon Source is supported by the U.S. Department of Energy, Office of Science, Office of Basic Energy Sciences, under Contract No. W-31-109-ENG-38.

DIFFUSE SCATTERING FROM THE LIQUID-VAPOR INTERFACE OF GA

Scientists from The University of Chicago, using the ChemMatCARS-CAT beamline 15-ID at the APS, determined the wave-vector (q) dependence of the liquid-vapor interfacial tension (γ) of gallium (Ga). Their experimental data (Fig. 1) was used to test the Mecke-Dietrich theory of liquid-vapor interfacial tension, originally developed for dielectrics. The Mecke-Dietrich theory incorporates fluctuations of all wavelengths from the smallest to the largest. It predicts that surface tension is wave-vector dependent for a dielectric liquid with asymptotic form of the pair interaction with form r^{-6} . In a dielectric, the liquid-vapor interfacial density profile is monotone. However, in a metal such as gallium, the liquid-vapor interface density profile is stratified and the asymptotic form of the pair interaction is different from r^{-6} .

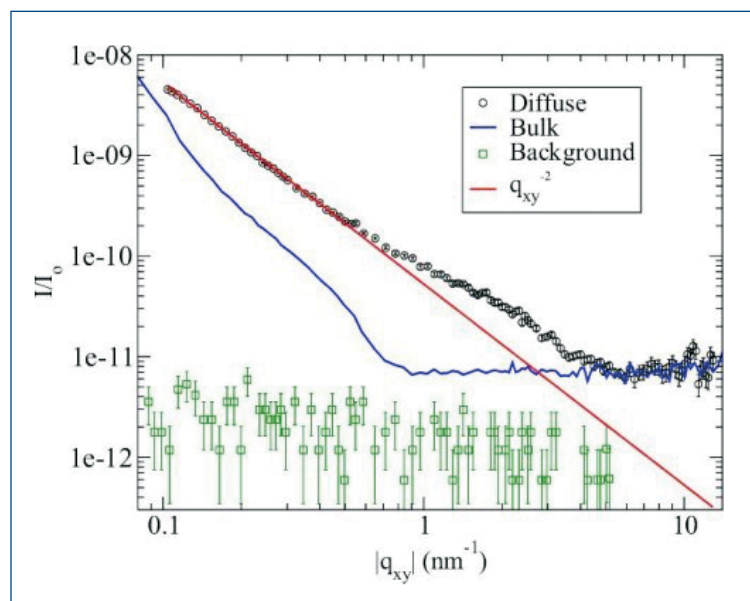
Before the measurements were made, a sample of liquid Ga was prepared from pure metal ingots, sent through a capillary feeder system and into an evacuated sample chamber; heated to a constant 35° C (95° F); and subjected to argon ion sputtering in order to remove contamination. Collection of the diffuse x-ray scattering was accomplished with a static incident angle of 0.13°—smaller than the critical angle of 0.19°. The q resolution was calculated to be 0.002 inverse-Angstroms (\AA^{-1}) with horizontal slits installed in front of the detector. Background scattering from the direct beam was greatly diminished by using large detector pickup angles of 1.0°, 1.5°, and 3.0°. Empty chamber background x-ray scattering and bulk scattering were measured appropriately.

All the experiments were carried out at the ChemMatCARS-CAT 15-ID beamline. The q -dependent sur-

face tension was calculated from the diffuse scattering pattern. Several models—screened Coulomb, Van der Waals, energy independent model pseudopotential, and individual local pseudopotential (ILP)—were used to predict the behavior of $\gamma(q)$ and then compared with the experimental data. The ILP potential produced the best agreement between the observed and calculated $\gamma(q)$ when the correct stratified interfacial density profile was used.

Before this study, the existing theory of the effective Hamiltonian and the experimental diffuse x-ray scattering measurements of liquid-vapor interfaces were mainly focused on dielectric liquids. While liquid gallium and water have very different forms of inter-particle potentials and longitudinal density profiles across the interfaces, the wave-vector dependency of surface tension turns out to be quite similar, and this similarity

Fig. 1. The diffuse x-ray scattering from the liquid-vapor interface of liquid Ga measured by grazing incidence x-ray diffraction. The diffuse scattering intensity is shown as circles; the background scattering that was measured by moving the sample out of the x-ray beam is shown as green squares; the bulk liquid scattering intensity is shown as a blue solid line; and the red solid line shows a diffuse scattering intensity predicted by a classical capillary wave theory.



suggests that the reduction of surface tension in the intermediate q range could be a more general phenomenon than previously conceived. — William Arthur Atkins and Dongxu Li

See: D. Li, B. Yang, B. Lin, M. Meron, J. Gebhardt, T. Graber, and S.A. Rice, "Wavelength Dependence of Liquid-Vapor Interfacial Tension of Ga," *Phys. Rev. Lett.* **92**(13), 136102-1 (2 April 2004).

Author Affiliations: The University of Chicago
Correspondence: sarice@uchicago.edu

The research was supported by a grant from the National Science Foundation. All of the experiments described were carried out at the

ChemMatCARS-CAT beamline at the APS. ChemMatCARS-CAT is supported by grants from the National Science Foundation and the Department of Energy. Use of the Advanced Photon Source was supported by the U.S. Department of Energy, Office of Science, Office of Basic Energy Sciences, under Contract No. W-31-109-ENG-38.

SHEDDING LIGHT ON THE MACHINERY OF PHOTOSYNTHESIS

Square-planar molecules known as porphyrins are at the heart of natural and artificial photosynthesis. They provide a molecular springboard that captures photons of sunlight and bounces out energetic electrons. Porphyrins also have potential as light-powered catalysts and as components of photonics devices, such as information storage materials, that use light, rather than electrons, as their currency. To help illuminate the inner workings of porphyrins, an Argonne National Laboratory (ANL) research group used the BESSRC/XOR 11-ID beamline to determine how different porphyrin molecules respond to being excited by light under different chemical conditions. Their findings could help scientists fine tune the chemical structure of porphyrins by changing the attached side groups and the metal ions at their center to make them respond to different wavelengths of light. Such modified porphyrins may one day form the building blocks of novel catalysts, photonic devices, and efficient solar-power units.

Experimenters have previously used Raman and other forms of visible-light spectroscopy to study the excited states of porphyrins. While these techniques provide useful information, they cannot reveal crucial structural details. For instance, Raman spectroscopy tells scientists only indirectly about the bond distances between the central metal ion and the chemical groups around the porphyrins' ring bond distance, a key property that could be tweaked for optimum effect in a modified porphyrin. Raman spectroscopy also fails to reveal the number of bonds to the metal, the coordination number, how many electrons have been lost or gained in forming those bonds, and the oxidation state.

New x-ray techniques, such as time-resolved pump-probe x-ray absorption near edge and fine structure (XANES and

XAFS), on the other hand, can reach into the core of such molecules and pull out information when the porphyrin is in solution phase. By carrying out experiments using the pulsed synchrotron source available on beamline 11-ID, the ANL team was able to obtain information even for porphyrin molecules that exist only fleetingly, with lifetimes of about 100 picoseconds. On this time scale, it is possible to freeze the action as a porphyrin absorbs a photon and is excited, allowing researchers to determine its structure precisely in this state.

The ANL team has focused on a derivative of the basic porphyrin molecule that carries eight hydrocarbon groups on the outside of the ring and a copper ion at the center: the copper(II) octaethylporphyrin, CuOEP, molecule. CuOEP is an archetypal

Continued on next page

synthetic porphyrin that is essentially free from the interference of other complex chemical groups that are attached to the porphyrin ring in its natural counterparts. The researchers can therefore use CuOEP as a skeletal porphyrin model.

Knowledge of the structural changes induced by photon absorption is key to tailoring the physical properties of these porphyrins. The ANL group carried out studies with two different solvent systems, one comprising the aromatic hydrocarbon toluene and the second containing both toluene and the oxygen-containing polar solvent tetrahydrofuran (THF). They found that toluene alone did not affect the way the copper-porphyrin system responds to light. However, in the mixed-solvent system, the researchers found that a THF molecule can become attached temporarily through the copper atom to the porphyrin ring. The result is the formation of an excited porphyrin in which the bonds between the copper atom and the porphyrin ring are stretched (Fig. 1). The formation of such a “pyramidal” shaped, short-lived excited chemical species provides new insights into earlier spectroscopic studies—such as lifetimes of the excited state and photoluminescence quantum yields—and will help researchers with the design of new versions of the basic structure that have particular absorption properties. —
David Bradley

See: L.X. Chen, G.B. Shaw, T. Liu, G. Jennings, and K. Attenkofer “Exciplex Formation of Copper(II) Octaethylporphyrin Revealed by Pulsed X-rays,” *Chem. Phys.* **299**, 215 (2004).

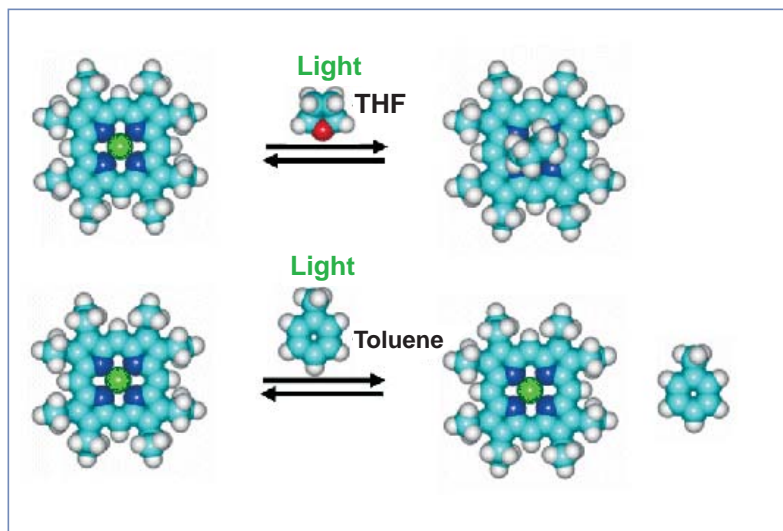


Fig. 1. Photoinduced ligation of excited-state CuOEP with solvent molecules studied by time-domain X-ray absorption. Top: Formation of the THF-CuOEP adduct at the photoexcited state. Bottom: The adduct does not form with toluene even at the photoexcited state of CuOEP.

Author Affiliations: Argonne National Laboratory
Correspondence: lchen@anl.gov

Work supported by the Division of Chemical Sciences and Materials Science, Office of Basic Energy Sciences, U.S. Department of Energy (DOE) under Contract No. W-31-109-ENG-38. Use of the Advanced Photon Source was supported by the U.S. DOE, Office of Science, Office of Basic Energy Sciences under Contract No. W-31-109-ENG-38.

BRINGING SENSORS INTO THE FOLD



A new class of sensors for important biomolecules, pollutants, and compounds relevant to defense is on the horizon, thanks to studies of the way proteins fold into their active shape. Researchers from the University of California, Santa Barbara; Stanford University; The University of Chicago; Argonne National Laboratory; Princeton University; and The Johns Hopkins University used BESSRC/XOR beamline 12-ID and Bio-CAT beamline 18-ID at the APS and beamline 4-2 at the Stanford Synchrotron Radiation Laboratory to probe the nature of the random coiling of proteins and to compare the dimensions of these coils with chemically unfolded proteins. Their research offers important clues about the behavior of these proteins, which appear to have random structures. These results will advance efforts to exploit proteins in real-time optical and electronic sensors for the biotechnology industry and in biomedicine.

Previous research using various spectroscopic techniques, such as nuclear magnetic resonance (NMR) spectroscopy, led to the tantalizing conclusion that many proteins can keep their shape even under chemical conditions that would quickly denature, or break down, the structure of lesser proteins. For instance, NMR showed that even in urea or guanidine hydrochloride, two strongly denaturing chemical reagents, several proteins display ordered structure. These findings suggested that this residual structure might play a role

in the initial folding kinetics and thermodynamics of certain proteins.

However, small-angle x-ray scattering studies appear to give a different picture of these proteins, revealing them as behaving in certain respects as random coils completely devoid of any organized structure.

The group hoped to explain this discrepancy by using a detailed study of several proteins that, it has been claimed, were robust in withstanding denaturation. If there were residual struc-

ture, as the spectroscopic studies suggested, then the dimensions of these tough proteins would not follow the same rules as a randomly coiled peptide chain. A hallmark of random-coil behavior is a power-law relationship between peptide chain length and the ensemble average radius of gyration.

There is a highly characteristic relationship between the length of a polymer and the dimensions of the bundle it forms. This power-law relationship can be used to distinguish between a random coil and a coil with structure. A simple analog would be to take the mean distance between the two ends of a piece of yarn floating in a swimming pool; they will naturally increase for longer pieces of yarn. But, if the yarn is wrapped into a tight ball, the end-to-end distance will be related to the cube-root of the length of the piece of yarn. If, on the other hand, the yarn is unwound and adopts an expanded, random structure, the increase in end-to-end distance will follow, not the cube-root, which would be to the $1/3$ power, but instead to the 0.588 power. This 0.588-power rule holds for any fully random polymer, whether a length of yarn or a sub-microscopic protein molecule.

The group investigated 28 proteins that had a claim to denaturation resilience and found that only two deviated from the expected 0.588 behavior of a random coil. If there were true resilience, one would expect all of the proteins to deviate significantly from this relationship.

Their data suggest that, if there is residual structure in the unfolded states—structure that might guide the folding process—it is too subtle to affect the mean overall dimensions of the unfolded state. This should put strong constraints on our mental model of the unfolded state and should have profound consequences for our understanding of folding.

A clearer understanding of protein folding could ultimately allow scientists to develop simple and efficient sensors based on the folding of proteins, peptides, and DNA when they come into contact with compounds of interest in a sample. Indeed, the motivation for this research was the research group's efforts to build optical sensors based on the binding-induced folding of

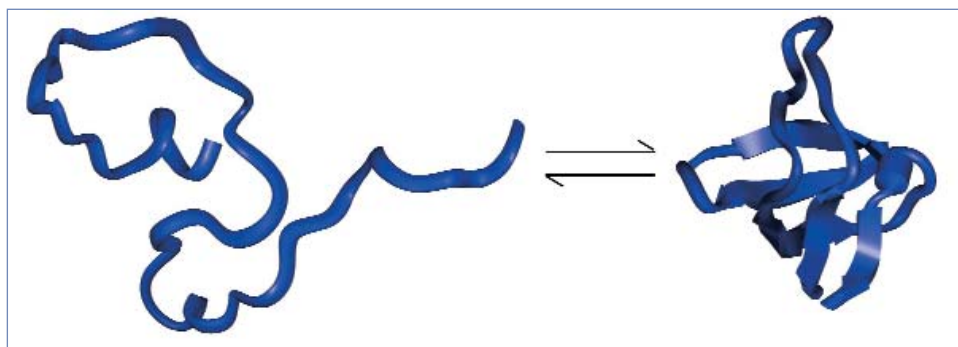


Fig. 1. Understanding the power of protein folding could lead to a new class of medical and environmental sensor.

normally unfolded proteins. If the unfolded state is truly random, then this binding-induced folding represents the largest possible change in protein conformation (from random to perfectly structured), suggesting an ideal means of coupling binding events with optical or electronic outputs.

Sensors based on this behavior would be inexpensive and easy to use and so might allow sensor technology to become more readily accessible in home testing kits and in the developing world. — David Bradley

See: J.E. Kohn¹, I.S. Millett², J. Jacob^{3,4}, B. Zagrovic², T.M. Dillon¹, N. Cingel¹, R.S. Dothager³, S. Seifert⁴, P. Thiyagarajan⁴, T.R. Sosnick³, M.Z. Hasan⁵, V.S. Pande², I. Ruczinski⁶, S. Doniach², and K.W. Plaxco^{1,2}, "Random-Coil Behavior and the Dimensions of Chemically Unfolded Proteins," *P. Natl. Acad. Sci. USA* **101**, 12491 (2004).

Author Affiliations: ¹University of California, Santa Barbara, ²Stanford University, ³The University of Chicago, ⁴Argonne National Laboratory, ⁵Princeton University, ⁶The Johns Hopkins University

Correspondence: kwp@chem.ucsb.edu

This research was supported by the National Institutes of Health (K.W.P. and V.S.P.), the Packard Foundation Interdisciplinary Science Program (T.R.S. and P.T.), and a faculty innovation award from The Johns Hopkins University (to I.R.). Use of the Advanced Photon Source was supported by the U.S. Department of Energy, Office of Science, Office of Basic Energy Sciences, under Contract No.W-31-109-ENG-38.



FINDING ACTIVE PROTEINS

When combinatorial chemistry produces new varieties of reagents, the tricky next step is figuring out whether those molecules will be biochemically active. While there are several methods for finding active molecules, they all have limitations. Researchers from Argonne National Laboratory, using the Bio-CAT beamline 18-ID, employed wide-angle x-ray scattering (WAXS) to develop a method for identifying drug candidates.

One way to identify active molecules is to design an assay for the desired function of a protein target and then test each small molecule variant. This approach is labor intensive and time consuming because it means that a different assay must be developed for each drug target of interest. Another approach is based on deriving a more general probe that would identify whether any protein structural change had occurred. A large number of samples could be screened in this way; those that showed promise could then be examined more closely for mechanistic details. Just such a general method, which uses x-ray scattering to detect functional drug candidates, is now available.

The APS served as a unique resource to aid the investigators in their study of WAXS of proteins in solution. The researchers are developing WAXS as a probe for detecting the structural changes that usually occur when a protein binds to a

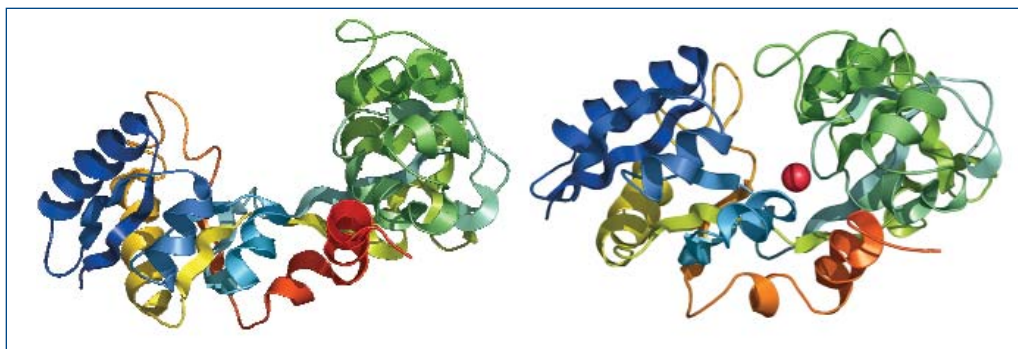


Fig. 1. Computer renditions (PyMOL) of the apo form of the protein transferrin (left) and the iron bound form (right) based upon crystallographic coordinates. From this angle, one can see the great extent to which the protein domains rotate relative to one another upon ligand binding.

functional ligand. Such activity encompasses a broad range of changes in secondary, tertiary, and quaternary structure of the protein. Although nuclear magnetic resonance can be used to characterize proteins in solution, this method requires extensive data collection and analyses. Small-angle x-ray scattering (SAXS) allows researchers to observe changes in the radius of gyration, but not all domain rotations and none of the small

side-chain interactions. Using the WAXS technique, data can be collected quickly and accurately using label-free ligands and targets, making the method well suited to moderate-throughput detection and analysis of protein-ligand interactions. The data collected permits direct estimate of the magnitude of the structural change, without reference to crystallographic coordinates. Although the exact form of the structural change at atomic resolution cannot be inferred from WAXS, both the magnitude and the class of

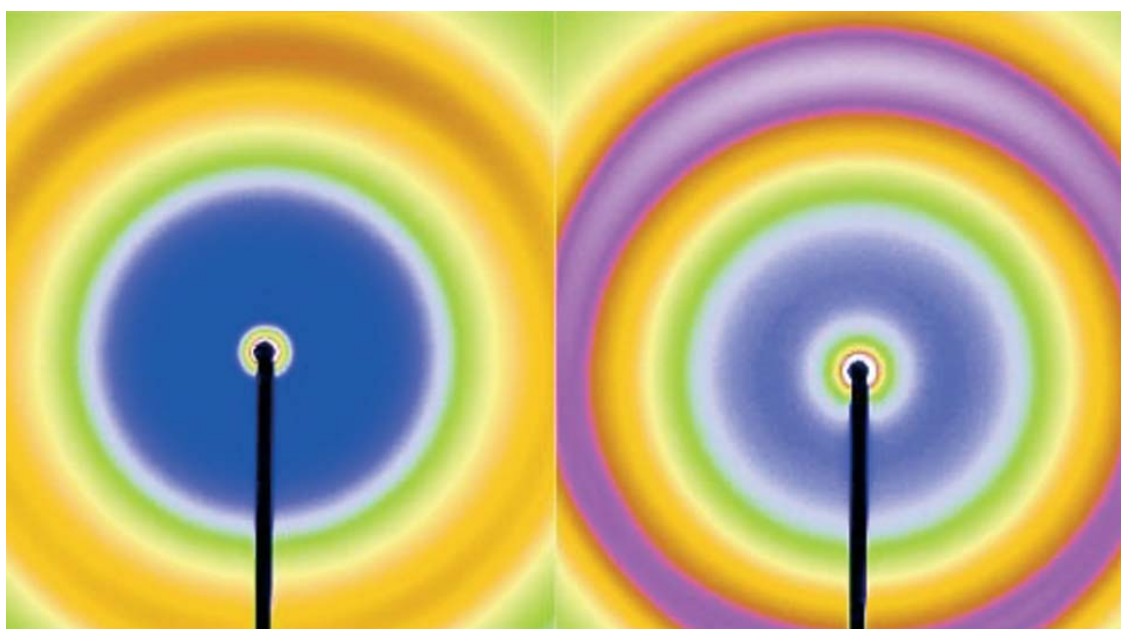


Fig. 2. False color images of the solution scattering patterns from the apo and ligand-bound forms of transferrin, highlighting the differences in diffraction between the structures.

the change can be elucidated. Even without crystallographic data, a combination of SAXS and WAXS has the potential to characterize what happens during ligand binding. As proof of concept, the data demonstrate that WAXS is a sensitive probe for identifying functional ligands through ligand-induced structural changes.

Using proteins in solution, five classes of structural change were studied: transferrin for ligand-induced domain rotation, maltose binding protein for hinge-bending motion, alcohol dehydrogenase for change of the shape of the binding cleft, calmodulin for ligand-induced refolding, and adipocyte lipid binding protein and ricin for side chain reorientations. To minimize damage to the proteins, thin aluminum foils were used as x-ray beam attenuators to control the incident beam flux. Protein concentrations ranged between 12.6 and 48 mg/mL. As a validation, the program CRY SOL was used to predict WAXS patterns from the proteins, using the atomic coordinates from the crystallographic structures.

The data showed that ligand-induced structural changes involving domain movements, as well as smaller ones (such as side chain rearrangements) are detected by WAXS, an *in vitro* biophysical probe. For the most part, measured scattering was in agreement with that predicted by applying the CRY SOL software to the atomic coordinates (Fig. 1). Ligand-induced domain movements, however, were larger than predicted on the basis

of x-ray crystallography alone, consistent with a previous finding that crystal-lattice domain positions may differ from those observed in solution (Fig. 2).

When binding a ligand, most proteins undergo some change in conformation, either local or global. Collecting the necessary WAXS data to characterize these changes takes about 30 s at a third-generation synchrotron source and can be carried out with a wide range of solution conditions for protein-ligand pairs, which do not have to be chemically modified. As such, WAXS can greatly improve the speed and accuracy with which drug candidates can be assessed for their therapeutic potential, enhancing the drug development process. — *Mona Mort*

See: R.F. Fischetti, D.J. Rodi, D.B. Gore, and L. Makowski, "Wide-Angle X-ray Solution Scattering as a Probe of Ligand-Induced Conformational Changes in Proteins," *Chem. Biol.* **11**, 1431 (October 2004).

Author Affiliation: Argonne National Laboratory
Correspondence: lmakowski@anl.gov

This work was supported by the Office of Biological and Environmental Sciences, DOE, to D.J.R.; NCRR, NIH, for Bio-CAT as a Health-supported Research Center. Use of the Advanced Photon Source was supported by the U.S. Department of Energy, Office of Science, Office of Basic Energy Sciences, under Contract No. W-31-109-ENG-38.

TRACKING THE CHEMISTRY WITHIN LIVING BACTERIA

Using a tiny device that focuses x-rays much as a lens focuses light, researchers from Argonne National Laboratory, Wichita State University, the University of Notre Dame, and the University of Southern California, working at the APS, have mapped the distributions of phosphorous, calcium, and other elements within a single hydrated bacterium. The measurements performed at beamline XOR 2-ID at the APS open the way for directly studying chemical interactions in and around bacteria. In particular, the technique might reveal how some bacteria bind toxic heavy metals into mineral deposits—a phenomenon that might be exploited to combat the spread of underground pollution.

To see precisely how an individual bacterium ticks, researchers must determine how different chemical elements are distributed within it. Techniques employing electron or proton beams possess the resolution to detect nanometer-sized features inside the cell and distinguish one element from another. However, these techniques work only in high vacuum, which kills the cells and can alter the distribution of elements. In contrast, the x-ray technique enables investigation of hydrated cells in their natural state.

Key to the technique is a device called a phase zone plate that works like a lens for x-rays. But whereas an ordinary lens relies on refraction to bend rays of visible light, the zone plate focuses x-rays through diffraction. Measuring 150 microns in diameter, the zone plate consists of gold etched into an elaborate bull's-eye pattern of concentric rings, or

zones, of various widths. When x-rays pass through the plate at a particular point, they experience a phase shift; the size of the shift depends on the thickness of the plate at that location. Thanks to the various phase shifts, the x-rays emerging from the other side of the plate will interfere in a way that focuses them in a spot 150 nanometers wide.

The researchers used these tightly focused x-rays to study *Pseudomonas fluorescens*, a bacterium commonly found in wetlands, water columns, and lakes. Fixing the x-ray energy at 10 keV, the researchers first scanned their tiny x-ray spotlight back and forth across samples of individual bacteria harvested from a suspension and bacteria growing in a film, their natural state. The high-energy x-rays excited inner-shell electrons in the various atoms inside and around the cells, which then fluoresced as outer-shell electrons fell into the vacancies. By track-

Continued on next page

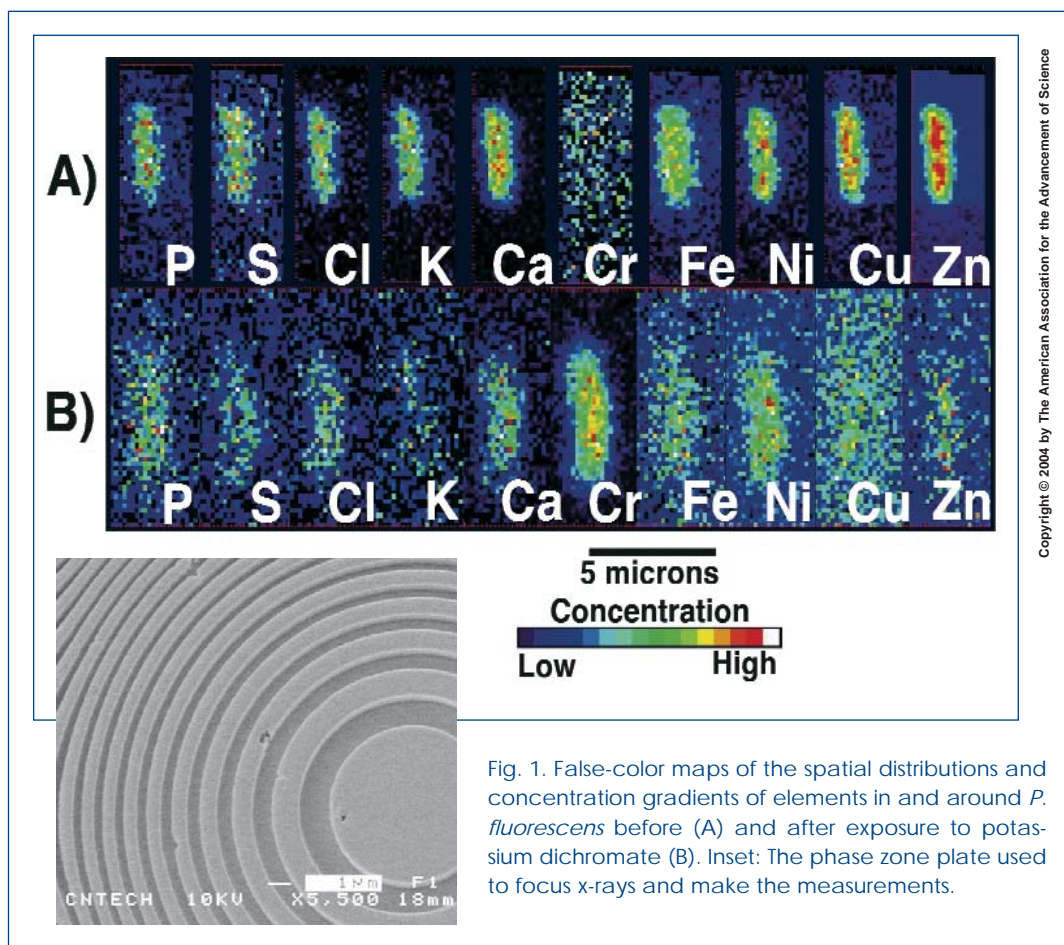


Fig. 1. False-color maps of the spatial distributions and concentration gradients of elements in and around *P. fluorescens* before (A) and after exposure to potassium dichromate (B). Inset: The phase zone plate used to focus x-rays and make the measurements.

ing and analyzing the fluorescence, the researchers found that they could locate individual cells and map the distribution of elements—ranging from lightweight phosphorous and sulfur to hefty copper and zinc—within them.

The researchers also examined samples of bacteria that had been exposed to the ion chromium-VI, a carcinogen and potent toxin. The chromium permeated and killed the isolated cells harvested from a floating suspension, but cells grown in a film did not absorb the toxin and continued to thrive. The chromium appeared to collect around the cells in the film, presumably in the cement of sugars the bacteria exuded to glue themselves to one another. To further study the fate of the chromium, the researchers fixed the x-ray beam on a chromium deposit and ramped the x-ray energy up slowly from about 6 keV. The precise energy at which the chromium began to fluoresce revealed its valance state and indicated that, through chemical interactions with the extra-cellular matrix, the chromium-VI was reduced to less pernicious chromium-III. In fact, the detailed shape of the “x-ray absorption near edge spectrum” indicated that the chromium was bound in a phosphate.

The measurements demonstrate that isolated bacteria do not necessarily behave in the same way as those grown in

films—an important caveat for microbiologists. The researchers now plan to turn their attention to bacteria that actively metabolize toxic metals. Such bacteria essentially breathe metal, and the new technique promises a breathtaking view of precisely how they do it. — *Adrian Cho*

See: K.M. Kemner¹, S.D. Kelly¹, B. Lai¹, J. Maser¹, E.J. O’Loughlin¹, D. Sholto-Douglas¹, Z. Cai¹, M.A. Schneegurt², C.F. Kulpa, Jr.³, and K.H. Neelson⁴, “Elemental and Redox Analysis of Single Bacterial Cells by X-ray Microbeam Analysis,” *Science* **306**, 686 (2004).

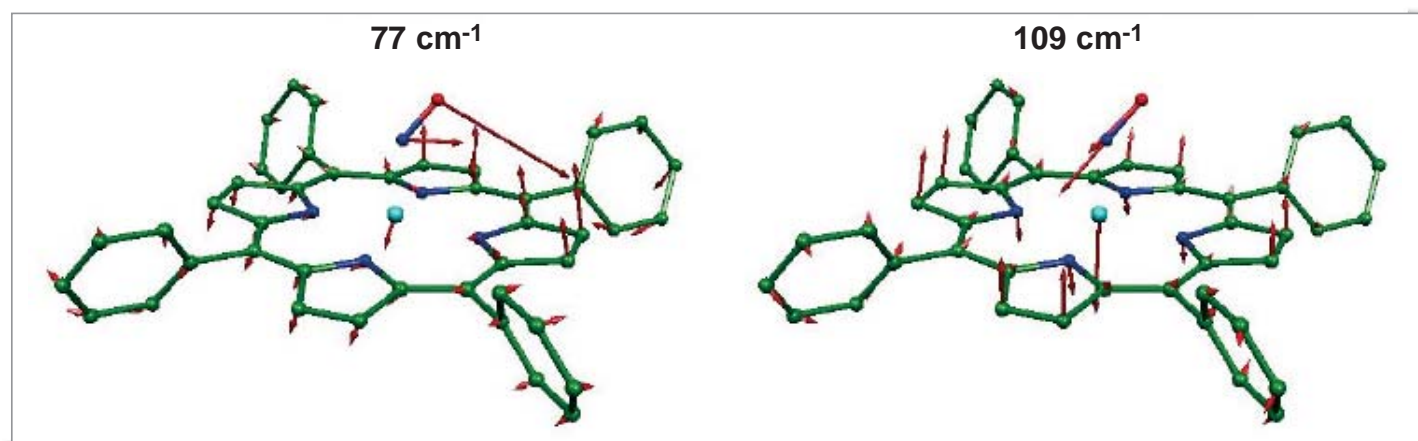
Author Affiliations: ¹Argonne National Laboratory, ²Wichita State University, ³University of Notre Dame, ⁴University of Southern California

Correspondence: kemner@anl.gov

This work supported by the Natural and Accelerated Bioremediation Research Program, Office of Biological and Environmental Research, Office of Science, U.S. Department of Energy. Additional support (K.M.K.) provided by the DOE Office of Science Early Career Scientist and Engineer Award. Use of the Advanced Photon Source was supported by the U.S. Department of Energy, Office of Science, Office of Basic Energy Sciences, under Contract No. W-31-109-ENG-38.

REBOUNDED ATOMIC NUCLEI TO PROBE LOW-FREQUENCY MOLECULAR VIBRATIONS

Unlike the rigid models chemistry students assemble from sticks and balls, real biomolecules readily flex and vibrate, and those vibrations may enable some molecules to perform their crucial tasks. But observing the low-frequency vibrations of jumbo biomolecules remains a challenge. X-ray measurements taken at XOR beamline 3-ID at the APS by researchers from Northeastern University, the National Research Council of Canada, the University of Notre Dame, Purdue University, and Argonne National Laboratory have revealed the low-frequency vibrations of molecules resembling heme proteins, which regulate blood pressure and enable blood to absorb oxygen. Combining the new spectroscopy with powerful computational techniques, researchers hope to deduce precisely how such molecules prefer to twist, bend, and stretch.



© 2004 American Chemical Society

A molecule will vibrate only at distinct frequencies, much as a soda bottle will resonate only certain tones if you blow across the top of it. To study molecular vibrations, researchers typically prod molecules with infrared light; the spectrum of the absorbed or scattered light then reveals the frequencies of the vibrations. Infrared techniques have limitations, however. The long wavelength light effectively interacts with all the atoms as a group. So while the techniques show that a molecule is rattling, they do not indicate how each individual atom is moving. Moreover, in accordance with quantum mechanical selection rules, infrared photons will only excite vibrations when the atoms move in patterns with certain symmetries.

To overcome such impediments, the research team employed an x-ray technique that excites a single atomic nucleus in a biomolecule. Known as nuclear resonance vibrational spectroscopy (NRVS), the technique works a bit like the famed Mössbauer effect, in which a nucleus embedded in a crystal can absorb x-rays of a very specific energy without recoiling. In NRVS, the targeted nucleus does recoil, but it can only do so by causing the entire molecule to vibrate. That means that an x-ray must pack precisely enough extra energy to excite a vibration, which according to quantum mechanics, is just Planck's constant times the frequency of vibration. The atom eventually emits an x-ray again, and by tracking such fluorescence as a function of x-ray energy, researchers can determine the molecule's vibrational spectrum. Moreover, the x-rays

Fig. 1. Low-frequency vibrations involve the same motions that take place on binding of the dumbbell-shaped NO molecule to the planar heme molecule. These motions include reorientation of the NO (left) and "doming" of the heme (right), where the heavy central iron atom moves out of the plane and the rest of the molecule flexes like a trampoline responding to a dropped cannonball.

can excite any mode in which the targeted nucleus moves, regardless of the mode's overall symmetry.

Using NRVS, the team studied the vibrations of disk-like molecules known as ferrous nitrosyl porphyrins, which resemble the reactive heart of heme proteins. The core of the porphyrin molecules consists of an iron atom surrounded by four pyrrole rings joined edge to edge like scales on a turtle shell. A nitrosyl group (NO) attaches to the iron and sticks up from the plane of the molecule. Taking advantage of a monochromatic x-ray beam with a flux 10^9 photons per second and an energy spread of 0.85 meV (in wavenumbers, 7 cm^{-1}), the researchers studied the fluorescence of both powder samples and samples consisting of many aligned crystals as they probed energies up to 75 meV (600 cm^{-1}) above the 14.413 keV resonance of the ^{57}Fe nuclei. They compared the observed spectra to those predicted by density functional theory, a computer-based technique that enables the calculation of the structure and dynamics of molecules. The researchers found they could match the spectra and identify several of the low-frequency vibrations of the molecules.

Continued on next page

In particular, the researchers observed low-frequency vibrations in which the iron nucleus moves in the plane of the molecule, which generally cannot be seen with infrared techniques. They also identified the “doming” mode, in which the disk like molecule bows like a rounded hubcap. Such motion may help control the reactions of iron in heme proteins with diatomic molecules such as nitric oxide, whose interactions with heme control blood pressure. The close agreement between the calculated and measured spectra suggest that by combining NRVS and density functional theory, researchers may be able to determine the spring constants and other dynamical parameters of biomolecules, which could help reveal precisely how the molecules function. That’s nothing to shake a stick at—or an atomic nucleus, either. — *Adrian Cho*

See: B.M. Leu¹, M.Z. Zgierski², G.R.A. Wyllie³, W.R. Scheidt³, W. Sturhahn⁴, E.E. Alp⁴, S.M. Durbin⁵, and J.T. Sage¹, “Quantitative Vibrational Dynamics of Iron in Nitrosyl Porphyrins,” *J. Am. Chem. Soc.* **126**, 4221 (2004).

Author Affiliations: ¹Northeastern University; ²Steacie Institute for Molecular Science, National Research Council of Canada; ³University of Notre Dame; ⁴Argonne National Laboratory; ⁵Purdue University

Correspondence: jtsage@neu.edu

This work supported by National Science Foundation grants 0240955 (J.T.S.) and 9988763 (S.M.D.) and National Institutes of Health grants GM-52002 (J.T.S) and GM-38401 (W.R.S.). Use of the Advanced Photon Source supported by the Department of Energy, Basic Energy Sciences, Office of Science, under Contract No. W-31-109-ENG.

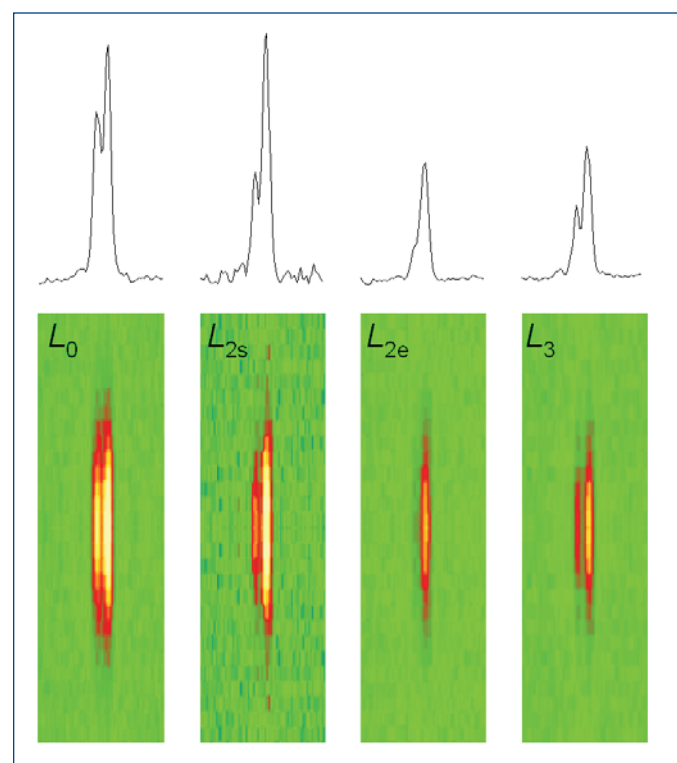
MEASURING THE EFFICIENCY OF THE MYOSIN MOTOR AT HIGH LOAD

The sliding filament model of muscle contraction is more than 50 years old, yet theories about the precise mechanisms of the motor function still generate some controversy. A group of researchers from Università di Firenze, Istituto Nazionale di Fisica della Materia, Brandeis University, King’s College London, the European Synchrotron Radiation Facility, Illinois Institute of Technology, and Argonne National Laboratory used insertion device beamlines at Bio-CAT at the APS and at the European Synchrotron Radiation Facility (ESRF) to take a closer look at the molecular structure of myosin II, the molecular motor in muscle, as it works under different loads. This study provides a more detailed understanding of the complex process responsible for the efficient chemomechanical transduction of energy.

Myosin II is a class of proteins found in skeletal muscle and heart cells. Myosin molecules aggregate to form the thick myosin filament, with the heads of the molecules protruding periodically from the filament. Myosin filaments overlap with the actin filaments in the 2.1- μm sarcomere, the elementary contracting structure in muscle. During contraction, the myosin heads act as tiny motors, drawing the thin actin filament toward the center of the sarcomere and then detaching from actin and returning to the original conformation, ready for another stroke cycle.

Studies using *in vitro* samples of muscle tissue have produced variable results in measuring the size of the stroke produced by the intermittent binding of myosin to actin. These puz-

Fig. 1. Two-dimensional (2-D) patterns in the region of the M3 reflection recorded on a charge-coupled device detector at the Bio-CAT beamline with 3-m camera-to-sample distance, normalized by X-ray exposure time. Total exposure times: L_0 , 25 ms; L_{2s} , 5.5 ms; L_{2e} , 21 ms; and L_3 , 25 ms. Fiber cross-sectional area equals $38 \cdot 10^3 \mu\text{m}^2$; isometric tension equals 230 kPa; sarcomere length equals 2.16 μm . On the top are shown the intensity profiles obtained by integrating 80 pixels on each side of the meridional axis of the 2-D patterns.



zing results are likely attributable to the nature of the samples, which do not retain their natural structure and function and thus are inaccurate measurements of events in a muscle fiber in actual physiological conditions.

To produce a more precise view of these molecular interactions, researchers have recently used an x-ray diffraction technique to measure the size of the working stroke *in vivo*, by using intact frog skeletal muscle cells. The researchers directed parallel synchrotron x-ray beams to the muscle cell. This produces a strong reflection called M3, which comes from the 14.5-nm repeat of the myosin heads along the filament (Fig. 1). The x-ray interference originating from the two arrays of myosin heads in each sarcomere allows measurements of the axial motion of the motors with ~ 1 Å spatial resolution and submillisecond time resolution.

At the 18-ID (APS) and ID-2 (ESRF) beamlines, the researchers measured changes in intensity and in the fine structure of the reflection during three phases of the motor cycle elicited at three different loads: 0.25, 0.50, and 0.75 times the isometric force (T_0). To eliminate the damaging effect of radiation, which eventually caused the fibers to fail, the samples were displaced vertically a few hundred micrometers between each contraction. A steady isometric force was obtained by electric stimulation of the fiber at the proper frequency—ranging from 18 to 25 Hz at the 4°C used in these experiments. Then the force was suddenly reduced in a stepwise manner through a force feedback control. During the filament sliding that follows this step, the two interference peaks into which the M3 x-ray

reflection is split change their relative intensities. First R, the ratio of the high-angle peak over the low-angle peak, decreases; then R increases as the myosin heads detach and return to their original axial position.

The recovery of R occurs at ~ 6 nm with $0.75 T_0$ and at ~ 11 nm with $0.25 T_0$, showing that the axial motion that drives filament sliding is smaller at high loads.

These observations help explain the efficiency of muscle fibers at the molecular level. — *Elise LeQUIRE*

See: M. Reconditi¹, M. Linari¹, L. Lucii¹, A. Stewart², Y.-B. Sun³, P. Boesecke⁴, T. Narayanan⁴, R.F. Fischetti⁵, T. Irving⁶, G. Piazzesi¹, M. Irving³, V. Lombardi¹, "The Myosin Motor in Muscle Generates a Smaller and Slower Working Stroke at Higher Load," *Nature* **428**(6982), 578 (1 April 2004).

Author Affiliations: ¹Università di Firenze, ²Brandeis University, ³King's College London, ⁴European Synchrotron Radiation Facility, ⁵Argonne National Laboratory, ⁶Illinois Institute of Technology

Correspondence: vincenzo.lombardi@unifi.it

This work was supported by Ministero dell'Istruzione, dell'Università e della Ricerca, Telethon-945 (Italy), the National Institutes of Health (NIH, USA), the Medical Research Council (UK), the European Molecular Biology Laboratory, the European Union, and the European Synchrotron Radiation Facility. Bio-CAT is an NIH-supported research center. Use of the Advanced Photon Source was supported by the U.S. Department of Energy, Office of Science, Office of Basic Energy Sciences, under Contract No.W-31-109-ENG-38.

AROUND THE EXPERIMENT HALL



> Lisa Keefe (The University of Chicago), director of IMCA-CAT, in the 17-ID research station at the controls of the ACTOR robot for high-throughput protein crystallography.

< Kevin Battaile and Kathleen Favale (both The University of Chicago) dispensing liquid nitrogen to be used in preparing samples that will be loaded into the ACTOR robot.



IDENTIFYING CRITICAL ENZYMES IN PATHOGENIC BACTERIA

Bacteria continue to cause disease in humans, despite, or perhaps because of, decades of antibiotic therapy. Two serious pathogens are *Staphylococcus aureus*, a major cause of hospital infections, and *Bacillus anthracis*, an anthrax agent of major bioterrorism concern. Because new strains have emerged that are resistant to known antibiotics, there is an urgent need to develop new means of combating these bacteria. One approach is to study their cell surface proteins, such as the sortases, which possess exposed functional domains easily accessible to drugs. Sortases anchor other proteins to the cell surface and have shown promise as drug targets. New studies of the sortase B (SrtB) crystal structure have been carried out by researchers from Argonne National Laboratory and The University of Chicago using SBC-CAT beamline 19-ID. Their results provide badly needed details about how it behaves in *S. aureus* and *B. anthracis*, thus fueling the search for ways to inhibit growth of these bacteria.

Sortases play a role in attaching surface proteins to the cell wall envelope of the bacteria during infection. C-terminal signals direct sorting and attachment of these proteins. In *S. aureus*, SrtB recognizes a motif NPQTN, cleaves the protein after the Thr residue, and then attaches it to the pentaglycine cross bridges. In *B. anthracis*, SrtB recognizes the NPKTG motif and attaches surface proteins to m-diaminopimelic acid cross bridges. The crystal structure of SrtB from *S. aureus* was determined at 2.0 Å resolution and that of *B. anthracis* at 1.6 Å. The structures exhibit a feature—a β -barrel fold with α -helical elements on the outside—that have to date been identified only in the sortase family. On the edge of the β -barrel is a putative active site consisting of a Cys-His-Asp catalytic triad thought to face the bacterial cell surface. The data also reveal a nearby putative binding site for the sorting signal.

Chromosomal DNA of *S. aureus* (strain Newman) was used to produce Sa-SrtB ORF by PCR amplification. The resulting construct encoded a protein 216 amino acids long with a 20-residue His tag at its N terminus. In a similar manner, chromosomal DNA of *B. anthracis* (strain Sterne) was used to obtain Ba-SrtB ORF, a protein consisting of 242 amino acids with a 24-residue His tag at its N terminus. The constructs did not include the N-terminal signal peptide. Vapor diffusion and hanging droplets produced crystals of Sa-SrtB and Ba-SrtB at room temperature. The 19-ID beamline was used to collect diffraction data on the Se-Met-labeled protein crystals at 100K. For Sa-SrtB, the space group was $P2_12_12$ with cell dimension of $a = 71.208$ Å, $b = 104.367$ Å, $c = 58.087$ Å, $\alpha = \beta = \gamma = 90^\circ$. For Ba-SrtB, the space group was $P2_1$ with cell dimension of $a = 40.47$ Å, $b = 64.60$ Å, $c = 42.96$ Å, $\alpha = 90^\circ$, $\beta = 105.77^\circ$, $\gamma = 90^\circ$. Multiwavelength anomalous dispersion phasing was used to determine and refine the structures of Sa-SrtB and Ba-SrtB.

The resulting high-resolution crystal structures of Sa-SrtB and Ba-SrtB show a high degree of similarity. The Sa-SrtB monomer exhibits an α/β fold containing a central β -barrel decorated on the outside with several α helices. An eight-stranded β -barrel containing mainly antiparallel β strands forms the core of the protein, which in Ba-SrtB shows some disorder in the loop region. Some difference between Sa-SrtB and Ba-SrtB also exists in the N-terminal region. Both proteins contain a fold unique to the sortase family—a β -barrel in a novel “double banner” design. The active site of SrtB is thought to point toward the cell wall surface, with the edge of the β -barrel

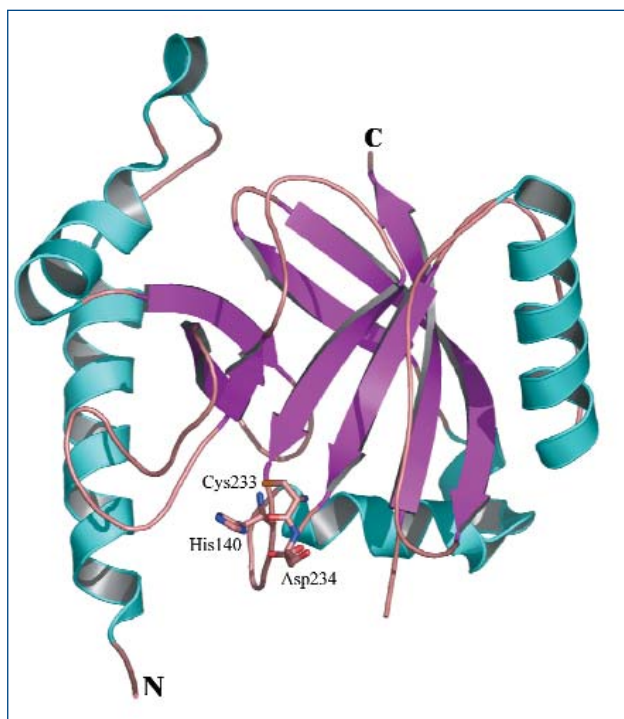


Fig. 1. The secondary structure diagram of Ba-SrtB; strands forming the barrel are in purple, helices are in aqua, loops and turns are in pink. N- and C-termini, as well as presumed active site residues in Ba-SrtB are labeled. The figure was prepared with PyMol.

containing a catalytic triad of Cys-His-Asp. The SrtB surface contains two grooves, in a V shape, that are potential substrate binding sites for the transpeptidation reaction.

The SrtB gene is located in the *isd* locus of staphylococci and other gram-positive bacteria, suggesting a capacity for heme-iron scavenging from hemoglobin that allows continued growth even in iron-restrictive mammalian tissues. Inhibiting SrtB could lead to insufficient decoration of the cell with surface proteins and subsequent decreased bacterial growth. With these new data on SrtB structure, and existing knowledge of its behavior, a detailed strategy for hindering pathogen success can now be undertaken. — Mona Mort

See: R. Zhang¹, R. Wu¹, G. Joachimiak¹, S.K. Mazmanian², D.M. Missiakas², P. Gornicki², O. Schneewind², and A. Joachimiak¹, "Structures of Sortase B from *Staphylococcus aureus* and *Bacillus anthracis* Reveal Catalytic Amino Acid Triad in the Active Site," *Structure* **12**, 1147 (July 2004).

Author Affiliations: ¹Argonne National Laboratory, ²The University of Chicago.

This work was supported by grants from NIH, NIGMS Protein Structure Initiative to A.J., D.M.M., and O.S.; by a University of Chicago-Argonne National Laboratory joint research grant; by the U.S. DOE, Office of Biological and Environmental Research; and by the Regional Center of Excellence in Biodefense and Emerging Infectious Diseases Program. Use of the Advanced Photon Source was supported by the U.S. Department of Energy, Office of Science, Office of Basic Energy Sciences under Contract No. W-31-109-ENG-38.

HIV FORCES THE IMMUNE SYSTEM OUTSIDE THE BOX

In the arms race between the human immunodeficiency virus (HIV) and the immune system, the virus usually comes out ahead. Studying the immune system's efforts, therefore, can reveal its most state-of-the-art weapons. Researchers from the National Institute of Allergy and Infectious Diseases and the National Cancer Institute at the National Institutes of Health; Columbia University; Brigham and Women's Hospital, Children's Hospital, the Dana-Farber Cancer Institute, and the Harvard School of Public Health at Harvard University; and the Tulane University Medical Center using the SER-CAT beamline 22-ID at the APS and the National Synchrotron Light Source (NSLS) have now solved the three-dimensional structures of a handful of antibodies that recognize HIV by mimicking the virus's point of entry into cells, resulting in some unique features. The group carrying out this study notes that the result highlights our immune system's extraordinary adaptivity in the face of a constantly changing foe.

The human immunodeficiency virus succeeds in confusing the legions of antibodies that scour the bloodstream in search of foreign agents. But one component that HIV can't hide completely is the sugar-covered protein gp120, which venture outside the envelope to bind so-called "co-receptors" on the surface of immune cells. Although HIV constantly varies and masks the structure of gp120, some antibodies manage to recognize the protein's binding site, although most of them are poor at stopping the virus. The researchers had already solved the structure of one of these antibodies and found that its binding site is highly acidic, as is the co-receptor on immune cells that grants access to HIV. To see if the other antibodies have similar features, the group analyzed the amino acid sequences of 12 gp120-binding antibodies isolated from five HIV-infected individuals.

The antibodies are highly selected to mimic the HIV co-receptor, the group reported. Seven of the 12 contain a sulfate group on their primary binding site—the same sulfate modification that decorates the cellular co-receptor (Fig. 1). The cell adds sulfate groups to a small percentage of proteins after it has synthesized them, but researchers had never before seen an antibody with such a modification. In three of the sulfated antibodies, removal of the sulfate group greatly reduced their ability to bind HIV, indicating that sulfation and perhaps direct co-receptor mimicry are key to binding. The other four, however, bound HIV equally well with or without the sulfate group. In explanation, the researchers note that HIV's co-receptor contains a highly negatively charged amino acid sequence that causes the cell to deposit a sulfate there. The researchers propose that in mimicking the cell receptor, the antibodies must adopt a similar sequence, which tends to attract sulfate but may be sufficient on its own to recognize the virus protein.

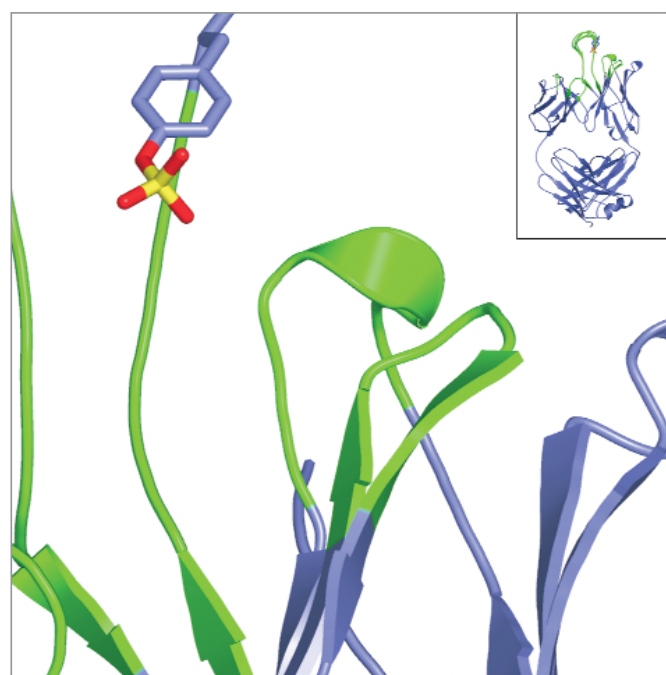


Fig. 1. Atomic details (main) of the binding fragment (insert) of the HIV-recognizing antibody 412d. A sulfate group (yellow, red) is attached to a tyrosine residue (blue). Mutation of the tyrosine to phenylalanine reduces 412d's ability to bind the HIV protein gp120.

Another unusual feature of the sulfated antibodies is that they all share the same "VH" gene, one of the genes that encodes their binding site. An antibody's binding site is made from the mixing and matching of dozens of genes. Such highly

Continued on next page

specific genetics is out of the ordinary and suggests that the gene contributes strongly to the antibodies' specificity for the virus. To determine the structure of the binding site at the VH region, the group crystallized five of the antibodies and determined their structures based on x-ray diffraction studies performed on the 22-ID and X4A beamlines. Of the 50 different VH genes that an antibody might contain, only the gene these antibodies share leads to a small, water-averse protuberance on the binding site that seems to be important for binding HIV.

The group is continuing to examine the structures of antibodies that neutralize HIV, which may reveal other peculiarities and suggest ways to develop an effective HIV vaccine.

— *JR Minkel*

See: C.-c. Huang¹, M. Venturi¹, S. Majeed^{1,2}, M.J. Moore³, S. Phogat⁶, M.-Y. Zhang⁶, D.S. Dimitrov⁶, W.A. Hendrickson², J. Robinson⁷, J. Sodroski^{5,8}, R. Wyatt^{1,5}, H. Choe⁴, M. Farzan², P.D. Kwong^{1,2}, "Structural Basis of Tyrosine Sulfation

and V_H-gene Usage in Antibodies that Recognize the HIV Type 1 co-receptor-binding Site on gp120," P. Natl. Acad. Sci. USA **101**(9), 2706 (2 March 2004).

Author Affiliations: ¹National Institute of Allergy and Infectious Diseases, National Institutes of Health; ²Columbia University; ³Brigham and Women's Hospital; ⁴Children's Hospital; ⁵Dana-Farber Cancer Institute; ⁶National Cancer Institute, National Institutes of Health; ⁷Tulane University Medical Center; ⁸Harvard School of Public Health

Correspondence: pdkwong@nih.gov

These studies were supported by grants from the National Institutes of Health. P.D.K. was a recipient of a Burroughs Wellcome Career Development Award. J.S. was supported by a Bristol-Myers Squibb research grant and by the International AIDS Vaccine Initiative. Beamline X4A at the National Synchrotron Light Source, a Department of Energy facility, was supported by the Howard Hughes Medical Institute. Use of the SER-CAT beamline and the APS was supported by the U.S. Department of Energy, Office of Science, Office of Basic Energy Sciences, under Contract No. W-31-109-ENG-38.

STRUCTURE OF A POSSIBLE DRUG TARGET FOR THE COMMON COLD

Researchers from Pfizer Global Research and Development have cracked the first three-dimensional structures of a protein that allows the common cold virus to reproduce. The group crystallized the RNA polymerase enzyme, which copies the viral genome, from three different strains and determined each structure via x-ray diffraction of the crystallized enzymes at the IMCA-CAT beamline 17-ID at the APS and beamline 5.0.1 at the Advanced Light Source. The structures are similar to those found in analogous proteins from other viruses, including polio and hepatitis C. The researchers say the result could aid in the design of antiviral drugs to combat the common cold.

The cold has defied vaccination because it is caused by many different strains of the same virus, called rhinovirus, and vaccines against one strain work poorly against others. An alternative strategy to keep the cold at bay is to develop antiviral drugs that kill the virus or stop its growth, analogous to antibiotics for bacterial infections. Researchers have tested a few such anti-rhinovirus compounds in human cells grown in the lab, but they are still looking for the best part of the virus to attack. One attractive potential drug target is RNA polymerase, because it plays two roles in copying the rhinovirus genome. In one role, it slides along an existing copy of the viral genome—namely, a single strand of RNA, which is similar to DNA—and constructs a complementary RNA strand one piece at a time. (RNA is a polymer, or string, of building blocks called nucleotides. The enzyme builds RNA molecules; hence "polymerase.") In its other role, the RNA polymerase prepares a protein that attaches to the genome and serves as a starting point for the copying process.

Rhinovirus RNA polymerase has the typical structure of enzymes that copy DNA and RNA (Fig. 1). The Pfizer group examined polymerase from three strains, including representatives of both major types of rhinovirus. All three structures are highly similar, resembling a right hand curled into an "O" shape,

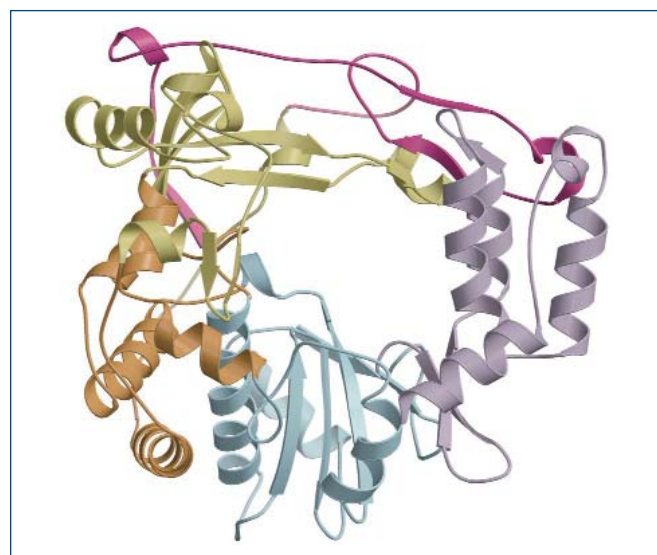


Fig. 1. The structure of the RNA polymerase of human rhinovirus, which causes the common cold, looks like a curled up right hand, made of thumb (purple), palm (blue) and fingers (orange, pink, gold) domains.

with distinct regions serving as thumb, palm, and fingers. The structure is most similar to the polymerase of poliovirus, which is closely related to rhinovirus.

The enzyme's active site, or the place where it catalyzes the fusion of a nucleotide to the growing RNA, lies in the palm. The reaction requires two magnesium ions in the active site. Although the researchers could not get the enzyme to crystallize with magnesium ions present, one structure contains an ion of samarium (an element used to solve the crystal structure) where a magnesium ion should be. The overall shape of the structure with samarium is the same as the others without it—implying that no large changes accompany metal binding. The thumb and fingers of the rhinovirus enzyme bind tightly, and this interaction may provide the rigidity that seems apparent in all RNA polymerases of this type.

A structure of the enzyme attached to an RNA molecule would be needed to determine whether it can bind an old RNA and elongate a new one in its observed state. Nevertheless, the Pfizer investigators modeled the enzyme bound to RNA based on the structure of the human immunodeficiency virus poly-

merase. The modeled RNA molecule does not clash with the enzyme, indicating a potential fit. The rhinovirus polymerase contains a bent structure called a “beta hairpin” between the palm and fingers, which is unique among enzymes of this type and may serve as a guide for the RNA molecule. — *JR Minkel*

See: R.A. Love, K.A. Maegley, X. Yu, R.A. Ferre, L.K. Lingardo, W. Diehl, H.E. Parge, P.S. Dragovich, and S.A. Fuhrman, “The Crystal Structure of the RNA-Dependent RNA Polymerase from Human Rhinovirus: A Dual Function Target for Common Cold Antiviral Therapy,” *Structure* **12**, 1533 (August 2004).

Author Affiliation: Pfizer Global Research and Development
Correspondence: robert.love@pfizer.com

The Advanced Light Source is supported by the Director, Office of Science, Office of Basic Energy Sciences, Materials Sciences Division, of the U.S. Department of Energy under Contract No. DE-AC03-6SF00098 at Lawrence Berkeley National Laboratory. The IMCA-CAT facilities are supported by the companies of the Industrial Macromolecular Crystallography Association. Use of the Advanced Photon Source was supported by the U.S. Department of Energy, Office of Science, Office of Basic Energy Sciences, under Contract No. W-31-109-ENG-38.

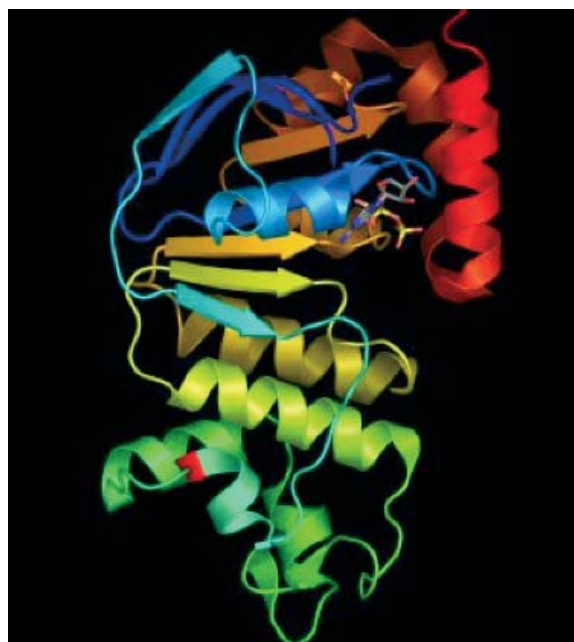
LINKING PROTEIN STRUCTURE AND CYSTIC FIBROSIS

Cystic fibrosis is a debilitating disease that causes malfunction of the lungs, liver, pancreas, and reproductive tract, typically leading to death by middle age. Knowing more about which cellular changes cause the disease would greatly aid the search for drugs to combat its effects. Deletion of a single amino acid in a membrane channel protein is known to cause cystic fibrosis, and the mechanism by which it does so was thought to be understood. However, new data collected by researchers from Structural GenomiX, Inc., Columbia University, and The Johns Hopkins University using the SGX-CAT 31-ID beamline at the APS are surprising in that they show the mutant protein to behave in a completely different way than previously proposed. These new data suggest promising ways in which to use pharmaceuticals against cystic fibrosis.

The research group in this study determined the crystal structure of the first nucleotide-binding domain (NBD1) of the human cystic fibrosis transmembrane conductance regulator (CFTR) containing deletion of residue F508 (Δ F508). This mutation in CFTR causes cystic fibrosis, presumably by reducing the number of functional channels at the epithelial cell surface. Previous studies, which used incomplete NBD1 domains, implicated abnormal folding of the mutant protein as the reason for the malfunction. In studying the complete NBD1 domain, however, the current research shows little change in protein folding but marked changes in surface topography at the site of the deletion. Because the deletion is in the region of NBD1 that is thought to interact with the first membrane-spanning domain of CFTR, the new results suggest the main effect of Δ F508 to be that of preventing proper interactions between CFTR domains.

Continued on next page

Fig. 1. Ribbon diagram of human NBD1. The region where Phe 580 is deleted is shown as a red patch in the lower left of the figure. Bound adenosine triphosphate, thought to participate in the regulation of CFTR, is shown as wireframe in the upper right.



Accompanying biophysical studies support this new model, which can now be used in designing pharmaceuticals effective against cystic fibrosis. The research also revealed that so-called suppressor mutations at a second site might work to compensate for the F508 mutation by increasing NBD1 folding efficiency in the full-length protein.

Human NBD1 (hNBD1) proteins, with and without the Δ F508 mutation, were expressed in *E. coli*, purified, and crystallized at 4°C. Crystals in space group C222₁ (protein without Δ F508 mutation, five molecules per asymmetric unit) and in space group P4₃2₁2 (protein with Δ F508 mutation, one molecule per asymmetric unit) were obtained by hanging drop vapor diffusion. The SGX-CAT 31-ID beamline was used to measure diffraction data. Equilibrium denaturations and tryptophan fluorescence measurements allowed observation of thermodynamic stability and folding mechanisms.

The high-resolution diffraction data acquired for the hNBD1 crystals showed that the protein has similar folding patterns, with or without the Δ F508 deletion (Fig. 1). The surface topography and chemical properties were markedly different, however, at this critical site where the domains interact, providing a possible explanation of how the deletion exerts its lethal effect. The equilibrium denaturation studies showed no apparent change in the *in vitro* stability of hNBD1 in the presence or absence of the Δ F508 mutation. The biophysical studies of intact hNBD1 domains were consistent with the structural data, showing only minor differences in folding for the mutant molecule. In contrast, biophysical studies of the suppressor muta-

tions showed that they may significantly enhance folding of NBD1 *in vitro*. Further work will be needed to show whether the folding effect explains how suppressor mutations improve CFTR efficiency *in vivo*.

The disruption of interdomain interactions could be related to the altered gating properties previously reported for Δ F508 CFTR channels. This effect might also be responsible for known malfunctions in the endoplasmic reticulum that are associated with cystic fibrosis. Designing a small molecule that could “correct” the Δ F508 mutation by reinforcing interdomain interactions in CFTR would be one possible pharmaceutical treatment for cystic fibrosis. These new data greatly advance the search for effective treatment of the disease. — *Mona Mort*

See: H.A. Lewis¹, X. Zhao¹, C. Wang², J.M. Sauder¹, I. Rooney¹, B.W. Noland¹, D. Lorimer¹, M.C. Kearins¹, K. Conners¹, B. Condon¹, P.C. Maloney³, W.B. Guggino³, J.F. Hunt², and S. Emtage¹, “Impact of the Δ F508 Mutation in NBD1 of Human CFTR on Domain Folding and Structure,” *J. Biol. Chem.* **280**(2), 1346 (14 January 2005).

Author Affiliations: ¹Structural GenomiX, Inc., ²Columbia University, ³The Johns Hopkins University
Correspondence: hlewis@stromix.com

This work was supported by a research contract from the Cystic Fibrosis Foundation Therapeutics, Inc. Use of the Advanced Photon Source was supported by the U.S. Department of Energy, Office of Science, Office of Basic Energy Sciences under Contract No. W-31-109-ENG-38.

CLOSE-UP OF A VIRAL SPIKE

Researchers from the Harvard Medical School, the Howard Hughes Medical Institute, and the Baylor College of Medicine have constructed a new model of the way the infectious rotavirus turns flexible proteins on its surface into rigid spikes that help it enter human cells. The researcher group made x-ray measurements of the spike proteins' three-dimensional structure at SBC-CAT beamline 19-ID at the APS and beamlines F1 and A1 of the Cornell High Energy Synchrotron Source. Their results revealed an unexpected umbrella-like shape. By comparing the x-ray crystal structure to structures obtained during previous electron microscopy studies of the rotavirus, the group concluded that, during cell entry, rotavirus spikes fold back on themselves, exposing regions that attack cell membranes. A better understanding of the spikes' structure and formation should help in the design of vaccines against the virus.

A virus uses proteins on its outer surface to recognize specific receptors on host cells and gain entry, like inserting a key into a lock. Rotavirus, responsible for digestive tract infections that kill half a million children each year, is studded with tiny, protruding protein spikes called VP4. Antibodies that attach to VP4 prevent the virus from entering and infecting cells. But knowing exactly how viruses like rotavirus breach a host cell's barrier could help in choosing a vaccine strategy.

In the case of rotavirus, VP4 starts out floppy and incapable of penetrating cells. The protein-degrading intestinal enzyme trypsin primes VP4 to enter cells by nicking its protein backbone, making it rigid. Electron microscopy studies indi-

cated that the resulting spike has approximately two-fold symmetry, meaning it seems to be composed of two symmetric, rigid subunits.

The research team crystallized a recombinant form of VP4 that was both primed by trypsin and inadvertently triggered to undergo an additional rearrangement that probably occurs during cell entry. They solved the structure of this form of the spike by using x-ray diffraction measurements. The crystal structure shows that, during this second rearrangement, the protein acquires a third rigid subunit, and the subunits bend back on themselves, like an umbrella shade around an inner post. Trypsin-primed VP4 is essentially straight, not bent, and hides a

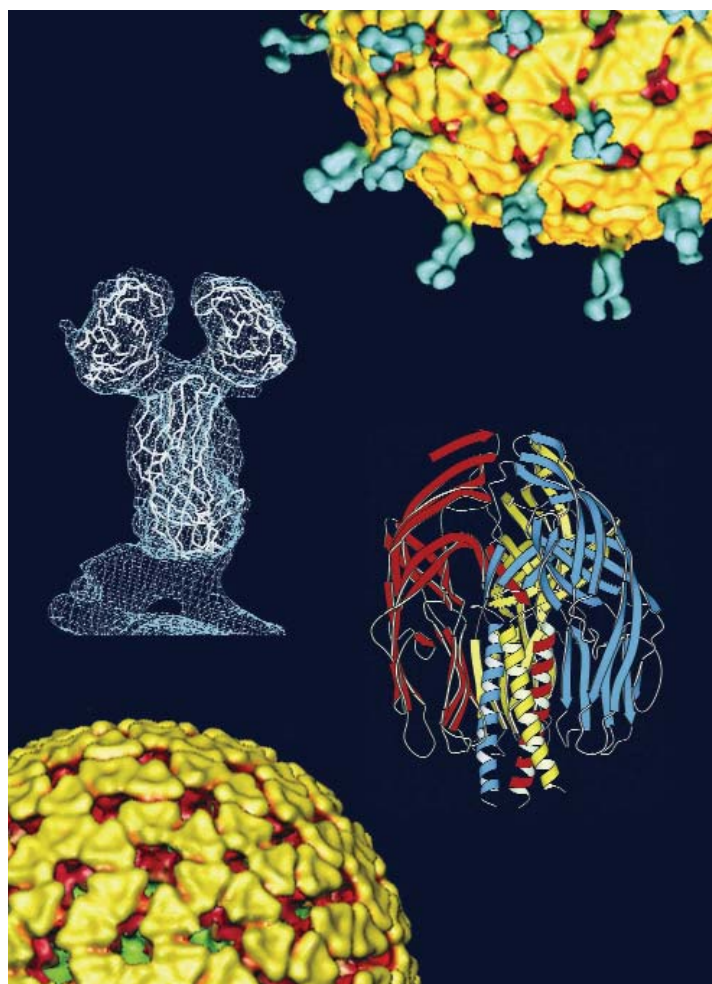


Fig. 1. Three forms of the rotavirus spike. Lower left: Before trypsin priming, the VP4 spikes are flexible and therefore absent from averaged image reconstructions based on electron cryomicroscopy. Upper right: After trypsin priming, two subunits of each VP4 spike become rigid and visible in a reconstruction. Middle left: Closer view of an image reconstruction of a primed spike, into which x-ray crystal structures of VP4 domains have been fit. Middle right: X-ray crystal structure shows that the primed spikes can rearrange to a “folded umbrella” shape with three subunits. This rearrangement probably occurs during cell entry.

greasy, water-averse region in its interior. The second rearrangement bends the protein and exposes the water-averse region, which moves from near the tip of the spike toward the base. Insertion of this region into a cell membrane, followed by bending-back of the protein, could breach the host membrane and give the virus entry to cells.

The researchers surmise that all three subunits must be there from the beginning. So, they conclude that, when trypsin primes the flexible VP4 protein, two subunits rigidify and one remains flexible, which would make it hard to detect in averaged image reconstructions based on electron microscopy. They further hypothesize that, when some second event triggers the primed spike, the third subunit also becomes rigid—bending back onto itself like the other two subunits. The prediction that the second rearrangement disrupts cell membranes must now be tested experimentally. — *JR Minkel*

See: P. R. Dormitzer¹, E.B. Nason³, B.V.V. Prasad³, and S.C. Harrison^{1,2}, “Structural Rearrangements in the Membrane Penetration Protein of a Non-Enveloped Virus,” *Nature* **430**, 1053 (26 August 2004).

Author Affiliations: ¹Harvard Medical School, ²Howard Hughes Medical Institute, ³Baylor College of Medicine
Correspondence: dormitze@crystal.harvard.edu

Use of electron cryomicroscopy facilities at the National Center for Macromolecular Imaging funded by NIH at Baylor College of Medicine. This work supported by an NIH grant and an Ellison Medical Foundation New Investigator in Global Infectious Diseases award to P.R.D., by an NIH grant to B.V.V.P., and by an NIH grant to S.C.H., who is a Howard Hughes Medical Institute Investigator. Use of the Advanced Photon Source supported by the U.S. Department of Energy, Office of Science, Office of Basic Energy Sciences, under Contract No. W-31-109-ENG-38.

NEW REVERSE TRANSCRIPTASE ON THE BLOCK

Investigators from the Indiana University School of Medicine have solved the crystal structure of an enzyme that a mouse virus uses to copy its genome. They crystallized the virus's "reverse transcriptase" enzyme and solved its structure via x-ray crystallography at IMCA-CAT beamline 17-ID and SBC-CAT beamline 19-ID at the APS, and beamline X25 at the National Synchrotron Light Source (NSLS). To gain insight into the enzyme's functioning, they compared its structure to that of the HIV reverse transcriptase and other related enzymes.

Enzymes that build polymers of DNA or its relative RNA are called polymerases. Most polymerases slide along a template strand of DNA and construct complementary strands of DNA or RNA from building blocks called nucleotides. Some types of polymerases, called reverse transcriptases, flip the process: they build double-stranded DNA molecules from a single-stranded RNA template. The resulting DNA inserts itself into the host cell's genome, often disrupting the cell's normal functioning. The human immunodeficiency virus (HIV) uses this strategy, as does the Moloney murine leukemia virus, a mouse virus that causes cancer in its host. So far, researchers have paid the most attention to the structure of HIV reverse transcriptase, which consists of two different subunits, compared to the mouse enzyme's single piece (Fig. 1). To try to understand how a single-subunit reverse transcriptase works, and how it differs from that of HIV, researchers from the Indiana University School of Medicine in Indianapolis performed x-ray crystallography on the mouse enzyme.

Both the HIV and mouse virus reverse transcriptases are shaped like cupped right hands, with a "thumb" on one side of the "palm," and "fingers" on the other side. The active site of each enzyme, where it catalyzes the joining of two nucleotide building blocks, lies where the palm and fingers meet. The enzymes also have extra portions for degrading RNA templates; connecting segments link these RNA-chewers to the hands. The thumbs of the two enzymes are slightly rotated relative to each other, and the connecting segments are almost perpendicular to each other. The result is that the mouse virus enzyme adopts more of a clamp shape than the HIV version, which may explain how it can grip a template strand of RNA without a second subunit, the researchers say.

From structural comparisons with other enzymes, the researchers conclude that the positions of the thumb, connecting segment, and RNA-chewer strongly control the trajectory of the DNA and RNA molecules as they pass through the mouse enzyme. When they superimposed the palm region of the mouse virus enzyme onto that of a conventional polymerase that builds DNA from a DNA template, the trajectory of the DNA template in the conventional enzyme clashes with the fingers, palm, and RNA-chewer of the mouse virus enzyme. And when

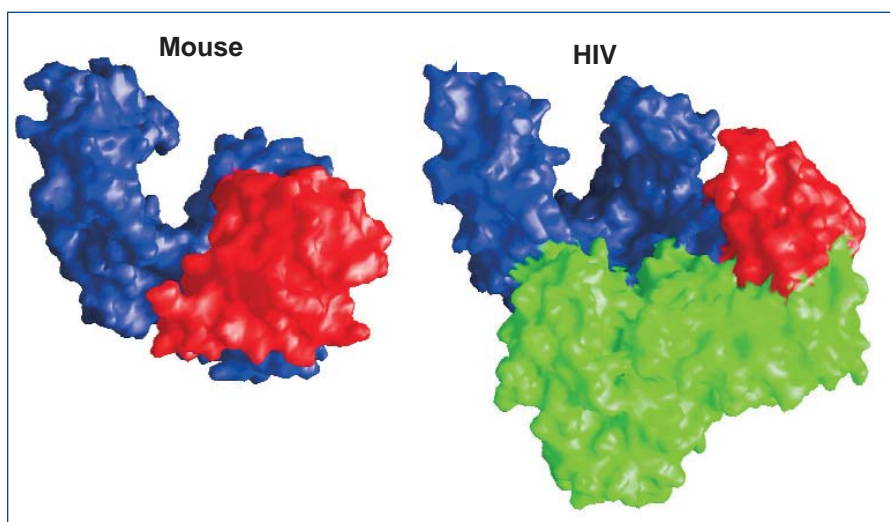


Fig. 1. Surface representations of the mouse and HIV reverse transcriptases. The mouse enzyme has one subunit (blue), including an RNA-degrading domain (red). The HIV enzyme has two subunits (blue, green), one of which (blue) is related in structure to the mouse enzyme.

they superimposed the palms and fingers of the mouse virus and HIV enzymes, the DNA template again clashes with the mouse enzyme's thumb and RNA-chewer.

The RNA-chewing part of the enzyme is potentially flexible, the researchers note. If it did move around, it might control the way that DNA and RNA project from the enzyme's binding site. The group is currently investigating the functional role of the movement of the RNA-chewer in reverse transcription.

— JR Minkel

See: D. Das and M.M. Georgiadis, "The Crystal Structure of the Monomeric Reverse Transcriptase from Moloney Murine Leukemia Virus," *Structure* **12**, 819 (May 2004).

Author Affiliation: Indiana University School of Medicine
Correspondence: mgeorgia@iupui.edu

This work was funded by a grant from the National Institutes of Health. The NSLS at Brookhaven National Laboratory is supported by the U.S. Department of Energy, Division of Materials Sciences and Division of Chemical Sciences. The IMCA-CAT facilities are supported by the companies of the Industrial Macromolecular Crystallography Association. Use of SBC-CAT and the Advanced Photon Source were supported by the U.S. Department of Energy, Office of Science, Office of Basic Energy Sciences, under Contract No. W-31-109-ENG-38.

HOW VIRUSES INVADE: PROTEIN FOLDING IN DENGUE

Before enveloped viruses can enter a cell, they must direct a fusion of their membrane with the cellular membrane. Viral surface proteins carry out an intricate set of steps by which interaction with the cell and subsequent membrane fusion occur. For flaviviruses, such as yellow fever, West Nile, and dengue, there is a distinct set of proteins that undergo folding and rearrangement to bring about fusion. Although much was already known about how these fusion proteins behaved, new research carried out by investigators from the Howard Hughes Medical Institute, Children's Hospital and Harvard Medical School; and Hawaii Biotech, Inc. using the BioCARS-CAT beamline 14-BM the APS provides what is considered a missing link in our understanding of the viral fusion process. It is now possible to describe the protein as it inserts into a target membrane, suggesting a strategy for preventing flaviviruses from entering in the first place.

In studying the structure of the dengue virus envelope after membrane fusion, the research group directed their attention to the viral envelope glycoprotein E, which binds to a receptor and undergoes conformational rearrangement in response to the lower pH of the endosome. The three-dimensional structure of the ectodomain of soluble E (sE) is markedly different after fusion, changing from a dimer to a trimer and bearing three "fusion loops" at one end. These loops are what allow insertion into the cell membrane, and they provide a model of precisely how this insertion occurs via protein folding. The study suggests a fusion mechanism driven by irreversible conformational changes in E. Certain features of the folded-back structure point to ways in which flavivirus entry could be prevented, such as by binding of peptides that block the required folding.

The protein sE from the dengue virus type 2 S1 strain was obtained after expression in *Drosophila melanogaster* using a pMt vector containing the dengue 2 prM and E genes (nucleotides 539-2121). The prM-E protein was processed during secretion to yield sE, the component purified from the cell culture medium by using immunoaffinity chromatography. Dengue sE trimers were obtained by using a method similar to that used for tick-borne encephalitis sE, then they were concentrated to about 15 mg ml⁻¹ for crystallization, and dialysed.

Hanging-drop vapor diffusion was used to grow crystals at 20°C, resulting in two forms: plates of space group *P*321 with cell dimensions $a=b=76.2$ Å, $c=131$ Å (the asymmetric unit contains one molecule of sE) and rhomboids of space group *P*3221 with cell dimensions $a=b=153$ Å, $c=143$ Å (the asymmetric unit contains one trimer of sE). Cryoprotection was achieved by raising the PEG400 concentration to 30%, after which the crystals were frozen in liquid nitrogen for data collection at 100K on beamline 14-BM. For electron microscopy, dengue sE trimers inserted into liposomes were adsorbed to copper grids with micrographs recorded at 100 kV and 64,000-fold magnification. To determine the crystal structure of dengue E in the post-fusion conformation, the group performed molecular replacement using individual domains from the prefusion E structure as search models, and the *P*321 data set.

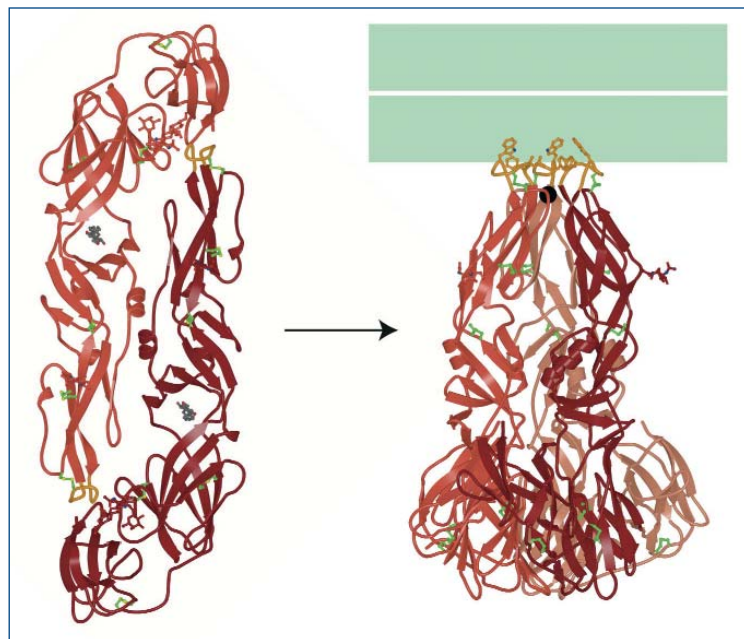


Fig. 1. The envelope protein of dengue virus undergoes a conformational change under the acidic conditions encountered early in the infection process. This change drives fusion of viral and cellular lipid membranes into a single membrane, a key event in the entry of a protein-coated virus into a host cell. The crystal structures of the dengue virus envelope protein before and after membrane fusion (on left and right, respectively) reveal the nature of the conformational change and suggest strategies for inhibiting viral entry into host cells. The green rectangles represent the fused lipid membrane.

The results provide a clear view of the crystal structure of the trimeric, postfusion conformation of the soluble ectodomain of dengue virus type 2 sE (Fig. 1). A membrane-insertable "aromatic anchor" is formed at the tip of the trimer when the fusion loops of the three subunits come together (Fig. 2). In this process, the fusion loop retains its prefusion conformation while the neighboring hydrophilic groups limit insertion to the near end of the outer lipid bilayer. Then the viral membrane anchor is directed toward the fusion loop when the ectodomain of the protein folds back on itself.

The researchers proposed a mechanism in which fusion is driven by an irreversible change in the conformation of sE and aided

Continued on next page

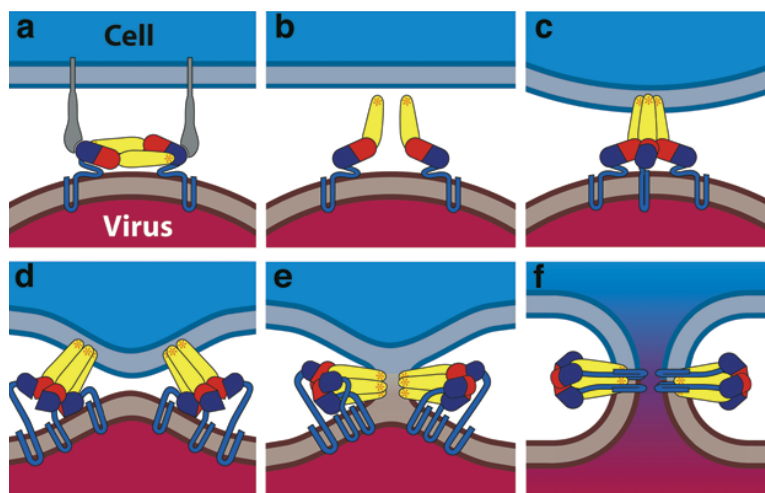


Fig. 2. Proposed mechanism for how class 2 enveloped viruses fuse membranes. The envelope protein, E, is composed of three domains (red, yellow, blue) and a stem (cyan), which is anchored in the viral membrane. (a) E binds to a receptor on the cell surface. (b) Acidic conditions cause the yellow domain to hinge outward from the virion surface, exposing the fusion loop (orange asterisk) at the tip of the yellow domain. (c) The fusion loop inserts into the cell membrane, promoting clustering of E. (d) Contacts between E proteins spread downward from the fusion loop. The blue domain shifts and rotates to create more contacts, causing the stem to fold back toward the fusion loop. Energy released by this refolding bends the two membranes. (e) Creation of additional contacts between the stem and yellow domain leads first to hemifusion and then (f) to complete fusion of the viral and cellular membranes. This creates a pore, through which viral genes enter the cell.

by membrane distortions that are imposed by insertion of the fusion loops. These data provide new knowledge about the features of the folded-back protein and are consistent with concurrently published results on an alphavirus fusion protein. The data also arm researchers in the fight against viral disease by suggesting exciting possibilities for ways in which viral entry—and the resulting diseases—can be prevented. — *Mona Mort*

See: Y. Modis¹, S. Ogata², D. Clements², and S.C. Harrison¹, “Structure of the Dengue Virus Envelope Protein after Membrane Fusion,” *Nature* **427**, 313 (2004).

Author Affiliations: ¹Howard Hughes Medical Institute Children’s Hospital and Harvard Medical School; ²Hawaii Biotech

Correspondence: harrison@crystal.harvard.edu

This work was supported by a long-term fellowship to Y.M. from the Human Frontier Science Program Organization and by an NIH grant to S.C.H. Use of the Advanced Photon Source was supported by the U.S. Department of Energy, Office of Science, Office of Basic Energy Sciences under Contract No. W-31-109-ENG-38.

SELECTIVE ESTROGEN MODULATORS HOLD THERAPEUTIC PROMISE

Using hormones to treat disease can often have unwanted side effects. One example is estrogen, successfully used in hormone replacement therapy to combat osteoporosis, but now linked to increased rates of uterine and breast cancer. Previous work revealed molecular modulators that enhance the positive effects of estrogen therapy while minimizing the negative ones. This is accomplished by selectively targeting the estrogen receptors in certain tissues. Investigators from Merck Research Laboratories and Karo Bio AB, using the IMCA-CAT 17-ID beamline at the APS, have discovered and synthesized dihydrobenzoxathiins, potent and selective estrogen receptor α (ER α) ligands. The study reveals an estrogen modulator with extremely high selectivity and great promise for clinical use.

Of these selective estrogen receptor modulators (SERMs), one analogue, 4-D, was the most active, showing 50-fold selectivity in competitive binding assay and 100-fold selectivity in transactivation assay in HEK-293 cells. The researchers also investigated the mechanism by which the 4-D ligand exhibits selectivity for ER α . This selectivity appears to be due to the interaction between the sulfur atom of the benzoxathiin ring and two critical residues in the binding pocket of the receptor. The discovery and synthesis of 4-D represents marked progress because previously synthesized modulators had shown either little preference for the ER α over ER β or had

shown a lower affinity for ER α . “Ideal SERMs”—those that show high affinity for one receptor subtype over another—are desirable in that they should lead to reduced side effects of hormone therapy. Because 4-D is so selective for ER α , it shows great promise for therapeutic use.

Following synthesis, the complex of 4-D and the ligand-binding domain of ER α (residues 307-554) was crystallized (space group $P6_5-22$, with cell dimensions $a = b = 58.48 \text{ \AA}$, $c = 276.08 \text{ \AA}$) and analyzed at beamline 17-ID to a resolution of 1.9 \AA . An ER binding assay allowed testing of the compounds for intrinsic activity. A cellular transactivation assay was used to

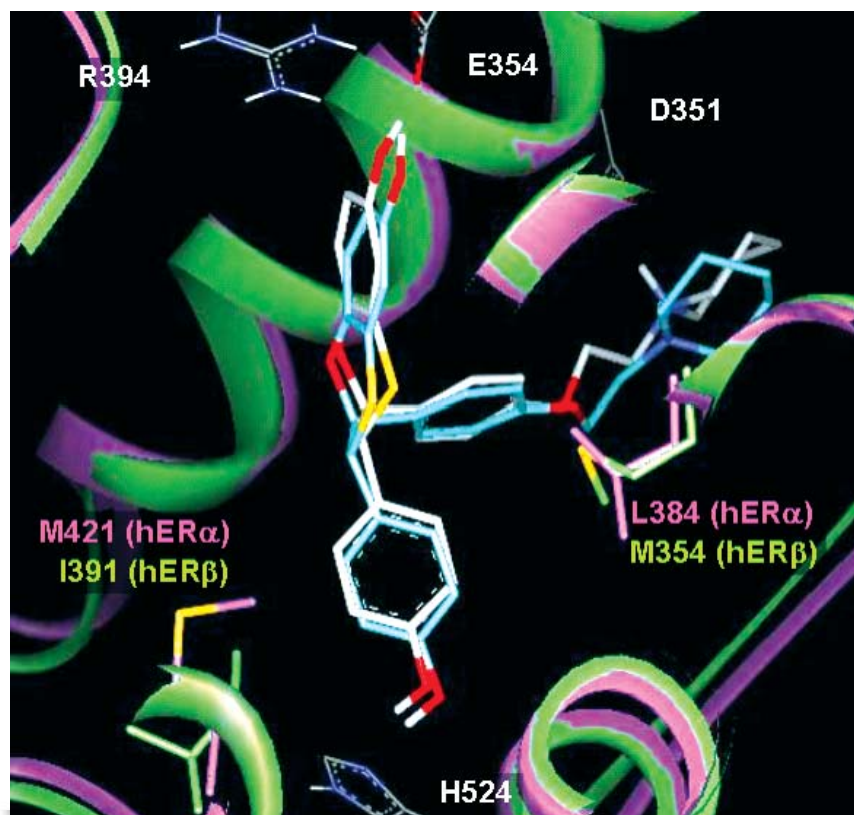


Fig. 1. Crystallographic (cyan) and molecular modeling (white) results for 4-D, shown with hER α (purple) and hER β (green).

test for potency and selectivity, using HEK-293 cells co-transfected with human ER α or ER β and the alkaline phosphatase reporter gene.

Previous work by the research team led them to propose that the α selectivity was related to the interaction in the carbonyl region of the ligand; the present work allowed a focused analysis of this interaction. By using the larger, more polar sulfur atom, a greater affinity for the α receptor over the β receptor was achieved (Fig. 1). A single enantiomer, 4-D, exhibited both high affinity for ER α and strong inhibition of estradiol-driven uterine growth in rats, thus showing that it could operate to enhance estrogen activity without the negative side effect of increasing uterine sensitivity. In rats, 4-D also inhibited bone resorption and lower serum cholesterol levels induced by ovariectomy. These activities clearly characterize this new class of compounds as a selective estrogen α receptor alpha modulator (SERAM), with low-nanomolar binding affinity and subnanomolar functional activity. The specificity that is so crucial to the beneficial effects of 4-D is most likely due to the sulfur moiety.

Critical to minimizing side effects of estrogen therapy, the SERAMs show great promise for use in treating diseases resulting from low estrogen activity, such as osteoporosis. The pres-

ent work fine-tunes the ways in which estrogen receptor modulators can be enlisted for maximum effectiveness and sets the stage for sophisticated synthesis of future pharmaceuticals.

— Mona Mort

See: S. Kim¹, J.Y. Wu¹, E.T. Birzin¹, K. Frisch¹, W. Chan¹, L.-Y. Pai¹, Y.T. Yang¹, R.T. Mosley¹, P.M.D. Fitzgerald¹, N. Sharma¹, J. Dahllund², A.-G. Thorsell², F. DiNinno¹, S.P. Rohrer¹, J.M. Schaeffer¹, and M.L. Hammond¹, "Estrogen Receptor Ligands. II. Discovery of Benzoxathiins as Potent, Selective Estrogen Receptor Modulators," *J. Med. Chem.* **47**(9), 2171 (2004).

Author Affiliations: ¹Merck Research Laboratories, ²Karo Bio AB

Correspondence: Seongkon_kim@merck.com

Use of the IMCA-CAT 17-ID beamline was supported by the companies of the Industrial Macromolecular Crystallography Association through a contract with the Illinois Institute of Technology. Use of the Advanced Photon Source was supported by the U.S. Department of Energy, Office of Science, Office of Basic Energy Sciences, under contract No.W-31-109-ENG-38.

HORMONE ASSEMBLY LINKS OBESITY AND DIABETES

Two major health problems—obesity and diabetes—tend to be associated. An obese individual has an increased risk of developing Type II diabetes. The molecular basis for this connection, however, remains elusive. Insulin resistance is one of the main characteristics of Type II diabetes, and understanding its origins has long been thought to be a promising area of study. When the hormone insulin works properly, it decreases blood glucose levels; in Type II diabetes, insulin can no longer achieve this function adequately, leading to dangerous elevations in blood glucose. A newly-discovered family of hormones, the resistins, may help explain the link between obesity and diabetes. Resistin, which is named for its ability to promote resistance to insulin, is secreted from fat cells. Studies suggest that it circulates in the blood at elevated levels in obese individuals, pointing to a potential molecular link between obesity and insulin resistance. Researchers from Columbia University and Albert Einstein College of Medicine used SGX-CAT and COM-CAT beamlines at the APS to obtain high-resolution crystal structures for resistin and a resistin-like molecule (RELM) β . These new studies provide a critical understanding of how resistin assembly affects its function and suggest new ways to understand insulin resistance and diabetes.

Detailed analyses of resistins revealed a multimeric structure, unusual in that it has highly exposed disulfide bonds linking the multimer together. The assembly of the hormones requires association of trimers to form hexamers, and some of both the assembled and unassembled forms are found in serum samples (Fig. 1). A mutant lacking the disulfide bonds between protomers appeared to inhibit insulin action to a far greater extent than the wild-type protein, suggesting that the trimer form may be an active species, and the hexamer a “storage form.” Thus, the disulfide bonds themselves appear to be important in controlling resistin activity.

Mammalian HEK-293T cells provided expressed mouse resistin and RELM β , resulting in two crystal forms of resistin, in space groups C2 and C22₁, and one form of RELM β in space group I222. Structural data were obtained by using beamlines 31-ID (SGX-CAT) and 32-ID (COM-CAT) at the APS, and beamlines X4, X9, and X25 at the National Synchrotron Light Source, Brookhaven National Laboratory. To analyze mouse serum for the presence of resistin, protein separation was performed on SDS gels and developed with antibodies against resistin. To study the importance of the disulfide bonds, the mutant version of resistin, lacking a critical cysteine residue, was tested for its ability to form multimers and assayed on non-reducing SDS gels.

The structures of resistin and RELM are similar—each has a C-terminal β -sandwich “head” domain, rich in disulfides, linked to a helical “tail” region at the N terminus. The head domain forms a unique six-stranded jelly-roll, in which the cysteine residues and, by inference, the disulfide pattern is conserved throughout the resistin family. The association of the protomers into the multimer occurs through formation of a coiled coil by the amino-terminal helical regions. The disulfide bonds between chains of resistin and RELM β are highly solvent exposed, a novel characteristic for such bonds in proteins. In serum, the proposed assembly mechanism was confirmed by the presence of about 80 to 90% of total resistin in the form exhibiting disulfide bonds, with the remainder lacking such bonds. After purification of the mutant from 293T cells, the covalently bound form was not present, confirming the critical



Fig. 1. Ribbon diagrams of (a) resistin and (b) RELM β are shown with each protomer shaded in a different hue and disulfide bonds shaded in yellow. In both structures, a protomer from the “top” trimer is covalently attached via a disulfide to a protomer from the “bottom” trimer.

nature of the missing cysteine residue in disulfide bond formation. In the presence of this mutant, using the pancreatic-insulin clamp technique, the researchers found that changes in hepatic insulin sensitivity levels were far greater than with wild-type resistin. Thus, the disulfide bonds appear to be critical for the bioactivity of resistin.

The investigators previously demonstrated a similar mechanism for bioactivation of adiponectin, another adipocyte-specific hormone that has the opposite physiological effect to that of resistin. Taken together, these data suggest a general mechanism for regulation of adipokine hormone secretion and contribute significantly to the search for a way to control obesity-related diabetes. — *Mona Mort*

See: S.D. Patel¹, M.W. Rajala², L. Rossetti², P.E. Scherer², and L. Shapiro¹, "Disulfide-Dependent Multimeric Assembly of Resistin Family Hormones," *Science* **304**, 1154 (21 May 2004).

Author Affiliations: ¹Columbia University, ²Albert Einstein College of Medicine.

Correspondence: lss8@columbia.edu

This work was supported by grants from NIH and the Research to Prevent Blindness Foundation; the NIGMS NYSGXRC; the U.S. DOE, Office of Basic Energy Science (W-31-109-ENG-38); and by Structural GenomiX, Inc. Use of the Advanced Photon Source was supported by the U.S. Department of Energy, Office of Science, Office of Basic Energy Sciences, under contract No.W-31-109-ENG-38.

ENZYME MUTATIONS AND MOTOR DISORDERS

In the 1920s, acetylcholine became the first neurotransmitter described in the scientific literature. It took another two decades to identify the enzyme, choline acetyltransferase (ChAT), that is responsible for the synthesis of acetylcholine, a molecule essential to the nervous system and other tissues. Decreased ChAT activity is associated with neurodegenerative disorders such as Alzheimer's disease, Huntington's disease, and amyotrophic lateral sclerosis (ALS). Knowledge about the crystal structure of ChAT and how mutations are distributed within this enzyme would provide important clues as to how these disease states arise. Just such a data set is now available, thanks to studies by researchers from the University of Kentucky, SYRRX, and the Mayo Clinic using the SER-CAT, SBC, and BioCARS-CAT beamlines at the APS to further their detailed studies of the structure of ChAT.

The crystal structure of the ChAT enzyme reveals two domains and a solvent-accessible site at the domain interface. When the enzyme is in complex with the substrate coenzyme A (CoA) and is viewed at low resolution, the binding site is apparent, as is another interaction not found in the related enzyme carnitine acetyltransferase (CrAT). Both electrostatic and steric blocks to carnitine binding appear to be responsible for the preference of choline over carnitine at the active site. About half of the mutations causing motor disorders are found at positions where they would affect enzyme activity directly, while the remaining mutations are at distant positions and are believed to exert indirect effects. The ChAT structure resulting from this extensive analysis also indicates how regulation occurs via phosphorylation and how surface patches may be involved in membrane association or macromolecular interactions.

To obtain ChAT, the recombinant rat enzyme in the protein expression vector pLENTY was overexpressed in DH5aF'IQ cells, collected, and purified. The isolation of selenomethionyl-ChAT, obtained by using the methionine pathway inhibition technique, used the same vector and similar purification procedure to that used for native ChAT. To determine ChAT activity during the purification procedure, a fluorometric assay was used to monitor the byproducts of the enzymatic pathway and its reverse. The research group used sitting-drop vapor diffusion to grow crystals of both native and selenomethionyl-ChAT at 4°C. Crystals were cryoprotected using glycerol, mounted in a nylon loop, and plunged into liquid nitrogen. The charge-cou-

Continued on next page

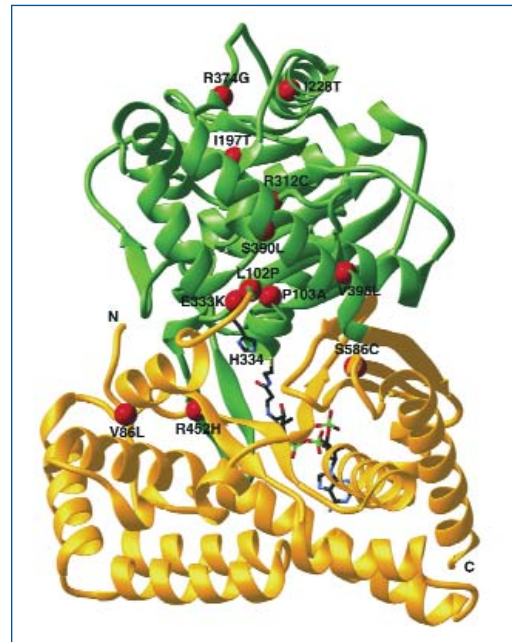


Fig. 1. Location of ChAT mutations that cause congenital myasthenic syndrome with episodic apnea. The positions of the 12 ChAT point mutations found in patients are shown as red spheres on a ribbons representation of the enzyme. Labels indicate the wild type and mutant residues. The two domains of ChAT are in green and gold, and the bound coenzyme A and catalytic histidine are shown in a wireframe representation.

pled device detectors at APS beamlines 22-ID (SER-CAT), 19-ID (SBC-CAT), and 14-BM (BioCARS-CAT) were used to collect x-ray diffraction data. Native ChAT forms crystals in space group $P2_1$ (unit cell dimensions: $a = 84.70 \text{ \AA}$, $b = 78.88 \text{ \AA}$, $c = 139.36 \text{ \AA}$, $\alpha = 90^\circ$, $\beta = 98.4^\circ$, and $\gamma = 90^\circ$). ChAT-CoA complex crystals (space group $P2_12_12_1$, unit cell dimensions: $a = 77.59 \text{ \AA}$, $b = 153.32 \text{ \AA}$, and $c = 152.83 \text{ \AA}$) were formed by hanging-drop vapor diffusion at 4°C . Molecular replacement was used to determine the ChAT structure by using coordinates of unliganded CrAT as a search object.

The crystal structure of recombinant rat ChAT, at 2.5-\AA resolution, shows that the enzyme contains a total of 22 α helices and 18 β strands divided into two structural domains: the N domain (residues 102-401) and the C domain (residues 18-101 and 402-617). Both of these domains, as in CrAT, are structurally similar to the monomers of trimeric acetyl transferases. At the domain interface, a $2,500\text{-\AA}^2$ surface area is home to a solvent-accessible tunnel running through the center of the molecule and reducing the contact area. This tunnel is the known substrate binding site for CrAT and other acetyltransferases; in ChAT, the crystal structure also reveals a metal-binding site in the C domain. No substantial conformational changes in ChAT were detected upon CoA binding. Although ChAT and CrAT have similar choline-binding sites, ChAT exhibits a strong pref-

erence to use choline as a substrate. Twelve point mutations were located in the ChAT three-dimensional structure; nine of these mutations are in the N domain, while three map to the C domain, close to the surface and the active site (Fig. 1). The mutations can now be characterized in some detail and related to known disease states, such as congenital myasthenic syndrome with episodic apnea. These data, along with knowledge about how ChAT is regulated in the cell, provide new tools with which to fight neurodegenerative disease. — *Mona Mort*

See: Y. Cai¹, C.N. Cronin², A.G. Engel³, K. Ohno³, L.B. Hersh¹, and D.W. Rodgers¹, "Choline Acetyltransferase Structure Reveals Distribution of Mutations that Cause Motor Disorders," *EMBO J.* **23**, 2047 (2004).

Author Affiliations: ¹University of Kentucky ²SYRRX Inc., ³Mayo Clinic

Correspondence: david.rodgers@uky.edu or lhersh@uky.edu

This work supported by: the United States Public Health Service to D.W.R. (NS38041), L.B.H. (AG05893), and A.G.E. (NS6277), the National Science Foundation to D.W.R. (MCB-9904886), the American Chemical Society Petroleum Research Fund to D.W.R. (37135-AC4), and the Muscular Dystrophy Association to A.G.E. Use of the Advanced Photon Source was supported by the U.S. Department of Energy, Office of Science, Office of Basic Energy Sciences under Contract No. W-31-109-ENG-38.

A RELAXED APPROACH TO FATTY ACID TRANSPORT

A protein in the outer membrane of *E. coli* seems to draw greasy molecules, such as fatty acids, into the cell just by "breathing" in and out, according to researchers from the Harvard Medical School and The Ordway Research Institute. The researchers solved the three-dimensional structure of the protein, called FadL, using the NE-CAT 8-BM beamline at the APS and the X25 beamline at the National Synchrotron Light Source (NSLS). Comparing two slightly different structures of FadL suggests that it operates by a mechanism unique among such transport proteins, in which the protein's natural undulations allow a long fatty acid molecule to burrow into the cell. The result may eventually help scientists engineer bacteria to better degrade industrial wastes.

Cells are coated in fatty membranes that keep most molecules out. But they still need sugars, proteins, and fatty acids for fuel and building materials. So the cells make proteins that reside in their membranes and ferry these materials across. Researchers still don't understand the workings of the proteins that transport fatty acids and other greasy, or water-averse, molecules in bacteria like *E. coli*. To gain fresh insight, the research team examined FadL, a fatty acid transporter that resides in the tough outer membrane of *E. coli*. They used x-ray diffraction to solve the crystal structure of the protein, which they purified with a fatty-acid-like detergent. The protein crystallized in two slightly different forms, called monoclinic and hexagonal, giving the researchers additional insight into how the protein wiggles from shape to shape.

On first inspection, the monoclinic structure contains no obvious channel through which fatty acids could enter the cell. The protein has a 50-\AA -long barrel made of 14 parallel protein

strands, like strips of wood in typical barrels (Fig. 1A). However, the barrel is not hollow; it has a compact "hatch" that plugs the space inside, preventing the passage of fatty acids. Two loops project out of the mouth of the barrel on the side that would face the cell's environment (outside). These loops form a water-averse groove with two fatty-acid-like detergent molecules sticking to it, suggesting that passing fatty acids may do the same. Inside the barrel, below the water-averse groove, is a pronounced pocket of even greasier amino acids, clinging to another detergent molecule. The researchers propose that this pocket is a strong binding site for fatty acids that diffuse into the barrel from the groove.

The pocket of the hexagonal structure is distorted slightly compared to the monoclinic structure. The detergent molecule is also 10 \AA closer to the barrel's inner mouth. This observation suggests that rearrangement of the pocket releases the fatty acid and creates more space underneath it on the barrel's inner

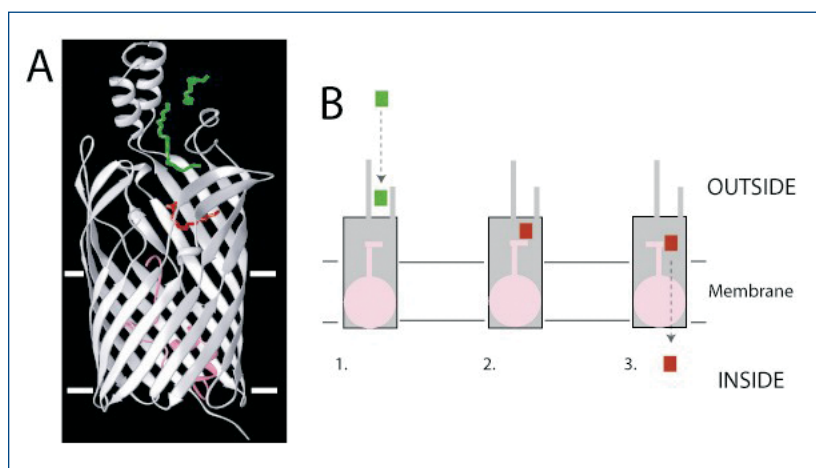


Fig. 1. (A) X-ray structure of FadL, shown in a schematic form. A hatch (pink) plugs the interior of the FadL barrel (gray). Fatty-acid-like detergents (green, red) are bound to a greasy groove (top) and pocket (middle). (B) Model of FadL-mediated fatty acid transport: (1) collection of fatty acids (green) from the external medium by the groove; (2) diffusion of fatty acids (red) into the pocket; (3) spontaneous expansions and contractions in the hatch (pink) knead the fatty acid to the inside of the cell. Horizontal lines indicate the position of the bacterial outer membrane.

side. The researchers hypothesize that additional shape changes, driven by spontaneous contractions and expansions in the protein's structure, or "breathing," knead the fatty acids through the hatch and into the cell (Fig. 1B).

Many bacteria use transporters like FadL to take in toxic greasy molecules, such as hydrocarbons, from oil spills and other industrial wastes. The bacteria then "biodegrade" these chemicals, making them harmless. The researchers hope that insights provided by the FadL structures could ultimately improve the efficiency of such transporters, and therefore enhance biodegradation. — *JR Minkel*

See: B. van den Berg¹, P.N. Black², W.M. Clemons, Jr.¹, T.A. Rapoport¹, "Crystal Structure of the Long-Chain Fatty Acid Transporter FadL," *Science* **304**, 1506 (4 June 2004).

Author Affiliations: ¹Harvard Medical School, ²The Ordway Research Institute.

Correspondence: lvandenberg@hms.harvard.edu

P.N.B. received support from the NSF. W.M.C. is supported by a fellowship from the Damon Runyon Cancer Research Foundation. T.A.R. is a Howard Hughes Medical Institute investigator. Use of the Advanced Photon Source was supported by the U.S. Department of Energy, Office of Science, Office of Basic Energy Sciences, under Contract No. W-31-109-ENG-38.

FORMIN CRYSTAL STRUCTURE SHEDS LIGHT ON HOW ACTIN FORMS

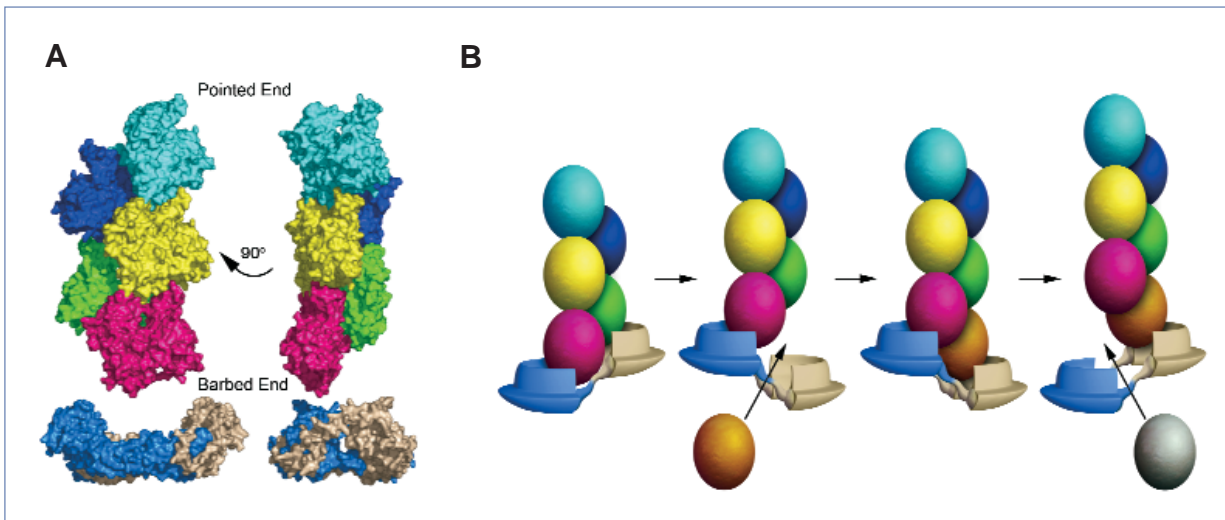
Formin proteins are often involved in building cytoskeletons (the combination of muscle and skeleton that is responsible for cell movement, cytokinesis, and the organization of the organelles within a cell) inside eukaryota, one of the two major cellular groups in living things. Formin proteins contain a conserved region, the Formin Homology-2 (FH2) domain, that nucleates actin filaments. New data obtained at NE-CAT beamline 8-BM at the APS and at the Cornell High Energy Synchrotron Source (CHESS) revealed the crystal structure of an FH2 domain from the yeast *S. cerevisiae*, providing much-needed details on the mechanism by which the actin filaments form, especially with respect to required conformational intermediates. These data, which greatly improve our understanding of how the final structure arises, suggest an elegant stair-step process by which formins aid the elongation of a new actin filament.

Investigators from Dana-Farber Cancer Institute, the Harvard Medical School, and Brandeis University studied the structure of the *S. cerevisiae* Bni1p FH2 domain. They found that the mostly α -helical FH2 forms a unique "tethered dimer." In this dimer, an unusual lasso and linker structure ties together two elongated actin binding heads at either end. Biochemical and crystallographic data proved the dimer to be stable but flexible, with flexibility between the two halves of the dimer produced by linker segments. Even though each half of the dimer can interact with the filament ends, actin nucleation and processive capping occur only when the dimer is intact. This tethered dimer architecture may facilitate a process by which

formins stair-step on the barbed end of a growing actin filament.

Three protein constructs, Z (residues 1348-1766 of the Bni1p FH2 domain), P (residues 1348-1750 of Bni1p plus a C-terminal 6-His tag), and ΔZ (identical to Z except that residues 1411-1416 were replaced with Glu-Phe via mutagenesis), were expressed as a fusion with a tobacco etch virus (TEV) protease site. The Z protein was concentrated to 8 mg/ml for crystallization and PCMBs was added to 2.5 mM. Hanging-drop diffusion was used to grow crystals (hexagonal space group P6₃22; unit cell dimensions $a = b = 101.4 \text{ \AA}$, $c = 265.7 \text{ \AA}$; asymmetric

Continued on next page



Cell 116, Fig. 7, Pg. 720, March 5, 2004, Copyright © 2004 by Cell Press

Fig. 1. Stair-stepping of the tethered FH2 (tan and blue) dimer on the elongating barbed end of F-Actin (subunits are colored ovals). (A) Orthogonal views of FH2 below the barbed end of a five-subunit actin filament. (B) Schematic illustration shows how FH2 might stair-step on the barbed end.

unit contains one FH2 polypeptide chain) at 20°C with 16% ethylene glycol as a precipitant. Hanging-drop vapor diffusion was used to crystallize the ΔZ protein (space group C2 with unit cell dimensions $a = 98 \text{ \AA}$, $b = 172.2 \text{ \AA}$, $c = 120.6 \text{ \AA}$, and $\beta = 112.3^\circ$, with two subunits per asymmetric unit). Crystal diffraction data for the Z construct were collected at CHESS. X-ray diffraction data for the ΔZ construct were collected on the NE-CAT beamline 8-BM at the APS. Rabbit skeletal muscle actin was used for actin assembly, filament elongation, and filament depolymerization reactions.

The FH2 dimer, when viewed from the top, forms a closed ring shaped like a parallelogram. The dimer can be separated into five subdomains: an N-terminal "lasso," a 17-residue "linker" segment, a globular "knob" subdomain, a coiled-coil region, and a carboxy-terminal "post" subdomain. A "hemidimer" is formed from the knob, coiled coil, and post of one subunit, together with the lasso. The tethered dimer architecture is formed when the two comparatively rigid hemidimers are leashed together by the linker segments. When viewed from the side, the molecule has a boat shape because the two knob regions of the dimer extend above the plane of the parallelogram. Biochemical studies of the deletions (constructs P and ΔZ , which perturb the arrangement of subunits observed in the crystal structure but still form dimers), along with earlier studies of deletions that cannot form dimers, show that the dimer is required for activity but that the two halves of the dimer are not held in a defined orientation. Rather, they are "flexibly tethered."

Dimerization creates the lasso/post interface, where actin binds. Actin filament assembly and disassembly are affected by capping proteins. In the resulting picture, the hemidimer can

bind actin but it blocks elongation, whereas with the intact FH2 dimer, normal actin nucleation and processive capping occur. From these results, the researchers have constructed a working model in which the formin molecule has a role in regulating activity at the barbed end of the actin molecule. As each half of the FH2 dimer dissociates in a stair-stepping fashion, the formin molecule could processively "ride" the elongating barbed end of an actin filament (Fig. 1). The tethered-dimer model would be a strikingly elegant mechanism for elongation of actin filaments and is consistent with data collected thus far. Further research will address whether the flexibility of the FH2 domain is required for function. In the meantime, these data allow a new way of looking at actin elongation. — *Mona Mort*

See: Y. Xu^{1,2}, J.B. Moseley³, I. Spagot⁴, F. Poy¹, D. Pellman⁴, B.L. Goode³, and M.J. Eck^{1,2}, "Crystal Structures of a Formin Homology-2 Domain Reveal a Tethered Dimer Architecture," *Cell* **116**, 711 (2004).

Author Affiliations: ¹Dana-Farber Cancer Institute, ²Harvard Medical School, ³Brandeis University, ⁴Dana-Farber Cancer Institute and Children's Hospital, Harvard Medical School.
Correspondence: eck@red.dfci.harvard.edu

M.J.E. and D.P. are Scholars of the Leukemia and Lymphoma Society. B.L.G. was supported by a Pew Scholars award. This work was supported in part by NIH proposals GM61345 (D.P.) and GM63691 (B.L.G.). Use of the Advanced Photon Source was supported by the U.S. Department of Energy, Office of Science, Office of Basic Energy Sciences under Contract No. W-31-109-ENG-38.

PROBING THE MOLECULAR STRUCTURE OF A BACTERIAL PHOTOSYNTHETIC REACTION CENTER

To convert photons from solar radiation into usable chemical energy, bacteria, algae, and the higher plants employ a membrane protein that acts as a photosynthetic reaction center. The reaction center accepts photons directly from the source of the light and from antennae proteins in the membrane, initiating a cascade of reactions that move electrons across the membrane, generating an electrochemical potential. A recent experiment by researchers from The University of Chicago using the BioCARS-CAT beamlines at the APS has disclosed new information about reaction center behavior. Freeze-trapping crystallographic probes of the reaction center from the bacteria *Rhodobacter sphaeroides* have revealed details of the molecular dynamics of secondary electron transfer, in which electrons are transferred to a ubiquinone molecule bound to an active site inside the reaction center. These studies indicate significant movement and rotation of native quinone during photoillumination.

In the dark (or inactive) state, the ubiquinone Q_B is bound to the distal site. Upon stimulation by light, it shifts about 4.5 Å to the proximal binding site. At the same time, the aromatic ring of the ubiquinone in *R. sphaeroides* has been observed to rotate 180° around the isoprene tail.

A recent experiment using third-generation-synchrotron techniques has explored this reaction in *Blastochloris viridis*, formerly *Rhodospseudomonas viridis*, the first organism in which the reaction center's structure was determined on the molecular scale. Using Laue diffraction and time-resolved crystallographic techniques, the researchers have found significant differences in the structural behavior and time frame of quinone exchange in the reaction center of *B. viridis* compared to that in *R. sphaeroides*.

The time-resolved Laue diffraction method, which has been employed in previous experiments to examine proteins such as myoglobin and a photoactive yellow protein, uses brief pulses of brilliant x-ray radiation after the sample has been stimulated by a short burst of visible light from a laser (Fig. 1). Using this technique, temporal resolution down to nanoseconds can be achieved.

Monochromatic x-ray data were collected on the reaction center of *B. viridis* in the dark stage, using a natural form of ubiquinone (UQ10) similar to one found in *R. sphaeroides*. Then, native ubiquinone in the *B. viridis* reaction center was replaced with a synthetic form (UQ2). Both phases of the experiments were conducted on samples at room temperature to avoid artifacts that may occur in freeze-trapping crystallographic studies. The Laue diffraction pump-probe data were collected at beamline 14-ID. Monochromatic diffraction measurements were collected at beamline 14-BM.

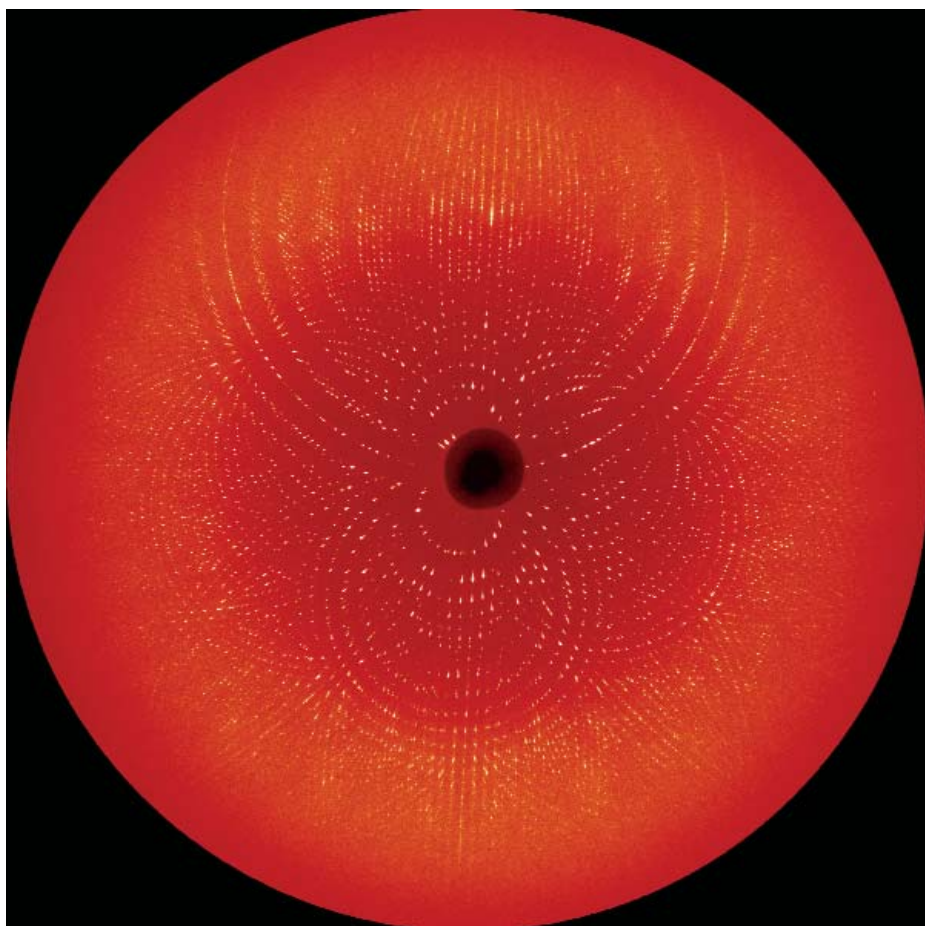


Fig. 1. The bacterial reaction center of *B. viridis* revealed by Laue diffraction with spatial resolution of 2.9 Å at the detector edge and with a temporal resolution of 2 ms.

To prepare the reaction center, protein was isolated and purified from wild-type bacteria grown in a semianaerobic medium, and protein crystals containing the two ubiquinones, UQ2 and UQ10, were grown in the dark at 18° C. The samples were analyzed by means of Laue diffraction at 15° C in the dark and 3 ms after illuminating the crystal with a pulsed laser at 630 nm. Analysis of the data revealed no discernible motion of

Continued on next page

ubiquinone from the distal to the proximal position in the shift from the dark to the illuminated state.

These results suggest that the distal position is not a stable state on the time scale of the experiment, or that the movement of ubiquinone from the distal to the proximal position is not reversible in *B. viridis*. In future time-resolved crystallographic studies of *B. viridis* and *R. sphaeroides*, the researchers might vary the time resolution between light and dark phases and further explore the effect of pH on electron transfer in order to pinpoint in greater detail the molecular dynamics of photosynthetic bacteria. — *Elise LeQuire*

See: R.H.G. Baxter¹, N. Ponomarenko¹, V. Šrajer¹, R. Pahl¹, K. Moffat¹, and J.R. Norris¹, "Time-resolved Crystallographic

Studies of Light-Induced Structural Changes in the Photosynthetic Center," *P. Natl. Acad. Sci. USA* **101**(16), 5982 (20 April 2004).

Author Affiliation: ¹The University of Chicago
Correspondence: jrnorris@uchicago.edu

This work was supported by U.S. Department of Energy Grant DE-FG02-96ER14675 (to J.R.N.), and by National Institutes of Health (NIH) Grant GM36452 (to K.M.). BioCARS-CAT is supported by NIH Grant RR07707 (to K.M.). R.H.G.B. was supported by the Brian Ledley Scholarship from the Gowrie Trust Fund of Australia and Fellowship 1001774 from the Burroughs-Wellcome Interfaces Program. We acknowledge the Burroughs Wellcome Fund Interfaces Cross-Disciplinary Training Program at The University of Chicago for partial support of the Chemistry Department computer cluster. Use of the Advanced Photon Source was supported by the U.S. Department of Energy, Office of Science, Office of Basic Energy Sciences, under Contract No. W-31-109-ENG-38.

STRUCTURE OF AN ESCAPE HATCH FOR RESTLESS PROTEINS

Researchers using APS and National Synchrotron Light Source (NSLS) beamlines have solved the three-dimensional (3-D) structure of a protein channel that allows other proteins to pass across cellular membranes or become lodged in them. The protein contains a funnel that leads into a channel blocked by a plug in the middle. When the plug moves out of the way, the opening forms a shape like an hourglass, with a ring of greasy amino acids in the middle that may act as a seal to prevent other molecules from passing through. The structure indicates how the channel recognizes the "signal sequence," the trigger in proteins that leads to plug movement and the opening of the channel.

Proteins are manufactured in the endoplasmic reticulum of eukaryotes (cells with a nucleus) or in the cytoplasm of bacteria. To eventually make it outside the cell or into a cellular membrane, a protein has to pass through a channel in the endoplasmic reticulum membrane (or the cytoplasmic membrane in bacteria). All organisms share a very similar channel, called SecY in bacteria, which is the target of outgoing proteins either during or after synthesis. The escaping protein's "open sesame" command normally consists of a sequence of amino acids, called the signal sequence, at its leading tip. Proteins destined to sit in a membrane contain sequences called transmembrane segments; these proteins are shunted sideways through an opening in the channel wall. To understand how the protein transport process works, a group of researchers from the Harvard Medical School, the Max Planck Institute of Biophysics, and University Luebeck crystallized SecY from a methane-producing "archaebacterium" and solved its 3-D structure, based on x-ray diffraction measurements obtained at beamlines 8-BM (NE-CAT), 14-BM (BioCARS-CAT), and 19-ID (SBC-CAT) at the APS, and NSLS beamline X25 at Brookhaven National Laboratory.

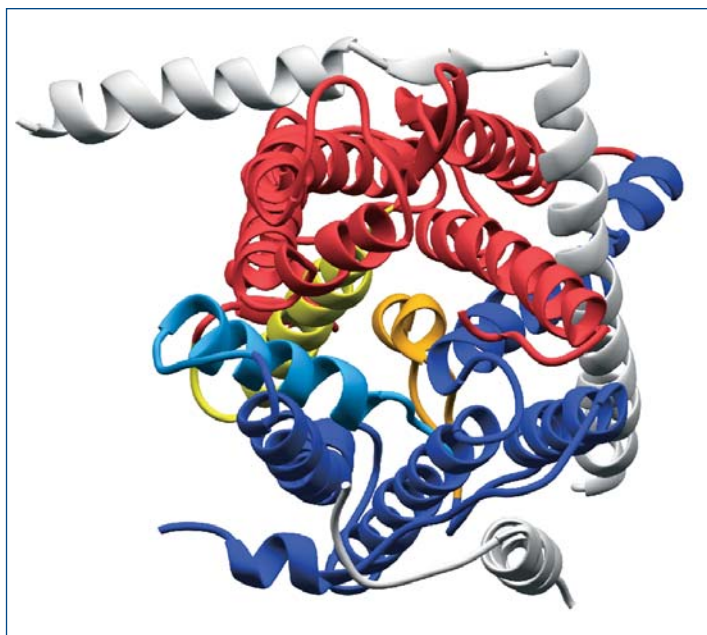
The group doing this study asserts that the channel is formed by one SecY molecule, not between multiple SecY proteins, as was previously suspected. SecY is dimpled on one end with a funnel-shaped cavity 20 to 25 Å wide at its mouth. The fun-

nel tapers to a close in the middle of the molecule, indicating that the structure may correspond to the closed channel. A short stretch of protein plugs the channel (Fig. 1), and the researchers propose that the channel opens when the plug swings toward the back of the protein. This unplugging would leave an hourglass-shaped channel—two funnels opening out from a central constriction. The 5- to 8-Å constriction is lined with flexible, water-averse amino acids, which may act as a gasket-like seal as a protein snakes through, preventing ions and other small molecules from rushing out. Previous models assumed that another cellular complex such as the protein-manufacturing ribosome sealed the mouth of the channel, but electron micrographs have observed gaps between the channel and ribosome.

The signal sequence-binding site is at the front of the channel. The researchers propose that the signal sequence wedges open the channel wall and contorts it so that the plug doesn't fit snugly into the constriction (Fig. 1). A transmembrane segment could also slip out into the surrounding membrane from that side, they suggest, and membrane-averse portions of the transmembrane protein could pass through the gap between channel and ribosome.

The belief was that SecY proteins collect in groups of between two and four to form a channel. Although the researchers say this is still a possibility, they consider it unlikely because the channel is known to contain water and the outsides

Fig. 1. View down the putative channel formed by the SecY protein, which spans the cell membrane and transports other proteins through or into the membrane. A small portion of the protein (orange) may act as a plug, becoming dislodged only when an outgoing protein wedges apart two faces of the channel (red and blue). Proteins destined to reside in the membrane may exit through the channel's front (yellow and light blue).



by a fellowship from the Damon Runyon Cancer Research Foundation to W.M.C., and by fellowships from the Human Frontier Science Program Organization to I.C. and Y.M. E.H. was supported by grants from the Deutsche Forschungsgemeinschaft and Fonds der Chemischen Industrie. T.A.R. and S.C.H. are Howard Hughes Medical Institute Investigators. Use of the Advanced Photon Source was supported by the U.S. Department of Energy, Office of Science, Office of Basic Energy Sciences under contract No. W-31-109-ENG-38.

of SecY proteins are greasy and could not combine together to form a water-filled pore. Grouping may instead facilitate regulation of the transport process by other molecules, they suggest.

— JR Minkel

See: B. van den Berg¹, W.M. Clemons, Jr.¹, I. Collinson², Y. Modis³, E. Hartmann⁴, S.C. Harrison³, and T.A. Rapoport¹, "X-ray Structure of a Protein-Conducting Channel," *Nature* **427**(1), 36 (January 2004).

Author Affiliations: ¹Harvard Medical School, ²Max Planck Institute of Biophysics, ³Children's Hospital and Harvard Medical School, ⁴University Luebeck

Correspondence: tom_rapoport@hms.harvard.edu

The National Synchrotron Light Source is supported by the U.S. Department of Energy, Division of Materials Sciences and Division of Chemical Sciences; SBC-CAT is supported by the U.S. Department of Energy, Office of Science, Office of Basic Energy Sciences; NE-CAT is supported by an award from the National Center for Research Resources at the National Institutes of Health. This work was supported

SIGNALING VIA CONFORMATIONAL PLASTICITY: SURPRISES FROM VINCULIN

It has long been known that the protein vinculin plays an important role in cellular junctions. The regulation of cell-cell and cell-matrix binding depended on vinculin, but its exact role remained a mystery. It was thought that vinculin remained largely passive in the adhesion process and served merely as a scaffold for other binding partners. New data, however, show that vinculin, in association with its partner molecule, talin, undergoes dramatic conformational changes, called "helical bundle conversion," that allow it to actively control critical cellular adhesion processes.

Vinculin orchestrates reorganization of the actin cytoskeleton following formation of cell-cell (adherens junctions) and cell-matrix (focal adhesions) contacts. In focal adhesions, vinculin links the actin cytoskeleton to integrin receptors through its interactions with talin, though vinculin's ability to bind to its partners is masked by an intramolecular interaction between its N-terminal head domain (Vh1) and its tail (Vt) domains, which clamp the molecule in a closed conformation. Severing the Vh1-Vt interaction thus activates vinculin and was thought mediated by the binding of acidic phospholipids to the Vt domain. But recent crystal structure determinations of the human Vh1:Vt complex and the Vh1:talin complex by investigators from St. Jude Children's Research Hospital, Global Phasing Limited, and the University of Tennessee revealed a new model, whereby talin vinculin binding sites (VBS) activate

vinculin by severing the extensive hydrophobic interactions between the helical bundles of Vh1 and Vt.

Using an array of data sets, most of which were collected at the APS (SBC-CAT, sector 19; SER-CAT, sector 22; and COM-CAT, sector 32), the research team determined the crystal structures of the human Vh1:Vt complex to 2.35-Å resolution, and that of the Vh1:talin-VBS3 complex to a resolution of 2.7 Å. Native and derivative crystals were extremely sensitive to radiation, especially the SeMet derivatives at the Se peak wavelength. Only the first few frames of several data sets were merged to provide a complete data set for phase determinations.

The structure of the Vh1:Vt complex revealed that the five-helical bundle of Vt changed little when in complex with the Vh1 domain. Further, the Vh1 domain was revealed as an elon-

Continued on next page

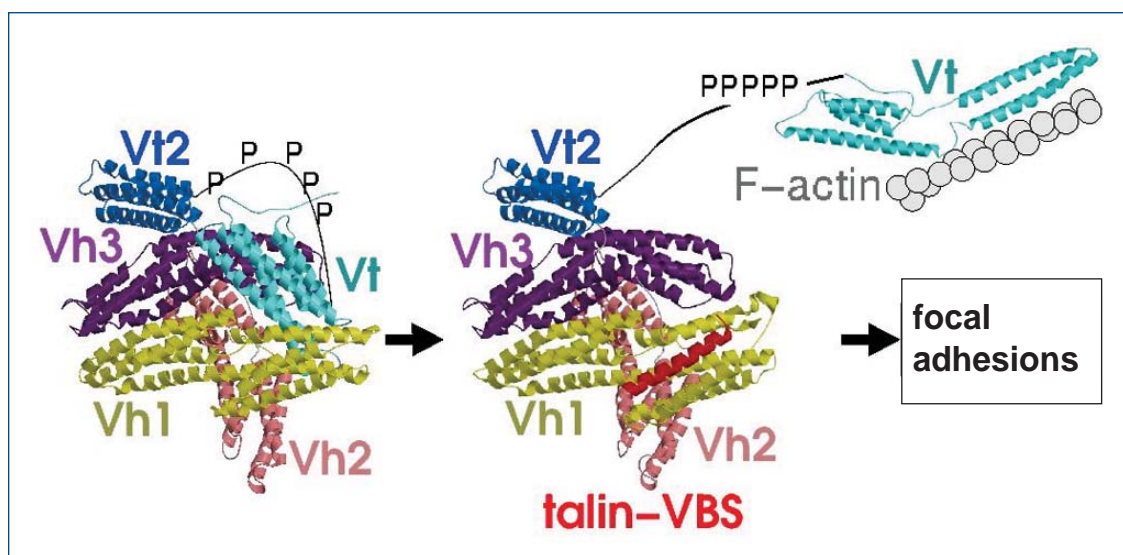


Fig. 1. Ribbon representation of the structure of the inactive conformation of vinculin is shown at left. The protein contains eight helical bundles that organize the protein into five distinct domains, with a seven-helical bundle at its head (Vh1, yellow), a five-helical bundle in its tail (Vt, light blue), and three globular-helical bundle domains in between that are structurally related to either Vh1 (Vh2, pink, and Vh3, magenta) or Vt (Vt2, dark blue). A proline-rich (P-P-P) and structurally disordered linker joins the Vt and Vt2 domains and is believed to function as a flexible hinge for the protein. The extensive hydrophobic interactions in the Vh1 and Vt domains clamp vinculin in a closed architecture, yet these interactions are abolished by the high-affinity binding of amphipathic-helical vinculin binding sites (VBS) present in the central rod of talin (talín-VBS, red).

gated seven-helical bundle with two four-helical bundle substructures joined by a long, centrally shared α -helix. The structure of the Vh1 domain was most similar to the β -catenin: α -catenin complex, which is another seven-helical bundle that forms when the β -catenin α -helix displaces the α -helices of the α -catenin homodimer by a helical exchange mechanism in which one helix swaps out for another.

A similar sequence of events was thus predicted for the Vh1:talín-VBS3 complex, but this structure established a totally new mechanism for altering protein structure: the binding of the amphipathic α -helix of talin VBS3 provoked dramatic movements and changes in the conformation of the α -helices of the *N*-terminal bundle of Vh1, by means of a process coined “helical bundle conversion.” Importantly, this structure also established talin as a direct trigger that activates vinculin as these drastic alterations in structure abolish the Vt binding site in Vh1.

The structure of the “active” Vh1:VBS3 complex paved the way for solving the crystal structure of the Vh1 domain in complex with talín-VBS1 to a resolution of 2.4 Å. This was accomplished by means of molecular replacement using data collected at the SBC-CAT 19-ID beamline. These analyses confirmed that all of the talin VBS provoke helical bundle conversion of vinculin's *N*-terminal helical bundle. Most recently, the group solved the full-length (116-kDa) structure of human vinculin to a 2.85-Å resolution from data sets collected at the APS (SBC-CAT 19-ID and SER-CAT 22-ID beamlines) by using single-wavelength

anomalous dispersion. This structure revealed three new globular α -helical bundle domains. Two are seven-helical bundles that are structurally highly related to Vh1, and were thus coined Vh2 and Vh3; the third bundle domain is a four-helical structure most closely related to Vt, and was thus denoted the Vt2 domain. Between the Vt and Vt2 domains is a highly disordered and flexible proline-rich linker. This structure established that the most extensive inter-domain interactions in vinculin indeed occurred between Vh1 and Vt, whereas the other helical bundles are loosely packed. Thus, when the Vh1-Vt interaction is severed, for example following talin binding, the Vt domain is predicted to swing free from the rest of the molecule to allow it to bind to other partners at sites of cell adhesion (Fig. 1). — *Mona Mort*

See: T. Izard¹, G. Evans², R.A. Borgon^{1,3}, C.L. Rush^{1,3}, G. Bricogne², and P.R.J. Bois¹, “Vinculin Activation by Talin through Helical Bundle Conversion,” *Nature* **427**, 171 (8 January 2004).

Author Affiliations: ¹St. Jude Children's Research Hospital, ²Global Phasing Limited, ³University of Tennessee
Correspondence: tina.izard@stjude.org

This work was supported in part by the Cancer Center Support (CORE) Grant and by the American Lebanese Syrian Associated Charities (ALSAC). Use of the Advanced Photon Source was supported by the U.S. Department of Energy, Office of Science, Office of Basic Energy Sciences under Contract No. W-31-109-ENG-38.

STRUCTURE OF TRANSLATION FACTOR REVEALED

Translating messenger RNA into protein is a complex process that requires a cast of hundreds of macromolecules. A large number of protein and RNA molecules assembles at the initiation codon of the mRNA, and there are at least 12 eukaryotic initiation factors (eIFs) involved, two of which hydrolyze GTP. Knowing more about how this process is regulated would aid in understanding cellular responses to environmental stressors, such as viral infection, nutrient deprivation, and radiation damage. eIF2—consisting of the three subunits α , β , and γ —is essential for viability in yeast and is highly conserved among all eukaryotes and archaeobacteria. New structural information on eIF2 γ from an archaeobacterium provides unexpected details that greatly increase understanding of translation initiation.

Investigators from The Rockefeller University and the National Institutes of Health used the SGX-CAT 31-ID beamline at the APS to determine the x-ray structure of eIF2 γ from *Methanococcus jannaschii* at 2.4-Å resolution. eIF2 γ , a GTPase that delivers the initiator tRNA during a rate-limiting step in initiation, exhibits a structure that is similar to those of known translation elongation factors. The main structural features of eIF2 γ include an N-terminal G domain and two β -barrel domains (II and III) in a closed configuration, with domain II packed against the G domain near the Switch regions. An unusual zinc ribbon motif, not yet found in other GTPases, was discovered within the G domain. Using structure-based site-directed mutagenesis, two adjacent features on the surface of eIF2 γ , responsible for binding the α -subunit of eIF2 and the Met-tRNA, were identified. The combined structural, biochemical, and genetic results provide a much more detailed picture of how the eIF2 heterotrimer assembles, suggesting starting points for further detailed study and understanding of translation initiation.

M. jannaschii genomic DNA encoding residues 35-437 of eIF2 γ were amplified using PCR and inserted into an expression vector, expressed in *E. coli*, and purified. Hanging drop vapor diffusion was used to grow native and Se-Met crystals in the monoclinic space group $P2_1$ with one protein molecule per asymmetric unit ($a = 52.8$ Å, $b = 52.4$ Å, $c = 74.1$ Å, $\beta = 92.5^\circ$, diffraction limit = 2.4 Å resolution), at room temperature. The SGX-CAT beamline was used to measure diffraction data. At

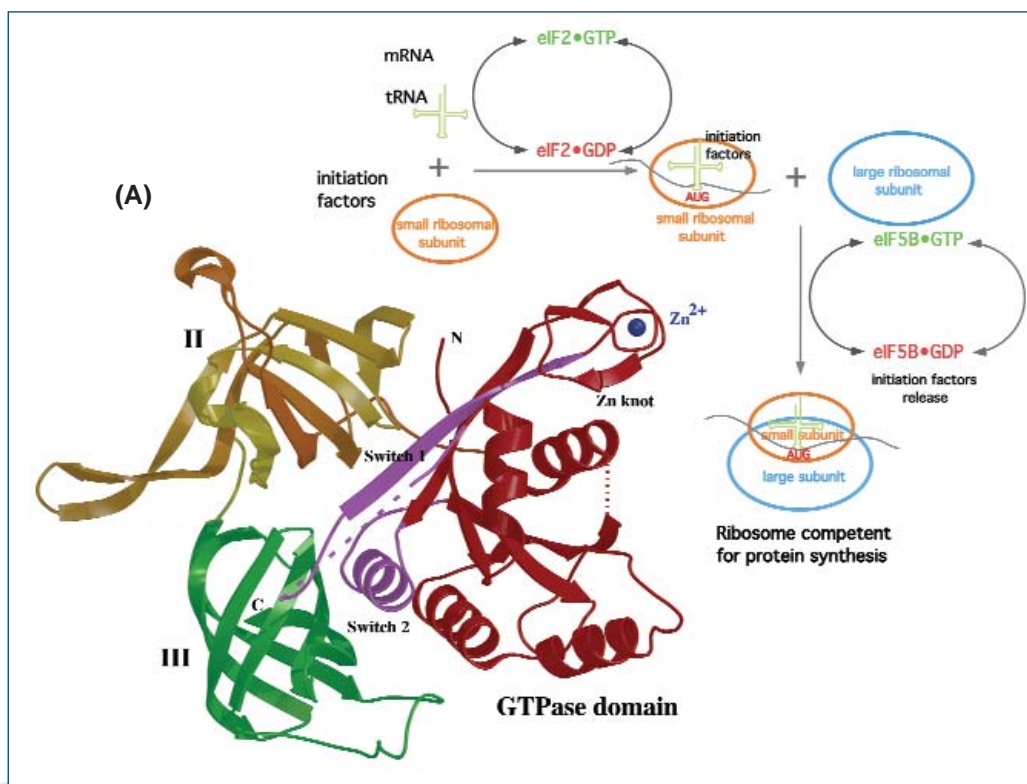


Fig. 1. Structure of eIF2 γ . (A) Ribbons diagram of eIF2 γ , with N- and C-termini and domains labeled. Domain color-coding is as follows: GTPase domain, red; domain II, yellow; and domain III, green. The Switch regions are shown in magenta and a dark blue sphere denotes the Zn ion. A simplified diagram of the translation initiation pathway is shown on the right.

an x-ray wavelength corresponding to the white line of the selenium K-absorption edge, Se-Met single wavelength anomalous dispersion (SAD) data were collected. To obtain mutant forms of eIF2 γ , the appropriate codons were mutated in the expression vector.

Structure- and sequence-based comparisons of *M. jannaschii* eIF2 γ to known eukaryotic and archaeal homologs showed that the conserved residues map to hydrophobic cores of the three domains (G, II, and III) and mutants map to random coil portions (Fig. 1). The data show that all known eIF2 γ s exhibit highly similar three-dimensional structures. A zinc rib-

Continued on next page

bon extends from the G domain and forms an overhang between the G domain and domain II. Domains II and III are β -barrels that show structural similarity to previously described elongation factors. Significant conformational changes appear to be restricted to two polypeptide chain segments, Switches 1 and 2. Switch 1, positioned at the interface of the G domain and domain II, stabilizes the relative orientations of the two domains. Switch 2, located at the heart of the structure, makes contact with domains II and III. Mutations in eIF2 γ affect eIF2 α binding, pointing to the overall importance of the γ subunit for eIF2 activity. Unlike mutations in yeast eIF2 γ , certain eIF2 γ mutations in *M. jannaschii* also impair the Met-tRNA binding, suggesting additional subtleties in archaeobacterial translation initiation.

Within eIF2, the α - and β -subunits and the Met-tRNA use the γ -subunit as a foundation for assembly. The detailed crystal structure studies of eIF2 γ allow location of conserved adjacent surfaces responsible for eIF2 α and tRNA binding. Further bio-

chemical, genetic, and structural studies can now be directed toward understanding interactions among eIF2 subunits, tRNA, mRNA, and the small ribosomal subunit. Such studies will greatly enhance our understanding of translation initiation.

— *Mona Mort*

See: A. Roll-Mecak¹, P. Alone², C. Cao², T.E. Dever², and S.K. Burley¹, "X-ray Structure of Translation Initiation Factor eIF2 γ " *J. Biol. Chem.* **279**, 10634 (2004).

Author Affiliations: ¹The Rockefeller University, ²National Institutes of Health

Correspondence: stephen_burley@stromix.com;
rolla@cmp.ucsf.edu

This work was supported by NIH grant GM61262 (to S.K. B.) and a Burroughs-Wellcome Fund Interfaces training grant (to A. R.-M.). Use of the Advanced Photon Source was supported by the U.S. Department of Energy, Office of Science, Office of Basic Energy Sciences, under contract No.W-31-109-ENG-38.

STRUCTURE OF A DNA SPELL CHECKER

Errors in DNA duplication are important fodder for evolution, but they can also lead to cancer or hereditary diseases in multicellular organisms. This tension plays out in the cellular machinery responsible for DNA duplication, which must be accurate but not too accurate. Researchers from Duke University Medical Center, using the BioCARS-CAT beamline 14-BM have determined how the enzyme that builds DNA molecules identifies errors along the way. They solved the structure of the enzyme in the presence of all the possible errors that could occur during DNA duplication. The results show how errors disrupt the enzyme's structure and force it to slow down.

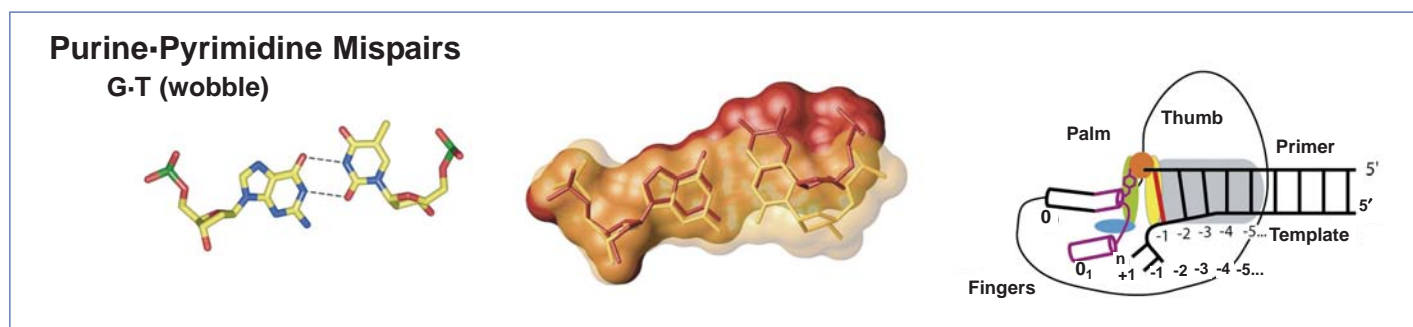


Fig. 1. Mismatched DNA base pairs distort the structure of the enzyme that synthesizes DNA, shown schematically on the right. When guanine and thymine come together, for example, the pair twists relative to its normal orientation (middle, red overlay vs. yellow), and the enzyme must adjust itself correspondingly (right, distorted regions in red and purple).

A DNA molecule is essentially a ladder. Each rung consists of a pair of the "bases" adenine, guanine, cytosine, and thymine. In normal DNA, bases pair together into a rung the same way: adenine with thymine or guanine with cytosine. When DNA is duplicated, an enzyme called polymerase reads the sequence of one strand, the template, and constructs a complementary strand base-by-base. Every guanine in the template is paired with a cytosine in the complementary strand, for example. Sometimes the wrong base finds its way into the duplicate strand. If it remains and the erroneous base is passed on to subsequent DNA molecules, a mutation occurs.

Polymerase plays a major role in proofreading the new strand as it's being built. If the enzyme adds the wrong base, it hesitates, giving other enzymes a chance to remove the mistake. Polymerase can sense errors up to four base pairs behind the one it is in the process of forming. To figure out how, the group crystallized and solved the structure of a commonly used bacterial polymerase bound to all of the possible base pair mismatches, such as guanine-thymine or guanine-guanine. They compared each structure's "active site," the place on the enzyme where a base is added to the growing DNA strand, based on x-ray diffraction measurements taken at 14-BM. No

one had solved the structure of a mismatch bound to polymerase before.

This study shows that a mismatch can disrupt the active site in one of four ways: It can cause the template strand or the duplicate (or both) to warp, or cause the two strands to split apart. For example, when a guanine is erroneously attached to a thymine in the template strand, the thymine positions itself normally but the guanine twists sideways (Fig. 1). The twisting disrupts the fit between template and polymerase so that the template is ejected from the active site. The distortion in the template extends back three base pairs from the mismatch. These structural deformations cause polymerase to hesitate, or stall. In most cases, the four categories of mismatch correlate with their observed abilities to stall polymerase. The structures should allow researchers to infer how different interactions contribute to the stalling process.

The group next extended the copy strands by soaking the crystals in free nucleotides, the source of new bases. The guanine-thymine mismatch, for example, moves down the line of new base pairs like a swallowed pill, changing its orientation a

little bit at each new position. Within three base pairs of the active site, the mismatch still distorts the DNA enough to pull the template away from the enzyme. At four base pairs distance, the mismatch causes the active site to fluctuate between a disrupted and undisrupted state, and by the time the mismatch is six nucleotides away and free of the enzyme entirely, the active site has returned to normal. — *JR Minkel*

See: S.J. Johnson and L.S. Beese, "Structures of Mismatch Replication Errors Observed in a DNA Polymerase," *Cell* **116**, 803 (March 19, 2004).

Author Affiliation: Duke University Medical Center
Correspondence: lsb@biochem.duke.edu

This research was carried out in part at the National Synchrotron Light Source, Brookhaven National Laboratory, which is supported by the U.S. Department of Energy, Division of Materials Sciences and Division of Chemical Sciences, under Contract No. DE-AC0298CH10886. Use of the BioCARS-CAT sector 14 was supported by the National Institutes of Health, National Center for Research Resources, under grant number RR07707. The work was supported by grants to L.S.B. from the Human Frontiers Science Program (RG0351/1998-M) and the National Cancer Institute (P01CA92584). Use of the Advanced Photon Source was supported by the U.S. Department of Energy, Office of Science, Office of Basic Energy Sciences under Contract No. W-31-109-ENG-38.

REP MARKS THE SPOT...OF VIRAL DNA INSERTION

Researchers from the National Institutes of Health, using the SER-CAT beamline 22-ID, have solved the three-dimensional (3-D) structure of the DNA binding domain of a protein that allows a virus to insert its DNA into a specific spot on a human chromosome. Multiple copies of the DNA binding domain of the viral protein, called Rep, latch onto a distinct pattern of DNA in an asymmetric way that prepares the viral genome for duplication and insertion into the host chromosome. These results may help scientists develop safer gene therapies to treat hereditary diseases.

Researchers typically exploit viruses as gene therapy vectors, or vehicles for replacement genes, because they enter cells selectively and cause the cells to express viral genes. A big problem with existing vectors is that they insert their DNA willy-nilly. Nothing prevents the replacement gene from landing in the middle of a host gene and disrupting it. The vectors also tend to place their contents near genes that the cell is actively copying, which poses a risk of causing cancer. In 2003, a retroviral gene therapy trial caused leukemia in two boys, apparently by this mechanism. Adeno-associated virus (AAV) is the only virus known to insert its DNA into the same location most of the time, on human chromosome 19. The Rep protein is key to this ability. Without it, AAV behaves like retroviruses such as HIV and integrates its DNA randomly. A better understanding of Rep could therefore help researchers engineer more precise vectors.

To understand how Rep binds to DNA, a group from the National Institutes of Health crystallized the DNA-binding portion of Rep attached to either of two binding sites on the viral DNA. AAV contains a single DNA strand, which folds back onto itself at the end, forming a double-stranded neck connected to a hairpin-like structure, each of which contains a different Rep

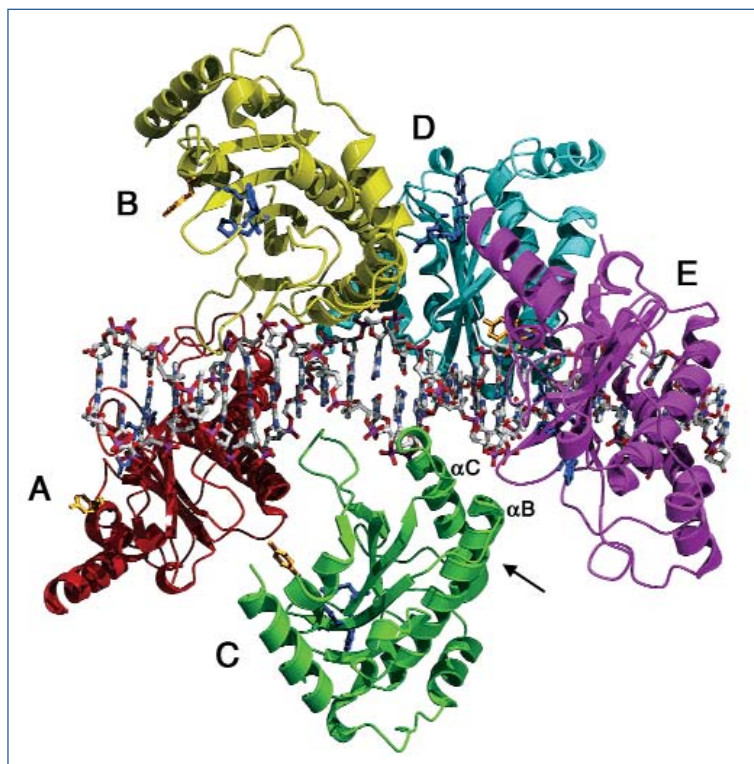
binding site. When bound to the neck (at a sequence called simply the Rep binding site), Rep unwinds a nearby section of double-stranded DNA and cuts one strand, which allows the duplication process to begin. The hairpin structure seems to help Rep perform the unwinding and cutting. The same Rep binding site found in the virus also appears on chromosome 19, implying that Rep is key for insertion of the viral genome, too.

Five Rep molecules spiral around the Rep binding site (Fig. 1), each grasping one strand of the DNA like tweezers, according to the group's 3-D structures, obtained from x-ray diffraction experiments carried out on SER-CAT beamline 22-ID at the APS. The hairpin structure binds to a pocket on the opposite side of the protein. The Rep binding site consists of several nearly identical repeated sequences of four "nucleotides," the building blocks of DNA. The group found that Rep grips the binding site at the junction between two repeated sequences with a strength that varies depending on the exact sequence.

The structure suggests a mechanism by which Rep initiates DNA duplication, the researchers say. Attached to Rep's DNA binding portion is an enzyme portion that unwinds double-

Continued on next page

Fig. 1. The structure of the Rep protein helps explain how adeno-associated virus inserts its DNA at a specific location on a human chromosome. Here, five Rep molecules (A-E) are attached to their binding sites on the viral DNA. One Rep is positioned to bind to a hairpin-like fold in the DNA (arrow).



stranded DNA, called a helicase. The crystallized proteins are oriented so that all of their nucleases would point toward the site at which Rep is known to cut the viral DNA. The researchers propose that Rep binding causes the helicases to join into a donut structure, which separates the strands of DNA and allows one to be cut. The hairpin DNA could bend to contact a Rep protein sitting on the binding site. Rep could bring two DNA molecules together by grabbing the Rep binding site of one molecule and the unwinding site of the other. — *JR Minkel*

See: A. Burgess Hickman, D.R. Ronning, Z.N. Perez, R.M. Kotin, and F. Dyda, "The Nuclease Domain of Adeno-Associated Virus Rep Coordinates Replication Initiation Using Two Distinct DNA Recognition Interfaces," *Molecular Cell* **13**, 403 (13 February 2004).

Author Affiliations: National Institutes of Health
Correspondence: dyda@ulti.niddk.nih.gov

Work supported in part by the NIH Intramural AIDS Targeted Antiviral Program. Use of the APS supported by the U.S. DOE, Office of Science, Office of Basic Energy Sciences, under Contract No. W-31-109-ENG-38.

FUNCTIONALLY SIMILAR RNA MOLECULES HAVE DIVERSE STRUCTURES

Some RNA molecules, known as ribozymes, serve as enzymes in the complex process of life. Of particular interest in this category of RNA is ribonuclease P (RNase P), integral to the maturation of transfer RNA (tRNA) and highly conserved across taxonomic kingdoms. RNase P contains both RNA and protein subunits. Bacterial RNase P is classified into two major types, A and B, depending on the sequence of the RNA subunit. Both types of bacterial RNase P have, in their RNA subunits, a catalytic domain and a specificity domain; the latter is responsible for recognizing and binding pre-tRNA. There are marked differences in how these specificity domains of types A and B are put together. The variance is large enough so that the two types would be expected to fold differently. Despite the underlying structural differences, new data obtained by investigators from Northwestern University and The University of Chicago show that types A and B end up having remarkably similar three-dimensional folds in the region that recognizes tRNA.

The group studied the crystal structure of the 161-nucleotide specificity domain of bacterial A-type RNase P and compared it to the previously described B-type RNase P. The A-type specificity domain showed major differences in secondary and tertiary structures from that of the B-type. But these underlying structural differences did not lead to disparate three-dimensional structures for the cores of the domains, which were remarkably similar in both the A and B types. The data

show that, even though there are different sets of interactions stabilizing the cores in the two RNase P types, the end result is a similar geometry in the pre-tRNA recognition region. These diverse ribozymes represent two different structural routes to the same end and create new respect for the diversity of RNA molecules.

The crystal structure of the *Thermus thermophilus* RNase P S domain (nucleotides 75 to 235) was determined to a reso-

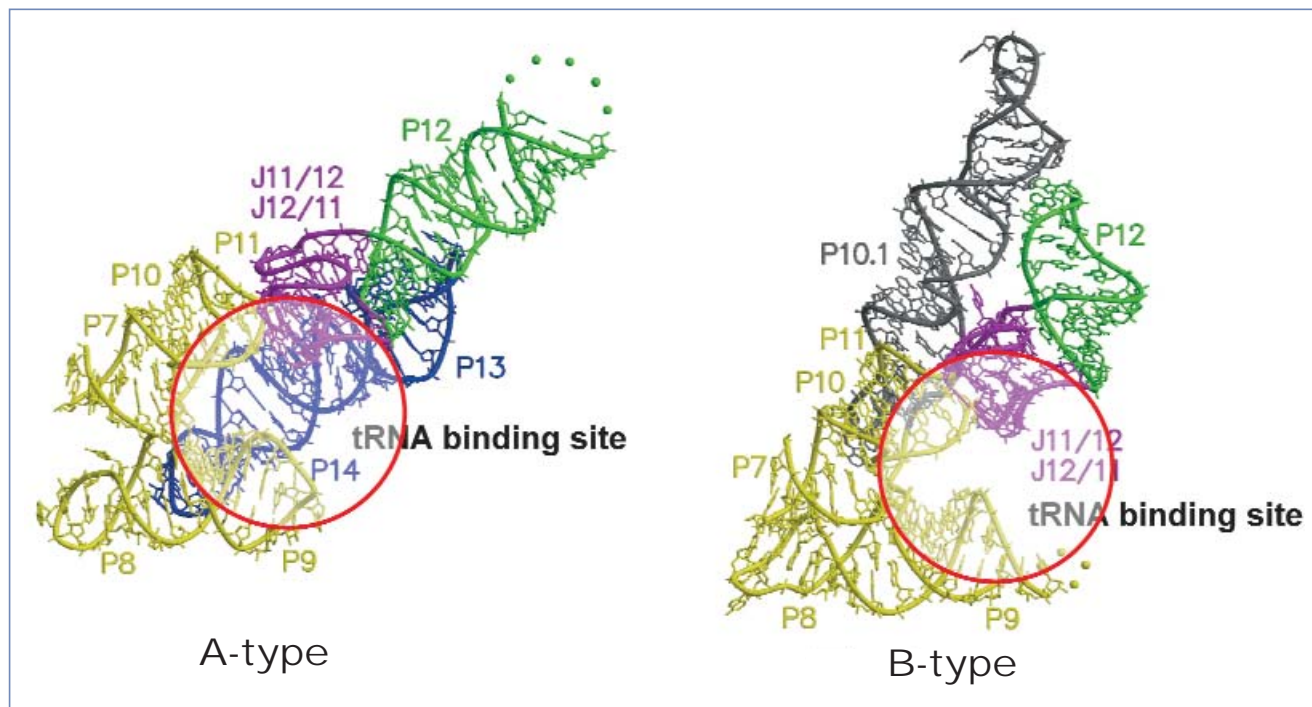


Fig. 1. The S-domains of the two bacterial types of RNase P have different architectures, but the overall structure of the tRNA binding site (circled in red) is conserved.

lution of 2.9 Å from single-wavelength anomalous diffraction using Ba^{+2} . The DND-CAT and LS-CAT beamlines (5-ID and 32-ID, respectively) at the APS were used to facilitate measurements.

The S domain from this A-type RNase P was compared to the S domain of a B-type RNase P previously reported by the same researchers for *Bacillus subtilis* and also solved by using data measured at beamline 5-ID. Certain differences between these two structures could affect the tertiary fold: the A-type J12/11 internal loop is interrupted by the insertion of the P13 and P14 stems, absent in the B-type; the B-type P10.1 stem involved in folding is absent in the A-type. These and other differences are large enough that they could be expected to lead to very different three-dimensional structures for the pre-tRNA recognition region (Fig. 1). But biochemical data from other laboratories show that the nucleotides recognized by these two types of RNase P are equivalent. Despite the substantially different underlying structures, when it comes to the three-dimensional folding of the region necessary for pre-tRNA recognition, types A and B appear to be quite similar.

The A and B types of RNase P do share a major common feature: an opening formed by stems P9, P10, and P11 and the nonhelical module J11/12-J12/11. The local positions of the nucleotides are remarkably similar and allow an understanding

of how the pre-tRNA orients in the opening. The high degree of structural conservation further underscores the finding that the type A and B RNase P molecules are two different large RNA molecules that have an identical function. The molecules look quite different but, because the functionally important regions are conserved, they behave in a similar fashion. The two RNase P subtypes are using different means to achieve the same end. The internal complexity of RNA molecules may contribute to their ability to perform the same function, even when their overall architecture is different. — *Mona Mort*

See: A.S. Krasilnikov¹, Y. Xiao¹, T. Pan², and A. Mondragón¹, "Basis for Structural Diversity in Homologous RNAs," *Science* **306**, 104 (1 October 2004).

Author Affiliations: ¹Northwestern University, ²The University of Chicago

Correspondence: a-mondragon@northwestern.edu

This work was supported by: NIH (A.M.) and an NIH National Research Service Award Fellowship (A.K.); the R.H. Lurie Cancer Center of Northwestern University to the Structural Biology Center; and DuPont, Dow, NSF, and DOE for the DND-CAT at the APS. Use of the Advanced Photon Source was supported by the U.S. Department of Energy, Office of Science, Office of Basic Energy Sciences, under Contract No. W-31-109-ENG-38.

DISSECTING THE ATOM

When a photon with low energy hits an atom, in most cases just a single electron is knocked loose from that atom. But higher energy photons, such as hard x-rays, can knock out two or more electrons at a time. Researchers from the University of Tennessee at Knoxville and Argonne National Laboratory used x-ray beams from the BESSRC/XOR wiggler beamline 11-ID at the APS to knock out electrons from krypton atoms in order to gain a new understanding of the fundamental physical processes of ionization and decay that can occur in atoms.

When hard x-rays interact with atoms, numerous processes can occur: electron excitation to different empty levels in the atom, recapture of electrons, and “bubbling” up to the outer shells of empty spaces (known as “holes”) where an electron might otherwise reside in an atom. These various phenomena provide different routes to the residual ion, which might ultimately have lost one, two, or even all of its original electrons.

Using the 11-ID beamline, the research group is delving into the depths of an atom's electron shells to discover what happens when hard x-ray photons ionize the atom. The charge on such ions depends strongly on the energy of the x-ray photons. The properties of the resulting ion can reveal new information about how atoms are organized and might one day lead to new applications in laser optics for medical and analytical uses.

The group studied the effects of x-ray photons on atoms of the noble gas krypton, which provides a replenishable, noncorrosive target of non-interacting atoms. Krypton has an atomic number of 36, which means there are 36 electrons in various shells around the atomic nucleus. An x-ray photon hitting a krypton atom can eject an electron to produce a krypton ion. This residual krypton ion also has a hole in a deep inner shell, which means it is in a highly energetic state and can release the absorbed photon energy via several paths. For instance, the hole can bubble up through the atom's energy levels, triggering the loss of additional electrons. These various energy decay paths involve a combination of radiative (fluorescence) and nonradiative (Auger) processes. The researchers hope their studies will ultimately lead to a predictive and quantitative map of these decay paths.

Earlier research examined the ion charge state distribution with the incident x-ray energy close to the so-called “K-edge.” (The K-edge is the energy required to eject the deepest electron, a 1s electron, from the atom's innermost shell.) In the vicinity of the K-edge, it is possible for the 1s electron to be excited to a vacant orbital, such as the “5p” (6p, 7p,...); the

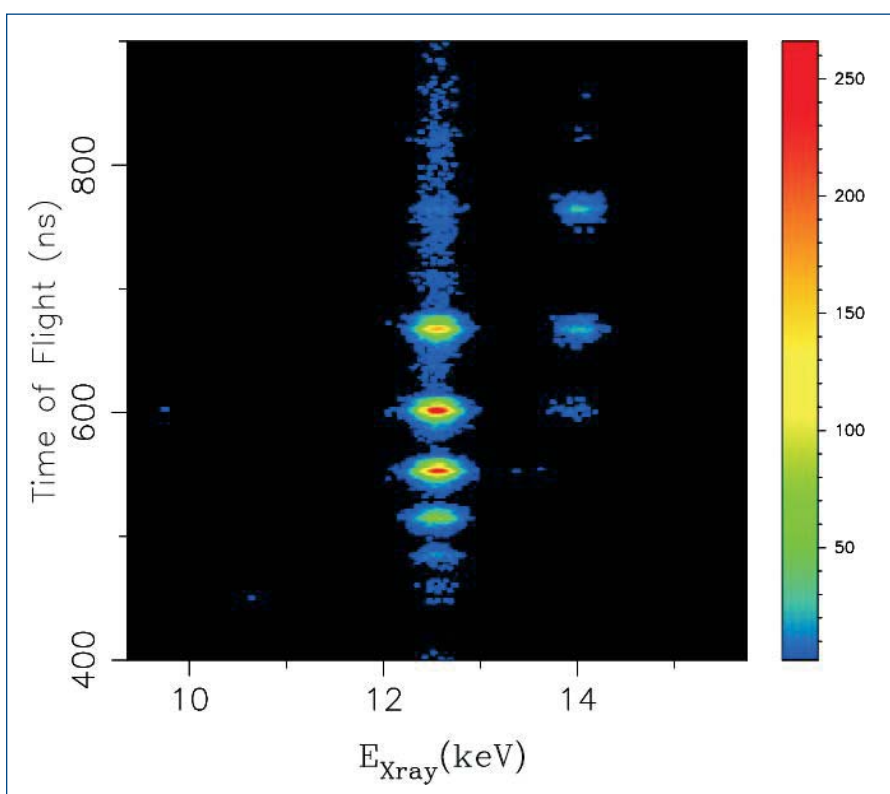


Fig. 1. Two-dimensional representation of the fluorescence energy vs. ion time-of-flight resulting from excitation of krypton at an x-ray energy 10 eV above the K-edge. The decay through the 2p hole state ($K\alpha$ at 12.6 keV) results in higher charge states than that proceeding through the 3p hole state ($K\beta$ at 14.1 keV).

researchers anticipated that the decay paths would be different here. In this earlier work, the researchers monitored the ion charge state for events in which K-fluorescence occurred.

The group's current work builds on this past research by using a new method that allows them to observe individual decay paths in isolation. They have now better defined the decay path by using a high-resolution x-ray detector, which can distinguish between decay paths proceeding through a 2p or a 3p hole.

The new experiments are feasible because the researchers are using a coincidence technique between fluorescence x-rays and ions. Figure 1 shows a map of the decay paths the team obtained by using this technique. On the basis of these results, they have developed a theory—the “spectator cascade decay” (SCD) model—to explain their findings. In the

SCD model, an excited electron acts as a spectator to the decay of the krypton ion's core. The model provides the means of predicting ionization effects, not only for krypton, but for many other atoms. The research bring us one step closer to understanding complex vacancy decay patterns in atoms. The understanding of such decay phenomena may suggest techniques to control or prevent the decay of highly energetic states, which could be exploited in a new type of laser that employs higher photon energy. Such lasers could have a variety of biomedical and analytical applications. — *David Bradley*

See: G.B. Armen¹, E.P. Kanter², B. Krässig², J.C. Levin¹, S.H. Southworth², and L. Young², "Spectator-Electron Behavior

During Cascade Decay in Krypton," *Phys. Rev. A* **69**, 062710 (2004).

Author Affiliations: ¹University of Tennessee, Knoxville; ²Argonne National Laboratory
Correspondence: young@anl.gov

Work supported by the National Science Foundation at the University of Tennessee. The ANL group was supported by the Chemical Sciences, Geosciences, and Biosciences divisions of the Office of Basic Energy Sciences, Office of Science, U.S. Department of Energy, under Contract No. W-31-109-ENG-38. Use of the Advanced Photon Source was supported by the U.S. Department of Energy, Office of Science, Office of Basic Energy Sciences, under Contract No. W-31-109-ENG-38.

METHANE PRODUCTION: NOT JUST FROM COWS

Hydrocarbons such as methane are believed to arise mainly from organic sources. Although it has been found in the Earth's crust, where there are no living systems, most methane is still assumed to originate in the biosphere, such as from bacterial metabolism in the rumen of cows. Challenging this assumption, new research shows that methane readily forms inorganically at the high pressure and temperature conditions encountered in the Earth's interior, forcing a new look at the planet's hydrocarbon budget. The HP-CAT beamline 16-ID at the APS aided investigators from Indiana University South Bend, the Carnegie Institution of Washington, Harvard University, and Lawrence Livermore National Laboratory in their study of hydrocarbon generation under conditions simulating those in the Earth's upper mantle.

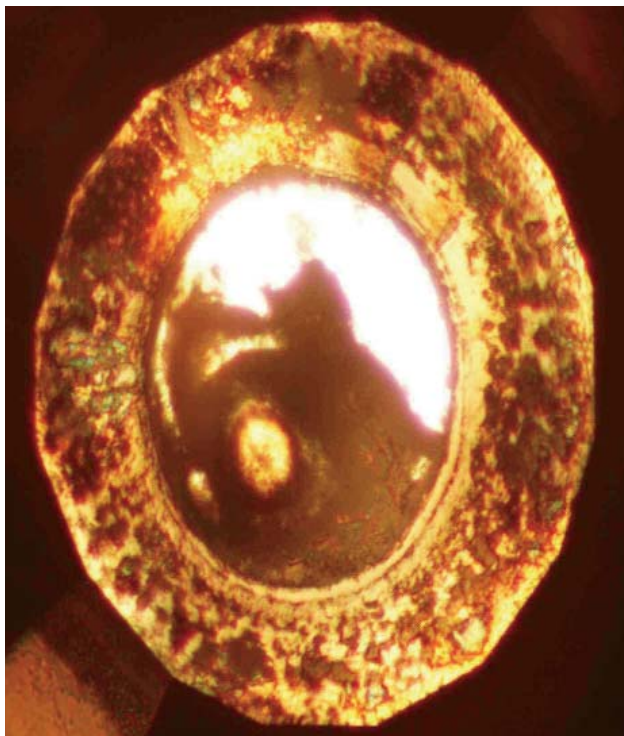


Fig. 1. A diamond anvil cell sample. View looking through the diamonds (using a microscope) to see the sample while it is at high pressure. The sample is in the center and surrounded by a metal foil that keeps it from flowing out.

Using carbonate reduction at high pressure and temperature (5-11 GPa; 500-1,500° C), the team documented *in situ* formation of methane (CH₄) from FeO-wüstite, CaCO₃-calcite, and water. The empirical results are supported by thermodynamic calculations on the statistical mechanics of soft particle mixtures. These data show that hydrocarbons can be formed via abiogenic pathways in the Earth's interior. Because this possible source has been generally ignored, the data also suggest that the Earth has a larger hydrocarbon budget than previously assumed.

Diamond anvil cells, with cutlets ranging between 350 and 700 μm in diameter, were used for the experiments. Simultaneous high pressure and temperature were produced by both resistive (T <600° C) and laser (T >1,000° C) heating. A combination of Raman spectroscopy-for detecting diagnostic C-H stretching vibrations and examining amorphous crystalline phases; synchrotron x-ray diffraction-to identify crystalline phases and help determine reactions; and optical microscopy allowed *in situ* analyses. This array of techniques was used for probing minute areas of the chamber, necessary because of the heterogeneous nature of the samples. The HP-CAT 16-ID beamline was used for x-ray measurements and double-sided Nd-YLF laser heating.

Raman spectra revealed hydrocarbon-rich regions—identified as methane on the basis of band position—

Continued on next page

after laser heating at $\sim 1,500^\circ\text{C}$ and 5.7 GPa. But such high temperatures were not necessary for methane formation, which also occurred *in situ* at 600°C , with resistive heating initiated at 5.1 GPa and temperature ramped at a rate of 50° per minute. Moreover, the amount of methane produced appeared to be greater in the experiments at lower temperatures. *In situ* synchrotron x-ray diffraction shed light on the principal reaction, which appears to be a chemically complex variant of FeO , CaCO_3 , and H_2O producing Fe_3O_4 , CH_4 , and CaO . Accompanying optical microscopy showed phenomena consistent with the presence of methane, such as extensive bubble formation when samples decompressed at room temperature (Fig. 1). Micro-Raman measurements indicate that the bubbles are predominantly methane. Analysis of the thermochemistry demonstrated that methane production is disfavored at higher temperatures: in a reaction of H_2 and CO_2 to produce CH_4 and H_2O , high temperatures favor the production of hydrogen gas and carbon dioxide, while low temperatures favor production of methane and water.

These data show that methane formation can occur at a broad range of pressure and temperature conditions, which

may be widespread in the Earth's mantle. The probable existence of large abiogenic hydrocarbon reservoirs inside the Earth can no longer be ignored. — *Mona Mort*

See: H.P. Scott^{1,2}, R.J. Hemley², H.-k. Mao², D.R. Herschbach³, L.E. Fried⁴, W.M. Howard⁴, and S. Bastea⁴, "Generation of Methane in the Earth's Mantle: *In situ* High Pressure-Temperature Measurements of Carbonate Reduction," P. Natl. Acad. Sci. USA **101**(39), 14023 (September 28, 2004).

Author Affiliations: ¹Indiana University South Bend, ²Carnegie Institution of Washington, ³Harvard University, ⁴Lawrence Livermore National Laboratory

Correspondence: hpscott@iusb.edu

This work was supported by the National Science Foundation, NASA Astrobiology Institute, and DOE/NNSA (Carnegie/DOE Alliance Center); the APS (DOE, BES, OER); a Green Fellowship (Carnegie Institution) to D.R.H.; and an Indiana University-South Bend Faculty Research Grant to H.P.S. Use of the Advanced Photon Source was supported by the U.S. Department of Energy, Office of Science, Office of Basic Energy Sciences, under Contract No. W-31-109-ENG-38.

PROBING IRON HYDRIDE UNDER HIGH PRESSURE

Seismic wave observations have established that Earth's "core" actually consists of a liquid outer core enveloping a solid inner core. From geophysical, cosmochemical, and geodynamic data, it is generally accepted that the core is primarily composed of an iron-rich iron-nickel alloy. Seismic observations, coupled with laboratory experiments, further indicate that the outer core—and to a lesser degree the inner core—is less dense than liquid iron, implying that elements lighter than iron must comprise a non-trivial fraction of the core. One element that might be present in significant quantities is hydrogen. Previous laboratory research had shown that, under high pressures and temperatures, hydrogen and iron combine to form a stable iron hydride. To gain greater insight into the properties of iron hydride, investigators from The University of Chicago, the Carnegie Institution of Washington, and Argonne National Laboratory subjected a sample of iron (Fe) and hydrogen (H) to the high pressures found deep inside the Earth.

The researchers probed the sample by using x-ray beams from the APS for the closely related techniques of nuclear resonant inelastic x-ray scattering (NRIXS) and synchrotron Mössbauer spectroscopy (SMS). Three APS beamlines were used in this research: the XOR 3-ID beamline for the NRIXS and SMS measurements; the GSECARS-CAT 13-ID beamline for pressure calibration; and the HP-CAT 16-ID beamline for obtaining x-ray diffraction patterns of iron hydride to determine its exact crystalline structure.

The sample examined in this research consisted of tiny amounts of iron (enriched in the isotope ^{57}Fe) and liquid hydrogen (H_2), which initially were inserted into a beryllium container (or gasket). The gasket was then squeezed within a diamond anvil cell to pressures up to 52 GPa. At pressures above 3 GPa, the iron and hydrogen combined to form nearly stoichiometric FeH_x (the "x" subscript indicates the proportion of hydrogen atoms to one iron atom in the compound; "nearly stoichiometric" means that $x \sim 1$). Excess hydrogen in the sample formed

a hydrostatic pressure-transmitting medium around the FeH_x , that evenly distributed the pressure (see the photomicrograph in the upper left-hand corner of Fig. 1). X-ray diffraction patterns of FeH showed that it possessed a double hexagonal close-packed (dhcp) structure over the entire range of pressures examined in the research.

The synchrotron x-rays used to probe the sample were focused to a diameter of approximately $10\ \mu\text{m}$ ($1\ \mu\text{m} = 1 \times 10^{-6}\ \text{m}$). As part of the NRIXS technique, the energies of the synchrotron x-rays were stepped in increments about the ^{57}Fe Mössbauer line. The NRIXS method can utilize the nuclear resonance of ^{57}Fe , which lies at the 14.1425-keV energy level. Nuclear resonance occurs, for instance, when an x-ray photon with an energy of 14.1425 keV is absorbed by the ^{57}Fe nucleus, thereby boosting the nucleus into an excited state; the process culminates in the excited nucleus emitting an x-ray photon (at an arbitrary angle to the absorbed photon) with the identical energy of 14.1425 keV. (Actually, NRIXS measures the inelas-

tic scattering of x-rays tuned slightly *off* the nuclear resonance energy because of the additional energy contributed by the lattice's phonon states).

The measurement of the emitted resonant x-rays (i.e., the NRIXS data) yielded information about the Fe-related phonon density of states (DOS) within the sample (see lower part of Fig. 1). The researchers combined their NRIXS results with the known equation of state (EOS) for FeH_x to yield its aggregate compressional velocity (V_p) and shear wave velocity (V_s) at various pressures. The shear wave velocity is especially difficult to determine at high pressure with methods other than NRIXS; the NRIXS data pegged its value at $V_s = 0.023 \cdot P \pm 3.2$ (V_s is in km/sec, while the pressure [P] is in GPa).

Previous research had established the ferromagnetic nature of FeH_x up to pressures of 10 GPa. In this research, the SMS technique was used to determine that FeH_x is actually magnetic up to a pressure of 22 GPa, after which it disappears altogether. (The SMS technique utilizes the elastic scattering of x-rays *exactly* at the nuclear resonance energy, which in this case is 14.1425 keV for ^{57}Fe). The loss of magnetism at 22 GPa corresponds to an abrupt change in the plotted values of V_p and V_s at that same pressure.

This research lends further credence to the case for iron hydride being a significant constituent of Earth's outer core. The researchers point out that a mass fraction of only 0.12–0.48% of hydrogen in the outer core could explain the so-called “core density deficit” in that region of Earth's interior. — Philip Koth

See: W.L. Mao^{1,2}, W. Sturhahn³, D.L. Heinz¹, H.-k. Mao^{1,2}, J. Shu², and R.J. Hemley², “Nuclear Resonant X-ray Scattering of Iron Hydride at High Pressure,” *Geophys. Res. Lett.* **31**, 15618 (2004).

Author Affiliations: ¹The University of Chicago, ²Carnegie Institution of Washington, ³Argonne National Laboratory
Correspondence: wmao@uchicago.edu

Use of the HP-CAT facility was supported by DOE-BES, DOE-NNSA (Carnegie/DOE Alliance Center), NSF, DOD-TACOM, and the W.M. Keck Foundation. GSECARS-CAT is supported by the NSF (EAR-0217473), DOE (DE-FG02-94ER14466), and the State of Illinois. Use of

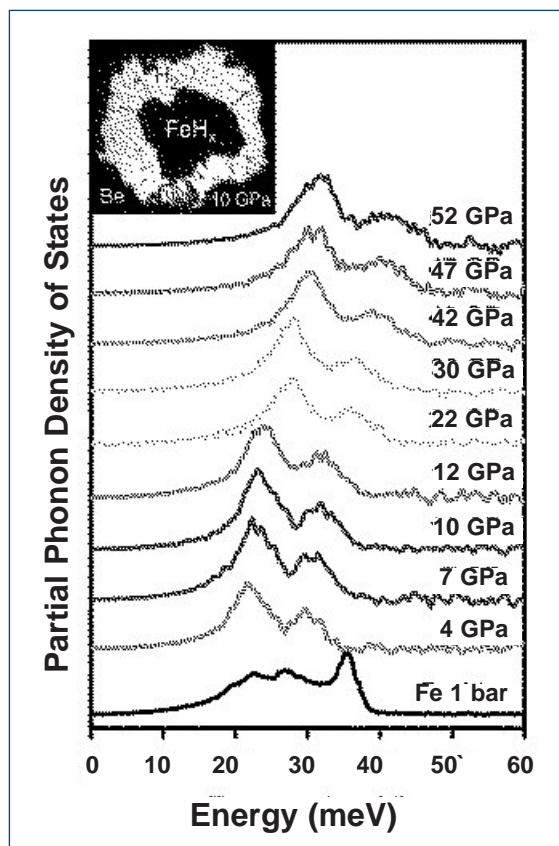


Fig. 1. The lower graphical portion of the figure displays the NRIXS spectra showing the partial phonon density of states (DOS) for FeH_x at selected high pressures. At the very bottom is shown the DOS of pure Fe at ambient pressure. The inset (upper left-hand corner) is a photomicrograph of FeH_x contained within a Beryllium gasket at a pressure of 10 GPa. Note the H_2 surrounding the FeH_x sample; the H_2 had crystallized at a pressure of 5.5 GPa.

the Advanced Photon Source was supported by the U.S. Department of Energy, Office of Science, Office of Basic Energy Sciences, under Contract No. W-31-109-ENG-38.



STRUCTURE OF LIQUID IRON AT PRESSURES UP TO 58 GPa

Both Earth and Mars have a large proportion of liquid iron in their cores, but the properties of that liquid have been almost impossible to study given the difficulties of reproducing the extreme pressure and temperature conditions of a planet's core. While crystalline iron has been examined at a wide range of pressures and temperatures, liquid iron has until now been analyzed only up to 5 GPa. Understanding the properties of liquid iron is crucial not only to understanding the internal make-up of the terrestrial planets, but also to understanding the dynamo action in Earth's fluid outer core that sustains the planet's magnetic field. Using a diamond anvil cell, which can create high pressures while still allowing analysis with synchrotron radiation, researchers from The University of Chicago used the GSECARS-CAT 13-ID beamline at the APS to obtain the first structural measurements of liquid iron up to 58 GPa and temperatures of 2900°K. This covers the entire range of pressure conditions of the Martian core and is almost halfway to Earth's outer core conditions.

X-ray diffraction patterns from beamline 13-ID showed that the atomic structure of liquid iron was remarkably stable under different pressure conditions and provided valuable information for both seismic and dynamo modeling. The researchers carrying out this study also found that the viscosity of liquid iron does not change significantly over the melting curve and is close to the value at ambient pressure. In addition, a new, unambiguous way to measure the melting point was determined by observing the change in x-ray diffraction patterns.

To create the samples, an iron flake was sandwiched between layers of NaCl and placed into a diamond anvil cell that could be heated under high pressure with a double-sided laser heating system. The sample was loaded in a glovebox in an argon atmosphere to avoid moisture, and then examined using x-ray diffraction. X-ray diffraction scattering patterns were recorded over a range of pressures as the temperature increased and the iron melted into pure liquid, thus providing information about the melting curve of iron.

Liquid transition metals can be interpreted as a simple fluid in which the arrangement of atoms is similar to the hard-sphere model (where atoms are packed like oranges in a grocery store) in which the structure factor is based on the average density of atoms and the hard-sphere diameter. These diffraction patterns were consistent with a packing structure in which the packing fraction essentially remained constant, while the hard-sphere diameter decreased with increasing pressure. The group also found that the structure factor retains the same shape throughout all of the measurements, suggesting that structure does not change for different pressures. This does not agree with the results from a previous study at pressures below 5 GPa where structural changes were seen. Since a stable local atomic configuration is consistent with close-packed structures, it was concluded that liquid iron at high pressure is consistent with the general characteristics of close-packed liquid metals.

Pertinent to modeling the geodynamo, these results suggest that viscosity remains consistent along the melting curve over a wide pressure range. This implies that the kinematic viscosity of the liquid outer core is comparable to that of water.

Thus the low-viscosity liquid permits vigorous convection as the core cools, implying fluid velocity rapid enough to sustain Earth's magnetic field.

The structural data can also be used to interpret the seismic parameter, Φ , which relates to longitudinal and shear sound velocities, and has been shown to be proportional to

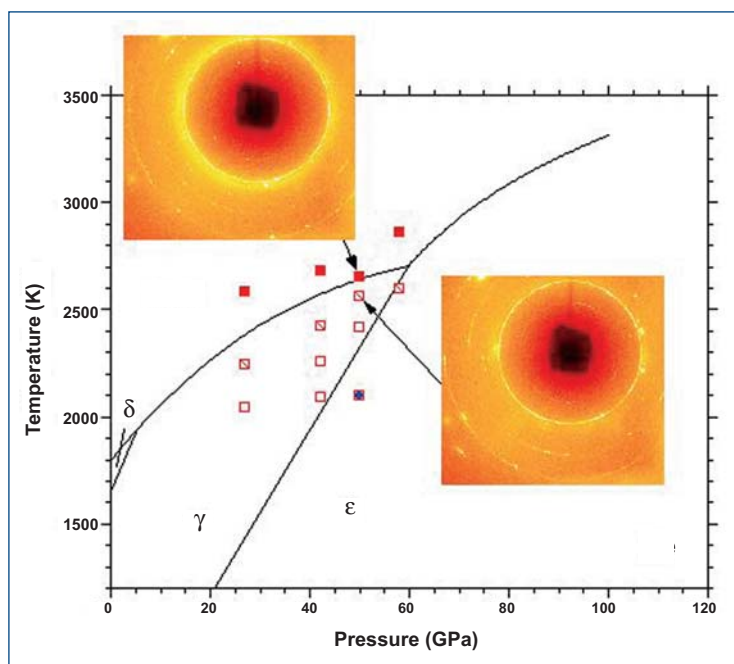


Fig. 1. Experimental points plotted in a phase diagram, showing clear evidence of melting point. Each point is defined by its measured pressure-temperature condition, and examined by x-ray diffraction/scattering (see the insert). The diffuse band arising from molten iron can be easily observed for liquid structure determination.

temperature and to be a function of the packing fraction. Because it was found that the packing fraction is constant, Φ along the melting curve can be shown to have a simple linear relationship to the melting temperature.

The study has implications for experimental techniques as well. Defining the onset of melting in a laser-heated diamond anvil cell has been the subject of a long-standing debate, since visual observations in such a small sample size—especially under the thermal glow of the laser—are incredibly difficult. Visual observations have provided melting temperatures that differ by more than 1000°. These studies showed that examining the difference between the x-ray diffraction pattern for a crystalline solid versus the pattern for a molten liquid is a much more reliable technique. — *Karen Fox*

See: G. Shen, V.B. Prakapenka, M.L.Rivers, and S.R. Sutton, "Structure of Liquid Iron at Pressures up to 58 GPa," *Phys. Rev. Lett.* **92**(18), 185701 (7 May 2004).

Author Affiliation: The University of Chicago
Correspondence: shen@cars.uchicago.edu

This work is supported by NSF-EAR Grant No. 0229987. The GSECARS-CAT sector is supported by the NSF (Earth Sciences Instrumentation and Facilities Program) and DOE (Geoscience Program). Use of the Advanced Photon Source was supported by the U.S. Department of Energy, Office of Science, Office of Basic Energy Sciences, under Contract No. W-31-109-ENG-38.

OXIDATION CONDITIONS IN THE FORMATION OF SOLAR SYSTEM VOLCANIC GLASSES

Vanadium is an abundant element found in basaltic glasses from terrestrial and planetary sources. Because it has an unusually large number of valences—four—vanadium can serve as a useful barometer to explore a wide range of oxidation conditions, thus providing a glimpse into the history of the formation of these materials in samples obtained from Earth, the Moon, and Mars. A major obstacle to exploring the properties of vanadium and other elements from natural samples, however, is that they occur as compounds rather than in a pure form. Researchers at APS recently applied a non-destructive technique—synchrotron x-ray absorption near-edge structure (XANES) spectroscopy—to explore the properties of six suites of experimental samples of basaltic glasses containing vanadium. Working with very small samples of a few millimeters, geochemists from The University of Chicago, the University of New Mexico, Rutgers University, and Mount Holyoke College used GSECARS-CAT beamline 13-ID at the APS to measure the XANES properties of these samples, a few of which had previously established valence values determined by traditional chemical and optical spectrometry techniques. The researchers used these known properties as a baseline to establish the accuracy of XANES probes in exploring the valence of natural samples of basaltic glasses.

The team used the undulator microprobe at 13-ID in two configurations, first analyzing the samples with Kirkpatrick-Baez microfocusing mirrors and a Canberra Industries, Inc., energy dispersive fluorescence detector with digital processing electronics; they then used a larger version of the mirror setup coupled with an Oxford Instruments, Inc., wavelength dispersive spectrometer.

Of the six experimental glass suites—*Schreiber*, *Hanson*, *Canil*, *Beckett*, *Karner*, and *Drake*—they first used the Schreiber suite of basaltic glasses with independently established valence states from V^{3+} to V^{5+} to calibrate the XANES measurements. The XANES measurements of this suite correlated well with measurements obtained by titration and optical spectrometry: an element with low valence (V^{2+}) displays a very weak pre-edge spectrum, while the intermediate valences (V^{3+} and V^{4+}) display multiplets. At the highest (V^{5+}) valence, the XANES probe confirmed the presence of an intense singlet. Using these data, the team was able to confirm a wide range of valences in samples from the other five experimental suites, which are in good agreement with predictions.

In addition, comparisons of the Schreiber glasses with high and low basicity demonstrated a slight valence increase with increased basicity, as expected from theory. The samples

with high concentrations of calcium were more oxidized than those with low concentrations at constant temperature and fugacity conditions.

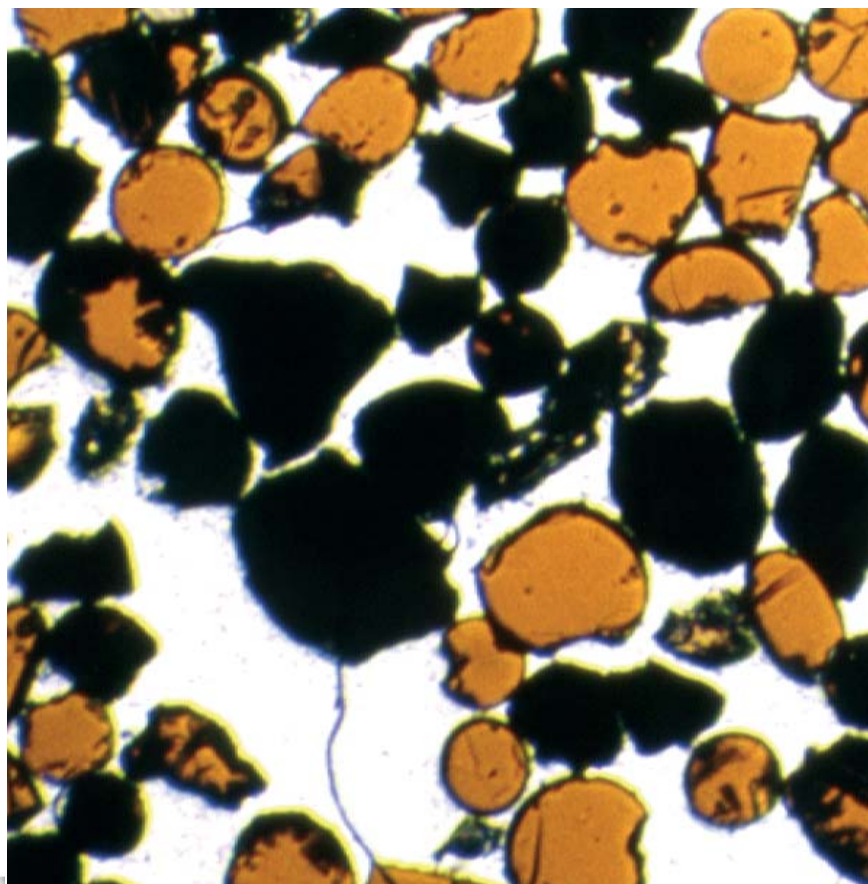
Further measurements analyzing the effects of temperature differences, using the Beckett suite and some of the Hanson samples, also revealed a slight increase in valence with lower temperatures. The calibration curve established in these probes can be used to infer oxygen fugacity from XANES peak intensity for unknown samples.

Since the measured pre-edge peak intensity can differ depending on molecular site geometry, the team also studied five natural and synthetic glass samples by means of extended x-ray absorption fine structure (microEXAFS) spectra with the undulator beam. These probes confirmed that synthetic glasses constitute suitable standards to determine the valences of naturally occurring vanadium under a range of redox conditions from 2+ to 5+.

Natural glass samples from volcanic sources on Earth, from lunar glass beads collected during the Apollo 15 and 17 missions (Fig. 1), and from a Martian meteorite collected in Antarctica were analyzed to compare the accuracy of the experimental measurements. The Martian sample, which was

Continued on next page

Fig. 1. Lunar beads from orange soil formed in a volcanic eruption, collected by Apollo 17 astronauts at the Taurus-Littrow Valley site. The sample contains volcanic glass (the orange particles) and the mineral ilmenite (the black particles). (Image courtesy of NASA and the Lunar and Planetary Institute.)



formed through meteorite impact rather than volcanic activity, was included because it may potentially reveal important information on the impact process.

Measurements of the natural glasses confirm that Mars has an intermediate oxidation state relative to the Earth (more oxidized) and the Moon (more reduced). These results demonstrate the great potential of XANES as a robust and non-destructive new oxybarometer to probe the conditions in which natural basaltic glasses from various solar system sources were formed.

— *Elise LeQuire*

See: S.R. Sutton¹, J.M. Karner², J.J. Papike², J.S. Delaney³, C.K. Shearer², M. Newville¹, P. Eng¹, M. Rivers¹, and M.D. Dyar⁴, "Oxygen Barometry of Basaltic Glasses based on Vanadium Valence Determinations Using Synchrotron MicroXANES," *Lunar and Planetary Science* **35**, 1725 (2004).

J.M. Karner², S.R. Sutton¹, J.J. Papike², J.S. Delaney³, C.K. Shearer², M. Newville¹, P. Eng¹, M. Rivers¹, and M.D. Dyar⁴, "A New Oxygen Barometer for Solar System Basaltic Glasses Based on Vanadium Valence," *Lunar and Planetary Science* **35**, 1269 (2004).

S.R. Sutton¹, J. Karner², J. Papike², J.S. Delaney³, C. Shearer², M. Newville¹, P. Eng¹, M. Rivers¹, and M.D. Dyar⁴, "Vanadium K Edge XANES of Synthetic and Natural Basaltic Glasses and

Application to Microscale Oxygen Barometry," *Geochim. Cosmochim. Acta*, in press (2004).

Author Affiliations: ¹The University of Chicago, ²University of New Mexico at Albuquerque, ³Rutgers University, ⁴Mount Holyoke College

Correspondence: sutton@cars.uchicago.edu

GeoSoilEnviroCARS is supported by the NSF, the DOE, and the State of Illinois. UNM group contribution (J.K., J.P., C.S.) was provided by a NASA Cosmochemistry grant to J.P. Support of D.D. was also provided by NASA (NAG5-12848). Use of the Advanced Photon Source was supported by the U.S. Department of Energy, Office of Science, Office of Basic Energy Sciences, under Contract No. W-31-109-ENG-38.



LOCAL STRUCTURE AROUND CHROMIUM IONS IN AQUEOUS ACETATE SOLUTIONS

When metal ions are released into the environment, how do they interact with the world they find? In particular, how do aqueous metals absorb on bacterial surfaces? Those are questions of great interest in environmental biogeochemistry. Studies carried out by researchers from Argonne National Laboratory and the University of Notre Dame using the MR-CAT 10-ID beamline at the APS provide an important first step toward understanding this process.

Contaminants such as chromium, cadmium, or uranium that leak into the environment generally become solvated in groundwater, increasing dramatically the contaminants' ability to move and spread. Along the way, these contaminants can meet various agents and surfaces, both mineralogical and biological, to which they can bind and that change their mobility. As a result, they stop somewhere and accumulate, which may or may not be desirable. Bacterial surfaces are rich in carboxyl functional groups COO^- , a radical that is typical of organic acids. The conditions under which significant adsorption/complexation can occur depend on the molecular binding mechanism. By beginning to understand how the metal behaves in the solution, and from there, how it binds to an acetate molecule (as a model of a carboxyl bond), science can explore important questions about metals in the environment.

To begin, the Argonne-Notre Dame team studied a model system of chromium salts dissolved in solution with and without an acetate ligand. They added acetic acid (CH_3COOH) to chromium solutions and observed how the metal behaves, i.e., whether or not it binds to the acetate. Acetic acid can bind to a metal in one of four ways: one is an electrostatic association that is not a strong bond, two are chemical bonds with a shared electron, and the fourth is a chemical bond in which two metal ions are bridged by the acetate group.

In the case of chromium ions, Cr^{3+} , three of them come together and form an aqueous trichromium acetate complex (Fig. 1) in which the acetate groups are in a bridging configuration between the chromium ions. The structure was derived by x-ray absorption fine structure (XAFS) spectroscopy as a function of pH, concentration, acetate-to-Cr ratio, and the age of the solution. The structure of hydrated Cr^{3+} ions was also obtained. Like most aqueous metals, the ions are not bare; they are surrounded by associated water molecules, called a hydration sphere. The first hydration sphere is the very inner circle of these hydrated molecules, which is quite structured. Going further out is another shell of more or less ordered waters—in this case, chromium, as a +3 ion, has a very strong interaction, and

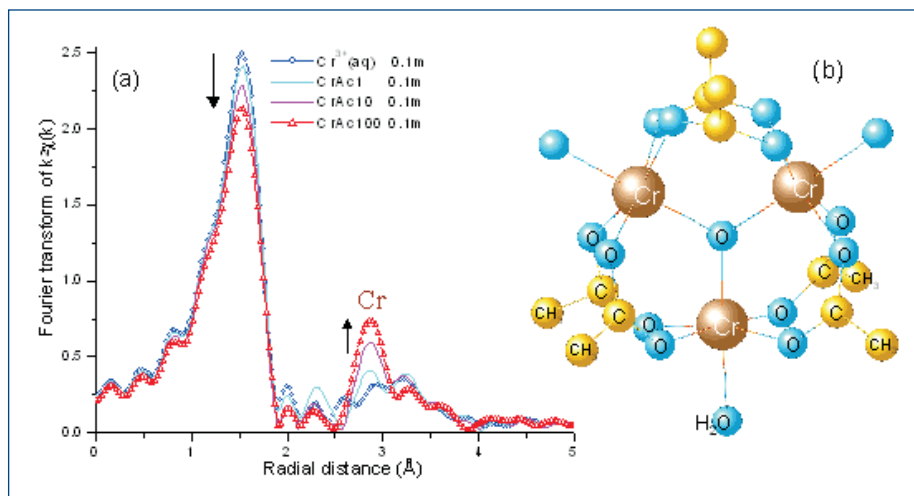


Fig. 1. (a) Results from EXAFS data for Cr acetate solutions; magnitude of the Fourier transform of $k^2 \chi(k)$. (b) Structure of the $\text{Cr}_3\text{O}(\text{CH}_3\text{COO})_6 \cdot 3\text{H}_2\text{O}$ solution complex

it is also able to order the second hydration sphere, forming a second shell of water molecules around the chromium ions.

This and other studies show that XAFS is an effective technique for investigating metal hydration and structure. Such information can also help in studies of the binding of dilute aqueous Cr to carboxyl ligands, as well as investigations of metal-metal interactions and polymerization in solution.

— David Appell

See: M.I. Boyanov^{1,2}, K.M. Kemner¹, T. Shibata², and B.A. Bunker², "Local Structure around Cr^{3+} Ions in Dilute Acetate and Perchlorate Aqueous Solutions," *J. Phys. Chem. A* **108**, 5131 (2004).

Author Affiliations: ¹Argonne National Laboratory, ²University of Notre Dame

Correspondence: mboyanov@nd.edu

M.B. acknowledges support from the Environmental Molecular Science Institute at University of Notre Dame (funded by NSF grant EAR-0221966), the United States Department of Energy, and the Bayer Corporation through a fellowship in environmental science. This work was supported in part by National Science Foundation grant EAR-0207169 and EAR-9905704, and the U.S. Department of Energy, Office of Science, Office of Biological and Environmental Research, Natural and Accelerated Bioremediation program. MR-CAT is supported by the U.S. Department of Energy under Contract No. DE-FG02-94-ER45525 and the member institutions. Use of the Advanced Photon Source was supported by the U.S. Department of Energy, Office of Science, Office of Basic Energy Sciences, under Contract No. W-31-109-ENG-38.

ASSESSING STRATEGIES FOR URANIUM CONTAMINATION REMEDIATION



accidental releases of liquid waste from U.S. nuclear weapons production facilities have included large quantities of radionuclides, such as cesium (^{137}Cs), cobalt (^{60}Co), europium ($^{152,154}\text{Eu}$), strontium (^{90}Sr), technetium (^{99}Tc), and uranium ($^{235,238}\text{U}$). Such subsurface leaks at several underground waste storage tanks, first built in the 1940s, have occurred throughout the Department of Energy's Hanford site in eastern Washington state. Many of these high- and low-level nuclear wastes have never been cleaned up and, thus, have caused complex subsurface contaminant plumes. As a result, many scientific studies have been performed to assess the future of such potentially harmful underground contaminants. One such study concerned the overflowing of tank BX-102 (on 20 March 1951) at the 200 East Area. This accident allowed the release and leakage of almost 350,000 liters (91,600 gallons) of caustic aqueous sludge—containing around 7.5 metric tons (16,500 pounds) of uranium metal—into the vadose zone.

In 2001, a borehole was drilled through the waste plume at the Hanford 200 East Area site to provide information on the depth distribution and inventory of uranium and technetium. Sediment samples drawn from this borehole and obtained by researchers from Stanford University, Stanford Synchrotron Radiation Laboratory, Argonne National Laboratory, and Pacific Northwest National Laboratory were analyzed to determine the speciation parameters for uranium that would ultimately determine its ability to move within the environment. These speciation parameters include uranium's: (1) valence state, (2) chemical form (e.g., precipitate and adsorption complex), (3) phase associations, and (4) spatial distribution within sediments (at the grain level). This information may be input into contaminant transport models to predict the future migration of uranium at this site.

The researchers applied synchrotron-based x-ray spectroscopic and diffraction techniques, including x-ray absorption near edge structure (XANES) spectroscopy, extended x-ray

absorption fine structure (EXAFS) spectroscopy, x-ray microdiffraction (μXRD), and microscanning x-ray fluorescence (μSXRF) to determine the key speciation parameters of uranium in the sediment samples. The measurement work was performed on the on the PNC/XOR 20-ID beamline at the APS and the Molecular Environmental Sciences beamline 11-2 at the Stanford Synchrotron Radiation Laboratory (SSRL).

The XANES spectroscopic measurements demonstrated that uranium occurs primarily in the hexavalent form in all samples examined. EXAFS spectroscopic studies showed that there was miniscule variation in the speciation of uranium among the samples. The studies also demonstrated that the main uranium species is probably a uranium (VI) silicate within the group of uranophane minerals. Because EXAFS techniques are unable to identify individual uranophane members, μXRD analyses were used to identify the specific phase present (Fig. 1), the only uranophane group mineral present in the sam-

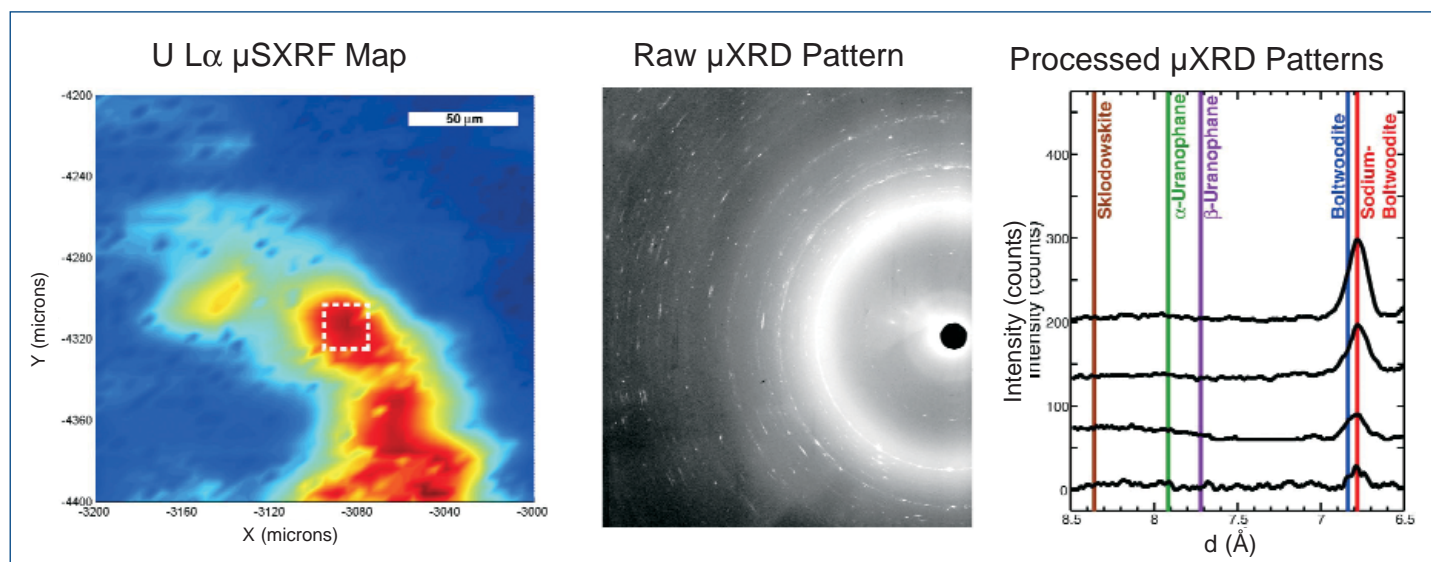


Fig. 1. Left: A μSXRF map showing the heterogeneous uranium distribution occurring at the micrometer scale. Center: A μXRD pattern taken of a $20 \times 20 \mu\text{m}$ area (white box in map at left) of high U concentration. Right: Integrated and background subtracted μXRD patterns demonstrating the presence of sodium-boltwoodite, $\text{Na}(\text{UO}_2)(\text{SiO}_3\text{OH}) \cdot 1.5\text{H}_2\text{O}$.

ples was sodium-boltwoodite $[\text{Na}(\text{UO}_2)(\text{SiO}_3\text{OH})\cdot 1.5\text{H}_2\text{O}]$. Electron microprobe and μSXRF analyses demonstrated that sodium-boltwoodite occurred as μm -size crystals inside fractures in plagioclase feldspar grains.

The researchers concluded that remediation of the contamination would likely be a difficult task because of the speciation and distribution of uranium within the sediments. They further concluded that future release of uranium from these sediments would be minimal because of the low moisture content of the sediments and the isolation of sodium-boltwoodite in microfractures. — *William Arthur Atkins*

See: J.G. Catalano¹, S.M. Heald², J.M. Zachara³, and G.E. Brown, Jr.⁴, "Spectroscopic and Diffraction Study of Uranium Speciation in Contaminated Vadose Zone Sediments from the Hanford Site, Washington State," *Environ. Sci. Technol.* **38**(10), 2822 (2004).

Author Affiliations: ¹Stanford University, ²Argonne National Laboratory, ³Pacific Northwest National Laboratory, ⁴Stanford Synchrotron Radiation Laboratory

Correspondence: catalano@pangea.stanford.edu

This research was supported by DOE-EMSP Grant FG07-ER0263495 (Stanford) and Battelle Contract 409089-A9E-P3623. SSRL is supported by the U.S. Department of Energy, Office of Basic Energy Sciences and Office of Biological and Environmental Research, and the National Institutes of Health, National Center for Research Resources, Biomedical Technology Program. PNC-CAT is supported by funding from the U.S. Department of Energy's Office of Basic Energy Sciences, the National Science Foundation, the University of Washington, the Natural Sciences and Engineering Research Council of Canada, and Simon Fraser University. Use of the Advanced Photon Source was supported by the U.S. Department of Energy, Office of Science, Office of Basic Energy Sciences, under Contract No. W-31-109-ENG-38.

MICROSCALE DISTRIBUTION OF CESIUM SORBED TO BIOTITE AND MUSCOVITE

Radioactive Cesium-137 is one of several contaminants in the soil at the Hanford Site in southeastern Washington, where numerous leaks of radioactive waste have accrued during synthesis of plutonium. About one million curies of ^{137}Cs seeped into the soil over the years, and much of it sits above the water table, chemically bound by sorption to the micaceous sediment. With a half-life of 30.2 years, leaving the ^{137}Cs to decay in place might well be the best option. However, the ^{137}Cs has, at times, migrated because of the mobilizing effects of interaction with concentrated wastes, so decisions about remediation require a better understanding of the sorption mechanisms. Researchers from the Pacific Northwest National Laboratory and The University of Chicago, using the GSECARS-CAT (sector 13) and PNC/XOR (sector 20) beamlines at the APS, have gained a clearer picture of these mechanisms and the mobility of ^{137}Cs at the Hanford site.

Previous research showed that ^{137}Cs at Hanford was sorbed specifically to the micas biotite and muscovite in preference to other minerals. When in contact with micaceous minerals, Cs had two rates of sorption and desorption. In addition, the longer the Cs had been present, the more resistant to desorption it was. These phenomena were thought to be caused by Cs binding to several kinds of sites on the mica structure composed of planar aluminosilicate sheets bound together by interplanar potassium ions. The hypothesized sites included cation exchange sites on mineral surfaces, frayed-edge sites formed by the removal of potassium from the mica structure during weathering, and interlayer sites where Cs could diffuse from the frayed edges, displacing potassium.

To study sorption in detail, the researchers hand-picked mica flakes taken from a borehole at the Hanford Site and separated them into dark biotite and colorless muscovite on the basis of appearance. The flakes were placed in a solution of CsNO_3 for either 14 or 28 days at room temperature. The surfaces of the mica were examined directly, and the mica interiors were examined by embedding the flakes in epoxy resin and cutting 60- μm -thick sections.

While the amounts of sorbed Cs varied from sample to sample, the researchers found no significant difference between those saturated for 14 or 28 days. Elemental abundances were examined by using an electron microprobe (EMP). Where Cs was concentrated, potassium was usually depleted, consistent with the formation of frayed edge sites caused by weathering reactions. Muscovite sorbed less total Cs than biotite, which could be explained by considering the differences between the two micaceous minerals. Because muscovite is both more weather-resistant and retains potassium more strongly than biotite, it develops fewer frayed edges that are hospitable to Cs sorption.

The spatial resolution of the EMP was superior, but its detection limit was 100 times that available using an x-ray microprobe (XMP, Fig. 1.). For more sensitive determinations of Cs residence on micas, measurements were made using the GSECARS-CAT and PNC/XOR beamlines. The XMP data showed that in muscovite, Cs was not limited to the edges, but had deeply penetrated the sample in distinct, concentrated areas, suggesting emplacement by processes other than diffu-

Continued on next page

sional replacement of potassium. Previous studies of mica weathering suggested that frayed-edge sites could occur deep within the mica structure, where structural defects acted as conduits for weathering fluids. These defects also could act as conduits for Cs migration and deposition on those internal frayed edges. Finding Cs on these sites was significant, because it implied that a much larger surface area was available for sorption than was otherwise apparent. It could also explain why desorption was slower after longer exposure to ^{137}Cs , corresponding to the migration over time of Cs from weaker surface sites onto the stronger sites in the interior.

Sorption of Cs onto biotite was significantly different. Cs was pervasive, but at much lower local abundance than in muscovite. Potassium was depleted and iron more abundant where Cs was concentrated, possibly because iron was oxidized and expelled from the crystal lattice along with interlayer potassium during weathering that created frayed-edge sites. Using x-ray absorption near-edge structure analysis, iron throughout the biotite was found to be oxidized. The Hanford biotites thus apparently included pervasive microchannels, accessible by Cs, formed by dissolution and oxidation; the iron-poor muscovites, on the other hand, developed clusters of internal frayed-edge sites after solution weathering along less numerous fractures, partings, or crystal defects.

In summary, Cs was sorbed to frayed-edge sites on the interior and exterior portions of mica minerals. Biotite had the ability to sorb a larger quantity of Cs than muscovite, but desorption from muscovite could be slower due to the restricted access of solutions to internal sites. The redistribution of Cs over time to internal frayed-edge sites may explain the slow desorption that has been observed for Cs associated with micaceous sediments. These results suggested that the ^{137}Cs at Hanford was relatively immobile.

— Karen Fox

See: "Microscale Distribution of Cesium Sorbed to Biotite and Muscovite," J.P. McKinley¹, J.M. Zachara¹, S.M. Heald¹, A. Dohnalkova¹, M.G. Newville², and S.R. Sutton², *Enviro. Sci. Tech.* **38**(4), 1017 (2004).

Author Affiliations: ¹Pacific Northwest National Laboratory, ²The University of Chicago

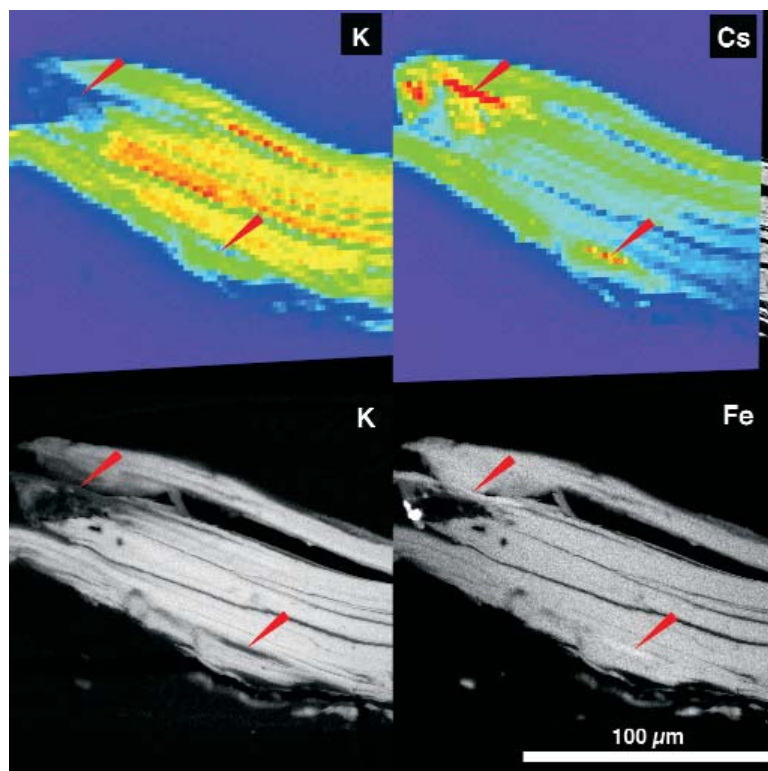


Fig. 1. The distribution of Cs in biotite: Comparative panels from XMP, above, and EMP, below, illustrate the relative advantages in detection and spatial resolution of the two techniques. Cesium was generally not detectable by EMP.

Correspondence: james.mckinley@pnl.gov

This research was supported by the U.S. Department of Energy Environmental Management Science Program. The PNC-CAT is supported by funding from the Office of Basic Energy Sciences, U.S. Department of Energy, and by the Canadian Natural Sciences and Research Council. The TEM work was performed at the W.R. Wiley Environmental Molecular Sciences Laboratory, a national scientific user facility sponsored by the U.S. Department of Energy's Office of Biological and Environmental Research and located at Pacific Northwest National Laboratory (PNNL). PNNL is operated for the U.S. Department of Energy by Battelle. Use of the Advanced Photon Source was supported by the U.S. Department of Energy, Office of Science, Office of Basic Energy Sciences, under Contract No. W-31-109-ENG-38.



METAL CONCENTRATIONS IN CEMENTUM RINGS AS AN AID TO BIOARCHAEOLOGY

Much as annual rings indicate the age of trees, the distinct ring structure of cementum—the tissue that surrounds the tooth root—may provide definite signals of an individual's long-term exposure to metals. That is the hypothesis put forward by researchers from the University of Western Ontario; Ludwig Maximilians University; and the National Institute of Culture, Peru based on experiments carried out at PNC/XOR beamline 20-ID. Such recorded concentrations within cementum are believed to be caused by the consumption of metals as part of the regular intake of nourishment and by the interaction of the body with the outside environment.

Beginning with the belief that no experimentation has ever been performed to resolve annual ring composition within cementum, the collaborators analyzed the metallic composition and distribution of cementum in human teeth from two mummies of the early sixteenth century. The mummies were retrieved from the archaeological "Stone Temple" burial site of Tucume, on the northern coast of Peru.

The technique employed, called micro-synchrotron radiation-induced x-ray fluorescence (μ -SRXRF), was used in this experiment because of its ability to accurately measure trace elements found in the cementum rings that are normally difficult to detect. Such measurements must have a trace element sensitivity of a few parts per billion and a spatial resolution of a few microns. μ -SRXRF provides these capabilities.

The experiments consisted of studying the lower right first incisor and the upper left first incisor of two female mummies selected from among 22 males and females found within an adobe platform at the Stone Temple ruins. The teeth were embedded in a slow-curing transparent epoxy resin, followed by cross-sectional cutting of the roots. Next, several thin sections of the teeth were cut at the cemento-enamel junction (the area where the cementum and enamel meet). The resulting surfaces were then polished with silicon carbide paper and diamond grit (both with appropriate lubricants) and later exposed to sound waves while submerged in methanol and distilled water in order to remove bacteria.

Continued on next page

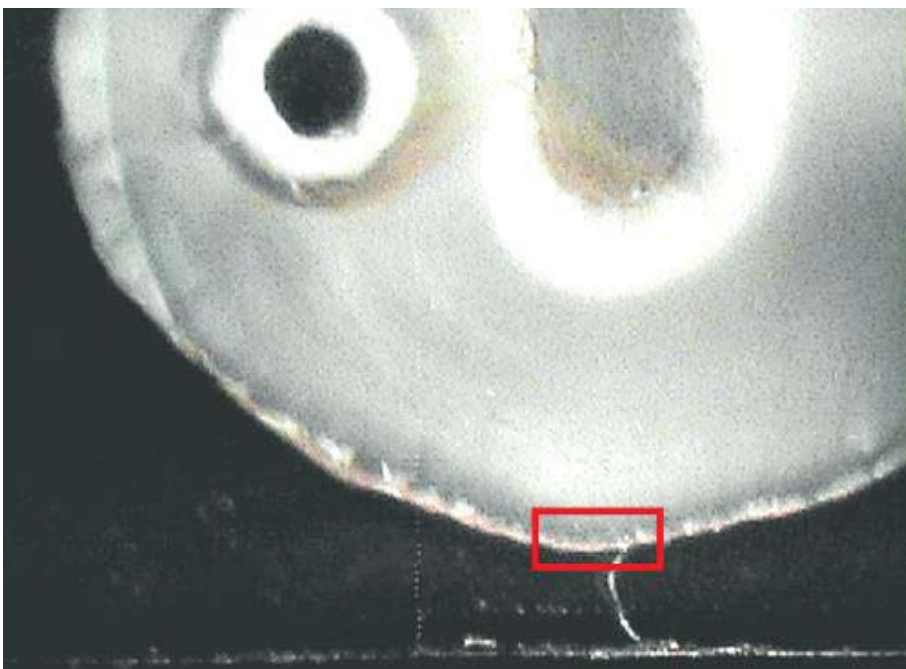


Fig. 1. Tooth cross section taken from one of the mummies. The figure is from a subsequent study done on mummies from the burial site at Tucume, Peru. The questions asked were essentially the same, although more detailed information was obtained because the collaborators achieved better resolution with the thin (approximately 50 μ m) sections. The small box indicates the area scanned with XRF (as shown in Fig. 2).

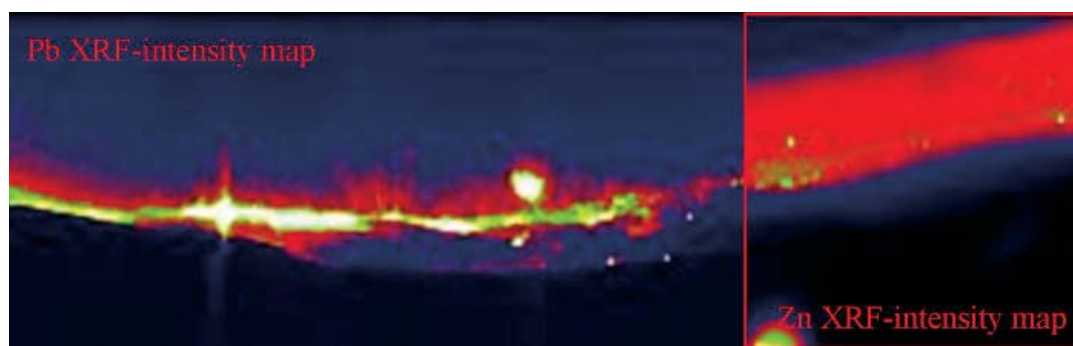


Fig. 2. X-ray fluorescence spectroscopy intensity maps for the tooth of the mummy shown in Fig. 1. The left hand side is the lead (Pb) image, while the right side shows the superimposed zinc (Zn) image.

The samples (Fig. 1) each had a thickness of 5 mm, which, when exposed to x-ray radiation, provides the most fluorescence from trace metals. The work was performed at beamline 20-ID using a pair of mirrors to focus the beam. Synchrotron x-ray fluorescence was collected at the K-alpha spectral line for the elements bromine (Br), calcium (Ca), copper (Cu), lead (Pb), nickel (Ni), strontium (Sr), and zinc (Zn).

The results show (Fig. 2) that Zn is regularly enriched in the cementum rings of both tooth samples, while Ca and Sr were found to be sometimes concentrated in the same two samples. The elements Pb and Br were at found concentrations very near the detection limits of the technique; thus, enrichment in only one individual could be demonstrated. No inferences could be made for Ni and Cu. Overall, the cementum rings were more enriched with the various metals than in other parts of the tooth material.

On the basis of these results, the collaborators feel that μ -SRXRF is an excellent method for examinations of the concentration of certain trace elements in archaeological samples such as teeth. Furthermore, the results indicate that μ -SRXRF can be exceptionally important in deciding whether the probable origin of a trace element is biogenic (from diet and disease that occur while humans are alive) or diagenetic (from postmortem condi-

tions). Further research may well provide additional insight into the historical measure and degree of absorption of metals and other substances into the human body.

— William Arthur Atkins

See: Ronald R. Martin¹, Steven J. Naftel¹, Andrew J. Nelson¹, Andrea B. Feilen², and Alfredo Narvaez³, "Synchrotron X-ray Fluorescence and Trace Metals in the Cementum Rings of Human Teeth," *J. Environ. Monit.* **6**, 783 (2004).

Author Affiliations:

¹University of Western Ontario, ²Ludwig Maximilians University,

³Instituto Nacional de Cultura, Peru

Correspondence: rrahm@uwo.ca

The Natural Science and Engineering Research Council of Canada provided support through operating grants and a major facility access grant. Experiments at PNC/XOR and use of the Advanced Photon Source are supported by the U.S. Department of Energy, Office of Science, Office of Basic Energy Sciences, under Contracts No. W-31-109-ENG-38 (APS) and DE-FG03-97ER45628 (PNC/XOR). Financial support was also received from The Social Sciences and Humanities Research Council of Canada, as well as The University of Western Ontario (ADF grant). A.J.N. and A.N. acknowledge the Instituto Nacional de Cultura, Peru.

SYNTHESIS OF ONE-DIMENSIONAL NANOSTRUCTURES



achieving the goal of coaxing highly branched, irregular, and flexible dendritic molecules to form uniform, stable, and robust shapes has been elusive. Fabricating long, thin supramolecular forms such as rods, fibers, and ribbons has, until recently, required multiple interventions in the composition of the branches and cores of the molecules. A new approach to manipulating the core-shell architecture of these molecules has produced intriguing results: exceptionally stable, one-dimensional structures ranging from a few nanometers to several micrometers long. Researchers from Iowa State University conducted grazing incidence x-ray diffraction and x-ray reflectivity experiments using the liquid surface refractometer at the MU-CAT 6-ID-B beamline at the APS, as well as bulk x-ray diffraction techniques at Iowa State University, to confirm the self-assembly of long, flexible, and robust one-dimensional nanofibers from highly branched, irregularly shaped molecules with hydrophobic tails and hydrophilic cores.

By manipulating the core-shell architecture and introducing amine groups to the core of these dendritic molecules, the team was able to boost polar interactions and stabilize surface structures. A critical condition for the formation of these long, thin structures is the crystallization of the alkyl tails in the outer shell.

The team submitted the hyperbranched core of the molecules to three modifications to produce molecules of different molecular weights. Molecules 1 and 3 are of particular interest. Molecule 1 has hydrophobic alkyl tails and hydroxyl and carboxyl groups in the outer shell, while molecule 3 has alkyl tails and hydroxyl groups in the outer shell, with the addition of amine groups in the inner core. Molecule 1, when applied to the substrate at different pressures, did not form long, robust structures but remained instead uniform and dense.

The introduction of the amine to molecule 3, however, enhanced the hydrogen bonding and polar interactions and

stabilized the surface structures at the silicon surface. When molecule 3 was deposited on a silicon substrate under increasing pressure using the Langmuir-Blodgett technique, the team observed a progression of morphological behaviors at the air-water interface. At the lowest pressure, a few curved and poorly branched nanofibers about 1 nm high and 500 nm long formed. With increasing pressure, the fibers multiplied, and some of these split and bent sharply. At medium high pressure, the nanofibers aggregated in groups of three or four, aligning themselves together and bending in the same direction. When evaporated from concentrated solutions, the fibers formed densely packed bundles several microns long and three to four microns tall across 60% of the silicon oxide surface, the upper limit for packing behavior.

Examination with a high-resolution atomic force microscope (AFM) confirmed that these nanofibers were between 0.8 and 1.0 nm high. Because of some distortion inherent in

AFM measurements, the exact width could not be determined, but was estimated to be about 4 to 10 nm, depending on the surface pressure and location of the molecules. Further confirmation of the structure and dimensions of molecule 3 was provided by x-ray reflectivity data, Langmuir isotherm data, and diffraction of the tail orientation. These probes suggest that this model is asymmetric and semispherical, with the hydrophilic cores compressed at the surface of the wafer and the hydrophobic branches concentrated in the top layer (Fig. 1).

The straightforward synthesis, robust stability, and potential versatility of these nanofibers and ribbons make these structures promising candidates for fabricating organic nanostructures in greater quantities than is possible with currently available models. — *Elise LeQuire*

See: M. Ornatska, S. Peleshanko, K.L. Genson, B. Rybak, K.N. Bergman, and V.V. Tsukruk, "Assembling of Amphiphilic Highly Branched Molecules in Supramolecular Nanofibers," *J. Am. Chem. Soc.* **126**(31), 9675 (9 July 2004).

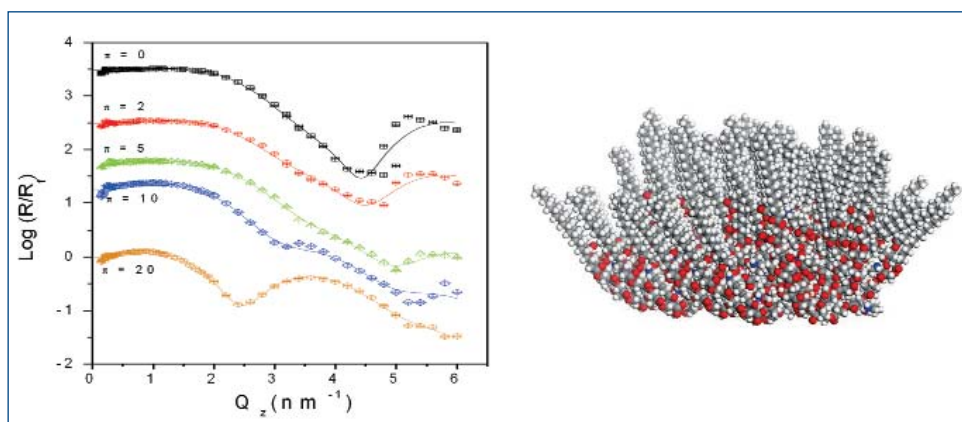


Fig. 1. Left: X-ray reflectivity data showing relative intensity versus wave number for molecule 3 at multiple surface pressures. Right: Molecular modeling reveals the architecture of molecule 3 at the higher pressure, as it assumed a compressed conformation with the alkyl tails slightly tilted from the surface normal and with limited short range ordering.

Author Affiliation: Iowa State University

Correspondence: vladimir@iastate.edu

This work supported by the NSF-DMR-0308982 project, AFOSRF496200210205 grant, and DOE Advanced Photon Source, GUP-660 award. Use of the Advanced Photon Source was supported by the U.S. Department of Energy, Office of Science, Office of Basic Energy Sciences, under Contract No. W-31-109-ENG-38, and Contract No. W-7405-ENG-82 for the MU-CAT beamline.

STRUCTURAL DISTORTIONS INSIDE NANOPARTICLES

Nanoparticles are not small bits of bulk material. They often exhibit internal structural disorder and complex strain interactions that can significantly modify their material and electronic properties relative to those of bulk materials. Understanding the reasons for these deviations from bulk behavior is key to expanding nanoparticle applications. But this understanding is hampered by the fact that the internal characteristics of nanoparticles are hard to study experimentally. Researchers from the University of California, Berkeley, and Lawrence Berkeley National Laboratory developed an approach to quantifying structural distortions inside nanoparticles and applied it to mercaptoethanol-coated zinc sulfide (ZnS) nanoparticles. The method is suitable for characterizing many nanoscale solids.

The structural analysis relied on wide-angle x-ray scattering (WAXS) patterns acquired from powders of bulk ZnS (sphalerite structure) and the mercaptoethanol-coated ZnS nanoparticles. Because WAXS requires high-brilliance, high-energy x-rays, this work was done at the APS, at BESSRC/XOR's 11-ID beamline. The researchers processed the WAXS data to obtain real-space interatomic distance correlation functions, commonly known as pair distribution functions (PDFs), for the bulk and nanoscale materials. They also demonstrated that structural differences in nanoparticles can be determined by a comparative approach, provided that the size of the nanoparticles is known accurately. So the researchers used fits to small-angle x-ray scattering (SAXS) data acquired at the Stanford Synchrotron Radiation Laboratory (SSRL) to measure the nanoparticles' average diameter at 3.4 nm. High-resolution

transmission electron microscope data confirmed the size determined by SAXS and showed that the nanoparticles were approximately spherical.

The analysis of disorder in the nanoparticles involved comparing the nanoparticle PDF to a simulated "ideal" PDF for ZnS sphalerite nanoparticles. This ideal nanoparticle PDF was obtained by truncating the PDF for bulk ZnS with a real-space curve associated with a 3.4-nm sphere; it corresponds to the PDF that would be expected for ZnS nanoparticles if their internal structure were identical to that of the bulk material. The approach allows finite particle size effects in the diffraction data to be separated from structural effects.

The researchers found evidence for the presence of two distinct forms of static disorder within the real nanoparticles rel-

Continued on next page

ative to the ideal bulk sphalerite particles: random-displacement disorder, in which individual atoms are randomly displaced from sites on a single lattice, and strain-driven distortion, in which local structure is maintained, but at larger interatomic distances, so that atoms lie farther from the positions expected for an undistorted lattice. The nanoparticle structure was also compressed relative to the bulk material, with a mean bond length contraction of 1%.

The loss of structural coherence and the inability of simple strain models to describe peak shifts in the PDF data point to the existence of complex strain fields within the nanoparticles. The researchers concluded that internal distortion is present throughout the nanoparticle interior, provoked by competing attempts of the structurally diverse surface regions of the nanoparticles to simultaneously adopt low-energy configurations.

Temperature-dependent extended x-ray absorption fine structure (EXAFS) showed that the structural modifications in the nanoparticles were associated with significantly altered material properties. To study the lattice dynamics of the ZnS samples, Zn K-edge EXAFS spectra (also acquired at SSRL) were obtained between 3K and 500K from the same bulk sphalerite and real ZnS nanoparticles used in the PDF analysis. The temperature dependence of the mean squared relative displacement was fitted to a theoretical expression for an anharmonic Einstein oscillator. The resultant zinc-sulfur Einstein vibration frequency was found to be substantially higher in the nanoparticles than that in bulk zinc sulfide, implying structural stiffening. Because the stiffening could not be explained by the observed 1% radial compression alone, it was attributed to the structural distortion observed by the PDF analysis.

The work demonstrates that nanoparticle size, structure, and properties are tightly linked. The method is an important

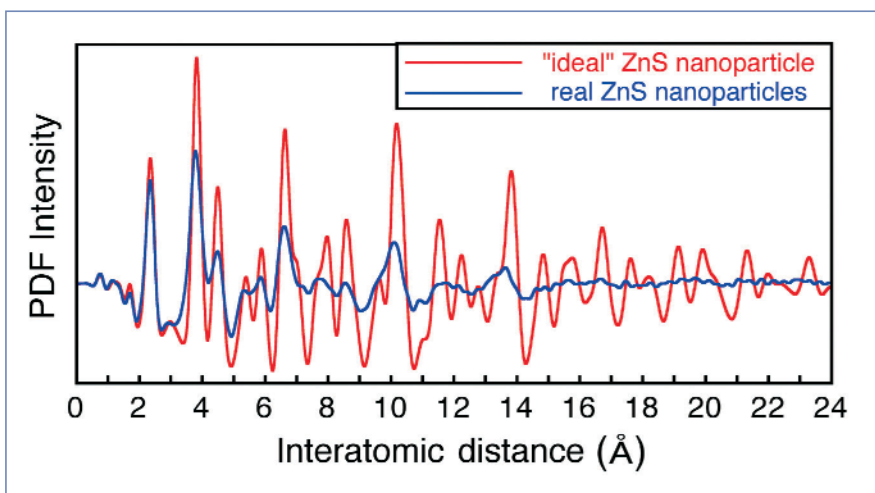


Fig. 1. A comparison between the pair distribution function (PDF) of 3.4-nm-diameter ZnS nanoparticles and a simulated PDF that represents ideal 3.4-nm nanoparticles having a perfect sphalerite structure. The simulated PDF is created by modifying data from bulk ZnS to account for small particle size. The reduced PDF peak intensities and peak shifts indicate the presence of strain and disorder within the real nanoparticles.

step toward more realistic descriptions of nanoparticle structure that include internal strain, which is likely to be a general feature of nanoscale solids. — *Vic Comello*

See: B. Gilbert¹, F. Huang¹, H. Zhang¹, G.A. Waychunas², J.F. Banfield^{1,2}, "Nanoparticles: Strained and Stiff," *Science* **305**, 651 (30 July 2004).

Author Affiliations: ¹University of California at Berkeley, ²Lawrence Berkeley National Laboratory
Correspondence: jill@eps.berkeley.edu

The U.S. Department of Energy, Office of Science, Office of Basic Energy Sciences supports use of the APS (Contract No. W-31-109-ENG-38) and the SSRL (Contract No. DE-AC03-76SF00515). HRTEM was performed at the National Center for Electron Microscopy. Financial support for this work came from the U.S. Department of Energy, the National Science Foundation, and Lawrence Berkeley National Laboratory.



DISCIPLINE FOR GOLD NANOCRYSTALS

Gold nanocrystals are not the most well-behaved of materials. Simply mixing the right ingredients will induce them to self-assemble, but the microscopic and mesoscopic organization of the nanocrystal superlattices is not predictable. Researchers from Argonne National Laboratory seeking to remedy this situation are using time-resolved small-angle x-ray scattering (SAXS) measurements on beamline XOR 1-BM at the APS to take a closer look at the physical processes taking place as gold nanocrystal superlattices form. They hope that their insights will allow researchers to better control these complex processes, allowing precise design of gold nanocrystal superlattices.

The formation of nanocrystal superlattices must be controlled before these materials can be used for a wide range of applications—from novel types of catalysts for speeding up useful chemical reactions to building tiny components for applications in optoelectronics and nanotechnology.

However, there are serious problems to be solved in trying to tame the structure of the nanocrystal superlattices as they form. The effect on structure of the numerous different forces between the clusters of gold atoms and the chemical reagents they use to make the nanocrystals cannot be predicted.

Conventional wisdom holds that gold nanocrystals can be condensed onto a substrate surface from an evaporating suspension of gold nanoparticles and a reactive organic molecule containing sulfur, a dodecanethiol ligand in organic solvent. As the liquid suspension dries, the nanoparticles coated with the ligands may self-assemble to produce so-called superlattices as the ligands act as a kind of spacer. Other researchers found that using this approach to nanocrystal construction leads to a wide range of superlattice structures—from ordered two-dimensional (2-D) and three-dimensional (3-D) patterns to fractal-like aggregates and even structures full of tunnels and channels.

One of the barriers to making desirable 2-D nanocrystal superlattices is a misunderstanding regarding the mechanism of their formation. Previous speculations had pointed to the idea that the self-assembly of nanocrystals occurs at the interface between the liquid and the substrate surface. At this interface, the nanocrystal particles can move freely at the substrate surface and, as the liquid evaporates and de-wets the surface, the superlattice structures are left behind.

The Argonne group used transmission electron microscopy to show that there is too much order for the dewetting idea to hold true. To prove this point, the team turned to the non-intrusive analytical SAXS technique, which allowed the group to

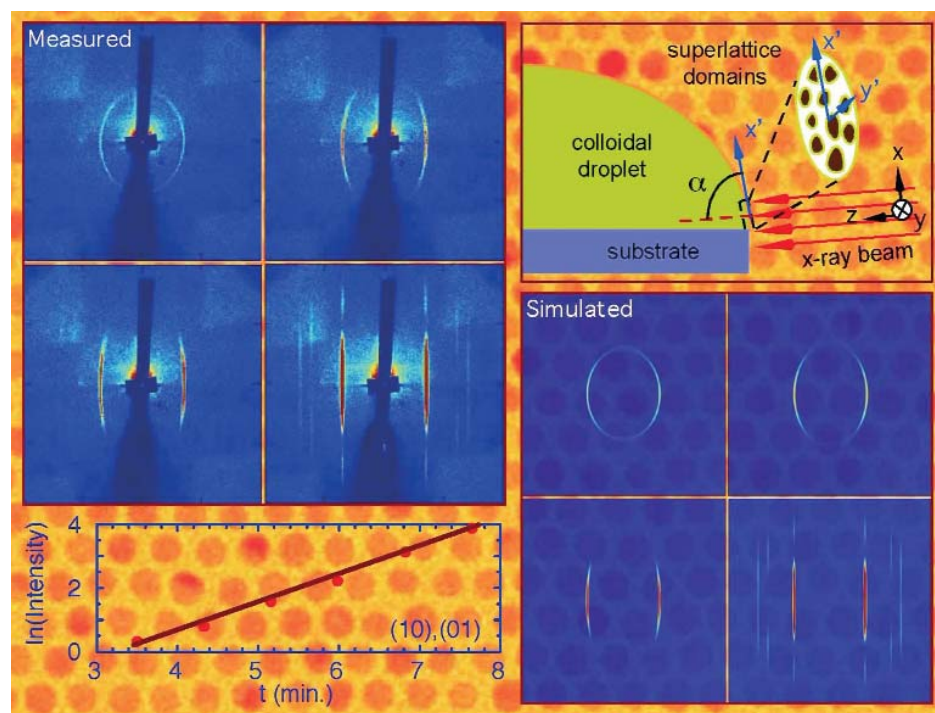


Fig. 1. X-ray experiments can reveal how the gold nanocrystal superlattices can form in real time. The four upper-left panels show the SAXS pattern from the superlattices during their ordering process as the liquid suspension is evaporated. The scattering patterns are collected by using the experimental setup shown in the upper-right panel, while the corresponding simulated scattering patterns are shown in the lower-right four panels. The match between the measured and simulated scattering patterns is striking, indicating the detailed understanding of superlattice formation. The lower-left panel shows a quantitative evaluation of the growth kinetics revealed by the scattering intensity change as a function of time.

watch the formation of nanocrystal superlattices as the nanoparticle suspension droplets evaporated (Fig. 1). Their results show that the self-assembly process does not occur at the interface between the liquid and the substrate but at the interface of the liquid surface and the surrounding air. They further demonstrated this to be the case by speeding up the rate of evaporation, showing that the same starting materials could produce either 2-D or 3-D lattices, depending on how quickly the liquid evaporated. The faster rate of evaporation produces 2-D structures; a slower rate of evaporation allows time for 3-D structures to form. The self-assembly of 2-D nanocrystal super-

Continued on next page

lattices at the liquid-air interface opens up the possibility of annealing out the defects and allowing ordered formation of 2-D superlattices in mesoscopic scale to form, which has not been proven possible in the past. — *David Bradley*

See: S. Narayanan, J. Wang, and X.-M. Lin, "Dynamical Self-Assembly of Nanocrystal Superlattices during Colloidal Droplet Evaporation by *in situ* Small Angle X-Ray Scattering," *Phys. Rev. Lett.* **93**, 135503 (2004).

Author Affiliation: Argonne National Laboratory
Correspondence: wangj@aps.anl.gov

This work and use of the APS are supported by the U.S. Department of Energy (DOE), BES-Materials Sciences, under Contract No. W-31-109-ENG-38, by DOE Center 135503-4 for Nanoscale Materials, and by the University of Chicago-Argonne National Laboratory Consortium for Nanoscience Research.

GETTING TO KNOW NANOPARTICLES

Ultrafine metal oxide particles are present in many widely used products, such as paints, cosmetics, and silicon rubber. Quality control of manufactured items depends largely on knowing how these nanoparticles behave. Agglomerates or clumps of very small particles can ruin paints and cosmetics but the same clumps would enhance the performance of silicon rubber. Existing methods for measuring the size and aggregation of ultra-fine silica particles are labor-intensive and time-consuming. Investigators from ETH Zurich and the University of Cincinnati used ultra-small-angle x-ray scattering (USAXS) at the UNI-CAT 33-ID beamline at the APS to determine particle size and degree of agglomeration of agglomerated and nonagglomerated flame-made silica nanoparticles.

With USAXS particle volume to surface ratio providing primary particle diameters, the researchers compared their results to diameters obtained from nitrogen adsorption (Brunauer-Emmett-Teller, BET). With both vapor phase and liquid silica precursors—at a range of production rates (5-1100 g/h), degree of agglomeration, and flame conditions (premixed, diffusion, or spray flame)—the USAXS average primary diameters were in excellent agreement with those obtained using BET. The USAXS data also showed how fuel and precursor flow rate affect product primary particle diameter and agglomerate size for various vapor- and liquid-fed flame reactors. USAXS distinguished between agglomerated and nonagglomerated flame-made silica particles; revealed that smaller agglomerates form in liquid-fed than in vapor-fed flames; and showed a reasonably constant mass-fractal dimension of SiO₂ ranging from 1.6 to 2.2 in vapor-fed flames and from 1.9 to 2.0 in liquid-fed flame aerosol reactors.

Silica nanoparticle production occurred in premixed and diffusion flame reactors, after which powder was collected on glass fiber filters. Nitrogen adsorption, using a five-point isotherm (relative pressure range, 0.05-0.25), was used to measure the BET specific surface area (SSA) of the powder; average primary particle diameter was calculated assuming spherical particles, SSA, and ρ_{SiO_2} of 2200 kg/m³. The UNI-CAT beamline and a Bonse-Hart camera covering a q range of 0.0001-0.4 Å⁻¹ and 10 keV were used to measure USAXS patterns of the powders under ambient pressure. Transmission electron microscopy (TEM) allowed a visual comparison of the degree of agglomeration.

Scattering patterns of a highly fractal (agglomerated) and commercially available powder, Aerosil 200, were compared to that of a nonfractal (nonagglomerated) SiO₂ powder synthesized in the premixed flame reactor (Fig. 1). The authors

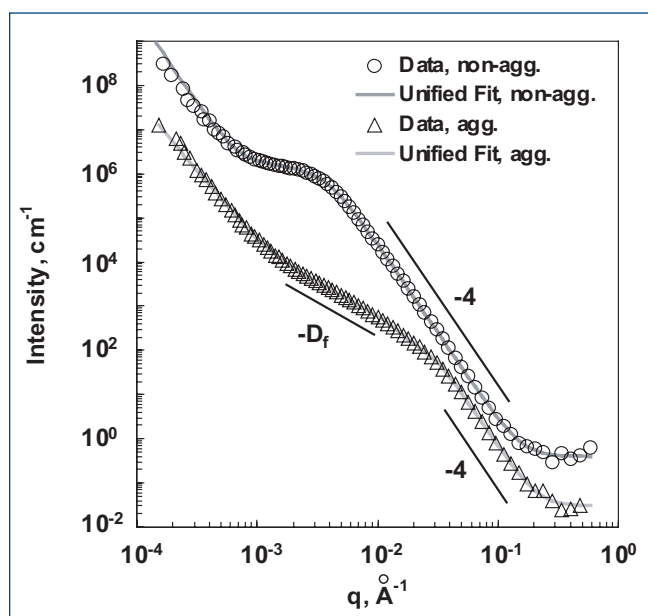


Fig. 1. Scattering curves recorded by ultra small-angle x-ray scattering (USAXS) of non-agglomerated (upper pattern) and agglomerated (lower pattern) flame-made silica nanoparticles. The use of third generation synchrotron radiation enables the detection over more than 4 orders of magnitude in q , resulting in information about primary particle and agglomerate size. The mass fractal dimension, D_f , can be determined from the slope of the intermediate power law dependence as indicated. The latter is absent for the upper pattern indicating non-agglomerated particles, as the correlation between the particles vanishes. This pattern was shifted by one order of magnitude in intensity for clarity. Primary particle size, agglomerate size, and D_f can be determined with the global unified fitting equation as described in the paper cited below, Kammler et al. (2004).

presented a set of equations allowing calculation of the volume to surface average primary particle diameter using USAXS measurements and the Porod invariant of the primary particles. For the agglomerated Aerosil 200, the data showed excellent agreement between USAXS and BET, which also provides volume to surface average primary particle diameter, and matched the manufacturer's specifications. Data resulting from analysis of the nonagglomerated particles showed that this type of nanostructured particle could be easily distinguished from the agglomerated type.

Previously, standard procedures to determine particle size distribution and degree of agglomeration used methods, such as TEM, that were time-consuming and resistant to automation. The current data show that USAXS provides similar information in an accurate and much more rapid fashion, thus constituting a

great leap forward with respect to efficiently characterizing silica nanoparticles and streamlining manufacturing. — *Mona Mort*

See: H.K. Kammler¹, G. Beaucage², R. Mueller¹, and S.E. Pratsinis¹, "Structure of Flame-Made Silica Nanoparticles by Ultra-Small-Angle X-ray Scattering," *Langmuir* **20**, 1915 (2004).

Author Affiliations: ¹ETH Zurich, ²University of Cincinnati

Correspondence: pratsinis@ptl.mavt.ethz.ch

This work was supported by the University of Illinois at Urbana-Champaign, Oak Ridge National Laboratory, the National Institute of Standards and Technology, and UOP LLC for the UNI-CAT facility; NSF to G.B.; and the Swiss National Science Foundation. Use of the Advanced Photon Source was supported by the U.S. Department of Energy, Office of Science, Office of Basic Energy Sciences, under Contract No. W-31-109-ENG-38.

SAXS AND THE WATER CHANNEL

Smart materials containing tiny channels, a thousandth the thickness of a human hair, could carry drug molecules directly to a target in the human body and release them when the material reaches body temperature. The heat-responsive materials would allow drugs that are otherwise inactive when taken by mouth to be administered without the patient requiring a shot. Related materials might also act as artificial enzymes, speeding up the conversion of the trapped molecules into useful products. A group of researchers from Argonne National Laboratory has designed several polymeric materials containing these tiny water and membrane channels. Their studies, using the BESSRC/XOR 12-ID beamline at the APS, are revealing how chemical fine-tuning of the polymer's structure can change the size of the channels so that different molecules can be held inside selectively for subsequent ejection.

The chemical driver behind the research is the possibility that certain molecules could self-assemble into more complex chemical structures, allowing chemists to design a building block that will then form itself into the desired material. This is one way of making nanoscale materials with a controlled structure that respond to different external stimuli, such as light, temperature, and pH. By fine-tuning the chemistry of the building blocks, scientists can tailor the nanostructures to have different response levels to a stimulus. For instance, when a polymer called PEG is mixed with a fatty, phospholipid molecule in water containing a surfactant (a soap-like molecule), the building blocks rearrange themselves into microscopic bubbles known as micelles. The resulting material is gel-like and doubly refracts light in slightly different directions—it is birefringent. By changing the length of the chemical side chains on the PEG component, it is possible to change the level of birefringence. Such materials are of interest for researchers working in optoelectronics.

The Argonne group, however, has uncovered the potential of a related polymer, N-isopropylacrylamide (PNIPAM), in mak-

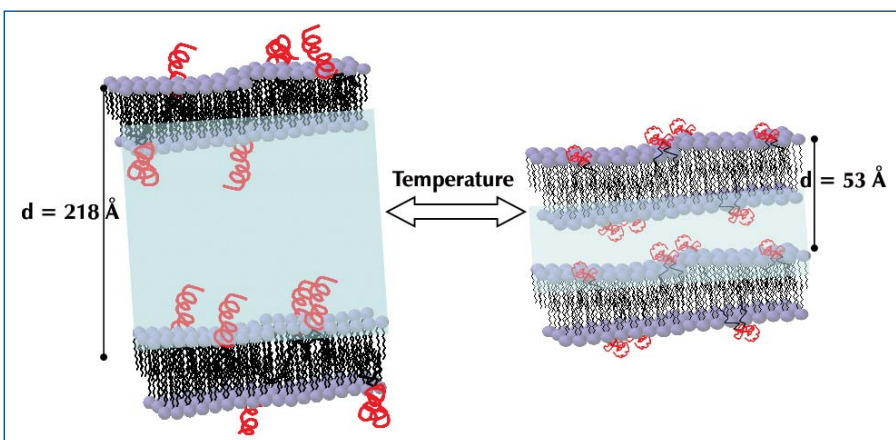


Fig. 1. Turning up the heat puts the squeeze on water channels.

ing, not microscopic bubbles, but channels in a similar mixture of ingredients. These channels are essentially "endless" bubbles into which water and other molecules can fit. While other researchers have been able to change the size of the micelles (one class of aggregate, formed by amphiphilic molecules, often in an aqueous environment) by tweaking the chemistry of

Continued on next page

the building blocks, the Argonne group set out to make the size of the water channels tunable using an external stimulus, such as a change in temperature. Other researchers have already demonstrated that PNIPAM undergoes dramatic changes in its chemical conformation when the temperature rises, so the polymer seemed to be the perfect choice for making a thermally responsive material.

A series of new materials was synthesized, in which a PNIPAM group was grafted on to the head of a phospholipid. The group used several spectroscopic techniques to demonstrate that the chemicals had self-assembled into the structures they were expecting, and they employed optical microscopy to confirm birefringence in these new materials. They found that the mixture was a transparent gel at room temperature (22°C), but when warmed to 32°C, it became an opaque fluid.

The researchers then turned to the BESSRC/XOR beamline, using small-angle x-ray scattering (SAXS) at different temperatures to obtain a detailed view of the water channels. At room temperature, the diffraction pattern for the material carries

three peaks, which are likely due to a lamellar structure composed of alternating layers of the PNIPAM-based material and water layers. The SAXS data also suggest that the stacking of these layers is directional, reflecting the channel-like nature of the layering. When the gel is warmed above 32°C, the diffraction pattern changes dramatically, indicating that the layered structure collapses and the size of the water channels is compressed. — *David Bradley*

See: D.N.T. Hay, P.G. Rickert, S. Seifert, and M.A. Firestone, "Thermoresponsive Nanostructures by Self-Assembly of a Poly(N-isopropylacrylamide)-Lipid Conjugate," *J. Am. Chem. Soc.* **126**, 2290 (2004).

Author Affiliations: Argonne National Laboratory

Correspondence: firestone@anl.gov

This work and use of the Advanced Photon Source supported by the U.S. Department of Energy, Office of Science, Office of Basic Energy Sciences, under Contract No. W-31-109-ENG-38.

UNRAVELING THE COMPLEXITY OF VANADIUM OXIDE NANOTUBES

Researchers from Central Michigan University, the State University of New York at Binghamton, and Argonne National Laboratory, using the XOR 1-ID beamline at the APS, have captured the most detailed picture yet of oxide-based nanotubes with potential industrial applications. The crystalline analogue of the nanotubes, vanadium pentoxide (V_2O_5), is a key technological material widely used in such applications as switches, chemical sensors, catalysts, and solid-state batteries. Vanadium pentoxide nanotubes have many of the useful physicochemical properties of the parent crystal significantly improved. In addition, their high surface area renders them even more attractive as positive electrodes in secondary Li batteries. Also, the nanotubes show good potential for completely novel applications, such as nanoactuators and nonlinear optical limiters.

To achieve better understanding and control of the useful properties of nanostructured materials, an accurate knowledge of their three-dimensional structure is needed. Usually the structure of materials is obtained from the Bragg peaks in their diffraction patterns. However, nanomaterials lack the three-dimensional order and periodicity of typical crystals and show diffraction patterns with only a few Bragg peaks and a pronounced diffuse component. This limits the applicability of traditional techniques for structure determination. Recently, researchers from Central Michigan University, the State University of New York at Binghamton, and Argonne National Laboratory extended an old method for analyzing x-ray data to vanadium pentoxide nanotubes. The method is the so-called "atomic pair distribution function" (PDF) technique, used in the past to study glasses and liquids and, more recently, crystalline materials. Nanomaterials are "somewhere in between" a perfect crystal and a completely disordered material. They tend to make highly intricate structures that, in the case of vanadium pentoxide nanotubes, resemble coils and scrolls (Fig. 1).

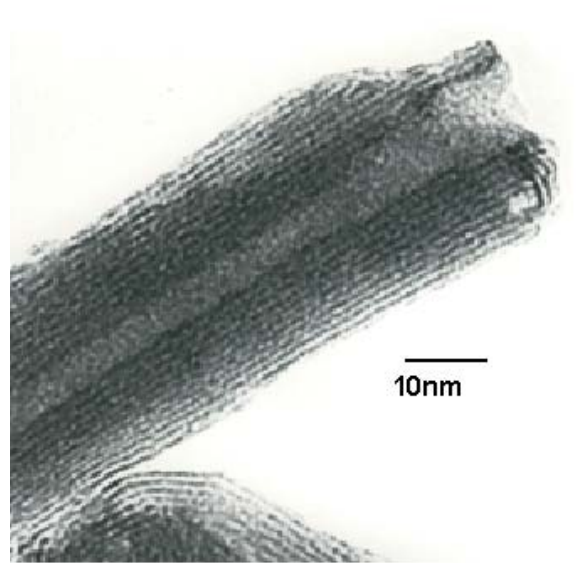


Fig. 1. TEM images of vanadium pentoxide nanotubes.

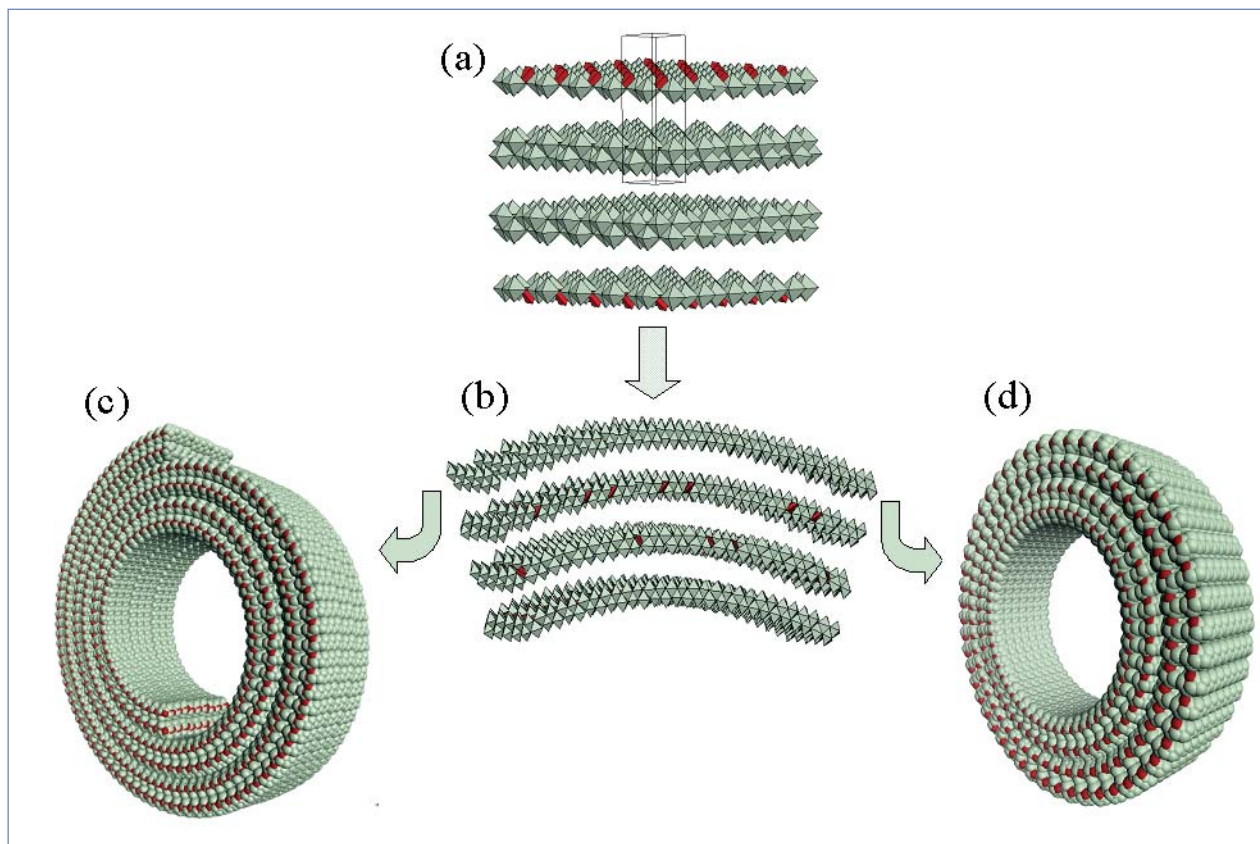


Fig. 2. Structure description of V_2O_5 nanotubes. Double layers of $V-O_6$ octahedral (green) and $V-O_4$ tetrahedral (red) units are undistorted and stacked in perfect registry with crystalline BaV_7O_{16} in H_2O (a). When bent (b.) such layers may form nanoscrolls (c) or closed nanotubes (d). Double layers of such complexity may sustain only a limited deformation. As a result, V_2O_5 nanotubes occur with inner diameters not less than 5 nm. The real-size models shown in (c) and (d) have an inner diameter of approximately 10 nm and involve 33,000 atoms. The bending of vanadium oxide layers into nanotubes can be explained by the presence of an anisotropy in the distribution of vanadium 4+ and 5+ ions.

The research team sent x-rays from the APS through the nanotubes and applied the PDF technique. They found that the nanotubes exhibited a very well-defined nanometer-scale structure and could be described in terms of such concepts as symmetry and unit cell [1]. By comparing the experimentally determined PDF with theoretical PDFs from various trial models, it was possible to create a real-space model for the nanotubes (Fig. 2) that accurately captures their atomic coordination properties. The unique capabilities of the PDF method, combined with the high brightness of the APS in the appropriate x-ray energy range, suggest that this technique should provide a sorely needed structural analysis technique for nanomaterials.

— David Voss

REFERENCE

[1] See below.

See: V. Petkov¹, P.Y. Zavali², S. Lutta², M.S. Whittingham², V. Parvanov¹, and S. Shastri³, "Structure Beyond Bragg: Study of V_2O_5 Nanotubes," *Phys. Rev. B* **69**, 085410-1 (2004).

Author Affiliations: ¹Central Michigan University, ²State University of New York at Binghamton, ³Argonne National Laboratory

Correspondence: petkov@phy.cmich.edu

The work was supported in part by NSF through Grant Nos. DMR0304391 (NIRT) and DMR0313963. Use of the Advanced Photon Source was supported by the U.S. Department of Energy, Office of Science, Office of Basic Energy Sciences, under Contract No.W-31-109-ENG-38.

NOVEL X-RAY TECHNIQUES & INSTRUMENTATION

THE MICROSTRUCTURE OF METALLIC THIN FILMS

The analysis of polycrystalline metals often uses x-ray diffraction geometry. However, many researchers prefer the method of grazing incidence small-angle x-ray scattering (GISAXS) because the scattered radiation that emerges from below the surface enables identification of average grain sizes as a function of depths within thin film samples. Collaborators from the Swiss Light Source at the Paul Scherrer Institute and the University of Illinois at Urbana-Champaign bounced coherent x-ray beams from the APS off the surface of metallic thin films so that the initial (incidence) angle (α_i) and the final (exit) angle (α_f) were both near the value of the critical angle for total external reflection (α_c). Measurements were made from the angular width of the scattering of the exit beam (as it emerged from various depths from within the thin film), specifically, those that fell below the value of α_c . As a result, the group was able to probe the fine internal structure of the sample. The coherence should allow imaging of the specific distribution of shapes and sizes within the grain structure.

The group carried out its experiments using the UNICAT 34-ID beamline at the APS. Gold film was deposited to a depth of 1,000 Å ($1 \text{ Å} = 10^{-8} \text{ cm}$) by thermal evaporation onto a $15 \times 15 \text{ mm}^2$ polished quartz substrate. Then the sample was positioned flat onto the primary axis of an ultra-high vacuum diffractometer, and slanted to accommodate the incidence angle. Two roller-blade slits were placed in front of the sample in order to achieve coherence of the x-ray beams. A charge-coupled device x-ray camera was positioned on the detector arm of the diffractometer. With the values of the incidence angle set at either 0.77° or 0.90° —both greater than the critical angle ($\sim 0.5^\circ$ for gold) in order to assure sufficient penetration inside the thin film—the reflected beam was measured within a range of $0 < \alpha_f < \alpha_c$.

The coherent x-ray diffraction produced a speckled modulation, with the speckle size inversely proportional to the beam size, but also affected by beam refraction. The speckle shape was used to interpret (1) distortions caused by emergence of the exit beam from the thin film and (2) distribution of identified grains within the film.

When using grazing exit geometry, three familiar parts of the scattering were observed (Fig. 1). First, a specular (mirror-like) beam occurred that exhibited identical geometric form and propagation properties as the incidence angle (α_i), but with decreased intensity caused by surface roughness. Second, a speckled ridge of pseudo-specular scattering appeared that was due directly to the surface roughness within the illuminated footprint. Third, diffuse scattering caused by the distribution of bulk grains within the thin film occurred. The scattering formed a triangular shape that became weaker when α_i was increased. Its intensity (along with the intensity of the ridge) was increased when the exit angle was approximately equal to the critical angle ($\alpha_f < \alpha_c$).

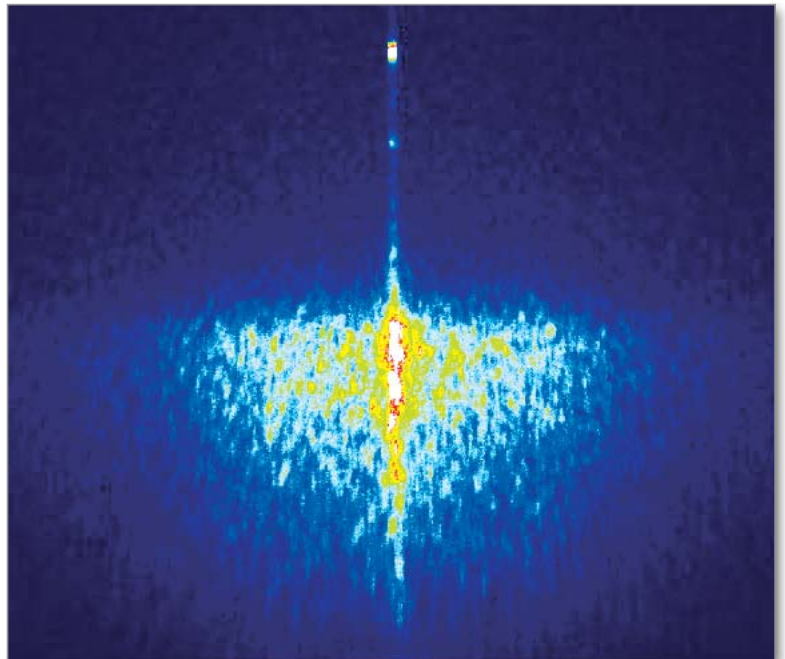


Fig. 1: Coherent x-ray diffraction pattern of a granular thin film of Au (gold) measured at 34-ID with an incidence angle greater than α_c . The specular beam is at the top, connected to the off-specular ridge, which falls to the horizon at $\alpha_f - \alpha_c$.

The shape of the speckles varied with the exit angle (α_f) becoming (1) more circular near $\alpha_f \approx \alpha_c$ and (2) longer in the vertical direction near the surface plane when $\alpha_f < \alpha_c$. The modification of the speckle shape was also dependent on the position of the beam on the sample. When the entrance slits

Continued on next page

were made wider in the vertical, the speckles became vertically contracted and *vice versa*.

The technique demonstrated here will be used to determine the microstructure of polycrystalline metallic thin films during their growth and subsequent processing.

— William Arthur Atkins

See: F. Pfeiffer¹, W. Zhang², and I.K. Robinson², "Coherent Grazing Exit X-ray Scattering Geometry for Probing the Structure of Thin Films," *Appl. Phys. Lett.* **84**(11), 1847 (15 March 2004).

Author Affiliations: ¹Swiss Light Source, ²University of Illinois at Urbana-Champaign Correspondence: ikr@uiuc.edu

Work supported by the NSF under Grant No. DMR03-08660. The 34-ID-C Coherent X-ray Diffraction facility built with funds from NSF DMR97-24294. UNI-CAT is supported by the U. of Illinois Materials Research Laboratory, funded by the U.S. DOE under DEFG02-91ER45439, Oak Ridge National Laboratory, the National Institute of Standards and Technologies, and UOP Research & Development. Use of the Advanced Photon Source was supported by the U.S. DOE, Office of Science, Office of Basic Energy Sciences under Contract No. W-31-109-ENG-38.

STUDYING VIBRATIONAL DYNAMICS OF HYDROGEN IN BIOMOLECULES, USING IRON (⁵⁷Fe) AS A PROBE



key element in understanding biological processes inside living cells involves determining how the behavior of lighter, smaller atoms, such as hydrogen, at certain active sites can influence the function of enzymes. Hydrogen, being the smallest and lightest atom, can be almost invisible to conventional x-ray scattering techniques, which is why scientists are exploring the possibility of studying hydrogen when it is bonded to other, larger elements, such as iron. Iron can often be found at positions on proteins that are important to the functioning of these biomolecules, and the stable ⁵⁷Fe isotope has a well-known Mössbauer resonance at 14.413 keV. Synchrotron x-rays can be tuned to the vicinity of this resonance to observe the vibrational dynamics of ⁵⁷Fe when paired with a hydrogen atom. Thus the iron isotope could serve as a "probe" that would enable researchers to study the associated hydrogen atoms. Researchers from the University of California, Davis; Lawrence Berkeley National Laboratory; Argonne National Laboratory; Indiana University; Purdue University; the University of Georgia; and Louisiana State University performed a study at the XOR beamline 3-ID, employing nuclear resonant vibrational spectroscopy (NRVS) to excite the nuclei in a sample in order to identify hydrogen and other ligands.

As ⁵⁷Fe nuclei decay, they resonate and generate a delayed signal that arrives at a detector shortly after the signals produced by the initial x-ray excitation of other nuclei in the sample. A computer program is used to extract the data and calculate the vibrational energy or resonant densities of the Fe atoms.

To investigate the potential for using nuclear resonant inelastic x-ray scattering to study iron and hydrogen atoms in complex biological samples, the researchers tested the technique on two simpler systems, tetrahedral Fe-S₄ in *Pyrococcus furiosus* (*Pf*) rubredoxin (Rd) and FeH(D)₆ in [FeH(D)₆][MgBr(THF)₂]₄. A high-resolution monochromator was used to select the exact x-ray energy (14.413 keV) needed to cause the Fe probes to resonate. The monochromator consisted of a series of perfect silicon crystals aligned in a specific geometry. The researchers could precisely tune the x-ray energy by mechanically rotating the crystals in mere fractions of a microradian, a unit of measure that describes extremely small tilt angles. (On a horizontal, perfectly rigid rod that is one kilometer long, raising one end of the rod by just one millimeter will tilt the rod by an angle of 1.0 microradian.) The perfect crystal optics produced an x-ray beam tunable through the E₀ = 14.413 keV ⁵⁷Fe nuclear resonance energy with 0.85 meV resolution. The 1.0-mm-square, monochromatized beam was aimed at samples held in a cryo-stand that kept the target cooled to

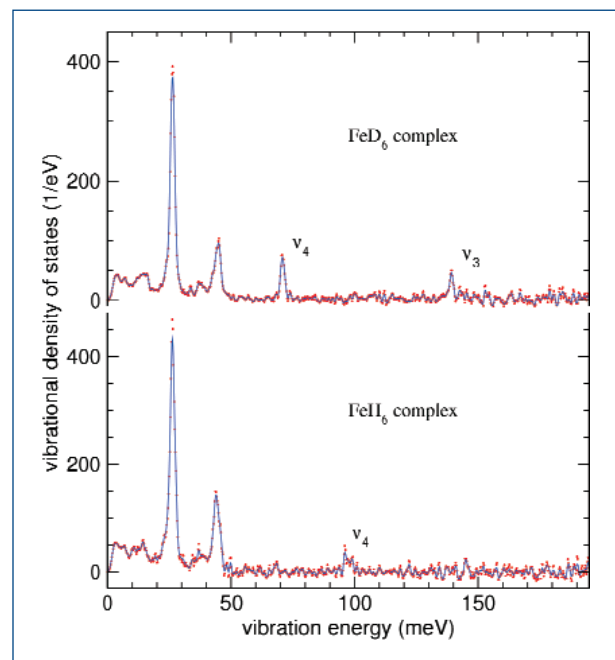


Fig. 1. The vibrational density of states of the FeH₆ and Fe(D)₆ complexes discussed in the text. The Fe-H and Fe-D bending modes (v_4) and the Fe-D stretch mode (v_3) are clearly identified.

about -370°F (50K), which minimized the radiation effects on the samples.

One Rd feature considered was the band near 60 cm^{-1} (in heme proteins and models, bands between 40 and 80 cm^{-1} are ascribed to heme doming modes). The NRIXS data revealed that the Pf Rd crystal structure has an Fe site enclosed in a loop at the far end of the protein. The Rd results showed that Fe–S vibrations in more complex enzymes will be easily observed but they will not interfere in the Fe H(D) bend regions. However, the researchers could not adequately observe Fe H stretches in $[\text{FeH(D)}_6] [\text{MgBr(THF)}_2]_4$, so the prospects for seeing Fe H stretches in proteins are not initially encouraging. The outlook is brightened by the fact that the Br in the sample (K-edge at 13.5 keV) reduced the penetration length for the 14.413 keV photons by about 200 fold versus what the effect would be in a protein sample. The observed count rate in the Fe D bend region of $\sim 1\text{ s}^{-1}$ would, for proteins, be $\sim 1750\text{ ppm}$ or $\sim 35\text{ mM}$ Fe. This means that observing Fe D bonds at the mM level would require several days, so that for this technique to become a routine experiment, better insertion devices, optics, and detectors are required.

Future studies include investigating other metal H bond properties, important in chemistry, industrial catalysis, and the mechanisms of enzymes such as hydrogenase and nitrogenase.

[Note: This highlight, based on a 2003 publication, was completed after the deadline for the 2003 APS annual report.]

See: U. Bergmann^{1,2,*}, W. Sturhahn³, D.E. Linn, Jr.⁴, F.E. Jenney, Jr.⁵, M.W.W. Adams⁵, K. Rupnik⁶, B.J. Hales⁶, E.E. Alp³, A. Mayse^{1,2}, and S.P. Cramer^{1,2}, "Observation of Fe-H/D Modes by Nuclear Resonant Vibrational Spectroscopy," J. Am. Chem. Soc. **125**, 4016 (2003).

Author Affiliations: ¹University of California, Davis; ²Lawrence Berkeley National Laboratory; ³Argonne National Laboratory; ⁴Indiana University-Purdue University, Fort Wayne; ⁵University of Georgia; ⁶Louisiana State University, *Now at the Stanford Synchrotron Radiation Laboratory

Correspondence: bergmann@slac.stanford.edu

This work was funded by NIHGM-44380 and GM-65440 (S.P.C.); NSFMCB-990424 (M.W.A.); CHE-0213952 (S.P.C.); USDA 1999-3695 (B.J.H.); ACS-PRF (D.E.L.); and DOE OBER (S.P.C.). Use of the Advanced Photon Source was supported by the U.S. Department of Energy, Office of Science, Office of Basic Energy Sciences, under Contract No. W-31-109-ENG-38.

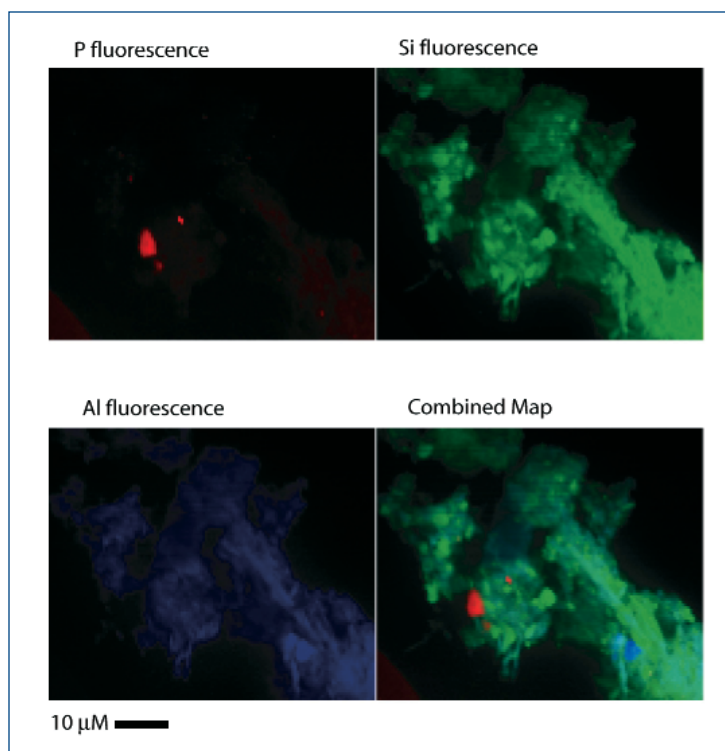
SPECTROMICROSCOPY IN THE 1- TO 4-KEV REGION: ENVIRONMENTAL STUDIES

Unique opportunities are opening up in an increasingly important energy region for environmental, biological, and advanced materials studies. Using brilliant focused x-ray beams at the APS, spectromicroscopy can be achieved in the 1- to 4-keV region at XOR beamline 2-ID-B. This energy region has traditionally been difficult to access, but recent application of multilayer coatings to the grating monochromator has increased available flux by 20-fold at key absorption edges.

Phosphorus and sulfur are key elements in environmental and biological studies. Chemical state analysis using near-edge spectroscopy combined with spatial resolution of 70 nm allows researchers to examine new science questions. Recent examples of research at XOR beamline 2-ID-B include the study of phosphorus within dissolved and particulate organic materials. Phosphorus in these forms is a significant, but poorly understood, source of bioavailable phosphorus in many aquatic environments [1]. Figure 1 shows high-resolution fluorescence maps

Continued on next page

Fig. 1. High-resolution fluorescence maps of dissolved marine organic material. Absorption mapping of marine organic phosphorus particulates shows that high-density regions are not necessarily phosphorus rich. Once the higher concentration regions of phosphorus are identified, the chemical state can be determined using spectromicroscopy.



of dissolved marine organic material locating phosphorus-rich regions. The chemical state of the phosphorus in sub-micron areas can then be determined using spectromicroscopy, as shown in Fig. 2.

A second example concerns sulfur, which is an indispensable nutrient for plants and microorganisms. Sulfur's speciation in soils is intimately linked with the chemical conditions of the soils, such as redox potential and acidity [2]. Changes in the speciation of sulfur in soils caused by pedogenetic processes and changes of the physicochemical temporary environment (e.g., water logging) can therefore result in considerable changes in soil fertility. In both these examples, knowledge of the chemical speciation at the sub-micron level and *in situ* is critical and can be provided by x-ray spectromicroscopy.

Contact: D. Paterson (paterson@aps.anl.gov)

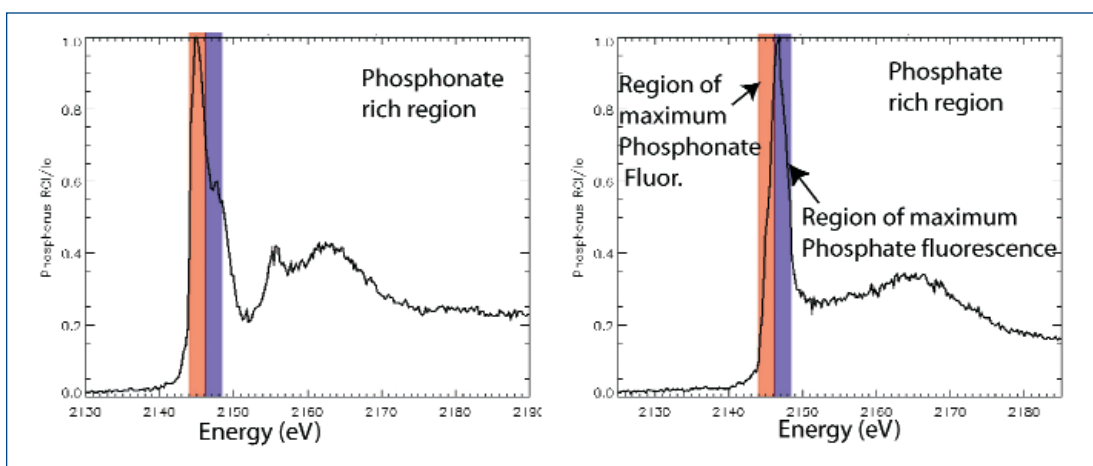


Fig. 2. Fluorescence spectromicroscopy from 100-nm areas of dissolved marine organic material.

REFERENCES

- [1] J. A. Brandes, C. Lee, S. Wakeham, M. Peterson, C. Jacobsen, S. Wirick, and G. Cody, *Marine Chemistry* 92, 107 (2004).
- [2] J. Priezel, J. Thieme, U. Neuhäusler, J. Susini, I. Kögel-Knabner, *Euro. J. Soil Sci.* 54, 1 (2003).

X-RAY NANODIFFRACTION: STRUCTURAL CHARACTERIZATION OF INDIVIDUAL NANOMATERIALS

X-ray scattering characterizations of nanoscale materials have been limited to averaging information obtained by illuminating a large number of objects. Detailed information, such as nanostructure, structure variation within individual nanomaterials, and dimension-dependent structural properties, was lost when conventional x-ray scattering was used. At the XOR 2-ID-D beamline, undulator radiation can be focused onto a spot measuring $150 \text{ nm} \times 150 \text{ nm}$, with a gold zone plate of $150\text{-}\mu\text{m}$ diameter, yielding a photon flux of better than 10^9 photons/s/0.01%BW from 5.5 keV to 12 keV, corresponding to a flux density of 4.5×10^4 photons/sec/nm²/0.01%BW. The x-ray microfocusing optics is further integrated with a six-circle diffractometer for full accessibility in reciprocal space [1].

Researchers studied the structure of individual tin oxide (Sn_2O_3) nanobelts synthesized via a thermal evaporation and condensation process in order to demonstrate the nanodiffraction capability. Figure 1 shows diffraction patterns of the (030) reflection obtained from a single 100-nm-wide nanobelt. The diffraction

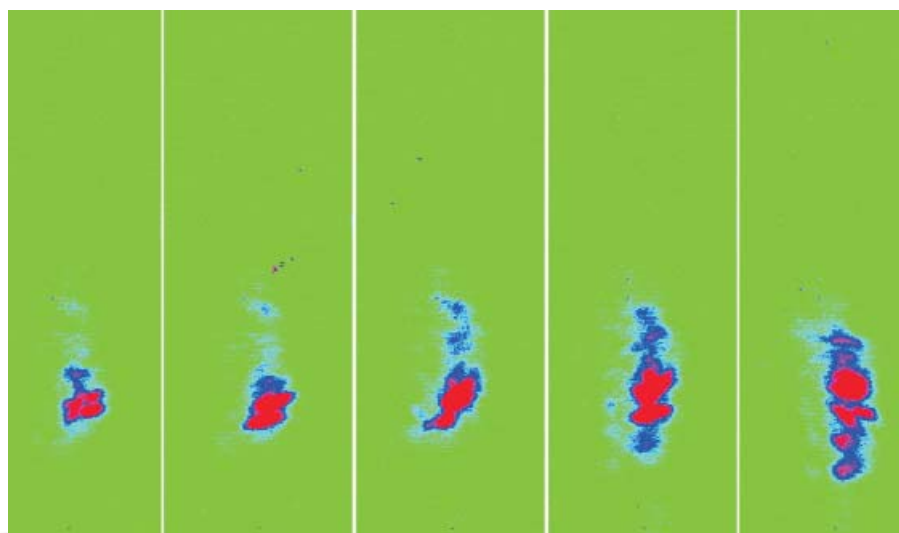


Fig. 1. X-ray diffraction spots of the (030) reflection from a 100 nm Sn_2O_3 nanobelt captured by a charge-coupled device detector. Each image was taken after moving the microbeam along the length of the nanobelt in steps of 200 nm. The horizontal axis represents the 2θ direction and ranges from 36.5 to 39.5 degrees. The vertical axis represents the χ direction and covers 8.5 degrees.

patterns are clearly composed of several sub-spots splitting along the χ direction in the range of degrees, indicating a highly textured subgrain structure. Studies of the orientation distribution of the grains revealed a broadening of 3 to 5 times in the χ axis compared to the θ axis.

Although scanning electron microscopy is an accurate tool for measuring lateral size, determination of the extent of the material along the third dimension often requires other techniques like x-ray scattering. Figure 2 shows an x-ray θ - 2θ profile along the (030) reflection of a nanobelt of lateral size $30 \mu\text{m} \times 100 \text{nm}$. A theoretical reflectivity profile based on the kinematic scattering was used to fit the measured profiles, which led to a thickness of 29 nm for the nanobelt.

The technique has enabled study of the size-dependent nanostructure of individual nanobelts of tin and zinc oxides with a minimum sampling volume down to $3 \times 10^{-5} \mu\text{m}^3$. With expected improvements in zone-plate optics, the detection limit will be pushed further, to $10^{-6} \mu\text{m}^3$ or smaller in the near future. Future research of the structure-related electrical, thermal, and optical transport processes in nanoscale materials will benefit from the development of the x-ray nanodiffraction technique.

Contact: Z. Cai (cai@aps.anl.gov)

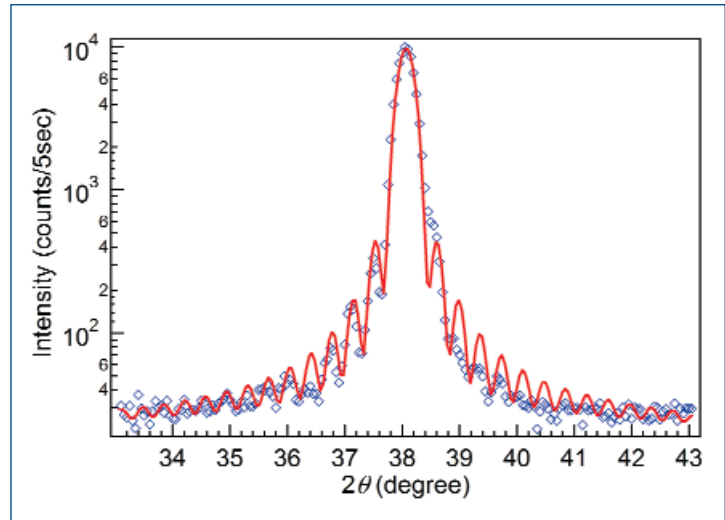


Fig. 2. Measured (open diamond) and calculated (solid line) x-ray θ - 2θ scan profiles of the (030) reflection from a 100-nm-wide triclinic tin-oxide nanobelt. The interference fringes and their frequency characterize the thickness of the nanobelt. Fitting the profile revealed a thickness of 29 nm.

REFERENCES

- [1] Z. Cai, B. Lai, Y. Xiao, S. Xu, J. Phys. IV France 104, 17-20 (2003).
- [2] Z. Pan, Z. Dai, Z. Wang, Science 291, 1947 (2001).

FLUCTUATION X-RAY MICROSCOPY FOR STUDYING DISORDERED MATERIALS

In recent years, materials research has increasingly sought to develop a better understanding of the disordered state of matter. Most of the effort in understanding amorphous materials has focused on structural models with an atomic pair distribution function (PDF) consistent with diffraction experiments. However, the PDF method has poor sensitivity to medium-range order (MRO). Recently, fluctuation electron microscopy (FEM) was developed and successfully used for probing MRO in amorphous materials [1]. This technique gains its sensitivity to MRO by examining fluctuations of speckle intensity from very small sample volumes. The speckle variance depends on higher-order correlation functions that are more sensitive to MRO [2].

Compared to electrons, x-rays provide access to longer length scales and offer greater sample penetration with less radiation damage. Consequently, we are developing fluctuation x-ray microscopy (FXM) at the 2-ID-B soft x-ray beamline to study MRO in bulk samples and films at nanometer and larger length scales [3]. A working definition of MRO in the x-ray regime is $5 \leq L/d \leq 20$, where d is the separation distance of unit objects and L is the correlation

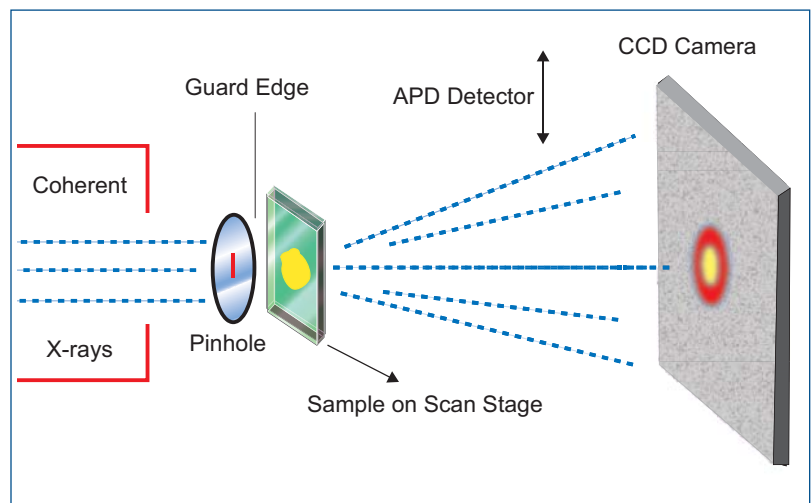


Fig. 1. Schematic outline of the FXM setup at 2-ID-B beamline.

length of these units [3]. FXM examines variations in coherent x-ray speckle patterns measured as a function of illumination radius R and sample position, where R is defined using either

Continued on next page

pinholes or zone plate optics with various numerical apertures. FXM produces a fluctuation map that contains information about the degree of MRO and the correlation length.

A disordered distribution of polystyrene latex spheres was studied to demonstrate this technique. Using various pinhole apertures to define R, a stage to scan the sample, and a CCD camera mounted on a two-circle diffractometer (Fig.1), speckle patterns were obtained over a range of illumination radii and sample positions. The mean data on the left of Fig. 2 are equivalent to the average (incoherent) small-angle scattering patterns from the sample. As predicted, the variance shown at right of Fig. 2 is far more sensitive to MRO. Changing the illumination radius allows direct extraction of the correlation length. The variance grows with increasing illumination radius up to 5.5 μm , implying a correlation length on the order of several μm for this latex sphere "glass" with sphere radius 140 nm.

This technique is still under development. With further development in x-ray nanofocusing optics, we can expect to study systems with characteristic length scales from 10 nm to 2 μm . Fluctuation x-ray microscopy can be used to explore medium-range order and subtle structural changes in a wide range of disordered materials, such as polymers, biological systems, self-assembled nanostructures, nanocomposites, and hybrid materials, as well as quantum dot arrays and magnetic materials. *Contact: L. Fan (lfan@anl.gov)*

[1] M.M.J. Treacy, P.M. Voyles, and J.M. Gibson, *J. Non-Cryst. Sol.* **150**, 266-269 (1990).

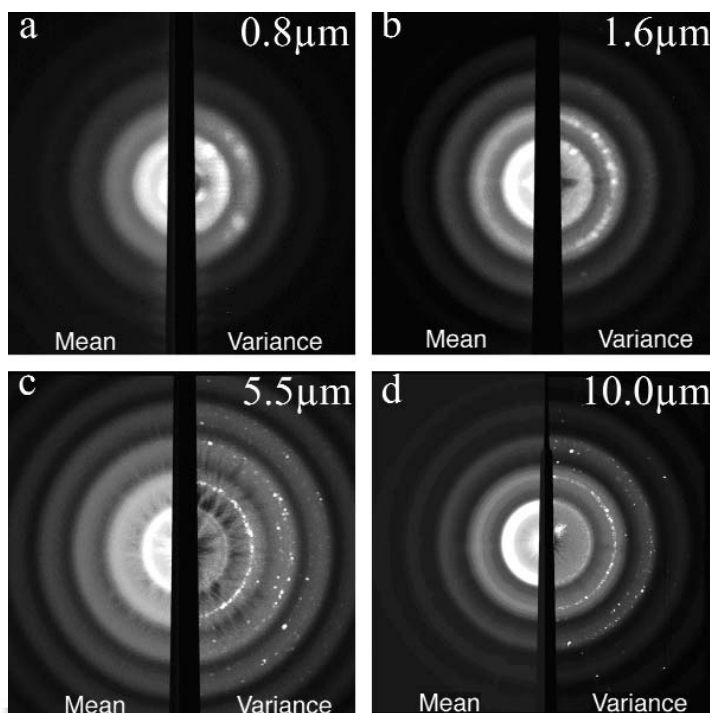


Fig. 2. Mean and variance data of 3721 speckle patterns from a film ($\sim 7 \mu\text{m}$ thick) of latex spheres, using 1.83-keV radiation and differing illumination diameters as indicated.

[2] M.M.J. Treacy and J.M. Gibson, *Acta Cryst.* **A52**, 212 (1996).

[3] L. Fan et al., *Nucl. Instrum. Methods B*, in press.

A NOVEL INSTRUMENT FOR THE MEASUREMENT OF q -DEPENDENT IXS

Inelastic x-ray scattering (IXS) at various energy ranges and resolutions is gradually becoming a more important part of the research done at the APS. As part of the continuing specialization of PNC-CAT sector 20 on scanning-energy x-ray spectroscopies, a new instrument has been constructed and commissioned for improved measurement of momentum- (q -) dependent IXS (q IXS) from the core-shell electrons of low-Z elements or the less tightly bound electrons in heavier elements.

This scattering, traditionally called nonresonant x-ray Raman scattering (XRS), provides several unique opportunities. First, in the low- q range, XRS measures the same transition matrix element as in x-ray absorption spectroscopies (XAS). However, where the direct XAS measurements require soft x-rays with energies comparable to the binding energy of the electron, the XRS measurements are performed with incident photon energies of approximately 10 keV. This enables measurements in environments incompatible with the high vacuum required in soft x-ray studies, such as low-Z elements in electrolytic reactions in aqueous solution or high-pressure

studies in diamond anvil cells. Second, unlike XAS measurements, XRS measurements provide a range of momentum transfer sufficient to escape the dipole scattering limit for many systems. This often permits a partial spectroscopy of the symmetry of the final-state wavefunction, information that can sometimes be inferred from measurement of multiple absorption edges in XAS studies for heavier elements but that cannot be obtained from XAS measurements for low- or intermediate-Z elements. Finally, momentum conservation in the system of the incident photon, outgoing photon, and photoelectron requires the use of the direction of the momentum transfer to further probe the symmetry of the final state, especially in strongly anisotropic, single-crystal samples.

Unfortunately, the small XRS cross section, combined with the frequently large background from Compton scattering, can make these measurements unduly time-consuming, even at a third-generation synchrotron such as the APS. Several groups, especially those of Uwe Bergmann (Lawrence Berkeley National Laboratory) and Peter Eng (GSECARS-CAT, APS

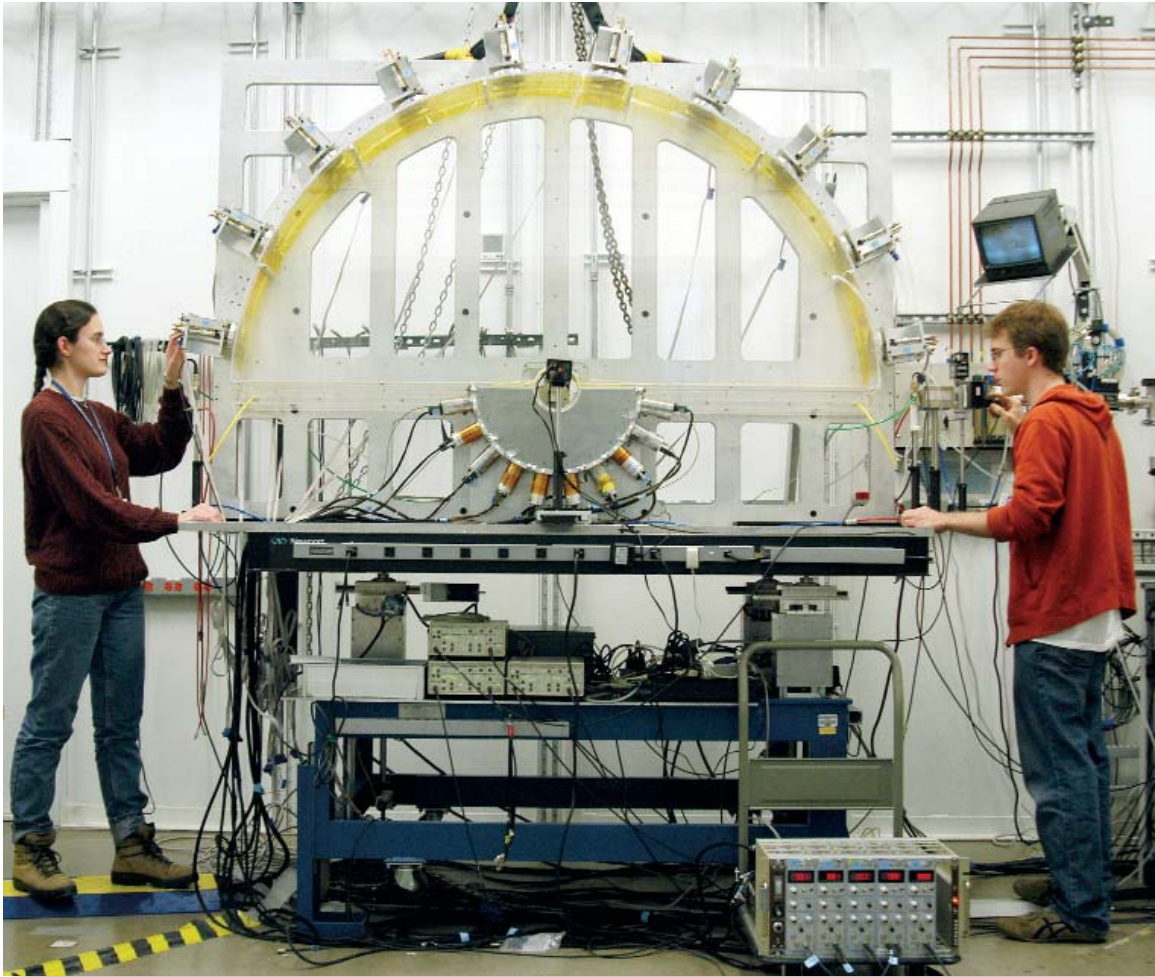


Fig. 1. University of Washington graduate students Adrienne Battle (left) Tim Fister inspect the alignment on the q IXS apparatus at sector 20-ID (PNC-CAT). This apparatus, which will soon become available to general users, is primarily used to measure the contribution to the dynamical structure factor from the core shells of low-Z elements or weakly-bound orbitals of higher-Z elements. This provides an alternative to and extension of x-ray absorption spectroscopy measurements performed with soft x-rays.

sector 13), have worked to overcome this problem by constructing instruments that can integrate the signal from several spherically bent Si analyzers at a single detector to improve the overall counting statistics.

The q IXS instrument at sector 20 was designed and constructed by graduate student Tim Fister in Assoc. Prof. Gerald Seidler's group at the University of Washington Physics Department, working in close association with Julie Cross (XFD-BES) and Al Macrander (XFD-OFM) of the APS and Trevor Tyson and Qing Qian (New Jersey Institute of Technology). Unlike all prior XRS apparatus, the new instrument consists of many independent sets of spherically bent Si analyzers and matching photon-counting detectors so that it simultaneously measures the IXS signal at many different momentum transfers, from 0.5 to 10 inverse Å. The present apparatus, which was commissioned in December 2004, consists of 10 such matched sets of analyzers and detectors with the scattering from the sample straddling the vertical plane (Fig.1). This vertical configuration maximizes the XRS signal by working in the plane perpendicular to the polarization of the incident x-rays. In addition, the

fact that the entire apparatus is stationary (energy loss is achieved by energy-scanning the monochromator for the incident radiation) allows for rapid sample exchange with no need to retune any of the analyzers. Finally, the coplanar arrangement for all the analyzers is an excellent fit with the goal of significantly broadening the range of materials for which XRS can be measured in diamond anvil cells, where scattering through the planar gasket is a convenient experimental geometry.

The commissioning run for this instrument was extremely successful, with manuscripts in preparation on the instrument and on the final state symmetry in several systems, and also with successful preliminary measurements on several other materials of interest in geophysics or in energy science research. Future plans include making this instrument available for general users by mid- to late-2005 and the installation of nine additional matched sets of spherically bent Si analyzers and photon-counting detectors to optimize the counting rate in the coplanar geometry and provide finer detail in the q IXS spectra.

Contact: S. Heald (heald@aps.anl.gov)

A VERSATILE, HIGH-RESOLUTION, ADAPTIVE-OPTIC X-RAY FLUORESCENCE ANALYZER

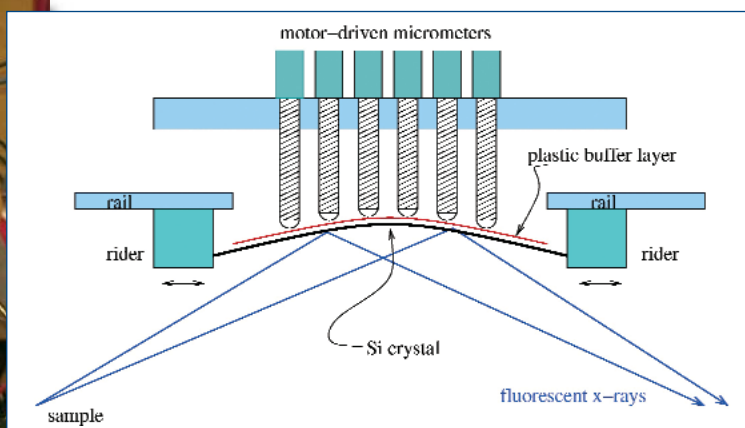
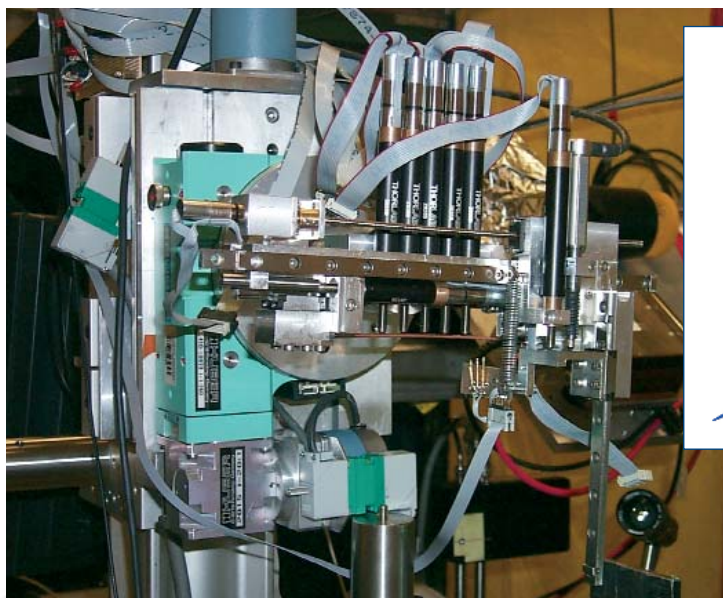


Fig. 1. Photo and schematic of the prototype x-ray fluorescence analyzer.

A high-resolution x-ray fluorescence analyzer with large solid-angle coverage has been developed as part of a project to implement a laser pump, x-ray probe spectroscopic technique for measuring the charge carrier dynamics in a photoexcited semiconductor. This new analyzer promises to be very useful in other applications as well, and will be further refined in the future. Currently, the energy resolution is 2.85 eV at a fluorescent photon energy of ~ 10 keV; the solid angle is of the order $5^\circ \times 2^\circ$, and the device can easily be tuned over several keV of pass energy. Development of this device was necessary because none of the existing technologies could provide the combination of eV energy resolution; large solid-angle collec-

tion of photons of one narrowly defined energy; and wide energy coverage required for the spectroscopy device. Figure 1 shows a schematic of the device: a strip cut from a silicon wafer is pushed from both ends to buckle up, and a row of (currently) eight shape correctors are adjusted to change the shape of the crystal to that of a logarithmic spiral matched to the pertinent photon energy.

Figure 2 shows the resolution and energy coverage range of the analyzer. These data were taken with the same experimental setup, but with the position and incidence angle of the analyzer (with the pass energy) changed. Figure 3 shows the raw data from one of the angular scans of the analyzer that

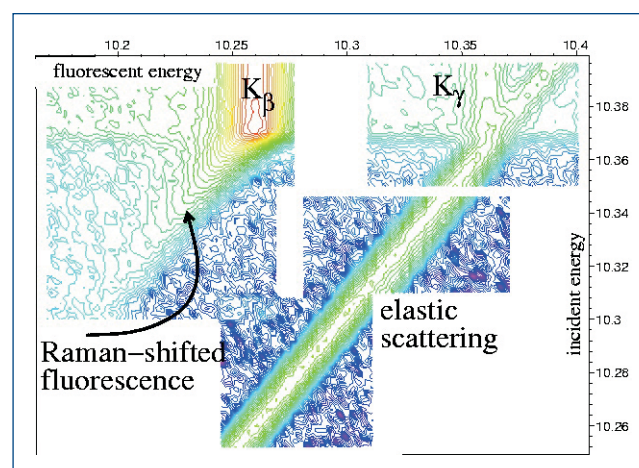
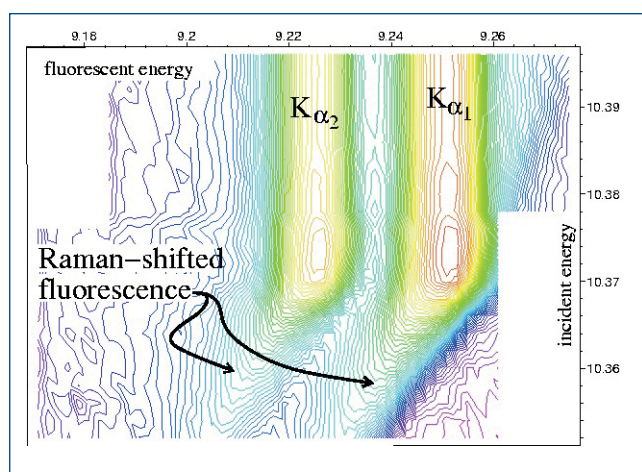


Fig. 2. Logarithmic contour plots of the detected intensity over the energies of the photons incident of the GaAs sample, and those of the fluorescent photons at 9.225 keV and 9.252 keV (Ga K_{α} lines), 10.264 keV (Ga K_{β}) and 10.367 keV (Ga K_{γ} and absorption edge).

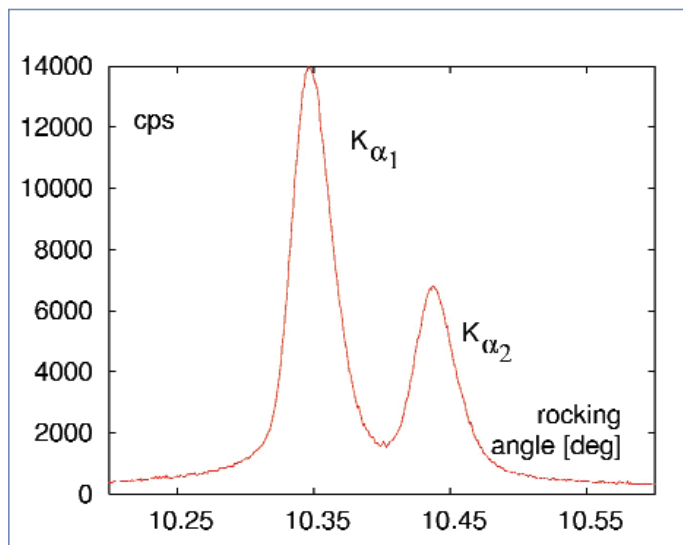


Fig. 3. Raw data, intensity [counts per second] over the rocking angle [degree] of the analyzer assembly, showing the Ga K_{α} line pair having a separation of 27 eV.

went into the contour plot of Fig. 2. The Ga $K_{\alpha_{1,2}}$ line pair is well resolved, and the count rate is consistent with >50% collection efficiency within the solid angle covered by the analyzer. The background intensity level is very low. The intensity incident on the GaAs sample was $\sim 10^{10}$ photons/s. The energy resolution of the analyzer was measured with elastically scattered x-rays and determined to be ~ 2.85 eV. Therefore, the line width in Fig. 3 is mostly intrinsic, and is not attributable to the resolution.

An interesting detail is seen in the region where the K_{γ} fluorescence line intersects the elastic scattering line (upper right-hand corner of Fig. 2). The left-hand side of Fig. 4 shows a side view of this region in Fig. 2. This data set corresponds to an orientation of the sample with the surface normal along the (001) direction pointing up, and the x-rays coming at grazing incidence along the (110) direction. The right-hand side of Fig. 4 shows the same view for a sample orientation with (001) pointing up and the x-rays incident along (100). The difference in fluorescent yield between the two orientations is probably due to the directionality of the Ga-As bond, giving rise to an anisotropic pattern of near-resonant elastic scattering.

Contact: B.W. Adams (adams@aps.anl.gov) and K. Attenkofer (klaus.attenkofer@anl.gov)

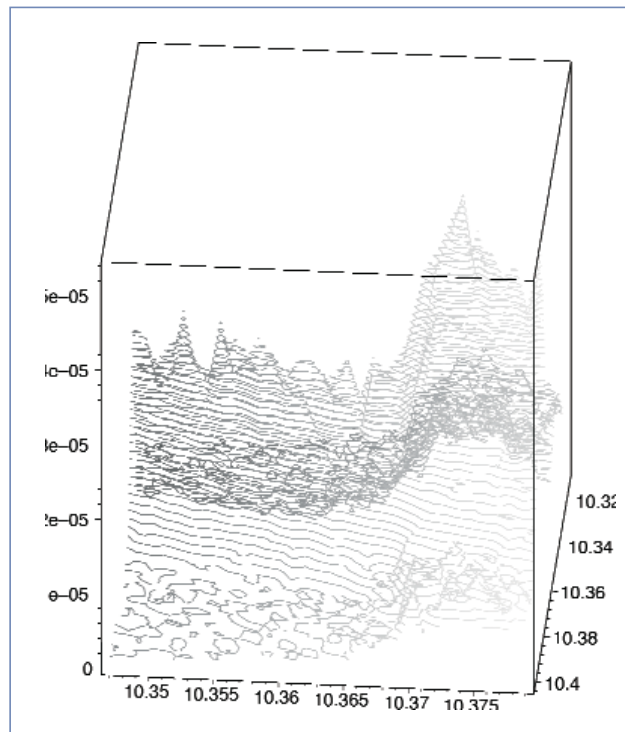
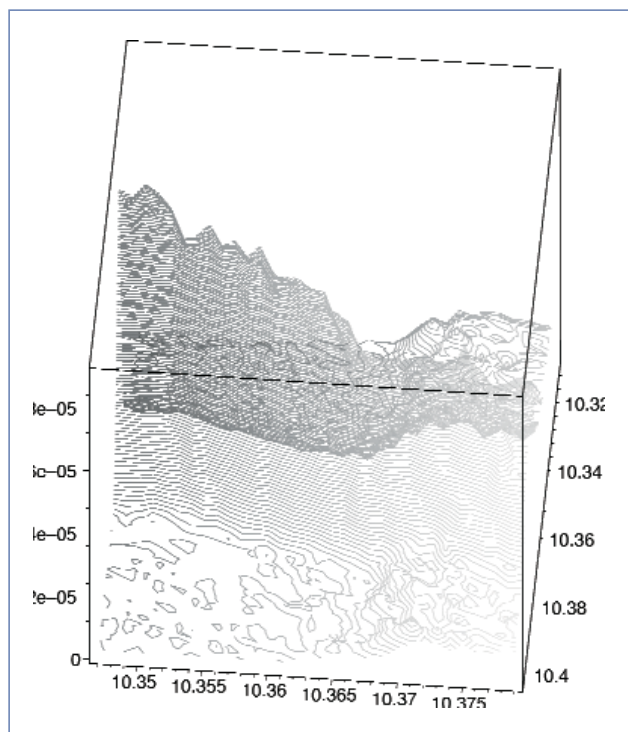


Fig. 4. Side view of the upper left-hand corner of Fig. 2. Incident energy along bottom and fluorescent energy into the paper plane. Left, with x-rays incident along (110); right: x-rays incident along (100).

A CONTROLLED-ATMOSPHERE SYSTEM FOR *IN SITU* MATERIALS PROCESSING AT THE APS

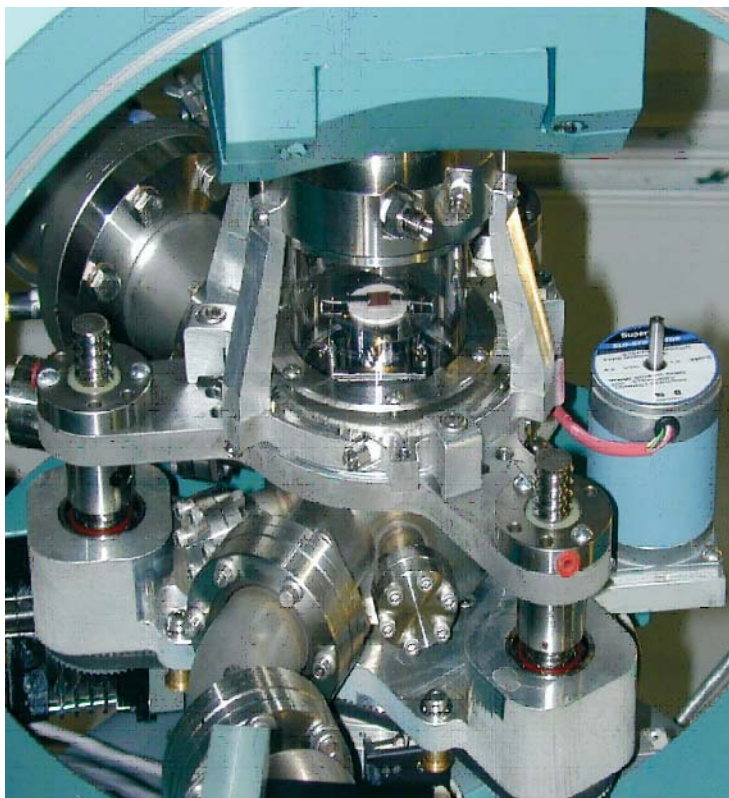


Fig. 1. The environmental cell mounted on the diffractometer at BESSRC/XOR beamline 12-ID. The sample height can be adjusted with sub-micron resolution by the use of three high-precision, pre-loaded ball screws driven by a common belt.

Synchrotron x-ray scattering techniques are particularly well-suited for providing *in situ* information during materials processing. In addition to having sufficiently low absorption to readily penetrate chamber walls and chemically reactive environments, high-energy x-rays are useful for determining atomic-scale structure and following microstructural and chemical evolution. However, application of these capabilities has been limited due to the lack of a suitable chamber capable of producing an appropriate chemical environment and sample temperatures. For this reason, a state-of-the-art, controlled-atmosphere system was constructed by a group from the ANL Materials Science Division for use at the APS.

This system creates oxidizing/reducing atmospheres maintained within a quartz-walled chamber, as shown in Fig. 1. The chamber is mounted on a Huber six-circle diffractometer (BESSRC/XOR beamline 12-ID) and is evacuated with a compact turbomolecular pump backed by an oil-free scroll pump. The base pressure is approximately 1×10^{-7} Torr; the partial pressure of the reactive gas can be varied from 1×10^{-11} Torr up to one atmosphere using a controlled flow of purified gases (e.g., Ar, O₂, CO, CO₂, H₂, etc.). The temperature can be tightly

maintained from 0 to $\sim 1000^\circ\text{C}$. A rectangular single crystal specimen is shown in the center of Fig. 1, mounted, via two high-T-alloy metal clips, onto a ceramic furnace faceplate. The sample temperature is monitored using a thermocouple in contact with the back side of the faceplate. The thermocouple readings are calibrated to the actual sample temperatures by comparing measured and known lattice parameter values for materials with well-characterized thermal expansion behavior. A residual gas analyzer for monitoring the sample environment and a plasma source for surface cleaning/reduction can be mounted on the chamber. Fine control of the oxidizing/reducing environment is achieved by adjusting gas flows via a series of mass-flow controllers and admitting the purified gas into the chamber through a controlled leak valve. All gas flows can be controlled remotely during x-ray measurements. Both grazing-incidence and high-angle diffraction x-ray scattering geometries can be accessed, and an easily mountable area detector facilitates rapid analysis of new specimens.

The initial research using this system is aimed at understanding oxidation processes in pure and alloyed metals. Such understanding has been limited by the dearth of structural, chemical, and kinetic information during the early stages of oxidation, exactly the type of information that an *in situ* study can elucidate. Early-stage oxidation studies are particularly demanding, requiring high-purity, single-crystal films or bulk samples, selected so that thermodynamic processes can be reversibly explored and surfaces can be reproducibly

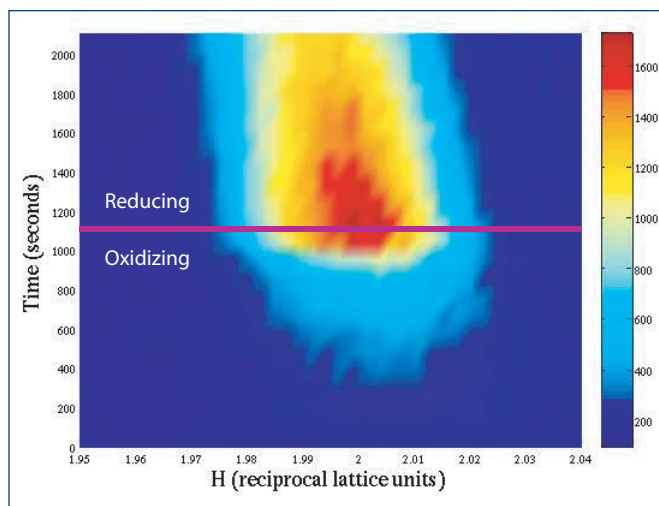


Fig. 2. Oxidation of (001) Cu single-crystal thin films produces cube-on-cube-aligned Cu₂O islands. The Cu/Cu₂O phase boundary is determined by monitoring the Cu₂O (200) Bragg reflection and observing the pressure at which the behavior changes from oxidizing to reducing. The horizontal line marks a change between O₂ and Ar atmospheres.

cleaned and characterized. Figure 2 is from an ongoing study of the oxidation behavior of thin copper films epitaxially grown on SrTiO_3 . It shows the intensity of the Cu_2O (200) Bragg peak, as a function of time, for various partial pressures of oxygen, while oriented oxide nanoislands grow (oxidize) or shrink (reduce). A reversible phase boundary is present between an oxidizing regime and a reducing regime. Interestingly, this phase bound-

ary is many orders of magnitude higher in oxygen partial pressure than predicted from bulk thermodynamic data. Using *in situ* techniques, phase diagrams and kinetic information can be rapidly and accurately determined for these complex systems.

P.H. Fuoss, J.A. Eastman, L.E. Rehn, P. Baldo, G-W. Zhou, D.D. Fong, L. Thompson / Contact: P.H. Fuoss (fuoss@anl.gov)

A NEW 2-M INELASTIC X-RAY SCATTERING SPECTROMETER AT 9-ID

A new spectrometer for momentum-resolved, resonant inelastic x-ray scattering (RIXS) with medium-energy resolution has been designed and commissioned at CMC-CAT beamline 9-ID (Fig. 1). The instrument features a 2-m-long vertical scattering arm with dynamic balancing of mechanical twist moments caused by its payload. An overall energy resolution of 118 meV full-width half-maximum was achieved by using an Si(444) monochromator and a newly fabricated Ge(733) spherical analyzer. The mechanical stability of the instrument is excellent.

The design of the spectrometer was guided by the need for an analyzer-to-sample distance of 2 m to provide adequate energy resolution, a vertical scattering geometry to minimize polarization losses, and good mechanical stability in terms of twisting and bending of the $2-\theta$ arm as it is moved over its angular range from 0° to $\sim 120^\circ$. Using Huber components, the new instrument incorporates a 3-circle sample stage in Eulerian geometry and two coupled $2-\theta$ rotation stages to provide the load-bearing capacity and bearing stiffness for operating the scattering arm. A finite-element analysis was performed for this arm and revealed that, as a consequence of its length and load requirements, significant mechanical deformations would still occur as a function of scattering angle. Thus, a novel anti-twist system was designed to dynamically counteract these deformations. The system consists of an adjustable, transverse counterweight and a large torsional cylinder running down the rear side of the arm. This cylinder both stiffens the arm against bending and transmits the torque from the counter weight to the tip of the arm, where it dynamically balances the twisting torques generated by the payload.

The effectiveness of this anti-twist system was tested in operation with a laser and position-sensitive PIN diode detector. Its compensatory mechanism was found to work exceptionally well.

The RIXS analyzer-detector setup includes a number of new features to facilitate the precision, ease of alignment, and ease of use of the instrument. Both the sample-to-analyzer and analyzer-to-detector distances can now be independently adjusted under computer control. Modular analyzer mounts and changeable detector slits enable easy energy and resolution configuration. An He-filled flight tank with telescoping snouts reduces air gaps in the optical path to a minimum and, as a result, background count rates are less than one count per minute.

Contact: J. Hill (hill@bnl.gov)



Fig. 1. John Hill (BNL), Nalaka Kodituwakku (Western Michigan University) and Thomas Gog (CMC-CAT) inspect the spherical analyzer on the detector arm of the new IXS spectrometer in sector 9.

X-RAY TRANSPARENT WINDOWS SUSTAINABLE TO HIGH PRESSURE FOR IMAGING APPLICATIONS

With the advent of third-generation synchrotron sources, emerging x-ray imaging techniques have shown the capability of acquiring ultrafast, two-dimensional x-ray images of extended size with high spatial resolution. The subject of the experiments can be fast transient phenomena, including but not limited to supercritical fluids, high-pressure liquid and gas injection, and plasma-material interactions. The materials involved in the phenomena are normally opaque to visible light due to the highly dense droplets surrounding the core region of the events.

The x-ray images are made quantitative and yet nonintrusive by utilizing monochromatic x-radiography to probe the characteristics of these events. Therefore, the fundamental problem that must now be solved in order to make these experiments possible is the development of techniques to make the critical sample environmental chamber x-ray accessible for quantitative and time-resolved x-ray analysis.

The development of practical x-ray windows for a high-pressure chamber has been a key undertaking requiring significant effort and creativity. New types of materials have been sought to meet the rigorous requirements imposed by the pressurized conditions. A series of simulations and bench testing have revealed that polymer-based thin films are able to provide the pressure and temperature resistance required by the proposed chamber. More important, these thin films feature superior safety operational properties, compared with beryllium-based windows.

Such a design concept has been realized during the past two years, and windows have been fabricated that can withstand up to 1000 psi of pressure with a window size of 3 mm \times 21 mm (see Fig. 1) for imaging applications. A test of fuel sprays under pressurized conditions at XOR sector 1 using the windows has been accomplished. In Fig. 2, a fuel spray to an injection chamber filled with 10 bar of N_2 gas was imaged through these x-ray transparent windows.

This research was funded in part by the DOE Office of FreedomCAR and Vehicle Technology.

Contact: D. Shu (shud@aps.anl.gov) and
J. Wang (wangj@aps.anl.gov)



Fig. 1. A set of high-pressure x-ray transparent windows, maximum size 4 \times 27 mm².

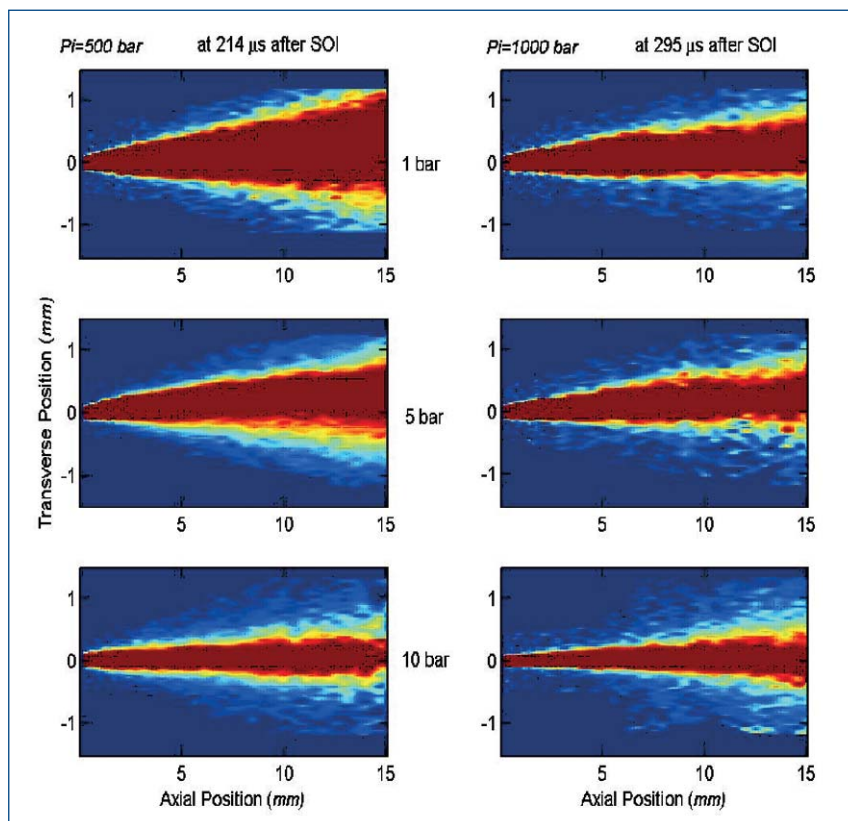


Fig. 2. A series of near-nozzle images of fuel sprays injected into a chamber with N_2 pressure up to 10 bars.

ULTRAFAST 4-D TOMOGRAPHY: HOW INSTANT FUEL SPRAYS ARE CAPTURED AND RECONSTRUCTED

Detailed analysis of the internal structure of fuel sprays has been recognized as an important step for optimizing the operation of internal-combustion engines in order to improve efficiency and reduce emissions.

By using an ultrafast x-ray pixel array detector (PAD) developed at Cornell University and intense monochromatic x-ray beam from XOR 1-BM and pink beam from the Cornell High Energy Synchrotron Source (CHESS), the fine structures and dynamics of 1-ms direct-injection gasoline fuel sprays were elucidated for the first time by a newly developed, ultrafast, computed microtomography technique. The temporal and spatial resolutions of the current measurement are $5.1 \mu\text{s}$ and $150 \mu\text{m}$, respectively.

Many features associated with the transient liquid flows are readily observable in the reconstructed spray, such as “sac” (a small volume of fuel near the spray’s leading edge caused by transient nonequilibrium pressures at the instance of the injection pintle lift), streaks, and highly axial asymmetry. Furthermore, an accurate time-resolved, three-dimensional fuel density distribution was obtained as a result of the computed tomography.

These results not only reveal the characteristics of automotive fuel sprays with unprecedented detail, but will also facilitate realistic computational fluid dynamic simulations in complex multiphase flows. The researchers believe that the methodology demonstrated here is also a sensitive probe and diagnostic tool for investigating other highly transient phenomena. *Contact: J. Wang (wangj@aps.anl.gov)*

See: X. Liu¹, J. Liu¹, X. Li¹, S.-K. Cheong¹, D. Shu¹, J. Wang¹, M.W. Tate², A. Ercan², D.R. Schuette², M.J. Renzi², A. Woll², S.M. Gruner²,

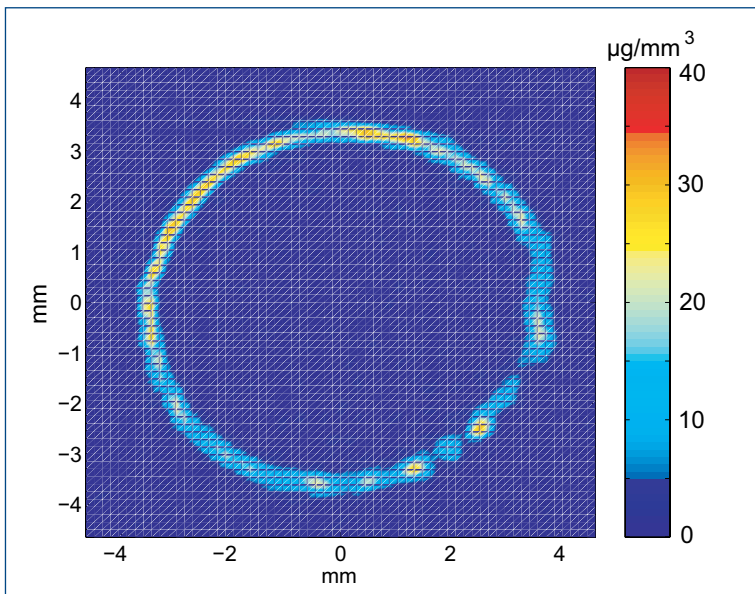


Fig. 2. Reconstructed hollow-cone fuel spray cross section (3.6 mm from nozzle and 820 ns after start of injection).

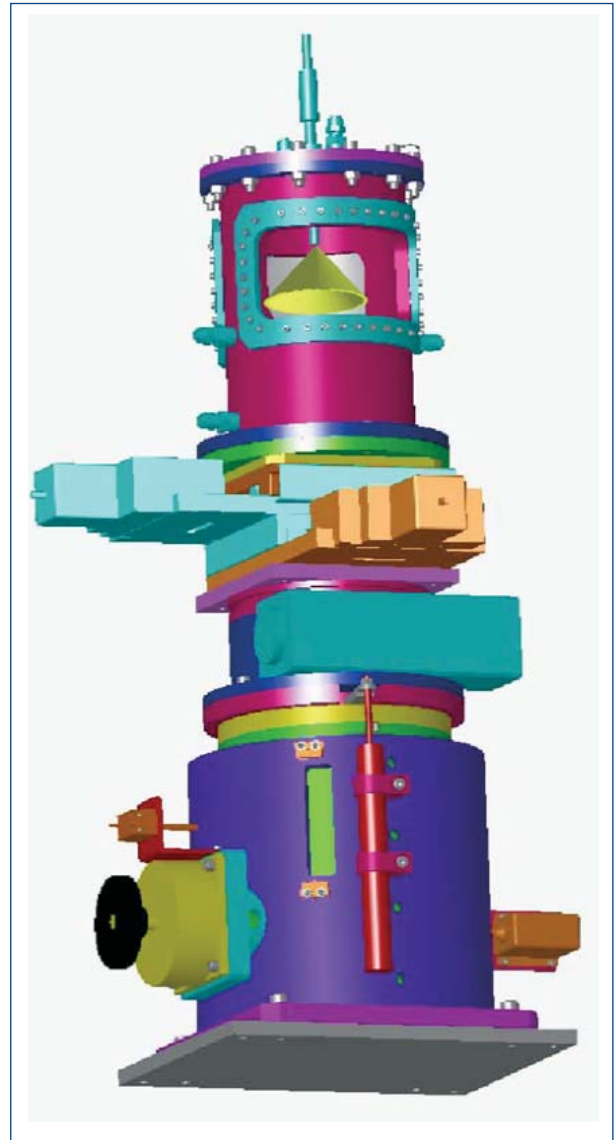


Fig. 1. Tomography fuel chamber.

“Development of Ultrafast Computed Tomography of Highly Transient Fuel Sprays,” Proc. of SPIE **5535**, 21 (invited) (4 August 2004).

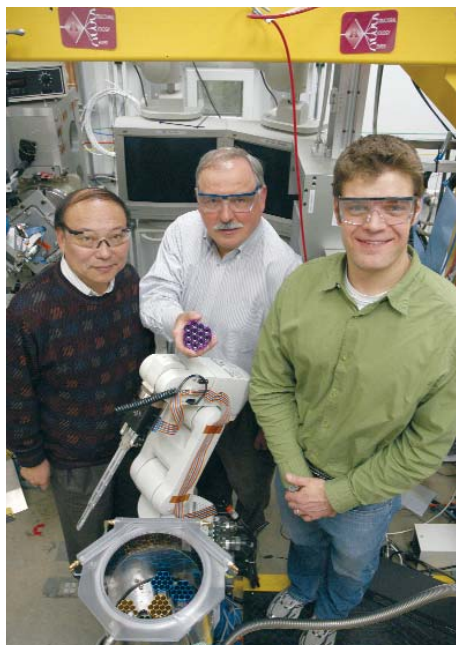
Author Affiliations: ¹Argonne National Laboratory, ²Cornell University

This work was supported by the U.S. Department of Energy under Contract W-31-109-ENG-38. PAD detector development was funded by DOE grants DE-FG-0297ER14805 and DE-FG-0297ER62443. Staff support at CHESS, which is funded by the U.S. National Science Foundation and the U.S. National Institute of General Medical Sciences via NSF under award DMR-9713424.

INTEGRATION OF A ROBOTIC SYSTEM AND AN X-RAY CRYSTALLOGRAPHY STATION

Researchers at the APS and the Argonne Structural Biology Center (SBC-CAT, sector 19) have met the continually increasing demand for macromolecular x-ray crystallography beam time by increasing the productivity of the SBC bending magnet beamline with an automated, cryogenic sample-mounting system in the 19-BM-D enclosure. The higher-throughput experimental station will reduce the need for users to enter the hutch and will take advantage of improved data collection quality control and online structure determination. Improvements in the past year centered on efficient robot-to-beamline control integration and on providing SBC users with a reliable piece of equipment.

In collaboration with SBC scientists, XOR engineers designed and implemented many improvements in order to make the system more robust and reliable. The equipment protection system was augmented with the installation of miniature encoders and an optical sample sensor. Thermal compensation circuitry was designed to improve robot finger function at liquid nitrogen temperatures. Milestones met during the first two APS runs of 2004 included demonstration of protein sample viability during system use (Fig. 1) and operation of the system by an SBC user. *Contact: D. Shu (shud@aps.anl.gov) and A. Joachimiak (andrzej@anl.gov)*



< Deming Shu (left) and Curt Preissner (right; both XFD-XOR) with Andrzej Joachimiak (center; ANL-BIO and Director, SBC-CAT) in the 19-BM-D research station. In the foreground is the receptacle for sample holders, one of which Joachimiak is holding just above the robotic arm. The sample stage and detector are behind Shu.

Photo sequence below, from top right: The robotic arm removes a sample from the cryogenic receptacle; precisely positions the sample; and then places the sample in the sample stage.

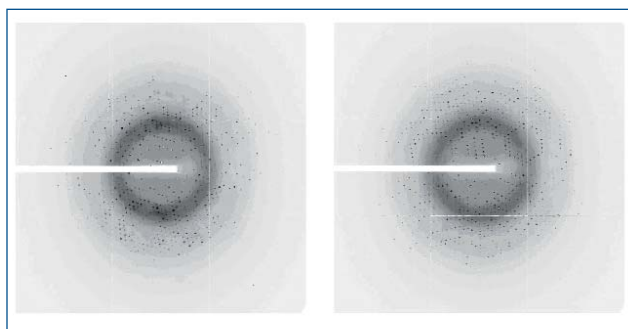
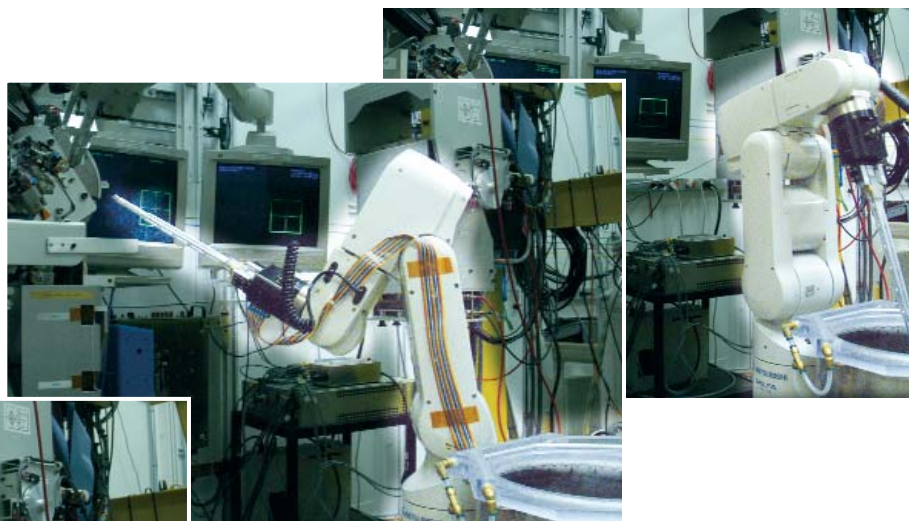
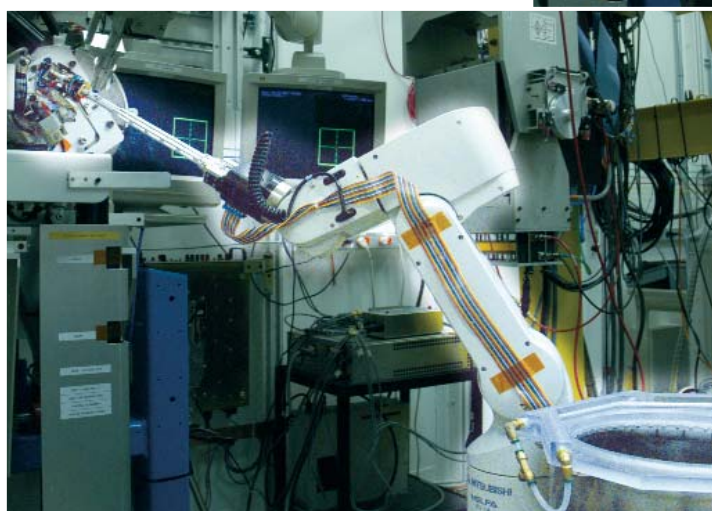


Fig. 1. Diffraction images of the same cryo-sample using the APS 19-BM-D robot for automatic sample mounting. Left side; image after the first mounting; right side; image after seven automatic mounting cycles.

INTERMEDIATE-FIELD MAGNETS FOR SCATTERING AND SPECTROSCOPY

In the study of electronic, magnetic, and structural properties of complex materials, magnetic field plays a fundamental role. It directly couples to the spin and orbital degrees of freedom and can act as an experimental “knob” to tune-in novel phases of matter. Correlated electron systems—such as cuprates and manganites, magnetocaloric and magnetoelectric compounds, and metamagnetic materials—all require the use of magnetic fields to explore their phase diagrams.

In order to meet users' demands, instrumentation has been developed that will expand the capabilities of XOR sector 4 in order to facilitate scattering and spectroscopic studies in magnetic field. Two cryogen-free magnets are available at the XOR 4-ID-D beamline that can provide a maximum magnetic field of 4 T: one in the horizontal (“H-magnet”) and the other in the vertical (“V-magnet”) direction. Both of them are user-friendly, versatile, and have significant optical access. A variable temperature insert (VTI) is used to control the sample temperature (4.2–325K). The magnets are placed on a three-circle Huber goniometer. The goniometer allows for scattering experiments in the horizontal plane. Depending on the magnet, the range of scattering angles accessible varies, as described below.

Figure 1 shows the H-magnet. The magnet has two round Be windows aligned along the field, one on either side of the magnet. These windows allow for transmission of x-rays and are particularly useful for magnetic dichroism measurements. The windows are large enough to permit scattering up to 30°. This range of scattering angle is sufficient for magnetic reflectivity measurements using a three-circle Huber diffractometer (right panel); high-energy (~40 keV) diffuse scattering and diffraction studies can also be performed. Such measurements are needed to study phenomena such as competing electronic and magnetic phases in cuprates in the presence of vortices and magnetostriction in metamagnetic materials. There are two other windows at 90° with respect to the magnetic-field axis, with an opening of 10°. These windows can be used to monitor fluorescence signals in circular or linear mag-



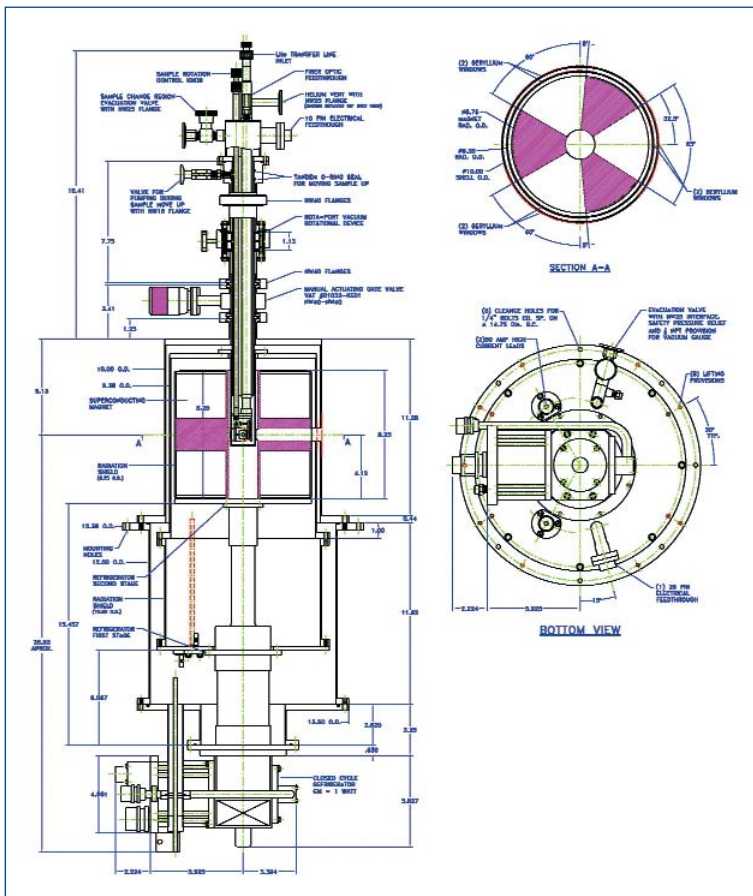
Fig. 1. The 4-T H-magnet at the XOR sector 4-ID-D beamline.

netic dichroism measurements. Such windows also allow scattering at 90°; because the charge scattering goes to zero for x-rays polarized in the horizontal plane, this geometry is, in some cases, useful for magnetic scattering investigations.

The V-magnet (Fig. 2) is designed for diffraction measurements. Reflectivity and high-energy diffuse scattering can be performed as well. The V-magnet, which can be easily swapped with the H-magnet, has three windows, each of which spans 60°–65° at the center of the magnet (see right side of Fig. 2). A scattering angle as high as 120° can be accessed. The V-magnet is well suited for resonant scattering studies of magnetic, multipolar, and structural transitions induced by a field.

Both magnets are cooled to an operating temperature of 3.2K by a closed-cycle refrigerator. The compressor

Continued on next page



requires chilled water for operation. Because it takes ~13 h for initial cool-down before the magnet can be operated, the cooling is done off-line. The magnet and VTI control units are mounted in a single rack for ease of operation and transport. Fields can be switched between +4 and -4 T in ~5 min. For precise alignment of crystals, a small tilt stage has been mounted at the VTI tip. A height-adjustable magnet mount with an arc ($\pm 12^\circ$) makes it possible to align and orient any crystal with a high degree of precision. In addition, a rotation stage allows for rotation of the VTI and sample around the vertical axis in order to change the sample angle with respect to the x-ray beam while keeping the field direction fixed.

In summary, the horizontal and vertical 4-T magnets at beamline 4-ID-D offer the user community new capabilities for magnetism studies at the APS.

Contact: Z. Islam (zahir@aps.anl.gov)

Fig. 2. The XOR beamline 4-ID-D 4-T V-magnet.

EPICS MOTOR RECORD DEVELOPMENT AT 8-ID

The requirement for closed-loop control of the sub-micron-accuracy positioning stage in station 8-ID-E led to enhancements in the capability of the Experimental Physics and Industrial Control System motor record (EPICS MR). The user readback feature of the EPICS MR was designed to allow closed-loop control using external position feedback devices. In fact, any EPICS input record could be used as the user readback device [Fig. 1(a)], except another MR. This was because the EPICS MR would not communicate with a motion controller unless the motor was in motion.

The 8-ID-E positioning stage comprises an open-loop precision-spatial-resolution actuator and a separate nanometer-resolution position-feedback encoder. Support for the encoder was available from the EPICS MR, but a separate EPICS MR was needed to support the actuator. Enhancements to the EPICS MR allowed for a position feedback status update on request. The EPICS MR can now be used as a user readback device [Fig. 1(b)].

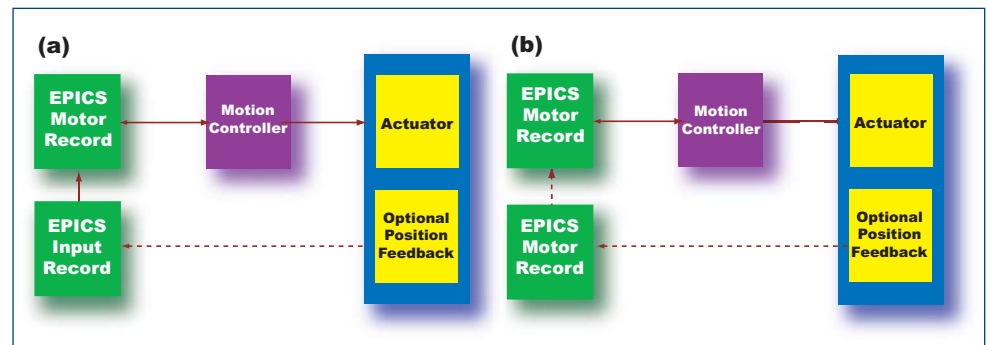


Fig. 1. (a) The existing functional EPICS Motor Record. Only position feedback devices supported by other EPICS records could be utilized for user feedback. (b) The enhanced functional EPICS Motor Record. Now optional position feedback devices that are only supported by the EPICS Motor Record can also be used for software closed-loop control.

The status update enhancement to the EPICS MR has other benefits. The feedback devices supported by the EPICS MR are now available as input to all EPICS records. And information such as limit switch states and position feedback is available for display even if the motor is not in motion.

— Contact: R. Sluiter (sluiter@aps.anl.gov)

ADDITION OF A HIGH-FIELD MAGNET TO THE SOFT X-RAY BEAMLINE 4-ID-C

The use of polarized x-rays in the study of magnetism in complex materials offers unique capabilities for probing physical and electronic structure, as well as phase behavior, with element selectivity. In particular, resonant absorption and scattering of x-rays at transition metal L and rare-earth M lines are very attractive techniques for studying multielement materials such as manganites, metamagnetic materials, permanent magnets, ferromagnetic semiconductors, and many layered systems. In many cases, these materials display rich behavior at significant magnetic fields and at cryogenic temperatures, thus indicating the need for sample services to access this region of phase space.

Recently, the beamline staff at XOR sector 4 have upgraded the magnetic field capabilities of the soft x-ray beamline (4-ID-C) with a new electromagnet designed for soft x-ray absorption, optical luminescence, and reflectivity in fields of up to 7 T. This is a split-coil, windowless, UHV-compatible, liquid-He bath superconducting magnet with horizontal field along the beam direction. The geometry of this system is shown schematically in Fig. 1. The input and output ports allow beam angles of $\pm 5^\circ$ with respect to the field direction. The split-coil design allows two radial detector ports at 90° with respect to the field for x-ray fluorescence and optical luminescence measurements, while a scattered beam detector can be mounted on the output port for reflectivity measurements with 2θ up to 26° . The sample may also be isolated for electron yield measurements, thus providing depth selectivity via the difference in escape depths between the electron and fluorescence measurements (-5 nm and 100 nm, respectively). The coil can be operated in either persistent mode for static field experiments or in non-persistent mode for hysteresis loops. The system is equipped with a variable temperature insert (VTI) capable of achieving temperatures from 4.2K to 325K with liquid-He cooling. The VTI is mounted on a translation/rotation stage so that the sample angle can be varied between $\pm 120^\circ$ with respect to the beam direction. Finally, the magnet system is enclosed in a 20-L liquid-He dewar and liquid-nitrogen shroud with a static hold time of 24 h.

Figure 2 shows the magnet chamber at the end of the 4-ID-C beamline. The magnet chamber was received in August 2003 and was made available to general users after its first

Continued on next page

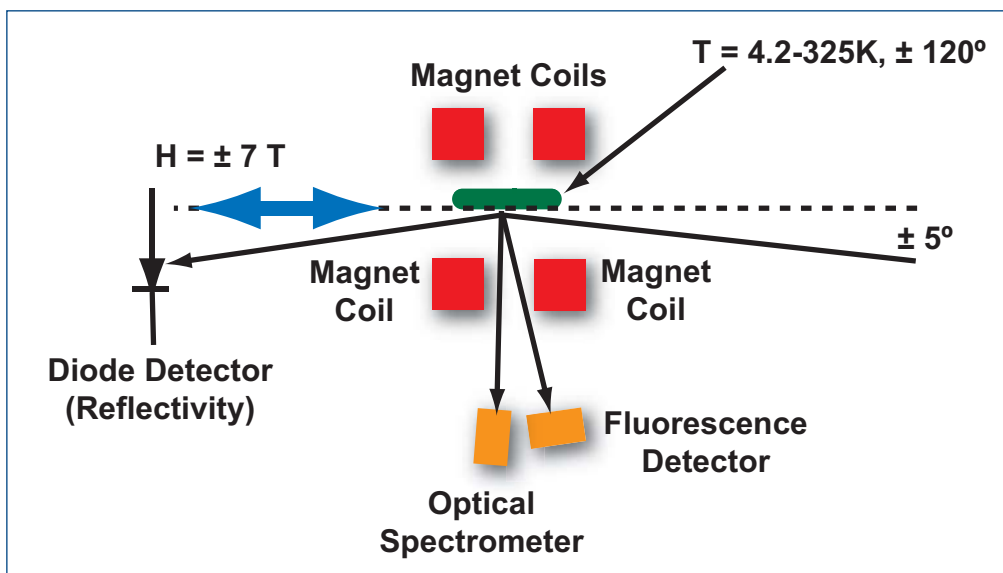


Fig. 1. Schematic diagram of the high-field magnet, showing the split-coil 7-T superconducting magnet and three detectors for photon-in photon-out techniques. The chamber is also equipped with a variable-temperature sample insert for sample temperatures of 4.2K to 325K.

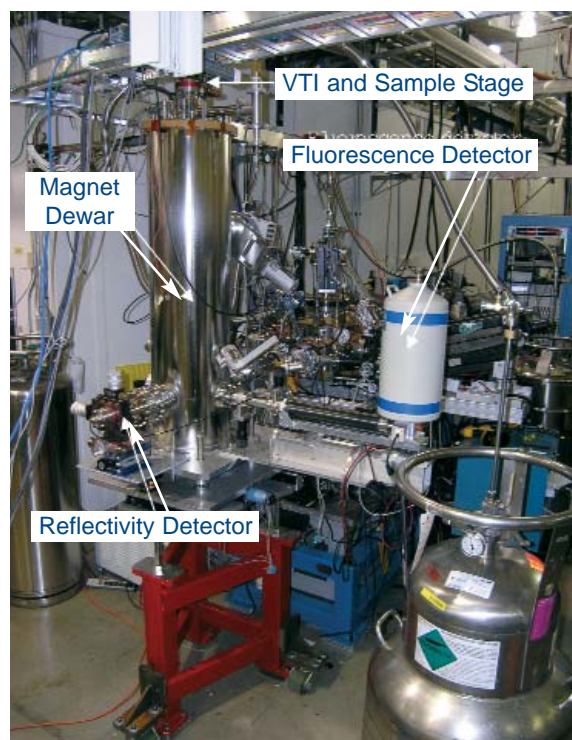


Fig. 2. The 7-T magnet system at the end of beamline 4-ID-C. Reflectivity and fluorescence detectors are indicated. The optical spectrometer is not mounted in this picture.

commissioning run in December 2003. In subsequent commissioning work, the fluorescence and optical detectors were fitted to the magnet chamber, and the magnet controls and power supplies were integrated into the beamline controls. During that time, use of the high-field magnet grew to account for approximately 30% of the beam time on 4-ID-C and has impacted several user groups' research programs. Users perform experi-

ments in areas including exchange-biased layered systems, colossal magnetoresistive manganites, ferromagnetic semiconductors, and exchange-spring magnets.

The 7-T magnet offers the users of beamline 4-ID-C greatly enhanced sample environments and the flexibility to perform a wide range of measurements not previously available at the APS.

Contact: D. Keavney (keavney@aps.anl.gov)

DIGITAL LOCK-IN DETECTION OF DICHOIC DIFFRACTION OF CIRCULARLY POLARIZED X-RAYS

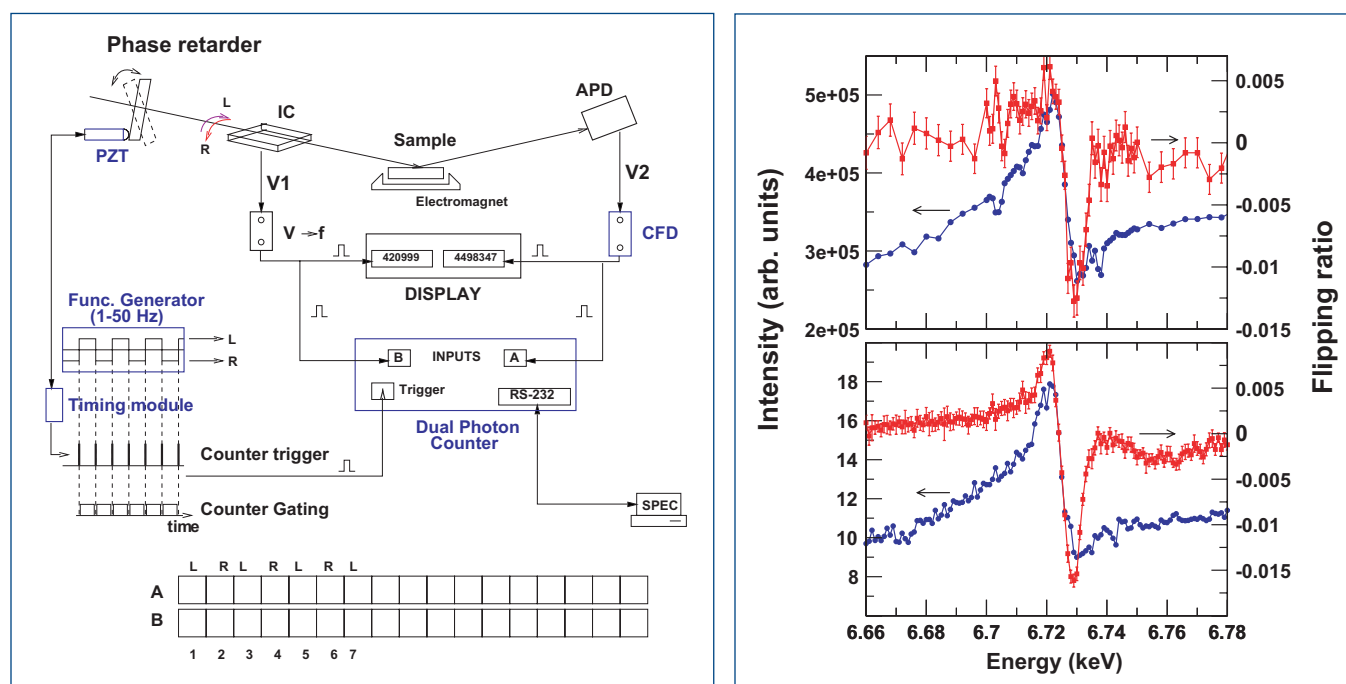


Fig. 1. (Left): Schematic of the digital lock-in system. CFD = constant fraction discriminator; PZT = piezoelectric actuator; APD = avalanche photodiode. (Right): Chemical (blue) $(I^+ + I^-)$ and magnetic (red) $(I^+ - I^-)/(I^+ + I^-)$ resonant diffraction at the (110) Bragg peak of Nd₂Fe₁₄B single crystal. (I^+, I^-) denote diffracted intensities for opposite x-ray helicity. The (110) Bragg condition isolates one of the two inequivalent Nd sites in the structure [1]. Top panel shows conventional detection using a scintillator detector; bottom panel shows lock-in detection over 20 cycles of helicity switching using an APD detector. The lock-in data were taken two times faster.

The ability of x-ray-based techniques to separate magnetic contributions from different elements in heterogeneous samples is one of the most important advantages of x-rays over neutrons when probing magnetism. X-ray magnetic circular dichroism (XMCD) achieves this separation by tuning the x-ray energy to element-specific electron excitations whose absorption cross section depends on x-ray helicity (left or right). This dichroism arises from an imbalance between spin-up and spin-down density of electronic states near the Fermi energy, characteristic of ferro(ferri)magnetic materials. While x-ray dichroism is commonly measured in absorption, a related dichroic effect occurs in the resonant scattering/diffraction of circularly polarized x-rays, where the virtual photoelectron is sensitive to

that same spin imbalance in the intermediate state. Analog lock-in detection of XMCD in the absorption channel is already available at XOR sector 4 of the APS. Now, a digital lock-in detection scheme has been developed for measurements of dichroic scattering/diffraction.

Advantages of dichroic scattering/diffraction include the ability to exploit structure factor effects in crystals in order to separate magnetic contributions from elements of the same species in inequivalent crystal sites [1], to determine element-specific magnetization depth profiles in films and multilayers [2], and to separate magnetic signals from the same element in dissimilar crystal phases in multiphase materials such as nanocomposites.

The detection system shown in Fig. 1 allows measurements of the x-ray-diffracted intensity to be synchronized with the helicity modulation of a circularly polarized incoming x-ray beam, which alternates in the 1- to 50-Hz range. A square wave with half-duty cycle expands/contracts a piezoelectric actuator causing a phase-retarding optic to yield opposite helicities of circularly polarized x-rays. Upon helicity switching, a timing module triggers the incident and scattered intensity scalers of a dual photon counter for a time interval (gating) just below the half period of the square wave. This allows measurements of x-ray-incident and scattered intensities for opposite helicities to be performed over many helicity switchings in a short time, with the data for each type of helicity stored in even and odd addresses, respectively, of the photon counter's memory arrays. This detection scheme, coupled to a fast-counting avalanche photodiode detector, yields large improvements in signal-to-noise ratios and reduction of systematic errors over conventional detection, in which the helicity is switched only once.

The right panel of Fig. 1 compares data collected by using the conventional method (top) to that collected by using digital lock-in over 20 cycles of helicity switching (bottom). In addition to improvements in data quality, the lock-in measurement was done in half the time of the conventional measurement. This development extends the detectability of dichroic scattering/diffraction to 1 part in 10,000. It is especially suited for detection of dichroic diffraction from single crystals and small-angle dichroic reflectivity/scattering from layered nanostructures.

Contact: D. Haskel (haskel@aps.anl.gov)

References

- [1] D. Haskel et al., IEEE Transactions on Magnetics **40**, 2874 (2004).
 [2] Y. Hayasaki et al., J. Phys. Cond. Matt. **16**, 1915 (2004);
 D. Haskel et al., Phys. Rev. Lett. **87**, 207201 (2001).

AREA DETECTOR-BASED GIXD MEASUREMENTS FROM LIQUID SURFACE SAMPLES

Capabilities at CMC-CAT beamline 9-ID for investigating grazing incidence x-ray diffraction (GIXD) from liquid surfaces are now augmented by the use of a charge coupled device (CCD)-based area detector in conjunction with the liquid surface spectrometer (LSS). The CCD detector complements the two detectors routinely used with the LSS: a scintillation point detector used for reflectivity and a linear position-sensitive detector (PSD) equipped with Soller slits, normally used for GIXD. The area detector allows the GIXD pattern over a large range of reciprocal space to be captured simultaneously with exposures as brief as 10 s. This is especially advantageous for organic or biological specimens, which may be damaged by radiation during the longer exposures required to complete scans with the PSD. As an example, the new configuration was useful in observing the GIXD from a Langmuir monolayer composed of alpha-helical peptide bundles, which scatter weakly in the region near $q_{xy} \approx 0.55 \text{ \AA}^{-1}$ (Fig. 1). At this value of the momentum transfer, the effects of the decreasing Δq_{xy} resolution with increasing scattering angle are not so severe. To scan the same region of reciprocal space with the PSD (10 s/point) would have required approximately 600 s exposure for a Δq_{xy} resolution of 0.012 \AA^{-1} .

In the most recent configuration of CCD-based GIXD measurements, a Langmuir trough on the sample stage of the LSS contained the specimen. The CCD detector (Bruker SMART 1500) was

Continued on next page

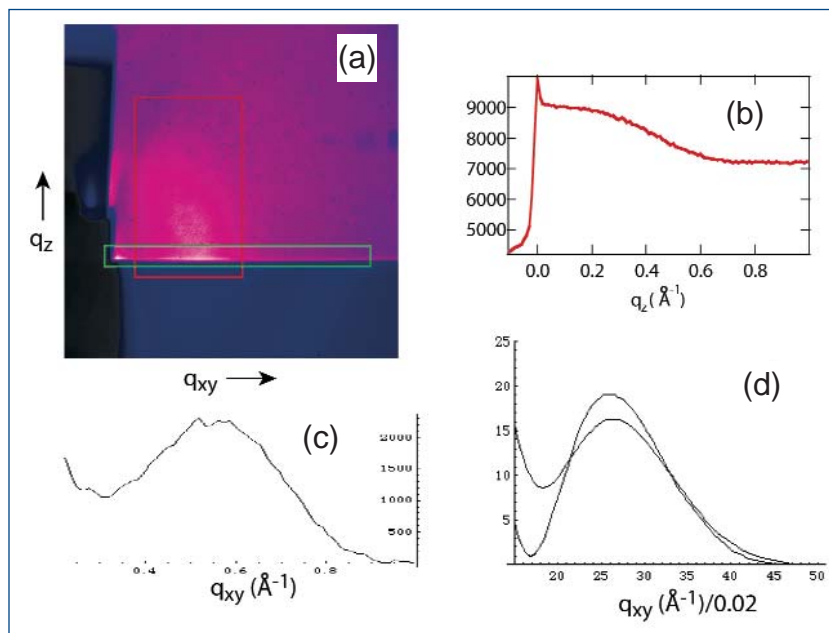


Fig. 1. Grazing incidence x-ray diffraction from peptide monolayers. (a) Two-dimensional CCD image of GIXD from a monolayer of a synthetic peptide designated AP2 at high surface pressure. Integration of the region bounded by the red rectangle along q_{xy} gives the intensity as a function of q_z (b), including background scattering. Integration of similar data from a monolayer of another peptide, designated AP0, along the q_z direction (as indicated by the green box), after background subtraction of otherwise equivalent GIXD from the pure subphase in the absence of the peptide monolayer, gives the background corrected GIXD as a function of q_{xy} (c). Model calculations for the q_{xy} dependence of the in-plane diffraction from a bundle of 4 cylinders show good agreement with the data in (c), especially once the experimental Δq_{xy} resolution is considered.

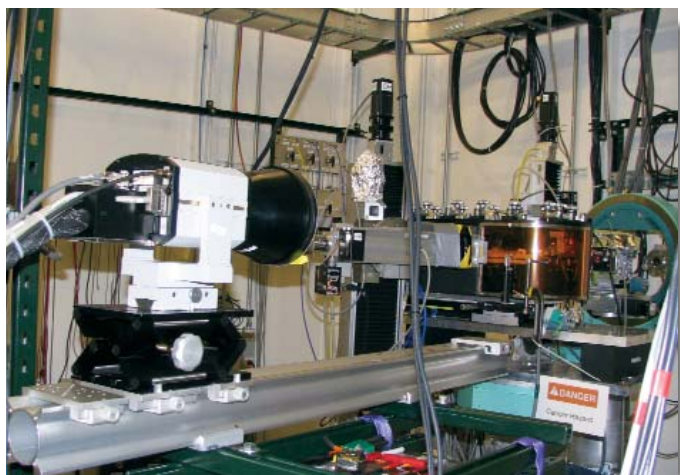


Fig. 2. Area detector-based GIXD setup. The CCD detector is shown in the foreground at the end of the X-95 rail, out of the way of the point detector. The beamstop is mounted against the kapton exit window of the canister enclosing the Langmuir trough on the sample stage of the liquid surface spectrometer.

mounted on an X-95 rail supported from the floor. This allows the specimen-detector distance to be varied from 26 to 120 cm; or, for x-ray energy of 13.474 keV, the corresponding q -ranges to be varied from more than 2 \AA^{-1} to about 0.5 \AA^{-1} . However, the CCD detector cannot be scanned. The beamstop at the exit window of the trough canister limited the minimum q to about 0.3 \AA^{-1} . Additional shielding upstream of the sample and a fixed aperture inside the entrance window of the canister reduced background. Alignment of the sample requires use of the point detector in reflectivity mode, with the CCD detector moved out of the way to the largest specimen-detector distance, so that the user must enter the hutch to return the CCD detector to the desired specimen-detector distance. The geometry prevents the PSD from being used when the rail is in position near the sample, but the point detector can still be scanned through angles up to approximately 15° , or $q_{xy} \sim 1.7 \text{ \AA}^{-1}$.

*J. Strzalka, I. Kuzmenko, T. Xu, T. Gog, J.K. Blasie.
Contact: J. Strzalka (strzalka@sas.upenn.edu)*

SILICON SAWTOOTH REFRACTIVE LENSES FOR HIGH-ENERGY X-RAY OPTICS

X-ray Operations and Research beamline 1-ID has been utilizing Si-based refractive lenses for vertical focusing of high-energy (50-100 keV) x-rays at both low and high source demagnification geometries ($\sim 1:0.6$ and $\sim 1:0.05$, respectively). The high x-ray intensity from vertical focusing has enhanced a number of sector 1 programs, including time-resolved diffraction, small-angle scattering, and high-pressure studies. Such lenses can also be used for x-ray angular collimation in order to improve the throughput of subsequent high-energy-resolu-

tion optics, as has been demonstrated with cylindrical aluminum lenses [1].

The Si lenses are based on a sawtooth geometry, described elsewhere [2], and exhibit a number of desirable properties. First, their effective profile closely approximates a single parabolic lens, eliminating cylindrical aberration. Second, by adjusting the taper between the top and bottom sets of the teeth, the focal length can be varied. For a given position downstream of the lens, this allows for tunability in the focused beam

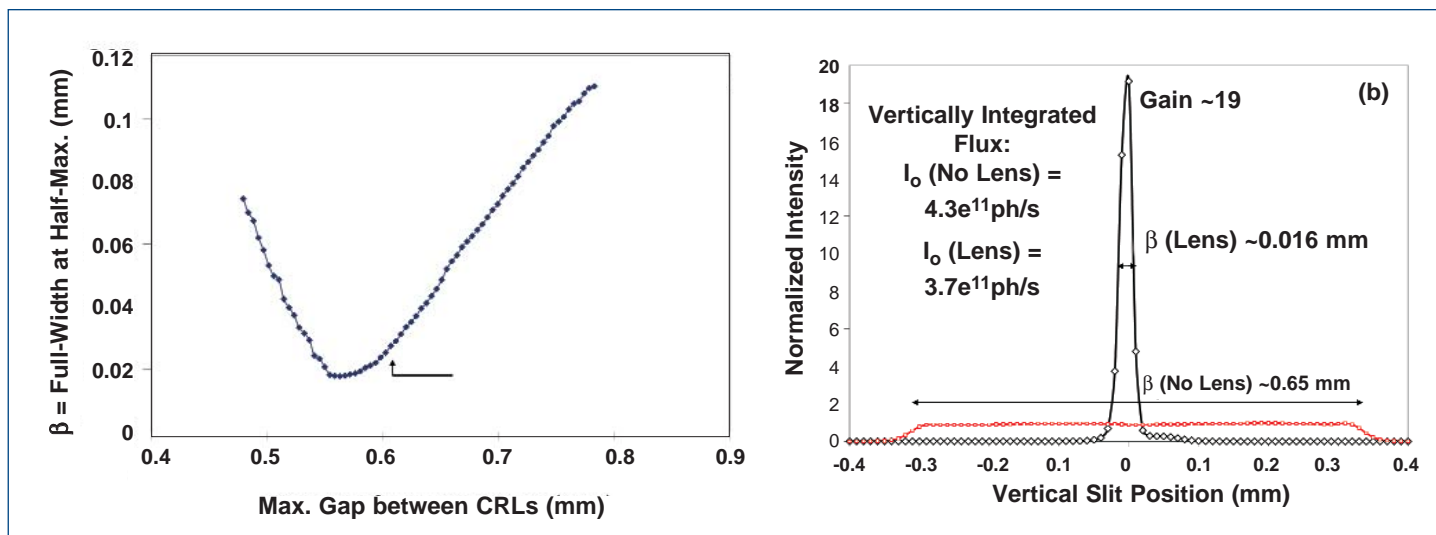


Fig. 1. (a) Variation in vertical beam size with taper end-gap between lens pieces and (b) beam profiles with and without the lens, as measured using a $0.005(v) \times 1(h) \text{ mm}^2$ aperture and PIN diode at the entrance to the C-hutch.

size or for adaptation to an energy change. Third, x-rays passing directly along the optical axis experience zero absorption. Finally, since they are composed of single-crystal Si, they produce little small-angle scattering, and thus a cleaner beam than that from lenses comprised of polycrystalline material.

The lenses were provided by C. Ribbing (Uppsala University, Sweden) and B. Cederström (KTH, Stockholm, Sweden). They consist of two 65-mm-long pieces of Si, each etched to produce an array of 230 triangular ridges (“teeth”) with slopes at 57° to the surface normal and a tooth depth of 0.2 mm. The pieces were serially mounted in the 1-ID-B station, approximately 0.2 m apart and 34 m from the source, with one piece inverted to form a maximum combined physical aperture of 0.4 mm. The lenses receive radiation from a bent double-Laue Si(111) monochromator [1] that preserves beam size and divergence, and hence source properties.

Figure 1a shows the tunability of the lenses at 81 keV by measuring the vertical beam size in the C-station 21 m downstream of the lenses ($\sim 1:0.6$ ratio) as a function of the taper end-gap between the two sawteeth. It is clear that the beam size can be continuously varied, with a minimum observed at a gap of 0.58 mm, which compares well with the expected value of 0.62 mm. The minimum beam width measured at that setting

is $16\ \mu\text{m}$ FWHM ($15\ \mu\text{m}$ expected), with Fig. 1b showing its profile compared to that of the unfocused beam. The result corresponds to a flux density gain of about 19, in reasonable agreement with the calculated value of 21. Finally, the total transmitted flux is approximately 85% of the unfocused value, which is evidence of a low lens attenuation loss. The lenses have also been used for greater demagnification ($\sim 1:0.05$), creating a line focus at 1.6 m away in the same station. A beam size of $1.8\ \mu\text{m}$ and flux density gain of 36 were achieved at 81 keV.

An important point is that the tails of the focused beam decrease rapidly, with no appreciable flux measured past ± 0.1 mm. This reduces parasitic scattering around the direct beam compared to apertures, and allows access to lower q-values for the high-energy small-angle scattering camera under development at 1-ID. Contact: J. Almer (almer@aps.anl.gov) and S. Shastri (shastri@aps.anl.gov)

[1] S.D. Shastri, “Combining Flat Crystals, Bent Crystals and Compound Refractive Lenses for High-Energy X-ray Optics,” *J. Synchrotron Rad.* **11**, 150 (2004).

[2] B. Cederstrom, M. Lundqvist, and C. Ribbing, “Multiprism X-ray Lens,” *Appl. Phys. Lett.* **81**(8), 1399 (2002).

UPGRADE OF THE HIGH-RESOLUTION INELASTIC SPECTROMETER AT 3-ID

High-resolution inelastic x-ray scattering (HRIXS) provides microscopic information about the dynamics of atoms inside materials, from ordered crystalline solids to disordered solids and even liquids. Because the typical energy scale involved for dynamical excitations (meV) is substantially less than x-ray energies, using x-rays to probe these excitations requires a spectrometer with high resolving power. To achieve this, synchrotron radiation must be highly monochromatized, and then the scattered x-rays must be analyzed with approximately the same level of energy resolution. The need for highly monochromatic x-rays means only a narrow spectral region of synchrotron radiation is actually used. Consequently, incident photon flux is low and typical measurements involve low signal rates and long data-collection times. The HRIXS

Continued on next page



Fig. 1. XOR staff member Tom Toellner at the new monochromator used for HRIXS. The cryogenically-cooled, high-resolution monochromator transmits a 1.2 meV-bandwidth x-ray beam with 60% spectral efficiency.

spectrometer at the XOR beamline 3-ID, which operates using 21.7-keV x-rays, is the only one currently available at the APS with meV-resolving capability.

To improve the data-collection rate it is necessary to optimize the efficiency of every aspect of the spectrometer. To this end, XOR staff have recently upgraded the high-resolution monochromator of the HRIXS spectrometer to a cryogenically-cooled six-reflection design (Fig. 1). This replaces a room-temperature four-reflection design that was underperforming due to thermal influences. Thermal effects arise from various heat sources, including the x-ray beam itself. High-resolution monochromatization generally encounters problems associated with thermal loading, given the present x-ray power loads (0.1 W per eV-bandwidth) in premonochromated x-ray beams at third-generation synchrotron sources. A solution developed by XOR staff to mitigate thermal problems involves the use of cryogenics to operate the more sensitive crystal components at a temperature where the crystalline material experiences no thermal deformations. For silicon, which is the crystal material used for the monochromator components, the coefficient for thermal expansion vanishes around 123K and then again below 30K. Cooling the silicon crystal components to such cryogenic temperatures mitigates the thermal problems, but it poses a technical challenge in that the crystal components need to have their angle relative to the beam controlled with a stability of 0.01 μ rad. XOR staff have recently developed a low-vibration cryostat for this purpose that is light enough to be mounted on a high-resolution rotation stage.

In addition to the use of cryogenics to improve monochromator efficiency, a new crystal design has been developed that uses six crystal reflections to achieve a highly efficient in-line

monochromator that reduces the bandwidth of the x-ray beam down to the "meV" level. The layout of the crystal components is shown in Fig. 2. The first pair of reflectors is aligned to the silicon (2 2 0) crystal reflection, and their surfaces are chosen to successively collimate the x-ray beam so its divergence matches the reflection width of the second pair of reflectors that are mounted in a low-vibration cryostat and oriented to diffract from the silicon (15 11 3) crystal reflection. While the second, high-index crystal reflection pair transmits an x-ray beam with a

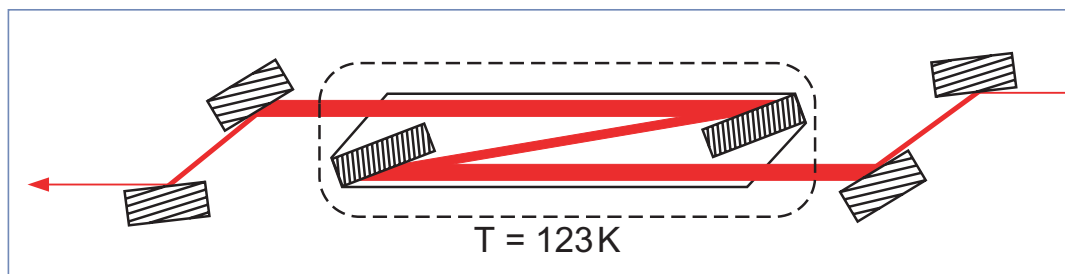


Fig. 2. Crystal configuration of the six-reflection CHRM.

bandpass of 1.2 meV, the first pair makes the CHRM perform more efficiently by reducing the beam divergence and funneling the radiation into the inherently narrow angular acceptance of this small-bandpass reflection. The third and last pair of reflectors is identical to the first pair, but placed in reverse order to return the beam back to its original size and divergence.

Performance tests demonstrate that the monochromator transmits an x-ray beam with a bandwidth of 1.2 meV and an exceptionally high spectral efficiency of 60%. This is a fivefold improvement over the previous monochromator and is the highest efficiency achieved for an inline x-ray monochromator with an energy resolution in excess of 10^7 . This is achieved both by the use of cryogenic cooling and by the newly-developed six-reflection design. A similar CHRM is currently being designed for the IXS-CDT beamline 30-ID that is now under construction.

Contact: T.S. Toellner (toellner@aps.anl.gov)



HIGH-RESOLUTION, HIGH-ENERGY X-RAY SCATTERING IN HIGH MAGNETIC FIELDS

The availability of synchrotron-generated high-flux photons with energies greater than 60 keV has significantly advanced the field of materials research because of the great penetration and low absorption of high-energy x-rays. The capability of reaching high resolution in high-energy x-ray scattering provides further research opportunities, especially in the study of bulk samples for both fundamental research and practical applications. Recently, a user facility for high-resolution, high-energy x-ray scattering studies of materials under high magnetic fields has been developed at BESSRC beamline 11-ID-C. This facility combines all the advantages of high-energy photons (high penetration, low absorption, small scattering angle, and greater access to the reciprocal space) with the high-Q resolution of the triple-axis diffractometer at 11-ID-C.

The magnetic interaction is one of the most fundamental forces affecting the physical properties and functionalities of materials and devices. While the effect of a magnetic field on the structures and properties of magnetic compounds has been extensively studied over the last century because of its importance in broad applications, our knowledge about the magneto-lattice interactions is still limited. Recent efforts to understand the newly discovered phenomena (e.g., high temperature superconductivity, colossal magneto-resistance, multiple electric-magnetic effects, magnetic-shape-memory-alloys) in complex materials have resulted in increased research into the charge and structural lattice effects of an external magnetic field. Magnetic fields can alter magnetic structures and significantly modify the charge carriers and their short- and long-range distributions—especially in the vicinity of competing phases, where fascinating new properties are often found. Understanding magnetic-field-induced structural modifications, phase transitions, and domain reorientations is of crucial importance in fundamental research, as well as in the search for materials that function more efficiently. In this research area, high-resolution, high-energy x-ray scattering in high magnetic fields offers unique advantages.

The user facility at the BESSRC/XOR 11-ID-C beamline consists of a cryomagnet (Oxford Instrumentation) installed on the heavy-duty sample stage of a triple-axis diffractometer. The cryomagnet can provide magnetic fields up to 7 T in a temperature range from 1.5K to 325K. The magnetic field can be applied either parallel or perpendicular to the incoming beam. The diffractometer allows ω and χ angle rotations up to 10 degrees. The Q-resolution can reach 10^{-5} \AA^{-1} perpendicular to the reciprocal lattice vector. The access in the reciprocal space is up to 15 \AA^{-1} . Three pre-monochromators provide three different photon energies: 60, 98, and 115 keV. A single-element Ge solid-state detector located more than 2 m from the sample position has an energy resolution better than 0.7 keV at 122 keV and is very sensitive to weak signals caused by diffuse scattering and subtle structural changes. An image plate (Mar345) is available for two-dimensional data collection for both single crystals and powder samples.

This facility has opened the door to new and unique scientific opportunities, has attracted scientific interest from a broad user community, and has begun to produce important results.

Contact: Y Ren (yren@anl.gov)



Haluk E Karaca, a graduate student from Texas A&M University, at the 11-ID-C high-resolution, high-energy x-ray scattering facility, which he uses to study ferromagnetic shape-memory alloys. (Photo: Y. Ren)

ULTRA-HIGH-SPEED PHASE-ENHANCED RADIOGRAPHY

Real-time phase-enhanced radiography has proven to be an extremely useful technique for the study of small animal biomechanics and physiology [1]. In this technique, the partial coherence of an APS x-ray beam, coupled with a suitable sample-detector distance, allows for image edge enhancement. Edge enhancement greatly increases the image contrast and makes it much easier to discern features that would otherwise not be discernable. Adding the high x-ray intensity available at the APS, real-time recording of the images at 30 Hz (with exposure times of $\sim 1/60$ s) was demonstrated using silicon crystals and monochromatic radiation with an energy bandpass of about 10^{-4} . Recently, this technique has been advanced to utilize filtered white beam, which allows for exposure times of $1 \mu\text{s}$ (10^{-6} s).

The ability to do phase-enhanced imaging with very broad energy bandpass x-ray beams is facilitated by two facts. On one hand, the positions of the maximum and minimum of the first fringe in a Fresnel diffraction pattern are not very sensitive to energy. On the other hand, the secondary fringes are smeared out, making the complex holographic pattern disappear and the image much easier to understand. Thus, even with broadband radiation, there is still excellent edge enhancement in the image. Ultra-high-speed phase-enhanced radiography has been demonstrated by using filtered white beam at the MHATT/XOR beamline 7-ID to examine the dynamics of a fuel injector.

Fuel sprays from a fuel injector are an integral part of internal combustion engines. X-rays have been used to study the properties of the fuel sprays, and asymmetric density variations have been observed [2]. However, the internal dynamics of the injector itself, and how they relate to the spray, have never been measured, because the fuel injector is made of stainless steel (several millimeters thick) and the entire injection cycle period is only about 1 ms or less. Until now, no technique has been able to afford a view of the inside of the injector with the necessary time and spatial resolution.

Figure 1 shows a four-exposure image of the fuel injector, taken with 10- μs exposure each, separated by 100 μs . The

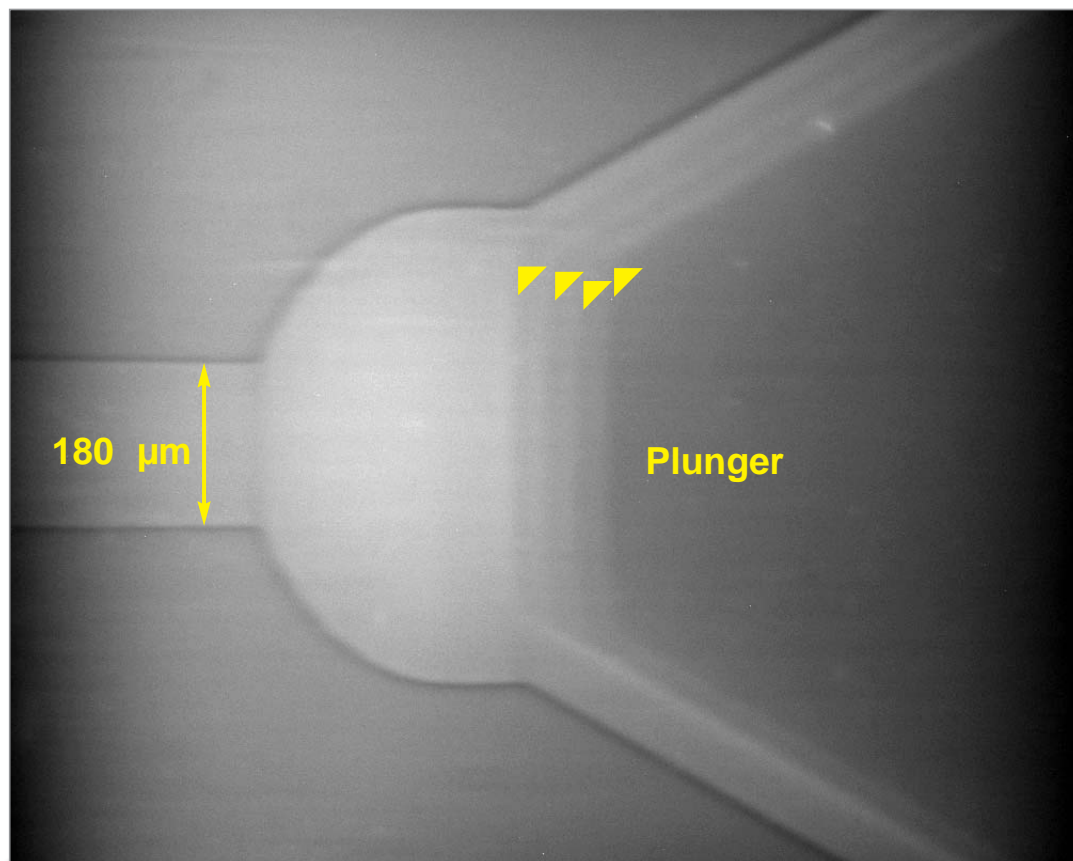


Fig. 1. A four-exposure phase-enhanced radiograph of the fuel injector. The field of view is about $1 \times 1 \text{ mm}^2$. Each exposure is $10 \mu\text{s}$, separated by $100 \mu\text{s}$. The wobble of the plunger is clearly seen: the four positions of the plunger corner are indicated with white triangles. The concave shape of the injector body gives the dark edge enhancement, while the convex shape of the plunger gives the lighter edge enhancement.

image allows for calculation of instantaneous velocity, and also clearly shows a wobble in the motion. The motion of the plunger is highly reproducible and, as a result, x-ray movies of the entire injection cycle have been made.

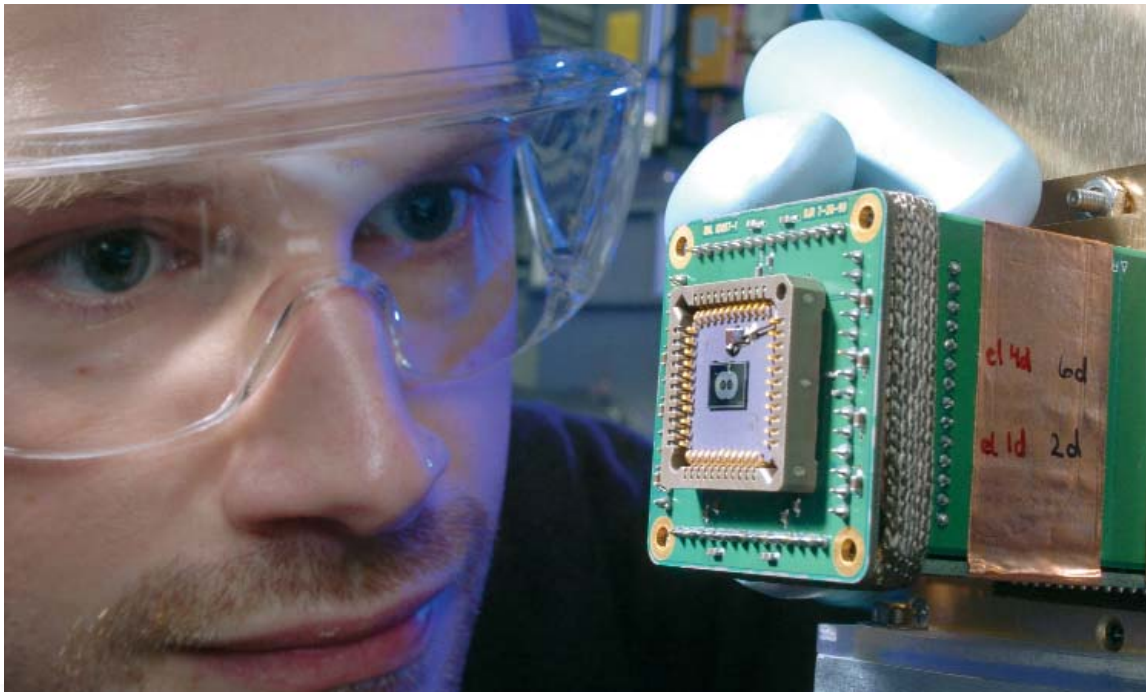
Filtered white-beam, phase-enhanced radiography at the APS opens new avenues of research. This technique allows for μs time and μm spatial resolutions. It will be a very useful tool for the study of dynamics in small systems, including microexplosions, fluid flow, cavitations, and micromachines.

Contact: W.-K. Lee (wkleee@aps.anl.gov) & K. Fezzaa (fezzaa@aps.anl.gov)

REFERENCES

- [1] M. W. Westneat, O. Betz, R. W. Blob, K. Fezzaa, W. J. Cooper, and W. Lee. *Science* **299**(5606), 558 (2004).
- [2] A.G. MacPhee, M.W. Tate, C.F. Powell, Y. Yue, Renzi MJ, A. Ercan, S. Narayanan, E. Fontes, J. Walther, J. Schaller, S.M. Gruner, and J. Wang. *Science* **295**(5558), 1261 (2002).

DIFFERENTIAL PHASE CONTRAST USING A CONFIGURED DETECTOR



Stefan Vogt (XOR-XMG) with the configured detector installed at XOR beamline 2-ID-E.

The importance of trace elements in biological, medical, and environmental sciences has received increased recognition (e.g., see [1]). Synchrotron-based x-ray fluorescence (XRF) microscopy is a powerful technique to study the elemental distributions. Due to its low background, XRF is particularly well suited to detect elements in trace quantities, down to the level of attograms. However, a substantial part of the specimen is typically made up of light elements that are difficult to map using XRF because of their small photo-electric absorption cross section and low fluorescence yield. The small x-ray absorption also makes direct visualization in absorption contrast difficult at higher x-ray energies. However, the real part δ of the complex index of refraction $n = 1 - \delta - i\beta$ is several orders of magnitude larger than the imaginary part β , and this difference can be used advantageously to visualize such material in phase contrast instead of absorption contrast [2-4].

In collaboration with SUNY-Stony Brook [5], beamline scientists at XOR beamlines 2-ID-B and 2-ID-E are developing a configured detector optimized for the detection of differential phase contrast at intermediate and hard x-ray energies. Differential phase contrast (DPC) makes direct use of x-rays that were refracted by the specimen and does not require changes to existing

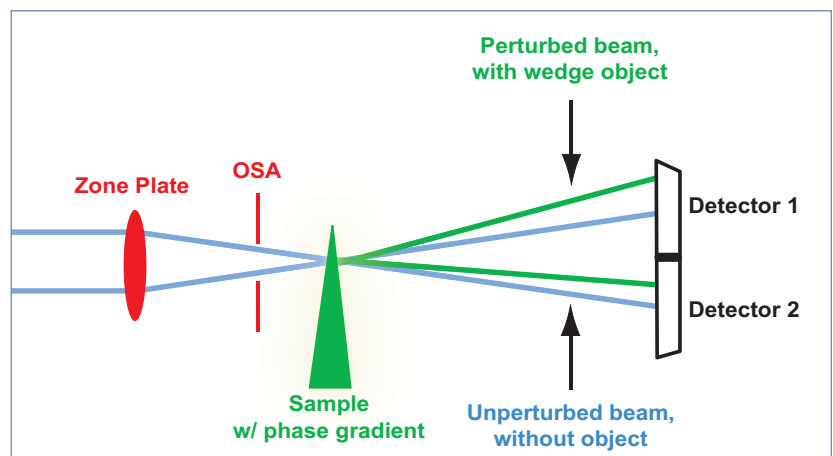


Fig. 1. Illustration of differential phase contrast in a scanning microprobe setup. The zone plate focuses hard x-rays into a focal spot on the sample. The order sorting aperture (OSA) suppresses any x-rays not diffracted into the first (focusing) order. Here, the presence of a wedge shaped phase object causes an angular shift of the center of the transmitted beam. By using a set of spatially resolving detectors, this shift can be measured.

focusing optics. While the total transmitted flux is insensitive to these phase effects, they lead to spatial variations in the far-field diffraction pattern, which can be registered with appropriate detectors. Figure 1 illustrates how a wedge-like object would perturb the x-ray beam.

Continued on next page

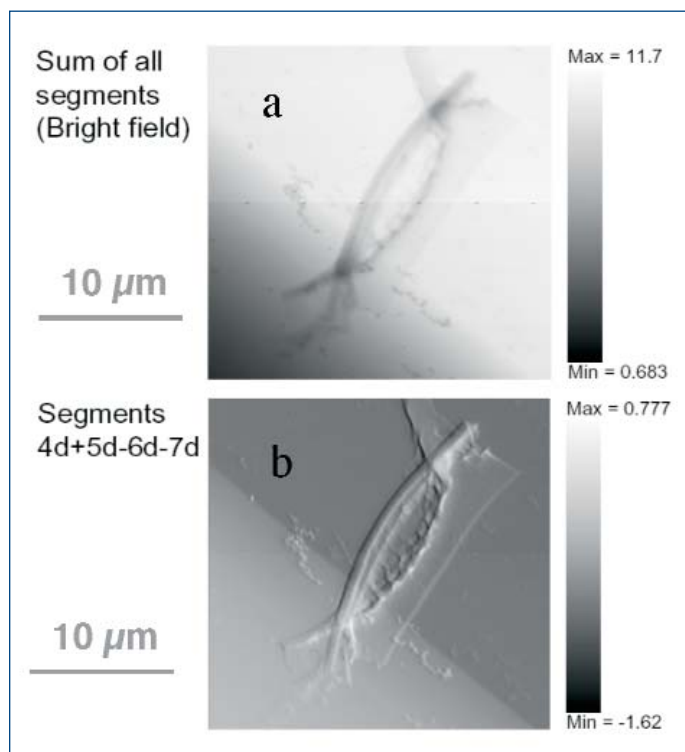


Fig. 2. Scanning microscope images of a diatom taken at an incident x-ray energy of 1.8 keV at 2-ID-B: (a) Bright field image, showing the absorption contrast; (b) Differential phase contrast image, showing the horizontal differential phase contrast. The fine structure of the specimen is much more visible in the DPC contrast.

In addition to improved contrast for the visualization of “soft” organic materials, as shown in Figures 2 and 3 (see also [6]), this new detection scheme allows the fast imaging of environmental and biological samples by moving the sample continuously through the focal spot while acquiring the detector signal “on the fly” using a hardware multi-channel scaler. This substantially increases the throughput by avoiding the overhead associated with the step and probe approach used for conventional scans. *Contact: S. Vogt (vogt@aps.anl.gov), D. Paterson (paterson@aps.anl.gov)*

REFERENCES

- [1] Science (9 May 2003) with Focus: “Metals: Impacts on Health and Environment.”
- [2] G. Schmahl, D. Rudolph, G. Schneider, P. Guttman, and B. Niemann, *Optik* **97**, 181 (1994).
- [3] B. Kaulich, F. Polack, U. Neuhaeusler, J. Susini, E. di Fabrizio, and T. Wilhein, *Optics Expr.* **10**(20), 1111 (2002).
- [4] Y. Kagoshima et al., *J. Phys IV France* **104**, 49 (2003).
- [5] B. Hornberger, C. Jacobsen, M. Feser, SUNY Stony Brook.
- [6] S. Vogt, M. Feser, D. Legnini, J. Kirz, and J. Maser, *Synchrotron Radiation Instrumentation*, 1348 (2004).

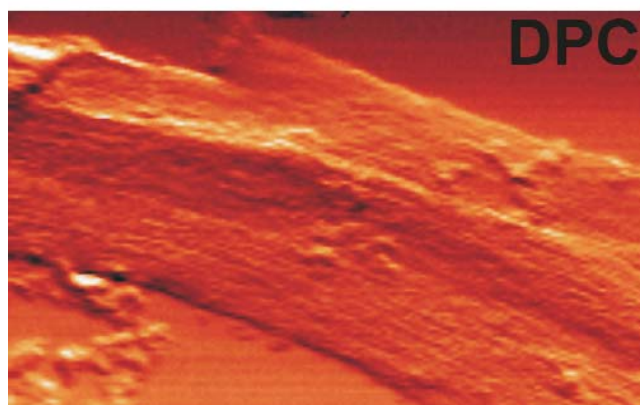
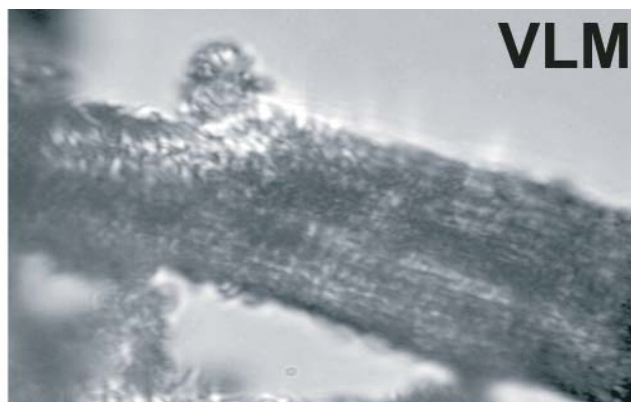
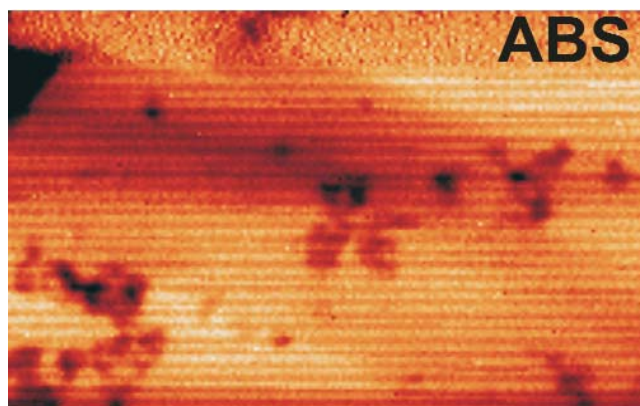


Fig. 3. Scans of a cardiac myocyte, taken at 10 keV incident x-ray energy at beamline 2-ID-E: ABS is an absorption contrast image showing mostly salt deposits that remained from sample preparation; DPC shows the differential phase contrast that visualizes the biological structure of the cell; VLM is a visible light micrograph of the same cell. DPC image gives a significantly better representation of the biological mass of the specimen than do the absorption contrast.

A HARD X-RAY NANOPROBE BEAMLINE AT THE CENTER FOR NANOSCALE MATERIALS

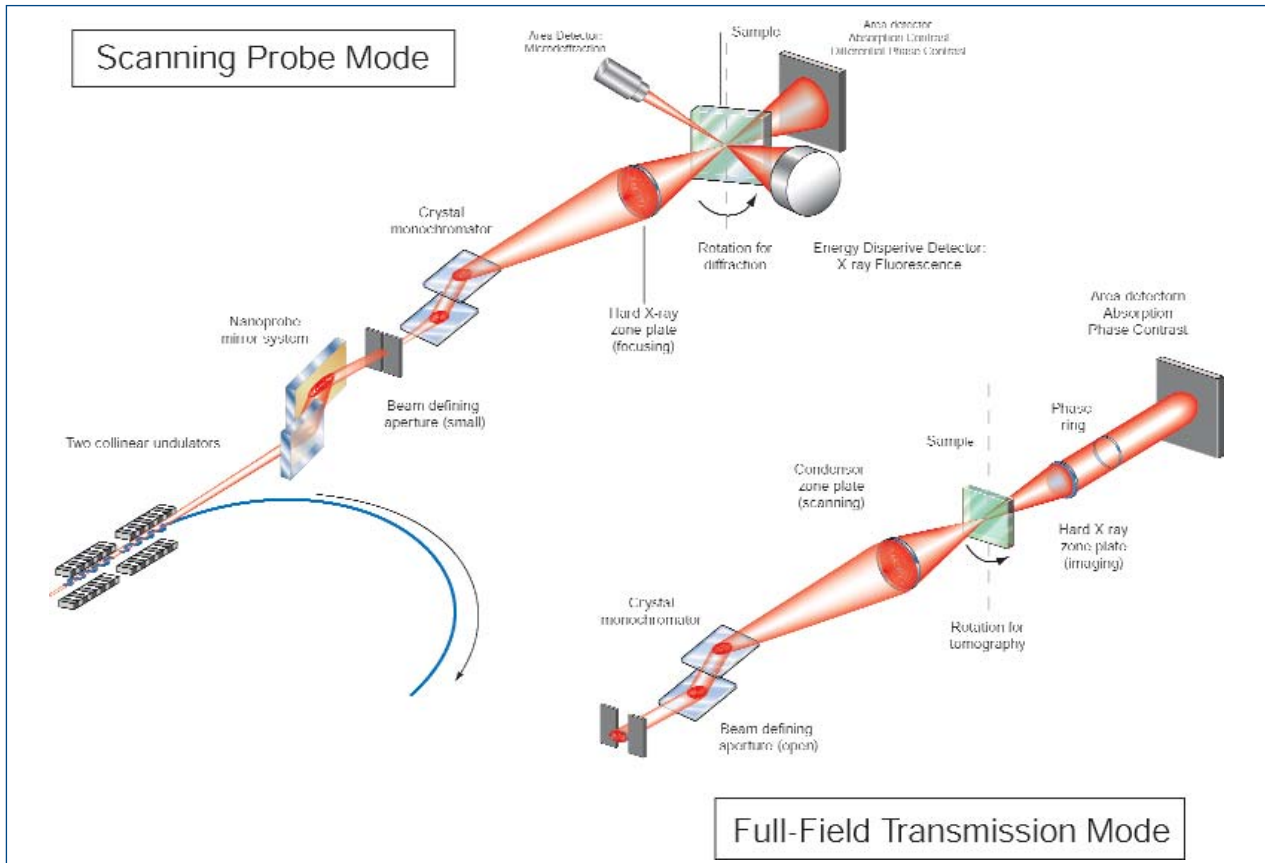


Fig. 1. Schematic of the hard x-ray nanoprobe beamline with the major beamline components.

Construction of the hard x-ray Nanoprobe beamline for the Argonne National Laboratory Center for Nanoscale Materials (CNM) on APS sector 26 has begun. The beamline is designed to characterize nanoscale systems and devices at a spatial resolution of 30 nm, using x-ray fluorescence spectroscopy, x-ray diffraction, and transmission imaging. Two collinear insertion devices with periods of 3.3 cm are used as the x-ray source, providing a brilliance of 10^{20} photons/s/mm²/mrad²/0.1%BW at photon energies between 3 and 10 keV. The nanoprobe beamline will deliver x-rays with photon energies between 3 keV and 30 keV to the nanoprobe instrument, thus allowing x-ray fluorescence spectroscopy of most elements in the periodic system. The beamline optics are designed to provide a spatially coherent wavefront for illumination of the focusing optics in the nanoprobe instrument, allowing imaging with diffraction-limited resolution.

Fresnel zone plates are planned as high-resolution x-ray optics. They will be used as focusing optics in scanning probe mode and as imaging optics in full-field transmission mode. In scanning probe mode, the zone plate is placed upstream of the

specimen and focuses the incident coherent wavefront, defined by the vertical source size and a horizontal beam-defining aperture, into a diffraction-limited spot on the specimen. In full-field transmission mode, the zone plate is placed downstream of the specimen to create a magnified image of the specimen on an area detector. In this case, the beamline is configured to accept a large fraction of the undulator beam, and a condenser system is placed upstream of the specimen to provide partially coherent illumination of the specimen.

Figure 1 shows a schematic of the beamline in scanning probe mode and in full-field transmission mode. Major beamline components are a double mirror system, a beam-defining aperture, and a crystal monochromator. The mirror system, located 30 m from the source, focuses the undulator beam in the horizontal direction on a beam-defining aperture located 40 m from the source. To provide a spatially coherent source for operating in scanning probe mode, the beam-defining aperture is closed to a horizontal size of 20–25 μm . For operation in full-field transmission mode, the beam-defining aperture is opened, allowing

Continued on next page

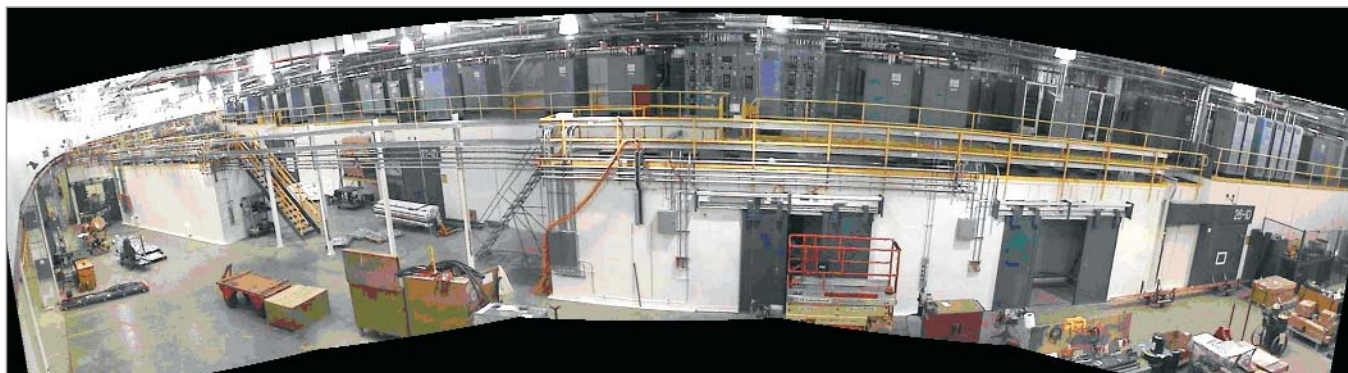


Fig. 2. The Nanoprobe beamline at APS sector 26 as of late 2004, with hutch construction complete. The first optical enclosure is in the center of the photo; the second optical enclosure and the Nanoprobe end station are at left. (Photo: R. Winarki, XFD-XMG)

partially coherent beam accepted by the mirror system to illuminate the condenser system. A crystal monochromator will select the required photon energy.

Figure 2 is a photo of sector 26 with completed radiation enclosures. Shielding verification is planned for March and April 2005. The enclosures are based on a standard APS design. The beamline spans the entire length of sector 26 in order to maximize the working distance of the nanoprobe instrument. Measurements made at high resolution require good temperature stability for the nanoprobe instrument. The final enclosure will, therefore, have a temperature-controlled environment.

Figure 3 shows an engineering drawing of components inside the first optical enclosure (FOE). Design of the safety shutters, photon shutters, beamline masks, and shielded transport pipes between the FOE and the second optical enclosure is complete. APS technical design reviews of most of these components have been concluded and procurement is proceeding as of late 2004. Installation of required vacuum components and shutters will be completed in early 2005 to allow shielding verification of all nanoprobe beamline hutches.

The CNM hard x-ray nanoprobe beamline is scheduled to be completed in June 2007. To provide initial x-ray microscopy

capabilities before availability of the nanoprobe instrument, an Early User Instrument (Fig. 4, next page) has been developed. This system incorporates a prototype of the required high-precision scanning stage and specimen stage. The system is designed to provide a mechanical repeatability of ± 2 nm over a travel range of 12 mm for lateral zone plate and specimen position and to maintain the lateral position to better than 15 nm during the focusing motion of the zone plate. The latter is required to allow spectroscopy of a single specimen point of 30 nm diameter. The zone plate is mounted on a piezo-driven flexure stage with a range of 1 μ m, which in turn is mounted on a motorized x/y/z stage. The specimen is mounted on a motorized x/y/z/θ stage. High-precision positioning is achieved by measuring the position of both zone plate and specimen stages in the x and y directions with individual laser Doppler interferometers with respect to a reference frame. Deviations of the position from the desired values are corrected by using the flexure stage. A feedback loop operating at a frequency of 100 Hz allows correction for drifts and provides active vibration control. First measurements of the system performance at 8-ID have yielded a source-size limited resolution of 70 nm at a photon energy of 7.4 keV.

Contact: J. Maser (maser@aps.anl.gov) and G. B. Stephenson (stephenson@anl.gov)

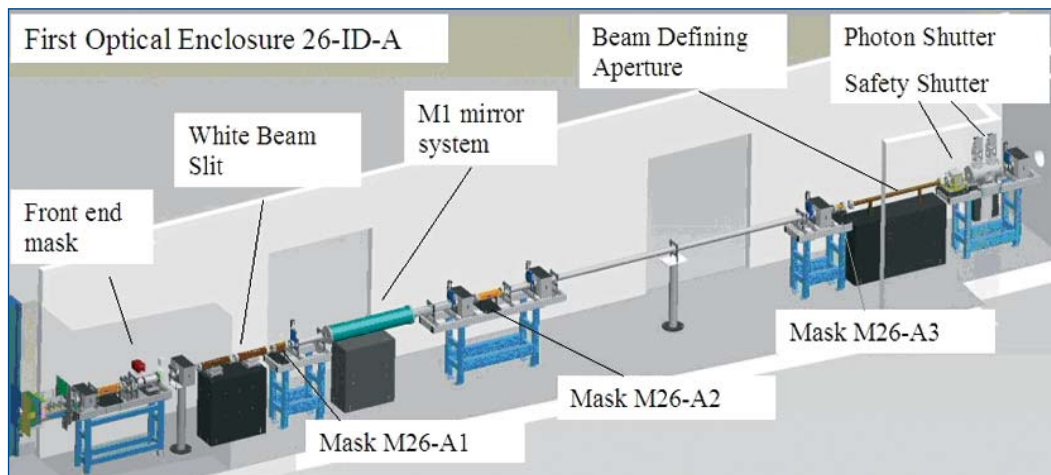


Fig. 3. First optical enclosure of the Nanoprobe beamline.

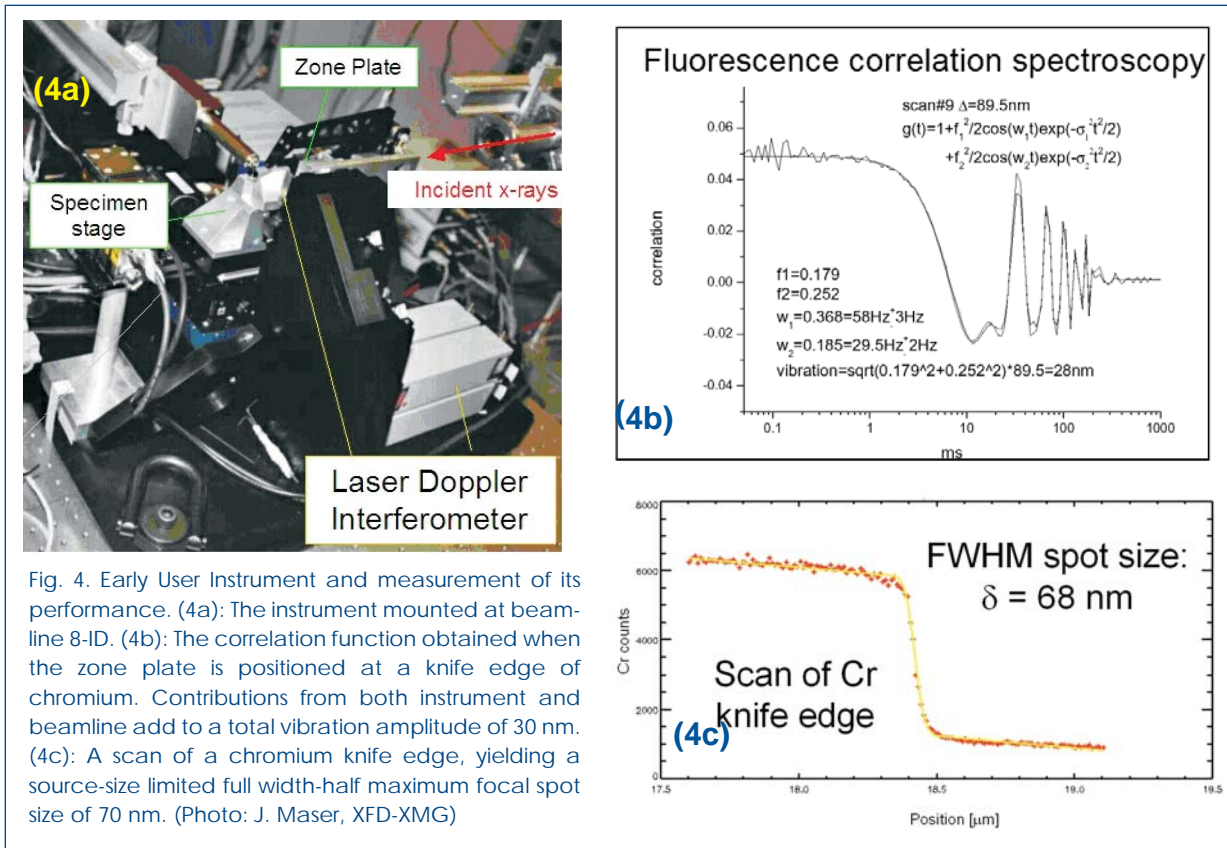


Fig. 4. Early User Instrument and measurement of its performance. (4a): The instrument mounted at beamline 8-ID. (4b): The correlation function obtained when the zone plate is positioned at a knife edge of chromium. Contributions from both instrument and beamline add to a total vibration amplitude of 30 nm. (4c): A scan of a chromium knife edge, yielding a source-size limited full width-half maximum focal spot size of 70 nm. (Photo: J. Maser, XFD-XMG)

THE DEDICATED INELASTIC X-RAY SCATTERING BEAMLINE AT APS SECTOR 30-ID

Construction of a dedicated inelastic x-ray scattering (IXS) beamline (Figs. 1a and b, next page) is under way at APS sector 30. This IXS beamline was developed by a collaborative development team (IXS-CDT) comprising several universities, national laboratories, and private companies. The beamline will have two dedicated instruments: a high-energy-resolution inelastic x-ray spectrometer (HERIX) with a resolution of 1-2 meV to study collective excitations such as phonons, and a medium-energy-resolution inelastic x-ray spectrometer (MERIX) with a resolution of 50-100 meV to study collective electronic excitations.

The HERIX spectrometer is designed to work in the 21 keV to 5 keV energy range, while the MERIX instrument will operate in the 5 keV to 12 keV energy range. Both instruments will have dedicated, state-of-the-art, bimorph Kirkpatrick-Baez focusing mirror pairs to provide a spot size under 20 μm , with full spatial efficiency.

Construction of the beamline began in 2003. The first beam is expected in the spring of 2005. Beamline commissioning is planned to start in the fall of 2005, with completion in the fall of 2006. Funding for the construction was obtained from the U.S. Department of Energy (75%) and the National Science

Foundation (15%), with matching funds from the member institutions (10%).

The HERIX spectrometer (Fig. 2, next page) is served by a state-of-art, in-line, six-crystal, cryogenically cooled high-resolution monochromator. The energy range is 21.6 to 25.7 keV, and overall energy resolution is under 2 meV. It has a 9-m-long horizontal arm to provide momentum transfer in the range of 0.5 to 78 nm^{-1} . Current plans call for nine analyzers, allowing data to be collected at multiple q values simultaneously. This number may be increased in the future.

The MERIX spectrometer, shown in Fig. 3 (next page), will also be served by a state-of-art, in-line, no-offset, four-crystal, constant-bandpass monochromator. The instrument has a 2-m-long spectrometer that is capable of both vertical and horizontal scans, allowing it to take full advantage of polarized x-rays. It will perform both resonant and non-resonant IXS measurements. Initial energy resolution will be around 120 meV, and analyzers will be available for a number of transition metal absorption edges.

The Experimental Facilities Division Engineering Group designed a new front end to handle a total power of 21 kW

Continued on next page

and a maximum normal incidence peak power density of 2,100 W/mm² at about 17.2 m from the center of the straight section. This precaution is taken to accommodate up to three insertion devices, if it becomes possible in the future to extend the straight section length from the current 5 m to 8.5 or 12 m. Planners also foresee a dedicated superconducting undulator that will deliver 20-25 keV x-rays in the first harmonic.

Contact: E. Alp (eea@aps.anl.gov)

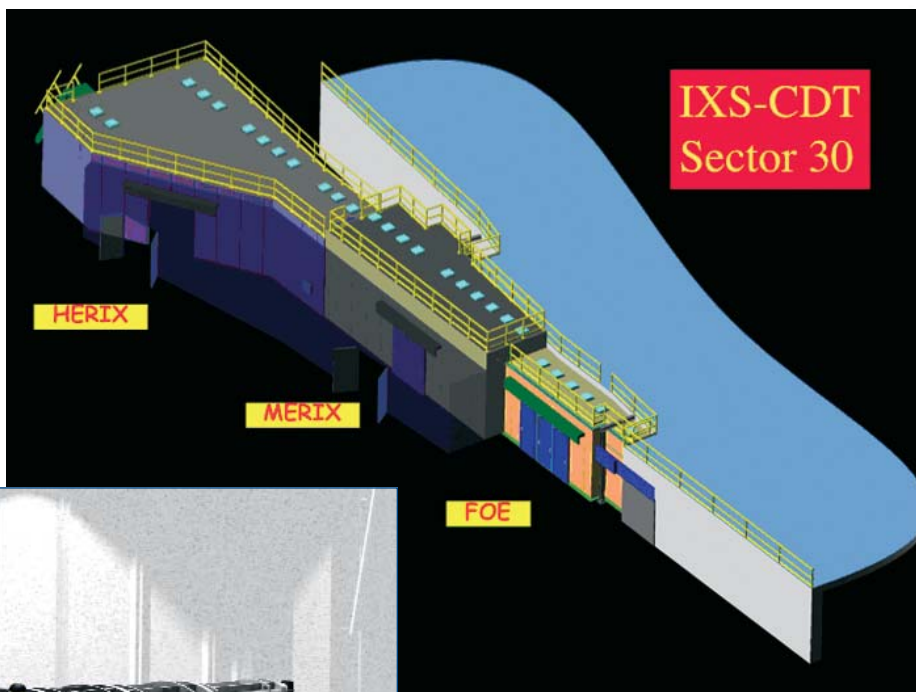
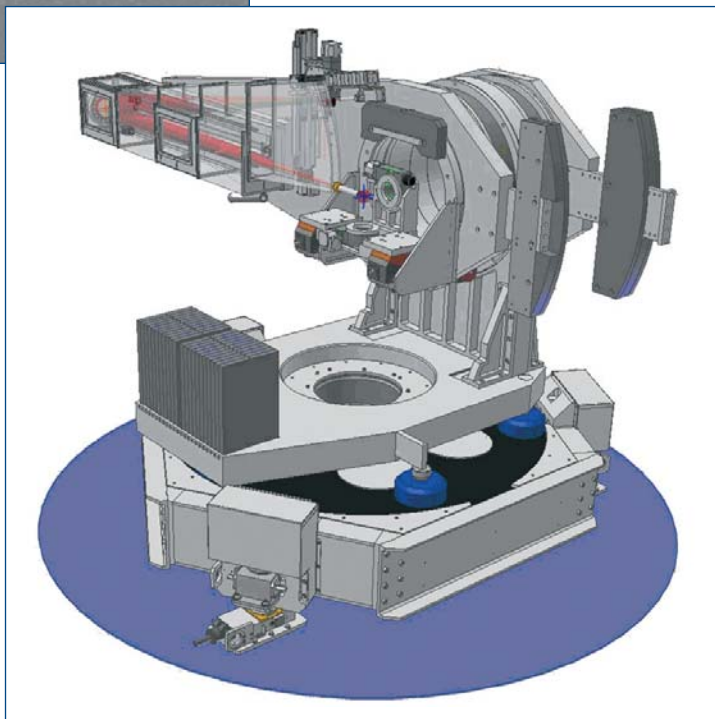


Fig. 1 (top right). Overall layout of the new IXS beamline at sector 30 of the APS. The first optics enclosure houses a water-cooled diamond double-crystal monochromator and a Be-compound refractive lens. The second station (MERIX) houses the high-resolution monochromators for both the MERIX and HERIX spectrometers, as well as the MERIX instrument itself. The last station downstream (HERIX) includes a state-of-the-art microfocusing system and the HERIX spectrometer. The control room acts as a buffer to provide exceptional temperature stability during access to the stations.

Fig. 2 (above left). The HERIX spectrometer for sector 30. The 19-m horizontal arm swings up to 30°, enabling momentum transfer from 0.5 to 78 nm⁻¹.

Fig. 3 (right). The MERIX instrument for sector 30. The instrument features vertical and horizontal scattering geometries and the provision for extreme sample environments, such as high magnetic field.



THE BioCARS-CAT BSL-2/BSL-3 FACILITY: A RESOURCE FOR SOLVING THE STRUCTURES OF VIRUSES AND TOXINS

BioCARS-CAT, a National User Facility at sector 14 of the APS, fosters frontier research in the field of macromolecular crystallography. It provides state-of-the-art facilities and scientific and technical support for structure determination of macromolecules by means of standard x-ray diffraction techniques, such as multiple-wavelength anomalous diffraction.

But the facility is also designed for two special tasks that set it apart from other centers for macromolecular crystallography at the APS and nationwide. The BioCARS-CAT insertion device beamline 14-ID

can serve as both a monochromatic and a polychromatic x-ray source. The

polychromatic capability is essential for conducting time-resolved x-ray diffraction experiments that utilize the Laue technique. These experiments result in molecular movies depicting biologically important macromolecules as they carry out their functions. The other special feature of the BioCARS-CAT facility is that all three experimental stations are embedded in a Biosafety Level 3 (BSL-3) containment, the only one of its kind in the U.S. This permits safe research with biohazardous materials classified as Biosafety Level 2 or 3 agents, such as human, animal, or plant viruses and toxins.

Agents classified as BSL-2 include a broad range of indigenous moderate-risk agents that are present in the community and associated with human diseases of varying severity. Immunization or treatment for these agents is available. Examples include the measles virus, *Salmonellae*, and the Hepatitis B virus. Agents classified as BSL-3 are indigenous or exotic agents that may cause serious human diseases as a result of exposure by inhalation. Examples of BSL-3 agents include *M. tuberculosis*, the St. Louis encephalitis virus and *Coxiella burnetii*. The guidelines for BSL-2 and BSL-3 facilities, described in "Biosafety in Microbiological and Biomedical



Left to right; Vukica Srajer (BioCARS-CAT), Bärbel Kaufmann, Susan Hafenstein, and Michael Rossmann (all Purdue University) in the BioCARS-CAT BSL-3 facility. (Photo: Reinhard Pahl/The University of Chicago)

Laboratories" (U.S. Department of Health and Human Services, Centers for Disease Control and Prevention and National Institutes of Health, Fourth Edition, May 1999), require special safety equipment, as well as a special facility design for handling BSL-2 and BSL-3 materials. All of these requirements are fulfilled by the BioCARS-CAT facility, originally designed by Wilfried Schildkamp and recently upgraded for BSL-3 operation in a joint effort by BioCARS-CAT staff (led by Vukica Srajer and Reinhard Pahl) and the APS. The facility was approved for BSL-3 operation on November 2, 2004, by the ANL Institutional Biosafety Committee. The

first BSL-3 experiment was conducted on November 12, 2004.

Manipulation of all BSL-3 agents is done in a Class II Biosafety Cabinet that serves as the primary protection barrier. The facility is physically separated from the access corridors and is maintained under negative pressure (with respect to the APS experiment hall) while BSL-2 and BSL-3 experiments are under way. Air flows into the facility and is exhausted, via a high-efficiency particle air filter, out of the APS experiment hall building. Mandatory special operating procedures for BioCARS-CAT users and staff have been developed. These procedures describe in detail the rules for conducting BSL-2 and BSL-3 experiments, the required responses to incidents and emergencies, as well as safe disposal methods for any waste generated during such experiments.

Many virus crystallographers nationwide already use the BioCARS-CAT facility for their research projects. In this expanding field of national importance, BioCARS-CAT is in a position to play an important role as the only synchrotron-based x-ray diffraction laboratory that can be used for safe study of BSL-3 samples.

Contact: V. Srajer (v-srajer@uchicago.edu)

APS USERS

THE APS USER PROGRAM

During 2004, access opportunities for APS users increased substantially as new beamlines began hosting general users (GUs), and partner users continued to develop new capabilities and introduce new communities of users to APS research. (General users are investigators who apply for beam time through the APS GU peer-review proposal process; partner users are individuals or groups whose work involves a greater degree of collaboration with the APS than is generally expected of GUs.) By the end of 2004, a total of 42 beamlines (28 insertion device and 14 bending magnet) were supporting GUs, with commitments of beam time on each ranging from 25% to 80%. Overall, during 2004, more than 10,500 8-h shifts of beam time were available for GUs.

To access the APS as GUs, researchers submit proposals—either individual (good for one allocation of beam time) or programmatic (good for multiple beam-time allocations over a two-year period). These proposals are reviewed and rated by one of nine proposal review panels (scientific peers, generally not affiliated with the APS). Beam time is then allocated by either of two APS Beam Time Allocation Committees. During 2004, 1,392 requests for beam time were submitted through the GU system; of those, 67% received time.

Those users who proposed to carry out research programs beyond the scope of the GU program may apply to become partner users on any beamline operated by the APS. APS-operated beamlines generally provide 80% of their beam time to general users. Prospective partner users can compete for up to 30% of the total beam time over a 3-year period by submitting proposals that are peer-reviewed by a subset of the APS Scientific Advisory Committee. Final decisions on the appointment of partner users are made by APS management. The two most significant criteria for successful partner user proposals are the significance/impact of the proposed science and the ultimate benefit to the APS general user community. To date, 33 partner user proposals have been submitted, 17 of which have been approved for some percentage of time. A list of successful partner user proposals and their time and beamline allocations appears in Table 1 (next page).



Table 1. Partner User Proposals Approved for Beam Time

Investigators	Partner User Proposal Title (PUP number)	Beamline	Beam Time Award
T.A. Calcott D.L. Ederer J. Freeland G. Srajer	Soft X-ray Spectroscopy for the Study of Complex Magnetic Materials (PUP-1)	4-ID-C	10%/run for three years beginning with run 2003-3 through 2006-2
J. Wang S. E. Parrish R. Poola P.V. Farrell M.-C. Lai S. Gruner	Fuel Spray Research at the 1-BM Beamline at the APS (PUP-3)	1-BM	30%/run for three years beginning with run 2003-3 through 2006-2
J. Lang D. Haskel Z. Islam G. Srajer	Enhanced Sensitivity of X-ray Magnetic Circular Dichroism Measurements Using Phase Lock-in Detection (PUP-7)	4-ID-D	15%/run for two years beginning with run 2003-3 through 2005-2
D. Keavney J. Freeland R. Rosenberg	Incorporation of a High-Field Magnet on Beamline 4-ID-C (PUP-8)	4-ID-C	15%/run for one year beginning with run 2003-3 through 2004-2 (completed)
S. Shastri D. Haeffner W.-K. Lee U. Lienert	High-Energy X-ray Optics Development (50-100 keV) at the XOR 1-ID Beamline at the APS (PUP-9)	1-ID	10%/run for three years beginning with run 2003-3 through 2005-2
W. Sturhan J. Zhao J.-F. Lin J. Jackson G. Shen	Nuclear Resonant Scattering under High Pressure and High Temperature (PUP-10)	3-ID	15%/run for one year beginning with run 2003-3 through 2004-2 (completed)
S. Mochrie L. Lurio A. Sandy S. Narayanan	Development of X-ray Photon Correlation Techniques to Probe Soft Matter and Complex Fluids (PUP-17)	8-ID-I	15%/run for one year beginning with run 2003-3 through 2004-2 (completed)
U. Lienert H. Poulson R. Suter	<i>In Situ</i> Structural Characterization of Bulk Polycrystalline Materials on the Single-Grain Length Scale by High-Energy Synchronization (PUP-19)	1-ID	10%/run for two years beginning with run 2004-1 through 2005-3
D. Reis P. Bucksbaum R. Clarke E. Dufresne	Ultrafast X-ray Science: A Partner User Proposals for Establishing a User Base for Time-Resolved Science at MHATT-CAT, Sector 7 (PUP-20)	7-ID	20%/run for one year beginning with run 2004-1 through 2004-3
E.D. Crozier	Pacific Northwest Consortium Synchrotron Radiation Facility-XOR Partnership Proposal (PUP-21)	20-ID	15%/run for three years beginning with run 2004-1 through 2006-3
E. Stern E.D. Crozier S. Heald G. Seidler Y. Yacoby D. Brewe J. Cross	Novel X-ray Spectroscopies and Microscopies for the Determination of Structure with Atomic Resolution (PUP-24)	20-ID 20-BM	30% for two years on both lines beginning with run 2004-3 through 2006-2
S. Mochrie A. Sandy L. Lurio S. Narayanan	Development of Small-Angle X-ray Photon Correlation Spectroscopy for Studies of the Dynamics of Soft Matter (PUP-35)	8-ID-I	20% for three years beginning with run 2004-3 through 2007-2
L. Young S. Southworth D. Ederer E. Landahl E. Kanter B. Kraessig R. Dunford	Ultrafast and Ultrasmall Laser X-ray Techniques (PUP-37)	7-ID	15% for three years beginning with run 2004-3 through 2007-2
L. Soderholm S. Skanthakumar J. Neufeind P. Burns M. Beno	Short-range Order in Solution: Development of a Dedicated Beam Line for Pair-Distribution Functions Studies at the APS (PUP-42)	11-ID-B	10% per run for two years beginning with run 2005-1
Y. Lee B. Khaykovich Z. Islam G. Srajer J. Hill J. Lang	Establishing a High-Magnetic-Field Capability at the APS (PUP-43)	4-ID-D	10% per run for two years beginning with run 2005-1
D. Keavney	Implementation of Low-Temperature Magnetic Imaging Using Photoemission Electron Microscopy at 4-ID-C (PUP-44)	4-ID-C	10%/run for one year beginning with run 2005-1
D. Reis R. Clarke P. Bucksbaum D. Arms E. Landahl D. Walko	Ultrafast X-ray Science: a Partner User Proposal for Establishing a User Base for Time-Resolved Science at MHATT-CAT, Sector 7 (update of PUP-20) (PUP-47)	7-ID	15% of each run for one year

THE 2004 APS USERS MEETING

The 2004 APS Users Meeting, held May 4 to 6, attracted the largest number of attendees (more than 650 people) of any APS user meeting to date; featured the most posters (140) of any Users Meeting to date; had the largest student population (more than 50 registered, 41 submitting posters); offered the most adjunct workshops (8); and had the largest number of exhibitors (40). Highlights of the meeting included the newly established Rosalind Franklin Young Investigator Award (see sidebar), three \$500 student poster prizes, and a "Midwestern Country Evening" featuring a pig roast and a bluegrass band.

The opening session began with a welcome from Argonne's Director, Hermann Grunder. Ellen Burns, congressional staffer and Ph.D. chemist, described the process and prospects for science funding in Congress, while Pat Dehmer, Director of the DOE Office of Basic Energy Sciences, added her perspective on science funding in today's climate, urging APS users to pay attention not only to their own particular experiments and facilities, but also to the broader scientific picture. Associate Laboratory Director for Scientific User Facilities and

APS Director Murray Gibson recapped the past year's scientific accomplishments and offered a glimpse into the future, echoing Dehmer's comments about the need for "grand challenge, visionary goals."

Efim Gluskin, Director of the APS Experimental Facilities Division (XFD), described advances in undulator technology, with an emphasis on how these new instruments can help drive the APS vision. Finally, Gabrielle Long, Associate Director of XFD, explained the structure and evolution of the scientific programs on APS-managed beamlines and described the workshops planned in 2005 as part of the strategic planning process.

Wednesday afternoon opened with a warm and informative retrospective by Gene Ice (Oak Ridge National Laboratory) on the life of synchrotron pioneer and colleague Cullie Sparks, a charter member of the APS user community who died not long before the meeting. Richard Reeder (State University of New York at Stony Brook) followed with a glimpse into the geophysical world via his talk entitled, "Mineral Surfaces: Bridging Adsorption and Co-Precipitation." Next came a look into the future with Ronald Ruth of Lyncean Technologies, Inc., who described plans for a compact light source that could easily fit



May 4, 2004, just prior to the opening session of the 2004 APS Users Meeting. **Left to right:** Hermann Grunder (Director, ANL), Dan Arvizu (Director, National Renewable Energy Laboratory), Ellen Burns, aide to Congressman Vern Ehlers (R-MI 3rd), Murray Gibson (Director, APS), Patricia Dehmer (Associate Director of Science for Basic Energy Sciences [BES], U.S. Department of Energy [DOE], Office of Science), Eric Isaacs (Director, Center for Nanoscale Materials, ANL), Stephen Durbin (Purdue University and outgoing Chair, APS Users Organization), and Pedro Montano (Director, Scientific User Facilities, DOE-BES).

into a home laboratory. The final speaker for this session was George Flynn, who moved farther afield with his look at interplanetary dust particles, including challenges in chemical analysis and preparation for the first samples to be returned from a comet.

Thursday morning's scientific session focused on structural biology and geology. The first presentation, by Dinshaw Patel of Memorial Sloan-Kettering Cancer Center, was entitled "Molecular Recognition Events in RNA Interference and Glycolipid Transfer Processes." The second, by Jonathan Greer of Abbott Laboratories, described progress in designing drugs to fit targets—that is, the process of structure-based drug discovery. The final talk in the structural biology sequence was by Wei-Jen Tang of The University of Chicago on anthrax adenylyl cyclase toxin. Next, Thomas Duffy moved into the geophysical realm in his talk on the role of synchrotron experiments in understanding deep planetary interiors. The morning ended on a high note with the presentation of the three student-poster prizes to Jennifer Jackson ("(Mg,Fe)SiO₃ Perovskite to 120 GPa Using Synchrotron Mössbauer Spectroscopy"), Jason Key ("Time-Resolved Crystallographic Studies of the Heme-Based Sensor Protein FixLH") and Mark Pfeifer ("3-D Mapping of Strain Using Coherent X-Ray Diffraction"). ○



Above: Scenes from the 2004 APS Users Meeting.

THE FIRST APSUO ROSALIND FRANKLIN YOUNG INVESTIGATOR AWARD

The APS Users Organization (APSUO) awarded its first Rosalind Franklin Young Investigator Award to Alexis S. Templeton for her work as a graduate student at Stanford University and more recent studies as a Postdoctoral Research Associate at Scripps Institution of Oceanography, University of California, San Diego. Franklin was presented with the award, which consists of a plaque and \$1,000, on May 6 at the 2004 APS User Meeting. She presented a talk on her work at the close of the meeting.

Templeton's research centers around the influence of microorganisms in the speciation of heavy metals in environmental systems, as well as the role of bacteria in the weathering of basaltic glasses in deep ocean environments. She has relied on a diverse array of spectroscopic and microscopic techniques. A particularly novel development was her combination of the long-period x-ray standing wave technique with x-ray absorption near-edge structure spectroscopy to provide depth-sensitive speciation of selenium within bio-film coatings on mineral surfaces. The methods she used to provide a fully three-dimensional characterization of trace element distribution and speciation represents a major advance in the investigation of such systems.



Alexis Templeton

The award was established by the APSUO in conjunction with the APS to recognize an important technical or scientific accomplishment by a young investigator that depended on, or is beneficial to, the APS. The award is open to senior graduate students and those whose Ph.D. was awarded no more than two years prior to nomination. The award is presented every other year (alternating with the Compton Award) at the APS Users Meeting.

Rosalind Franklin was born in 1920 and graduated from Cambridge University in 1941. Before she was 26 years old, she published five papers on the composition of coal and charcoal, work that is still quoted today, and helped launch the field of high-strength carbon fibers. Franklin later pioneered the use of x-ray diffraction in analyzing complex, unorganized matter such as large biological molecules. Working as a research associate for John Randall at King's College, she performed x-ray crystallographic studies of DNA that were a critical contribution to the solution of the molecule's structure. Franklin's career was cut short by her untimely death at age 37.

USER SUPPORT

NEW USER SUPPORT RESOURCES

During 2004, the Experiment Floor Operations and Beamline Technical Support groups in the APS Operations Division were merged to form the Experiment Operations Support (EOS) group. Among other responsibilities, the new group provides 24/7 coverage for beamline operations and manages work on configuration control components through the Floor Coordinators. The group also manages and operates the APS Detector Pool. Consolidating the technical resources of both groups into the new EOS group has allowed for a more efficient use of resources in support of user operations.

The APS Experiment Floor Project Specialist (EFPS) position was created in April 2004. This person acts as the main interface between the APS Conventional Facilities Engineering (CFE) staff and the research groups undertaking construction and upgrade projects in the experiment hall, while also providing electrical design and installation oversight capability to CFE. Among other responsibilities, the EFPS serves as the contract officer technical representative and construction field representative for shielding projects.

The new User ESH Support Group was formed in 2004. The group leader also serves as the APS User Safety Officer overseeing user activities on the experiment hall floor. The group's responsibilities include direct environment, safety, and health support for the APS beamline staff and users; experiment safety reviews; and compliance issues related to DOE and other federal regulatory requirements; health physics support for the users as well as for all of the APS; and maintenance of user safety related information, policies, procedures, Experiment Safety Assessment system, and tracking of experiment-related user statistics. In addition, members of the group are involved in dosimetry measurements pertaining to the study of radiation damage to insertion devices and beamline and accelerator components. The dosimetry activity has recently been extended to assist several users in determining x-ray doses at the sample position during experiments.

THE APS DETECTOR POOL AND OTHER DETECTOR ACTIVITIES

The APS continues to expand its activities in the arena of x-ray detectors. The APS Detector Pool became fully operational as a centralized source of x-ray detectors for the beamlines (Fig. 1), and detector development efforts are ongoing. The mission of the Detector Pool is to provide high-end x-ray detectors and instrumentation on short-term loan to the APS beamlines. In this way, the Detector Pool allows access to expensive detectors that can be used as backup detectors or to satisfy specific requirements of beamline users. The Detector Pool staff surveys the needs of the APS scientific community, researches detector options, evaluates commercial systems,

provides equipment loans via a Web-based reservation system, promotes sharing of equipment between beamlines, and assists beamline staff in the repair and maintenance of useful systems. This past year, use of the equipment has been very high, with some 20 detectors almost continually out on loan. New systems added to the pool this year included large-area charge-coupled device systems, image plates, and silicon drift detectors. As gaps show up between what types of detectors



Fig. 1. Steve Ross (AOD-TBS) with a germanium energy dispersive detector, one of several detector types that users can check out from the APS Detector Pool.

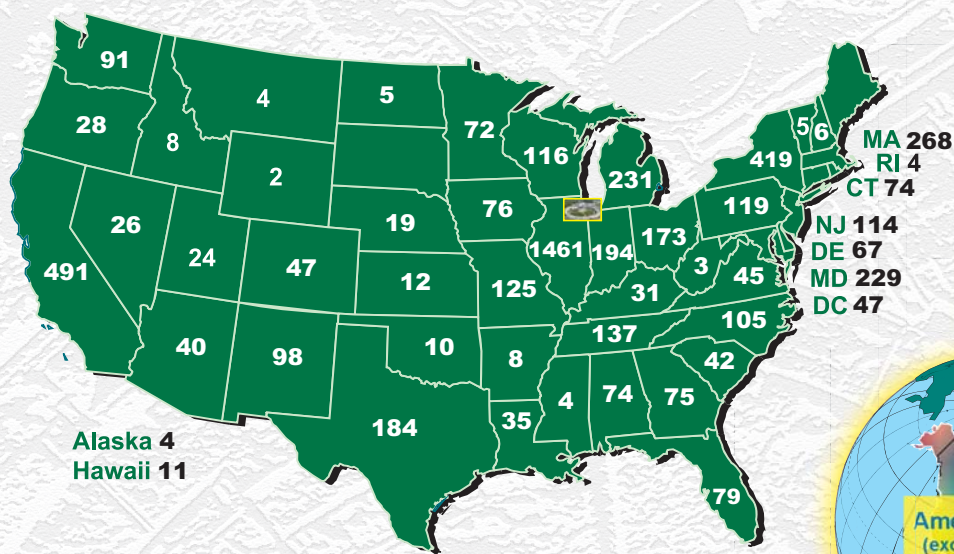
are needed and what can be purchased, and to enhance the scientific productivity of the beamlines, EOS personnel continue to develop detectors. This effort is now growing thanks to an expanded staff.

In the past year, the EOS group has hired two persons to work on the detector effort. In support of beamline operations, this past year the EOS staff continued to deliver and install electrometer-based beam-position monitors, provided sets of custom shaping amplifiers, worked to develop high-speed avalanche photodiode systems, and installed several custom digital timing systems.

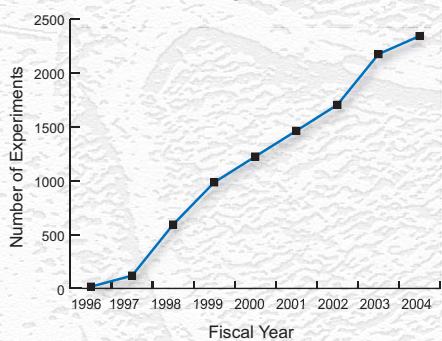
USER SHIPPING SUPPORT

The EOS group has begun processing User Shipping Requests in an effort to provide support to beamline personnel by expediting the transportation offsite of material brought to the APS by visiting scientists. The program began with the processing of dry shippers for SBC-CAT; NE-CAT and IMCA-CAT have also utilized this service. Each week approximately 5 to 20 different shipments are sent out from the APS. Future plans are to incorporate an online shipping request system to handle notification and tracking of items shipped. ○

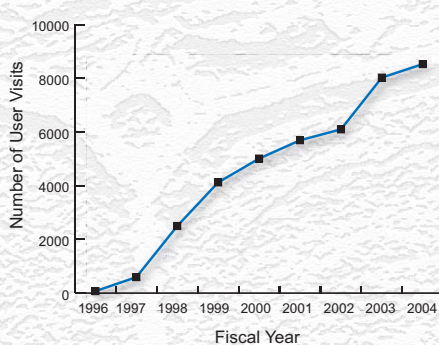
APS Badged Users by Region and U.S. State



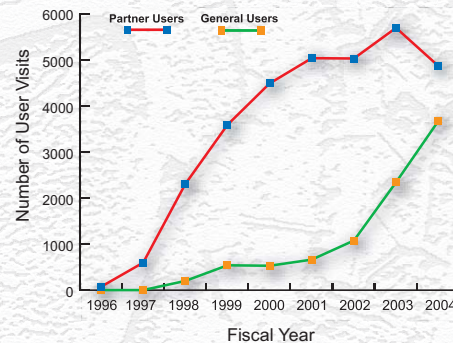
Number of APS Experiments Per Year



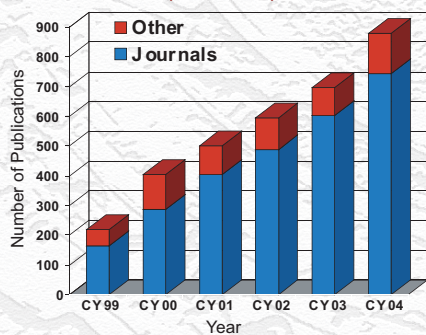
Number of Visits to APS by Users



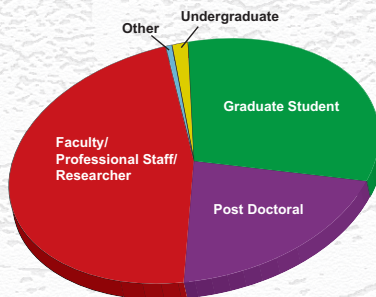
Number of Visits to APS by User Type



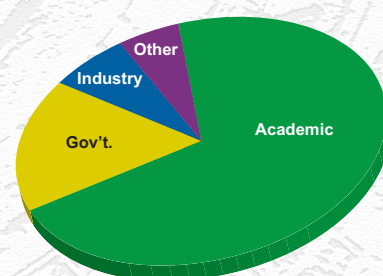
Number of APS User Publications (CY99-CY04)



APS Users by Profession



APS Users by Institution Type



THE APS LIGHT SOURCE

TYPICAL APS MACHINE OPERATIONS PARAMETERS

LINAC

Output energy	325 MeV
Output beam charge	1–3 nC
Normalized emittance	10–20 mm-mrad
Frequency	2.856 GHz
Modulator pulse rep rate	30 Hz
Gun rep rate (1–6 pulses, 33.3 ms apart every 0.5 sec)	2–12 Hz
Beam pulse length	8–30 ns
Bunch length	1–10 ps FWHM

PARTICLE ACCUMULATOR RING (PAR)

Nominal energy	450 MeV
Circumference	30.66 m
Cycle time	500 ms
Fundamental rf frequency (RF1)	9.77 MHz
12th harmonic rf frequency (RF12)	117.3 MHz
RMS bunch length (after compression)	0.28 ns

INJECTOR SYNCHROTRON (BOOSTER)

Nominal extraction energy	7.0 GeV
Injection energy	325 MeV
Circumference	368.0 m
Lattice structure	10 FODO cells/ quadrant
Ramping rep rate	2 Hz
Natural emittance	65 nm-rad
Radio frequency	351.930 MHz

STORAGE RING SYSTEM

Nominal energy	7.0 GeV
Circumference	1,104 m
Number of sectors	40
Length available for insertion device	5.0 m
Nominal circulating current, multibunch	100 mA
Natural emittance	2.5 nm-rad
Momentum spread	0.096%
Effective emittance	3.1 nm-rad
Vertical emittance	0.025 nm-rad
Coupling	1%
Revolution frequency	272 kHz
Radio frequency	351.930 MHz
Number of bunches	24 to 324
Time between bunches	153 to 11.3 ns
Bunch length	45 ps to 23 ps

THE ACCELERATOR

In calendar year (CY) 2004, the APS scheduled 5,128.25 h for user operations and delivered 5039.3 h. The emphasis on meeting established availability and reliability goals continues to yield impressive results. This is the first year in which the reliability, expressed as the mean time between faults (MTBF), exceeded project goals. The long-term goal for the APS was to be able to deliver beam without interruption for 50 h or greater, on average. Orbit stability is also a very high priority, and this year progress was made in this area (see related article, following). The APS continues to utilize a schedule of three long runs and three extended maintenance periods, first employed in 2002.

BEAM AVAILABILITY & MTBF

During 2004, accelerator operations, as quantified by availability and MTBF, exceeded the high levels obtained in 2003 (see Table 1). The APS has, since 2000, routinely exceeded the goal of 95% availability. Efforts have focused on maintaining this level of availability while reducing the number of faults. These efforts have resulted in a reliability figure of merit of 68.1 h MTBF—a truly remarkable accomplishment. The MTBF in the final run of 2004 was 110.7 h.

These improvements can be attributed, in large part, to the pragmatic and rigorous approach taken in analyzing and addressing problems and the proactive efforts to identify and resolve potential problems before they cause downtime. Causes (and duration) of user-beam downtime due to accelerator equipment problems have been tracked and analyzed since the inception of operations. To this end, the APS made increased use of periodic machine intervention periods to resolve problems. Examples of such rigor include detailed daily monitoring of rf system behavior to detect potential problems early and the automatic replacement of storage ring converters following transient trips so as to prevent recurring trips. A great deal of effort has also gone into identifying and replacing weak components, such as power-converter-control power supplies, and to reducing susceptibility to electromagnetic interference in the rf systems. As engineering improvements have been identified and implemented, they have been subjected to ever-increasing quality assurance and workmanship standards, in order to minimize the chance of introducing new problems as the old problems are resolved.

Table 1. Operations statistics—CY 2004.

	CY2003	Run 04-1	Run 04-2	Run 04-3	CY2004
Run number					
Start		1/29/04	5/25/04	10/05/04	
End		4/19/04	8/25/04	12/21/04	
Total hours scheduled (h)	5,129.0	1647	1,911.6	1,569.7	5,128.3
Beam available for users (h)	4,959.6	1,610.0	1,880.1	1,549.2	5,039.3
Beam availability (%)	96.7	97.8	98.4	98.7	98.3
Total downtime (h)	169.4	37.0	31.5	20.4	88.9
Average current (mA)	99.8	99.2	99.3	99.6	99.4
Number of faults	116	28	32	14	74
Mean time between faults (h)	42.8	57.5	58.8	110.7	68.1
Mean time to recovery (h)	1.46	1.32	0.98	1.46	1.20
Injector availability in top-up (%)	97.1	97.5	98.7	98.9	98.4

Table 2. APS beam parameters at radiation points, 2.5-nm horizontal emittance, 1% coupling.

	ID	BM
Horiz. beta function (m)	19.5	2.12
Horiz. dispersion (m)	0.172	0.058
Horiz. rms beam size (μm)	275.3	91.6
Horiz. rms divergence (mrad)	11.3	56.4
Vert. beta function (m)	2.87	25.97
Vert. rms beam size (μm)	8.5	25.5
Vert. rms divergence (mrad)	3.0	1.1

USER OPERATION FILL PATTERNS

Various storage ring operation modes have been developed to meet different user-beam requirements. The operating modes used in 2004 were:

- Top-up, low emittance, 24 singlets fill pattern
- Top-up, low emittance, 1 + 7 × 8 hybrid (singlet) fill pattern
- Non-top-up, low emittance, 324 multibunch

Note that all operations now utilize the low-emittance lattice developed over the last several years. See Table 2. CY2004 is the first year for which this is the case.

The most common fill pattern is 24 singlets spaced by 154 ns. Top-up injection (injecting beam into the storage ring every two minutes) is utilized for this fill pattern.

The hybrid singlet pattern is used by the timing community to perform dynamic biological, chemical, and condensed matter/materials science studies. This pattern is defined as a single bunch containing a maximum of 8 mA isolated from the remaining bunches by symmetrical 1.59-μsec gaps. The remaining current is distributed in 8 groups of 7 consecutive bunches with a maximum current of 12 mA per group and a spacing of 48 ns between groups. Top-up injection is also utilized in this mode.

Non-top-up operation (refilling the storage ring twice every 24 h) is mainly used to provide injector beam time for parasitic injector study, operator training, and injector maintenance and improvement. A 324-multibunch fill pattern (bunch spacing of 11.4 ns) is utilized. Experimentation with filling all 1,296 buckets for this mode began in 2004 and will be evaluated during operation in 2005.

The percentages of scheduled hours in 2004 for each of the operation modes are shown in Fig. 1.

Beam current is 100 mA for all modes. The APS previously explored a program of raising the current during short periods of operation as part of a strategy for raising normal operational current. This program has been put on hold while a thorough analysis is done on all front-end and beamline components that are exposed to insertion device x-rays. When this analysis is completed, it will lead to an understanding of the limitations and a plan for moving forward.

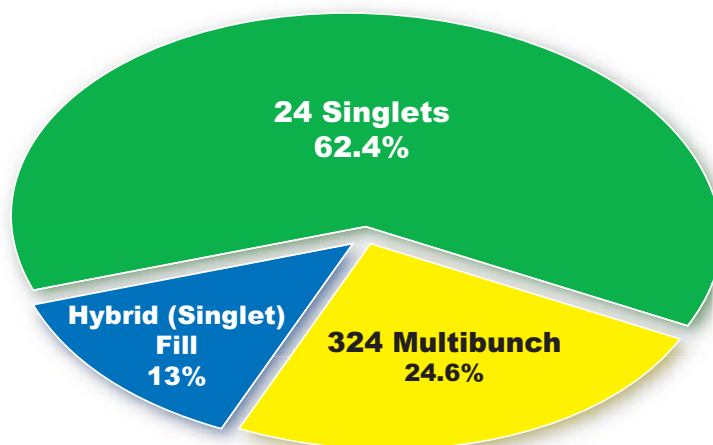


Fig. 1. Calendar year 2004 scheduled time for different APS operating modes.

THE DECKER DISTORTION: AT LONG LAST, SUCCESS

During the summer of 1997, in the “bad old days” of storage ring beam stabilization efforts, I bemoaned the myriad systematic errors affecting our now-endearing monopulse radio frequency (rf) beam-position monitor (BPM) system. The problems were manifold: fill pattern dependence, intensity dependence (this was before top-up), timing problems—not to mention the periodic mode changes between high-emittance and low-emittance machine optics. With each change in fill pattern and/or optics, one dreaded the effort needed to restore the trajectory at dozens of source points, each having four independent degrees of freedom.

I was determined to include the insertion device (ID) photon BPMs in closed-loop orbit correction in order to ease the burden of reproducing the orbit. After a few intense machine studies shifts, despair ruled there, as well. The number of stray sources of radiation co-propagating down the ID beamlines made the correction of systematic gap-dependent errors in these devices a completely intractable problem. There were something like 22 separate sources of ultraviolet radiation. Every dipole, quadrupole, sextupole, and corrector magnet located in every ID straight section was a potential source of erroneous signal.

An idea then occurred: realign the accelerator in such a way as to steer all but two of these stray sources away from the field of view of the ID photon BPMs (now commonly referred to as the “Decker Distortion”). To that end, round about September 1997, I formed the Experimental Facilities Division/Accelerator Systems Division (ASD) X-ray Stability Task Force (XAXSTF). Quite fortuitously, Om Singh joined the Diagnostics Group of the APS Operations Division (AOD) around this time, coming from the National Synchrotron Light Source at Brookhaven National Laboratory. Although his background was in electrical engineering, he ended up doing things such as running accelerator modeling codes to extract survey coordinates, among dozens of other organizational and technical tasks necessary to move my idea forward. In October of 1998, the APS Operations Directorate gave formal approval to the plan, and the first two storage ring sectors (34 and 35) were realigned by Horst Friedsam's Survey and Alignment Group (ASD) during the December 1998 shutdown.

This represented the culmination of more than a year of detailed studies to find and solve numerous problems, including ray tracing, mechanical engineering, thermal analysis, power supply technology, accelerator physics, beam mis-steering interlock configuration, potential impact on top-up operation, *ad infinitum*. Fortunately, the idea had merit, and the effort was successful, opening the door to the possibility of long-term pointing stabil-

ity at or below the 500-nrad level. The results from beamline 34-ID were published in November of 1999 [1].

Now, after six years, nearly the entire APS storage ring has been displaced, allowing closed-loop feedback using photon BPMs at about 20 ID beamlines. Many hurdles still remained, even after the reduction of stray radiation effects, that resulted in significant residual gap-dependent systematic errors requiring



The author in the (almost) fully displaced APS storage ring.

compensation. Judicious use of sophisticated feed-forward algorithms pioneered by Michael Borland's Operations Analysis Group (AOD) have allowed the use of these monitors, while still retaining the ability of users to make gap changes on demand.

Having recently (December 2004) returned from an international workshop on beam stabilization in Switzerland, it is clear that the APS is the only facility in the world to have solved the stray radiation problem, making good use of ID photon BPMs. My personal goal is to compensate residual systematic errors to provide long-term pointing stability at the 100- to 200-nanoradian level, making individual beamline steering requests (as someone once stated in another context) “impotent and obsolete.”

Contact: G. Decker (decker@aps.anl.gov)

REFERENCE

[1] G. Decker, O. Singh, "A Method for Reducing X-ray Background Signals from Insertion Device X-ray Beam Position Monitors," *Phys. Rev. ST Accel. Beams* **2**, 112801 (1999).

STORAGE RING OPERATION AT HIGHER STORED CURRENT

THERMAL AND STRESS ANALYSIS OF MASKS AND SHUTTERS FOR THE V1.2 AND V1.5 FRONT ENDS

New front ends at the APS have been designed to operate with two undulators and stored beam current of up to 200 mA; ongoing R&D seeks to extend operation to 300 mA. Finite element analysis of the older existing front end (FE v1.2 and FE v1.5) masks and shutters was carried out to establish the maximum beam current allowed for each type of front end. Earlier analysis was adequate for operations up to 100 mA of stored beam, but operation beyond this level required more extensive analysis. The analysis of each component was comprehensive, employed three-dimensional (3-D) models with precise thermal loading, and covered all relevant beam steering scenarios.

Analysis Procedure. A typical mask analysis starts with a 3-D model that is read directly by ANSYS via an ANSYS/ProE geometry connection that is part of the ANSYS package (an example is shown in Fig. 1). Next, a mesh is generated in ANSYS. The mesh control is set for a fine mesh in the aperture region (where the beam may strike) and a coarse mesh elsewhere. The heat load (calculated based on the source parameters) is fitted into a fourth-order Gaussian formula. The Gaussian formula is then applied as the heat flux distribution in ANSYS. The temperature field is calculated (see Fig. 2), then, using the temperature as the body load, the stress field is calculated. The beam was moved within the aperture to simulate vertical, horizontal, and corner mis-steering, with temperature and stress calculations repeated to cover all load cases. Sample results for the FE components at 100 mA are shown in Table 1.

Once the results for 100 mA were calculated, a linear extrapolation to higher stored beam currents was obtained.

Failure Criteria. The APS has, over the past 10 years, used conservative criteria for establishing the maximum thermal load acceptable for x-ray beam intercepting components:

Please see "Stress" on page 154

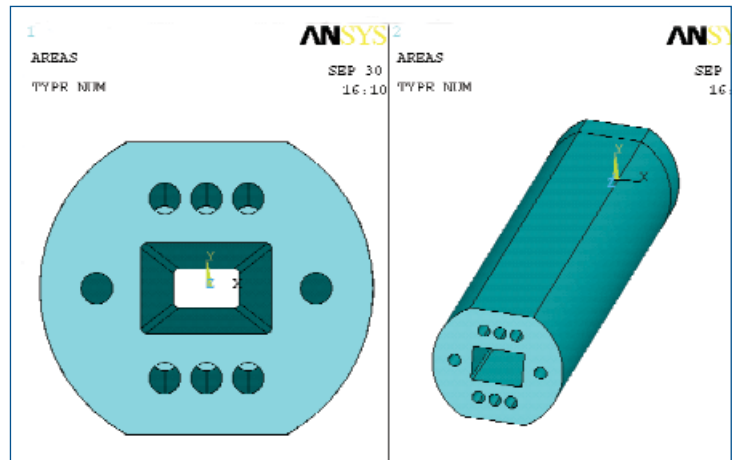


Fig. 1. M1-40 ProE model read in by ANSYS.

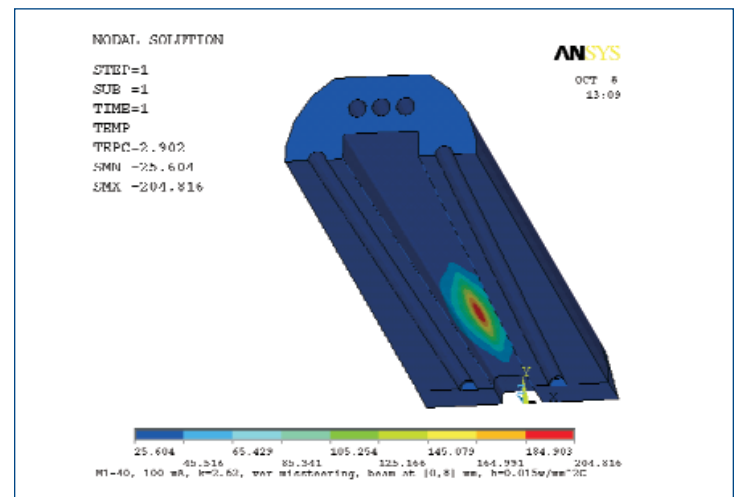


Fig. 2. M1-40 temperature (°C) at 100 mA, k = 2.62, vertical mis-steering.

Table 1. Sample results of FE components at 100 mA ($h = 0.015 \text{ W/mm}^2 \text{ }^\circ\text{C}$, $T_{\text{water}} = 25.6 \text{ }^\circ\text{C}$)

FE type	Components	T_{max} (°C)	T_{wall} (°C)	Max. σ_{vm} (MPa)
One undulator A K=2.62 (11 mm gap)	FE v1.2u	FM1 (M1-30)	245.8	96.8372.2
	FM2 (M2-20)	201.6	89.1	294.0
	PS1 (P1-20)	228.1	118.6	308.3
	PS2 (P2-20)	238.1	126.9	309.4
	Exit Mask (L5-83)	189.6	86.6	328.7
FE v1.5 One undulator A K=2.62 (11 mm gap)	FM1(M1-40)	204.8	88.2	349.1
	FM2 (M2-40)	191.2	83.2	326.5
	FM3 (M2-50)	184.0	79.8	308.9
	PS1 (P2-30)	140.9	59.3	176.2
	PS2 (P2-30)	Same component as PS1 further downstream		
3-ID, one 2.7-cm N=88, plus one 2.7-cm N=74, k=1.655	PS1 (P1-20)	246	111	359
	PS2 (P2-20)	261	121	370
4-ID, one undulator A, k=3.175, plus CPU at k=2.75	PS1 (P1-20)	297	147	410
	PS2 (P2-20)	308	158	403

APS SOURCE PARAMETERS

UNDULATOR A

Period: 3.30 cm
 Length: 2.4 m
 K_{max} : 2.74 (effective; at minimum gap)
 Minimum gap: 10.5 mm
 Tuning range: 3.0–13.0 keV (1st harmonic)
 3.0–45.0 keV (1st-5th harmonic)
 On-axis peak brilliance:
 5.0×10^{19} ph/s/mrad²/mm²/0.1%bw at 7 keV
 Source size and divergence at 8.0 keV:
 Σ_x : 275 μ m Σ_y : 9 μ m
 $\Sigma_{x'}$: 12.6 μ rad $\Sigma_{y'}$: 6.4 μ rad

3.0-CM UNDULATOR (SECTOR 30)

Period: 3.00 cm
 Length: 2.4 m
 K_{max} : 2.11 (effective; predicted at minimum gap)
 Minimum gap: 10.5 mm
 Tuning range: 4.8–14.5 keV (1st harmonic)
 4.8–50.0 keV (1st-5th harmonic)
 On-axis peak brilliance:
 6.0×10^{19} ph/s/mrad²/mm²/0.1%bw at 7.5 keV
 Source size and divergence at 8.0 keV:
 Σ_x : 275 μ m Σ_y : 9 μ m
 $\Sigma_{x'}$: 12.6 μ rad $\Sigma_{y'}$: 6.4 μ rad

2.70-CM UNDULATOR (SECTOR 3)

Period: 2.70 cm
 Length: 2.4 m
 K_{max} : 1.69 (effective; predicted at minimum gap)
 Minimum gap: 10.5 mm
 Tuning range: 7.0–16.0 keV (1st harmonic)
 7.0–60.0 keV (1st-5th harmonic, non-contiguous)
 On-axis peak brilliance:
 7.0×10^{19} ph/s/mrad²/mm²/0.1%bw at 8 keV
 Source size and divergence at 8.0 keV:
 Σ_x : 275 μ m Σ_y : 9 μ m
 $\Sigma_{x'}$: 12.6 μ rad $\Sigma_{y'}$: 6.4 μ rad

5.50-CM UNDULATOR (SECTOR 2)

Period length: 5.50 cm
 Length: 2.4 m
 K_{max} : 6.57 (effective; at minimum gap)
 Minimum gap: 10.5 mm
 Tuning range: 0.4–7.0 keV (1st harmonic)
 0.4–25.0 keV (1st-5th harmonic)
 On-axis peak brilliance:
 2.0×10^{19} ph/s/mrad²/mm²/0.1%bw at 4 keV
 Source size and divergence at 4.0 keV:
 Σ_x : 275 μ m Σ_y : 9 μ m
 $\Sigma_{x'}$: 13.9 μ rad $\Sigma_{y'}$: 8.6 μ rad

APS INSERTION DEVICES:

NEW INSERTION DEVICES

Two planar hybrid permanent-magnet APS insertion device (ID) designs with period lengths of 2.7 cm and 3.0 cm, and with a nominal length of 2.4 m, have recently been completed. While most APS ID beamlines use the 3.3-cm-period Undulator A, some users require other period lengths to optimize the brilliance in a particular energy region or to reach specific K edges in the first harmonic with sufficient brilliance. In Fig. 1, the on-axis brilliance tuning curves for the new devices are compared with the tuning curve for Undulator A for a minimum undulator gap of 10.5 mm.

The 2.7-cm-period device is used for generation of relatively high-energy x-rays with a minimum energy of 7.0 keV in the first harmonic. The 3.0-cm-period device, with a tuning range from 4.8 keV to 14.5 keV in the first harmonic (which covers the important bromine K edge at 13.5 keV), will be used for inelastic x-ray scattering and for biological research.



Mike Merritt (XFD-XFE) with one of the new planar hybrid IDs (period length 2.7 cm) after testing and just prior to installation.

RECENT DEVELOPMENTS

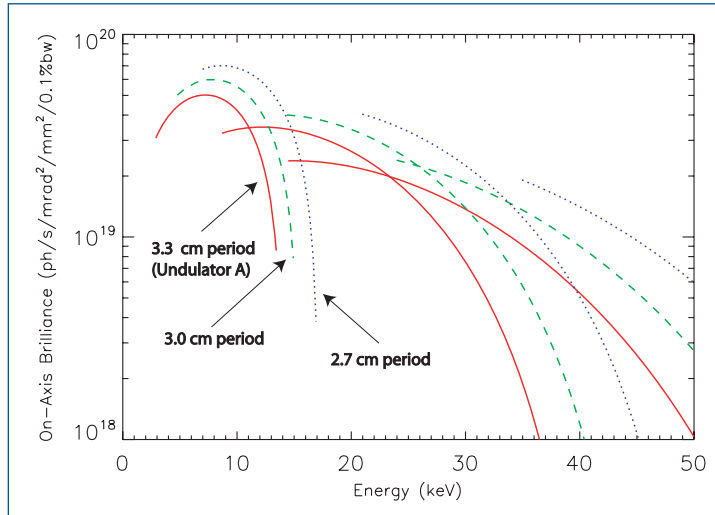


Fig. 1. On-axis brilliance tuning curves for the first, third, and fifth harmonics of the 3.3-cm-period, 3.0-cm-period, and 2.7-cm-period undulators at 7.0-GeV beam energy and 100-mA beam current. The minimum gap was set to 10.5 mm for all devices, and all devices are 2.4 m long. The tuning curves intersect for the 3.3-cm-period undulator, providing a continuous spectrum. The shorter the period length, the higher the brilliance, but the spectrum may then no longer be continuous.

FEATURES OF THE NEW DESIGNS

The primary goals of the new ID designs were lower cost, ease of magnetic tuning, compatibility with both types of existing gap separation mechanisms, commonality of as many parts as possible, and adaptability for use in both full 2.4-m length and in nominal 2.1-m length for the dual-canted-undulator sectors (where two IDs are used in a common straight section to provide two radiation sources with a small angular separation between them). Several design studies were performed for the initial 2.7-cm-period device to investigate the utility and feasibility of various design features. Then a parametric solid model for the initial device was developed and value engineered, in consultation with APS experts in undulator assembly and tuning and with ANL experts in manufacturing processes. This process resulted in a design that minimized the overall cost of manufacturing, assembling, and tuning the ID. The optimized parametric model facilitated the very rapid design of subsequent devices of similar periods and allowed economies of scale in producing components common to all of the devices.

This design family incorporates a low-cost method of pole retention and registration. Poles are secured by screws in two holes tapped into each pole. Pole location is registered by means of two small dowel pins for each pole in mating holes

APS SOURCE PARAMETERS

CIRCULARLY POLARIZED UNDULATOR (SECTOR 4)

Period: 12.8 cm

Length: 2.1 m

Circular mode:

K_{\max} : 2.65 (effective; for both horizontal and vertical fields at maximum currents of 1.2 kA horizontal and 0.34 kA vertical)

B_{\max} : 0.26 T (peak fields)

Tuning range: 0.5–3.0 keV (1st harmonic)

On-axis peak circular brilliance:

3.6×10^{18} ph/s/mrad²/mm²/0.1%bw at 1.8 keV

Linear mode:

K_{\max} : 2.80 (effective; for both horizontal and vertical fields at maximum currents 1.4 kA horizontal and 0.40 kA vertical)

B_{\max} : 0.29 T (peak fields)

Tuning range: 0.8–3.0 keV (1st harmonic)

0.8–10.0 keV (1st–5th harmonic)

On-axis peak linear brilliance:

2.7×10^{18} ph/s/mrad²/mm²/0.1%bw at 2.1 keV

Switching frequency: 0–5 Hz

Switching rise time: 20 ms

Source size and divergence at 1.5 keV:

Σ_x : 275 μm

Σ_y : 9 μm

Σ_x' : 18.0 μrad

Σ_y' : 14.3 μrad

ELLIPTICAL MULTIPOLE WIGGLER (SECTOR 11)

Period length: 16.0 cm

Number of poles: 34 permanent magnets,
36 electromagnets

Length: 2.8 m

$K_{x-\max}$: 1.3 (effective; at maximum current 1.15 kA)

$K_{y-\max}$: 14.4 (peak; at minimum gap 24.0 mm)

Switching frequency: 0–10 Hz

Critical energy: 31.4 keV (at minimum gap)

Energy range: 5–200 keV

Elliptical mode ($K_x = 1.3$, $K_y = 14.4$)

Degree of circular polarization (P_c) ~90%

On-axis peak brilliance:

1.0×10^{17} ph/s/mrad²/mm²/0.1%bw at 7 keV

On-axis peak angular flux density:

1.6×10^{15} ph/s/mrad²/mm²/0.1%bw at 7 keV

Linear mode ($K_x = 0$, $K_y = 14.4$)

On-axis peak brilliance:

2.0×10^{17} ph/s/mrad²/mm²/0.1%bw at 26 keV

On-axis peak angular flux density:

3.1×10^{15} ph/s/mrad²/mm²/0.1%bw at 26 keV

Source size and divergence at the critical energy:

Σ_x : 275 μm

Σ_y : 9 μm

Σ_x' : 820 μrad (FWHM 1.9 mrad; non-Gaussian; linear mode)

Σ_y' : 47 μrad (linear mode)

APS BENDING MAGNET

Critical energy: 19.51 keV

Energy range: 1–100 keV

On-axis peak brilliance:

6.5×10^{15} ph/s/mrad²/mm²/0.1%bw at 16 keV

On-axis peak angular flux density:

9.6×10^{13} ph/s/mrad²/0.1%bw at 16 keV

On-axis peak horizontal angular flux density:

1.6×10^{13} ph/s/mrad²/0.1%bw at 6 keV

Source size and divergence at the critical energy:

Σ_x : 92 μm

Σ_y : 26 μm

Σ_x' : 6 mrad

Σ_y' : 47 μrad

reamed into each pole and a base plate common to the poles and the magnets. This base plate is flexible so that shimming can be used behind it to accurately change the height of a pair of poles for tuning. This design approach is feasible because of the reasonable cost for high accuracy in machining the poles and base plate and the assembly time saved by having the accuracy of the assembly "machined into" the components rather than achieved through high-precision assembly techniques. Several of the features of the design are shown in Fig. 2.

Another feature of the design is the modular construction that allows each device to be used full length or shortened to a nominal 2.1-m length by removal of the end modules. The shorter length is needed for use in the APS dual-canted-undulator sectors.

STATUS

The 2.7-cm- and 3.0-cm-period devices are currently being fabricated for installation in the APS storage ring in mid-2005.

Contact: J. Grimmer (grimmer@aps.anl.gov) and R. Dejus (dejus@aps.anl.gov)

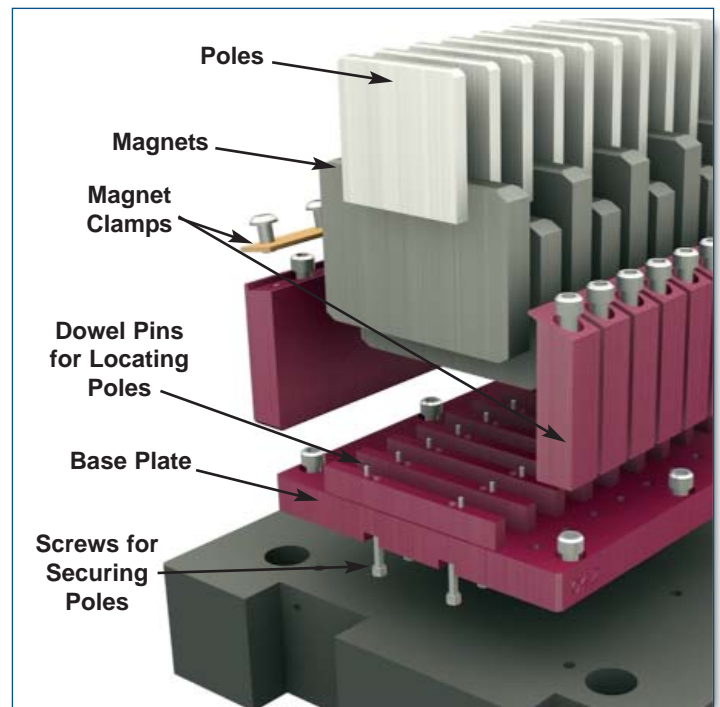


Fig. 2. Exploded view of the new undulator assembly.

A COMPUTATIONAL TOOL FOR UNDULATOR PHASE TUNING AND APPLICATIONS FOR THE LINAC COHERENT LIGHT SOURCE

The undulator segments of the 130-m-long undulator line for the Linac Coherent Light Source project must have a deflection parameter K_{eff} that matches the nominal value for that segment to within $\Delta K_{eff}/K_{eff} < 1.5 \times 10^{-4}$. A canted-pole geometry was chosen, allowing the K value to be changed by lateral translation of the entire undulator segment [1]. This scheme also facilitates step-wise tapering of the undulator line to accommodate electron beam energy loss. Changing the K value in this manner can also be used as a way to tune the phase between devices.

To be able to set the K value to the very high accuracy required and to evaluate whether the correct phasing between undulator segments is achieved, we calculate and use a quantity called the complex amplitude of radiation. This value is extremely sensitive to break length errors between undulator segments (they cause a phase error) and to any other unmatched condition that may arise, either from a change of the K value or from the particle energy loss. The complex amplitude of radiation is plotted in polar coordinates, making it easy to visualize small errors that cause the phase to be wrong.

The phase slippage along the undulator can be calculated using the following [2]:

$$\varphi(z) = \frac{k}{2\gamma^2} \left[z + \int_0^z I_{1x}^2(z') dz' + \int_0^z I_{1y}^2(z') dz' \right]$$

where k is the fundamental harmonic wave vector of the radiation, γ is the relativistic factor, and I_{1x} and I_{1y} are the normalized

particle angles in the vertical and horizontal directions, respectively, derived from magnetic measurement data. In free space, with zero field and zero angle we have:

$$\varphi(z) = \frac{k}{2\gamma^2} z, \quad L_{free} = n\lambda_u (1 + K_{eff}^2 / 2)$$

where L_{free} is the required distance in free space for n periods of phase slippage. An initial magnetic tuning will be required for each undulator segment to match its end phasing to the standard mechanical break length. The complex radiation amplitude A is defined as:

$$A(z) = \int_0^z I_{1y}(z') e^{-i\varphi(z')} dz'$$

In the polar plot, the magnitude of A is plotted as the radius, and the complex phase angle of A is plotted as the angle. These values, calculated for a sequence of points along the undulator, are plotted. A properly phased undulator will be represented as a straight line drawn radially outward from the center of the graph. Phasing errors appear as curved lines or kinks (see Fig. 1). The absolute value of the complex radiation amplitude at the undulator segment end $A(L)$ is represented in the polar plot as the distance between the initial and final points of the vector. The radiation intensity is proportional to $|A|^2$.

Three examples are shown in Fig. 1. Consider the scenario with a long line of ideal undulators and ideal particle beam energy, followed by two undulators separated by a long break section with three periods of phase slippage in the drift

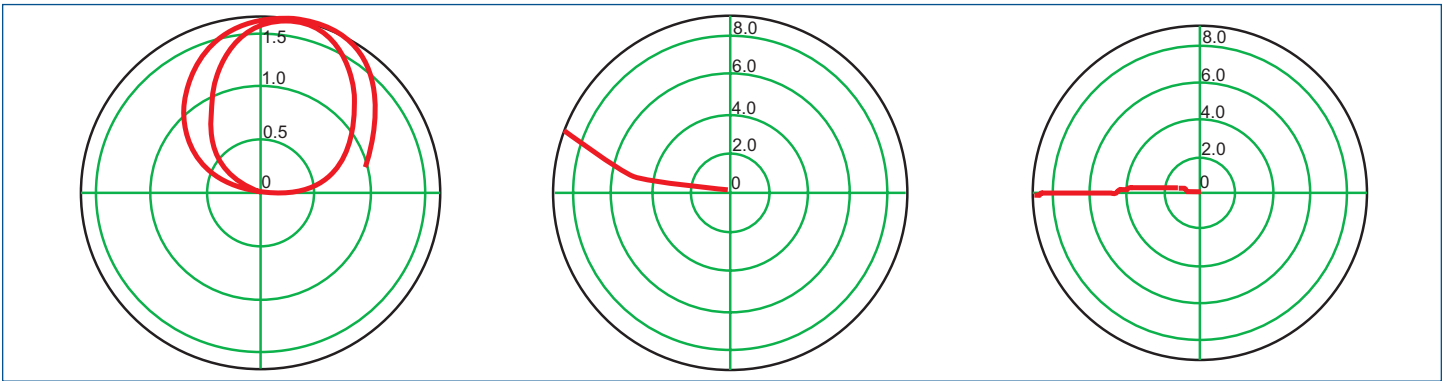


Fig. 1. Left: After passing through a line of undulator segments where the undulators are perfect and the beam energy is ideal, the beam loses 0.4% of its energy prior to passage through two undulators that are separated by a drift space with three periods of phase slippage. The magnitude and complex phase angle of $|A|$ are plotted in polar coordinates at points along the two undulators. The radiation amplitude from those two undulators, represented by the length of a vector from the beginning to the end of the trace, is very small. Middle: The K_{eff} of the two undulators has been adjusted so that the spontaneous radiation is at the nominal wavelength, despite the beam energy loss. The lines through the undulators are straight, and the kink between them indicates a phasing error in the drift space. The radiation amplitude from these undulators is now 98.2% of ideal. Right: The K_{eff} of the two undulators has been adjusted to maximize the overall $|A|$. The K_{eff} through the undulators is not perfect, as can be seen by the slight curvature, but the overall $|A|$ is 99.1% of ideal. The radial scale for the leftmost figure is different from that for the other two.

space. Also, assume that the particle beam energy is 0.4% too low through those two undulators, because of a beam energy loss. Figure 1 (left) shows a polar plot of the complex amplitude of radiation through those two undulators and the drift space between them. The line curvature is so extreme that the radiation intensity from the two undulators is sharply reduced. The performance of the undulator is seen to be very sensitive to the particle energy. Figure 1(middle) shows what happens when the magnetic field strength of the two undulators is adjusted so that the spontaneous radiation is at the nominal wavelength, despite the reduced beam energy. The traces through the two undulators are straight, as they should be, but now there is a kink between the two undulators, showing that the drift space is not the right length for the reduced beam energy. This type of plot can clearly show and help diagnose the origin of an effect that

only impacts the final radiation amplitude by 2% of the ideal value. An additional improvement can be obtained if, instead of adjusting K_{eff} to match the spontaneous radiation to the nominal wavelength, K_{eff} is adjusted to maximize the overall $|A|$, as in Fig. 1 (right). As shown by the curvature in the traces through the undulators, there is a small phase slippage in the undulator segments, but the net effect is that the radiation amplitude is 99.1% of ideal. *Contact: I. Vasserman (isaac@aps.anl.gov) and R. Dejus (dejus@aps.anl.gov)*

- [1] I. Vasserman, R. Dejus, P. Den Hartog, E. Moog, S. Sasaki, E. Trakhtenberg, M. White, in *Proceedings of the 26th International Free Electron Conference*, August 29-September 3, 2004, Trieste, Italy.
- [2] E. Gluskin et al., *Nucl. Instrum. Methods A* **475**, 323 (2001).

“Stress” continued from page 150

- 1) Maximum temperature on Glidcop <300°C to prevent material creep.
- 2) Maximum temperature on the cooling wall is less than the water boiling temperature at the channel pressure. The typical pressure after going through two-thirds of the length of a component is 60 psig, and the corresponding boiling temperature at 60 psig is 153°C.
- 3) Maximum von Mises stress is less than the yield stress of Glidcop at room temperature (300 MPa to ~450 MPa, depending on the Glidcop stock size).

Efforts are under way to reexamine these criteria. A committee has been formed to re-evaluate the failure criteria, especially the stress limit. Tests are also under way in collaboration with the European Synchrotron Radiation Facility, to obtain operational fatigue strength data.

Conclusion. On the basis of existing failure criteria that have been used at the APS for more than 10 years, the maximum beam current presently allowed for each type of front end is as follows:

- 1) FE v1.2u can operate with one undulator A at $k = 2.62$ (11 mm gap) and at a maximum current of 130 mA.
- 2) The photon shutters (P2-30) of FE v1.5 can operate at more than 200 mA, but the masks can only operate at up to 130 mA. Overall, the FE v1.5 can operate with one undulator A at $k = 2.62$ at 130 mA.
- 3) 3-ID can operate at 115 mA.
- 4) 4-ID with undulator A at $k = 3.175$ (9.5 mm gap) and CPU can only operate at 100 mA. Gap restrictions on undulator A are necessary at higher current.
- 5) Water flow trip points should be set so the h value is greater than or equal to $0.01 \text{ W/mm}^2 \text{ } ^\circ\text{C}$.

Contact: Y. Jaski (jaskiy@aps.anl.gov)

SUPERCONDUCTING UNDULATOR R&D

INTRODUCTION

A planar superconducting undulator (SCU) with a period of 15 mm has been designed to achieve a peak field of 0.8 T on the beam axis with an 8 mm pole gap and a current density of 1 kA/mm² in the NbTi superconducting (SC) coil. The tunable range of the undulator's photon energy in the APS 7-GeV storage ring would be from 19 to 28 keV for the first harmonic. Further extensions of this energy range to higher harmonics would require a high field quality in the SCU. Because of the high current density in the coil and low Cu/SC ratio, quenches propagate rapidly even at current densities well below the intended design value or critical current density. However, two R&D short sections were fully "trained" by means of quenches to reach the critical currents so as to measure the stability margins.

DESIGN

The peak field in the midplane of the undulator, B_o , and the coil maximum field, B_m , are calculated for an undulator period of 15 mm and a coil cross section of 4.32 mm × 3.89 mm deep. In Fig. 1, for pole gaps of 6.0 mm, 7.5 mm, and 8.0 mm, B_o and B_m are plotted as functions of the current density j in the coil. As seen in the figure, B_m differs by less than 1% for the three values of the gap. The peak field, on the other hand, depends significantly on the gap. The critical current density, $j_c(\text{coil})$, for the NbTi SC wire is about 1.43 kA/mm² at $B_m = 3.6$ T, which limits the highest peak fields to 1.5 T and 1.0 T for pole gaps of 6.0 mm and 8.0 mm, respectively.

FABRICATION AND TESTS

A core for a 12-period upper-half SCU ($\lambda = 15$ mm) was machined from 1008 low-carbon steel. Formvar-insulated rec-

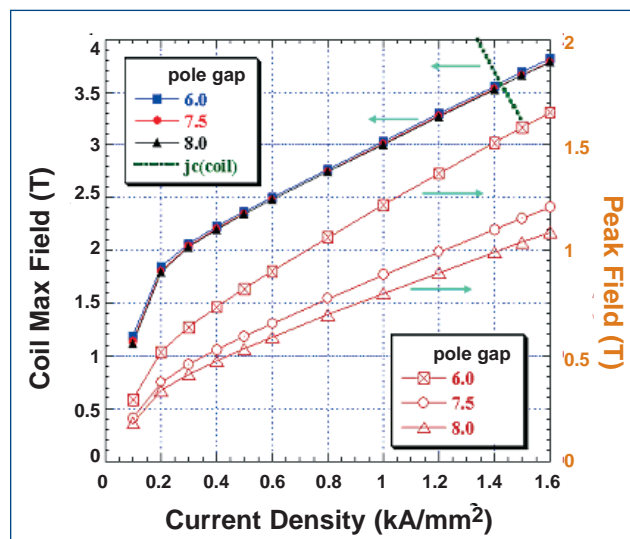


Fig. 1. For an undulator period of 15 mm, the maximum field in the coil, B_m , (left axis) and the on-axis peak field, B_o , (right axis) are calculated as functions of the average current density in the coil.

tangular NbTi SC wire with dimensions of 1.05 mm × 0.77 mm was used for the 20-turn coil in each groove. Another upper-half SCU ($\lambda = 14.5$ mm) with 22 periods was fabricated. The grooves for the cross-over winding in the core were modified from the 12-period one. Figure 2 shows the flat side of the magnetic poles and coil (a) and the outer side of the cross-over windings (b). The core is designed to wind the coil first in one direction into every other groove for the full length. The alter-

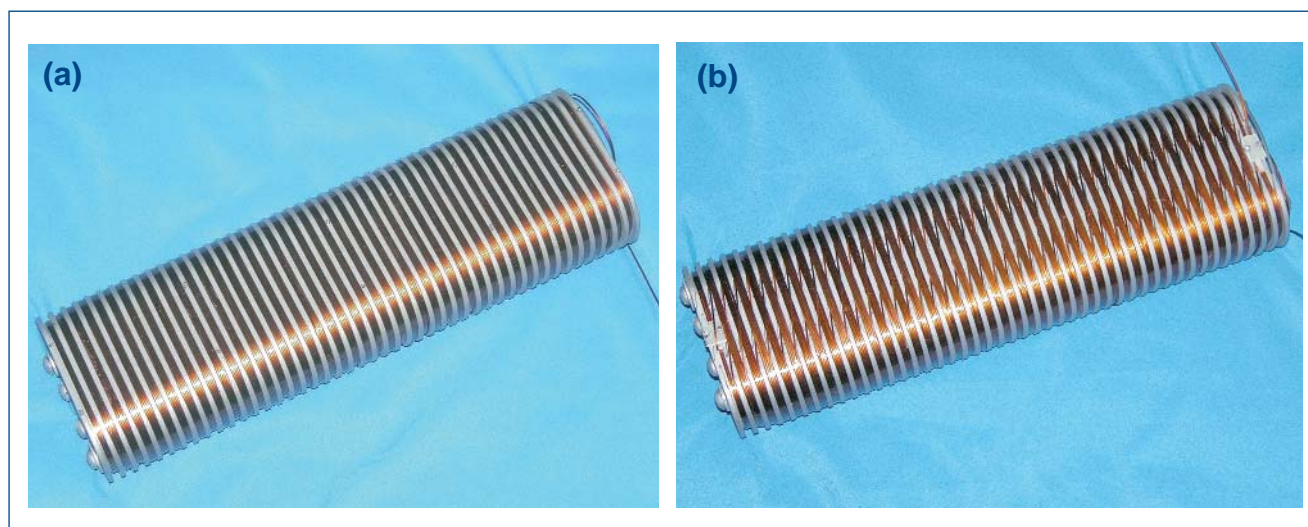


Fig. 2. Coil winding on a core for the 22-period upper-half SCU. (a): Flat bottom side shows the magnetic poles and coil. (b): Top side shows the cross-over windings. After the full 20 turns are wound in one groove, the wire skips one groove before continuous winding. The alternate (skipped) grooves are subsequently wound in the opposite direction.

nate coil grooves are then similarly wound in the opposite direction.

The two upper-half SCUs ($\lambda = 15$ mm and 14.5 mm) were tested at 4.2K. The peak fields, B_0 , were measured using a Hall probe at a fixed distance from a magnetic pole face. The measured peak fields, as well as the calculated fields, are plotted in Fig. 3 after normalizing to a pole gap of 8.0 mm. Because of the differences in the g/λ ratio between the two, the peak fields for the 15-mm SCU are higher compared with those for the 14.5-mm SCU. When the 14.5-mm SCU was trained by means of quenches during the charging process, it nearly reached the critical current density.

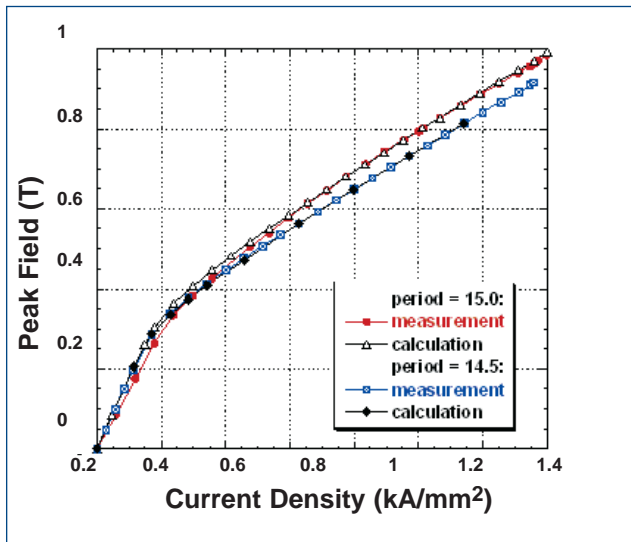


Fig. 3. The peak fields B_0 for the two upper-half SCUs are plotted for a pole gap of 8 mm.

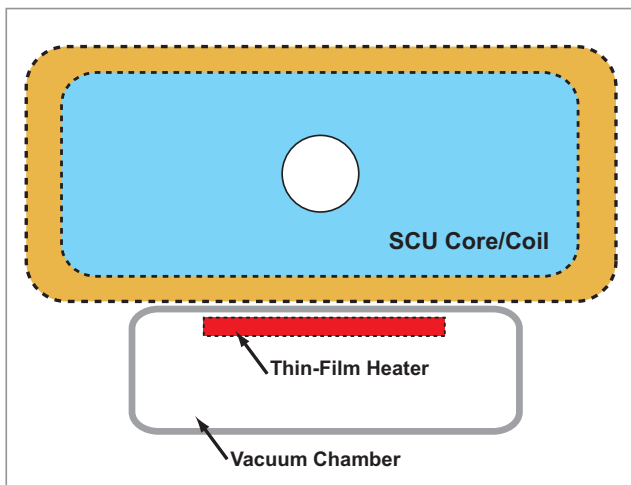


Fig. 4. A two-dimensional sketch of the setup for the heat-load tests in a plane perpendicular to the undulator axis. A thin-film heater was attached to the inner wall of a vacuum chamber, which was attached to the SCU core/coil flat face.

THERMAL STABILITY TESTS

Once the current density required to achieve the desired peak field is attained, the issue becomes one of stability at the operating current despite the heat load from the electron beam and elsewhere. A test setup for the heat load is sketched in Fig. 4. A thin-film heater is attached to the 0.6-mm-thick inner wall of a vacuum chamber that presses against the coil/pole face. The SCU axis was in the vertical direction during the tests in a pool-boiling LHe dewar at 4.2K.

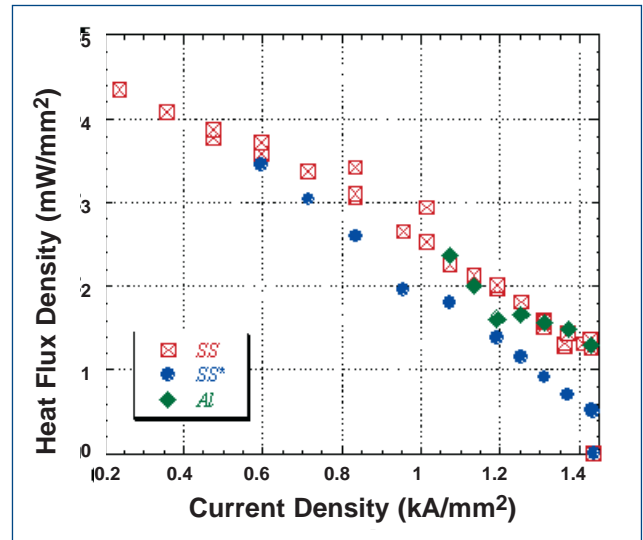
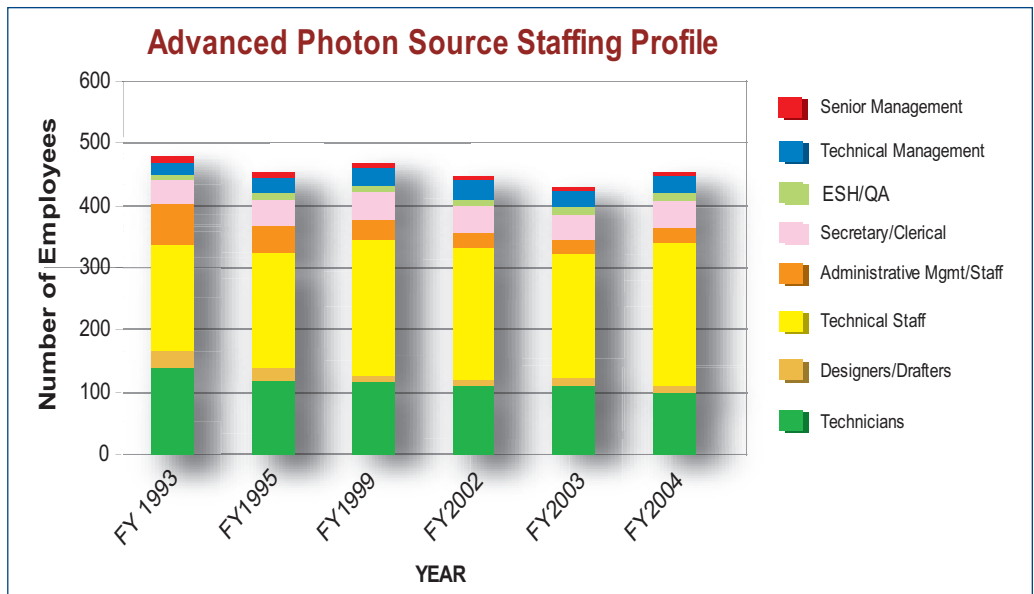
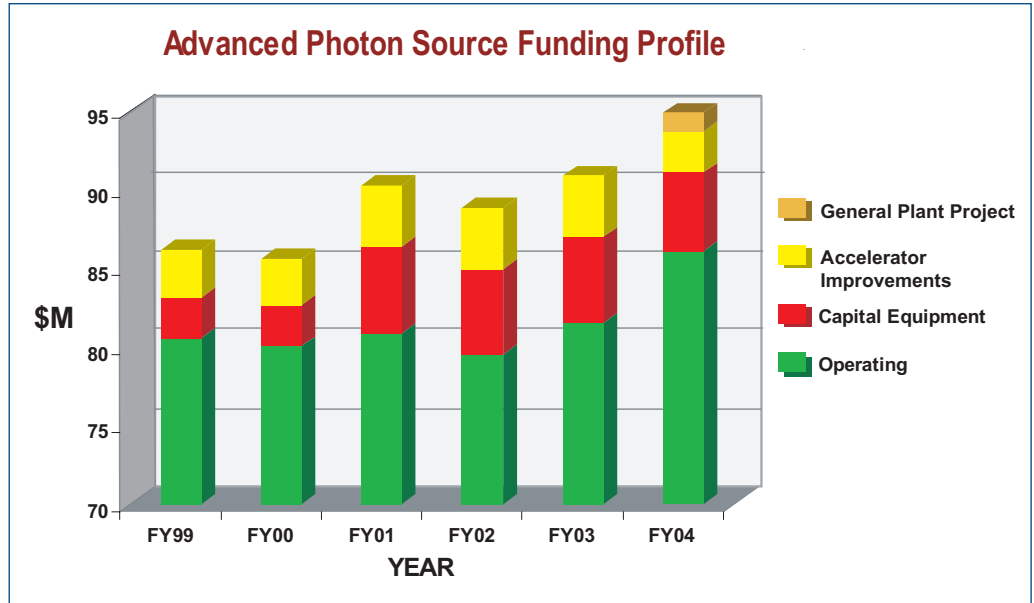


Fig. 5. Steady-state heat loads that quench the SC coil were measured as a function of the current density in 4.2K pool-boiling LHe. *SS*: the thin film heater was attached inside a stainless-steel chamber as depicted in Fig. 4. *SS**: same as *SS* except that a thin layer of vacuum grease was applied between the SCU and the chamber to exclude any LHe at this interface. *Al*: same as *SS* except that an aluminum chamber was used instead of a stainless-steel one.

The steady-state heat flux densities were measured when the SCU quenched. The measured data are plotted in Fig. 5 for three different cases, two with LHe at the interface and one without it. Since the temperature margin between 4.2K and the quench temperature should increase from zero at j_c to about 5K at zero current, the heat flux densities needed to quench the SCU increase as the current density is reduced. Near the critical current density of 1.43 kA/mm^2 the heat flux densities are about 1.3 mW/mm^2 and 0.5 mW/mm^2 for the cases of *SS* (or *Al*) and *SS**, respectively. When LHe is excluded at the interface (*SS**), the vacuum chamber and the interface conduct away a heat flux of 0.5 mW/mm^2 so that it never reaches the superconductor, as indicated by the heat flux near the critical current density at $0.998 j_c$. When LHe is allowed into the interface (*SS* and *Al*), an additional 0.8 mW/mm^2 of heat flux density is carried away, making a total of 1.3 mW/mm^2 . The results imply that LHe offers an efficient heat absorber for the SCU because of the relatively large latent heat of vaporization for LHe (2.6 mJ/mm^3).

Contact: S.H. Kim (shkim@aps.anl.gov)

APS DATA



ARGONNE NATIONAL LABORATORY

SCIENTIFIC USER FACILITIES

J. M. GIBSON

ASSOCIATE LABORATORY DIRECTOR

D. M. MILLS

Deputy Associate Laboratory Director

INTENSE PULSED NEUTRON SOURCE

R. G. TELLER

DIVISION DIRECTOR

J. W. RICHARDSON

Deputy Division Director

EXTERNAL REVIEW COMMITTEES

ACCELERATOR SAFETY REVIEW COMMITTEE
B. MICKLICH, CHAIR

THE U OF C REVIEW COMMITTEE
Y. PETROFF, CHAIR

ADVANCED PHOTON SOURCE

J. M. GIBSON

DIRECTOR

D. M. MILLS

Deputy Director

APS USER ORGANIZATION STEERING COMMITTEE
M. RIVERS, CHAIR
SCIENTIFIC ADVISORY COMMITTEE
M. ROWE, CHAIR
PARTNER USER COUNCIL
J. VICCIARO, CHAIR

Linac Coherent Light Source
S. MILTON
Project Director

Accelerator Systems Division

R. GERIG
Division Director

APS Operations Division

W. RUZICKA
Division Director

User Admin. and Support
S. STRASSER
Group Leader

Experimental Facilities Division

E. GLUSKIN

Division Director

M. BENO

Deputy Division Director

Mechanical Systems
J. NOONAN
Assoc. Div. Dir.

Electrical Systems
J. CARWARDINE
Assoc. Div. Dir.

APS Accelerator & User Operations
JOHN QUINTANA
Assoc. Div. Dir.

APS Site Operations
J. MACLEAN
Assoc. Div. Dir.

X-Ray Operation & Research
G. LONG
Assoc. Div. Dir.

Experimental Facilities Engineering
P. DEN HARTOG
Group Leader

Mechanical Engineering
S. SHARMA
Group Leader

Accelerator Physics
K. HARKAY
Group Leader

Power Systems
J. WANG
Group Leader

MCR Operations
G. BANKS
Group Leader

Operations Analysis
M. BORLAND
Group Leader

Information Technology
K. SIDOROWICZ
Group Leader

High Resolution X-Ray Scattering
W. STURHAHN
Group Leader

Magnetic Devices
E. MOOG
Group Leader

Survey & Alignment
H. FRIEDSAM
Group Leader

Safety Interlocks
G. MARKOVICH
Group Leader

Diagnostics
O. SINGH
Group Leader

Experiment Operations Support
P. FERNANDEZ
Group Leader

Information Solutions
S. LEATHERMAN
Group Leader

Polarization Studies
G. SRAJER
Group Leader

Optics Fabrication & Metrology
A. MACRANDER
Group Leader

Vacuum Technology
G. GOEPPNER
Group Leader

Controls
N. ARNOLD
Group Leader

Beamline Control & Data Acquisition
J. MACLEAN
Group Leader

User ESH Support
B. GLAGOLA
Safety Officer

X-Ray Physics
D. HAEFFNER
Group Leader

Time-Resolved X-Ray Research
J. WANG
Group Leader

Design & Drafting
P. CHOI
Group Leader

RF
G. PILE
Group Leader

X-Ray Microscopy
B. LAI
Group Leader
(Acting)

BESSRC
M. BENO
Group Leader
(Acting)

SYNCHROTRON RELATED THEORY

As of April 4, 2005

APS BEAMLINE GUIDE

As of 2.17.05 Source: http://beam.aps.anl.gov/pls/apsweb/beamline_display_pkg.beamline_dir

(KEY: UA = 3.3 Undulator A; BM = Bending Magnet; CPU = Circularly Polarized Undulator; EMW = Elliptical Multipole Wiggler; GU = Accepting General Users)

Beamline	Sector	Discipline	Supported Techniques	Source	Status
1-BM	XOR	Physics, Materials Sci.	Powder diffraction Reflectivity	BM	Operational/GU
1-ID	XOR	Materials Sci., Physics	Phase contrast imaging High-energy x-ray scattering	UA	Operational/GU
2-BM	XOR	Physics, Life Sci.	Phase contrast imaging Tomography Microdiffraction General diffraction	BM	Operational/GU
2-ID-B	XOR	Physics	Microfluorescence Phase contrast imaging Coherent x-ray scattering	5.5 Undulator	Operational/GU
2-ID-D	XOR	Life Sci., Materials Sci.	Microfluorescence Microdiffraction Microprobe	UA	Operational/GU
2-ID-E	XOR	Life Sci., Enviro. Sci.	Microfluorescence Imaging: X-ray fluorescence	UA	Operational/GU
3-ID	XOR	Physics	Inelastic scattering Nuclear resonant scattering	2.7 Undulator	Operational/GU
4-ID-C	XOR	Physics, Materials Sci.	Photoemission electron microscopy Photoemission spectroscopy X-ray magnetic circular dichroism Magnetic x-ray scattering	CPU	Operational/GU
4-ID-D	XOR	Physics	X-ray magnetic circular dichroism Anomalous and resonant scattering Magnetic x-ray scattering Magnetic microscopy	UA	Operational/GU
5-BM-C	DND-CAT	Materials Sci., Polymer Sci.	Tomography Powder diffraction	BM	Operational/GU
5-BM-D	DND-CAT	Materials Sci., Polymer Sci.	X-ray absorption fine structure High-energy x-ray scattering Polymer	BM	Operational/GU
5-ID	DND-CAT	Materials Sci., Polymer Sci.	Macromolecular crystallography Powder diffraction Small-angle x-ray scattering X-ray optics development Polymer Inorganic crystallography	UA	Operational/GU
6-ID	MU-CAT	Materials Sci.	Liquid scattering Magnetic x-ray scattering Powder diffraction Surface diffraction	UA	Operational/GU
6-ID-D	MU-CAT	Materials Sci.	High-energy x-ray scattering Magnetic x-ray scattering Powder diffraction Time-resolved x-ray scattering	UA	Operational/GU
7-ID	MHATT/XOR	Materials Sci.	Time-resolved x-ray scattering Microprobe General diffraction Ultrafast laser excitations	UA	Operational/GU
8-BM	NE-CAT	Life Sci.	Macromolecular crystallography Multiwavelength anomalous dispersion	BM	Operational

(KEY: UA = 3.3 Undulator A; BM = Bending Magnet; CPU = Circularly Polarized Undulator; EMW = Elliptical Multipole Wiggler; GU = Accepting General Users)

Beamline	Sector	Discipline	Supported Techniques	Source	Status
8-ID	IMMY/XOR	Materials Sci.	Coherent x-ray scattering Small-angle x-ray scattering Time-resolved x-ray scattering Wide-angle x-ray scattering	UA	Operational/GU
9-BM	CMC-CAT	Materials Sci.	X-ray absorption fine structure Surface diffraction General diffraction	BM	Operational/GU
9-ID	CMC-CAT	Materials Sci.	Grazing incidence diffraction & reflectometry Liquid scattering Small-angle x-ray scattering General diffraction	UA	Operational/GU
10-ID	MR-CAT	Materials Sci., Enviro. Sci.	X-ray absorption fine structure microscopy X-ray absorption fine structure Diffraction anomalous fine structure	UA	Operational/GU
11-ID-B	BESSRC/XOR	Materials Sci., GeoSci.	High-energy x-ray scattering	EMW	Operational/GU
11-ID-C	BESSRC/XOR	Materials Sci., GeoSci.	High-energy x-ray scattering	EMW	Operational/GU
11-ID-D	BESSRC/XOR	Materials Sci., GeoSci.	X-ray absorption fine structure General diffraction	EMW	Operational/GU
12-BM	BESSRC/XOR	Materials Sci., GeoSci.	X-ray absorption fine structure Powder diffraction General diffraction	BM	Operational/GU
12-ID	BESSRC/XOR	Materials Sci., Physics	Intensity fluctuation spectroscopy Photoemission spectroscopy Small-angle x-ray scattering	UA	Operational/GU
13-BM	GSECARS-CAT	GeoSci., Enviro. Sci.	Tomography X-ray absorption fine structure Diamond anvil cell Multi anvil press	BM	Operational/GU
13-ID	GSECARS-CAT	GeoSci., Enviro. Sci.	X-ray absorption fine structure Microdiffraction Static & time-dependent surface scattering Microprobe Diamond anvil cell Multi-anvil press	UA	Operational/GU
14-BM-C	BioCARS-CAT	Life Sci.	Macromolecular crystallography Time-resolved x-ray scattering	BM	Operational/GU
14-BM-D	BioCARS-CAT	Life Sci.	Macromolecular crystallography Microdiffraction Multiwavelength anomalous dispersion Time-resolved x-ray scattering	BM	Operational/GU
14-ID	BioCARS-CAT	Life Sci.	Macromolecular crystallography Multiwavelength anomalous dispersion Time-resolved x-ray scattering Laue crystallography	UA	Operational/GU
15-ID	ChemMatCARS-CAT	Materials Sci., Chemistry	Anomalous and resonant scattering Liquid scattering Time-resolved x-ray scattering Wide-angle x-ray scattering Microcrystallography Liquid and solid surface scattering	UA	Operational/GU
16-BM	HP-CAT	Materials Sci., GeoSci.	Powder diffraction Single-crystal diffraction	BM	Construction

(KEY: UA = 3.3 Undulator A; BM = Bending Magnet; CPU = Circularly Polarized Undulator; EMW = Elliptical Multipole Wiggler; GU = Accepting General Users)

Beamline	Sector	Discipline	Supported Techniques	Source	Status
16-ID-B	HP-CAT	Materials Sci., GeoSci.	X-ray absorption fine structure Compton scattering Inelastic scattering Microdiffraction Nuclear resonant scattering Powder diffraction Diamond anvil cell	UA	Operational/GU
16-ID-D	HP-CAT	Materials Sci., GeoSci.	Nuclear forward scattering Nuclear resonant inelastic x-ray scattering Inelastic x-ray scattering X-ray Raman scattering X-ray emission spectroscopy Resonant inelastic x-ray scattering	UA	Operational
17-BM	IMCA-CAT	Life Sci.	Macromolecular crystallography Multiwavelength anomalous dispersion	BM	Commissioning
17-ID	IMCA-CAT	Life Sci.	Macromolecular crystallography Multiwavelength anomalous dispersion	UA	Operational/GU
18-ID	Bio-CAT	Life Sci.	X-ray absorption fine structure Fluorescence spectroscopy Small-angle x-ray scattering Time-resolved x-ray scattering General diffraction	UA	Operational/GU
19-BM	SBC-CAT	Life Sci.	Macromolecular crystallography Multiwavelength anomalous dispersion	BM	Operational/GU
19-ID	SBC-CAT	Life Sci.	Macromolecular crystallography Multiwavelength anomalous dispersion	UA	Operational/GU
20-BM	PNC/XOR	Materials Sci., Enviro. Sci.	X-ray absorption fine structure Diffraction anomalous fine structure General diffraction	BM	Operational/GU
20-ID	PNC/XOR	Materials Sci., Enviro. Sci.	X-ray absorption fine structure microscopy Microfluorescence X-ray absorption fine structure Diffraction anomalous fine structure Microprobe General diffraction	UA	Operational/GU
22-BM	SER-CAT	Life Sci.	Macromolecular crystallography	BM	Commissioning
22-ID	SER-CAT	Life Sci.	Macromolecular crystallography Multiwavelength anomalous dispersion	UA	Operational/GU
31-ID	SGX-CAT	Life Sci.	Macromolecular crystallography	UA	Operational/GU
32-ID	COM-CAT	Materials Sci.	X-ray absorption fine structure Powder diffraction Single-crystal diffraction Small-angle x-ray scattering	UA	Operational
33-BM	UNI-CAT	Materials Sci.	Topography Powder diffraction Single-crystal diffraction General diffraction	BM	Operational/GU
33-ID	UNI-CAT	Materials Sci.	Anomalous and resonant scattering Inelastic scattering Small-angle x-ray scattering Surface diffraction Ultras-small-angle x-ray scattering General diffraction	UA	Operational/GU
34-ID	UNI-CAT	Materials Sci.	Coherent x-ray scattering Microdiffraction Microprobe	UA	Operational/GU

APS TECHNIQUES DIRECTORY

As of 2.17.05 Source: http://beam.aps.anl.gov/pls/apsweb/beamline_display_pkg.technique_dir

Technique	Beamline
Absorption/Spectroscopy	
Fluorescence spectroscopy	18-ID
Intensity fluctuation spectroscopy	12-ID, 7-ID
Photoemission spectroscopy	4-ID-C
X-ray absorption fine structure	10-ID, 11-ID-D, 12-BM, 13-BM, 13-ID, 16-ID-B, 18-ID, 20-BM, 20-ID, 5-BM-D, 9-BM
X-ray magnetic circular dichroism	4-ID-C, 4-ID-D
High Pressure	
Diamond Anvil Cell	13-BM, 13-ID, 16-ID-B
Multi-Anvil Press	13-BM, 13-ID
Imaging	
X-ray absorption fine structure microscopy	10-ID, 20-ID
Microfluorescence	2-ID-B, 2-ID-D, 2-ID-E, 20-ID
Microprobe	13-ID, 2-ID-D, 20-ID, 34-ID, 7-ID
Phase contrast imaging	1-ID, 2-BM, 2-ID-B
Photoemission electron microscopy	4-ID-C
Tomography	13-BM, 2-BM, 5-BM-C
Topography	33-BM
Protein Crystallography	
Macromolecular crystallography	14-BM-C, 14-BM-D, 14-ID, 17-ID, 19-BM, 19-ID, 22-ID, 31-ID, 5-ID
Multiwavelength anomalous dispersion	14-BM-D, 14-ID, 17-ID, 19-BM, 19-ID, 22-ID
Scattering	
Anomalous and resonant scattering	15-ID, 33-ID, 4-ID-D
Coherent x-ray scattering	2-ID-B, 34-ID, 8-ID
Compton Scattering	16-ID-B
Diffraction anomalous fine structure	10-ID, 20-BM, 20-ID
General diffraction	11-ID-D, 12-BM, 2-BM, 13-BM, 2-BM, 20-BM, 20-ID, 33-BM, 33-ID, 7-ID
High-energy x-ray scattering	1-ID, 11-ID-B, 11-ID-C, 5-BM-D, 6-ID-D
Inelastic scattering	13-ID, 16-ID-B, 3-ID, 33-ID
Liquid scattering	15-ID, 6-ID, 9-ID
Magnetic x-ray scattering	4-ID-C, 4-ID-D, 6-ID, 6-ID-D
Microdiffraction	13-ID, 14-BM-D, 16-ID-B, 2-BM, 2-ID-D, 34-ID
Nuclear resonant scattering	16-ID-B, 3-ID
Polymer	5-BM-D, 5-ID
Powder diffraction	1-BM, 12-BM, 16-ID-B, 33-BM, 5-BM-C, 5-ID, 6-ID, 6-ID-D
Reflectivity	1-BM
Small-angle x-ray scattering	12-ID, 18-ID, 33-ID, 5-ID, 8-ID, 9-ID
Surface diffraction	33-ID, 6-ID
Time-resolved x-ray scattering	14-BM-C, 14-BM-D, 14-ID, 15-ID, 18-ID, 6-ID-D, 7-ID, 8-ID
Ultra-small-angle x-ray scattering	33-ID
Wide-angle x-ray scattering	15-ID, 8-ID
Miscellaneous	
X-ray optics development	5-ID

APS USER COMMITTEES

2004 APS SCIENTIFIC ADVISORY COMMITTEE

William A. Bassett

*Director, Mineral Physics Laboratory
Cornell University*

Paul M. Bertsch

*Director, Savannah River Ecological Laboratory;
Technical Director, Advanced Analytical Center for
Environmental Sciences
University of Georgia*

Howard Birnbaum

*Director Emeritus, Materials Research Laboratory,
University of Illinois at Urbana-Champaign*

John R. Helliwell

*Department of Chemistry
University of Manchester*

Wayne A. Hendrickson

*Department of Biochemistry and Molecular Biophysics
Columbia University*

Peter Ingram

*Department of Pathology
Duke University Medical Center*

Gerhard T. Materlik

*Director, Diamond Light Source
Rutherford Appleton Laboratory*

Denis B. McWhan

*Associate Laboratory Director (Retired)
Brookhaven National Laboratory*

James R. Norris

*Department of Chemistry
The University of Chicago*

Paul S. Peercy

*College of Engineering
University of Wisconsin-Madison*

Michael J. Rowe (*Chair*)

*Director [Retired], Center for Neutron Research,
National Institute of Standards and Technology*

Joachim Stöhr

*Professor and Deputy Director, Stanford Accelerator Center,
Stanford Synchrotron Radiation Laboratory
Stanford University*

Kathleen Taylor

*Director (Retired), Materials and Processes Laboratory
General Motors Research & Development
and Processing Center*

Pierre E. Wiltzius

*Director, Beckman Institute for Advanced Science
and Technology, and Professor, Departments of
Materials Science & Engineering and Physics
University of Illinois at Urbana-Champaign*

APS USERS ORGANIZATION STEERING COMMITTEE

Mark L. Rivers (*The University of Chicago*), *Chair*

Carol Thompson (*Northern Illinois University*), *Vice-Chair*

Keith E. Brister (*The University of Chicago*)

Malcolm S. Capel (*Cornell University*)

Julie O. Cross (*Argonne National Laboratory*)

Stephan L. Ginell (*Argonne National Laboratory*)

Thomas Gog (*Argonne National Laboratory*)

Tim J. Graber (*The University of Chicago*)

Gene E. Ice (*Oak Ridge National Laboratory*)

Ward W. Smith (*Argonne National Laboratory*)

Ex-officio: Stephen M. Durbin (*Purdue University*)

Source: http://www.aps.anl.gov/About/Committees/APS_Users_Organization/Members/index.html

PARTNER USER COUNCIL

Dean R. Haeffner (*sector 1, Argonne National Laboratory*)

Barry P. Lai (*sector 2, Argonne National Laboratory*)

Wolfgang Sturhahn (*sector 3, Argonne National Laboratory*)

George Srajer (*sector 4, Argonne National Laboratory*)

Denis T. Keane (*sector 5, Northwestern University*)

Douglas S. Robinson (*sector 6, Iowa State University*)

Roy Clarke (*sector 7, University of Michigan*)

Simon G.J. Mochrie (*sector 8, Yale University*)

J. Kent Blasie (*sector 9, University of Pennsylvania*)

Bruce A. Bunker (*sector 10, University of Notre Dame*)

Mark A. Beno (*sector 11, Argonne National Laboratory*)

Randall E. Winans (*sector 12, Argonne National Laboratory*)

Mark L. Rivers (*sector 13, The University of Chicago*)

Keith Moffat (*sector 14, The University of Chicago*)

P. James Viccaro (*sector 15, The University of Chicago*) *Chair*

David Mao (*sector 16, Carnegie Institution of Washington*)

Lisa J. Keefe (*sector 17, The University of Chicago*)

Thomas C. Irving (*sector 18, Illinois Institute of Technology*)

Andrzej Joachimiak (*sector 18, Argonne National Laboratory*)

Edward A. Stern (*sector 20, University of Washington*)

Wayne F. Anderson (*sector 21, Northwestern University*)

John J. Chrzas (*sector 22, University of Georgia*)

Robert F. Fischetti (*sector 23, Argonne National Laboratory*)

Malcolm Capel (*sector 24, Cornell University*)

John P. Hill (*sector 30, Brookhaven National Laboratory*)

Kevin L. D'Amico (*sector 31, Structural GenomiX, Inc.*)

Paul Zschack (*sector 33-34,
University of Illinois at Urbana-Champaign*)

Source: http://www.aps.anl.gov/About/Committees/Partner_Users_Council/Members/puc_list.htm

PROPOSAL REVIEW PANELS

HIGH PRESSURE

Guoyin Shen, *Chair*
Jay Bass
Kurt Leinenweber
Surendra Saxena
Viktor Struzhkin/Wilfried Schildkamp
Sarvjit Shastri

INSTRUMENTATION

Eric Dufresne, *Chair*
Peter Eng
Sarvjit Shastri

IMAGING/MICROBEAM

Mark Rivers, *Chair*
George Cody
Barry Lai
Al Thompson

MACROMOLECULAR CRYSTALLOGRAPHY

Karl Volz, *Chair*
Craig Ogata
Amy Rosenzweig

SCATTERING/APPLIED MATERIALS

Paul Fuoss, *Chair*
I. Cev Noyan
Carol Thompson
Robert A. Winholtz

SCATTERING/CONDENSED MATTER

Joel Brock, *Chair*
Paul Evans
John Hill
Ben Larson
Young S. Lee
Haskell Taub

SCATTERING/CHEMISTRY/BIOLOGY/ ENVIRONMENTAL SCIENCE

Neil Sturchio, *Chair*
Fred Stevens
David Tiede
Angus Wilkinson

SMALL-ANGLE SCATTERING

Larry Lurio, *Chair*
Andrew Allen
Jyotsana Lal
David Londono
Pappannan Thiyagarajan
Hiro Tsuruta

SPECTROSCOPY (EXAFS)

Joe Woicik, *Chair*
Simon Bare
Lin X. Chen
Lisa M. Miller
Matt Newville

Source:

http://www.aps.anl.gov/About/Committees/Proposal_Review_Panel/index.html

BEAM TIME ALLOCATION COMMITTEES

MACROMOLECULAR CRYSTALLOGRAPHY

Keith Brister
Robert Fischetti
Stephan Ginell
Andy Howard
Zdzislaw Wawrzak

ALL OTHER SCIENCE

Jon Tischler
Steve Heald
Brian Stephenson
Denis Keane

Source:

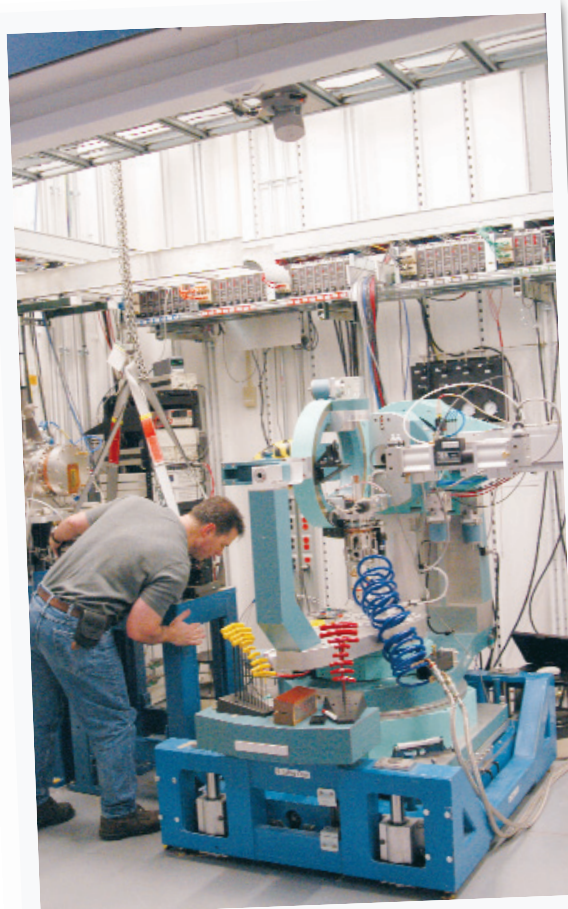
http://www.aps.anl.gov/About/Committees/Beam_Time_Allocation_Committees/index.html

APS INTERCAT

TECHNICAL WORKING GROUP

Eric Dufresne, *Co-Chair*
Reinhard Pahl, *Co-Chair*

Source: <http://www.aps.anl.gov/cats/twg/>



APS PUBLICATIONS—2004*

*As of 2.25.05. For an up-to-date listing, see the searchable, publicly available database of all APS-related scientific and technical publications from APS users and personnel at:

http://beam.aps.anl.gov/pls/apsweb/pub_v2_0006.review_start_page

EXPERIMENTAL RESULTS: JOURNAL ARTICLES

P. Abbamonte, K. D. Finkelstein, M. D. Collins, S. M. Gruner, "Imaging Density Disturbances in Water with a 41.3-Attosecond Time Resolution," *Phys. Rev. Lett.* 92 (23), June, 237401-1-237401-4 (2004).

Jan Abendroth, Michael Bagdasarian, Maria Sandkvist, Wim G. J. Hol, "The Structure of the Cytoplasmic Domain of EpsL, An Inner Membrane Component of the Type II Secretion System of *Vibrio cholerae*: An Unusual Member of the Actin-like ATPase Superfamily," *J. Mol. Biol.* 344 (3), November, 619-633 (2004).

Sugat Abeygunaratne, Antal Jakli, Goetz Milkereit, Hans Sawade, Volkmar Vill, "Antiferroelectric ordering of amphiphilic glycolipids in bent-core liquid crystals," *Phys. Rev. E* 69, 021703-1-021703-6 (2004).

Sara L. Adamski-Werner, Satheesh K. Palaninathan, James C. Sacchettini, Jeffery W. Kelly, "Diflunisal Analogues Stabilize the Native State of Transthyretin. Potent Inhibition of Amyloidogenesis," *J. Med. Chem.* 47, 355-374 (2004).

Iana Agmon, Maya Amit, Tamar Auerbach, Anat Bashan, David Baram, Heike Bartels, Rita Berisio, Inbal Greenberg, Joerg Harms, Harly A. S. Hansen, Maggie Kessler, Erez Pyetan, Frank Schluenzen, Assa Sittner, Ada Yonath, Raz Zarivach, "Ribosomal crystallography: a flexible nucleotide anchoring tRNA translocation, facilitates peptide-bond formation, chirality discrimination and antibiotics synergism," *FEBS Lett.* 567 (1), June, 20-26 (2004).

F. S. Aguirre-Tostado, A. Herrera-Gomez, J. C. Woicik, R. Droopad, Z. Yu, D. G. Schlom, J. Karapetrova, P. Zschack, P. Pianetta, "Displacive phase transition in SrTiO₃ thin films grown on Si(001)," *J. Vac. Sci. Technol.* 22 (4), July, 1356-1360 (2004).

M. J. Ahrens, L. E. Sinks, B. Rybtchinski, W. Liu, B. A. Jones, J. M. Giaimo, A. V. Gusev, A. J. Goshe, D. M. Tiede, M. R. Wasielewski, "Self-Assembly of Supramolecular Light-Harvesting Arrays from Covalent Multi-Chromophore Perylene-3,4:9,10-bis(dicarboximide) Building Blocks," *J. Am. Chem. Soc.* 126, June, 8284-8294 (2004).

Maher Al-Ayyoubi, Peter G. W. Gettins, Karl Volz, "Crystal Structure of Human Maspin, a Serpin with Antitumor Properties," *J. Biol. Chem.* 279 (53), December, 55540-55544 (2004).

H. A. Al-Khayat, L. Hudson, M. K. Reedy, T.C. Irving, J. M. Squire, "Modelling oriented macromolecular assemblies from low-angle x-ray fibre diffraction data with the program MOVIE: Insect flight muscle as an example," *Fibre Diffraction Rev.* 12, 50-60 (2004).

Mayssam H. Ali, Ezra Peisach, Karen N. Allen, Barbara Imperiali, "X-ray structure analysis of a designed oligomeric miniprotein reveals a discrete quaternary architecture," *Proc. Natl. Acad. Sci.* 101 (33), 12183-12188 (2004).

R. W. Alkire, R. Schuessler, F. J. Rotella, J. D. Gonczy, G. Rosenbaum, "Re-thinking the role of the beamstop at a synchrotron-based protein crystallography beamline," *J. Appl. Crystallogr.* 37 (5), 836-840 (2004).

R. D. Allan, J. Greenwood, T. Hambley, D. Hibbs, J. Hanrahan, S. Itani, H. Tran, P. Turner, "Studies on Pyridazine Azide Cyclisation Reactions," *Org. Biomol. Chem.* 2, 1782-1788 (2004).

John S. Allingham, Junichi Tanaka, Gerard Marriott, Ivan Rayment, "Absolute Stereochemistry of Ulupalide A," *Org. Lett.* 6 (4), 597-599 (2004).

P. M. Almond, R. E. Sykora, S. Skanthakumar, L. Soderholm, T. E. Albrecht-Schmitt, "Hydrothermal Synthesis, Structure, and Magnetic Properties of the Mixed-Valent Np(IV)/Np(V) Selenite Np(NpO₂)₂(SeO₃)₃," *Inorg. Chem.* 43 (3), January, 958-963 (2004).

G. M. Amulele, M. H. Manghnani, B. Li, D. J. H. Errandonea, M. Somayazulu, Y. Meng, "High pressure ultrasonic and x-ray studies on monolithic SiC composite," *J. Appl. Phys.* 95 (4), February, 1806-1810 (2004).

R. Anand, P. A. Kaminski, S. E. Ealick, "Structures of Purine 2'-Deoxyribosyltransferase, Substrate Complexes, and the Ribosylated Enzyme Intermediate at 2.0 Å Resolution," *Biochemistry-US* 43 (9), 2384-2393 (2004).

R. Anand, A.A. Hoskins, E.M. Bennett, M.D. Sintchak, J. Stubbe, S.E. Ealick, "A Model for the *Bacillus subtilis* Formylglycinamide Ribonucleotide Amidotransferase Multiprotein Complex," *Biochemistry-US* 43, 10343-10352 (2004).

M. Anastasio, D. Shi, F. De Carlo, X. Pan, "Analytic image reconstruction in local phase-contrast tomography," *Phys. Med. Biol.* 49, January, 121-144 (2004).

S. Anderson, S. Crosson, K. Moffat, "Short hydrogen bonds in photoactive yellow protein," *Acta Crystallogr. D* 60, 1008-1016 (2004).

S. Anderson, V. Srajer, R. Pahl, S. Rajagopal, F. Schotte, P. Anfinrud, M. Wulff, K. Moffat, "Chromophore Conformation and the Evolution of Tertiary Structural Changes in Photoactive Yellow Protein," *Structure* 12 (6), 1039-1045 (2004).

Spencer Anderson, Vukica Srajer, Keith Moffat, "Structural Heterogeneity of Cryotrapped Intermediates in Photoactive Yellow Protein," *Photochem. Photobiol.* 80 (1), 7-14 (2004).

Brent A. Appleton, Arianna Loregian, David J. Filman, Donald M. Coen, James M. Hogle, "The Cytomegalovirus DNA Polymerase Subunit UL44 Forms a C Clamp-Shaped Dimer," *Molecular Cell* 15 (2), 233-244 (2004).

G. B. Armen, B. Kraessing, E. P. Kanter, J. C. Levin, S. H. Southworth, L. Young, "Spectator-electron behavior during cascade decay in krypton," *Phys. Rev. A* 69, June, 062710-1-062710-12 (2004).

- Kelly L. Arnett, Stephen C. Harrison, Don C. Wiley, "Crystal structure of a human CD3- ζ dimer in complex with a UCHT1 single-chain antibody fragment," *Proc. Natl. Acad. Sci.* 101 (46), 16268-16273 (2004).
- Benjamin J. Ash, Richard W. Siegel, Linda S. Schadler, "Mechanical Behavior of Alumina/Poly(methyl methacrylate) Nanocomposites," *Macromolecules* 37, 1358-1369 (2004).
- Shane Atwell, Jason M. Adams, John Badger, Michelle D. Buchanan, Ingeborg K. Feil, Karen J. Froning, Xia Gao, Jorg Hendle, Kevin Keegan, Barbara C. Leon, Hans J. Muller-Dieckmann, Vicki L. Nienaber, Brian W. Noland, Kai Post, K.R. Rajashankar, Aurora Ramos, Marijane Russell, Stephen K. Burley, Sean G. Buchanan, "A Novel Mode of Gleevec Binding Is Revealed by the Structure of Spleen Tyrosine Kinase," *J. Biol. Chem.* 279 (53), December, 55827-55832 (2004).
- Kerim Babaoglu, Jianjun Qi, Richard E. Lee, Stephen W. White, "Crystal Structure of 7,8-Dihydropoteroate Synthase from *Bacillus anthracis* Mechanism and Novel Inhibitor Design," *Structure* 12 (9), September, 1705-1717 (2004).
- Euiyoung Bae, George N. Phillips Jr., "Structures and Analysis of Highly Homologous Psychrophilic, Mesophilic, and Thermophilic Adenylate Kinases," *J. Biol. Chem.* 279 (27), 28202-28208 (2004).
- Ranjini Bandyopadhyay, Dennis Liang, Hasan Yardimci, David A. Sessoms, Matthew A. Borthwick, Simon G. J. Mochrie, James L. Harden, Robert L. Leheny, "Evolution of Particle-Scale Dynamics in an Aging Clay Suspension," *Phys. Rev. Lett.* 93 (22), November, 228302-1-288302-4 (2004).
- O. M. Barabash, J. A. Horton, S. S. Babu, J. M. Vitek, S. A. David, J. W. Park, G. E. Ice, R. I. Barabash, "Evolution of dislocation structure in the heat affected zone of a nickel-based single crystal," *J. Appl. Phys.* 96 (7), October, 3673-3679 (2004).
- R. I. Barabash, G. E. Ice, J. Pang, W. Liu, "Characterization of the Dislocation Density Tensor with White Beam Diffraction," *TMS Lett.* 1 (1), 13-14 (2004).
- L. Basile, Hawoong Hong, P. Czoschke, T.-C. Chiang, "X-ray studies of the growth of smooth Ag films on Ge(111) - c(2X8)," *Appl. Phys. Lett.* 84 (24), June, 4995-4997 (2004).
- Kevin P. Battaile, Tien V. Nguyen, Jerry Vockley, Jung-Ja P. Kim, "Structures of Isobutyryl-CoA Dehydrogenase and Enzyme-Product Complex: Comparison with Isovaleryl- and Short-Chain Acyl-coa Dehydrogenases," *J. Biol. Chem.* 279, 16526-16534 (2004).
- J. A. Bauer, E. M. Bennett, T. P. Begley, S. E. Ealick, "Three-dimensional structure of YaaE from *Bacillus subtilis*, a glutaminase implicated in pyridoxal-5'-phosphate biosynthesis," *J. Biol. Chem.* 279, 2704-2711 (2004).
- Richard H.G. Baxter, Nina Ponomarenko, Vukica Srajer, Reinhard Pahl, Keith Moffat, James R. Norris, "Time-resolved crystallographic studies of light-induced structural changes in the photosynthetic reaction center," *Proc. Natl. Acad. Sci.* 101 (16), 5982-5987 (2004).
- J. K. Bell, G. A. Grant, L. J. Banaszak, "Multiconformational states in phosphoglycerate dehydrogenase," *Biochemistry-US* 43 (12), March, 3450-3458 (2004).
- F. Berkovitch, E. Behshad, K.-H. Tang, E.A. Enns, P.A. Frey, C.L. Drennan, "A locking mechanism preventing radical damage in the absence of substrate, as revealed by the x-ray structure of lysine 5, 6-aminomutase," *Proc. Natl. Acad. Sci.* 101, 15870-15875 (2004).
- Ricardo A. Bernal, Susan Hafenstein, Raquel Esmeralda, Bentley A. Fane, Michael G. Rossmann, "The [phi] X174 Protein J Mediates DNA Packaging and Viral Attachment to Host Cells," *J. Mol. Biol.* 337 (5), 1109-1122 (2004).
- Matthew J. Bennett, Thayumanasamy Somasundaram, Michael Blaber, "An atomic resolution structure for human fibroblast growth factor 1," *Proteins* 57 (3), 626-634 (2004).
- Douglas A. Bernstein, Julie M. Eggington, Michael P. Killoran, Ana M. Mistic, Michael M. Cox, James L. Keck, "Crystal structure of the *Deinococcus radiodurans* single-stranded DNA-binding protein suggests a mechanism for coping with DNA damage," *Proc. Natl. Acad. Sci.* 101 (22), 8575-8580 (2004).
- M.F. Bertino, J.F. Hund, J. Sosa, G. Zhang, C. Sotiriou-Leventis, N. Leventis, A.T. Tokuhira, J. Terry, "High resolution patterning of silica aerogels," *J. Non-Cryst. Solids* 333, January, 108-110 (2004).
- S. Bhattacharjee, J. H. Booske, C. L. Kory, D. W. van der Weide, S. Limbach, S. Gallagher, J. Welter, M. R. Lopez, R. M. Gilgenbach, R. L. Ives, M. E. Read, R. Divan, D. C. Mancini, "Folded waveguide traveling wave tube sources for THz radiation," *IEEE T. Plasma Sci.* 32 (3, pt. 1), 1002-1014 (2004).
- Pradip K. Bhowmik, Haesook Han, James J. Cebe, Ivan K. Nedeltchev, Shin-Woong Kang, Satyendra Kumar, "Synthesis and Characterization of Poly(pyridinium salt)s with Organic Counterions Exhibiting Both Thermotropic Liquid-Crystalline and Light-Emitting Properties," *Macromolecules* 37, March, 2688-2694 (2004).
- S. J. L. Billinge, M. G. Kanatzidis, "Beyond crystallography: The study of disorder, nanocrystallinity and crystallographically challenged materials with pair distribution functions," *Chem. Comm.* 2004, 749-760 (2004).
- Julio Blanco, Roger A. Moore, Christopher R. Faehle, David M. Coea, Ronald E. Viola, "The role of substrate-binding groups in the mechanism of aspartate-[beta]-semialdehyde dehydrogenase," *Biological Crystallography* 60 (8), 1388-1395 (2004).
- Julio Blanco, Roger A. Moore, Christopher R. Faehle, Ronald E. Viola, "Critical catalytic functional groups in the mechanism of aspartate--semialdehyde dehydrogenase," *Biological Crystallography* 60 (10), 1808-1815 (2004).
- Jaroslawn Blaszczyk, Jianhua Gan, Joseph E. Tropea, Donald L. Court, David S. Waugh, Xinhua Ji, "Noncatalytic Assembly of Ribonuclease III with Double-Stranded RNA," *Structure* 12, March, 457-466 (2004).
- N. K. Blute, D. J. Brabander, H. F. Hemond, S. R. Sutton, M. G. Newville, M. L. Rivers, "Arsenic sequestration by ferric iron plaque on cattail roots," *Environ. Sci. Technol.* 38, November, 6074-6077 (2004).
- D.N. Bolon, R.A. Grant, T.A. Baker, R.T. Sauer, "Nucleotide-dependent Substrate Handoff from the SspB Adaptor to the AAA+ ClpXP Protease," *Mol. Cell* 16 (3), November, 343-350 (2004).
- C. H. Booth, S.-W. Han, S. Skanthakumar, J. L. Sarrao, "Lattice disorder and magnetism in f-electron intermetallics," *Physica B* 354 (1-4), December, 313-319 (2004).

- Robert A. Borgon, Clemens Vornrhein, Gerard Bricogne, Philippe R. J. Bois, Tina Izard, "Crystal Structure of Human Vinculin," *Structure* 12, 1189-1197 (2004).
- Ivan Bosanac, Haruka Yamazaki, Toru Matsu-ura, Takayuki Michikawa, Katsuhiko Mikoshiba, Mitsuhiko Ikura, "Crystal Structure of the Ligand Binding Suppressor Domain of Type 1 Inositol 1,4,5-Trisphosphate Receptor," *Mol. Cell* 17 (2), January, 193-203 (2004).
- Christopher A. Bottoms, Jonathan P. Schuermann, Sayeh Agah, Michael T. Henzl, John J. Tanner, "Crystal structure of rat [alpha]-parvalbumin at 1.05 Å resolution," *Protein Sci.* 13, 1724-1734 (2004).
- M. Boyanov, K. M. Kemner, T. Shibata, B. A. Bunker, "Local structure around Cr [superscript3+] in dilute acetate and perchlorate aqueous solutions," *J. Phys. Chem. A* 108, 5131-5138 (2004).
- A. Braun, F. E. Huggins, S. Seifert, J. Ilavsky, N. Shah, K. Kelly, A. Sarofim, G. P. Huffman, "Size-range analysis of diesel soot powders and pellets with ultra small angle X-ray scattering," *Combust. Flame* 137 (1/2), April, 63-72 (2004).
- Chad A. Brautigam, Yogarany Chelliah, Johann Deisenhofer, "Tetramerization and ATP Binding by a Protein Comprising the A, B, and C Domains of Rat Synapsin I," *J. Biol. Chem.* 279 (12), March, 11948-11956 (2004).
- Chad A. Brautigam, Barbara S. Smith, Zhiquan Ma, Maya Palnitkar, Diana R. Tomchick, Mischa Machius, Johann Deisenhofer, "Structure of the photolyase-like domain of cryptochrome 1 from *Arabidopsis thaliana*," *Proc. Natl. Acad. Sci.* 101 (33), August, 12142-12147 (2004).
- Luis G. Brieba, Brandt F. Eichman, Robert J. Kokoska, Sylvie Doublé, Tom A. Kunkel, Tom Ellenberger, "Structural basis for the dual coding potential of 8-oxoguanosine by a high-fidelity DNA polymerase," *EMBO J.* 23 (17), September, 3452-3461 (2004).
- D.E. Brown, T.S. Toellner, W. Sturhahn, E.E. Alp, M. Hu, R. Kruk, K. Rogacki, P.C. Canfield, "Partial phonon density of states of dysprosium and its compounds measured using inelastic nuclear resonant scattering," *Hyperfine Interact.* 153 (1-4), 17-24 (2004).
- J. Brownlee, K. Johnson-Winters, D.H.T. Harrison, G.R. Moran, "Structure of the Ferrous Form of (4-Hydroxyphenyl)Pyruvate Dioxygenase from *Streptomyces avermitilis* in Complex with the Therapeutic Herbicide, Ntbc," *Biochemistry-US* 43 (21), 6370-6377 (2004).
- Joseph S. Brunzelle, Ruiying Wu, Sergey V. Korolev, Frank R. Collart, Andrzej Joachimiak, Wayne F. Anderson, "Crystal structure of *Bacillus subtilis* YdaF protein: A putative ribosomal N-acetyltransferase," *Proteins* 57, December, 850-853 (2004).
- J. Daniel Bryan, Steve M. Heald, Scott A. Chambers, Daniel R. Gamelin, "Strong Room-Temperature Ferromagnetism in Co[superscript 2+]-Doped TiO[subscript 2] Made from Colloidal Nanocrystals," *J. Am. Chem. Soc.* 126, 11640-11647 (2004).
- J. D. Budai, W. Yang, B. C. Larson, J. Z. Tischler, W. Liu, H. Weiland, G. E. Ice, "Three-Dimensional Micron-Resolution X-Ray Laue Diffraction Measurement of Thermal Grain-Evolution in Aluminum," *Mater. Sci. Forum* 467-470, 1373-1378 (2004).
- Christopher G. Bunick, Melanie R. Nelson, Sheryll Mangahas, Michael J. Hunter, Jonathan H. Sheehan, Laura S. Mizoue, Gerard J. Bunick, Walter J. Chazin, "Designing Sequence to Control Protein Function in an EF-Hand Protein," *J. Am. Chem. Soc.* 126, 5990-5998 (2004).
- Yiyi Cai, Ciarán N. Cronin, Andrew G. Engel, Kinji Ohno, Louis B. Hersh, David W. Rodgers, "Choline acetyltransferase structure reveals distribution of mutations that cause motor disorders," *EMBO J.* 23, 2047-2058 (2004).
- J. M. Calo, P. J. Hall, "The application of small angle scattering techniques to porosity characterization in carbons," *Carbon* 42 (7), February, 1299-1304 (2004).
- B. J. Campbell, T. R. Welberry, R. W. Broach, H. Hong, A. K. Cheetham, "Elucidation of zeolite microstructure by synchrotron X-ray diffuse scattering," *J. Appl. Crystallogr.* 37, 187-192 (2004).
- Nino Campobasso, Mehul Patel, Imogen E. Wilding, Howard Kallender, Martin Rosenberg, Michael N. Gwynn, "*Staphylococcus aureus* 3-Hydroxy-3-methylglutaryl-CoA Synthase," *Biol. Chem.* 279 (43), October, 44883-44888 (2004).
- Bertram Canagarajah, Federico Coluccio Leskow, Jonathan YewSeng Ho, Harald Mischak, Layla F. Saidi, Marcelo G. Kazanietz, James H. Hurley, "Structural Mechanism for Lipid Activation of the Rac-Specific GAP, β 2-Chimaerin," *Cell* 119, October, 407-418 (2004).
- K. A. Carrado, R. Kizilel, G. Sandi, S. Seifert, C. L. Marshall, M. J. Castagnola, "Catalytic Nanocomposite Membranes for CO Abatement in Fuel Cell Applications," *American Chemical Society, Division of Fuel Chemistry* 49, 199-200 (2004).
- Christopher J. Carrell, Xiaotang Wang, Limei Jones, William L. Jarrett, Victor L. Davidson, F. Scott Mathews, "Crystallographic and NMR Investigation of Cobalt-Substituted Amicyanin," *Biochemistry-US* 43 (29), 9381-9389 (2004).
- Christopher J. Carrell, Dapeng Sun, Shoulei Jiang, Victor L. Davidson, F. Scott Mathews, "Structural Studies of Two Mutants of Amicyanin from *Paracoccus denitrificans* that Stabilize the Reduced State of the Copper," *Biochemistry-US* 43 (29), 9372-9380 (2004).
- M. J. Castagnola, M. K. Neylon, C. L. Marshall, "Coated bifunctional catalysts for NOx SCR with C3H6: Part II. *In situ* spectroscopic characterization," *Catal. Today* 96 (1-2), October, 61-70 (2004).
- C. Castro, A. A. Gratson, J. C. Evans, J. Jiracek, M. Collinsova, M. L. Ludwig, T. A. Garrow, "Dissecting the Catalytic Mechanism of Betaine-Homocysteine S-Methyltransferase Using Intrinsic Tryptophan Fluorescence and Site-Directed Mutagenesis," *Biochemistry-US* 43 (18), 5341-5351 (2004).
- J. G. Catalano, S. M. Heald, J. M. Zachara, G. E. Brown, Jr., "Spectroscopic and Diffraction Study of Uranium Speciation in Contaminated Vadose Zone Sediments from the Hanford Site, Washington State," *Environ. Sci. Technol.* 38 (10), May, 2822-2828 (2004).
- R. G. Cavell, E. M. Barnes, P. H. Arboleda, P. A. Cavell, R. Feng, R. A. Gordon, M. A. Webb, "An X-ray and electron microprobe study of Fe, Ni, Ga and Ge distribution and local structure in a section of the Canyon Diablo iron meteorite," *Am. Mineral.* 89, April, 519-526 (2004).
- Benoy M. Chacko, Bin Y. Qin, Ashutosh Tiwari, Genbin Shi, Suvana Lam, Lawrence J. Hayward, Markde Caestecker, Kai Lin, "Structural basis of heteromeric smad protein assembly in TGF-beta signaling," *Molecular Cell* 15 (5), 813-8923 (2004).

- G. Chai, J. M. Brewer, L. L. Lovelace, T. Aoki, W. Minor, L. Lebioda, "Expression, purification and the 1.8 angstroms resolution crystal structure of human neuron specific enolase," *J. Mol. Biol.* 341 (4), August, 1015-1021 (2004).
- Brian R. Chapados, David J. Hosfield, Seungil Han, Junzhuan Qiu, Biana Yelent, Binghui Shen, John A. Tainer, "Structural Basis for FEN-1 Substrate Specificity and PCNA-Mediated Activation in DNA Replication and Repair," *Cell* 116, 39-50 (2004).
- D. Chelazzi, M. Ceppatelli, M. Santoro, R. Bini, V. Schettino, "High-pressure synthesis of crystalline polyethylene using optical catalysis," *Nat. Mater.* 3, July, 470-475 (2004).
- L. X. Chen, L. M. Utschig, S. L. Schesselman, D. M. Tiede, "Temperature and Light-induced Structural Changes in Photosynthetic Reaction Center Proteins Probed by X-ray Absorption Fine Structure," *J. Phys. Chem. B* 108, March, 3912-3924 (2004).
- L. X. Chen, "Taking Snapshots of Photoexcited Molecular Structures in Disordered Media Using Pulsed X-rays," *Angew. Chem. Int. Ed.* 43, May, 2886-2905 (2004).
- Lin X. Chen, George B. Shaw, Tao Liu, Guy Jennings, Klaus Attenkofer, "Exciplex formation of copper(II) octaethylporphyrin revealed by pulsed x-rays," *Chem. Phys.* 299 (2-3), April, 215-223 (2004).
- Liqing Chen, Enrico DiGammarino, Xiaoyin E. Zhou, Yujun Wang, Diana Toh, Thomas W. Hodge, Edward J. Meehan, "High Resolution Crystal Structure of Human Rab9 GTPase: A Novel Antiviral Drug Target," *J. Biol. Chem.* 279 (38), September, 40204-40208 (2004).
- Liqing Chen, Li-Rong Chen, Xiaoyin E. Zhou, Yujun Wang, Mebrahtu A. Kahsai, Andrew T. Clark, Stephen P. Edmondson, Zhi-Jie Liu, John P. Rose, Bi-Cheng Wang, Edward J. Meehan, John W. Shriver, "The Hyperthermophile Protein Sso10a is a Dimer of Winged Helix DNA-binding Domains Linked by an Antiparallel Coiled Rod," *J. Mol. Biol.* 341, 73-91 (2004).
- Yuan Cheng, Sonia M. Sequeira, Lucy Malinina, Valentina Tereshko, Thomas H. Söllner, Dinshaw J. Patel, "Crystallographic identification of Ca[superscript 2+] and Sr[superscript 2+] coordination sites in synaptotagmin I C[subscript 2]B domain," *Protein Sci.* 13, 2665-2672 (2004).
- M.-H. Chiang, M. R. Antonio, C. W. Williams, L. Soderholm, "A unique coordination environment for an ion: EXAFS studies and bond valence model approach of the encapsulated cation in the Preyssler anion," *Dalton T.* 5, January, 801-806 (2004).
- M.-H. Chiang, M. R. Antonio, L. Soderholm, "Energetics of the Preyssler anions molecular orbitals: Quantifying the effect of the encapsulated cations charge," *Dalton T.* 21, October, 3562-3567 (2004).
- Kyung H. Choi, James M. Groarke, Dorothy C. Young, Richard J. Kuhn, Janet L. Smith, Daniel C. Pevear, Michael G. Rossmann, "The structure of the RNA-dependent RNA polymerase from bovine viral diarrhea virus establishes the role of GTP in *de novo* initiation," *Proc. Natl. Acad. Sci.* 101 (13), 4425-4430 (2004).
- Y. Choi, D. Haskel, D. R. Lee, J. C. Lang, G. Srajer, J. S. Im, "Measurement of local magnetization in the buried layer of a pseudo-spin-valve submicron wire," *J. Appl. Phys.* 95 (11), June, 7028-7030 (2004).
- Y. Choi, D. Haskel, R.E. Camley, D.R. Lee, J.C. Lang, G. Srajer, J.S. Jiang, S.D. Bader, "Temperature evolution of the Gd magnetization profile in strongly coupled Gd / Fe multilayers," *Phys. Rev. B* 70, 134420: 1-10 (2004).
- C. R. Christensen, J. N. Cutler, D. A. Christensen, "Using X-ray absorption near edge structure (XANES) spectroscopy to determine selenium oxidation states in animal mineral supplements and feeds," *Can. J. Anim. Sci.* 84, 171-175 (2004).
- Y. S. Chu, A. Tkachuk, S. Vogt, P. Ilinski, D. A. Walko, D. C. Mancini, E. M. Dufresne, L. He, F. Tsui, "Structural investigation of CoMnGe combinatorial epitaxial thin films using microfocused synchrotron radiation," *Appl. Surf. Sci.* 223, February, 175-182 (2004).
- P. J. Chupas, S. Chaudhuri, J. C. Hanson, X. Qiu, P. L. Lee, S. D. Shastri, S. J. L. Billinge, C. P. Grey, "Probing local and long-range structure simultaneously: An *in situ* study of the high-temperature phase transition of alpha-AlF[subscript 3]," *J. Am. Chem. Soc.* 126, 4756-4757 (2004).
- Michael P. Clark, Steven K. Laughlin, Matthew J. Laufersweiler, Roger G. Bookland, Todd A. Brugel, Adam Golebiowski, Mark P. Sabat, Jennifer A. Townes, John C. VanRens, Jane F. Djung, Michael G. Natchus, Biswanath De, Lily C. Hsieh, Susan C. Xu, Rick L. Walters, Marlene J. Mekel, Sandra A. Heitmeyer, Kimberly K. Brown, Karen Juergens, Yetunde O. Taiwo, Michael J. Janusz, "Development of Orally Bioavailable Bicyclic Pyroazolones as Inhibitors of Tumor Necrosis Factor- α Production," *J. Med. Chem.* 47, 2724-2727 (2004).
- Todd Clark, Sandra Haddad, Ellen Neidlea, Cory Momany, "Crystallization of the effector-binding domains of BenM and CatM, LysR-type transcriptional regulators from *Acinetobacter* sp. ADP1," *Acta Crystallogr. D* 60, 105-108 (2004).
- Eric W. Cochran, Frank S. Bates, "Shear-Induced Network-to-Network Transition in a Block Copolymer Melt," *Phys. Rev. Lett.* 93, 087802-1-087802-4 (2004).
- N. Coker, J. Krause, R. Elder, "Emission Energy Correlates with Inverse of Gold-Gold Distance for Various [Au(SCN)₂] -Salts," *J. Am. Chem. Soc.* 126, 12-13 (2004).
- Brandon K. Collins, Stephen J. Tomanicek, Natasha Lyamicheva, Michael W. Kaiser, Timothy C. Mueser, "A preliminary solubility screen used to improve crystallization trials: crystallization and preliminary X-ray structure determination of *Aeropyrum pernix* flap endonuclease-1," *Acta Crystallogr. D* 60 (9), 1674-1678 (2004).
- Adam B. Conway, Thomas W. Lynch, Ying Zhang, Gary S. Fortin, Cindy W. Fung, Lorraine S. Symington, Phoebe A. Rice, "Crystal structure of a Rad51 filament," *Nat. Struct. Mol. Biol.* 11, August, 791-796 (2004).
- P. Coppens, I. Vorontsov, T. Graber, A. Kovalevsky, Y. Chen, G. Wu, M. Gembicky, I. V. Novozhilova, "Geometry Changes of a Cu(I) Phenanthroline Complex on Photoexcitation in a Confining Medium by Time-Resolved X-ray Diffraction," *J. Am. Chem. Soc.* 126 (19), 5980-5981 (2004).
- Philip Coppens, Oksana Gerlits, Ivanl. Vorontsov, Andrey Yu. Kovalevsky, Yu-Sheng Chen, Tim Graber, Milan Gembicky, Irina V. Novozhilova, "A very large Rh-Rh bond shortening on excitation of the [Rh[subscript 2](1,8-diisocyno-p-menthane)[subscript 4][superscript 2+] ion by time-resolved synchrotron X-ray diffraction," *Chem. Comm.* 19, 2144-2145 (2004).

- Abbie M. Coros, Lora Swenson, William T. Wolodko, Marie E. Fraser, "Structure of the CoA transferase from pig heart to 1.7 Å resolution," *Acta Crystallogr. D* 60, 1717-1725 (2004).
- C. K. Costello, J. Guzman, J. H. Yang, Y. M. Wang, M. C. Kung, B. C. Gates, H. H. Kung, "Activation of Au/[math>\gamma]-Al₂O₃ Catalysts for CO Oxidation: Characterization by X-ray Absorption Near Edge Structure and Temperature Programmed Reduction," *J. Phys. Chem. B* 108 (33), 12529-12536 (2004).
- B.R. Crane, S.A. Kang, "Electron Transfer between Cytochrome C and Cytochrome C Peroxidase in Single Crystals," *J. Am. Chem. Soc.* 126, 10836-10837 (2004).
- R.A. Crowell, R. Lian, I.A. Shkrob, J. Qian, D.A. Oulianov, S. Pommeret, "Light-induced temperature jump causes power-dependent ultrafast kinetics of electrons generated in multiphoton ionization of liquid water," *J. Phys. Chem. A* 108, 9105-9114 (2004).
- James D. Crowley, Andrew J. Goshe, Ian M. Steele, Brice Bosnich, "Supramolecular Recognition: Protonmotive-Driven Switches or Motors?," *Chem.-Eur. J.* 10 (8), April, 1944-1955 (2004).
- M. E. Cuff, D. J. Miller, S. Korolev, X. Xu, W. F. Anderson, A. Edwards, A. Joachimiak, A. Savchenko, "Crystal Structure of a Predicted Precorrin-8x Methylmutase from *Thermoplasma acidophilum*," *Proteins* 58, 751-754 (2004).
- K. A. Culligan, D. Wildenschild, B. S. B. Christensen, W. G. Gray, M. L. Rivers, A. F. B. Thompson, "Interfacial Area Measurements for Unsaturated Flow Through a Porous Medium," *Water Resour. Res.* 40 (12), W12413 (2004).
- J. J. Curry, H. G. Adler, A. MacPhee, S. Narayanan, J. Wang, "X-ray absorption imaging of Hg vapour in a ceramic metal-halide lamp using synchrotron radiation," *Plasma Sources Sci. T.* 13 (3), August, 403-408 (2004).
- P. Czoschke, Hawoong Hong, L. Basile, T.-C. Chiang, "Quantum Beating Patterns Observed in the Energetics of Pb Film Nanostructures," *Phys. Rev. Lett.* 93 (3), July, 036103-1-036103-4 (2004).
- D. Das, M.M. Georgiadis, "The crystal structure of the monomeric reverse transcriptase from Moloney murine leukemia virus," *Structure* 12, 819-829 (2004).
- Kalyan Das, Arthur D. Clark, Jr., Paul J. Lewi, Jan Heeres, Marc R. de Jonge, Lucien M. H. Koymans, H. Maarten Vinkers, Frederik Daeyaert, Donald W. Ludovici, Michael J. Kukla, Bart De Corte, Robert W. Kavash, Chih Y. Ho, Hong Ye, Mark A. Lichtenstein, Koen Andries, Rudi Pauwels, Marie-Pierre Bethune, Paul L. Boyer, Patrick Clark, Stephen H. Hughes, Paul A. J. Janssen, Eddy Arnold, "Roles of Conformational and Positional Adaptability in Structure-Based Design of TMC125-R165335 (Etravirine) and Related Non-nucleoside Reverse Transcriptase Inhibitors that are Highly Potent and Effective against Wild-Type and Drug-Resistant HIV-1 Variants," *J. Med. Chem.* 47 (10), 2550-2560 (2004).
- Dayna L. Daubaras, Eileen M. Wilson, Todd Black, Corey Strickland, Brian M. Beyera, Peter Orth, "Crystallization and preliminary X-ray analysis of the acyl carrier protein synthase (AcpS) from *Staphylococcus aureus*," *Biological Crystallography* 60 (4), April, 773-774 (2004).
- Srini DeMel, Jin Shi, Philip Martin, Barry P. Rosen, Brian F.P. Edwards, "Arginine 60 in the ArsC arsenate reductase of *E. coli* plasmid R773 determines the chemical nature of the bound As(III) product," *Protein Sci.* 13 (9), September, 2330-2340 (2004).
- Glen B. Deacon, Peter C. Junk, Peter Turner, "The X-ray crystal structure of Hg(p-MeC₆H₄)(O₂CC₆F₅) from synchrotron radiation," *J. Chem. Crystallogr.* 34 (7), 405-408 (2004).
- A. Deb, U. Bergmann, E. J. Cairns, S. P. Cramer, "X-ray absorption spectroscopy study of the Li_xFePO₄ cathode during cycling using a novel electrochemical *in situ* reaction cell," *J. Synchrotron Rad.* 11, 497-504 (2004).
- C. Degueldre, D. Reed, A. J. Kropf, C. Mertz, "XAFS Study of Americium Sorbed Onto Groundwater Colloids," *J. Synchrotron Rad.* 11, 198-203 (2004).
- Ranjit K. Deka, Lori Neil, Kayla E. Hagman, Mischa Machius, Diana R. Tomchick, Chad A. Brautigam, Michael V. Norgard, "Structural Evidence That the 32-Kilodalton Lipoprotein (Tp32) of *Treponema pallidum* Is an L-Methionine-binding Protein," *J. Biol. Chem.* 279 (53), December, 55644-55650 (2004).
- Louis T. J. Delbaere, Athena M. Sudom, Lata Prasad, Yvonne Leduc, Hughes Goldie, "Structure/function studies of phosphoryl transfer by phosphoenolpyruvate carboxykinase," *Biochim. Biophys. Acta* 1697, 271-278 (2004).
- Alexey Dementiev, Maurice Petitou, Jean-Marc Herbert, Peter G. W. Gettins, "The ternary complex of antithrombin-anhydrothrombin-heparin reveals the basis of inhibitor specificity," *Nat. Struct. Mol. Biol.* 11, September, 863-867 (2004).
- Lu Deng, Zhi-Jie Liu, Hisashi Ashida, Su-Chen Li, Yu-Teh Li, Peter Horanyi, Wolfram Tempel, John Rose, Bi-Cheng Wang, "Crystallization and preliminary X-ray analysis of GlcNAc[math>\alpha1,4Gal-releasing endo- β -galactosidase from *Clostridium perfringens*," *Acta Crystallogr. D* 60 (3), March, 537-538 (2004).
- I. G. Denisov, Y. V. Grinkova, A. A. Lazarides, S. G. Sligar, "Directed Self-Assembly of Monodisperse Phospholipid Bilayer Nanodiscs with Controlled Size," *J. Am. Chem. Soc.* 126 (11), 3477-3487 (2004).
- Shahab Derakhshan, Abdeljalil Assoud, Katja M. Kleinke, Enkhtsetseg Dashjav, Xiangyun Qiu, Simon J. L. Billinge, Holger Kleinke, "Planar Nets of Ti Atoms Comprising Squares and Rhombs in the New Binary Antimonide Ti₂[Sb]," *J. Am. Chem. Soc.* 126, 8295-8302 (2004).
- Yancho Devedjiev, Yogesh Surendranath, Urszula Derewenda, Alexandra Gabrys, David R. Cooper, Rong-guang Zhang, Lour Lezondra, Andrzej Joachimiak, Zygmunt S. Derewenda, "The Structure and Ligand Binding Properties of the *B. subtilis* YkoF Gene Product, a Member of a Novel Family of Thiamin/HMP-binding Proteins," *J. Mol. Biol.* 343, 395-406 (2004).
- M. L. Dietz, M. P. Jensen, "EXAFS investigations of strontium complexation by a polymer-supported crown ether," *Talanta* 62 (1), January, 109-113 (2004).
- N. M. Dimitrijevic, T. Rajh, Z.V. Saponjic, L. de la Garza, D. M. Tiede, "Light-Induced Charge Separation and Redox Chemistry at the Surface of TiO₂/Host-Guest Hybrid Nanoparticles," *J. Phys. Chem. B* 108 (26), July, 9105-9110 (2004).
- R. Divan, D. C. Mancini, S. M. Gallagher, J. Booske, D. Van Der Weide, "Improvements in graphite-based x-ray mask fabrication for ultradeep x-ray lithography," *Microsystems Technologies* 10 (10), December, 728-734 (2004).

- Dal-Hyun Do, P. G. Evans, E. D. Isaacs, D. M. Kim, C. B. Eom, E. M. Dufresne, "Structural visualization of polarization fatigue in epitaxial ferroelectric oxide devices," *Nat. Mater.* 3, June, 365-369 (2004).
- D. Dodatko, A. A. Fedorov, M. Grynberg, Y. Patskovsky, D. A. Rozwarski, L. Jaroszewski, E. Aronoff-Spencer, E. Kondrashkina, T. C. Irving, A. Godzik, S. C. Almo, "Crystal Structure of the Actin-binding domain of the Cyclase Associated Protein," *Biochemistry-US* 43 (33), 10628-10641 (2004).
- Julie A. Dohm, Sarah J. Lee, J. Marie Hardwick, R. Blake Hill, Apostolos G. Gittis, "Cytosolic domain of the human mitochondrial fission protein fis1 adopts a TPR fold," *Proteins* 54 (1), 153-156 (2004).
- Ying Dong, Leonard F. Lindoy, Peter Turner, Gang Wei, "Three-ring, branched cyclam derivatives and their interaction with nickel(II), copper(II), zinc(II) and cadmium(II)," *Dalton T.* 8, 1264-1270 (2004).
- Philip R. Dormitzer, Emma B. Nason, B.V. Venkataram Prasad, Stephen C. Harrison, "Structural rearrangements in the membrane penetration protein of a non-enveloped virus," *Nature* 430, August, 1053-1058 (2004).
- T. C. Droubay, S. M. Heald, V. Shutthanandan, S. Thevuthasan, S. A. Chambers, J. Osterwalder, "Cr-doped TiO₂: Anatase- A Ferromagnetic Insulator," *J. Appl. Phys.* 97, 046103-1-046103-3 (2004).
- L. S. Dubrovinsky, N. A. Dubrovinskaia, V. Prakapenka, F. Seifert, F. Langenhorst, V. Dmitriev, H.-P. Weber, T. LeBihan, "A class of new high-pressure silica polymorphs," *Phys. Earth Planet. In.* 143, 231-240 (2004).
- Y. I. Dudchik, N. N. Kolchevsky, F. F. Komarov, M. A. Piestrup, J. T. Cremer, C. K. Gary, H. Park, A. M. Khounsary, "Microspot x-ray focusing using a short focal-length compound refractive lenses," *Rev. Sci. Instrum.* 75 (11), 4651-4655 (2004).
- R. W. Dunford, E. P. Kanter, B. Krässig, S. H. Southworth, L. Young, "Higher-order processes in X-ray photoionization and decay," *Radiat. Phys. Chem.* 70 (1-3), May, 149-172 (2004).
- Collin M. Dyerb, Michael L. Quillina, Andres Campos, Justine Lu, Megan M. McEvoy, Andrew C. Hausrath, Edwin M. Westbrook, Philip Matsumura, Brian W. Matthews, Frederick W. Dahlquist, "Structure of the Constitutively Active Double Mutant CheY^[superscript D13K Y106W] Alone and in Complex with a FliM Peptide," *J. Mol. Biol.* 342 (4), September, 1325-1335 (2004).
- Susanne C. Edavettal, Karen A. Lee, Masahiko Negishi, Robert J. Linhardt, Jian Liu, Lars C. Pedersen, "Crystal Structure and Mutational Analysis of Heparan Sulfate 3-O-Sulfotransferase Isoform 1," *J. Biol. Chem.* 279 (24), June, 25789-25797 (2004).
- M. Egli, "Deoxyribo Nanonucleic Acid: Antiparallel, Parallel and Unparalleled," *Chem. Biol.* 11, 1027-1035 (2004).
- Ossama El-Kabbani, Connie Darmanin, ThomasR. Schneider, Isabelle Hazemann, Federico Ruiz, Mitsuru Oka, Andrzej Joachimiak, Clemens Schulze-Briese, Takashi Tomizaki, Andre Mitschler, Alberto Podjarny, "Ultrahigh resolution drug design. II. Atomic resolution structures of human aldose reductase holoenzyme complexed with fidarestat and minalrestat: Implications for the binding of cyclic imide inhibitors," *Proteins* 55, 805-813 (2004).
- E. J. Elzinga, C. D. Tait, R. J. Reeder, K. D. Rector, R. J. Donohoe, D. E. Morris, "Spectroscopic investigation of U(VI) sorption at the calcite-water interface," *Geochim. Cosmochim. Acta* 68 (11), June, 2437-2448 (2004).
- M. I. Eremets, A. G. Gravriliuk, N. R. Serebryanaya, I. A. Trojan, D. A. Dzivenko, R. Boehler, H.-k. Mao, R. J. Hemley, "Structural transformation of molecular nitrogen to a single-bonded atomic state at high pressures," *J. Chem. Phys.* 121 (22), December, 11296-11300 (2004).
- A. A. Escudero, D. M. Goodner, J. S. Okasinski, M. J. Bedzyk, "X-ray standing wave analysis of the Sn/Si(111)- [square root]3 x [square root]3 surface," *Phys. Rev. B* 70, December, 235416-1-235416-7 (2004).
- Lothar Esser, Byron Quinn, Yong-Fu Li, Minquan Zhang, Maria Elberry, Linda Yu, Chang-An Yu, Di Xia, "Crystallographic Studies of Quinol Oxidation Site Inhibitors: A Modified Classification of Inhibitors for the Cytochrome bc₁ Complex," *J. Mol. Biol.* 341 (1), 281-302 (2004).
- J. C. Evans, D. P. Huddler, M. T. Hilgers, G. Romanchuk, R. G. Matthews, M. L. Ludwig, "Structures of the N-Terminal Modules Imply Large Domain Motions during Catalysis by Methionine Synthase," *Proc. Natl. Acad. Sci.* 101 (11), March, 3729-3726 (2004).
- Carme Fabrega, Stephane Hausmann, Vincent Shen, Stewart Shuman, Christopher D. Lima, "Structure and Mechanism of mRNA Cap (Guanine-N7) Methyltransferase," *Molecular Cell* 13, January, 77-89 (2004).
- P. Falus, H. Xiang, M. A. Borthwick, T. P. Russell, S. G. J. Mochrie, "Symmetric-to-Asymmetric Transition in Triblock Copolymer-Homopolymer Blends," *Phys. Rev. Lett.* 93 (14), October, 145701-1-145701-4 (2004).
- P. Falus, M. A. Borthwick, S. G. J. Mochrie, "Fast CCD camera for x-ray photon correlation spectroscopy," *Rev. Sci. Instrum.* 75 (11), November, 4383-4400 (2004).
- R. Feng, E. H. Conrad, M. C. Tringides, C. Kim, P. F. Miceli, "Wetting Layer Transformation for Pb nanocrystals grown on Si(111)," *Appl. Phys. Lett.* 85 (17), October, 3866-3868 (2004).
- Y. Feng, G. T. Seidler, J. O. Cross, A. T. Macrander, J. J. Rehr, "Role of inversion symmetry and multipole effects in nonresonant x-ray Raman scattering from icosahedral B₄C," *Phys. Rev. B* 69, 125402: 1-8 (2004).
- Timothy D. Fenn, Dagmar Ringe, Gregory A. Petsko, "Xylose Isomerase in Substrate and Inhibitor Michaelis States: Atomic Resolution Studies of a Metal-Mediated Hydride Shift," *Biochemistry-US* 43 (21), 6464-6474 (2004).
- P. Fenter, C. Park, "Termination interference along crystal truncation rods of layered crystals," *J. Appl. Crystallogr.* 37 (6), December, 977-987 (2004).
- P. Fenter, N. C. Sturchio, "Mineral-water interfacial structure revealed by synchrotron X-ray scattering," *Prog. Surf. Sci.* 77, 177-258 (2004).
- R. Fischetti, S. Stepanov, G. Rosenbaum, R. Barrea, E. Black, D. Gore, R. Heurich, E. Kondrashkina, A. J. Kropf, S. Wang, K. Zhang, T. C. Irving, G. B. Bunker, "The BioCAT undulator beamline 18ID: A facility for biological non-crystalline diffraction and x-ray absorption spectroscopy at the APS," *J. Synchrotron Rad.* 11, 399-405 (2004).

- R. F. Fischetti, D. J. Rodi, D. B. Gore, L. Makowski, "Wide-angle x-ray solution scattering as a probe of ligand-induced conformational changes in proteins," *Chem. Biol.* 11, October, 1431-1443 (2004).
- Pamela Focia, Irina Shepotinovskaya, James Seidler, Douglas Freymann, "Heterodimeric GTPase core of the SRP targeting complex," *Science* 303, January, 373-377 (2004).
- Pamela J. Focia, Hena Alam, Thanh Lu, Ursula D. Ramirez, Douglas M. Freymann, "Novel protein and Mg[²⁺] configurations in the Mg[²⁺] GDP Complex of the SRP GTPase ffh," *Proteins* 54, February, 222-230 (2004).
- D. D. Fong, G. B. Stephenson, S. K. Streiffer, J. A. Eastman, O. Auciello, P. H. Fuoss, Carol Thompson, "Ferroelectricity in Ultrathin Perovskite Films," *Science* 304, June, 1650-1653 (2004).
- D. D. Fong, C. Thompson, S. K. Streiffer, J. A. Eastman, O. Auciello, P. H. Fuoss, G. B. Stephenson, "In Situ Synchrotron X-ray Studies of PbTiO₃ Thin Films," *Ann. Phys-Berlin* 13, 27-30 (2004).
- Katrina T. Forest, Kenneth A. Satyshur, Gregory A. Worzalla, Johanna K. Hansen, Timothy J. Herdendorf, "The pilus-retraction protein PilT: ultrastructure of the biological assembly," *Acta Crystallogr. D* 60, 978-982 (2004).
- J. A. Fortner, R. J. Finch, A. J. Kropf, J. C. Cunnane, "Re-evaluating Neptunium in Uranyl Phases Derived from Corroded Spent Fuel," *Nucl. Technol.* 148 (2), 174-180 (2004).
- James K. Fredrickson, John M. Zachara, David W. Kennedy, Ravi K. Kukkadapu, James P. McKinley, Steve M. Heald, Chongxuan Liu, Andrew E. Plymale, "Reduction of TcO₄ by sediment-associated biogenic Fe(II)," *Geochim. Cosmochim. Acta* 68 (15), August, 3171-3187 (2004).
- J. W. Freeland, R. H. Kodama, M. Vedpathak, S. C. Erwin, D. J. Keavney, R. Winarski, P. Ryan, R. A. Rosenberg, "Induced Ge spin polarization at the Fe/Ge interface," *Phys. Rev. B* 70, 033201-1-033201-4 (2004).
- Anatoly I. Frenkel, Douglas M. Pease, Jayne Giniewicz, Edward A. Stern, Dale L. Brewster, Million Daniel, Joseph Budnick, "Concentration-dependent short-range order in the relaxor ferroelectric (1-x)Pb(Sc,Ta)O₃-xPbTiO₃," *Phys. Rev. B* 70, 014106-1-014106-12 (2004).
- S.P. Frigo, I. McNulty, R.C. Richmond, C.F. Ehret, "Photoabsorption study of *Bacillus megaterium*, DNA and related biological materials in the phosphorus K-shell edge region," *Radiat. Res.* 162, 464-468 (2004).
- G. E. Fryxell, H. Wu, Y. Lin, W. Shaw, J. C. Birnbaum, J. C. Linehan, Z. Nie, K. M. Kemner, S. D. Kelly, "Lanthanide selective sorbents: self-assembled monolayers on mesoporous supports (SAMMS)," *J. Mater. Chem.* 14 (22), 3356-3363 (2004).
- Bruce X. Fu, Andre Lee, Timothy S. Haddad, "Styrene-Butadiene-Styrene Triblock Copolymers Modified with Polyhedral Oligomeric Silsesquioxanes," *Macromolecules* 37, 5211-5218 (2004).
- N. Fukuda, H. Granzier, "Role of the giant elastic protein titin in the Frank-Starling mechanism of the heart," *Curr. Vas. Pharmacol.* 2, 135-139 (2004).
- J.L. Fulton, Y. Chen, S.M. Heald, M. Balasubramanian, "High-pressure, High-temperature X-ray Absorption Fine Structure Transmission Cell for the Study of Aqueous Ions with Low Absorption-edge Energies," *Rev. Sci. Instrum.* 75 (12), 5228-5231 (2004).
- M. S. Gagliardi, Y. Ren, J. F. Mitchell, M. A. Beno, "Magnetic-field-induced structural homogeneity of a phase-separated manganite," *Appl. Phys. Lett.* 84 (22), May, 4538-4540 (2004).
- Dahai Gai, Rui Zhao, Dawei Li, Carla V. Finkielstein, Xiaojiang S. Chen, "Mechanisms of Conformational Change for a Replicative Hexameric Helicase of SV40 Large Tumor Antigen," *Cell* 119 (1), 47-60 (2004).
- Andrey Galkin, Liudmila Kulakova, Elif Sarikaya, Kap Lim, Andrew Howard, Osnat Herzberg, "Structural Insight into Arginine Degradation by Arginine Deiminase, an Antibacterial and Parasite Drug Target," *J. Biol. Chem.* 279 (14), April, 114001-14008 (2004).
- Vannakambadi K. Ganesh, Scott A. Smith, Girish J. Kotwal, Krishna H.M.M. Murthy, "Structure of vaccinia complement protein in complex with heparin and potential implications for complement regulation," *Proc. Natl. Acad. Sci.* 101 (24), June, 8924-8929 (2004).
- Robert G. Garces, Ning Wu, Wanda Gillon, Emil F. Pai, "*Anabaena* circadian clock proteins KaiA and KaiB reveal a potential common binding site to their partner KaiC," *EMBO J.* 23, April, 1688-1698 (2004).
- Scott C. Garman, David N. Garboczi, "The Molecular Defect Leading to Fabry Disease: Structure of Human alpha-Galactosidase," *J. Mol. Biol.* 337, 319-335 (2004).
- M. Gateshki, S.-J. Hwang, D. H. Park, Y. Ren, V. Petkov, "Structure of Nanocrystalline Alkali Metal Manganese Oxides by the Atomic Pair Distribution Function Technique," *J. Chem. Phys.* 108, September, 14956-14963 (2004).
- M. Gateshki, S.-J. Hwang, D. H. Park, Y. Ren, V. Petkov, "Structure of Exfoliated Titanate Nanosheets Determined by Atomic Pair Distribution Function Analysis," *Chem. Mater.* 16 (24), November, 5153-5157 (2004).
- J.L. Gattis, E. Ruben, M.O. Fenley, W.R. Ellington, M.S. Chapman, "The Active Site Cysteine of Arginine Kinase: Structural and Functional Analysis of Partially Active Mutants," *Biochemistry-US* 43 (27), 8680-8689 (2004).
- P. Geissbühler, P. Fenter, E. DiMasi, G. Srajer, L. B. Sorensen, N. C. Sturchio, "Three-Dimensional Structure of the Calcite-Water Interface," *Surf. Sci.* 573 (20), October, 191-203 (2004).
- Francoise Gellibert, James Woolven, Marie-Helene Fouchet, Neil Mathews, Helen Goodland, Victoria Lovegrove, Alain Laroze, Van-Loc Nguyen, Stephane Sautet, Ruolan Wang, Cheryl Janson, Ward Smith, Gael Krysa, Valerie Boullay, Anne-Charlotte de Gouville, Stephane Huet, David Hartley, "Identification of 1,5-Naphthylidene Derivatives as a Novel Series of Potent and Selective TGF- β Type I Receptor Inhibitors," *J. Med. Chem.* 47 (18), 4494-4506 (2004).
- B. Gilbert, H. Zhang, F. Huang, J. F. Banfield, Y. Ren, D. Haskel, J. C. Lang, G. Srajer, A. Jürgensen, G. A. Waychunas, "Analysis and simulation of the structure of nanoparticles that undergo a surface-driven structural transformation," *J. Chem. Phys.* 120 (24), June, 11785-11795 (2004).

- B. Gilbert, F. Huang, H. Zhang, G. A. Waychunas, J. F. Banfield, "Nanoparticles: Strained and Stiff," *Science* 305 (5684), July, 651-654 (2004).
- P. Glatzel, U. Bergmann, J. Yano, H. Visser, J. H. Robblee, W. Gu, M. F. de Groot, G. Christou, V. L. Pecoraro, S. P. Cramer, V. K. Yachandra, "The Electronic Structure of Mn in Oxides, Coordination Complexes, and the Oxygen-Evolving Complex of Photosystem II Studied by Resonant Inelastic X-ray Scattering," *J. Am. Chem. Soc.* 126 (32), 9946-9959 (2004).
- T. Gnaeupel-Herold, H.J. Prask, R.J. Fields, T.J. Foecke, Z.C. Xia, U. Lienert, "A synchrotron study of residual stresses in a Al6022 deep drawn cup," *Mat. Sci. Eng. A366*, 104-113 (2004).
- Arhonda Gogos, Jason Gorman, Lawrence Shapiro, "Structure of *Escherichia coli* YfdW, a type III CoA transferase," *Acta Crystallogr. D D60*, 507-511 (2004).
- Gali Golan, Dmitry O. Zharkov, Andrea S. Fernandes, Elena Zaika, Jadwiga H. Kycia, Zdzislaw Wawrzak, Arthur P. Grollman, Gil Shoham, "Crystallization and preliminary crystallographic analysis of endonuclease VIII in its uncomplexed form," *Biological Crystallography* 60 (8), 1476-1480 (2004).
- Barbara L. Golden, Hajeong Kim, Elaine Chase, "Crystal structure of a phage Twort group I ribozyme—product complex," *Nat. Struct. Mol. Biol.* 12, 82-89 (2004).
- G. B. Gonzalez, T. O. Mason, J. P. Quintana, P. Warshkow, D. E. Ellis, J.-H. Hwang, J. P. Hodges, J. D. Jorgenson, "Defect structure studies of bulk and nano-indium-tin oxide (ITO)," *J. Appl. Phys.* 96 (7), 3912-3920 (2004).
- Jason Gorman, Lawrence Shapiro, "Structure of serine acetyltransferase from *Haemophilus influenzae* Rd," *Acta Crystallogr. D* 60, 1600-1605 (2004).
- Ty A. Gould, William T. Watson, Kyoung-Hee Choi, Herbert P. Schweizer, Mair E. A. Churchill, "Crystallization of *Pseudomonas aeruginosa* AHL synthase LasI using [beta]-turn crystal engineering," *Acta Crystallogr. D* 60, 518-520 (2004).
- Ty A. Gould, Herbert P. Schweizer, Mair E.A. Churchill, "Structure of the *Pseudomonas aeruginosa* acyl-homoserinelactone synthase LasI," *Mol. Microbiol.* 53 (4), 1135-1146 (2004).
- E. Gregoryanz, C. Sanloup, M. Somayazulu, J. Badro, G. Fiquet, H.-k. Mao, R. Hemley, "Synthesis and characterization of a binary noble metal nitride," *Nat. Mater.* 3, May, 294-297 (2004).
- S. Grenier, K. J. Thomas, Young-June Kim, J. P. Hill, Doon Gibbs, V. Kiryukhin, Y. Tokura, Y. Tomioka, D. Casa, T. Gog, C. Venkataraman, "Resonant X-ray scattering as a probe of the valence and magnetic ground state and excitations in Pr_{0.6}Ca_{0.4}MnO₃," *Physica B* 345, 6-10 (2004).
- S. Grenier, J. P. Hill, D. Gibbs, K. J. Thomas, M. V. Zimmermann, C. S. Nelson, V. Kiryukhin, Y. Tokura, Y. Tomioka, D. Casa, T. Gog, C. Venkataraman, "Resonant x-ray diffraction of the magnetoresistant perovskite Pr_{0.6}Ca_{0.4}MnO₃," *Phys. Rev. B* 69, 134419: 1-16 (2004).
- Meigang Gu, Carme Fabrega, Shin-Wu Liu, Hudan Liu, Megerditch Kiledjian, Christopher D. Lima, "Insights into the Structure, Mechanism, and Regulation of Scavenger mRNA Decapping Activity," *Molecular Cell* 14, April, 67-80 (2004).
- Maxwell J. Gunter, Tyrone P. Jaynes, Peter Turner, "Structural Homology and Dynamic Variation in a Series of Porphyrin Bipyridinium Receptors and Their [2]Catenanes," *Eur. J. Org. Chem.* 2004 (1), 193-208 (2004).
- Qing Guo, Yuequan Shen, Natalia L. Zhukovskaya, Jan Florián, Wei-Jen Tang, "Structural and Kinetic Analyses of the Interaction of Anthrax Adenylyl Cyclase Toxin with Reaction Products cAMP and Pyrophosphate," *J. Biol. Chem.* 279 (28), July, 29427-29435 (2004).
- M. Guthrie, C. A. Tulk, J. Benmore, J. Xu, J. L. Yarger, D. D. Klug, J. S. Tse, H.-k. Mao, R. J. Hemley, "Formation and Structure of a Dense Octahedral Glass," *Phys. Rev. Lett.* 93 (11), September, 115502-1-115502-4 (2004).
- M. Guthrie, C. A. Tulk, C. J. Benmore, D. D Klug, "A structural study of very high-density amorphous ice," *Chem. Phys. Lett.* 397, September, 335-339 (2004).
- Pamela R. Hall, Run Zheng, Marianne Pusztai-Carey, Focovanden Akker, Paul R. Carey, Vivien C. Yee, "Expression and crystallization of several forms of the *Propionibacterium shermanii* transcarboxylase 5S subunit," *Biological Crystallography* 60 (3), March, 521-523 (2004).
- K. Ham, J. Hua, R. I. Al-Raoush, X. Xie, C. S. Willson, G. R. Byerly, L. S. Simeral, M. L. Rivers, R. L. Kurtz, L. G. Butler, "Three-Dimensional Chemical Analysis with Synchrotron Tomography at Multiple X-ray Energies: Brominated Aromatic Flame Retardant and Antimony Oxide in Polystyrene," *Chem. Mater.* 16 (21), 4032-4042 (2004).
- Bing Hao, Gang Zhao, Patrick T. Kang, Jitesh A. Soares, Tsuneo K. Ferguson, Judith Gallucci, Joseph A. Krzycki, Michael K. Chan, "Reactivity and Chemical Synthesis of L-Pyrrolysine- the 22nd Genetically Encoded Amino Acid," *Chem. Biol.* 11, 1317-1324 (2004).
- C. Harman, C. J. Rieke, R. M. Garavito, W. L. Smith, "Crystal Structure of Arachidonic Acid Bound to a Mutant of Prostaglandin Endoperoxide Synthase-1 that Forms Predominantly 11-HPETE," *J. Biol. Chem.* 279 (41), October, 42929-42935 (2004).
- Jörg M. Harms, Frank Schlünzen, Paola Fucini, Heike Bartels, Ada Yonath, "Alterations at the peptidyl transferase centre of the ribosome induced by the synergistic action of the streptogramins dalbopristin and quinupristin," *BMC Biology* 2 (4), April, 1-10 (2004).
- R.T. Hart, J.W. Zwanziger, P.L. Lee, "The crystalline phase of (K₂O)₁₅(Nb₂O₅)₁₅(TeO₂)₇₀ glass ceramic is a polymorph of K₂Te₄O₉," *J. Non-Cryst. Solids* 337, 48-53 (2004).
- D. Haskel, J. Lang, Z. Islam, G. Srajer, J. Cross, P. Canfield, "Beyond element-specific magnetism: Resolving inequivalent Nd crystal sites in Nd₂Fe₁₄B," *IEEE T. Magn.* 40 (4), July, 2874-2876 (2004).
- D. Haskel, Z. Islam, J. Lang, C. Kmety, G. Srajer, K.I. Pokhodnya, A.J. Epstein, J.S. Miller, "Local structural order in the disordered V[TCNE]_x room-temperature molecule-based magnet," *Phys. Rev. B* 70, 054422: 1-9 (2004).
- D.N.T. Hay, P.G. Rickert, S. Seifert, M.A. Firestone, "Thermoresponsive Nanostructures by Self-Assembly of a Poly(N-isopropylacrylamide)-Lipid Conjugate," *J. Am. Chem. Soc.* 126, February, 2290-2291 (2004).

- Y. Hayasaki, K. Ishiji, H. Hashizume, N. Hosoito, K. Omote, M. Kuribayashi, G. Srajer, J. C. Lang, D. Haskel, "Measurement of resonant x-ray magnetic scattering from induced Cu polarizations in exchange-coupled Co/Cu multilayers," *J. Phys. Condens. Matter* 16 (12), 1915-1925 (2004).
- Franklin A. Hays, Zebulon J. R. Jones, P. Shing Ho, "Influence of Minor Groove Substituents on the Structure of DNA Holliday Junctions," *Biochemistry-US* 43 (30), 9813-9822 (2004).
- W. M. Heijboer, P. Glatzel, K. R. Sawant, R. F. Lobo, U. Bergmann, R. A. Barrea, D. C. Koningsberger, B. M. Weckhuysen, F. M. F. de Groot, "K[super-script [beta]]-Detected XANES of Framework-Substituted FeZSM-5 Zeolites," *J. Phys. Chem. B* 108 (28), 10002-10011 (2004).
- Begoña Heras, Melissa A. Edeling, Horst J. Schirra, Satish Raina, Jennifer L. Martin, "Crystal structures of the DsbG disulfide isomerase reveal an unstable disulfide," *Proc. Natl. Acad. Sci.* 101, 8876-8881 (2004).
- J. Hershberger, O. O. Ajayi, J. Zhang, H. Yoon, G. R. Fenske, "Formation of austenite during scuffing failure of SAE 4340 steel," *Wear* 256 (1-2), January, 159-167 (2004).
- J. Hershberger, O. O. Ajayi, G. R. Fenske, "Nondestructive Characterization of Surface Chemical-Wear Films via X-rays, Part 1: Technique," *Thin Solid Films* 446 (2), January, 248-257 (2004).
- Alison B. Hickman, Donald R. Ronning, Zhanita N. Perez, Robert M. Kotin, Fred Dyda, "The Nuclease Domain of Adeno-Associated Virus Rep Coordinates Replication Initiation Using Two Distinct DNA Recognition Interfaces," *Molecular Cell* 13, February, 403-414 (2004).
- Altor Hierro, Ji Sun, Alexander S. Rusnak, Jaewon Kim, Gali Prag, Scott D. Emr, James H. Hurley, "Structure of the ESCRT-II endosomal trafficking complex," *Nature* 431, September, 221-225 (2004).
- Y. Hochman, X.-M. Gong, Y. Lifshitz, G. Bunker, C. Carmeli, "EXAFS analysis of the structure of Ca and Ca-nucleotides bound to chloroplasts ATP synthase," *BBA-Bioenergetics* 1658 (Suppl.1) (1-2), July, 113 (2004).
- Todd Holyoak, Charles A. Kettner, Gregory A. Petsko, Robert S. Fuller, Dagmar Ringe, "Structural Basis for Differences in Substrate Selectivity in Kex2 and Furin Protein Convertases," *Biochemistry-US* 43, 2412-2421 (2004).
- N. Hosoito, H. Sano, T. Tanaka, S. Miya, Y. Yamaguchi, H. Hashizume, G. Srajer, J.C. Lang, "Twisted-type magnetic structures of thin Dy layers in an Fe/Dy multilayer film determined by resonant x-ray magnetic diffraction," *J. Phys. Soc. Jpn.* 73 (7), July, 1962-1969 (2004).
- S. Hosokawa, W.-C. Pilgrim, H. Sinn, E.E. Alp, "Microscopic dynamics in trivalent liquid Ga," *Physica B* 350, 262-2648 (2004).
- Ming-Hon Hou, Howard Robinson, Yi-Gui Gao, Andrew H.-J. Wang, "Crystal structure of the [Mg²⁺-(chromomycin A₃)₂]-d(TTGGCCAA)₂ complex reveals GGCC binding specificity of the drug dimer chelated by a metal ion," *Nucleic Acids Res.* 32 (7), 2214-2222 (2004).
- P. Y. Hou, A. P. Paulikas, B. W. Veal, "Growth Strains and Stress Relaxation in Alumina Scales During High Temperature Oxidation," *Mater. Sci. Forum* 461-464, September, 671-680 (2004).
- E. I. Howard, R. Sanishvili, R. E. Cachau, A. Mitschler, B. Chevrier, P. Barth, V. Lamour, M. Van Zandt, E. Sibley, C. Bon, D. Moras, T. R. Schneider, A. Joachimiak, A. Podjarny, "Ultra-high resolution drug design I: Details of interactions in human aldose reductase-inhibitor complex at 0.66 Å," *Proteins* 55, 7982-804 (2004).
- Gerald W. Hsu, Matthias Ober, Thomas Carell, Lorena S. Beese, "Error-prone replication of oxidatively damaged DNA by a high-fidelity DNA polymerase," *Nature* 431, September, 217-221 (2004).
- Tengjiao Hu, Ronald L. Jones, Wen-li Wu, Eric K. Lin, Qinghuang Lin, Denis Keane, Steve Weigand, John Quintana, "Small angle x-ray scattering metrology for sidewall angle and cross section of nanometer scale line gratings," *J. Appl. Phys.* 96 (4), 1983-1987 (2004).
- Z. W. Hu, Y. S. Chu, B. Lai, B. R. Thomas, A. A. Chernov, "Diffraction and imaging study of imperfections of crystallized lysozyme with coherent x-rays," *Acta Crystallogr. D* 60, 621-629 (2004).
- Qing Huai, Yudong Liu, Sharron H. Francis, Jackie D. Corbin, Hengming Ke, "Crystal Structures of Phosphodiesterases 4 and 5 in Complex with Inhibitor 3-Isobutyl-1-methylxanthine Suggest a Conformation Determinant of Inhibitor Selectivity," *J. Biol. Chem.* 279 (13), 13095-13101 (2004).
- Chin-chin Huang, Miro Venturi, Shahzad Majeed, Michael J. Moore, Sanjay Phogat, Mei-Yun Zhang, Dimiter S. Dimitrov, Wayne A. Hendrickson, James Robinson, Joseph Sodroski, Richard Wyatt, Hyeryun Choe, Michael Farzan, Peter D. Kwong, "Structural basis of tyrosine sulfation and VH-gene usage in antibodies that recognize the HIV type 1 coreceptor-binding site on gp120," *Proc. Natl. Acad. Sci.* 101 (9), March, 2706-2711 (2004).
- Danny T. Huang, David W. Miller, Rose Mathew, Robert Cassell, James M. Holton, Martine F. Roussel, Brenda A. Schulman, "A unique E1-E2 interaction required for optimal conjugation of the ubiquitin-like protein NEDD8," *Nat. Struct. Mol. Biol.* 11 (10), October, 927-935 (2004).
- Feng Huang, Benjamin Gilbert, Hengzhong Zhang, Jillian F. Banfield, "Reversible, Surface-Controlled Structure Transformation in Nanoparticles Induced by an Aggregation State," *Phys. Rev. Lett.* 92 (15), April, 155501-1-155501-4 (2004).
- Hugh E. Huxley, "Recent X-ray diffraction studies of muscle contraction and their implications," *Phil. Trans. R. Soc. Lond. B* 359 (1452), December, 1879-1556 (2004).
- Gene Ice, Bennett Larson, "Three-Dimensional X-Ray Structural Microscopy Using Polychromatic Microbeams," *MRS Bull.* 29, March, 170-176 (2004).
- Eugene S. Ilton, Anca Haiduc, Carl O. Moses, Steve M. Heald, David C. Elbert, David R. Veblen, "Heterogeneous reduction of uranyl by micas: Crystal chemical and solution controls," *Geochim. Cosmochim. Acta* 68 (11), June, 2417-2435 (2004).
- Robert M. Immormino, D. Eric Dollins, Paul L. Shaffer, Karen L. Soldano, Melissa A. Walker, Daniel T. Gewirth, "Ligand-Induced Conformational Shift in the N-terminal Domain of GRP94, an Hsp90 Chaperone," *J. Biol. Chem.* 279 (44), October, 46162-46171 (2004).
- H. Interthal, P.M. Quigley, W.G.J. Hol, J.J. Champoux, "The Role of Lysine 532 in the Catalytic Mechanism of Human Topoisomerase I," *J. Biol. Chem.* 279 (4), 2984-2992 (2004).

- V. Iota, J.-H. Park, C. S. Yoo, "Phase diagram of nitrous oxide: Analogy with carbon dioxide," *Phys. Rev. B* 69, February, 064106-1-064106-6 (2004).
- Z. Islam, X. Liu, S.K. Sinha, J.C. Lang, S.C. Moss, D. Haskel, G. Srajer, P. Wochner, D.R. Lee, D.R. Haefner, U. Welp, "Four-unit-cell superstructure in the optimally doped YBa₂Cu₃O_{6.92} superconductor," *Phys. Rev. Lett.* 93 (15), October, 157008: 1-4 (2004).
- Robert A. Ivey, Yong-Mei Zhang, Kristopher G. Virga, Kirk Hevener, Richard E. Lee, Charles O. Rock, Suzanne Jackowski, Hee-Won Park, "The Structure of the Pantothenate Kinase-ADP-Pantothenate Ternary Complex Reveals the Relationship between the Binding Sites for Substrate, Allosteric Regulator and Antimetabolites," *J. Biol. Chem.* 279 (34), August, 35622-35629 (2004).
- Tina Izard, Clemens Vonrhein, "Structural Basis for Amplifying Vinculin Activation by Talin," *J. Biol. Chem.* 279 (26), June, 27667-27678 (2004).
- Tina Izard, Gwyndaf Evans, Robert A. Borgon, Christina L. Rush, Gerard Bricogne, Philippe R. J. Bois, "Vinculin activation by talin through helical bundle conversion," *Nature* 427, 171-175 (2004).
- Laurie K. Jackson, Jeffrey Baldwin, Radha Akella, Elizabeth J. Goldsmith, Margaret A. Phillips, "Multiple Active Site Conformations Revealed by Distant Site Mutation in Ornithine Decarboxylase," *Biochemistry-US* 43 (41), 12990-12999 (2004).
- J. Jacob, B. Krantz, R. S. Dothager, P. Thiyagarajan, T. R. Sosnick, "Early Collapse is not an Obligate Step in Protein Folding," *J. Mol. Biol.* 338 (2), April, 369-382 (2004).
- Izabela Janda, Yancho Devedjiev, Urszula Derewenda, Zbigniew Dauter, Jakub Bielnicki, David R. Cooper, Paul C. F. Graf, Andrzej Joachimiak, Ursula Jakob, Zygmunt S. Derewenda, "The Crystal Structure of the Reduced, Zn²⁺-Bound Form of the *B. subtilis* Hsp33 Chaperone and Its Implications for the Activation Mechanism," *Structure* 12 (10), October, 1901-1907 (2004).
- Izabela Janda, Yancho Devedjiev, David Cooper, Maksymilian Chruszcz, Urszula Derewenda, Aleksandra Gabrys, Wladek Minor, Andrzej Joachimiak, Zygmunt S. Derewenda, "Harvesting the high-hanging fruit: the structure of the YdeN gene product from *Bacillus subtilis* at 1.8 Å resolution," *Acta Crystallogr. D* 60, 1101-1107 (2004).
- B.H. Jeon, S.D. Kelly, K.M. Kemner, M.O. Barnett, W.D. Burgos, B.A. Dempsey, E.E. Roden, "Microbial reduction of U(VI) at the solid-water interface," *Environ. Sci. Technol.* 38, 5649-5655 (2004).
- J.S. Jiang, J.E. Pearson, Z.Y. Liu, B. Kabius, S. Trasobares, D.J. Miller, S.D. Bader, D.R. Lee, D. Haskel, G. Srajer, J.P. Liu, "Improving exchange-spring nanocomposite permanent magnets," *Appl. Phys. Lett.* 85 (22), November, 1-3 (2004).
- S. Jin, D. M. Kurtz Jr., Z.-J. Liu, J. Rose, B.-C. Wang, "Displacement of Iron by Zinc at the Di-iron Site of *Desulfovibrio Vulgaris* Rubrerythrin: X-Ray Crystal Structure and Anomalous Scattering Analysis," *J. Inorg. Biochem.* 98 (5), 786-796 (2004).
- C. H. Johnson, M. Egli, "Visualizing a Biological Clockwork's Cogs," *Nat. Struct. Mol. Biol.* 11, 584-585 (2004).
- J.E. Johnson, "Virus structure analysis with synchrotron radiation: methods and results," *J. Synchrotron Rad.* 11, 89-92 (2004).
- Sean J. Johnson, Lorena S. Beese, "Structures of Mismatch Replication Errors Observed in a DNA Polymerase," *Cell* 116, 803-816 (2004).
- A. C. Jupe, S. R. Stock, P. L. Lee, N. N. Naik, K. E. Kurtis, A. P. Wilkinson, "Phase composition depth profiles using spatially resolved energy dispersive x-ray diffraction," *J. Appl. Crystallogr.* 37, October, 967-976 (2004).
- A. Jürgensen, J. R. Widmeyer, R. A. Gordon, L. I. Bendell-Young, M. M. Moore, E. D. Crozier, "The structure of the manganese oxide on the sheath of the bacterium *Leptothrix discophora*: An XAFS study," *Am. Mineral.* 89, July, 1110-1118 (2004).
- J. A. Kaduk, "Crystal structure of guaifenesin, 3-(2-methoxyphenoxy)-1,2-propanediol," *Powder Diffr.* 19 (2), 127-132 (2004).
- Hendrik K. Kammler, Gregory Beaucage, Roger Mueller, Sotiris E. Pratsinis, "Structure of Flame-Made Silica Nanoparticles by Ultra-Small-Angle X-ray Scattering," *Langmuir* 20, February, 1915-1921 (2004).
- C. Karanfil, D. Chapman, C. U. Segre, G. Bunker, "A device for selecting and rejecting X-ray harmonics in synchrotron radiation beams," *J. Synchrotron Rad.* 11 (5), September, 393-398 (2004).
- Bärbel Kaufmann, Alan A. Simpson, Michael G. Rossmann, "The structure of human parvovirus B19," *Proc. Natl. Acad. Sci.* 101 (32), 11628-11633 (2004).
- A. Kavner, W. R. Panero, "Temperature gradients and evaluation of thermoelastic properties in the synchrotron-based laser heated diamond cell," *Phys. Earth Planet. In.* 143, 527-539 (2004).
- K. M. Kemner, S. D. Kelly, B. Lai, J. Maser, E. J. O'Loughlin, D. Sholto-Douglas, Z. Cai, M. A. Schneegurt, C.F. Kulpa, Jr., K.H. Neelson, "Elemental and redox analysis of single bacterial cells by x-ray microbeam analysis," *Science* 306, October, 686-687 (2004).
- C. Kennedy, D. S. Smith, L. A. Warren, "Surface chemistry of synthetic Mn oxyhydroxides under variable wetting and drying regimes and their relative sorptive capacities for nickel," *Geochim. Cosmochim. Acta* 68 (3), 443-454 (2004).
- John T. M. Kennis, Ivo H. M. van Stokkum, Sean Crosson, Magdalena Gauden, Keith Moffat, Rienkvan Grondelle, "The LOV2 domain of phototropin: A reversible photochromic switch," *J. Am. Chem. Soc.* 126 (14), 4512-4513 (2004).
- M. S. Kent, H. Yim, D. Y. Sasaki, S. Satija, J. Majewski, T. Gog, "Analysis of Myoglobin Adsorption to Cu(II)-IDA and Ni(II)-IDA Functionalized Langmuir Monolayers by Grazing Incidence Neutron and X-ray Techniques," *Langmuir* 20, 2819-2829 (2004).
- W. Keune, T. Ruckert, B. Sahoo, W. Sturhahn, T. S. Toellner, E. E. Alp, R. Röhlberger, "Atomic vibrational density of states in crystalline and amorphous Tb_{1-x}Fe_x alloy thin films studied by nuclear resonant inelastic x-ray scattering (NRIXS)," *J. Phys. Condens. Matter* 16, S379-S393 (2004).
- Pavel P. Khil, Galina Obmolova, Alexey Teplyakov, Andrew J. Howard, Gary L. Gilliland, R. Daniel Camerini-Otero, "Crystal structure of the *Escherichia coli* YjiA protein suggests a GTP-dependent regulatory function," *Proteins* 54 (2), 371-374 (2004).

- C. S. Kim, M. F. Toney, G. A. Waychunas, J. R. Rustad, J. F. Banfield, "Synchrotron-based studies of nanoparticulate iron oxyhydroxide growth and metal uptake," *Geochim. Cosmochim. Acta* 68 (11), June, A101 (2004).
- Hyunjung Kim, A. Rühm, L. B. Lurio, J. K. Basu, J. Lal, S. G. J. Mochrie, S. K. Sinha, "Synchrotron radiation studies of the dynamics of polymer films," *J. Phys. Condens. Matter* 16 (33), August, S3491-S3497 (2004).
- J.Y. Kim, J.C. Hanson, A.I. Frenkel, P.L. Lee, J.A. Rodriguez, "Reaction of CuO with hydrogen studied by using synchrotron-based x-ray diffraction," *J. Phys. Condens. Matter* 16, S3479-S3484 (2004).
- Myung Hee Kim, David R. Cooper, Arkadiusz Oleksy, Yancho Devedjiev, Urszula Derewenda, Orly Reiner, Jacek Otlewski, Zygmunt S. Derewenda, "The Structure of the N-Terminal Domain of the Product of the Lissencephaly Gene Lis1 and Its Functional Implications," *Structure* 12, June, 987-998 (2004).
- P.-S. G. Kim, P. Zhang, T. K. Sham, "Reductive Deposition of Rh Nanostructures on n-type Porous Silicon: X-ray Absorption and X-Ray Excited Optical Luminescence," *Langmuir* 20, 4690-4695 (2004).
- S. Kim, J.Y. Wu, E.T. Birzin, W. Chan, L.Y. Pai, Y.T. Yang, R.T. Mosley, P.M. Fitzgerald, N. Sharma, F. Dinunno, S.P. Rohrer, J.M. Schaeffer, M.L. Hammond, K. Frisch, J. Dahllund, A.-G. Thorsell, "Estrogen Receptor Ligands. II. Discovery of Benzoxathiins as Potent, Selective Estrogen Receptor Alpha Modulators," *J. Med. Chem.* 47 (9), 2171-2175 (2004).
- Y.-J. Kim, J.P. Hill, H. Benthien, F.H.L. Essler, E. Jeckelmann, H.S. Choi, T.W. Noh, N. Motoyama, K.M. Kojima, S. Uchida, D. Casa, T. Gog, "Resonant Inelastic X-Ray Scattering of the Holon-Antiholon Continuum in SrCuO₂," *Phys. Rev. Lett.* 92 (13), April, 137402-1-137402-4 (2004).
- Y.-J. Kim, J.P. Hill, F.C. Chou, D. Casa, T. Gog, C.T. Venkataraman, "Charge and orbital excitations in Li₂CuO₂," *Phys. Rev. B* 69, 155105-1-155105-6 (2004).
- Youngchang Kim, Alexander F. Yakunin, Ekaterina Kuznetsova, Xiaohui Xu, Micha Pennycooke, Jun Gu, Fred Cheung, Michael Proudfoot, Cheryl H. Arrowsmith, Andrzej Joachimiak, Aled M. Edwards, Dinesh Christendat, "Structure- and Function-based Characterization of a New Phosphoglycolate Phosphatase from *Thermoplasma acidophilum*," *J. Biol. Chem.* 279, 517-526 (2004).
- M. J. Kipper, S. Seifert, P. Thiyagarajan, B. Narasimhan, "Understanding Polyanhydride Blend Phase Behavior Using Scattering, Microscopy and Molecular Simulations," *Polymer* 45 (10), May, 3329-3340 (2004).
- D.J. Klein, P.B. Moore, T.A. Steitz, "The Roles of Ribosomal Proteins in the Structure Assembly, and Evolution of the Large Ribosomal Subunit," *J. Mol. Biol.* 340 (1), June, 141-177 (2004).
- Vadim A. Klenchin, Dawn M. Schmidt, John A. Gerlt, Ivan Rayment, "Evolution of Enzymatic Activities in the Enolase Superfamily: Structure of a Substrate-Ligated Complex of the L-Ala-D/L-Glu Epimerase from *Bacillus subtilis*," *Biochemistry-US* 43 (32), 10370-10378 (2004).
- James E. Knapp, Vukica Srajer, Reinhard Pahl, William E. Royer Jr., "Immobilization of Scapharca Hbl crystals improves data quality in time-resolved crystallographic experiments," *Micron* 35, 107-108 (2004).
- H. Kobayashi, T. Kamimura, D. Alfe, W. Sturhahn, J. Zhao, E. E. Alp, "Phonon density of states and compression behavior in iron sulfide under pressure," *Phys. Rev. Lett.* 93 (19), November, 195503: 1-4 (2004).
- J. E. Kohn, I. S. Millett, J. Jacob, B. Zagrovic, T. M. Dillon, N. Cingel, R. S. Dothager, S. Seifert, P. Thiyagarajan, T. R. Sosnick, M. Z. Hasan, V. S. Pande, I. Ruczinski, S. Doniach, K. W. Plaxco, "Random-Coil Behavior and the Dimensions of Chemically Unfolded Proteins," *Proc. Natl. Acad. Sci.* 101 (34), August, 12491-12496 (2004).
- Junichi Komoto, Taro Yamada, Kikuko Watanabe, Fusao Takusagawa, "Crystal Structure of Human Prostaglandin F Synthase (AKR1C3)," *Biochemistry-US* 43, 2188-2198 (2004).
- Dmitry A. Kondrashov, Sue A. Roberts, Andrzej Weichsel, William R. Montfort, "Protein Functional Cycle Viewed at Atomic Resolution: Conformational Change and Mobility in Nitrophorin 4 as a Function of pH and NO Binding," *Biochemistry-US* 43 (43), October, 13637-13647 (2004).
- Michael Kostelansky, Bettina Bolliger-Stucki, Laurie Betts, Oleg V. Gorkun, Susan T. Lord, "BBGlu397 and BBAsp398 but not BBAsp432 Are Required for 'B:b' Interactions," *Biochemistry-US* 43, 2465-2474 (2004).
- Rhett A. Kovall, Wayne A. Hendrickson, "Crystal structure of the nuclear effector of Notch signaling, CSL, bound to DNA," *EMBO J.* 23 (17), 3441-3451 (2004).
- R. Koynova, R. C. MacDonald, "Columnar DNA superlattices in lamellar O-ethylphosphatidylcholine lipoplexes. Mechanism of the gel-liquid crystalline lipid phase transition," *Nano Lett.* 4, 1475-1479 (2004).
- R. Koynova, H. S. Rosenzweig, L. Wang, M. Wasielewski, R. C. MacDonald, "Novel Fluorescent Cationic Phospholipid, O-4-Naphthylimido-1-Butyl-DOPC, Exhibits Unusual Foam Morphology, Forms Hexagonal and Cubic Phases in Mixtures, and Transfects DNA," *Chem. Phys. Lipids* 129, 184-194 (2004).
- Paul Kraft, Daniel Kümmel, Andrea Oeckinghaus, George H. Gauss, Blake Wiedenheft, Mark Young, C. Martin Lawrence, "Structure of D-63 from Sulfolobus Spindle-Shaped Virus 1: Surface Properties of the Dimeric Four-Helix Bundle Suggest an Adaptor Protein Function," *J. Virol.* 78 (14), 7438-7442 (2004).
- Paul Kraft, Andrea Oeckinghaus, Daniel Kümmel, George H. Gauss, John Gilmore, Blake Wiedenheft, Mark Young, C. Martin Lawrence, "Crystal Structure of F-93 from Sulfolobus Spindle-Shaped Virus 1, a Winged-Helix DNA Binding Protein," *J. Virol.* 78 (21), 11544-11550 (2004).
- Andrey S. Krasilnikov, Yinghua Xiao, Tao Pan, Alfonso Mondragon, "Basis for Structural Diversity in Homologous RNAs," *Science* 306, October, 104-107 (2004).
- Romana Kristelly, Guang Gao, John J. G. Tesmer, "Structural Determinants of RhoA Binding and Nucleotide Exchange in Leukemia-associated Rho Guanine-Nucleotide Exchange Factor," *J. Biol. Chem.* 279 (45), November, 47352-47362 (2004).
- A. Kulkarni, H. Herman, F. De Carlo, R.J. Subramanian, "Microstructural characterization of electron beam-physical vapor deposition thermal barrier coatings through high-resolution computed microtomography," *Metall. Mater. Trans. A* 35A (7), July, 1945-1952 (2004).

- A. A. Kulkarni, H. Herman, J. Almer, U. Lienert, D. Haeffner, J. Ilavsky, S. Fang, P. Lawton, "Depth-resolved porosity investigation of EB-PVD thermal barrier coatings using high-energy x-rays," *J. Am. Ceram. Soc.* 87 (2), 268-274 (2004).
- R. Kumar, H. Kohlmann, B. E. Light, A. L. Cornelius, V. Raghavan, T. W. Darling, J.L. Sarrao, "Anisotropic elastic properties of CeRhIn [subscript 5]," *Phys. Rev. B* 69, January, 014515-1-014515-6 (2004).
- R. S. Kumar, A. L. Cornelius, "Compressibility of CeMn[subscript 5] and Ce[subscript 2] Mn[subscript 8] (M=Rh, Ir, and Co) compounds," *Phys. Rev. B* 70, December, 214526-1-214526-8 (2004).
- Muthiah Kumaraswami, Martha M. Howe, Hee-Won Park, "Crystal Structure of the Mor Protein of Bacteriophage Mu, a Member of the Mor/C Family of Transcription Activators," *J. Biol. Chem.* 279 (16), April, 16581-16590 (2004).
- J. Kung, B. Li, T. Uchida, Y. Wang, D. Neuville, R.C. Liebermann, "*In situ* measurements of sound velocities and densities across the orthopyroxene - high-pressure clinopyroxene transition in MgSiO[subscript 3] at high pressure," *Phys. Earth Planet. In.* 147, 27-44 (2004).
- H. Kusunoki, R.I. Macdonald, A. Mondragon, "Structural Insights into the Stability and Flexibility of Unusual Erythroid Spectrin Repeats," *Structure* 12, 645-656 (2004).
- C. L'abbe, J. Meersschat, W. Sturhahn, J.S. Jiang, T.S. Toellner, E.E. Alp, S.D. Bader, "Nuclear resonant magnetometry and its application to Fe/Cr multilayers," *Phys. Rev. Lett.* 93 (3), July, 037201: 1-4 (2004).
- Nicole LaRonde-LeBlanc, Alexander Wlodawer, "Crystal Structure of *A. fulgidus* Rio2 Defines a New Family of Serine Protein Kinases," *Structure* 12 (9), September, 1585-1594 (2004).
- Jane E. Ladner, James F. Parsons, Chris L. Rife, Gary L. Gilliland, Richard N. Armstrong, "Parallel Evolutionary Pathways for Glutathione Transferases: Structure and Mechanism of the Mitochondrial Class Kappa Enzyme rGSTK1-1," *Biochemistry-US* 43, 352-361 (2004).
- Sushmita D. Lahiri, Guofeng Zhang, Jianying Dai, Debra Dunaway-Mariano, Karen N. Allen, "Analysis of the Substrate Specificity Loop of the HAD Superfamily Cap Domain," *Biochemistry-US* 43, 2812-2820 (2004).
- J. C. Lang, D. Lee, D. Haskel, G. Srajer, "Imaging spiral magnetic domains in Ho metal using circularly polarized Bragg diffraction," *J. Appl. Phys.* 95 (11), June, 6537-6539 (2004).
- B. C. Larson, W. Yang, J. Z. Tischler, G. E. Ice, J. D. Budai, W. Liu, H. Weiland, "Micron-resolution 3-D measurement of local orientations near a grain-boundary in plane-strained aluminum using X-ray microbeams," *Int. J. Plasticity* 20, 543-560 (2004).
- Bennett C. Larson, Bruno Lengeler, "High-Resolution Three-Dimensional X-Ray Microscopy," *MRS Bull.* 29, March, 152-155 (2004).
- Matthew Laufersweiler, Todd Brugel, Michael Clark, Adam Golebiowski, Roger Bookland, Steven Laughlin, Mark Sabat, Jennifer Townes, John VanRens, Biswanath De, Lilly Hsieh, Sandra Heitmeyer, Karen Juergens, Kimberly Brown, Marlene Mekel, Richard Walter, Michael Januz, "The development of novel inhibitors of tumor necrosis factor-alpha production based on substituted [5,5]-bicyclic pyroazolones," *Bioorgan. Med. Chem.* 14, 4267-4272 (2004).
- Michael C. Lawrence, Natalie A. Borg, Victor A. Streltsov, Patricia A. Pilling, V. Chandana Epa, Joseph N. Varghese, Jennifer L. McKimm-Breschkin, Peter M. Colman, "Structure of the Haemagglutinin-neuraminidase from Human Parainfluenza Virus Type III," *J. Mol. Biol.* 335, 1343-1357 (2004).
- C. Lee, B. Hong, J.M. Choi, Y. Kim, S. Watanabe, Y. Ishimi, T. Enomoto, S. Tada, Y. Kim, Y. Cho, "Structural Basis for Inhibition of the Replication Licensing Factor Cdt1 by Geminin," *Nature* 430, August, 913-917 (2004).
- D. R. Lee, J. W. Freeland, G. Srajer, V. Metlushko, C.-Y. You, "Domain-specific magnetization reversals on a permalloy square ring array," *J. Appl. Phys.* 95 (11), June, 7016-7018 (2004).
- G. W. Lee, A. K. Gangopadhyay, K. F. Kelton, R. W. Hyers, T. J. Rathz, J. R. Rogers, D. S. Robinson, "Difference in Icosahedral Short-Range Order in Early and Late Transition Metal Liquids," *Phys. Rev. Lett.* 93 (3), 037802-1-037802-4 (2004).
- J.E. Lee, E.C. Settembre, K.A. Cornell, M.K. Riscoe, J.R. Sufrin, S.E. Ealick, P.L. Howell, "Structural Comparison of MTA Phosphorylase and MTA/AdoHcy Nucleosidase Explains Substrate Preferences and Identifies Regions Exploitable for Inhibitor Design," *Biochemistry-US* 43, 5159-5169 (2004).
- K. K. Lee, B. O'Neill, R. Jeanloz, "Limits to resolution in composition and density in ultra high-pressure experiments on natural mantle-rock samples," *Phys. Earth Planet. In.* 143, 241-253 (2004).
- K. M. Lee, B. O'Neill, W. R. Panero, S.-H. Shim, L. R. Benedetti, R. Jeanloz, "Equations of state of the high-pressure phases of a natural peridotite and implications for the Earth's lower mantle," *Earth Planet Sc. Lett.* 223 (3-4), 381-393 (2004).
- S.-H. Lee, D. Louca, H. Ueda, S. Park, T.J. Sato, M. Isobe, Y. Ueda, S. Rosenkranz, P. Zschack, J. Iniguez, Y. Qiu, R. Osborn, "Orbital and Spin Chains in ZnV[subscript 2]O[subscript 4]," *Phys. Rev. Lett.* 93 (15), October, 156407-1-156407-4 (2004).
- W.-K. Lee, P. Cloetens, M. Schlenker, "Dispersion corrections of the copper K-edge measured by Fresnel diffraction," *Acta Crystallogr. A* 60 (Pt. 1), January, 58-63 (2004).
- Christopher Lehmann, Victoria Doseeva, Sadhana Pullalarevu, Wojciech Krajewski, Andrew Howard, Osnat Herzberg, "YbdK is a Carboxylate-Amine Ligase with a gamma-Glutamyl:Cysteine Ligase Activity:Crystal Structure and Enzymatic Assays," *Proteins* 56 (2), August, 376-383 (2004).
- B. M. Leu, M. Z. Zgierski, G. R. A. Wyllie, W.R. Scheidt, W. Sturhahn, E. E. Alp, S. M. Durbin, J. T. Sage, "Quantitative vibrational dynamics of iron in nitrosyl porphyrins," *J. Am. Chem. Soc.* 126, 4211-4227 (2004).
- L. E. Levine, G. G. Long, "X-ray imaging with ultra-small-angle X-ray scattering as a contrast mechanism," *J. Appl. Crystallogr.* 37, June, 757-765 (2004).
- Z. H. Levine, S. Grantham, D. Paterson, I. McNulty, I. C. Noyan, T. M. Levin, "Imaging material components of an integrated circuit interconnect," *J. Appl. Phys.* 95 (1), January, 405-407 (2004).

- Hal A. Lewis, Sean G. Buchanan, Stephen K. Burley, Kris Connors, Mark Dickey, Michael Dorwart, Richard Fowler, Xia Gao, William B. Guggino, Wayne A. Hendrickson, John F. Hunt, Margaret C. Kearins, Don Lorimer, Peter C. Maloney, Kai W. Post, Kanagalaghatta R. Rajashankar, Marc E. Rutter, J. Michael Sauder, Stephanie Shriver, Patrick H. Thibodeau, Philip J. Thomas, Marie Zhang, Xun Zhao, Spencer Emtage, "Structure of nucleotide-binding domain 1 of the cystic fibrosis transmembrane conductance regulator," *EMBO J.* 23 (2), 282-293 (2004).
- J.A. Libera, R.W. Gurney, S.T. Nguyen, J.T. Hupp, C. Liu, R. Conley, M.J. Bedzyk, "X-ray nanoscale profiling of layer-by-layer assembled metal/organophosphonate films," *Langmuir* 20, 8022-8029 (2004).
- D. Li, B. Yang, B. Lin, M. Meron, J. Gebhardt, T. Graber, S. Rice, "Wavelength Dependence of Liquid-Vapor Interfacial Tension of Ga," *Phys. Rev. Lett.* 92 (13), April, 136102-1-136102-2 (2004).
- J. Li, V. Struzhkin, H.-k. Mao, J. Shu, R. Hemley, Y. Fei, B. Mysen, D. Przemek, V. Parapenka, G. Shen, "Electronic spin state of iron in lower mantle perovskite," *Proc. Natl. Acad. Sci.* 101 (39), September, 14027-14030 (2004).
- Jun Li, R. Max Wynn, Mischa Machius, Jacinta L. Chuang, Subramanian Karthikeyan, Diana R. Tomchick, David T. Chuang, "Cross-talk between Thiamin Diphosphate Binding and Phosphorylation Loop Conformation in Human Branched-chain [alpha]-Keto Acid Decarboxylase/Dehydrogenase," *J. Biol. Chem.* 279 (31), July, 32968-32978 (2004).
- X. Li, L. E. Sinks, B. Rybtchinski, M. R. Wasielewski, "Ultrafast Aggregate-to-Aggregate Energy Transfer within Self-Assembled Light-Harvesting Columns of Zinc Phthalocyanine Tetrakis(Perylenediimide)," *J. Am. Chem. Soc.* 126 (35), September, 10810-10811 (2004).
- Y. Li, P. A. Montano, J. F. Mitchell, B. Barbiellini, P. E. Mijnders, S. Kaprzyk, A. Bansil, "Temperature-Dependent Orbital Degree of Freedom of a Bilayer Manganite by Magnetic Compton Scattering," *Phys. Rev. Lett.* 93 (20), November, 207206-1-207206-4 (2004).
- Yuanhe Li, David Karnak, Borries Demeler, Ben Margolis, Arnon Lavie, "Structural basis for L27 domain-mediated assembly of signaling and cell polarity complexes," *EMBO J.* 23 (14), 2723-2733 (2004).
- Dennis Liang, Matthew A. Borthwick, Robert L. Leheny, "Smectic Liquid Crystals in Anisotropic Colloidal Silica Gels," *J. Phys. Condens. Matter* 16, S1989-S2002 (2004).
- U. Lienert, T.S. Han, J. Almer, R.R. Dawson, T. Leffers, L. Margulies, S.F. Nielsen, H.F. Poulsen, S. Schmidt, "Investigating the effect of grain interaction during plastic deformation of copper," *Acta Mater.* 52 (15), 4461-4467 (2004).
- H. P. Liermann, A. K. Singh, B. Manoun, S. K. Saxena, V. B. Prakapenka, G. Shen, "Compression behavior of VC0.85 up to 53 GPa," *Int. J. Refract. Met. H.* 22, 129-132 (2004).
- Kap Lim, Elif Sarikaya, Andrey Galkin, Wojciech Krajewski, Sadhana Pullalarevu, Jae-Ho Shin, Zvi Kelman, Andrew Howard, Osnat Herzberg, "Novel structure and nucleotide binding properties of HI1480 from *Haemophilus influenzae*: A protein with no known sequence homologues," *Proteins* 56 (3), 564-571 (2004).
- J. Lin, W. Sturhahn, J. Zhao, G. Shen, H.-k. Mao, R. J. Hemley, "Absolute temperature measurement in the diamond anvil cell," *Geophys. Res. Lett.* 31, L14611 (2004).
- J.-F. Lin, O. Degtyareva, C. T. Prewitt, D. Przemyslaw, N. Sata, E. Gregoryanz, H.-k. Mao, R. J. Hemley, "Crystal structure of a high-pressure/high-temperature phase of alumina by in situ X-ray diffraction," *Nat. Mater.* 3, June, 389-393 (2004).
- J.-F. Lin, W. Sturhahn, J. Zhao, G. Shen, H.-k. Mao, R. J. Hemley, "Absolute temperature measurement in a laser-heated diamond anvil cell," *Geophys. Res. Lett.* 31, L14611-L14615 (2004).
- J.-F. Lin, Y. Fei, W. Sturhahn, J. Zhao, H.-k. Mao, R. J. Hemley, "Magnetic transition and sound velocities of Fe₃S at high pressure: implications for Earth and planetary cores," *Earth Planet Sc. Lett.* 226, 33-40 (2004).
- Jung-Fu Lin, Mario Santoro, Viktor V. Struzhkin, Ho-kwang Mao, Russell J. Hemley, "*In situ* high pressure-temperature Raman spectroscopy technique with laser-heated diamond anvil cells," *Rev. Sci. Instrum.* 75 (10), October, 3302-3306 (2004).
- Jung-Fu Lin, Burkhard Militzer, Viktor V. Struzhkin, Eugene Gregoryanz, Russell J. Hemley, Ho-kwang Mao, "High pressure-temperature Raman measurements of H₂O melting to 22 GPa and 900 K," *J. Chem. Phys.* 121 (17), November, 8423-8427 (2004).
- Jung-Fu Lin, Viktor V. Struzhkin, Ho-kwang Mao, Russell J. Hemley, Paul Chow, Michael Y. Hu, Jie Li, "Magnetic transition in compressed Fe₃C from x-ray emission spectroscopy," *Phys. Rev. B* 70, 212405-1-212405-4 (2004).
- Chongxua Liu, John M. Zachara, Odeta Qafoku, James P. McKinley, Steve M. Heald, Zheming Wang, "Dissolution of uranyl microprecipitates in subsurface sediments at Hanford Site, USA," *Geochim. Cosmochim. Acta* 68 (22), November, 4519-4537 (2004).
- H. Liu, H.-k. Mao, M. Somayazulu, Y. Ding, Y. Meng, D. Hausermann, "B1-to-B2 phase transition of transition-metal monoxide CdO under strong compression," *Phys. Rev. B* 70, September, 094114-1-094114-5 (2004).
- H. Liu, J. Hu, J. Shu, D. Hausermann, H.-k. Mao, "Lack of critical pressure for weakening of size-induced stiffness in 3C-SiC nanocrystals under hydrostatic compression," *Appl. Phys. Lett.* 85, September, 1973-1975 (2004).
- H. Liu, J. Hu, J. Xu, Z. Liu, J. Shu, H.-k. Mao, J. Chen, "Phase transition and compression behavior of gibbsite under high-pressure," *Phys. Chem. Miner.* 31, 240-246 (2004).
- Jun Liu, Mary C. Reedy, Yale E. Goldman, Clara Franzini-Armstrong, Hiroyuki Sasaki, Richard T. Tregear, Carmen Lucaveche, Hanspeter Winkler, Bruce A. J. Baumann, John M. Squire, Thomas C. Irving, Michael K. Reedy, Kenneth A. Taylor, "Electron tomography of fast frozen, stretched rigor fibers reveals elastic distortions in the myosin crossbridges," *J. Struct. Biol.* 147 (3), 268-282 (2004).
- Ping Liu, Yuan-Fang Wang, Hosam E. Ewis, Ahmed T. Abdelal, Chung-Dar Lu, Robert W. Harrison, Irene T. Weber, "Covalent Reaction Intermediate Revealed in Crystal Structure of the *Geobacillus stearothermophilus* Carboxylesterase Est30," *J. Mol. Biol.* 342, 551-561 (2004).

- S. Liu, Z. Lu, Y. Han, Y. Jia, A.. Howard, D. Dunaway-Mariano, O. Herzberg, "Conformational Flexibility of PEP Mutase," *Biochemistry-US* 43 (15), April, 4447-4453 (2004).
- Y. Liu, D. Berti, A. Faraone, W.-R. Chen, A. Alatas, H. Sinn, E. Alp, A. Said, P. Baglioni, S.-H. Chen, "Inelastic x-ray scattering studies of phonons in liquid crystalline DNA," *Phys. Chemm. Chem. Phys.* 6, 1499-1505 (2004).
- Zhenxian Liu, Jian Xu, Henry P. Scott, Quentin Williams, Ho-kwang Mao, Russell J. Hemley, "Moissanite (SiC) as windows and anvils for high-pressure infrared spectroscopy," *Rev. Sci. Instrum.* 75 (11), November, 5026-5029 (2004).
- C.-T. Lo, S. Seifert, P. Thiyagarajan, B. Narasimhan, "Phase Behavior of Semicrystalline Polymer Blends," *Polymer* 45 (11), May, 3671-3679 (2004).
- A. J. Locock, S. Skanthakumar, P. C. Burns, L. Soderholm, "Syntheses, Structures, Magnetic Properties and X-ray Absorption Spectra of Carnotite-type Uranyl Chromium (V) Oxides: $A[(UO_2)_2]_2[Cr_2O_8](H_2O)_n$ ($A = K_2, Rb_2, Cs_2, Mg; [n] = 0, 4$)," *Chem. Mater.* 16, March, 1384-1390 (2004).
- Bradley C. Logsdon, John F. Vickrey, Philip Martin, Gheorghe Proteasa, Jay I. Koepke, Stanley R. Terlecky, Zdzislaw Wawrzak, Mark A. Winters, Thomas C. Merigan, Ladislav C. Kovari, "Crystal Structures of a Multidrug-Resistant Human Immunodeficiency," *J. Virol.* 78 (6), March, 3123-3132 (2004).
- Karin Loscha, Aaron J. Oakley, Bogdan Bancia, Patrick M. Schaeffer, Pavel Prosselkov, Gottfried Otting, Matthew C. J. Wilce, Nicholas E. Dixon, "Expression, purification, crystallization, and NMR studies of the helicase interaction domain of *Escherichia coli* DnaG primase," *Protein Expres. Purif.* 33, 304-310 (2004).
- George T. Lountos, Bettina R. Riebel, William B. Wellborn, Andreas S. Bommarius, Allen M. Orville, "Crystallization and preliminary analysis of a water-forming NADH oxidase from *Lactobacillus sanfranciscensis*," *Acta Crystallogr. D* 60, 2044-2047 (2004).
- Robert A. Love, Karen A. Maegley, Xiu Yu, RoseAnn Ferre, Laura K. Lingardo, Wade Diehl, Hans E. Parge, Peter S. Dragovich, Shella A. Fuhrman, "The Crystal Structure of the RNA-Dependent RNA Polymerase from Human Rhinovirus A Dual Function Target for Common Cold Antiviral Therapy," *Structure* 12 (8), August, 1533-1544 (2004).
- Shanyun Lu, Jindrich Symersky, Songlin Li, Mike Carson, Liqing Chen, Edward Meehan, Ming Luo, "Structural Genomics of *Caenorhabditis elegans*: Crystal Structure of the Tropomodulin C-Terminal Domain," *Proteins* 56, 384-386 (2004).
- Anthony V. Ludlam, Brian A. Moore, Zhaohui Xu, "The crystal structure of ribosomal chaperone trigger factor from *Vibrio cholerae*," *Proc. Natl. Acad. Sci.* 101 (37), September, 13436-13441 (2004).
- Wenjun Lui, Gene E. Ice, Bennett Larson, Wenge Yang, "The Three-Dimensional X-ray Crystal Microscope: A New Tool for Materials," *Metall. Mater. Trans. A* 35A (7), July, 1963 (2004).
- Che Ma, Geoffrey Chang, "Structure of the multidrug resistance efflux transporter EmrE from *Escherichia coli*," *Proc. Natl. Acad. Sci.* 101, 2852-2857 (2004).
- Jin-Biao Ma, Keqiong Ye, Dinshaw J. Patel, "Structural basis for overhang-specific small interfering RNA recognition by the PAZ domain," *Nature* 429, May, 318-322 (2004).
- Q. Ma, P. Ryan, J.W. Freeland, R.A. Rosenberg, "Thermal effect on the oxides on Nb(100) studied by synchrotron radiation x-ray photoelectron spectroscopy," *J. Appl. Phys.* 96 (12), December, 7675-7680 (2004).
- Y. Ma, M. Somayazulu, G. Shen, H.-k. Mao, J. Shu, R. J. Hemley, "*In situ* X-ray diffraction studies of iron to Earth-core conditions," *Phys. Earth Planet. In.* 143, 455-467 (2004).
- Kevin P. Madauss, Su-Jun Deng, Robert J.H. Austin, Millard H. Lambert, Iain McLay, John Pritchard, Steven A. Short, Eugene L. Stewart, IanJ. Uings, Shawn P. Williams, "Progesterone Receptor Ligand Binding Pocket Flexibility: Crystal Structures of the Norethindrone and Mometasone Furoate Complexes," *J. Med. Chem.* 47 (13), 3381-3387 (2004).
- Estelle M. Maes, Andrzej Weichsel, John F. Andersen, Donald Shepley, William R. Montfort, "Role of Binding Site Loops in Controlling Nitric Oxide Release: Structure and Kinetics of Mutant Forms of Nitrophorin," *Biochemistry-US* 43 (21), 6679-6690 (2004).
- N. Makhharashvili, O. Koroleva, S. Bera, D. Grandgenett, S. Korolev, "A novel structure of DNA repair protein RecO from *Deinacoccus radiodurans*," *Structure* 12 (10), October, 1881-1889 (2004).
- L. Malinina, M. L. Malakhova, A. Teplov, R. E. Brown, D. J. Patel, "Structural Basis for Glycosphingolipid Transfer Specificity," *Nature* 430, August, 1048-1053 (2004).
- W. L. Mao, W. Sturhahn, D. L. Heinz, H.-k. Mao, J. Shu, R. J. Hemley, "Nuclear resonant x-ray scattering of iron hydride at high pressure," *Geophys. Res. Lett.* 31 (15), August, L15618: 1-4 (2004).
- W. L. Mao, G. Shen, V. V. Prakapenka, Y. Meng, A. J. Campbell, D. L. Heinz, J. Shu, R. J. Hemley, H.-k. Mao, "Ferromagnesian postperovskite silicates in the D" Layer of the Earth," *Proc. Natl. Acad. Sci.* 101 (45), November, 15867-15869 (2004).
- Yuxin Mao, Nand K. Vyas, MeenakshiN Vyas, Dong-Hua Chen, Steven J. Ludtke, Wah Chiu, Florante A. Quioco, "Structure of the bifunctional and Golgi-associated formiminotransferase cyclodeaminase octamer," *EMBO J.* 23 (15), 2963-2971 (2004).
- R. R. Martin, S. J. Naftel, A. J. Nelson, A. B. Feilen, A. Narvaez, "Synchrotron X-ray Fluorescence and Trace Metals in the Cementum Rings of Human Teeth," *J. Environ. Monitor.* 6 (10), 783-786 (2004).
- E. Mathew, A. Mirza, N. Menhart, "Liquid-chromatography-coupled SAXS for accurate sizing of aggregating proteins," *J. Synchrotron Rad.* 11, 314-318 (2004).
- Michael R. Maurizi, Di Xia, "Protein Binding and Disruption by Clp/Hsp100 Chaperones," *Structure* 12, 175-183 (2004).
- J. A. McCourt, R. Tyagi, L. W. Guddat, V. Biou, R. G. Duggleby, "Facile crystallization of *Escherichia coli* ketol-acid reductoisomerase," *Acta Crystallogr. D* 60 (8), 1432-1434 (2004).

- M. J. McKelvy, A. V. G. Chizmeshya, J. Diefenbacher, H. Bearat, "Exploration of the Role of Heat Activation in Enhancing Serpentine C Sequestration Reaction," *Environ. Sci. Technol.* 38 (24), 6897-6903 (2004).
- James P. McKinley, John M. Zachara, Steven M. Heald, Alice Dohnalkova, Matt G. Newville, Steve R. Sutton, "Microscale distribution of cesium sorbed to biotite and muscovite," *Environ. Sci. Technol.* 38 (4), 1017-1023 (2004).
- William J. McKinstry, Yu Wan, Julian J. Adams, Richard J. Brown, Michael J. Waters, Michael W. Parker, "Crystallization and preliminary X-ray diffraction analysis of the unliganded human growth hormone receptor," *Acta Crystallogr. D* 60, 2380-2382 (2004).
- S. E. McLain, C. J. Benmore, J. Siewenie, J. Urquidi, J. F. C. Turner, "On the Structure of Liquid Hydrogen Fluoride," *Angew. Chem. Int. Ed. web publ.* (43), February, 1952-1955 (2004).
- S. E. McLain, C. J. Benmore, J. E. Siewenie, J. J. Molaison, J. F. C. Turner, "On the variation of the structure of liquid deuterium fluoride with temperature," *J. Chem. Phys.* 121 (13), October, 6448-6455 (2004).
- Q. Mei, P. Ghalsasi, C. J. Benmore, J. L. Yarger, "The local structure of triphenyl phosphite studied using spallation neutron and high energy x-ray diffraction," *J. Phys. Chem. B* 108 (52), December, 20076-20082 (2004).
- Y. Meng, H.-k. Mao, P. J. Eng, T. P. Trainor, M. Newville, M. Y. Hu, C.-C. Kao, J. Shu, D. Hausermann, R. J. Hemley, "The formation of sp³ binding in compressed BN," *Nat. Mater.* 3, February, 111-114 (2004).
- S. Merkel, H.-R. Wenk, P. Gillet, H.-k. Mao, R. J. Hemley, "Deformation of polycrystalline iron up to 30 GPa and 1000K," *Phys. Earth Planet. In.* 145, May, 239-251 (2004).
- S. Merkel, H.-R. Wenk, P. Gillet, H.-k. Mao, R. J. Hemley, "Deformation mechanisms of iron under high pressure," *Phys. Earth Planet. In.* 209, 351-360 (2004).
- J. T. Miller, M. Schreier, A. J. Kropf, J. R. Regalbutto, "A Fundamental Study of Platinum Tetraammine Impregnation of Silica 2. The Effect of Method of Preparation, Loading and Calcination Temperature on (Reduced) Particle Size," *J. Catal.* 225, 203-212 (2004).
- X. Min, B.H. Lee, M.H. Cobb, E.J. Goldsmith, "Crystal Structure of the Kinase Domain of Wnk1, a Kinase that Causes a Hereditary Form of Hypertension," *Structure* 12 (7), July, 1303-1311 (2004).
- Y. Mishina, L. X. Chen, C. He, "Preparation and Characterization of the Native Iron(II)-Containing DNA Repair AlkB Protein Directly from *Escherichia coli*," *J. Am. Chem. Soc.* 126 (51), December, 16930-16936 (2004).
- Daniel D. Mitchell, Jason C. Pickens, Konstantin Korotkov, Erkan Fan, Wim G. J. Hol, "3,5-Substituted phenyl galactosides as leads in designing effective cholera toxin antagonists: synthesis and crystallographic studies," *Bioorgan. Med. Chem.* 12 (5), March, 907-920 (2004).
- H. Mo, S. Trogisch, H. Taub, S. N. Ehrlich, U. G. Volkmann, F. Y. Hansen, M. Pino, "Studies of the Structure and Growth Mode of Dotriacontane Films by Synchrotron X-ray Scattering and Molecular Dynamics Simulations," *J. Phys. Condens. Matter* 16, S2905-S2910 (2004).
- H. Mo, S. Trogisch, H. Taub, S.N. Ehrlich, U.G. Volkmann, F.Y. Hansen, M. Pino, "Structure and Growth of Dotriacontane Films on SiO₂ and Ag(111) Surfaces: Synchrotron X-ray Scattering and Molecular Dynamics Simulations," *Phys. Status Solidi. a.* 201, 2375-2380 (2004).
- Yorgo Modis, Steven Ogata, David Clements, Stephen C. Harrison, "Structure of the dengue virus envelope protein after membrane fusion," *Nature* 427, 313-319 (2004).
- P. A. Montano, Y. Li, J. F. Mitchell, B. Barbiellinid, P. E. Mijnders, S. Kaprzyk, A. Bansil, "Inelastic magnetic X-ray scattering from highly correlated electron systems: La_{1.2}Sr_{1.8}Mn₂O₇, La_{0.7}Sr_{0.3}MnO₃ and Fe₃O₄," *J. Phys. Chem. Solids* 65 (1), December, 1999-2004 (2004).
- Marc C. Morais, Megan Fisher, Shuji Kanamaru, Laralynne Przybyla, John Burgner, Bentley A. Fane, Michael G. Rossmann, "Conformational Switching by the Scaffolding Protein D Directs the Assembly of Bacteriophage [phi] X174," *Molecular Cell* 15 (6), 991-997 (2004).
- M. A. Morales, D. S. Williams, P. M. Shand, C. Stark, T. M. Pekarek, L. P. Yue, V. Petkov, D. L. Leslie-Pelecky, "Disorder-induced depression of the Curie temperature in mechanically milled GdAl₂," *Phys. Rev. B* 70, November, 184407: 1-8 (2004).
- J. Morse, C. J. Kenney, E. M. Westbrook, I. Naday, S. I. Parker, "The spatial and energy response of a 3d architecture silicon detector measured with a synchrotron X-ray microbeam," *Nucl. Instrum. Methods A* 524, May, 236-244 (2004).
- L. E. Moyer, G. S. Cargill, W. Yang, B. C. Larson, G. E. Ice, "X-ray Microbeam Diffraction Measurements in Polycrystalline Aluminum and Copper Thin Films," *MRS Bull.* 795, March, U1.71-U1.7.5 (2004).
- David M. Mueller, Neeti Puri, Venkataraman Kabaleeswaran, Cassandra Terry, Andrew G. W. Leslie, John E. Walker, "Crystallization and preliminary crystallographic studies of the mitochondrial F₁-ATPase from the yeast *Saccharomyces cerevisiae*," *Acta Crystallogr. D* 60 (8), August, 1441-1444 (2004).
- A. M. Mulichak, W. Lu, H. C. Losey, C.T. Walsh, R. M. Garavito, "Crystal Structure of Vancosaminyltransferase GtfD from the Vancomycin Biosynthetic Pathway: Interactions with Acceptor and Nucleotide Ligands," *Biochemistry-US* 43, 5170-5180 (2004).
- C.E. Murray, I.C. Noyan, B. Lai, Z. Cai, "Strain effects in thin film/Si substrates revealed by x-ray microdiffraction," *Powder Diffr.* 19 (1), March, 56-59 (2004).
- A. Nagpal, M. P. Valley, P. F. Fitzpatrick, A. M. Orville, "Crystallization and preliminary analysis of active nitroalkane oxidase in three crystal forms," *Acta Crystallogr. D* 60 (8), 1456-1460 (2004).
- Deepak T. Nair, Robert E. Johnson, Satya Prakash, Louise Prakash, Aneel K. Aggarwal, "Replication by human DNA polymerase-[iota] occurs by Hoogsteen base-pairing," *Nature* 430, July, 377-380 (2004).

- Narayanasamy Nandhagopal, Alan A. Simpson, Marc C. Johnson, Adam B. Francisco, Gisela W. Schatz, Michael G. Rossmann, Volker M. Vog, "Dimeric Rous Sarcoma Virus Capsid Protein Structure Relevant to Immature Gag Assembly," *J. Mol. Biol.* 335 (1), 275-282 (2004).
- S. Narayanan, J. Wang, X.-M. Lin, "Dynamical self-assembly of nanocrystal superlattices during colloidal droplet evaporation by *in situ* small angle x-ray scattering," *Phys. Rev. Lett.* 93 (13), September, 135503: 1-4 (2004).
- C. S. Nelson, J. P. Hill, D. Gibbs, M. Rajeswari, A. Biswas, S. Shinde, R. L. Greene, T. Venkatesan, A. J. Millis, F. Yokaichiya, C. Giles, D. Casa, C. T. Venkataraman, T. Gog, "Substrate-induced strain effects on Pr_{0.6}Ca_{0.4}MnO₃ films," *J. Phys. Condens. Matter* 16 (1), January, 13-27 (2004).
- J. Neuefeind, S. Skanthakumar, L. Soderholm, "Structure of the UO₂-SO₄ Ion Pair in Aqueous Solution," *Inorg. Chem.* 43, 2422-2426 (2004).
- J. Neuefeind, L. Soderholm, S. Skanthakumar, "Experimental Coordination Environment of Uranyl(VI) in Aqueous Solution," *J. Phys. Chem. A* 108 (14), 2733-2739 (2004).
- B. Newbury, B. Stephenson, J. Almer, M. Notis, G.S. Cargill III, G.B. Stephenson, D. Haeffner, "Synchrotron applications in archaeometallurgy: analysis of high zinc brass astrolabes," *Powder Diffr.* 19 (1), March, 12-15 (2004).
- Nathan I. Nicely, Justin Kosak, Vesna de Serrano, Carla Mattos, "Crystal Structures of Ras-GppNHp and Ras-GDP Reveal Two Binding Sites that Are Also Present in Ras and Rap," *Structure* 12, November, 2025-2036 (2004).
- Dierk Niessing, Stefan Huttelmaier, Daniel Zenklusen, Robert H. Singer, Stephen K. Burley, "She2p Is a Novel RNA Binding Protein with a Basic Helical Hairpin Motif," *Cell* 119 (4), November, 491-502 (2004).
- Ryo Nitta, Masahide Kikkawa, Yasushi Okada, Nobutaka Hirokaw, "KIF1A Alternately Uses Two Loops to Bind Microtubules," *Science* 305, July, 678-683 (2004).
- Claire J. O'Neal, Edward I. Amaya, Michael G. Jobling, Randall K. Holmes, Wim G.J. Hol, "Crystal Structures of an Intrinsically Active Cholera Toxin Mutant Yield Insight into the Toxin Activation Mechanism," *Biochemistry-US* 43 (13), 3772-3782 (2004).
- Aaron J. Oakley, Martin Klvaa, Michal Otyepka, Yuji Nagata, Matthew C. J. Wilce, Jii Damborsky, "Crystal Structure of Haloalkane Dehalogenase LinB from *Sphingomonas paucimobilis* UT26 at 0.95 Å Resolution: Dynamics of Catalytic Residues," *Biochemistry-US* 43 (4), 870-878 (2004).
- Gilad Ofek, Min Tang, Anna Sambor, Hermann Katinger, John R. Mascola, Richard Wyatt, Peter D. Kwong, "Structure and Mechanistic Analysis of the Anti-Human Immunodeficiency Virus Type 1 Antibody 2F5 in Complex with Its gp41 Epitope," *J. Virol.* 78, September, 10724-10735 (2004).
- Haruo Ogawa, Yue Qiu, Craig M. Ogata, Kunio S. Misono, "Crystal Structure of Hormone-bound Atrial Natriuretic Peptide Receptor Extracellular Domain," *J. Biol. Chem.* 279 (27), July, 28625-28631 (2004).
- J. S. Okasinski, C.-Y. Kim, D. A. Walko, M. J. Bedzyk, "X-ray standing wave imaging of the 1/3 monolayer Sn/Ge(111) surface," *Phys. Rev. B* 69, 041401-1-041401-4 (2004).
- Linda J. Olson, Rama D. Yammani, Nancy M. Dahms, Jung-Ja P. Kim, "Structure of uPAR, plasminogen, and sugar-binding sites of the 300 kDa mannose 6-phosphate receptor," *EMBO J.* 23, 2019-2028 (2004).
- S.M. Oppenheimer, J.G. O'Dwyer, D.C. Dunand, "Initial Investigations of Porous, Superelastic NiTi Produced by Powder-Metallurgy," *TMS Lett.* 1 (5), 93-94 (2004).
- Maryna Ornatska, Sergiy Peleshanko, Kirsten L. Genson, Beth Rybak, Kathy N. Bergman, Vladimir V. Tsukruk, "Assembling of Amphiphilic Highly Branched Molecules in Supramolecular Nanofibers," *J. Am. Chem. Soc.* 126, 9675-9684 (2004).
- Allen M. Orville, Linda Manning, David S. Blehert, Joey M. Studts, Brian G. Fox, Glenn H. Chambliss, "Crystallization and preliminary analysis of xenobiotic reductase A and ligand complexes from *Pseudomonas putida* II-B," *Acta Crystallogr. D* 60, 957-961 (2004).
- Andrew R. Osborne, William M. Clemons, Tom A. Rapoport, "A large conformational change of the translocation ATPase SecA," *Proc. Natl. Acad. Sci.* 101 (30), July, 10937-10942 (2004).
- Svetlana Pakhomova, Chris L. Rife, Richard N. Armstrong, Marcia E. Newcomer, "Structure of fosfomycin resistance protein FosA from transposon Tn2921," *Protein Sci.* 13, 1260-1265 (2004).
- D. Paktunc, A. Foster, S.M. Heald, G. LaFlamme, "Speciation and characterization of gold ores and cyanidation tailing using x-ray absorption spectroscopy," *Geochim. Cosmochim. Acta* 68 (5), 969-983 (2004).
- Bradley M. Palmer, Bradley K. McConnell, Guo Hua Li, Christine E. Seidman, J. G. Seidman, Thomas C. Irving, Norman R. Alpert, David W. Maughan, "Reduced cross-bridge dependent stiffness of skinned myocardium from mice lacking cardiac myosin binding protein-C," *Mol. Cell Biochem.* 263, 73-80 (2004).
- Siew Siew Pang, Ronald G. Duggleby, Richard L. Schowen, Luke W. Guddat, "The Crystal Structures of *Klebsiella pneumoniae* Acetolactate Synthase with Enzyme-bound Cofactor and with an Unusual Intermediate," *J. Biol. Chem.* 279, 2242-2253 (2004).
- A.B. Papandrew, A.F. Yue, B. Fultz, W. Sturhahn, T.S. Toellner, E.E. Alp, H.-k. Mao, "Vibrational modes in nanocrystalline iron under high pressure," *Phys. Rev. B* 69, 144301: 1-5 (2004).
- C. Park, P. Fenter, Z. Zhang, L. Cheng, N. C. Sturchio, "Structure of Naturally Grown Fluorapatite (100)-Water Interface by High-Resolution X-ray Reflectivity," *Am. Mineral.* 89 (11-12), December, 1647-1654 (2004).
- Frances Park, Ketan Gajiwala, Galina Eroshkina, Eva Furlong, Dongmei He, Yelena Batiyenko, Rich Romero, Jon Christopher, John Badger, Jorg Hendle, Johann Lin, Tom Peat, Sean Buchanan, "Crystal structure of YIGZ, a conserved hypothetical protein from *Escherichia coli* k12 with a novel fold," *Proteins* 55 (3), May, 775-777 (2004).

Frances Park, Ketan Gajiwala, Brian Noland, Lydia Wu, Dongmei He, Janessa Molinari, Kim Loomis, Barbra Pagarigan, Peggy Kearins, Jon Christopher, Tom Peat, John Badger, Jorg Hendle, Johann Lin, Sean Buchanan, "The 1.59 Å resolution crystal structure of TM0096, a flavin mononucleotide binding protein from *Thermotoga maritima*," *Proteins* 55 (3), 772-774 (2004).

S.-H. Park, H. Liu, M. Kleinsorge, C. P. Grey, B. H. Toby, J. B. Parise, "[Li-Si-O]-MFI: A new microporous lithosilicate with the MFI topology," *Chem. Mater.* 16, 2605-2614 (2004).

S.-J. Park., A. A. Lazarides, J. J. Storhoff, L. Pesce, C. A. Mirkin, "The Structural Characterization of Oligonucleotide-Modified Gold Nanoparticle Networks Formed by DNA Hybridization," *J. Phys. Chem. B* 108, 12375-12380 (2004).

Sagita B. Patel, Jeffrey P. Varnerin, Michael R. Tota, Scott D. Edmondson, Emma R. Parmee, Joseph W. Becker, Giovanna Scapin, "Crystallization and preliminary x-ray diffraction analysis of the catalytic domain of recombinant human phosphodiesterase 3B," *Acta Crystallogr. D* D60 (1), January, 169-171 (2004).

Saurabh D. Patel, Michael W. Rajala, Luciano Rossetti, Philipp E. Scherer, Lawrence Shapiro, "Disulfide-Dependent Multimeric Assembly of Resistin Family Hormones," *Science* 304, May, 1154-1158 (2004).

Rekha Pattanayek, Jimin Wang, Tetsuya Mori, Yao Xu, Carl Hirschie Johnson, Martin Egli, "Visualizing a Circadian Clock Protein: Crystal Structure of KaiC and Functional Insights," *Molecular Cell* 15, August, 375-388 (2004).

R. B. Payne, L. Casalot, T. Rivere, J. Terry, L. Larsen, B. J. Giles, J. D. Wall, "Interaction between uranium and the cytochrome c3 of *Desulfovibrio desulfuricans* strain G20," *Arch. Microbiol.* 181 (6), June, 398-406 (2004).

A.G. Peele, K.A. Nugent, A.P. Mancuso, D. Paterson, I. McNulty, J.P. Hayes, "X-ray phase vortices: theory and experiment," *J. Opt. Soc. Am. A* 21 (8), August, 1575-1584 (2004).

N. R. Pereira, E. M. Dufresne, R. Clarke, D. A. Arms, "Parabolic lithium refractive optics for x-rays," *Rev. Sci. Instrum.* 75 (1), January, 37-41 (2004).

D. Perkins, L. Lindhoy, G. Meehan, P. Turner, "Inherent helicity in an extended tris-bipyridyl molecular cage," *Chem. Comm.* 2, 152-153 (2004).

V. Petkov, D. Qadir, S. D. Shastri, "Rapid structure determination of disordered materials: study of GeSe₂ glass," *Solid State Commun.* 129, January, 239-243 (2004).

V. Petkov, P. Y. Zavalij, S. Lutta, M. S. Whittingham, V. Parvanov, S. Shastri, "Structure beyond Bragg: Study of V₂O₅ nanotubes," *Phys. Rev. B* 69, 085410 1-6 (2004).

Franz Pfeiffer, Wei Zhang, Ian.K. Robinson, "Coherent grazing exit x-ray scattering geometry for probing the structure of thin films," *Appl. Phys. Lett.* 84 (11), March, 1847-1849 (2004).

Jason Phan, Joseph E. Propea, David S. Waugh, "Structure of the *Yersinia pestis* type III secretion chaperone SycH in complex with a stable fragment of YscM2," *Acta Crystallogr. D* 60, 1591-1599 (2004).

Kulwadee Phannachet, Raven H. Huang, "Conformational change of pseudouridine 55 synthase upon its association with RNA substrate," *Nucleic Acids Res.* 32 (4), 1422-1429 (2004).

Agustin O. Pineda, Christopher J. Carrell, Leslie A. Bush, Swati Prasad, Sonia Caccia, Zhi-Wei Chen, F. Scott Mathews, Enrico Di Cera, "Molecular dissection of Na⁺ binding to thrombin," *J. Biol. Chem.* 279 (30), 31842-31853 (2004).

Agustin O. Pineda, Zhi-Wei Chen, Sonia Caccia, Angelene M. Cantwell, Savvas N. Savvides, Gabriel Waksman, F. Scott Mathews, Enrico Di Cera, "The anticoagulant thrombin mutant W215A/E217A has a collapsed primary specificity pocket," *J. Biol. Chem.* 279, 39824-39828 (2004).

A. Podjarny, R. E. Cachau, T. Schneider, M. Van Zandt, A. Joachimiak, "Subatomic and atomic crystallographic studies of aldose reductase: implications for inhibitor binding," *Cell Mol. Life Sci.* 61 (7-8), April, 763-773 (2004).

Larissa M. Podust, Liudmila V. Yermalitskaya, Galina I. Lepesheva, Vladimir N. Podust, Enrique A. Dalmasso, Michael R. Waterman, "Estradiol Bound and Ligand-free Structures of Sterol 14α-Demethylase," *Structure* 12 (11), November, 1937-1945 (2004).

Larissa M. Podust, Haracio Bach, Youngchang Kim, David C. Lamb, Maharu Arase, David H. Sherman, Steven L. Kelly, Michael R. Waterman, "Comparison of the 1.85 Å structure of CYP154A1 from *Streptomyces coelicolor* A3(2) with the closely related CYP154C1 and CYPs from antibiotic biosynthetic pathways," *Protein Sci.* 13, 255-268 (2004).

Galina Polekhina, Kara Sue Giddings, Rodney K. Tweten, Michael W. Parker, "Crystallization and preliminary X-ray analysis of the human-specific toxin intermedilysin," *Acta Crystallogr. D* 60, 347-349 (2004).

R. Poulsen, A. Bentien, T. Graber, B. Iversen, "Synchrotron charge density studies in materials chemistry: 16K X-ray charge density of new magnetic metal-organic framework material, [Mn₂(C₈H₄O₄)₂(C₃H₇NO₂)₂]," *Acta Crystallogr. A* A60, 382-389 (2004).

Edwin Pozharski, Mark A. Wilson, Anura Hewagama, Armen B. Shanafelt, Gregory Petsko, Dagmar Ringe, "Anchoring a Cationic Ligand: The Structure of the Fab Fragment of the Anti-morphine Antibody 9B1 and its Complex with Morphine," *J. Mol. Biol.* 337, 691-697 (2004).

Adam Prah, Marzena Pazgier, Mahdi Hejazi, Wolfgang Lockau, Jacek Lubkowski, "Structure of the isoaspartyl peptidase with L-asparaginase activity from *Escherichia coli*," *Acta Crystallogr. D* D60, 1173-1176 (2004).

V. B. Prakapenka, G. Shen, L. S. Dubrovinsky, "Carbon transport in diamond anvil cells," *High Temp.-High Press.* 35/6 (2), 237-249 (2004).

T. P. Prakash, A. Puschl, E. Lesnik, V. Mohan, V. Tereshko, M. Egli, M. Manoharan, "2'-O-[2-(guanidinium)ethyl]-modified oligonucleotides: stabilizing effect on duplex and triplex structures," *Org. Lett.* 6 (12), 1971-1974 (2004).

Lata Prasad, Yvonne Leduc, Koto Hayakawa, Louis T. J. Delbaere, "The structure of a universally employed enzyme: V8 protease from *Staphylococcus aureus*," *Acta Crystallogr. D* 60, 256-259 (2004).

- Veena Prasad, Antal Jakli, "Achiral bent-core azo compounds: observation of photoinduced effects in an antiferroelectric tilted smectic mesophase," *Liq. Cryst.* 31 (4), April, 473-479 (2004).
- Veena Prasad, Shin-Woong Kang, Xianghong Qi, Satyendra Kumar, "Photo-responsive and electrically switchable mesophases in a novel class of achiral bent-core azo compounds," *J. Mater. Chem.* 14, April, 1495-1502 (2004).
- M. Predota, Z. Zhang, P. Fenter, D. J. Wesolowski, P. T. Cummings, "Electric Double Layer at the Rutile (110) Surface. 2. Adsorption of Ions from Molecular Dynamics and X-ray Experiments," *J. Phys. Chem. B* 108 (32), August, 12061-12072 (2004).
- Xiayang Qiu, Cheryl A. Janson, "Structure of apo acyl carrier protein and a proposal to engineer protein crystallization through metal ions," *Biological Crystallography* 60 (9), May, 1545-1554 (2004).
- Paulene M. Quigley, Konstantin Korotkov, François Baneyx, Wim G. J. Hol, "The 1.6-Å crystal structure of the class of chaperones represented by *Escherichia coli* Hsp31 reveals a putative catalytic triad," *Proc. Natl. Acad. Sci.* 100 (6), March, 3137-3142 (2004).
- S. Rajagopal, K. Kostov, K. Moffat, "Analytical trapping: Extraction of time-independent structures from time-dependent crystallographic data," *J. Struct. Biol.* 147 (3), 211-222 (2004).
- Sudarshan Rajagopal, Marius Schmidt, Spencer Anderson, Hyotcherl Ihee, Keith Moffat, "Analysis of experimental time-resolved crystallographic data by singular value decomposition," *Acta Crystallogr. D* 60 (5), 860-871 (2004).
- S. S. Rajan, X. Yang, F. Collart, V. L. Y. Yip, S. G. Withers, A. Varrot, J. Thompson, G. J. Davies, W. F. Anderson, "Novel catalytic mechanism of glycoside hydrolysis based on the structure of an NAD⁺/Mn²⁺-dependent phospho- α -glucosidase from *Bacillus subtilis*," *Structure* 12 (9), September, 1619-1629 (2004).
- Shyamala S. Rajan, Xiaojing Yang, Ludmilla Shuvalova, Frank Collart, Wayne F. Anderson, "YfiT from *Bacillus subtilis* Is a Probable Metal-Dependent Hydrolase with an Unusual Four-Helix Bundle Topology," *Biochemistry-US* 43 (49), December, 15472-15479 (2004).
- S. Ramakrishnan, Y-L Chen, K. S. Schweizer, C. F. Zukoski, "Elasticity and clustering in concentrated depletion gels," *Phys. Rev. E* 70 (4), 040401-1-040401-4 (2004).
- Paul A. Ramsland, William Farrugia, Tessa M. Bradford, P. Mark Hogarth, Andrew M. Scott, "Structural Convergence of Antibody Binding of Carbohydrate Determinants in Lewis Y Tumor Antigens," *J. Mol. Biol.* 340 (4), 809-818 (2004).
- Kallol Ray, Christina S. Hines, Jerry Coll-Rodriguez, David W. Rodgers, "Crystal Structure of Human Thimet Oligopeptidase Provides Insight into Substrate Recognition, Regulation, and Localization," *J. Biol. Chem.* 279 (19), May, 20480-20489 (2004).
- Massimo Reconditi, Marco Linari, Leonardo Lucii, Alex Stewart, Yin-Biao Sun, Peter Boesecke, Theyencheri Narayanan, Robert F. Fischetti, Tom Irving, Gabriella Piazzesi, Malcolm Irving, Vincenzo Lombardi, "The myosin motor in muscle generates a smaller and slower working stroke at higher load," *Nature* 428 (6982), 578-581 (2004).
- Catherine Regni, Laura Naught, Peter A. Tipton, Lesa J. Beamer, "Structural Basis of Diverse Substrate Recognition by the Enzyme PMM/PGM from *P. aeruginosa*," *Structure* 12, 55-63 (2004).
- Scott T. Reid, Lorena S. Beese, "Crystal Structures of the Anticancer Clinical Candidates R115777 (Tipifarnib) and BMS-214662 Complexed with Protein Farnesyltransferase Suggest a Mechanism of FTI Selectivity," *Biochemistry-US* 43 (22), 6877-6884 (2004).
- T. Scott Reid, Stephen B. Long, Lorena S. Beese, "Crystallographic Analysis Reveals that Anticancer Clinical Candidate L-778,123 Inhibits Protein Farnesyltransferase and Geranylgeranyltransferase-I by Different Binding Modes," *Biochemistry-US* 43 (28), 9000-9008 (2004).
- T. Scott Reid, Kimberly L. Terry, Patrick J. Casey, Lorena S. Beese, "Crystallographic Analysis of CaaX Prenyltransferases Complexed with Substrates Defines Rules of Protein Substrate Selectivity," *J. Mol. Biol.* 343 (2), 417-433 (2004).
- D.A. Reis, P.H. Bucksbaum, M.F. DeCamp, "Ultrafast x-ray physics," *Radiat. Phys. Chem.* 70, 605-609 (2004).
- S. Rendon, W.R. Burghardt, A. New, R.A. Bubeck, L.S. Thomas, "Effect of Complex Flow Kinematics on the Molecular Orientation Distribution in Injection Molding of Liquid Crystalline Copolyesters," *Polymer* 45, 5341-5352 (2004).
- David Reverter, Christopher D. Lima, "A Basis for SUMO Protease Specificity Provided by Analysis of Human Senp2 and a Senp2-SUMO Complex," *Structure* 12, August, 1519-1531 (2004).
- Gordon B. Riddle, David A. Grossie, Kenneth Turnbull, "3-(2-Biphenyl)sydnone," *Acta Crystallogr. E* 60, o977-o978 (2004).
- Rachel E. Rigsby, Chris L. Rife, Kerry L. Fillgrove, Marcia E. Newcomer, Richard N. Armstrong, "Phosphonoformate: A Minimal Transition State Analogue Inhibitor of the Fosfomycin Resistance Protein, FosA," *Biochemistry-US* 43 (43), October, 13666-13673 (2004).
- S. Rihs, N. Sturchio, K. Orlandini, L. Cheng, H. Teng, P. Fenter, M. J. Bedzyk, "The Interaction of Uranyl with the Calcite Surface: Batch Sorption and Synchrotron X-ray Standing Wave Studies," *Environ. Sci. Technol.* 38 (19), October, 5078-5086 (2004).
- Ian K. Robinson, Jianwei Miao, "Three-Dimensional Coherent X-Ray Diffraction Microscopy," *MRS Bull.* 29 (3), March, 177-181 (2004).
- Antonina Roll-Mecak, Pankaj Alone, Chune Cao, Thomas E. Dever, Stephen K. Burley, "X-ray Structure of Translation Initiation Factor eIF2[γ]: Implications for tRNA and eIF2[α] Binding," *J. Biol. Chem.* 279, March, 10634-10642 (2004).
- Donald R. Ronning, Ying Li, Zhanita N. Perez, Philip D. Ross, Alison Burgess Hickman, Nancy L. Craig, Fred Dyda, "The carboxy-terminal portion of TnsC activates the Tn7 transposase through a specific interaction with TnsA," *EMBO J.* 23, August, 2972-2981 (2004).
- Donald R. Ronning, Varalakshmi Vissa, Gurdyal S. Besra, John T. Belisle, James C. Sacchettini, "*Mycobacterium tuberculosis* Antigen 85A and 85C Structures Confirm Binding Orientation and Conserved Substrate Specificity," *J. Biol. Chem.* 279, 36771-36777 (2004).

- John P. Rose, Zhi-Jie Liu, Wolfram Temple, Lirong Chen, Doowon Lee, M. Gary Newton, Bi-Cheng Wang, "Practical Aspects of SAS Structure Determination Using Chromium X-Rays," *Rigaku J.* 21 (2), 3-11 (2004).
- S. Rosenkranz, R. Osborn, "Prospects and Challenges in Single Crystal Diffuse Scattering," *Neutron News* 15 (4), December, 21-24 (2004).
- J. Rothe, C. Walther, M. A. Denecke, Th. Fanghänel, "XAFS and LIBD Investigation of the Formation and Structure of Pu(IV) Hydrolysis Products," *Inorg. Chem.* 43 (13), July, 4708-4718 (2004).
- Federico Ruiz, Isabelle Hazemann, Andre Mitschler, Andrzej Joachimiak, Thomas Schneider, Martin Karplus, Alberto Podjarny, "The crystallographic structure of the aldose reductase-IDD552 complex shows direct proton donation from tyrosine 48," *Acta Crystallogr. D* 60 (8), August, 1347-1354 (2004).
- W. Ruland, B. Smarsly, "SAXS of self-assembled oriented lamellar nanocomposite films: an advanced method of evaluation," *J. Appl. Crystallogr.* 37, 575-584 (2004).
- C. L. Rush, T. Izard, "Rhombohedral crystals of the human vinculin head domain in complex with a vinculin-binding site of talin," *Acta Crystallogr. D* 60, 945-947 (2004).
- P. Ryan, R. P. Winarski, D. J. Keavney, J. W. Freeland, R. A. Rosenberg, S. Park, C. M. Falco, "Enhanced magnetic orbital moment of ultrathin Co films on Ge (100)," *Phys. Rev. B* 69, February, 054416 1-6 (2004).
- B. Rytchinski, L. E. Sinks, M. R. Wasielewski, "Combining Light-Harvesting and Charge Separation in a Self-Assembled Artificial Photosynthetic System Based on Peryleneimide Chromophores," *J. Am. Chem. Soc.* 126, September, 12268-12269 (2004).
- S. Kamtekar, A.J. Berman, J. Wang, J.M. Lazaro, M. de Vega, L. Blanco, M. Salas, T.A. Steitz, "Insights into strand displacement and processivity from the crystal structure of the protein-primed DNA polymerase of bacteriophage phi 29," *Mol. Cell* 16, 609-618 (2004).
- R.K. Sani, B.M. Peyton, J.E. Amonette, G.G. Geesey, "Reduction of uranium(VI) under sulfate-reducing conditions in the presence of Fe(III)-(hydr)oxides," *Geochim. Cosmochim. Acta* 68 (12), 2639-2648 (2004).
- R. Sanishvili, R. Wu, D. E. Kim, J. D. Watson, F. Collart, A. Joachimiak, "Crystal structure of *Bacillus subtilis* YckF: structural and functional evolution," *J. Struct. Biol.* 148 (1), October, 98-109 (2004).
- Ruslan Sanishvili, Steven Beasley, Tania Skarina, David Glesne, Andrzej Joachimiak, Aled Edwards, Alexei Savchenko, "The Crystal Structure of *Escherichia coli* MoaB Suggests a Probable Role in Molybdenum Cofactor Synthesis," *J. Biol. Chem.* 279 (40), July, 42139-42146 (2004).
- Vivian Saridakis, Alexander Yakunin, Xiaohui Xu, Ponni Anandakumar, Micha Pennycooke, Jun Gu, Frederick Cheung, Jocelyne M. Lew, Ruslan Sanishvili, Andrzej Joachimiak, Cheryl H. Arrowsmith, Dinesh Christendat, Aled M. Edwards, "The Structural Basis for Methylmalonic Aciduria: The Crystal Structure of Archaeal ATP:Colbalamin Adenosyltransferase," *J. Biol. Chem.* 279 (22), May, 23646-23653 (2004).
- Kenneth Sauer, Vittalk. Yachandra, "The water-oxidation complex in photosynthesis," *BBA-Bioenergetics* 1655, April, 140-148 (2004).
- Alexei Savchenko, Tatiana Skarina, Elena Evdokimova, James D. Watson, Roman Laskowski, Cheryl H. Arrowsmith, Aled M. Edwards, Andrzej Joachimiak, Rong-guang Zhang, "X-ray crystal structure of CutA from *Thermotoga maritima* at 1.4 Å resolution reveals potential ligand site," *Proteins* 54, 162-165 (2004).
- Savvas N. Savvides, Srinivasan Raghunathan, Klaus Fütterer, Alex G. Kozlov, Timothy M. Lohman, Gabriel Waksman, "The C-terminal domain of full-length *E. coli* SSB is disordered even when bound to DNA," *Protein Sci.* 13, 1942-1947 (2004).
- S. K. Saxena, H.-P. Liermann, G. Shen, "Formation of iron hydride and high-magnetite at high pressure and temperature," *Phys. Earth Planet. In.* 146, 313-317 (2004).
- G. Scapin, S. B. Patel, C. Chung, J. P. Varnerin, S. D. Edmondson, A. Mastracchio, E. R. Parmee, S.B. Singh, J. W. Becker, L. L. T. Van der Ploeg, M. R. Tota, "Crystal Structure of Human Phosphodiesterase 3B: Atomic Basis for Substrate and Inhibitor Specificity," *Biochemistry-US* 43 (20), 6091-6100 (2004).
- Giovanna Scapin, Sangita B. Patel, Patricia M. Cameron, Betsy Frantz-Wattley, Edward O'Neill, Joseph W. Becker, "Lattice stabilization and enhanced diffraction in human p38 γ crystals by protein engineering," *Biochim. Biophys. Acta* 1696, January, 67-73 (2004).
- K. G. Scheckel, C. A. Impellitteri, J. A. Ryan, "Lead Sorption on Ruthenium Oxide: A Macroscopic and Spectroscopic Study," *Environ. Sci. Technol.* 38 (10), May, 2836-2842 (2004).
- K. G. Scheckel, E. Lombi, S. A. Rock, M. J. McLaughlin, "*In Vivo* Synchrotron Study of Thallium Speciation and Compartmentation in *Iberis intermedia*," *Environ. Sci. Technol.* 38 (19), 5095-5100 (2004).
- Marius Schmidt, Reinhard Pahl, Vukica Srajer, Spencer Anderson, Zhong Ren, Hyotcherl Ihee, Sudarshan Rajagopal, Keith Moffat, "Protein kinetics: Structures of intermediates and reaction mechanism from time-resolved x-ray data," *Proc. Natl. Acad. Sci.* 101 (14), 4799-4804 (2004).
- Florian D. Schubot, David S. Waugh, "A pivotal role for reductive methylation in the *de novo* crystallization of a ternary complex composed of *Yersinia pestis* virulence factors YopN, SycN and YscB," *Acta Crystallogr. D* 60, 1981-1986 (2004).
- Robert Schwarzenbacher, Frankvon Delft, Polat Abdubek, Eileen Ambing, Tanja Biorac, Linda S. Brinen, Jaume M. Canaves, Jamison Cambell, Hsui-Ju Chiu, Xiaoping Dai, Ashley M. Deacon, Mike DiDonato, Marc-André Elsliger, Said Eshagi, Ross Floyd, Adam Godzik, Carina Grittini, SlawomirK. Grzechnik, Eric Hampton, Lukasz Jaroszewski, Cathy Karlak, Heath E. Klock, Eric Koesema, John S. Kovarik, Andreas Kreis, Peter Kuhn, Scott A. Lesley, Inna Levin, Daniel McMullan, Timothy M. McPhillips, Mitchell D. Miller, Andrew Morse, Kin Moy, Jie Ouyang, Rebecca Page, Kevin Quijano, Alyssa Robb, Glen Spraggon, Raymond C. Stevens, Henryvanden Bedem, Jeff Velasquez, Juli Vincent, Xianhong Wang, Bill West, Guenter Wolf, Qingping Xu, Keith O. Hodgson, John Wooley, Ian A. Wilson, "Crystal structure of a putative PII-like signaling protein (TM0021) from *Thermotoga maritima* at 2.5 Å resolution," *Proteins* 54 (4), 810-813 (2004).
- H. P. Scott, R. J. Hemley, H.-k. Mao, D. R. Herschback, L. E. Fried, W. M. Howard, S. Bastea, "Generation of methane in the Earth's mantle: *In situ* high pressure-temperature measurements of carbonate reduction," *Proc. Natl. Acad. Sci.* 101 (39), September, 14023-14026 (2004).

- Dario Segura-Pena, Nikolina Sekulic, Stephan Ort, Manfred Konrad, Arnon Lavie, "Substrate-Induced Conformational Changes in Human UMP/CMP Kinase," *J. Biol. Chem.* 279 (32), August, 33882-33889 (2004).
- R. Senter, C. Pantea, Y. Wang, H. Liu, T. Zerda, J. Coffey, "Structural influence of erbium centers on silicon nanocrystal phase transitions," *Phys. Rev. Lett.* 93 (17), October, 175502-1-175502-4 (2004).
- E.C. Settembre, P.C. Dorrestein, H. Zhai, A. Chatterjee, F.W. McLafferty, T.P. Begley, S.E. Ealick, "Thiamin Biosynthesis in *Bacillus subtilis*: Structure of the Thiazole Synthase/Sulfur Carrier Protein Complex," *Biochemistry-US* 43, 11647-11657 (2004).
- Paul L. Shaffer, Arif Jivan, D. Eric Dollins, Frank Claessens, Daniel T. Gewirth, "Structural basis of androgen receptor binding to selective androgen response elements," *Proc. Natl. Acad. Sci.* 101 (14), April, 4758-4763 (2004).
- T.K. Sham, S.J. Naffel, P.-S.G. Kim, R. Sammynaiken, Y.H. Tang, I. Coulthard, A. Moewes, J.W. Freeland, Y.-F. Hu, S.T. Lee, "Electronic structure and optical properties of silicon nanowires: A study using x-ray excited optical luminescence and x-ray emission spectroscopy," *Phys. Rev. B* 70, 045313: 1-8 (2004).
- S. D. Shastri, "Combining flat crystals, bent crystals, and compound refractive lenses for high-energy x-ray optics," *J. Synchrotron Rad.* 11, 150-156 (2004).
- G. Shen, V. B. Prakapenka, M. L. Rivers, S. R. Sutton, "Structure of Liquid Iron at Pressures up to 58 GPa," *Phys. Rev. Lett.* 92 (18), May, 185701-1-185701-4 (2004).
- G. Shen, M. L. Rivers, S. R. Sutton, N. Sata, V. B. Prakapenka, J. Oxley, K. S. Suslick, "The structure of amorphous iron at high pressures to 67 GPa measured in a diamond anvil cell," *Phys. Earth Planet. In.* 143, 481-495 (2004).
- G. Shen, W. Sturhahn, E. E. Alp, J. Zhao, T. S. Toellner, V. B. Prakapenka, Y. Meng, H.-k. Mao, "Phonon density of states in iron at high pressures and high temperatures," *Phys. Chem. Miner.* 31, 353-359 (2004).
- Yuequan Shen, Natalia L. Zhukovskaya, Michael I. Zimmer, Sandriyana Soelaiman, Pamela Bergson, Chung-Ru Wang, Craig S. Gibbs, Wei-Jen Tang, "Selective inhibition of anthrax edema factor by adefovir, a drug for chronic hepatitis B virus infection," *Proc. Natl. Acad. Sci.* 101, 3242-3247 (2004).
- Yuequan Shen, Qing Guo, Natalia L. Zhukovskaya, Chester L. Drum, Andrew Bohm, Wei-Jen Tang, "Structure of anthrax edema factor-calmodulin-adenosine 5'-(alpha,beta-methylene)-triphosphate complex reveals an alternative mode of ATP binding to the catalytic site," *Biochem. Biophys. Res. Commun.* 317 (2), 309-314 (2004).
- S. R. Shieh, T. S. Duffy, G. Shen, "Elasticity and strength of calcium silicate perovskite at lower mantle pressures," *Phys. Earth Planet. In.* 143, 93-105 (2004).
- S.-H. Shim, T. S. Duffy, R. Jeanloz, G. Shen, "Stability and crystal structure of MgSiO₃ perovskite to the core-mantle boundary," *Geophys. Res. Lett.* 31, May, L10603-L10607 (2004).
- O. Shpyrko, M. Fukuto, P. Pershan, B. Ocko, I. Kuzmenko, T. Gog, M. Deutsch, "Surface layering of liquids: The role of surface tension," *Phys. Rev. B* 69, 245423-1-245423-5 (2004).
- O.G. Shpyrko, A.Yu. Grigoriev, C. Steimer, P.S. Pershan, B. Lin, M. Meron, T. Graber, J. Gebhardt, B. Ocko, M. Deutsch, "Anomalous Layering at the Liquid Sn Surface," *Phys. Rev. B* 70 (22), December, 224106-1-224106-7 (2004).
- V. Shutthanandan, S. Thevuthasan, S. M. Heald, T. Droubay, M. H. Engelhard, T.C. Kaspar, D. E. McCready, L. Saraf, S. A. Chambers, B. S. Mun, N. Hamdan, P. Nachimuthu, B. Taylor, R. P. Sears, B. Sinkovic, "Room-temperature ferromagnetism in ion-implanted Co-doped TiO₂(110) rutile," *Appl. Phys. Lett.* 84 (22), May, 4466-4468 (2004).
- E. Allen Sickmier, Kenneth N. Kreuzer, Stephen W. White, "The Crystal Structure of the UvsW Helicase from Bacteriophage T4," *Structure* 12, April, 583-592 (2004).
- Alex U. Singer, Darrell Desveaux, Laurie Betts, Jeff H. Chang, Zachary Nimchuk, Sarah R. Grant, Jeffery L. Dangel, John Sondek, "Crystal Structures of the Type III Effector Protein AvrPphF and Its Chaperone Reveal Residues Required for Plant Pathogenesis," *Structure* 12 (9), September, 1669-1681 (2004).
- A. Singh, H. Liermann, S. Saxena, "Strength of magnesium oxide under high pressure: evidence for the grain-size dependence," *Solid State Commun.* 132, October, 795-798 (2004).
- J.T.Graham Solomons, Ella M. Zimmerly, Suzanne Burns, N. Krishnamurthy, Michael K. Swan, Sandra Krings, Hilary Muirhead, John Chirgwin, Christopher Davies, "The Crystal Structure of Mouse Phosphoglucose Isomerase at 1.6 Å Resolution and its Complex with Glucose 6-Phosphate Reveals the Catalytic Mechanism of Sugar Ring Opening," *J. Mol. Biol.* 342 (3), September, 847-860 (2004).
- M. Sommerhalter, W.C. Voegtli, D.L. Perlstein, J. Ge, J. Stubbe, A.C. Rosenzweig, "Structures of the Yeast Ribonucleotide Reductase Rnr2 and Rnr4 Homodimers," *Biochemistry-US* 43, 7736-7742 (2004).
- D.J. Sordelet, E. Rozhkova, M.F. Besser, M.J. Kramer, "Meta-stable quasicrystal formation in vitrified and solid state synthesized amorphous Zr-based alloys," *J. Non-Cryst. Solids* 334 & 335, 263-269 (2004).
- M.K. Sorenson, S.S. Ray, S.A. Darst, "Crystal structure of the flagellar σ /anti- σ complex σ^{28} /FlgM reveals an intact σ factor in an inactive conformation," *Molecular Cell* 14 (1), April, 127-138 (2004).
- S. H. Southworth, R. W. Dunford, D. L. Ederer, E. P. Kanter, B. Krässig, L. Young, "Inner-shell photoionization in weak and strong radiation fields," *Radiat. Phys. Chem.* 70 (4-5), July, 655-660 (2004).
- E. D. Specht, P. F. Tortorelli, P. Zschack, "In situ measurement of growth stress in alumina scale," *Powder Diffr.* 19 (1), March, 69-73 (2004).
- E. A. Stern, S.-W. Han, D. Haskel, "Dynamic inhomogeneities in the La₂CuO₄-based superconductors," *J. Superconduct.* 17 (12), February, 97-102 (2004).

- S.R. Stock, K. Ignatiev, P.L. Lee, K. Abbott, L.M. Pachman, "Pathological calcification in Juvenile Dermatomyositis (JDM): MicroCT and synchrotron x-ray diffraction reveal hydroxyapatite with varied microstructures," *Connect Tissue Res.* 45, 248-256 (2004).
- Kristen Strand, James E. Knapp, Balaji Bhyravbhatla, William E. Royer Jr., "Crystal Structure of the Hemoglobin Dodecamer from *Lumbricus Erythrocytorin*: Allosteric Core of Giant Annelid Respiratory Complexes," *J. Mol. Biol.* 344 (1), November, 119-134 (2004).
- J. Stremper, I. Zegkinoglou, U. Ruett, M. V. Zimmermann, C. Bernhard, C. T. Lin, Th. Wolf, B. Keimer, "Oxygen superstructures throughout the phase diagram of $(Y,Ca)Ba_2Cu_3O_{6+x}$," *Phys. Rev. Lett.* 93 (15), October, 157007-1-157007-4 (2004).
- J. Stremper, U. Ruett, S. P. Bayrakci, Th. Brueckel, W. Jauch, "Magnetic properties of transition metal fluorides MF_2 (M = Mn, Fe, Co, Ni) via high-energy photon diffraction," *Phys. Rev. B* 69, 014417-1-014417-9 (2004).
- V. V. Struzhkin, H.-k. Mao, D. Errandonea, W. L. Mao, R. J. Hemley, W. Sturhahn, E. E. Alp, C. L'Abbe, M. Y. Hu, "Phonon density of states and elastic properties of Fe-based materials under compression," *Hyperfine Interact.* 153, 3-15 (2004).
- Viktor V. Struzhkin, Russell J. Hemley, Ho-kwang Mao, "New condensed matter probes for diamond anvil cell technology," *J. Phys. Condens. Matter* 16, S1071-S1086 (2004).
- Joseph Strzalka, Elaine DiMasi, Ivan Kuzmenko, Thomas Gog, J. Kent Blasie, "Resonant x-ray reflectivity from a bromine-labeled fatty acid Langmuir monolayer," *Phys. Rev. E* 70, November, 051603-1-051603-5 (2004).
- Joseph Strzalka, Brian R. Gibney, Sushil Satija, J. Kent Blasie, "Specular neutron reflectivity and the structure of artificial protein maquettes vectorially oriented at interfaces," *Phys. Rev. E* 70, December, 061905 (2004).
- W. Sturhahn, "Nuclear resonant spectroscopy," *J. Phys. Condens. Matter* 16, S497-S530 (2004).
- W. Sturhahn, C. L'abbe, T. S. Toellner, "Exo-interferometric phase determination in nuclear resonant scattering," *Europhys. Lett.* 66 (4), 506-512 (2004).
- K. Suino, L. Peng, R. Reynolds, Y. Li, J. Cha, J.J. Repa, S.A. Kliewer, H.E. Xu, "The Nuclear Xenobiotic Receptor CAR: Structural Determinants of Constitutive Activation and Heterodimerization," *Mol. Cell* 16 (5), December, 893-905 (2004).
- X.H. Sun, N.B. Wong, C.P. Li, S.T. Lee, P.S.G. Kim, T.K. Sham, "Reductive Self-assembling of Pd and Rh Nanoparticles on Silicon Nanowire Templates," *Chem. Mater.* 16, 1143-1152 (2004).
- B. Svensson, D. M. Tiede, D. R. Nelson, B. A. Barry, "Structural Studies of the Manganese-stabilizing Subunit of Photosystem II," *Biophys. J.* 86 (32), March, 1807-1812 (2004).
- Michael K. Swan, Thomas Hansen, Peter Schonheit, Christopher Davies, "A Novel Phosphoglucose Isomerase (PGI)/Phosphomannose Isomerase from the Crenarchaeon *Pyrobaculum aerophilum* Is a Member of the PGI Superfamily," *J. Biol. Chem.* 279 (38), September, 39838-39845 (2004).
- Michael K. Swan, Thomas Hansen, Peter Schonheit, Christopher Davies, "Structural Basis for Phosphomannose Isomerase Activity in Phosphoglucose Isomerase from *Pyrobaculum aerophilum*: A Subtle Difference between Distantly Related Enzymes," *Biochemistry-US* 43, October, 14088-14095 (2004).
- Mark R. Swingle, Richard E. Honkanen, Ewa M. Ciszak, "Structural Basis for the Catalytic Activity of Human Serine/Threonine Protein Phosphatase-5," *J. Biol. Chem.* 279 (32), August, 33992-33999 (2004).
- R.E. Sykora, L. Deakin, A. Mar, S. Skanthakumar, L. Soderholm, T. E. Albrecht-Schmitt, "Isolation of Intermediate-Valent Ce(III)/Ce(IV) Hydrolysis Products in the Preparation of Cerium Iodates: Electronic and Structural Aspects of $Ce_2(IO_3)_6(OH)_x$ ($x=0$ and 0.44)," *Chem. Mater.* 16 (7), 1343-1349 (2004).
- J. Symersky, Y. Zhang, N. Schormann, S. Li, R. Bunzel, P. Pruet, C.-H. Luan, M. Luo, "Structural genomics of *Caenorhabditis elegans*: structure of the BAG domain," *Acta Crystallogr. D* 60, 1606-1610 (2004).
- Keiji Takamoto, Rhiju Das, Qin He, Sebastian Doniachhttp, Michael Brenowitz, Daniel Herschlag, Mark R. Chance, "Principles of RNA Compaction: Insights from the Equilibrium Folding Pathway of the P4-P6 RNA Domain in Monovalent Cations," *J. Mol. Biol.* 343 (5), November, 1195-1206 (2004).
- R. Tanaka, E. Sato, J. E. Hunt, R. E. Winans, S. Sato, T. Takanohashi, "Characterization of Asphaltene Aggregates Using X-ray Diffraction and Small-Angle X-ray Scattering," *Energ. Fuel* 18 (6), November, 1118-1125 (2004).
- B. Taneja, S. Maar, L. Shuvalova, F. Collart, W. Anderson, A. Mondragon, "Structure of the *Bacillus subtilis* YYCN protein: a putative N-acetyltransferase," *Proteins* 53 (4), 950-952 (2004).
- Y. S. Tarahovsky, R. Koynova, R. C. MacDonald, "DNA release from lipoplexes by anionic lipids: correlation with lipid mesomorphism, interfacial curvature, and membrane fusion," *Biophys. J.* 87, 1054-1064 (2004).
- Wolfram Tempel, Zhi-Jie(James) Liu, Florian D. Schubot, Ashit Shah, Michael V. Weinberg, Francis E. Jenney Jr., W. Bryan Arendall III, Michael W.W. Adams, Jane S. Richardson, David C. Richardson, John P. Rose, Bi-Cheng Wang, "Structural Genomics of *Pyrococcus furiosus*: X-Ray Crystallography Reveals 3D Domain Swapping in Rubrerythrin," *Proteins* 57, October, 878-882 (2004).
- Mohammed Terrak, Frederic Kerff, Knut Langsetmo, Terence Tao, Roberto Dominguez, "Structural basis of protein phosphatase 1 regulation," *Nature* 429, 780-784 (2004).
- Michael J. Theisen, Ila Misra, Dana Saadat, Nino Campobasso, Henry M. Miziorko, David H. T. Harrison, "3-hydroxy-3-methylglutaryl-CoA synthase intermediate complex observed in real time," *Proc. Natl. Acad. Sci.* 101 (47), November, 16442-16447 (2004).
- J.B. Thoden, E.A. Taylor-Ringia, J.B. Garrett, J.A. Gerlt, H.M. Holden, I. Rayment, "Evolution of Enzymatic Activity in the Enolase Superfamily: Structural Studies of the Promiscuous O-Succinylbenzoate Synthase from *Amycolatopsis*," *Biochemistry-US* 43 (19), 5716-5727 (2004).
- James B. Thoden, Xinyi Huang, Jungwook Kim, Frank M. Raushel, Hazel M. Holden, "Long-range allosteric transitions in carbamoyl phosphate synthetase," *Protein Sci.* 13, 2398-2405 (2004).

- C.J. Thomas, X. Du, P. Li, Y. Wang, E.M. Ross, S.R. Sprang, "Uncoupling Conformational Change from GTP Hydrolysis in a Heterotrimeric G Protein [Alpha]-Subunit," *Proc. Natl. Acad. Sci.* 101 (20), March, 7560-7565 (2004).
- Yunfeng Tie, Peter I. Boross, Yuan-Fang Wang, Laquasha Gaddis, Azhar K. Hussain, Sofiya Leshchenko, Arun K. Ghosh, John M. Louis, Robert W. Harrison, Irene T. Weber, "High Resolution Crystal Structures of HIV-1 Protease with a Potent Non-peptide Inhibitor (UIC-94017) Active Against Multi-drug-resistant Clinical Strains," *J. Mol. Biol.* 338, 341-352 (2004).
- D. M. Tiede, R. Zhang, L. X. Chen, L. Yu, J. S. Lindsey, "Structural Characterization of Modular Supramolecular Architectures in Solution," *J. Am. Chem. Soc.* 126, November, 14054-14062 (2004).
- A. M. Tikhonov, S. Venkatesh Pingali, M. Schlossman, "Molecular ordering and phase transitions in alkanol monolayers at the water-hexane interface," *J. Chem. Phys.* 120 (24), June, 11822-11838 (2004).
- D. Tinker, C. E. Leshner, G. M. Baxter, T. Uchida, Y. Wang, "High-pressure viscometry of polymerized silicate melts and limitations of the Eyring equation," *Am. Mineral.* 89 (11-12), November, 1701-1708 (2004).
- T. K. Tokunaga, J. Wan, J. Pena, S. R. Sutton, M. Newville, "Hexavalent uranium diffusion into soils from concentrated acidic and alkaline solutions," *Environ. Sci. Technol.* 38, 3056-3062 (2004).
- Y. V. Tolmachev, A. Menzel, A. V. Tkachuk, Y. S. Chu, H. You, "*In Situ* Surface X-ray Scattering Observation of Long-range Ordered $\sqrt{19} \times \sqrt{19}$ R23.4 degrees - 13CO Structure on Pt(111) in Aqueous Electrolytes," *Electrochem. Solid St.* 7 (3), January, E23-E26 (2004).
- A.V. Toms, C. Kinsland, D.E. McCloskey, A.E. Pegg, S.E. Ealick, "Evolutionary Links as Revealed by the Structure of *Thermotoga maritima* S-adenosyl-methionine Decarboxylase," *J. Biol. Chem.* 279, 33837-33846 (2004).
- Jennifer Townes, Adam Golebiowski, Michael Clark, Matthew Laufersweiler, Todd Brugel, Mark Sabat, Roger Bookland, Steve Laughlin, John VanRens, Biswanath De, Lily Hsieh, Susan Xu, Michael Janusz, Richard Walters, "The development of new bicyclic pyrazole-based cytokine synthesis inhibitors," *Bioorg. Med. Chem. Lett.* 14, 4945-4948 (2004).
- S.A. Townson, J.C. Samuelson, E.S. Vanamee, T.A. Edwards, C.R. Escalante, S.Y. Xu, A.K. Aggarwal, "Crystal structure of BstYI at 1.85Å resolution: a thermophilic restriction endonuclease with overlapping specificities to BamHI and BglII," *J. Mol. Biol.* 338 (4), May, 725-733 (2004).
- T.P. Trainor, A. M. Chaka, P. J. Eng, M. Newville, G. A. Waychunas, J.G. Catalano, G.E. Brown, "Structure and reactivity of the hydrated hematite (0001) surface," *Surf. Sci.* 573, 204-224 (2004).
- Jose Trincão, Robert E. Johnson, William T. Wolfle, Carlos R. Escalante, Satya Prakash, Louise Prakash, Aneel K. Aggarwal, "Dpo4 is hindered in extending a GoT mismatch by a reverse wobble," *Nat. Struct. Mol. Biol.* 11, April, 457-462 (2004).
- F. Tsui, Y. S. Chu, "The combinatorial approach: A useful tool for studying epitaxial processes in doped magnetic semiconductors," *Macromol. Rapid Commun* 25, January, 189-195 (2004).
- F. Tsui, L. He, A. Tkachuk, S. Vogt, Y. S. Chu, "Evidence for strain compensation in stabilizing epitaxial growth of magnetically doped germanium," *Phys. Rev. B* 69, 081304 1-4 (2004).
- L.D. Turner, B.B. Dahl, J.P. Hayes, A.P. Mancuso, K.A. Nugent, D. Paterson, R.E. Scholten, C.Q. Tran, A.G. Peele, "X-ray phase imaging: Demonstration of extended conditions with homogeneous objects," *Opt. Express* 12 (13), June, 2960-2965 (2004).
- Steve Tuske, Stefan G. Sarafianos, Arthur D. Clark Jr., Jianping Ding, Lisa K. Naeger, Kirsten L. White, Michael D. Miller, Craig S. Gibbs, Paul L. Boyer, Patrick Clark, Gang Wang, Barbara L. Gaffney, Roger A. Jones, Donald M. Jerina, Stephen H. Hughes, Eddy Arnold, "Structures of HIV-1 RT-DNA complexes before and after incorporation of the anti-AIDS drug tenofovir," *Nat. Struct. Mol. Biol.* 11 (5), 469-474 (2004).
- B.S. Twining, S.B. Baines, N.S. Fisher, M.R. Landry, "Cellular iron contents of plankton during the Southern Ocean Iron Experiment (SOFeX)," *Deep-Sea Res. Pt. I* 51, 1827-1850 (2004).
- B.S. Twining, S.B. Baines, N.S. Fisher, "Element stoichiometries of individual plankton cells collected during the Southern Ocean Iron Experiment (SOFeX)," *Limnol. Oceanogr.* 49 (6), 2115-2128 (2004).
- Sacha N. Uljon, Robert E. Johnson, Thomas A. Edwards, Satya Prakash, Louise Prakash, Aneel K. Aggarwal, "Crystal Structure of the Catalytic Core of Human DNA Polymerase Kappa," *Structure* 12 (8), 1395-1404 (2004).
- J. Urquidí, C. J. Benmore, P. A. Egelstaff, M. Guthrie, S. E. McLain, C. Tulk, D. D. Klug, J. F. C. Turner, "A Structural Comparison of Supercooled Water and Intermediate Density Amorphous Ices," *Mol. Phys.* 102 (19-20), October, 2007-2014 (2004).
- D. Vaknin, S. Dahlke, A. Travesset, G. Nizri, S. Magdassi, "Induced Crystallization of Polyelectrolyte-Surfactant Complexes at the Gas-Water Interface.," *Phys. Rev. Lett.* 93 (21), November, 218302-1-218302-4 (2004).
- Bert Van Den Berg, William M. Clemons Jr., Ian Collinson, Yorgo Modis, Enno Hartmann, Stephen C. Harrison, Tom A. Rapoport, "X-ray structure of a protein-conducting channel," *Nature* 427, 36-44 (2004).
- Robert M. Vanacore, Sivananthaperumal Shanmugasundararaj, David B. Friedman, Olga Bondar, Billy G. Hudson, Munirathinam Sundaramoorthy, "The a1.a2 Network of Collagen IV," *J. Biol. Chem.* 279 (43), October, 44723-44730 (2004).
- K. Venkataraman, A. J. Kropf, C. U. Segre, Q. Jia, A. Goyal, S. Chattopadhyay, V. A. Maroni, "Detection of interfacial strain and phase separation in $\text{MBA}_{2}\text{Cu}_{3}\text{O}_{7-x}$ thin films using Raman spectroscopy and X-ray diffraction space mapping," *Physica C* 402, February, 1-16 (2004).
- R. Vidal-Michel, K. L. Hohn, "Effect of crystal size on the oxidative dehydrogenation of butane on V/MgO catalysts," *J. Catal.* 221 (1), January, 127-136 (2004).
- D. Vigil, D. K. Blumenthal, W. T. Heller, S. Brown, J. M. Canaves, S. S. Taylor, J. Trewhell, "Conformational Differences Among Solution Structures of the Type I[alpha], II[alpha], and II[beta] Protein Kinase A Regulatory Subunit Homodimers: Role of the Linker Regions," *J. Mol. Biol.* 337 (5), 1183-1194 (2004).

- D. Vigil, D. K. Blumenthal, S. Brown, S. S. Taylor, J. Trehwella, "Differential Effects of Substrate on Type I and Type II PKA Holoenzyme Dissociation," *Biochemistry-US* 43, 5629-5636 (2004).
- S. Vijay, E. E. Wolf, J. T. Miller, A. J. Kropf, "A Highly Active and Stable Platinum-Modified Sulfated Zirconia Catalyst - Part 2. EXAFS Studies of the Effect of Pretreatment on the State of Platinum," *Appl. Catal. A-Gen.* 264, 125-130 (2004).
- Erik M. Vogan, Cornelia Bellamacina, Xuemei He, Hung-wen Liu, Dagmar Ringe, Gregory A. Petsko, "Crystal Structure at 1.8 Å Resolution of CDP-D-Glucose 4,6-Dehydratase from *Yersinia pseudotuberculosis*," *Biochemistry-US* 43, 3057-3067 (2004).
- S. Vogt, Y. S. Chu, A. Tkachuk, P. Ilinski, D. A. Walko, F. Tsui, "Composition characterization of combinational materials by scanning X-ray fluorescence microscopy using microfocused synchrotron X-ray beam," *Appl. Surf. Sci.* 223, February, 214-219 (2004).
- Zhuli Wan, Bin Xu, Kun Huang, Ying-Chi Chu, Biaoru Li, Satoe H. Nakagawa, Yan Qu, Shi-Quan Hu, Panayotis G. Katsoyannis, Michael A. Weiss, "Enhancing the Activity of Insulin at the Receptor Interface: Crystal Structure and Photo-Cross-Linking of A8 Analogue," *Biochemistry-US* 43 (51), 16119-16133 (2004).
- J. Wang, S.E. Ealick, "Observation of time-resolved structural changes by linear interpolation of highly redundant X-ray diffraction data," *Acta Crystallogr. D* 60, 1579-1585 (2004).
- Y. Wang, T. Uchida, J. Zhang, M. L. Rivers, S. R. Sutton, "Thermal equation of state of akimotoite MgSiO₃ and effects of the akimotoite-garnet transformation on seismic structure near the 660 km discontinuity," *Phys. Earth Planet. In.* 143, 57-80 (2004).
- Yanbin Wang, Takeyuki Uchida, Robert Von Dreele, Mark L. Rivers, Norimasa Nishiyama, Ken-ichi Funakoshi, Akifumi Nozawac, Hiroshi Kanekod, "A new technique for angle-dispersive powder diffraction using an energy-dispersive setup and synchrotron radiation," *J. Appl. Crystallogr.* 37, 947-956 (2004).
- Jeffrey Watson, Franklin A. Hays, P. Shing Ho, "Definitions and Analysis of DNA Holliday Junction Geometry," *Nucleic Acids Res.* 32 (10), 3017-3027 (2004).
- Andrew I. Webb, Michelle A. Dunstone, Weisan Chen, Marie-Isabel Aguilar, Qiyuan Chen, Heather Jackson, Linus Chang, Lars Kjer-Nielsen, Travis Beddoe, James McCluskey, Jamie Rossjohn, Anthony W. Purcell, "Functional and Structural Characteristics of NY-ESO-1-related HLA A2-restricted Epitopes and the Design of a Novel Immunogenic Analogue," *J. Biol. Chem.* 279 (22), May, 23438-23446 (2004).
- Andrew I. Webb, Natalie A. Borg, Michelle A. Dunstone, Lars Kjer-Nielsen, Travis Beddoe, James McCluskey, Francis R. Carbone, Stephen P. Bottomley, Marie-Isabel Aguilar, Anthony W. Purcell, Jamie Rossjohn, "The Structure of H-2Kb and Kbm8 Complexed to a *Herpes simplex* Virus Determinant: Evidence for a Conformational Switch That Governs T Cell Repertoire Selection and Viral Resistance," *J. Immunol.* 173, 402-409 (2004).
- N.A. Webb, A.M. Mulichak, J.S. Lam, H.L. Rocchetta, R.M. Garavito, "Crystal structure of a tetrameric GDP-D-mannose 4,6-dehydratase from a bacterial GDP-D-rhamnose biosynthetic pathway," *Protein Sci.* 13, 529-539 (2004).
- J. K. R. Weber, C. J. Benmore, J. Siewenie, J. Urquidi, T. S. Key, "Structure and bonding in single- and two-phase alumina-based glasses," *Phys. Chemm. Chem. Phys.* 6, March, 2480-2483 (2004).
- T.-C. Weng, W.-Y. Hiseh, E. S. Uffelman, S. W. Gordon-Wylie, T. J. Collins, V. L. Pecoraro, J. E. Penner-Hahn, "XANES Evidence Against a Manganyl Species in the S₃ State of the Oxygen-Evolving Complex," *J. Am. Chem. Soc.* 126 (26), 8070-8071 (2004).
- H.-R. Wenk, I. Lonardelli, J. Pehl, J. Devine, V. Prakapenka, G. Shen, H.-k. Mao, "*In situ* observation of texture development in olivine, ringwoodite, magnesiowustite and silicate perovskite at high pressure," *Earth Planet Sc. Lett.* 226, October, 507-519 (2004).
- Ph. Wernet, D. Nordlund, U. Bergmann, M. Cavalleri, M. Odelius, H. Ogasawara, L. Å. Näslund, T. K. Hirsch, L. Ojamäe, P. Glatzel, L. G. M. Pettersson, A. Nilsson, "The Structure of the First Coordination Shell in Liquid Water," *Science* 304, May, 995-999 (2004).
- Eric Westhof, Christian Massire, "Evolution of RNA Architecture," *Science* 306, 62-63 (2004).
- M. C. Wilding, C. J. Benmore, J. A. Tangeman, S. Sampath, "Coordination changes in magnesium silicate glasses," *Europhys. Lett.* 67 (2), July, 212-218 (2004).
- M. C. Wilding, C. J. Benmore, J. A. Tangeman, S. Sampath, "Evidence of Different Structures in Magnesium Silicate Liquids: Coordination Changes in Forsterite-to-Enstatite Composition Glasses," *Chem. Geol.* 213, December, 218-291 (2004).
- Jeffrey J. Wilson, Margarita Malakhova, Rongguang Zhang, Andrzej Joachimiak, Rashmi S. Hegde, "Crystal Structure of the Dachshund Homology Domain of Human SKI," *Structure* 12 (5), May, 785-792 (2004).
- R. E. Winans, S. Vajda, B. Lee, S. J. Riley, S. Seifert, G. Y. Tikhonov, N. A. Tomczyk, "Thermal Stability of Supported Platinum Clusters Studied by In situ GISAXS," *J. Phys. Chem. B* 108 (47), November, 18105-18107 (2004).
- Eric L. Wise, Julie Akana, John A. Gerltb, Ivan Rayment, "Structure of D-ribulose 5-phosphate 3-epimerase from *Synechocystis* to 1.6 Å resolution," *Acta Crystallogr. D* 60 (9), September, 1687-1690 (2004).
- Eric L. Wise, Wen Shan Yew, John A. Gerlt, Ivan Rayment, "Evolution of Enzymatic Activities in the Orotidine 5'-Monophosphate Decarboxylase Suprafamily: Crystallographic Evidence for a Proton Relay System in the Active Site of 3-Keto-L-gulonate 6-Phosphate Decarboxylase," *Biochemistry-US* 43 (21), 6438-6446 (2004).
- Dennis W. Wolan, Cheom-Gil Cheong, Samantha E. Greasley, Ian A. Wilson, "Structural Insights into the Human and Avian IMP Cyclohydrolase Mechanism via Crystal Structures with the Bound XMP Inhibitor," *Biochemistry-US* 43 (5), 1171-1183 (2004).
- G. H. Wolf, A. V. G. Chizmeshya, J. Diefenbacher, M. J. McKelvy, "*In Situ* Observation of CO₂ Sequestration Reactions using a Novel Microreaction System," *Environ. Sci. Technol.* 38 (3), 932-936 (2004).
- Joe Wong, M. Wall, A. J. Schwartz, R. Xu, M. Holt, Hawoong Hong, P. Zschack, T.-C. Chiang, "Imaging phonons in a fcc Pu-Ga alloy by thermal diffuse x-ray scattering," *Appl. Phys. Lett.* 84 (19), May, 3747-3749 (2004).

- Beili Wu, Pengyun Li, Yiwei Liu, Zhiyong Lou, Yi Ding, Cuiling Shu, Sheng Ye, Mark Bartlam, Beifen Shen, Zihe Rao, "3D structure of human FK506-binding protein 52: Implications for the assembly of the glucocorticoid receptor/Hsp90/immunophilin heterocomplex," *Proc. Natl. Acad. Sci.* 101 (22), 8348-8353 (2004).
- Di Xia, Lothar Esser, Satyendra K. Singh, Fusheng Guo, Michael R. Maurizi, "Crystallographic investigation of peptide binding sites in the N-domain of the ClpA chaperone," *J. Struct. Biol.* 146 (1-2), 166-179 (2004).
- Tsan Xiao, Junichi Takagi, Barry S. Collier, Jia-Huai Wang, Timothy A. Springer, "Structural basis for allostery in integrins and binding to fibrinogen-mimetic therapeutics," *Nature* 432, November, 59-67 (2004).
- Y. Xiao, D. Wittmer, S. Mini, T. Graber, P.J. Viccaro, Fujio Izumi, "Determination of cations distribution in Mn[subscript 3]O[subscript 4] by anomalous x-ray powder diffraction," *Appl. Phys. Lett.* 85 (5), August, 736-738 (2004).
- Xu Xing, Charles E. Bell, "Crystal Structures of *Escherichia coli* RecA in a Compressed Helical Filament," *J. Mol. Biol.* 342 (5), October, 1471-1485 (2004).
- Yi Xing, Dan Liu, Rongguang Zhang, Andrzej Joachimiak, Zhou Songyang, Wenqing Xu, "Structural Basis of Membrane Targeting by the Phox Homology Domain of Cytokine-independent Survival Kinase (CISK-PX)," *J. Biol. Chem.* 279 (29), 30662-30669 (2004).
- Y. Xiong, T.A. Steitz, "Mechanism of transfer RNA maturation by CCA-adding enzyme without using an oligonucleotide template," *Nature* 430, 640-645 (2004).
- J. Xu, H.-k. Mao, R. J. Hemley, "Large volume high-pressure cell with supported moissanite anvils," *Rev. Sci. Instrum.* 75 (4), March, 1034-1038 (2004).
- J. Xu, Y. Ding, S. D. Jacobsen, H.-k. Mao, R. J. Hemley, J. Zhang, J. Qian, C. Pantea, S. C. Vogel, D. J. Williams, Y. Zhao, "Powder neutron diffraction of wustite (Fe[subscript 0.93]O) to 12 GPa using large moissanite anvils," *High Pressure Res.* 24 (2), June, 247-253 (2004).
- Ting Xu, Naomi J. Logsdon, Mark R. Walter, "Crystallization and X-ray diffraction analysis of insect-cell-derived IL-22," *Acta Crystallogr. D* 60 (7), July, 1295-1298 (2004).
- Y. Xu, J.B. Moseley, I. Sagot, F. Poy, D. Pellman, B.L. Goode, M.J. Eck, "Crystal structures of a formin homology-2 domain reveal a tethered dimer architecture," *Cell* 116 (5), March, 711-723 (2004).
- Yibin Xu, Rongguang Zhang, Andrzej Joachimiak, Paul D. Carr, Thomas Huber, Subhash G. Vasudevan, David L. Ollis, "Structure of the N-Terminal Domain of *Escherichia coli* Glutamine Synthetase Adenylyltransferase," *Structure* 12 (5), 861-869 (2004).
- W. Yang, B. Larson, G. Pharr, G. Ice, J. Budai, J. Tischler, W. Liu, "Deformation microstructure under microindents in single-crystal Cu using three-dimensional x-ray structural microscopy," *J. Mater. Res.* 19 (1), January, 66-72 (2004).
- W. Yang, B.C. Larson, J.Z. Tischler, G.E. Ice, J.D. Budai, W. Liu, "Differential-aperture x-ray structural microscopy: a submicron-resolution three-dimensional probe of local microstructure and strain," *Micron* 35, 431-439 (2004).
- Yuting Yang, Chang-Duk Jun, Jin-huan Liu, Rongguang Zhang, Andrzej Joachimiak, Timothy A. Springer, Jia-huai Wang, "Structural Basis for Dimerization of ICAM-1 on the Cell Surface," *Mol. Cell* 14 (2), April, 269-276 (2004).
- Jiqing Ye, Bert Van Den Berg, "Crystal structure of the bacterial nucleoside transporter Tsx," *EMBO J.* 23, July, 3187-3195 (2004).
- Sheng Ye, Ioannis Vakonakis, Thomas R. Ioerger, Andy C. LiWang, James C. Sacchettini, "Crystal Structure of Circadian Clock Protein KaiA from *Synechococcus elongatus*," *J. Biol. Chem.* 279 (19), 20511-20518 (2004).
- Hye-Jeong Yeo, Shane E. Cotter, Sven Laarmann, Twyla Juehne, Joseph W. St. Geme, Gabriel Waksman, "Structural basis for host recognition by the *Haemophilus influenzae* Hia autotransporter," *EMBO J.* 23, 1245-1256 (2004).
- A. Yilmazbayhan, A. T. Motta, R. J. Comstock, G. P. Sabol, B. Lai, Z. Cai, "Structure of zirconium alloy oxides formed in pure water studied with synchrotron radiation and optical microscopy: relation to corrosion rate," *J. Nucl. Mater.* 324, January, 6-22 (2004).
- Y. Whitney Yin, Thomas A. Steitz, "The Structural Mechanism of Translocation and Helicase Activity in T7 RNA Polymerase," *Cell* 116 (3), February, 393-404 (2004).
- Danielle Zernich, Anthony W. Purcell, Whitney A. Macdonald, Lars Kjer-Nielsen, Lauren K. Ely, Nihay Laham, Tanya Crockford, Nicole A. Mifsud, Mandvi Bharadwaj, Linus Chang, Brian D. Tait, Rhonda Holdsworth, Andrew G. Brooks, Stephen P. Bottomley, Travis Beddoe, Chen Au Peh, Jamie Rossjohn, James McCluskey, "Natural HLA Class I Polymorphism Controls the Pathway of Antigen Presentation and Susceptibility to Viral Evasion," *J. Exp. Med.* 200, 13-24 (2004).
- Jianzhong Zhang, Yusheng Zhao, "Formation of zirconium metallic glass," *Nature* 430, July, 332-335 (2004).
- K. Zhang, R. Lui, T. Irving, D. S. Auld, "A versatile rapid-mixing and flow device for X-ray absorption spectroscopy," *J. Synchrotron Rad.* 11 (2), March, 204-208 (2004).
- Min Zhang, Tommi A. White, Jonathan P. Schuermann, Berevan A. Baban, Donald F. Becker, John J. Tanner*, "Structures of the *Escherichia coli* PutA Proline Dehydrogenase Domain in Complex with Competitive Inhibitors," *Biochemistry-US* 43 (5), October, 12539-12548 (2004).
- R. Zhang, R. Wu, G. Joachimiak, S.K. Mazmanian, D.M. Missiakas, P. Gornicki, O. Schneewind, A. Joachimiak, "Structures of Sortase B from *Staphylococcus aureus* and *Bacillus anthracis* Reveal Catalytic Amino Acid Triad in the Active Site," *Structure* 12, July, 1147-1156 (2004).
- X. Zhang, M. Chodakowski, J. M. Shaw, "Dynamic Interfacial Zone and Local Phase Concentration Measurements in Emulsions, Dispersions, Slurries," *J Disper. Sci. Technol.* 25 (3), 277-285 (2004).
- Y. Zhang, M. Dougherty, D. M. Downs, S.E. Ealick, "Crystal structure of an aminoimidazole riboside kinase from *Salmonella enterica*: Implications for the evolution of the ribokinase superfamily of proteins," *Structure* 12 (10), October, 1809-1821 (2004).

- Y. Zhang, S.E. Cottet, S.E. Ealick, "Structure of *E. coli* AMP Nucleosidase Reveals Similarity to Nucleoside Phosphorylases," *Structure* 12, 1383-1394 (2004).
- Ying Zhang, Alan A. Simpson, Rebecca M. Ledford, Carol M. Bator, Sugoto Chakravarty, Gregory A. Skochko, Tina M. Demenczuk, Adiba Watanyar, Daniel C. Pevear, Michael G. Rossmann, "Structural and Virological Studies of the Stages of Virus Replication That Are Affected by Antirhinovirus Compounds," *Virology* 78, 11061-11069 (2004).
- Ying Zhang, Wei Zhang, Steven Ogata, David Clements, James H. Strauss, Timothy S. Baker, Richard J. Kuhn, Michael G. Rossmann, "Conformational Changes of the Flavivirus E Glycoprotein," *Structure* 9, 1607-1618 (2004).
- Z. Zhang, P. Fenter, L. Cheng, N. C. Sturchio, M. J. Bedzyk, M. L. Machesky, D. J. Wesolowski, "Model-independent X-ray imaging of adsorbed cations at the crystal-water interface," *Surf. Sci.* 554, April, L95-L100 (2004).
- Z. Zhang, P. Fenter, L. Cheng, N. C. Sturchio, M. J. Bedzyk, M. Predota, A. Bandura, J. D. Kubicki, S. N. Lvov, P. T. Cummings, A. A. Chialvo, M. K. Ridley, P. Benezeth, L. Anovitz, D. A. Palmer, M. L. Machesky, D. J. Wesolowski, "Ion Adsorption at the Rutile-Water Interface: Linking Molecular and Macroscopic Properties," *Langmuir* 12 (20), May, 4954-4969 (2004).
- H. L. Zhao, M. J. Kramer, M. Akinc, "Thermal expansion behavior of intermetallic compounds in the Mo-Si-B system," *Intermetallics* 12 (5), 493-498 (2004).
- J. Zhao, G. Shen, W. Sturhahn, E. E. Alp, "Highly efficient gaseous sample loading technique for diamond anvil cells," *Rev. Sci. Instrum.* 75 (12), December, 5149-5151 (2004).
- Kehao Zhao, Xiaomei Chai, Ronen Marmorstein, "Structure and Substrate Binding Properties of cobB, a Sir2 Homolog Protein Deacetylase from *Escherichia coli*," *J. Mol. Biol.* 337 (3), March, 731-741 (2004).
- Rui Zhao, Jingping Shen, Michael R. Green, Margaret MacMorris, Thomas Blumenthal, "Crystal Structure of UAP56, a DEXD/H-Box Protein Involved in Pre-mRNA Splicing and mRNA Export," *Structure* 12 (8), August, 1373-1381 (2004).
- Yiwei Zhao, Zhong Li, Sandra Drozd, Yi Guo, Robert Stack, Hauer Charles, Hongmin Li, "Crystallization and preliminary crystallographic analysis of *Mycoplasma arthritidis*-derived mitogen complexed with peptide/MHC class II antigen," *Acta Crystallogr. D* 60, 353-356 (2004).
- L. Zhong, F. Chen, S.A. Campbell, W.L. Gladfelter, "Nanolaminates of zirconia and silica using atomic layer deposition," *Chem. Mater.* 16, 1098-1103 (2004).
- M. Zhu, F. Shao, R. W. Innes, J. E. Dixon, Z. Xu, "The crystal structure of *Pseudomonas avirulence* protein AvrPphB: A papain-like fold with a distinct substrate binding site," *Proc. Natl. Acad. Sci.* 101, 302-307 (2004).
- Xueyong Zhu, Paul Wentworth Jr., Anita D. Wentworth, Albert Eschenmoser, Richard A. Lerner, Ian A. Wilson, "Probing the antibody-catalyzed water-oxidation pathway at atomic resolution," *Proc. Natl. Acad. Sci.* 101 (8), February, 2247-2252 (2004).
- E. Zolotoyabko, J. Quintana, "Control of synchrotron x-ray diffraction by means of standing acoustic waves," *Rev. Sci. Instrum.* 75 (3), 699-708 (2004).
- E. Zolotoyabko, B. Pokroya, J. P. Quintana, "Depth-resolved strain measurements in polycrystalline materials by energy-variable X-ray diffraction," *J. Synchrotron Rad.* 11, 309-313 (2004).
- Y. Zong, T.W. Bice, H. Ton-That, O. Schneewind, S.V. Narayana, "Crystal Structure of *Staphylococcus Aureus* Sortase a and its Substrate Complex," *J. Biol. Chem.* 279 (30), July, 31383-31389 (2004).
- M. D. de Jonge, Z. Barnea, C. Q. Tran, C. T. Chantler, "Full-foil x-ray mapping of integrated column density applied to the absolute determination of mass attenuation coefficients," *Meas. Sci. Technol.* 15 (9), September, 1811-1822 (2004).
- M. D. de Jonge, Z. Barnea, C. Q. Tran, C. T. Chantler, "X-ray bandwidth: Determination by on-edge absorption and effect on various absorption experiments," *Phys. Rev. A* 69, 022717-1-022717-12 (2004).
- Anne-Marie M. van Roon, Navraj S. Pannu, Johannes P.M. de Vrind, Gijs A. van der Mare, Jacques H. van Boom, Cornelis H. Hokke, André M. Deelder, Jan Pieter Abrahams, "Structure of an Anti-Lewis X Fab Fragment in Complex with Its Lewis X Antigen," *Structure* 12 (7), July, 1227-1236 (2004).
- B. van den Berg, P. N. Black, W. M. Clemons Jr., T. A. Rapoport, "Crystal Structure of the Long-Chain Fatty Acid Transporter FadL," *Science* 304, 1506-1509 (2004).

EXPERIMENTAL RESULTS: CONFERENCE PAPERS

- M. R. Antonio, M.-H. Chiang, C. W. Williams, L. Soderholm, "In situ actinide X-ray absorption spectroelectrochemistry," 2003 Fall MRS Proceedings, L. Soderholm, John J. Joyce, Malcolm F. Nicol, David K. Shuh, J.G. Tobin, eds., 802, MRS (2004) 157 - 168.
- R. Barabash, W. Pantleon, "Characterization of Dislocation Boundary Evolution with Monochromatic X-Ray Diffraction," Evolution of Deformation Microstructures in 3D, C. Gundlach, K. Haldrup, N. Hansen, X. Huang, D. J. Jensen, T. Leffers, Z. J. Li, S. F. Nielsen, W. Pantleon, J. A. Wert, G. Winther, eds., Riso National Laboratory (2004) 233 - 238.
- J.V. Beitz, S. Skanthakumar, S. Seifert, P. Thiyagarajan, "f-Element Influence on the Size of Nanophase Phosphate Inclusions in Silica," MRS Proceedings, J. B. Tobin, J. Joyce, M. F. Nicol, D. Shuh, L. Soderholm, eds., 802, MRS (2004) 125 - 130.
- M. A. Beno, U. Ruett, C. Kurtz, G. Jennings, "High-energy Bragg and Laue monochromators for an APS wiggler beam line," Proc. of the 8th Int'l. Conf. on Synchrotron Radiation Instrumentation, T. Warwick, J. Arthur, H.A. Padmore, J. Stoehr, eds., 705, AIP (2004) 675 - 678.
- T. Buonassisi, M.A. Marcus, A.A. Istratov, M. Heuer, T.F. Ciszek, B. Lai, Z. Cai, E.R. Weber, "Distribution and chemical state of Cu-rich clusters in silicon," 14th Workshop on Crystalline Silicon Solar Cells & Modules: Materials and Processes, NREL (2004) 161 - 164.
- T. Buonassisi, A.A. Istratov, T.F. Ciszek, D.W. Cunningham, A.M. Gabor, R. Jonczyk, R. Schindler, M. Sheoran, A. Upadhyaya, A. Rohatgi, B. Lai, Z. Cai, M.A. Marcus, E.R. Weber, "Differences and similarities between metal clusters in mc-Si materials from different manufacturers," 14th Workshop on Crystalline Silicon Solar Cells & Modules: Materials and Processes, NREL (2004) 226 - 229.

- S.-K. Cheong, J. Liu, D. Shu, J. Wang, C. F. Powell, "Effects of ambient pressure on dynamics of near-nozzle diesel sprays studied by ultrafast x-radiography," 2004 SAE Fuels & Lubricants Meeting and Exhibition, SAE International (2004) 2004-01-2026.
- G. N. Chestnut, B. D. Streetman, D. Schiferl, R. S. Hixson, W. M. Anderson, M. Nicol, Y. Meng, "Static x-ray diffraction study of cerium: The standard approach & magic-angle approach," Proc. of 13th APS Conf. on Shock Compression of Condensed Matter 2003, M.D. Furnish, Y.M. Gupta, J.W. Forbes, eds., 706, American Institute of Physics (2004) 37 - 40.
- D.-H. Do, D.M. Kim, E.-B. Eom, E.M. Dufresne, E.D. Isaacs, P.G. Evans, "Synchrotron x-ray microdiffraction images of polarization switching in epitaxial PZT capacitors with Pt and SrRuO₃ top electrodes," Mat. Res. Soc. Symp. Proc. Vol. 784, MRS (2004) C6.4.1 - C6.4.6.
- D. S. Ebel, M. K. R. Joungh, M.-M. McLow, "Chondrule formation by current sheets in protoplanetary disks," Lunar and Planetary Science XXXV, LPI (2004) 1971.
- M. Egli, V. Tereshko, "Lattice- and Sequence-Dependent Binding of Mg^[superscript 2+] in the Crystal Structure of a B-DNA Dodecamer," Curvature and Deformation of Nucleic Acids: Recent Advances, New Paradigms, N. Stellwagen, U. Mohanty, eds., 884, American Chemical Society (2004) 87 - 109.
- P. Fenter, C. Park, L. Cheng, Z. Zhang, N. C. Sturchio, "New Insights into the Orthoclase Dissolution Mechanism with X-ray Reflectivity," Proceedings of the Eleventh International Symposium on Water-Rock Interaction, R. B. Wanty, R. R. Seal II, Balkema Publishers (2004) 749 - 751.
- G. J. Flynn, L. P. Keller, S. R. Sutton, "Sub-micrometer scale minor element mapping in interplanetary dust particles: a test for stratospheric contamination," Lunar and Planetary Science XXXV, LPI (2004) 1334.
- G. J. Flynn, D. D. Durda, "Chemical and mineralogical size segregation in the impact disruption of anhydrous stone meteorites," Lunar and Planetary Science XXXV, LPI (2004) 1072.
- J. A. Fortner, A. J. Kropf, R. J. Finch, C. J. Mertz, J. L. Jerden, M. G. Goldberg, J. C. Cunnane, "Analysis of Trace Elements in Commercial Spent Nuclear Fuel using X-ray Absorption Spectroscopy," ANS Transactions, 89, American Nuclear Society (2004) CD-ROM.
- Magdalena Gauden, Sean Crosson, I. H. van Stokkum, Rienkvan Grondelle, Keith Moffat, John T. Kennis, "Low-temperature and time-resolved spectroscopic characterization of the LOV2 domain of Avena sativa phototropin," Proceedings of SPIE, 5463, Sigrid Avriillier, Jean-Michel Tualle, eds., 5463, SPIE (2004) 97 - 104.
- U. Geiser, H. H. Wang, C. Y. Han, G. A. Willing, "The role of organic conductors in a world of nanoscience," Proc. of Conf. on Organic Conductors, Superconductors and Magnets: From Synthesis to Molecular Electronics, L. Ouahab, E. Yagubskii, eds., Kluwer Academic Publishers (2004) 231 - 239.
- K. Ham, C. S. Willson, M. L. Rivers, R. L. Kurtz, L. G. Butler, "Algorithms for three-dimensional chemical analysis with multi-energy tomographic data," Proceedings of SPIE : Developments in X-Ray Tomography IV, 5535, SPIE (2004) 286 - 292.
- R. J. Hemley, H.-k. Mao, "New findings in static high-pressure science," Proceedings of the 13th APS Conference on Shock-compression of Condensed Matter, M. D. Furnish, Y. M. Gupta, J. W. Forbes, eds., 706, American Institute of Physics (2004) 17 - 26.
- G.E. Ice, R. Barabash, "Polychromatic X-Ray Microdiffraction Characterization of Local Crystallographic Microstructure Evolution in 3D," Proceedings of the 25th Symposium on Materials Science: Evolution of Deformation Microstructures in 3D, C. Gundlach, K. Haldrup, N. Hansen, X. Huang, D. Juul Jensen, T. Letters, Z. J. Lui, S. F. Nielsen, W. Pantelon, J. A. Wert, G. Winther, eds., Riso National Laboratory (2004) 351 - 356.
- K. Ignatiev, W.-K. Lee, K. Fezzaa, F. De Carlo, S.R. Stock, "Phase contrast stereometry: fatigue crack mapping in 3D," Proc. SPIE, U. Bonse, ed., 5535, SPIE (2004) 253 - 260.
- H. C. Kang, G. B. Stephenson, C. Liu, R. Conley, A. T. Macrander, J. Maser, S. Bajt, H. N. Chapman, "Synchrotron x-ray study of multilayers in Laue geometry," Proc. SPIE, 5537, SPIE (2004) 127 - 132.
- J. M. Karner, S. R. Sutton, J. J. Papike, J. S. Delaney, C. K. Shearer, M. Newville, P. Eng, M. Rivers, M. D. Dyar, "A new oxygen barometer for solar system basaltic glasses based on vanadium valence," Lunar and Planetary Science XXXV, LPI (2004) 1269.
- M. J. Kramer, D. J. Sordelet, "Metastable states during devitrification of a Zr₇₀Pd₂₀Cu₁₀ metallic glass," Amorphous and Nanocrystalline Metals, Ralf Busch, Todd C. Hufnagel, Jurgen Eckert, Akihisa Inoue, William L. Johnson, Alain Reza Yavari, eds., 806, Materials Research Society Symposium Proceedings (2004) 213 - 223.
- P. L. Lee, M. A. Beno, D. Shu, M. Ramanathan, J. F. Mitchell, J. D. Jorgensen, R. B. Von Dreele, "Dedicated high-resolution powder diffraction beamline U. Lienert, J. Almer, D. Haefner, Y. Gao, W. Carter, "Nondestructive strain tensor scanning within samples of cylindrical symmetry," Proc. of the 8th Int'l. Conf. on Synchrotron Radiation Instrumentation, 705, AIP (2004) 1074 - 1077.
- Kun Lu, Vincent P. Conticello, David G. Lynn, "Templating Colloidal Metal Nanoparticle Assemblies: Use of the A[β] Amyloid Peptide Nanotube," Symposium V, Proteins as Materials, V.P. Conticello, A. Chilkoti, E. Atkins, D.G. Lynn, eds., 826E, Mater. Res. Soc. (2004) V1.6.
- L. B. Lurio, X. Hu, S. Narayanan, X. Jiao, J. Lal, "Dynamics of Buried Polymer-Polymer Interfaces in Thin Films," Dynamics in Small Confining Systems-2003, J.T. Fourkas, P. Levitz, M. Urbakh, K.J. Wahl, eds., 790, Materials Research Society (2004) P7.43.1 - P7.43.6.
- M. J. McKelvy, A.V. G. Chizmeshya, J. Diefenbacher, H. Bearat, G. Wolf, "Exploration of the Role of Heat Activation in Enhancing Serpentine Carbon Sequestration Reactions," The Clearwater Coal Conference, National Energy Technology Laboratory, U.S. Dept. of Energy (2004) 47 - 58.
- K. L. Nagy, N. C. Sturchio, M. L. Schlegel, P. Fenter, "Cation Sorption at the Muscovite-Water Interface Using X-ray Reflectivity," Proceedings of the Eleventh International Symposium on Water-Rock Interaction, R. B. Wanty and R. R. Seal II, eds., Balkema Publishers (2004) 767 - 769.
- R.T. Ott, F. Sansoz, J.F. Molinari, J. Almer, C. Fan, T.C. Hufnagel, "Synchrotron strain measurements for in situ formed metallic glass matrix composites," Mat. Res. Soc. Symp. Proc., 806, MRS (2004) MM8.12.1 - 64.
- D. Paktunc, D. Smith, R. Lastra, A. Pratt, "Assessment of Uncertainties in Modal Analysis and Liberation Measurements by Synchrotron-based X-Ray Microtomography," Proceedings of 8th International Congress on Applied Mineralogy, M. Peccio et al., eds., 2, (2004) 1021 - 1024.

D. Paktunc, "Molecular-scale Characterization of Arsenic in Metallurgical Wastes," Proceedings of 8th International Congress on Applied Mineralogy, M. Peccio et al., eds., 1, (2004) 446 - 450.

M. L. Rivers, Y. Wang, T. Uchida, "Microtomography at GeoSoilEnviroCARS," Proceedings of SPIE : Developments in X-Ray Tomography IV, Ulrich Bonse, 5535, SPIE (2004) 783 - 791.

G. Robert, D. R. Baker, M. L. Rivers, E. Allard, J. Larocque, "Comparison of the bubble size distribution in silicate foams using 2-dimensional images and 3-dimensional x-ray microtomography," Proceedings of SPIE : Developments in X-Ray Tomography IV, Ulrich Bonse, 5535, SPIE (2004) 505 - 513.

C. K. Shearer, J. Karner, J. J. Papike, S. R. Sutton, "Oxygen fugacity of mare basalts and the lunar mantle application of a new microscale oxybarometer based on the valence state of vanadium," Lunar and Planetary Science XXXV, LPI (2004) 1617 - 16177.

S. Stock, K. Ignatiev, A. Veis, F. De Carlo, J.D. Almer, "MicroCT of sea urchin ossicles supplemented with microbeam diffraction," Proc. SPIE, U. Bonse, ed., 5535, SPIE (2004) 11 - 20.

S.R. Stock, K.I. Ignatiev, H.G. Simon, F. De Carlo, "Newt limb regeneration studied with synchrotron microCT," Proc. SPIE, U. Bonse, ed., 5535, SPIE (2004) 748 - 756.

S. R. Sutton, J. M. Karner, J. J. Papike, J. S. Delaney, C. K. Shearer, M. Newville, P. Eng, M. Rivers, M. D. Dyar, "Oxygen barometry of basaltic glasses based on vanadium valence determinations using synchrotron microXANES," Lunar and Planetary Science XXXV, LPI (2004) 1725.

V. Tirumala, D. Mancini, G. T. Caneba, "Synthesis of ultrafast response smart microgel structures," Proc. SPIE, V.K. Varadan, ed., 5389, SPIE (2004) 221 - 228.

V. R. Tirumala, D. C. Mancini, G. T. Caneba, "In situ fabrication of thermoreversible microgels," Proceedings of the International Conference on Intelligent Sensing and Information Processing - 2004, M. Palaniswami, C. C. Sekhar, G. K. Venayagamoorthy, S. Mohan, M. K. Ghantasala, eds., IEEE (2004) 196 - 200.

M. Weigl, M. A. Denecke, A. Geist, K. Gompfer, "X-ray Absorption Fine Structure Spectroscopy Investigations of the Structure of Cm(III)/Eu(III)," Advances in Nuclear and Radiochemistry, S.M. Qaim and H.H. Coenen, eds., 794, Research Centre Jülich (2004) 526 - 528.

D. J. Wesolowski, L. M. Anovitz, P. Bénézech, A. A. Chialvo, D. A. Palmer, P. Fenter, L. Cheng, N. C. Sturchio, Z. Zhang, M. J. Bedzyk, J. D. Kubicki, M. V. Fedkin, S. N. Lvov, D. Sykes, P. T. Cummings, M. K. Ridley, M. L. Machesky, M. Predota, A. Bandura, "Temperature-Effects and Structure at the Rutile-Water Interface," Proceedings of the Eleventh International Symposium on Water-Rock Interaction, R. B. Wanty and R. R. Seal II, Balkema Publishers (2004) 775 - 779.

D. Wildenschild, K. A. Culligan, B. S. B. Christensen, "Application of x-ray microtomography to environmental fluid flow problems," Proceedings of SPIE, Developments in X-Ray Tomography IV, Ulrich Bonse, 5535, SPIE (2004) 432 - 441.

C. S. Willson, K. Ham, K. A. Thompson, "Investigating the correlation between residual nonwetting phase liquids and pore-scale geometry and topology using synchrotron x-ray tomography," Proceedings of the 2004 SPIE Annual Conference, 5535, SPIE (2004) 13 - 14.

B. Yan, T. Abrajano, M. Newville, S. Sutton, N. C. Sturchio, H. Ehrlich, "Anaerobic bacterial reduction of ferric iron in pisolites," Water-Rock Interaction: Proceedings of the Eleventh International Symposium on Water-Rock Interaction, R. B. Wanty, R. R. Seal II, Balkema Publishers (2004) 1165 - 1169.

EXPERIMENTAL RESULTS: BOOK CHAPTERS

T. Ressler, J. A. van Bokhoven, G. Knop-Gericke, F. M. F. de Groot, "Time-Resolved X-ray Absorption Spectroscopy Methods," *In-situ spectroscopy of catalysis*, B. M. Weckhuysen, ed., American Scientific Publishers, 2004, 107 - 122.

T. Ressler, J. A. van Bokhoven, A. Knop-Gericke, F. M. F. de Groot, "X-ray absorption near edge spectroscopy," *In-situ spectroscopy of catalysis*, B. M. Weckhuysen, ed., American Scientific Publishers, 2004, 123 - 144.

P. H. Santschi, A. B. Burd, J.-F. Gaillard, A. A. Lazarides, "Transport of Materials and Chemicals by Nano-scale Colloids and Micro to Macro-scale Flocs in Marine, Freshwater, and Engineered Systems," *Flocculation in Natural and Engineered Environmental Systems*, I.G. Droppo, G.G. Leppard, S.N. Liss, T.G. Milligant, eds., CRC Press, 2004, 191 - 209.

Y. Wang, T. Uchida, "Thermal Expansion Measurements under High Pressure using X-ray Diffraction," *Thermal Conductivity 27 / Thermal Expansion 15*, DEStech Publications, Inc., 2004, 538 - 553.

EXPERIMENTAL RESULTS: TECHNICAL REPORTS

G.E. Brown, S.R. Sutton, J.R. Bargar, D.K. Shuh, W.A. Bassett, P.M. Bertsch, J. Bisognano, W.F. Bleam, D.L. Clark, P. DeStasio, S.E. Fendorf, P.A. Fenter, E. Fontes, J. Hormes, K.M. Kemner, S.C.B. Myneni, P.A. O'Day, K.H. Pecher, R.J. Reeder, A. Roy, S.J. Traina, C. Willson, J.M. Zachara, "Molecular Environmental Science: An assessment of research accomplishments, available synchrotron radiation facilities, and needs," SLAC 704, (February 2004).

M. C. Duff, D. B. Hunter, W. R. Wilmarth, A. Jurgensen, "Characterization of Uranium in Archived 2H Evaporator Scale," WSRC-TR-2004-00016, (February 2004).

ACCELERATOR & BEAMLINE TECHNOLOGY AND THEORY: JOURNAL ARTICLES

B. W. Adams, "Time-dependent Takagi-Taupin eikonal theory of x-ray diffraction in rapidly changing crystal structures," *Acta Crystallogr. A* 60 (2), March, 120-133 (2004).

B.W. Adams, "Time-dependent Takagi-Taupin eikonal theory and applications in the subpicosecond manipulation of x-rays," *Chem. Phys.* 299 (2-3), April, 193-201 (2004).

B.W. Adams, "Diffraction sub-picosecond manipulation of x-rays," *Radiat. Phys. Chem.* 70 (4-5), July, 469-477 (2004).

M. Lerotic, C. Jacobsen, T. Schäfer, S. Vogt, "Cluster analysis of soft x-ray spectromicroscopy data," *Ultramicroscopy* 100, 35-57 (2004).

- C. Liu, R. Conley, A.T. Macrander, "Functional profile coatings and film stress," *J. Vac. Sci. Technol. A* 22 (4), 1610-1614 (2004).
- A. H. Lumpkin, J. W. Lewellen, W. J. Berg, Y.-C. Chae, R. J. Dejus, M. Erdmann, Y. Li, S. V. Milton, D. W. Rule, "On-line SASE FEL Gain Optimization using COTRI Imaging," *Nucl. Instrum. Methods A* 528 (1-2), August, 179-183 (2004).
- A. H. Lumpkin, M. Erdmann, J. W. Lewellen, Y.-C. Chae, R. J. Dejus, P. Den Hartog, Y. Li, S. V. Milton, D.W. Rule, G. Wiemerslage, "First Observations of COTR due to a Microbunched Beam in the VUV at 157 nm," *Nucl. Instrum. Methods A* 528 (1-2), August, 194-198 (2004).
- O. V. Makarova, D. C. Mancini, N. Moldovan, R. Divan, V. N. Zyryanov, C.-M. Tang, "Fabrication of focused two-dimensional grids," *Microsystems Technologies* 10 (6-7), October, 540-543 (2004).
- S. D. Shastri, "Combining flat crystals, bent crystals, and compound refractive lenses for high-energy x-ray optics," *J. Synchrotron Rad.* 11, 150-156 (2004).
- G.K. Shenoy, "Advanced Photon Source: Science Retrospect and Prospect," *Radiat. Phys. Chem.* 70 (4-5), July, 619-630 (2004).
- G. Waldschmidt, A. Taflove, "Three-Dimensional CAD-Based Mesh Generator for the Dey-Mittra Conformal FDTD Algorithm," *IEEE T. Antennas Propag.* 52 (7), July, 1658-1664 (2004).
- C.-x. Wang, K.-J. Kim, "Beam-Envelope Theory of Ionization Cooling," *Nucl. Instrum. Methods A* 532, October, 260-269 (2004).
- C.-x. Wang, "Untangling mixed modes in model-independent analysis of beam dynamics in circular accelerators," *Phys. Rev. Spec. Top., Accel. Beams* 7, November, 114001 (2004).

ACCELERATOR & BEAMLINE TECHNOLOGY AND THEORY: CONFERENCE PAPERS

- B.W. Adams, "Femtosecond coherent control of x-rays," *Proc. SPIE*, 5194, SPIE (2004) 46 - 55.
- B.W. Adams, "Subpicosecond coherent manipulation of x-rays," *Proc. of the 8th Int'l. Conf. on Synchrotron Radiation Instrumentation*, 705, AIP (2004) 1395 - 1398.
- L. Assoufid, M. Bray, D. Shu, J. Qian, C. Preissner, B. Tieman, "Experience with stitching interferometry for evaluation of x-ray mirrors at the Advanced Photon Source," *Proc. 2nd Workshop for Metrology of X-ray Optics, ESRF (2004) CD - ROM*.
- L. Assoufid, M. Bray, D. Shu, "Development of a linear stitching interferometric system for evaluation of very large x-ray synchrotron radiation substrates and mirrors," *Proc. of the 8th Int'l. Conf. on Synchrotron Radiation Instrumentation*, 705, AIP (2004) 851 - 854.
- K. Attenkofer, B. W. Adams, M. A. Beno, "Instrumentation for time-dependent x-ray resonant Raman scattering," *Proc. of the 8th Int'l. Conf. on Synchrotron Radiation Instrumentation*, T. Warwick, J. Arthur, H.A. Padmore, J. Stoehr, 705, AIP (2004) 1138 - 1141.
- M. A. Beno, U. Ruett, C. Kurtz, G. Jennings, "High-energy Bragg and Laue monochromators for an APS wiggler beam line," *Proc. of the 8th Int'l. Conf. on Synchrotron Radiation Instrumentation*, T. Warwick, J. Arthur, H.A. Padmore, J. Stoehr, eds., 705, AIP (2004) 675 - 678.
- C. Benson, E. Trakhtenberg, Y. Jaski, B. Brajuskovic, J. Collins, P. Den Hartog, M. Erdmann, E. Rossi, O. Schmidt, W. Toter, G. Wiemerslage, "Mechanical design of a front end for canted undulators at the Advanced Photon Source," *Proc. of the 8th Int'l. Conf. on Synchrotron Radiation Instrumentation*, 705, AIP (2004) 466 - 469.
- B. Brajuskovic, P. Den Hartog, E. Trakhtenberg, "Mechanical analysis of the prototype undulator for the Linac Coherent Light Source," *Proceedings of the 2003 Particle Accelerator Conference*, J. Chew, P. Lucas, and S. Webber, eds., IEEE (2003) 1017 - 1019.
- A. Brunetti, F. De Carlo, "A robust procedure for determination of center of rotation in tomography," *Proc. SPIE*, U. Bonse, ed., 5535, SPIE (2004) 652 - 659.
- T. Buonassisi, A.A. Istratov, T.F. Ciszek, D.W. Cunningham, A.M. Gabor, R. Jonczyk, R. Schindler, M. Sheoran, A. Upadhyaya, A. Rohatgi, B. Lai, Z. Cai, M.A. Marcus, E.R. Weber, "Differences and similarities between metal clusters in mc-Si materials from different manufacturers," *14th Workshop on Crystalline Silicon Solar Cells & Modules: Materials and Processes, NREL (2004)* 226 - 229.
- S.-K. Cheong, J. Liu, D. Shu, J. Wang, C. F. Powell, "Effects of ambient pressure on dynamics of near-nozzle diesel sprays studied by ultrafast x-radiography," *2004 SAE Fuels & Lubricants Meeting and Exhibition, SAE International (2004)* 2004-01-2026.
- S.-K. Cheong, J. Liu, C.F. Powell, J. Wang, "Application of an avalanche photodiode in synchrotron-based ultra-fast x-radiography," *Proc. of the 8th Int'l. Conf. on Synchrotron Radiation Instrumentation*, 705, AIP (2004) 961 - 964.
- J. T. Cremer, M. A. Piestrup, C. K. Gary, R. H. Pantell, "Large-aperture compound refractive lenses," *Fourth-Generation X-ray Sources and Ultrafast X-ray Detectors*, 5194, SPIE (2004) 62 - 89.
- F. De Carlo, B. Tieman, "High-throughput x-ray microtomography system at the Advanced Photon Source beamline 2-BM," *Proc. SPIE*, U. Bonse, ed., 5535, SPIE (2004) 644 - 651.
- P. Den Hartog, G.A. Decker, L.J. Emery, "Dual canted undulators at the Advanced Photon Source," *Proceedings of the 2003 Particle Accelerator Conference*, J. Chew, P. Lucas, and S. Webber, eds., IEEE (2003) 833 - 835.
- D. A. Dohan, N. D. Arnold, "Integrated Relational Modeling of Software, Hardware, and Cable Databases at the APS," *Proceedings of ICALEPCS2003, Pohang Accelerator Laboratory (2004)* 365 - 367.
- Y. I. Dudchik, N. N. Kolchevsky, F. F. Komarov, M. A. Piestrup, J. T. Cremer, C. K. Gary, R. H. Pantell, "Short-focal-length compound refractive lenses for x-rays," *Fourth-Generation X-ray Sources and Ultrafast Detectors*, R.O. Tatchyn, Z. Chang, J.-C. Kieffer, J.B. Hastings, eds., 5194, SPIE (2004) 56 - 61.
- E.M. Dufresne, J.A. Guzman, S.B. Dierker, R. Clarke, D.A. Arms, D.A. Walko, "Experience with a fluorescence-based beam position monitor at the APS," *Proc. of the 8th Int'l. Conf. on Synchrotron Radiation Instrumentation*, 705, AIP (2004) 679 - 682.
- E.M. Dufresne, D.A. Arms, N.R. Pereira, P. Ilinski, R. Clarke, "An imaging system for focusing tests of Li multiprism x-ray refractive lenses," *Proc. of the 8th Int'l. Conf. on Synchrotron Radiation Instrumentation*, 705, AIP (2004) 780 - 783.

- H. Halloin, P. von Ballmoos, J. Ervard, G.K. Skinner, M. Hernanz, N.V. Abrosimov, P. Bastie, B. Hamelin, V. Lonjou, J.M. Alvarez, A. Laurens, P. Jean, J. Knödseder, R.K. Smither, G. Vedrenne, "CLAIRE gamma-ray lens: flight and long-distance test results," Proc. SPIE, O. Citterio, S.L. O'Dell, eds., 5168, SPIE (2004) 471 - 481.
- Y. Jaski, "New front-end design for multiple in-line undulators at the Advanced Photon Source," Proc. of the 8th Int'l. Conf. on Synchrotron Radiation Instrumentation, 705, AIP (2004) 356 - 359.
- P. K. Job, J. Alderman, "Radiation Levels Experienced by the Insertion Devices of the Third-Generation Synchrotron Radiation Sources," Proceedings of the Sixth Meeting of the Task Force on Shielding Aspect of Accelerators, Targets and Irradiation Facilities, Nuclear Energy Agency, OECD (2004) 299.
- P. K. Job, J. Alderman, "A Neutron Detection System for Electron Accelerators," Proc. of the Sixth International Topical Meeting on Nuclear Applications of Accelerator Technology, ANS (2004) 380 - 383.
- R. Khachatryan, A. Tkachuk, Y. S. Chu, J. Qian, A. Macrander, "Open-faced Z-shaped channel-cut x-ray monochromator," X-ray Sources and Optics, Proc. SPIE, C.A. MacDonald, A.T. Macrader, T. Ishikawa, C. Morawe, J.L. Wood, eds., 5537, SPIE (2004) 171 - 176.
- A. Khounsary, P.J. Eng, L. Assoufid, A. Macrander, J. Qian, "Recoating mirrors having a chromium underlayer," Proc. SPIE, 5193, SPIE (2004) 177-181.
- S.H. Kim, C. Doose, R.L. Kustom, E.R. Moog, K.M. Thompson, "Experimental study of the stability margin with beam heating in a short-period superconducting undulator for the APS," Proc. of EPAC 2004, European Physical Society Accelerator Group (EPS-AG) (2004) 470 - 472.
- M. R. Kraimer, "EPICS: Operating-System-Independent Device/Driver Support," Proceedings of ICALEPCS2003, Pohang Accelerator Laboratory (2004) 205 - 207.
- P. L. Lee, M. A. Beno, D. Shu, M. Ramanathan, J. F. Mitchell, J. D. Jorgensen, R. B. Von Dreele, "Dedicated high-resolution powder diffraction beamline at the Advanced Photon Source," Proc. of the 8th Int'l. Conf. on Synchrotron Radiation Instrumentation, T. Warwick, J. Arthur, H. A. Padmore, J. Stoehr, eds., Proc. of the 8th Int'l. Conf. on Synchrotron Radiation Instrumentation, 705, AIP (2004) 388 - 391.
- S.-H. Lee, E. Trakhtenberg, P. Den Hartog, "Insertion device vacuum chamber for the Linac Coherent Light Source," Proceedings of the 2003 Particle Accelerator Conference, J. Chew, P. Lucas, and S. Webber, eds., IEEE (2003) 824 - 826.
- J.W. Lewellen, "High-Brightness Injector Modeling," Proc. of the Eleventh Advanced Accelerator Concepts Workshop, AIP 737, AIP (2004) 483 - 493.
- Y. Li, A. Khounsary, J. Maser, S. Nair, "Cooled mirror for a double undulator beamline," Proc. SPIE, A.M. Khounsary, U. Dinger, K. Ota, 5193, SPIE (2004) 204 - 210.
- Y. Li, A. Khounsary, M. Gosz, "Effect of silicon anisotropy on mirror substrate design," Proc. SPIE, A.M. Khounsary, U. Dinger, K. Ota, eds., 5533, SPIE (2004) 124 - 130.
- Y. Li, A. Khounsary, S. Nair, "How and why side cooling of high-heat-load optics works," Proc. SPIE, A.M. Khounsary, U. Dinger, K. Ota, eds., 5533, SPIE (2004) 157 - 162.
- Y. Li, A. Khounsary, S. Narayanan, A. Macrander, R. Khachatryan, L. Lurio, "Design and analysis of a cooled Z-shaped germanium x-ray monochromator," SPIE Proc., C.A. MacDonald, A.T. Macrander, T. Ishikawa, C. Morawe, J.L. Woods, eds., 5537, SPIE (2004) 189 - 192.
- R. Lill, A. Pietryla, E. Norum, F. Lenkszus, "APS Storage Ring Monopulse RF BPM Upgrade Proposal," Proc. of the Beam Instrumentation Workshop 2004: Eleventh Beam Instrumentation Workshop, Thomas Shea, R. Coles Sibley III, eds., 732, AIP (2004) 358 - 365.
- C. Liu, R. Conley, L. Assoufid, Z. Cai, J. Qian, A.T. Macrander, "From flat substrate to elliptical KB mirror by profile coating," Proc. of the 8th Int'l. Conf. on Synchrotron Radiation Instrumentation, 705, AIP (2004) 704 - 707.
- C. Liu, R. Conley, A.T. Macrander, T. Graber, Ch. Morawe, C. Borel, E.M. Dufresne, "Small d-spacing WSi₂/Si narrow bandpass multilayers," Proc. SPIE, C.A. MacDonald, A.T. Macrander, T. Ishikawa, C. Morawe, J.L. Woods, eds., 5537, SPIE (2004) 154 - 160.
- J. Liu, J. Wang, B. Shan, C. Wang, Z. Chang, "X-ray streak camera with 30-fs timing jitter," Proc. SPIE Vol., 5194, SPIE (2004) 123 - 127.
- A.H. Lumpkin, B.X. Yang, M. Borland, "Measurements of the APS Storage Ring Beam Stability at 225 mA," Proc. of the Beam Instrumentation Workshop 2004: Eleventh Beam Instrumentation Workshop, Thomas Shea, R. Coles Sibley III, eds., 732, AIP (2004) 366 - 372.
- A.H. Lumpkin, R.J. Dejus, D.W. Rule, "Applications with Intense OTR Images II: Microbunched Electron Beams," Proc. of the Eleventh Advanced Accelerator Concepts Workshop, AIP 737, AIP (2004) 379 - 385.
- A.H. Lumpkin, V.E. Scarpine, "Applications with Intense OTR Images I: 120-GeV Protons," Proc. of the Eleventh Advanced Accelerator Concepts Workshop, AIP 737, AIP (2004) 359 - 364.
- O.V. Makarova, G. Yang, C.-M. Tang, D.C. Mancini, R. Divan, J. Yaeger, "Fabrication of collimators for gamma-ray imaging," Proc. SPIE, A.A. Snigirev, D.C. Mancini, eds., 5539, SPIE (2004) 126 - 132.
- J. Maser, G.B. Stephenson, D. Shu, B. Lai, S. Vogt, A. Khounsary, Y. Li, C. Benson, G. Schneider, "Conceptual design for a hard x-ray nanoprobe beamline with 30 nm resolution," Proc. of the 8th Int'l. Conf. on Synchrotron Radiation Instrumentation, 705, AIP (2004) 470 - 473.
- W.E. Norum, "New Capabilities of the EPICS IOC Shell," Proceedings of ICALEPCS2003, Pohang Accelerator Laboratory (2004) 60 - 62.
- L.E. Ocola, J. Maser, S. Vogt, B. Lai, R. Divan, G.B. Stephenson, "Tapered tilted linear zone plates for focusing hard x-rays," Proc. SPIE, A.A. Snigirev, D.C. Mancini, eds., 5539, SPIE (2004) 165 - 173.
- M. Petra, P.K. Den Hartog, E.R. Moog, S. Sasaki, N. Sereno, I.B. Vasserman, "Radiation effects studies at the Advanced Photon Source," Nucl. Instrum. Methods A 507, 422-425 (2003).
- M. Ramanathan, M. Smith, J. Grimmer, M. Merritt, "A Four-Motor Insertion Device Control System at the Advanced Photon Source," Proc. of the 8th Int'l. Conf. on Synchrotron Radiation Instrumentation, T. Warwick et al., eds., Proc. of the 8th Int'l. Conf. on Synchrotron Radiation Instrumentation, 705, AIP (2004) 286 - 289.

- V. Sajaev, "Measurement of Bunch Length Using Spectral Analysis of Incoherent Radiation Fluctuations," Proc. of the Beam Instrumentation Workshop 2004: Eleventh Beam Instrumentation Workshop, Thomas Shea, R. Coles Sibley III, eds., 732, AIP (2004) 73 - 87.
- V. Sajaev, Z. Huang, S. G. Biedron, P. K. Den Hartog, E. Gluskin, K.-J. Kim, J. W. Lewellen, Y. Li, O. Makarov, S. V. Milton, E. R. Moog, "Z-dependent Spectral Measurements of SASE FEL Radiation at APS," Nucl. Instrum. Methods A 506, 304-315 (2003).
- M. Sanchez del Rio, R.J. Dejus, "XOP 2.1 - A new version of the x-ray optics software toolkit," Proc. of the 8th Int'l. Conf. on Synchrotron Radiation Instrumentation, 705, AIP (2004) 784 - 787.
- S. Sasaki, "Conceptual design for superconducting planar helical undulator," Proc. of the 8th Int'l. Conf. on Synchrotron Radiation Instrumentation 705, AIP (2004) 278 - 281.
- G.K. Shenoy, J.W. Lewellen, D. Shu, N.A. Vinokurov, "Variable-period undulators - a potential source for storage ring, ERL and FEL applications," Proc. of the 8th Int'l. Conf. on Synchrotron Radiation Instrumentation, 705, AIP (2004) 274 - 277.
- D. Shu, C. Preissner, D. Nocher, Y. Han, J. Barraza, P. Lee, W.-K. Lee, Z. Cai, S. Ginell, R. Alkire, K. Lazarski, R. Schuessler, A. Joachimiak, "Design and development of a robot-based automation system for cryogenic crystal sample mounting at the Advanced Photon Source," Proc. of the 8th Int'l. Conf. on Synchrotron Radiation Instrumentation, 705, AIP (2004) 1201 - 1204.
- D. Shu, J. Maser, B. Lai, S. Vogt, "Design for an x-ray nanoprobe prototype with a sub-10-nm positioning requirement," Proc. of the 8th Int'l. Conf. on Synchrotron Radiation Instrumentation, 705, AIP (2004) 1287 - 1290.
- R.K. Smither, A.M. Khounsary, D.C. Mancini, K. Abu Saleem, "Performance of a Be refractive lens," Proc. of the 8th Int'l. Conf. on Synchrotron Radiation Instrumentation, 705, AIP (2004) 716 - 719.
- L. C. Teng, "Emittance and Cooling," Accelerator Physics, Technology and Applications - Selected Lectures of OCPA International Accelerator School 2002, Alexander Wu Chao, Herbert O. Moser, and Zhentang Zhao, eds., World Scientific (2004) 394 - 414.
- Lee C. Teng, "Synchrotron Radiation," Accelerator Physics, Technology and Applications -- Selected Lectures of OCPA International Accelerator School 2002, Alexander Wu Chao, Herbert O. Moser, and Zhentang Zhao, eds., World Scientific (2004) 176 - 204.
- E. Trakhtenberg, G. Wiemerslage, P. Den Hartog, B. Brajuskovic, "New insertion device vacuum chambers at the Advanced Photon Source," Proceedings of the 2003 Particle Accelerator Conference, J. Chew, P. Lucas, and S. Webber, eds., IEEE (2003) 830 - 832.
- S. Vogt, M. Feser, D. Legnini, J. Kirz, J. Maser, "Fast differential phase-contrast imaging and total fluorescence yield mapping in a hard x-ray fluorescence microprobe," Proc. of the 8th Int'l. Conf. on Synchrotron Radiation Instrumentation, 705, AIP (2004) 1348 - 1351.
- P. von Ballmoos, H. Halloin, G. Skinner, B. Smither, et al., "MAX: a gamma-ray lens for nuclear astrophysics," Proc. SPIE, O. Citterio, S.L. O'Dell, 5168, SPIE (2004) 482 - 491.
- C.-x. Wang, K. Harkay, "New Characteristics of a Single-Bunch Instability in the APS Storage Ring," Proceedings of EPAC 2004, European Physical Society Accelerator Group (EPS-AG) and CERN (2004) 2170 - 2172.
- C.-x. Wang, R. Calaga, "Transverse Coupling Measurement using SVD Modes from Beam Histories," Proceedings of EPAC 2004, European Physical Society Accelerator Group (EPS-AG) and CERN (2004) 1470 - 1472.
- C.-x. Wang, "Techniques to Extract Physical Modes in Model-Independent Analysis of Rings," Proceedings of EPAC 2004, European Physical Society Accelerator Group (EPS-AG) and CERN (2004) 1473 - 1475.
- J. Wang, "A New Current Regulator for the APS Storage Ring Correction Magnet Bipolar Switching Mode Converters," Proceedings of EPAC 2004, European Physical Society Accelerator Group (EPS-AG) and CERN (2004) 1768 - 1779.
- S. Xu, R. F. Fischetti, "A Ray-Tracing Study of the Dependence of Focal Properties on Surface Figure Error for a Kirkpatrick-Baez (K-B) Mirror System," Proc. of the 8th Int'l. Conf. on Synchrotron Radiation Instrumentation, 705, AIP (2004) 776 - 779.
- Y. Yacoby, D. A. Walko, D. Brewes, M. Bretschneider, M. Sowwan, R. Clarke, R. Pindak, E. A. Stern, "Diffractometer-control software for Bragg-rod measurements," Proc. of the 8th Int'l. Conf. on Synchrotron Radiation Instrumentation, 705, AIP (2004) 1221 - 1224.
- C. Y. Yao, G. Banks, G. Decker, R. Klaffky, "How We Do Business at APS," Proceedings of the 4th Workshop on Accelerator Operation WAO2003, KEK Proc. 2003-19, KEK (2004) 5 - 7.
- K. Young, A. Khounsary, "Extrusion of compound refractive x-ray lenses," Proc. SPIE, A.A. Snigirev, D.C. Mancini, eds., 5539, SPIE (2004) 31 - 37.
- K. Zhang, G. Rosenbaum, R. Liu, C. Liu, C. Carmeli, G. Bunker, D. Fischer, "Development of multilayer analyzer array detectors for x-ray fluorescence at the third generation synchrotron source," Proc. of the 8th Int'l. Conf. on Synchrotron Radiation Instrumentation, 705, AIP (2004) 957 - 960.
- L. Zhang, W.-K. Lee, M. Wulff, L. Eybert, "Performance prediction of cryogenically cooled silicon crystal monochromator," Proc. of the 8th Int'l. Conf. on Synchrotron Radiation Instrumentation, 705, AIP (2004) 623 - 626.

ACCELERATOR & BEAMLINE TECHNOLOGY AND THEORY: TECHNICAL REPORTS

- J. Alderman, E. Semones, P.K. Job, "Radiation Dose Measurements of the Insertion Devices Using Radiachromic Film Dosimeters," LS-283, rev. 1, (February 2004).
- J.T. Collins, C.L. Doose, J.N. Attig, M.M. Baehl, "Canted-undulator front-end exit-mask flow-induced vibration measurements," LS-306, (November 2004).
- R.J. Dejus, "Effect of emittance and rms phase error on angular flux density and pinhole flux-a simulation study of two undulators at 10.5 mm gap including very high harmonics," LS-304, (2004).
- R.W.C. Hansen, M. Severson, L. Assoufid, J. Qian, "UV/ozone cleaning of silicon carbide optics," SRC 210, (December 2004).
- K.-J. Kim (ed.), B. Carlsten, D. Dowell, K. Flottmann, K. Jensen, J. Petillo, A. Sessler, G. Stupakov, "Towards Advanced Electron Beam Brightness Enhancement and Conditioning," LS-305, (February 2004).

Y. Li, "Operation of the APS Photoinjector Drive Laser System," LS-307, (December 2004).

DISSERTATIONS

Richard Baxter, "Time-resolved crystallographic studies of the bacterial reaction center," Ph.D., The University of Chicago, 2004.

M. A. Borthwick, "Measurements of Dynamics in an Orientationally Anisotropic System," Ph.D., Massachusetts Institute of Technology, 2004.

Daniel P. Core, "Oxygen Sulfur Fugacities of Granetoids: Implications for Ore-Forming Processes," Ph.D., University of Michigan, 2004.

P. Falus, "X-ray photon correlation spectroscopy studies of the dynamics of self-assembling block copolymer structures," Ph.D., Massachusetts Institute of Technology, 2004.

R. T. Hart, "Structures and Optical Properties of Tellurite Glasses and Glass Ceramics," Ph.D., Indiana University, 2004.

Tiffany C. Kaspar, "Materials and Magnetic Studies of Cobalt-Doped Anatase Titanium Dioxide and Perovskite Strontium Titanate as Potential Dilute Magnetic Semiconductors," Ph.D., University of Washington, 2004.

Jiyuan Ke, "Crystal Structures and Mechanisms of Two Enzymes Involved in the Degradation of Tyrosine and Biphenyl," Ph.D., Purdue University, 2004.

Jason Key, "X-ray Crystallographic Studies of Bacterial Oxygen Sensor Proteins," Ph.D., The University of Chicago, 2004.

Craig P. McClure, "X-ray Absorption and X-ray Fluorescence Studies of Metalloproteins," Ph.D., University of Michigan, 2004.

S. E. McLain, "Structural Studies of Superacidic Systems Using Neutron and High Energy X-ray Diffraction," Ph.D., University of Tennessee - Knoxville, 2004.

H. Mo, "Neutron and X-ray Scattering Study of Intermediate-Length Alkane Films Adsorbed on Solid Surfaces," Ph.D., University of Missouri-Columbia, 2004.

Lindsay T. Odell, "The X-ray Crystallographic Structure of Phytanoyl-Coenzyme A Hydroxylase, an Fe(II) 2-Oxoglutarate Dependent Dioxygenase Involved in Refsum's Disease," Ph.D., Johns Hopkins University School of Medicine, 2004.

Christian Pantea, "Kinetics of diamond-silicon reaction under high pressure-high temperature conditions," Ph.D., Texas Christian University, 2004.

Samantha J. Perez-Miller, "Conformational selection of coenzyme bound to human mitochondrial aldehyde dehydrogenase," Ph.D., Indiana University, 2004.

Sudarshan Rajagopal, "Structural Pathways for Signaling in Photoactive Yellow Protein," Ph.D., The University of Chicago, 2004.

Kristen Strand, "Crystallographic Studies of Erythrocrucorin from Lumbricus Terrestris," Ph.D., University of Massachusetts Medical School, 2004.

Tsu-Chien Weng, "X-ray absorption spectroscopy studies on redox-active manganese," Ph.D., University of Michigan, 2004.

N. Yang, "Synchrotron diffraction studies of spontaneous magnetostriction in rare earth transition metal compounds," Ph.D., Iowa State University, 2004.

Shixin Ye, "Design, characterization of amphiphilic proteins and potential engineering applications," Ph.D., University of Pennsylvania, 2004.

The research highlights were written by:

David Appell (davidappell@comcast.net)
William Arthur Atkins (william.atkins@verizon.net)
David Bradley (david@sciencebase.com)
Yvonne Carts-Powell (yvonne@nasw.org)
Adrian Cho (hadriancho@yahoo.com)
Vic Comello (ANL-IPD)
Karen Fox (kfox@nasw.org)
Phil Koth (philkoth@insightbb.com)
Elise LeQuire (cygnete@mindspring.com)
JR Minkel (j_r_minkel@hotmail.com)
Mona A. Mort (mamort@nasw.org)
David Voss (dvoss@nasw.org)
Mark Wolverton (exetermw@earthlink.net)

Editorial advisors:

Mark A. Beno (XFD-ADM), Rodney Gerig (ASD-ADM), J. Murray Gibson (SUF-PA), Efim Gluskin (XFD-ADM), Gabrielle G. Long (XFD-ADM), Dennis M. Mills, (SUF-PA), William G. Ruzicka (AOD-ADM)

Mechanical editing:

Floyd Bennett (IPD-MED), Mary Fitzpatrick (IPD-MED), Catherine Eyberger (ASD-ADM), Madonna Pence (IPD-MED), Susan Picologlou (XFD-ADM)

Cover design: Aaron Ashley (Ranstad)

Photography: ANL Photography Group (IPD-MED)

Project coordination: Richard Fenner (SUF-PA), Susan Picologlou (XFD-ADM)

Publication design, photography: Richard Fenner (SUF-PA)

Our thanks to the corresponding authors who assisted in the preparation of the research highlights, and our apologies to anyone inadvertently left off this list. Your contributions are definitely appreciated.